



National Library  
of Canada

Acquisitions and  
Bibliographic Services Branch

395 Wellington Street  
Ottawa, Ontario  
K1A 0N4

Bibliothèque nationale  
du Canada

Direction des acquisitions et  
des services bibliographiques

395, rue Wellington  
Ottawa (Ontario)  
K1A 0N4

*Your file / Votre référence*

*Our file / Notre référence*

## NOTICE

The quality of this microform is heavily dependent upon the quality of the original thesis submitted for microfilming. Every effort has been made to ensure the highest quality of reproduction possible.

If pages are missing, contact the university which granted the degree.

Some pages may have indistinct print especially if the original pages were typed with a poor typewriter ribbon or if the university sent us an inferior photocopy.

Reproduction in full or in part of this microform is governed by the Canadian Copyright Act, R.S.C. 1970, c. C-30, and subsequent amendments.

## AVIS

La qualité de cette microforme dépend grandement de la qualité de la thèse soumise au microfilmage. Nous avons tout fait pour assurer une qualité supérieure de reproduction.

S'il manque des pages, veuillez communiquer avec l'université qui a conféré le grade.

La qualité d'impression de certaines pages peut laisser à désirer, surtout si les pages originales ont été dactylographiées à l'aide d'un ruban usé ou si l'université nous a fait parvenir une photocopie de qualité inférieure.

La reproduction, même partielle, de cette microforme est soumise à la Loi canadienne sur le droit d'auteur, SRC 1970, c. C-30, et ses amendements subséquents.

Canada

**UNIVERSITY OF ALBERTA**

**COMPRESSIVE BEHAVIOR AND STRENGTH OF STEEL GUSSET  
PLATE CONNECTIONS**

**BY**



**MICHAEL C. H. YAM**

**A thesis submitted to the Faculty of Graduate Studies and Research in partial fulfillment of  
the requirements for the degree of DOCTOR OF PHILOSOPHY.**

**DEPARTMENT OF CIVIL ENGINEERING**

**Edmonton, Alberta**

**Fall 1994**



National Library  
of Canada

Acquisitions and  
Bibliographic Services Branch

395 Wellington Street  
Ottawa, Ontario  
K1A 0N4

Bibliothèque nationale  
du Canada

Direction des acquisitions et  
des services bibliographiques

395, rue Wellington  
Ottawa (Ontario)  
K1A 0N4

*Your file* *Votre référence*

*Our file* *Notre référence*

THE AUTHOR HAS GRANTED AN IRREVOCABLE NON-EXCLUSIVE LICENCE ALLOWING THE NATIONAL LIBRARY OF CANADA TO REPRODUCE, LOAN, DISTRIBUTE OR SELL COPIES OF HIS/HER THESIS BY ANY MEANS AND IN ANY FORM OR FORMAT, MAKING THIS THESIS AVAILABLE TO INTERESTED PERSONS.

L'AUTEUR A ACCORDE UNE LICENCE IRREVOCABLE ET NON EXCLUSIVE PERMETTANT A LA BIBLIOTHEQUE NATIONALE DU CANADA DE REPRODUIRE, PRETER, DISTRIBUER OU VENDRE DES COPIES DE SA THESE DE QUELQUE MANIERE ET SOUS QUELQUE FORME QUE CE SOIT POUR METTRE DES EXEMPLAIRES DE CETTE THESE A LA DISPOSITION DES PERSONNE INTERESSEES.

THE AUTHOR RETAINS OWNERSHIP OF THE COPYRIGHT IN HIS/HER THESIS. NEITHER THE THESIS NOR SUBSTANTIAL EXTRACTS FROM IT MAY BE PRINTED OR OTHERWISE REPRODUCED WITHOUT HIS/HER PERMISSION.

L'AUTEUR CONSERVE LA PROPRIETE DU DROIT D'AUTEUR QUI PROTEGE SA THESE. NI LA THESE NI DES EXTRAITS SUBSTANTIELS DE CELLE-CI NE DOIVENT ETRE IMPRIMES OU AUTREMENT REPRODUITS SANS SON AUTORISATION.

ISBN 0-612-01666-8

Canada

Name YAM, MICHAEL CHI-HO

Dissertation Abstracts International is arranged by broad, general subject categories. Please select the one subject which most nearly describes the content of your dissertation. Enter the corresponding four-digit code in the spaces provided.

CIVIL ENGINEERING

0543 U·M·I

SUBJECT TERM

SUBJECT CODE

Subject Categories

**THE HUMANITIES AND SOCIAL SCIENCES**

<b>COMMUNICATIONS AND THE ARTS</b>	
Architecture	0729
Art History	0377
Cinema	0900
Dance	0378
Fine Arts	0357
Information Science	0723
Journalism	0391
Library Science	0399
Mass Communications	0708
Music	0413
Speech Communication	0459
Theater	0465
<b>EDUCATION</b>	
General	0515
Administration	0514
Adult and Continuing	0516
Agricultural	0517
Art	0273
Bilingual and Multicultural	0282
Business	0688
Community College	0275
Curriculum and Instruction	0727
Early Childhood	0518
Elementary	0524
Finance	0277
Guidance and Counseling	0519
Health	0680
Higher	0745
History of	0520
Home Economics	0278
Industrial	0521
Language and Literature	0279
Mathematics	0280
Music	0522
Philosophy of	0998
Physical	0523

Psychology	0525
Reading	0535
Religious	0527
Sciences	0714
Secondary	0533
Social Sciences	0534
Sociology of	0340
Special	0529
Teacher Training	0530
Technology	0710
Tests and Measurements	0288
Vocational	0747

**LANGUAGE, LITERATURE AND LINGUISTICS**

<b>Language</b>	
General	0679
Ancient	0289
Linguistics	0290
Modern	0291
<b>Literature</b>	
General	0401
Classical	0294
Comparative	0295
Medieval	0297
Modern	0298
African	0316
American	0591
Asian	0305
Canadian (English)	0352
Canadian (French)	0355
English	0593
Germanic	0311
Latin American	0312
Middle Eastern	0315
Romance	0313
Slavic and East European	0314

**PHILOSOPHY, RELIGION AND THEOLOGY**

Philosophy	0422
<b>Religion</b>	
General	0318
Biblical Studies	0321
Clergy	0319
History of	0320
Philosophy of	0322
Theology	0469

**SOCIAL SCIENCES**

American Studies	0323
<b>Anthropology</b>	
Archaeology	0324
Cultural	0326
Physical	0327
<b>Business Administration</b>	
General	0310
Accounting	0272
Banking	0770
Management	0454
Marketing	0338
Canadian Studies	0385
<b>Economics</b>	
General	0501
Agricultural	0503
Commerce-Business	0505
Finance	0508
History	0509
Labor	0510
Theory	0511
Folklore	0358
Geography	0366
Gerontology	0351
<b>History</b>	
General	0578

Ancient	0579
Medieval	0581
Modern	0582
Black	0328
African	0331
Asia, Australia and Oceania	0332
Canadian	0334
European	0335
Latin American	0336
Middle Eastern	0333
United States	0337
History of Science	0585
Law	0398
<b>Political Science</b>	
General	0615
International Law and Relations	0616
Public Administration	0617
Recreation	0814
Social Work	0452
<b>Sociology</b>	
General	0626
Criminology and Penology	0627
Demography	0938
Ethnic and Racial Studies	0631
Individual and Family Studies	0628
Industrial and Labor Relations	0629
Public and Social Welfare	0630
Social Structure and Development	0700
Theory and Methods	0344
Transportation	0709
Urban and Regional Planning	0999
Women's Studies	0453

**THE SCIENCES AND ENGINEERING**

**BIOLOGICAL SCIENCES**

<b>Agriculture</b>	
General	0473
Agronomy	0285
Animal Culture and Nutrition	0475
Animal Pathology	0476
<b>Food Science and Technology</b>	
Forestry and Wildlife	0478
Plant Culture	0479
Plant Pathology	0480
Plant Physiology	0817
Range Management	0777
Wood Technology	0746
<b>Biology</b>	
General	0306
Anatomy	0287
Biostatistics	0308
Botany	0309
Cell	0379
Ecology	0329
Entomology	0353
Genetics	0369
Limnology	0793
Microbiology	0410
Molecular	0307
Neuroscience	0317
Oceanography	0416
Physiology	0433
Radiation	0821
Veterinary Science	0778
Zoology	0472
<b>Biophysics</b>	
General	0786
Medical	0760
<b>EARTH SCIENCES</b>	
Biogeochemistry	0425
Geochemistry	0996

Geodesy	0370
Geology	0372
Geophysics	0373
Hydrology	0388
Mineralogy	0411
Paleobotany	0345
Paleoecology	0426
Paleontology	0418
Paleozoology	0985
Palynology	0427
Physical Geography	0368
Physical Oceanography	0415

**HEALTH AND ENVIRONMENTAL SCIENCES**

Environmental Sciences	0749
<b>Health Sciences</b>	
General	0500
Audiology	0300
Chemotherapy	0700
Dentistry	0700
Education	0700
Hospital Management	0700
Human Development	0700
Immunology	0982
Medicine and Surgery	0564
Mental Health	0347
Nursing	0569
Nutrition	0570
Obstetrics and Gynecology	0380
Occupational Health and Therapy	0354
Ophthalmology	0381
Pathology	0571
Pharmacology	0419
Pharmacy	0572
Physical Therapy	0382
Public Health	0573
Radiology	0574
Recreation	0575

Speech Pathology	0460
Toxicology	0383
Home Economics	0386

**PHYSICAL SCIENCES**

<b>Pure Sciences</b>	
<b>Chemistry</b>	
General	0485
Agricultural	0749
Analytical	0486
Biochemistry	0487
Inorganic	0488
Nuclear	0738
Organic	0490
Pharmaceutical	0491
Physical	0494
Polymer	0495
Radiation	0754
Mathematics	0405
<b>Physics</b>	
General	0605
Acoustics	0986
<b>Astronomy and Astrophysics</b>	
Astronomy and Astrophysics	0606
Atmospheric Science	0608
Atomic	0748
Electronics and Electricity	0607
Elementary Particles and High Energy	0798
Fluid and Plasma	0759
Molecular	0609
Nuclear	0610
Optics	0752
Radiation	0756
Solid State	0611
Statistics	0463
<b>Applied Sciences</b>	
Applied Mechanics	0346
Computer Science	0984

<b>Engineering</b>	
General	0537
Aerospace	0538
Agricultural	0539
Automotive	0540
Biomedical	0541
Chemical	0542
Civil	0543
Electronics and Electrical	0544
Heat and Thermodynamics	0348
Hydraulic	0545
Industrial	0546
Marine	0547
Materials Science	0794
Mechanical	0548
Metallurgy	0743
Mining	0551
Nuclear	0552
Packaging	0549
Petroleum	0765
Sanitary and Municipal	0554
System Science	0790
Geotechnology	0428
Operations Research	0796
Plastics Technology	0795
Textile Technology	0994

**PSYCHOLOGY**

General	0621
Behavioral	0384
Clinical	0622
Developmental	0620
Experimental	0623
Industrial	0624
Personality	0625
Physiological	0989
Psychobiology	0349
Psychometrics	0632
Social	0451



UNIVERSITY OF ALBERTA

RELEASE FORM

NAME OF AUTHOR: **Michael C. H. Yam**

TITLE OF THESIS: **Compressive Behavior and Strength of Steel Gusset Plate  
Connections**

DEGREE: **Doctor of Philosophy**

YEAR THIS DEGREE GRANTED: **1994**

Permission is hereby granted to the University of Alberta Library to reproduce single copies of this thesis and to lend or sell such copies for private, scholarly or scientific research purposes only.

The author reserves all other publication and other rights in association with the copyright in the thesis, and except as hereinbefore provided neither the thesis nor any substantial portion thereof may be printed or otherwise reproduced in any material form whatever without the author's prior written permission.



---

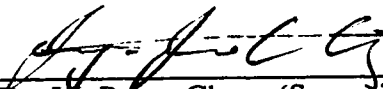
14842-43 Ave., Edmonton, Alberta  
Canada, T6H 5S1

Date: **7 Oct. 1994**

UNIVERSITY OF ALBERTA

FACULTY OF GRADUATE STUDIES AND RESEARCH

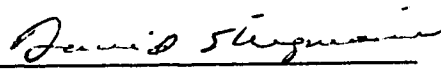
The undersigned certify that they have read, and recommend to the Faculty of Graduate Studies and Research for acceptance, a thesis entitled **COMPRESSIVE BEHAVIOR AND STRENGTH OF STEEL GUSSET PLATE CONNECTIONS** submitted by **MICHAEL C. H. YAM** in partial fulfillment of the requirements for the degree of **DOCTOR OF PHILOSOPHY**.

  
\_\_\_\_\_  
Dr. J.J. Roger Cheng (Supervisor)

  
\_\_\_\_\_  
Dr. D. H-K Chan

  
\_\_\_\_\_  
Dr. G. L. Kulak

  
\_\_\_\_\_  
Dr. D. W. Murray

  
\_\_\_\_\_  
Dr. D. J. Steigmann

  
\_\_\_\_\_  
Dr. J. A. Packer (External Examiner)

Date: *Oct. 6, 1994*

## ABSTRACT

Gusset plate connections are commonly used in bridge trusses and braced steel frames to transfer forces from one structural member to another. Due to the complexity of these connections, it is extremely difficult to evaluate the strength of gusset plate connections. Hence, a research program was initiated to investigate the compressive behavior and ultimate strength of gusset plate connections by testing full-scale diagonal bracing connections. In total, twenty-one tests were conducted on nineteen specimens. The test parameters included gusset plate thickness, size, brace angle ( $30^\circ$  and  $45^\circ$ ) and out-of-plane restraint boundary conditions. In addition, the effects of frame action on the compressive behavior of gusset plate connections were investigated by applying beam and column moment to the specimens. Out-of-plane loading eccentricity, which happens frequently in tubular bracing members with a slotted-in splice plate, was also examined by testing three eccentrically connected specimens.

In general, the gusset plate specimens were failed by sway buckling of the connection. However, for the specimens tested with out-of-plane restraint, local buckling of the free edges was observed. The failure mode of the eccentrically loaded specimens was the yielding of the splice member at the conjunction of gusset-to-splice. In general, except for the eccentrically loaded specimens, the test results indicated that significant yielding of the gusset plate specimens prior to reaching the ultimate load was observed. However, only limited yielding was observed for the specimens with a plate thickness of 6.5 mm. The ultimate load of the specimens increased almost linearly proportional to the gusset plate thickness and decreased with increasing plate size. While the out-of-plane restraint boundary condition had negligible effects on the ultimate load of the compact specimens (500 x 400), the ultimate load of the slender specimens (850 x 700) increased when out-of-plane restraint was applied. A slight decrease in the ultimate load of the specimens was observed when a  $30^\circ$  brace was used instead of a  $45^\circ$ . The beam and column moment had

only negligible effects on the ultimate load of the specimens; however, yielding of the specimens was detected at a load level significantly lower than that predicted by the Whitmore method. The out-of-plane loading eccentricity significantly reduced the ultimate load of the specimen.

The finite element analyses of the plastic bifurcation buckling loads of the test specimens carried out using the program ANSYS were in reasonable agreement with the test results. The elastic stress predicted by ANSYS at the gusset plate area beneath the splicing member agreed well with the experimental stress evaluated from the rosette readings. For the eccentrically loaded specimens, the load deflection analysis done by ANSYS also compared well with the experimental ultimate loads. Based on the available test data and the finite element analysis, a modified Thornton method is proposed to estimate the inelastic buckling strength of the gusset plate specimens. The beam-column equation is also recommended for the design of eccentrically loaded specimens.



## **ACKNOWLEDGEMENTS**

The author wishes to express his deep appreciation and gratitude to Dr. J.J. Roger Cheng for his supervision and guidance throughout the course of this study. The helpful advice and suggestions given by Drs. G. L. Kulak, J. A. Packer, D. W. Murray, D. H-K Chan and D. J. Steigmann are greatly acknowledged. Financial support was provided by the Natural Sciences and Engineering Research Council of Canada to Dr. Cheng under grant No. 4727.

The assistance of the technical staff of the I. F. Morrison Structural Laboratory at the University of Alberta is acknowledged.

The author deeply appreciates the encouragement, support and patience of his wife, Monica, throughout the course of this study.

## TABLE OF CONTENTS

<b>Chapter</b>	<b>Page</b>
1. INTRODUCTION.....	1
1.1 General.....	1
1.2 Objective and Scope.....	2
1.3 Literature Review.....	3
1.4 Current Design Methods.....	9
2. EXPERIMENTAL PROGRAM.....	21
2.1 Introduction.....	21
2.2 Scope.....	21
2.3 Specimen Description.....	22
2.4 Test Setup.....	25
2.4.1 General.....	25
2.4.2 Scheme I.....	25
2.4.3 Scheme II.....	25
2.5 Instrumentation.....	29
2.6 Test Procedure.....	31
2.7 Presentation of Test Results.....	33
3. TEST RESULTS OF GP TYPE SPECIMENS.....	55
3.1 General.....	55
3.2 Without Out-of-Plane Restraint at the Base of Test Frame.....	56
3.2.1 Behavior of Load vs. In-Plane Deformation.....	56
3.2.2 Behavior of Load vs. Out-of-Plane Displacement of Test Frame.....	56
3.2.3 Strain Gauge Results.....	57
3.2.4 Yielding Behavior of Specimens.....	58

3.2.5	Out-of-Plane Deflected Shapes of Free Edges and Along Centerline of Splicing Member .....	59
3.3	With Out-of-Plane Restraint at the Base of Test Frame.....	60
3.3.1	Behavior of Load vs. In-Plane Deformation.....	60
3.3.2	Behavior of Load vs. Out-of-Plane Displacement at Mid-Length of Long Free Edge .....	60
3.3.3	Yielding Behavior of Specimens .....	61
3.3.4	Out-of-Plane Deflected Shapes of Free Edges and Along Centerline of Splicing Member .....	61
4.	TEST RESULTS OF SP TYPE SPECIMENS .....	88
4.1	General .....	88
4.2	Without Out-of-Plane Restraint at the Base of Test Frame.....	88
4.2.1	Behavior of Load vs. In-Plane Deformation.....	88
4.2.2	Behavior of Load vs. Out-of-Plane Displacement of Test Frame .....	89
4.2.3	Strain Gauge Results .....	89
4.2.4	Yielding Behavior of Specimens.....	90
4.2.5	Out-of-Plane Deflected Shapes of Free Edges and Along Centerline of Splicing Member .....	91
4.3	With Out-of-Plane Restraint at the Base of Test Frame.....	91
4.3.1	General.....	91
4.3.2	Behavior of Load vs. In-Plane Deformation.....	92
4.3.3	Behavior of Load vs. Out-of-Plane Displacement at Mid-Length of Long Free Edge.....	92
4.3.4	Yielding Behavior of Specimens .....	93
4.3.5	Out-of-Plane Deflected Shapes of Free Edges and Along Centerline of Splicing Member .....	93
5.	TEST RESULTS OF AP TYPE SPECIMENS .....	114
5.1	General .....	114

5.2	Behavior of Load vs. In-Plane Deformation.....	114
5.3	Behavior of Load vs. Out-of-Plane Displacement .....	115
5.4	Strain Gauge Results .....	116
5.5	Yielding Behavior of Specimens.....	117
5.6	Out-of-Plane Deflected Shapes of Free Edges and Along Centerline of Splicing Member .....	118
6.	TEST RESULTS OF MP TYPE SPECIMENS.....	138
6.1	General .....	138
6.2	Behavior of Load vs. In-Plane Deformation.....	138
6.3	Behavior of Load vs. Out-of-Plane Displacement.....	140
6.4	Strain Gauge Results .....	142
6.5	Yielding Behavior of Specimens .....	144
6.6	Out-of-Plane Deflected Shapes of Free Edges and Along Centerline of Splicing Member .....	145
7.	TEST RESULTS OF EP TYPE SPECIMENS .....	182
7.1	General .....	182
7.2	Behavior of Load vs. In-Plane Deformation.....	182
7.3	Behavior of Load vs. Out-of-Plane Displacement of Test Frame .....	183
7.4	Strain Gauge Results .....	183
7.5	Out-of-Plane Deflected Shapes of Free Edges and Along Centerline of Splicing Member .....	185
8.	DISCUSSION AND COMPARISON OF TEST RESULTS .....	204
8.1	Introduction.....	204
8.2	General Discussion of Test Results.....	204
8.3	Effects of Gusset Plate Thickness and Size.....	207
8.4	Effects of Out-of-Plane Restraint at Conjunction of Gusset-to-Splice.....	208
8.5	Effects of Angle of the Diagonal Brace Member .....	209
8.6	Effects of Beam and Column Moments .....	210

8.7	Effects of Loading Eccentricity.....	213
9.	ANALYSIS OF TEST SPECIMENS .....	227
9.1	General .....	227
9.2	Finite Element Analysis - Plastic Bifurcation Buckling.....	227
9.3	Finite Element Model .....	229
9.4	Finite Element Analysis Results.....	231
9.4.1	General.....	231
9.4.2	GP and SP Type Specimens.....	232
9.4.2.1	In-Plane Stress Distribution .....	232
9.4.2.2	Principal Stress Vector and In-Plane Deformation Plots ....	234
9.4.3	AP Type Specimens .....	236
9.4.3.1	In-Plane Stress Distribution .....	236
9.4.3.2	Principal Stress Vector and In-Plane Deformation Plots.....	236
9.4.4	MP Type Specimens.....	237
9.4.4.1	In-Plane Stress Distribution .....	237
9.4.4.2	Principal Stress Vector and In-Plane Deformation Plots ....	237
9.4.5	Buckling Shapes of GP, SP, AP and MP Test Specimens .....	238
9.4.6	EP Type Specimens.....	239
9.4.6.1	Load Deflection Behavior.....	239
9.4.6.2	In-Plane Stress Distribution .....	239
9.4.6.3	Principal Stress Vector and Out-of-Plane Deformation Plots.....	241
9.5	Discussion and Comparison of Analytical Results.....	242
9.5.1	General .....	242
9.5.2	Effects of Gusset Plate Thickness and Size.....	242
9.5.3	Effects of Angle of Diagonal Brace Member (45° and 30°).....	243

9.5.4	Effects of Beam and Column Moments .....	244
9.5.5	Effects of Loading Eccentricity.....	245
9.6	Rigid-Plastic Analysis of Specimens EP1 and EP2.....	246
10.	PROPOSED DESIGN GUIDELINES AND METHODS.....	303
10.1	General.....	303
10.2	Elastic Parametric Studies of Gusset Plate Connections.....	303
10.2.1	General.....	303
10.2.2	Parametric Studies.....	304
10.2.2.1	General.....	304
10.2.2.2	Effects of Splice Plate Thickness.....	305
10.2.2.3	Effects of Splice Plate Length.....	306
10.2.2.4	Effects of Rotational Restraint at Conjunction of Bracing and Gusset Plate.....	307
10.2.2.5	General Design Guidelines.....	308
10.3	Modified Thornton Method.....	309
10.3.1	General.....	309
10.3.2	Proposed Design Method.....	311
10.4	Eccentrically Loaded Gusset Plates.....	313
10.4.1	General.....	313
10.4.2	General Design Guidelines.....	315
11.	SUMMARY AND RECOMMENDATIONS.....	329
11.1	Summary.....	329
11.2	Design Recommendations.....	330
11.2.1	Concentrically Loaded Gusset Plate Connections.....	330
11.2.2	Eccentrically Loaded Gusset Plate Connections.....	331
11.3	Recommendations for Future Research.....	332
	REFERENCES.....	335

APPENDIX.....	338
---------------	-----

## LIST OF TABLES

<b>Tables</b>	<b>Page</b>
2.1 Specimen Description .....	34
2.2 Types of Splicing Members.....	35
3.1 Test Results of GP Type Specimens.....	63
3.2 Material Properties .....	63
4.1 Test Results of SP Type Specimens .....	94
5.1 Test Results of AP Type Specimens .....	119
6.1 Test Results of MP Type Specimens.....	146
7.1 Test Results of EP Type Specimens .....	186
8.1 Summary of Test Results.....	215
9.1 Analytical Plastic Bifurcation Buckling Loads of Test Specimens .....	250
9.2 Rigid-Plastic Collapse Load for Specimens EP1 and EP2 .....	250
10.1 Buckling Loads of Test Specimens from Hu and Cheng (1987).....	316
10.2 Critical Splice Plate Thickness for 850 x 550 and 850 x 700 Specimens.....	316
10.3a Effects of Splice Plate Length on Buckling Loads for Specimens with a Plate Size of 850 x 550 .....	317
10.3b Effects of Splice Plate Length on Buckling Loads for Specimens with a Plate Size of 850 x 700 .....	317
10.4 Effects of Rotational Restraint at the Conjunction of Bracing Member and the Gusset Plate .....	318
10.5 Comparison of Test Loads with Analytical and Design Loads.....	319
10.6 Comparison of Elastic Buckling Loads with Whitmore Loads of Test Specimens.....	320
10.7 Design Loads for Test Specimens from Hu and Cheng (1987).....	321
10.8 Design Loads for EP Type Specimens.....	322



## LIST OF FIGURES

<b>Figure</b>	<b>Page</b>
1.1 Typical Gusset Plate Connection in a Warren Truss .....	12
1.2 Typical Braced Frames .....	13
1.3 Vertical Normal Stress Distribution Along the Critical Section .....	14
1.4 Whitmore Effective Width Concept .....	15
1.5 Block Shear Tear-Out Model.....	16
1.6 Typical Buckled Shapes for 45° Single Bracing Gusset (Williams and Richard 1986) .....	17
1.7 Schematic Test Setup (Hu and Cheng 1987).....	18
1.8 Schematic Test Setup and Specimen Configuration (Gross 1990); .....	19
1.9 Thornton Method.....	20
2.1 Typical Gusset Plate Configuration .....	36
2.2 Gusset Plate Connection of Tubular Section Bracing.....	37
2.3 Schematic of Test Specimens .....	38
2.4 Splice Members and Splicing Arrangement for GP, SP, MP and AP Type Specimens.....	39
2.5 Splice Member Arrangement for EP Type Specimens .....	40
2.6a Actual Braced Frame Behavior: Bracing Member and Gusset Plate Free Edges Deformed Out-of-Plane during Buckling .....	41
2.6b Test Frame Behavior: The Beam and Column and Gusset Plate Fixed Edges Deformed Out-of-Plane during Buckling.....	41
2.7 Schematic of Test Setup for Scheme I .....	42
2.8 Picture of Scheme I Test Setup .....	43
2.9 Schematic of Test Setup for Scheme II .....	44
2.10 Picture of Scheme II Test Setup .....	45
2.11 Picture of Test Setup for AP Type Specimens.....	46
2.12 Schematic of Loading System .....	47
2.13 Picture of Loading System .....	48
2.14 Schematic of Lateral Bracing for the Loading Unit.....	49
2.15 Schematic of LVDT Locations for GP, SP and MP Type Specimens .....	50
2.16 Schematic of LVDT Locations for EP Type Specimens .....	50
2.17 Schematic of Cable Transducers and LVDTs Locations for AP Type Specimens.....	51
2.18a LVDTs Arrangement on Supporting Frame.....	52
2.18b Close-up of LVDTs on Short Free Edge of Specimen.....	52
2.19 Location of Strain Gauges for GP, SP and EP Types Specimens.....	53

<b>Figure</b>	<b>Page</b>
2.20	Location of Strain Gauges for AP Type Specimens..... 53
2.21	Location of Strain Gauges of Splice Member for EP Type Specimens ..... 54
2.22	Location of Strain Gauges for MP Type Specimens ..... 54
3.1	Stress Strain Curve for the 9.8mm Thick Specimen ..... 64
3.2	Load vs. Vertical Displacement of Loading Head for Specimen GP1 ..... 65
3.3	Load vs. Vertical Displacement of Loading Head for Specimen GP2 ..... 66
3.4	Load vs. Vertical Displacement of Loading Head for Specimen GP3 ..... 67
3.5	Load vs. Out-of-Plane Displacement of Test Frame for Specimen GP1..... 68
3.6	Load vs. Out-of-Plane Displacement of Test Frame for Specimen GP2..... 69
3.7	Load vs. Out-of-Plane Displacement of Test Frame for Specimen GP3..... 70
3.8	Load vs. Strain Gauge Readings at Mid-Length of Long Free Edge for Specimen GP1..... 71
3.9	Load vs. Strain Gauge Readings at Mid-Length of Long Free Edge for Specimen GP2..... 72
3.10	Load vs. Strain Gauge Readings at Mid-Length of Long Free Edge for Specimen GP3..... 73
3.11	Load vs. Strain Gauge Readings at Mid-Length of Short Free Edge for Specimen GP1 ..... 74
3.12	Load vs. Strain Gauge Readings at Mid-Length of Short Free Edge for Specimen GP2..... 75
3.13	Load vs. Strain Gauge Readings at Mid-Length of Short Free Edge for Specimen GP3..... 76
3.14	Schematic of Yielding Process for Specimen GP1..... 77
3.15	Picture of Failed Specimen GP1..... 78
3.16	Out-of-Plane Deflected Shapes at Free Edges and Along Centerline of Splice for GP Type Specimens ..... 79
3.17	Picture of Out-of-Plane Deflected Shapes at Long Free Edge for Specimen GP1..... 80
3.18	Load vs. Vertical Displacement of Loading Head for Specimens GP1R..... 81
3.19	Load vs. Vertical Displacement of Loading Head for Specimens GP2R..... 82
3.20	Load vs. Vertical Displacement of Loading Head for Specimens GP3R..... 83
3.21	Load vs. Out-of-Plane Displacement at Mid-Length of Long Free Edge for Specimens GP1R..... 84
3.22	Load vs. Out-of-Plane Displacement at Mid-Length of Long Free Edge for Specimens GP2R..... 85
3.23	Load vs. Out-of-Plane Displacement at Mid-Length of Long Free Edge for Specimens GP3R..... 86
3.24	Out-of-Plane Deflected Shapes at Free Edges and Along Centerline of Splice for GP Type Specimens - With Restraint..... 87

<b>Figure</b>	<b>Page</b>
4.1 Load vs. Vertical Displacement of Loading Head for Specimen SP1 - Without Restraint .....	95
4.2 Load vs. Vertical Displacement of Loading Head for Specimen SP2 - Without Restraint .....	96
4.3 Load vs. Out-of-Plane Displacement of Test Frame for Specimen SP1 - Without Restraint .....	97
4.4 Load vs. Out-of-Plane Displacement of Test Frame for Specimen SP2 - Without Restraint .....	98
4.5 Load vs. Strain Gauge Readings at Mid-Length of Long Free Edge for Specimen SP1 - Without Restraint .....	99
4.6 Load vs. Strain Gauge Readings at Mid-Length of Long Free Edge for Specimen SP2 - Without Restraint .....	100
4.7 Load vs. Strain Gauge Readings at Mid-Length of Short Free Edge for Specimen SP1 - Without Restraint .....	101
4.8 Load vs. Strain Gauge Readings at Mid-Length of Short Free Edge for Specimen SP2 - Without Restraint .....	102
4.9 Load vs. Strain Readings at Rosette Location for Specimen SP1 - Without Restraint .....	103
4.10 Load vs. Strain Readings at Rosette Location for Specimen SP2 - Without Restraint .....	104
4.11 Picture of Failed Specimen SP1 .....	105
4.12 Out-of-Plane Deflected Shapes at Free Edges and Along Centerline of Splice for SP Type Specimens - Without Restraint .....	106
4.13 Load vs. Vertical Displacement of Loading Head for Specimen SP1 - With Restraint .....	107
4.14 Load vs. Vertical Displacement of Loading Head for Specimen SP2 - With Restraint .....	108
4.15 Load vs. Out-of-Plane Displacement at Mid-Length of Long Free Edge for Specimen SP1 - With Restraint .....	109
4.16 Load vs. Out-of-Plane Displacement at Mid-Length of Long Free Edge for Specimen SP2 - With Restraint .....	110
4.17 Yield Lines Observed Near South Corner of Splice for Specimen SP1 - With Restraint .....	111
4.18 Yield Lines Observed Near North Corner of Splice for Specimen SP1 - With Restraint .....	111
4.19 Yield Lines for Specimen SP1 - With Restraint .....	112
4.20 Out-of-Plane Deflected Shapes at Free Edges and Along Centerline of Splice for SP Type Specimens - With Restraint .....	113
5.1 Load vs. Vertical Strokes of Hydraulic Rams for Specimen AP1 .....	120
5.2 Load vs. Vertical Strokes of Hydraulic Rams for Specimen AP2 .....	121
5.3 Load vs. Vertical Strokes of Hydraulic Rams for Specimen AP3 .....	122

<b>Figure</b>	<b>Page</b>
5.4 Load vs. In-Plane Deformation Measured at End of Splice for Specimen AP2.....	123
5.5 Load vs. Out-of-Plane Displacement at Conjunction of Gusset-to-Splice for Specimen AP1.....	124
5.6 Load vs. Out-of-Plane Displacement at Conjunction of Gusset-to-Splice for Specimen AP2.....	125
5.7 Load vs. Out-of-Plane Displacement at Conjunction of Gusset-to-Splice for Specimen AP3.....	126
5.8 Load vs. Strain Gauge Readings at Mid-Length of Long Free Edge for Specimen AP1 .....	127
5.9 Load vs. Strain Gauge Readings at Mid-Length of Long Free Edge for Specimen AP2.....	128
5.10 Load vs. Strain Gauge Readings at Mid-Length of Long Free Edge for Specimen AP3 .....	129
5.11 Load vs. Average Strain Gauge Readings at Mid-Length of Short Free Edge for Specimen AP3.....	130
5.12 Load vs. Rosette Gauge Readings for Specimen AP1 .....	131
5.13 Load vs. Rosette Gauge Readings for Specimen AP2.....	132
5.14 Load vs. Rosette Gauge Readings for Specimen AP3.....	133
5.15 Yielding at West Side of Failed Specimen AP1.....	134
5.16 Yielding at East Side of Failed Specimen AP1.....	134
5.17 Yielding at West Side of Failed Specimen AP2.....	135
5.18 Yielding at East Side of Failed Specimen AP2.....	135
5.19 Out-of-Plane Deflected Shapes at Free Edges and Along Centerline of Splice for AP Type Specimens .....	136
5.20 Picture of Out-of-Plane Deflected Shapes at Long Free Edge for Specimen AP2.....	137
6.1 Load vs. In-Plane Deformation Measured at End of Splice for Specimen MP1 .....	147
6.2 Load vs. In-Plane Deformation Measured at End of Splice for Specimen MP2 .....	148
6.3 Load vs. In-Plane Deformation Measured at End of Splice for Specimen MP3 .....	149
6.4 Load vs. In-Plane Deformation Measured at End of Splice for Specimen MP3A .....	150
6.5 Load vs. In-Plane Deformation Measured at End of Splice for Specimen MP3B .....	151
6.6 Load vs. Vertical Strokes of Hydraulic Rams for Specimen MP1 .....	152
6.7 Load vs. Vertical Strokes of Hydraulic Rams for Specimen MP2 .....	153
6.8 Load vs. Vertical Strokes of Hydraulic Rams for Specimen MP3 .....	154

<b>Figure</b>	<b>Page</b>
6.9 Load vs. Vertical Strokes of Hydraulic Rams for Specimen MP3A .....	155
6.10 Load vs. Vertical Strokes of Hydraulic Rams for Specimen MP3B .....	156
6.11 Load vs. Out-of-Plane Displacement at Conjunction of Gusset-to-Splice for Specimen MP1 .....	157
6.12 Load vs. Out-of-Plane Displacement at Conjunction of Gusset-to-Splice for Specimen MP2.....	158
6.13 Load vs. Out-of-Plane Displacement at Conjunction of Gusset-to-Splice for Specimen MP3.....	159
6.14 Load vs. Out-of-Plane Displacement at Conjunction of Gusset-to-Splice for Specimen MP3A.....	160
6.15 Load vs. Out-of-Plane Displacement at Conjunction of Gusset-to-Splice for Specimen MP3B.....	161
6.16 Load vs. Strain Gauge Readings at Mid-Length of Long Free Edge for Specimen MP1.....	162
6.17 Load vs. Strain Gauge Readings at End of Long Free Edge for Specimen MP1.....	163
6.18 Load vs. Strain Gauge Readings at Mid-Length of Long Free Edge for Specimen MP2.....	164
6.19 Load vs. Strain Gauge Readings at End of Long Free Edge for Specimen MP2.....	165
6.20 Load vs. Strain Gauge Readings at Mid-Length of Long Free Edge for Specimen MP3.....	166
6.21 Load vs. Strain Gauge Readings at End of Long Free Edge for Specimen MP3.....	167
6.22 Load vs. Strain Gauge Readings at Mid-Length of Long Free Edge for Specimen MP3A.....	168
6.23 Load vs. Strain Gauge Readings at End of Long Free Edge for Specimen MP3A.....	169
6.24 Load vs. Strain Gauge Readings at Mid-Length of Short Free Edge for Specimen MP1.....	170
6.25 Load vs. Strain Gauge Readings at End of Short Free Edge for Specimen MP1.....	171
6.26 Load vs. Strain Gauge Readings at Mid-Length of Short Free Edge for Specimen MP2.....	172
6.27 Load vs. Strain Gauge Readings at End of Short Free Edge for Specimen MP2.....	173
6.28 Load vs. Strain Gauge Readings at Mid-Length of Short Free Edge for Specimen MP3.....	174
6.29 Load vs. Strain Gauge Readings at End of Short Free Edge for Specimen MP3.....	175

<b>Figure</b>	<b>Page</b>
6.30 Load vs. Strain Gauge Readings at Mid-Length of Short Free Edge for Specimen MP3A.....	176
6.31 Load vs. Strain Gauge Readings at End of Short Free Edge for Specimen MP3.....	177
6.32 Measured Strain Distribution Along Beam and Column Boundary at Gusset Plate for Specimen MP1.....	178
6.33 Picture of Failed Specimen MP1 .....	179
6.34 Out-of-Plane Deflected Shapes at Free Edge and Along Centerline of Splice for MP Type Specimens.....	180
6.35 Pictures of Out-of-Plane Deflected Shapes at Free Edges for Specimen MP3A .....	181
7.1 Picture of Failed Specimen EP3 .....	187
7.2 Load vs. Vertical Stroke of Loading Head for Specimen EP1.....	188
7.3 Load vs. Vertical Stroke of Loading Head for Specimen EP2.....	189
7.4 Load vs. Vertical Stroke of Loading Head for Specimen EP3.....	190
7.5 Load vs. Out-of-Plane Displacement of Test Frame for Specimen EP1 .....	191
7.6 Load vs. Out-of-Plane Displacement of Test Frame for Specimen EP2 .....	192
7.7 Load vs. Out-of-Plane Displacement of Test Frame for Specimen EP3 .....	193
7.8 Load vs. Strain Gauge Readings at the Conjunction of Gusset-to-Splice for Specimen EP1.....	194
7.9 Load vs. Strain Gauge Readings at Splice Member Near End of Brace for Specimen EP1.....	195
7.10 Schematic Yield Pattern on Splice Plate for EP Type Specimens.....	196
7.11 Yielding Observed in Specimen EP1.....	197
7.12a Failed Splice Members for Specimen EP1 .....	198
7.12b Failed Splice Members for Specimen EP2 .....	198
7.13 Load vs. Strain Gauge Readings at the Conjunction of Gusset-to-Splice for Specimen EP2.....	199
7.14 Load vs. Strain Gauge Readings at Splice Near End of Brace for Specimen EP2.....	200
7.15 Load vs. Strain Gauge Readings at Web of Tee-Section and Splice Plate for Specimen EP3.....	201
7.16 Strain Distribution Across the Depth of the Splice Section for Specimen EP3 .....	202
7.17 Out-of-Plane Deflected Shapes at Free Edges and Along Centerline of Splice for EP Type Specimens.....	203
8.1 Ratios of Ultimate Loads to Whitmore Loads vs. Gusset Plate Specimens Thickness.....	216

<b>Figure</b>	<b>Page</b>
8.2 Ratios of Ultimate Loads to Thornton Loads vs. Thickness of Gusset Plate Specimens .....	217
8.3 Ultimate Loads vs. Thickness of Gusset Plate Specimens .....	218
8.4 Effects of Out-of-Plane Restraint on the Ultimate Loads of GP and SP Type Specimens .....	219
8.5 Effects of Brace Angles on the Ultimate Loads of Specimens .....	220
8.6 Effects of Brace Angles on the Strain Readings Recorded at the Short Free Edge for Specimens AP3 and GP3 .....	221
8.7 Ratios of the Ultimate Loads of MP Type Specimens to GP Type Specimens vs. Beam Moment.....	222
8.8 Load vs. Strain Readings at Rosette underneath the Splice for Specimens MP3 and GP3.....	223
8.9 Load vs. In-Plane Deformation Measured at End of Splice for Specimens MP3, MP3A and MP3B .....	224
8.10 Load vs. Out-of-Plane Displacement at Conjunction of Gusset-to-Splice for Specimens MP3, MP3A and MP3B .....	225
8.11 Load vs. Out-of-Plane Displacement of Test Frame for EP Type Specimens.....	226
9.1 Flow Diagram for Plastic Bifurcation Buckling Analysis .....	251
9.2 Finite Element Model for GP and SP Type Specimens.....	252
9.3a Finite Element Model for AP and MP Type Specimens .....	253
9.3b Finite Element Model for EP Type Specimens.....	254
9.4 A Plot of Test to Predicted(ANSYS) Ratios for Various Specimens.....	255
9.5a In-Plane Stress Contour for Specimen GP1 at P = 1370 kN .....	256
9.5b In-Plane Stress Contour for Specimen GP1 at P = 1500 kN .....	257
9.5c In-Plane Stress Contour for Specimen GP1 at P = 1700 kN .....	258
9.5d In-Plane Stress Contour for Specimen GP1 at P = 1950 kN .....	259
9.5e In-Plane Stress Contour for Specimen GP1 at P = 2336 kN .....	260
9.6 In-Plane Stress Contour for Specimen GP1 at P = 1220 kN .....	261
9.7a Principal Stress Vector Plot for Specimen GP1 at P = 1370 kN .....	262
9.7b Principal Stress Vector Plot for Specimen GP1 at P =2336 kN .....	263
9.8a In-Plane Deformation Mode for Specimen GP1 at P = 1370 kN.....	264
9.8b In-Plane Deformation Mode for Specimen GP1 at P = 2336 kN.....	265
9.9 In-Plane Stress Contour for Specimen AP1 at P = 1380 kN.....	266
9.10 Principal Stress Vector Plot for Specimen AP1 at P = 1380 kN.....	267
9.11 In-Plane Deformation Mode for Specimen AP1 at P = 1380 kN.....	268
9.12a In-Plane Stress Contour for Specimen MP1 at P = 300 kN.....	269
9.12b In-Plane Stress Contour for Specimen MP1 at P = 1500 kN .....	270

<b>Figure</b>	<b>Page</b>
9.13a Principal Stress Vector Plot for Specimen MP1 at P = 300 kN.....	271
9.13b Principal Stress Vector Plot for Specimen MP1 at P = 1500 kN.....	272
9.14a In-Plane Deformation Mode for Specimen MP1 at P = 300 kN.....	273
9.14b In-Plane Deformation Mode for Specimen MP1 at P = 1500 kN.....	274
9.15a,b Typical Buckling Shapes for Specimens GP1 and AP1.....	275
9.15c,d Typical Buckling Shapes for Specimens MP1 and SP1.....	276
9.16 Analytical Load Deflection Curve for Specimen EP1.....	277
9.17 Analytical Load Deflection Curve for Specimen EP2.....	278
9.18 Analytical Load Deflection Curve for Specimen EP3.....	279
9.19 In-Plane Stress Distribution of Splice Plate Top Surface for Specimen EP1 at Ultimate.....	280
9.20 In-Plane Stress Distribution of Splice Plate Bottom Surface for Specimen EP1 at Ultimate.....	280
9.21 In-Plane Stress Distribution at Centerline Along Length of Splice Plate for Specimen EP1.....	281
9.22 In-Plane Stress Distribution of Gusset Plate Top Surface for Specimen EP1 at Ultimate.....	282
9.23 In-Plane Stress Distribution of Gusset Plate Bottom Surface for Specimen EP1 at Ultimate.....	282
9.24a In-Plane Stress Distribution of Splice Plate Top Surface for Specimen EP3 at Ultimate.....	283
9.24b In-Plane Stress Distribution of Splice Plate Bottom Surface for Specimen EP3 at Ultimate.....	283
9.25a In-Plane Stress Distribution of Gusset Plate Top Surface for Specimen EP3 at Ultimate.....	284
9.25b In-Plane Stress Distribution of Gusset Plate Bottom Surface for Specimen EP3 at Ultimate.....	284
9.26 Principal Stress Vector Plot of Gusset Plate Top Surface for Specimen EP1 at Ultimate.....	285
9.27 Principal Stress Vector Plot of Gusset Plate Bottom Surface for Specimen EP1 at Ultimate.....	285
9.28 Out-of-Plane Deformation for Specimen EP1.....	286
9.29 Out-of-Plane Deformation for Specimen EP2.....	286
9.30 Out-of-Plane Deformation for Specimen EP3.....	287



<b>Figure</b>	<b>Page</b>
9.31 Analytical Out-of-Plane Deflection at Centerline of Splice Plate for Specimen EP1 .....	288
9.32 Analytical Out-of-Plane Deflection at Centerline of Splice Plate for Specimen EP2 .....	289
9.33 Load vs. Gusset Plate Specimen Thickness.....	290
9.34a In-Plane Stress Contour for Specimen MP3 at P = 630 kN.....	291
9.34b In-Plane Stress Contour for Specimen MP3A at P = 630 kN.....	292
9.34c In-Plane Stress Contour for Specimen MP3B at P = 630 kN.....	293
9.35a Principal Stress Vector Plot for Specimen MP3 at P = 630 kN.....	294
9.35b Principal Stress Vector Plot for Specimen MP3A at P = 630 kN.....	295
9.35c Principal Stress Vector Plot for Specimen MP3B at P = 630 kN.....	296
9.36a In-Plane Deformation Mode for Specimen MP3 at P = 630 kN .....	297
9.36b In-Plane Deformation Mode for Specimen MP3A at P = 630 kN .....	298
9.36c In-Plane Deformation Mode for Specimen MP3B at P = 630 kN. ....	299
9.38 Rigid-Plastic Collapse Mechanism for Specimens EP1 and EP2 .....	300
9.39 Rigid-Plastic Unloading Line for Specimen EP1 .....	301
9.40 Rigid-Plastic Unloading Line for Specimen EP2.....	301
10.1 Finite Element Model and Typical Specimen Size and Shape from Cheng et al. (1994).....	323
10.2 Triangular Area of Gusset Plates .....	324
10.3 Effects of Splice Plate Thickness on the Elastic Buckling Loads of Gusset Plates .....	325
10.4 Various Splice Plate Lengths for Gusset Plate Specimens .....	326
10.5 Effects of Rotational Restraint on the Elastic Buckling Loads of Gusset Plates Specimens .....	327
10.6 Modified Thornton Method .....	328
11.1 Dimensions Required in the Design Method .....	334

## LIST OF SYMBOLS

$A_G$	=	gross area of section
$b_w$	=	Whitmore effective width
$e$	=	loading eccentricity
$F_{eff}$	=	effective tensile stress
$F_u$	=	ultimate strength of material
$F_y$	=	specified minimum yield strength of the material
$I$	=	moment of inertia
$k$	=	effective length factor for the unit column strip
$l$	=	total connection length
$l_b$	=	distance between the first row and the last row of bolts in a connection
$L$	=	length of column strip in modified Thornton method
$L_{1,2,3}$	=	length of column strips in Thornton method
$M_b$	=	applied beam moment
$M_c$	=	applied column moment
$M_p$	=	plastic moment capacity of a section in beam-column formula
$M_{pc}$	=	reduced plastic moment capacity in beam-column formula
$M_{pcG}$	=	reduced plastic moment capacity of gusset plate
$M_{pG}$	=	plastic moment capacity of gusset plate
$M_{pcS}$	=	reduced plastic moment capacity of splice plate
$M_{pS}$	=	plastic moment capacity of splice plate
$P$	=	ultimate load of test specimens
$P_a$	=	applied axial load in beam-column formula
$P_{ANSYS}$	=	plastic bifurcation buckling load of specimens by ANSYS
$P_{BC}$	=	analytical load based on beam-column equation with total eccentric moment
$P_{cr}$	=	compressive strength of gusset plate connections
$P_E$	=	elastic buckling load of specimens by ANSYS
$P_{MBC}$	=	analytical load based on beam-column equation with half of the eccentric moment
$P_{RBC}$	=	analytical load based on rigid-plastic analysis
$P_t$	=	Thornton load
$P_{TE}$	=	Thornton elastic buckling load
$P_{t30}$	=	Same as $P_t$ , used for clarity
$P_{t45}$	=	Thornton load with the effective width based on a 45° angle
$P_w$	=	Whitmore load
$P_y$	=	yield load of the section

$P_{yG}$	=	yield load of the gusset plate section
$P_{yS}$	=	yield load of the splice plate section
$r$	=	radius of gyration
$R_n$	=	nominal ultimate tensile resistance of connection
$s$	=	gauge of bolts
$S_c$	=	critical splice plate thickness
$SL$	=	length of splice plate member
$S_{net}$	=	net gauge between outside bolts
$V_r$	=	factored shear resistance
$[D]$	=	displacement vector
$\{R\}$	=	load vector
$[K]$	=	conventional stiffness matrix
$[K_\sigma]$	=	stress stiffness matrix
$\Delta$	=	out-of-plane displacement of eccentrically loaded specimens
$\lambda$	=	arbitrary scalar multiplier
$\sigma_\alpha$	=	critical stress of a column

# 1. INTRODUCTION

## 1.1 General

Gusset plate connections are frequently used in bridge trusses (Fig. 1.1) and braced steel frames in heavy industrial buildings. Typical braced frames, which are designed to resist lateral loads produced by wind and/or earthquake loads, are shown in Fig. 1.2. Depending on the particular connection detail, the gusset plate can be either bolted or welded to the diagonal bracing member and to the main framing members. The diagonal bracing member may transfer either a tensile or a compressive load to the gusset plate, according to the type of bracing system. Even though it is usually assumed that members of a gusset plate connection are loaded only in their axial direction, the delivery of these loads from the bracing member to the framing members through the gusset plate will produce bending, shear and normal force in the gusset plate.

Although gusset plate connections are widely used in a variety of steel structures, the current Canadian bridge design standard CAN/CSA-S6-88 only provides design philosophy and has no specific methods and formulas to design gusset plates. The conventional method of designing gusset plates (Kulak et al. 1987) is based on beam formula and elastic analysis, together with engineering judgement, past practice and experience. Recently, both the CAN/CSA-S16.1-M89 standard and the AISC-LFRD specification (1993) have provided a set of formulas developed by Hardash and Bjorhovde (1985), which are based on the block shear concept, to design gusset plates subject only to tension.

Recent research on the behavior and design of gusset plate connections (Hardash and Bjorhovde 1985, Williams and Richard 1986) concentrated on gusset plates loaded in tension. When gusset plates are subject to compressive loads, the local buckling of the gusset plate's free edges and the local crippling of the gusset plate area near the end of the

diagonal bracing member have to be examined. Because of the geometry of the connection, the boundary conditions, and complicated by the fact that stability failure caused by compressive loading applied to the connection may occur in the gusset plate, the compressive strength of the gusset plate connection is extremely difficult to evaluate. To date (1993) only a limited amount of research work on the compressive behavior of gusset plate connections (Hu and Cheng 1987, Gross 1990, Chakrabarti and Richard 1990, Kitipomchai et al. 1993, Cheng, Yam and Hu 1994) is available. Both experimental and analytical research work are still insufficient to provide a complete design guideline and recommendations for designing gusset plate connections loaded in compression. Hence, a research program was initiated to investigate the compressive behavior and strength of gusset plate connections.

## **1.2 Objective and Scope**

Based on the above discussion, it can be seen that much research work has to be done in the area of compressive strength and behavior of gusset plate connections in order to provide rational design guidelines and recommendations to the design engineer. Therefore, a research program was initiated to investigate experimentally the strength and behavior of gusset plate connections subject to compressive loads. The objectives of the program were as follows:

- 1) To provide experimental data for the behavior of gusset plate connections loaded in compression.
- 2) To evaluate the effects of the following variables on the compressive behavior and ultimate strength of gusset plate connections:
  - i) gusset plate size and thickness
  - ii) out-of-plane restraint at the base of the test frame (refers to test setup scheme I in chapter 2)
  - iii) brace angle

- iv) beam and column moments
  - v) out-of-plane loading eccentricity.
3. To examine the inelastic as well as elastic compressive behavior of gusset plate connections by the finite element program ANSYS.
  4. To compare the test results to the current design methods and to propose modified or refined design methods, if necessary.

A total of twenty-one tests were performed on nineteen specimens. Because of the significant number of test parameters, the scope of the program was limited to the following:

1. Single gusset plate connections of a braced steel frame were considered.
2. Three gusset plate thicknesses (13.3 mm, 9.8 mm and 6.5 mm) and two bracing angles ( $45^\circ$  and  $30^\circ$ ) were examined.
3. Only gusset plates with a rectangular shape were investigated. A practical size of 500 mm x 400 mm gusset plates was chosen to study the effects of various test parameters. A larger plate size of 850 mm x 700 mm was included for comparison.
4. The effect of framing members on the compressive behavior of gusset plate was examined. However, the influence of the axial force in the framing members was neglected. Two beam and column moment levels were considered and the ratio of column moment to the beam moment was kept at 0.5.

### **1.3 Literature Review**

Prior to the investigation by Whitmore in 1952, gusset plates were designed on the basis of simple beam theory combined with experience, general practice and engineering judgement. Whitmore (1952) performed tests of prototype gusset plates from a bottom chord connection in a Warren truss, as shown in Fig. 1.1. He investigated the elastic stress distribution in the gusset plate by using wire-bond strain gauges, brittle lacquers and

photoelastic procedures. He found from the tests that the maximum tensile and compressive stresses in the gusset plate were near the ends of the tension and compression diagonals, respectively. He also concluded that the use of simple beam theory to analyze gusset plates led to erroneous predictions, as shown in Fig. 1.3. Based on the test results, Whitmore proposed the well-known effective width concept (Whitmore 1952) to approximate the maximum normal stresses existing near the ends of diagonal members. The effective width of the gusset plate was defined as the length of the line passing through the bottom row of fasteners and intercepted by two  $30^\circ$  lines originating at the outside fasteners of the first row of the diagonal. The maximum normal stress was then calculated on the basis of this effective width. This concept is illustrated schematically in Fig. 1.4. This method of analyzing gusset plate connections is widely used in practice today. For purposes of this report, the Whitmore load will be defined as the product of the static yield strength of the material and the effective width and the thickness of the gusset plate.

Additional experimental work on gusset plates was done by Irvan (1957) and Hardin (1958). Irvan investigated the general stress distribution in a double gusset plate prototype of a Pratt truss. His findings were similar to those of Whitmore except that he slightly modified the Whitmore effective width concept. He proposed to extend the  $30^\circ$  lines from the center of gravity of the rivet group instead of from the outside fasteners of the first row of bolts, as had been suggested by Whitmore (1952). Hardin's work in 1958 substantiated the findings of Irvan. Davis (1967) and Vasarhelyi (1971) used the finite element method to analyze gusset plate connections. Davis's results confirmed Whitmore's experimental findings. Vasarhelyi tested specimens from a lower chord joint in a simple Warren truss and then employed the finite element method to analyze the test specimens. He found that the maximum normal stresses determined by various simplified methods were only slightly different from the analysis. However, the location of those maximums could vary quite significantly.

Analytical work performed by Struik (1972) involved the use of an elastic-plastic finite element program that could take into account the gusset plate behavior in the inelastic range. To estimate the effects of bolt holes in the gusset plate, Struik included the linear portion of the load vs. deformation relationship of the fasteners in the analysis. The result of his studies indicated that current design procedures produced a large and variable margin of safety against the ultimate capacity of the gusset plate. Bjorhovde (1985) performed full-scale testing of diagonal bracing connections in order to evaluate the behavior and ultimate strength of gusset plates in tension. A total of six tests were performed with two different thicknesses (3 mm and 9 mm) and three different angles of bracing ( $30^\circ$ ,  $45^\circ$ , and  $60^\circ$ , measured from the beam axis). He observed from the tests results that the primary failure mode was tearing across the last row of bolt holes of the gusset plate at the end of the splice plates. He also found that in-plane bending of the gusset plates caused plate buckling at the free edge of gusset plates. He suggested that this plate buckling might be a significant factor in developing the design criteria for gusset plates.

Richard et al. (1983) performed a finite element analysis to model the diagonal bracing used in Bjorhovde's experimental work. In order to include both the material and geometric nonlinearity of the complete connection, the load vs. deformation relationships of the fasteners, bolts, weldments and double framing angles determined from physical tests were used in the analysis. The measured strains from the tests compared well with the analytical predictions in areas of low strain gradients. However, the predictions at areas of high strain gradients differed significantly from the test results. This difference might be attributed to the improper mesh size in the finite element model (Richard et al. 1983).

Hardash and Bjorhovde (1985) performed a series of gusset plate tests aimed at developing an ultimate strength design criterion for gusset plate connections loaded in tension. Based on the test results, they modified the block shear concept used for coped beam-to-column connections in order to develop an ultimate tensile strength model for gusset plates. This



modified block shear concept incorporated the ultimate tensile stress on the net area between the bolts of the last row and an uniform effective shear stress on the gross area along the outside bolt lines, as shown in Fig. 1.5.

So far, the above discussion mainly has concerned the in-plane stress distribution and tensile behavior of gusset plate connections. When gusset plates are subject to compression, the problem of instability must also be addressed. Williams and Richard (1986) performed an elastic buckling analysis of gusset plates. They did this by excluding the beam and column framing members from the analysis. It was assumed that the bracing member would not buckle, and that the brace-to-gusset connection was restrained from out-of-plane translation. The parameters examined were types of bracing (single brace and K brace), brace angle, edge support, finite element mesh size, and plate size. They concluded from the finite element analysis that fixed edge supports increased the buckling strength of gusset plates significantly as compared to simply supported edge conditions. They also found that K-bracing gussets had a higher buckling strength than single-bracing gussets. Typical buckled shapes for a  $45^\circ$  single-brace gusset plate are shown in Fig. 1.6. Williams and Richard also demonstrated that frame action could significantly affect the behavior of gusset plates.

Hu and Cheng (1987) investigated the compressive behavior of gusset plate connections in the elastic range by testing full-scale diagonal bracing similar to the Bjorhovde tests (1985). A schematic of the test setup is shown in Fig. 1.7. As can be seen from this figure, any effect of loading the framing members on the gusset plate was neglected in the testing program. The test series consisted of six specimens with plate thickness and plate size as primary variables. The plate thicknesses examined were 6.7 mm and 3.1 mm, and the plate sizes examined were 850 x 550 and 850 x 700. The effects of load eccentricity were also investigated in this program by testing six more eccentrically loaded specimens. The test results showed that for the concentric loading cases, the primary failure mode for the gusset

plate was elastic buckling of the longer free edge of the plate. Depending on the out-of-plane restraints of the framing members, either local buckling or overall buckling of the gusset plate might occur. For the eccentric loading cases, failure was initiated at the splice plate due to excessive yielding. The maximum elastic normal compressive stress in the gusset plate obtained from the tests agreed quite well with Whitmore's predictions. However, using Whitmore's effective width concept to predict the test results would produce unconservative estimates, since the primary failure mode of the gusset plate was elastic buckling. The finite element program BASP, developed by Akay et al.(1977), was used to investigate analytically the elastic compressive behavior of gusset plates. The finite element solutions showed reasonable agreement with the test results. It was also found from the parametric studies by BASP that the rotational restraint from the boundary elements, the bending stiffness of the splice plates, and the distance between the end of the splice plate and the beam-column boundary significantly affected the elastic buckling strength of gusset plates.

Recently, Yamamoto et al. (1988) investigated the buckling strength of gusseted truss joint of the Warren type. Eight specimens with four different types of gusseted truss joints were tested. Strain gauges, rosette gauges and photoelastic coatings were used to measure the development of the plastic zone and strain distribution in the gusset plate. It was shown in the test results that all specimens yielded before reaching the buckling load. The buckling load in these tests was estimated as the load that caused strain bifurcation to occur in the gusset plate due to bending. Based on this test observation, Yamamoto et al. concluded that the buckling strength of the gusset plate specimens could be evaluated by considering only the elastic buckling load of a triangular area of the gusset plate that remained in the elastic range prior to buckling with various boundary conditions. A buckling analysis was then performed by a finite element method that utilizes an eigenvalue formulation. A design equation for the test specimens was proposed based on this analytical study. The test results also showed that the ratio of ultimate load to initial buckling load varied from 1.2 to

1.7. The increase in capacity was attributed to the postbuckling strength of the gusset plate connection.

The most recent (1990) experimental investigation of full-scale gusseted connections loaded in compression was performed by Gross. The testing program consisted of three diagonally braced steel subassemblages, as shown in Fig. 1.8. All the gusset plate specimens were 6.35 mm thick. The two main objectives of the testing program were:

1. to investigate the interaction between the intersection of the beam-column centroidal axes and the line of force in the diagonal member.
2. to investigate the orientation of the column strong axis in relation to the plane of the braced frame.

As can be seen in Fig. 1.8, the Gross test setup took into account the effects of the framing members on the gusset plate. According to Williams and Richard (1986), frame action can influence the gusset plate behavior significantly. However, the test setup did not permit the out-of-plane translation of the bracing member, which might have had a significant effect on the buckling strength of the gusset plate. The test results showed that the primary failure mode of the gusseted connection was gusset plate buckling. Gusset plate tearing was observed only when the weak axis was connected to the gusset plate. All specimens exhibited yielding before reaching the ultimate load. The first yield load of the specimens agreed well with the Whitmore predictions. For specimens failing by plate buckling, the ratio of the ultimate load to the first yield load ranged from 2.08 to 2.32.

Fung and Richard (1987) analyzed these test specimens using an inelastic finite program, INELAS. The analytical solutions compared well with the measured stress distribution. No attempt was made to determine the inelastic buckling strength of the gusset plate specimens by the finite element method. To estimate the inelastic buckling load of the specimens, Gross used the procedure proposed by Thornton (1984), which will be discussed later in this review. Nevertheless, the buckling loads of the gusset plates

evaluated by Thornton's method were very conservative. The ratio of the ultimate load to the predicted buckling load for the two specimens were 1.5 and 1.7.

Cheng et al. (1994) performed additional analyses of the test results from Hu and Cheng (1987) using the finite element program ANSYS. Reasonable predictions of the elastic buckling load of the test specimens were obtained. It was also found from the analytical results that the elastic buckling strength of the specimens increases with an increasing splice member connection length or splice member thickness. In addition, a large deflection analysis was performed on the specimen with a gusset plate thickness of 3.11 mm. It was found from the large deflection analysis that postbuckling strength existed in the specimen. The analytical load deflection curve obtained in this way agreed well with that of the test.

The cyclic behavior of gusset plate connections has been investigated by Rabinovitch and Cheng (1994) using total of five specimens. The testing program included parameters such as gusset plate shape necessary to accommodate the free formation of the plastic hinge, plate thickness, and gusset plate free edge stiffener. It was found from the tests that there was no rationale for providing an area for the free formation of plastic hinges in gusset plate connections attached to the framing members on two sides. On the other hand, this area for free plastic hinge formation reduced the compressive strength of the specimen due to buckling. In addition, the energy absorption capability of the gusset plate connection was significantly improved by the addition of plate edge stiffeners. The stiffened gusset plate also experienced a stable post-buckling response, whereas a sudden drop in compressive load carrying capacity was observed for the unstiffened gusset plates.

#### **1.4 Current Design Methods**

Current design specifications (e.g. AISC-LRFD, S16.1 and S6) do not have any specific formulas to evaluate the compressive strength of gusset plates. However, some design provisions are recommended in the S6 standard. The conventional method of designing a

gusset plate is to assume that the load distribution among the fasteners are equal; hence, the required number of fasteners can be determined. The gusset plate configuration is then selected to accommodate all the connecting elements and fasteners. Then, stresses are checked at the weakest and critical sections using beam formulas (Gaylord et al. 1992). The normal stress in the gusset plate should also be checked by the Whitmore effective width concept.

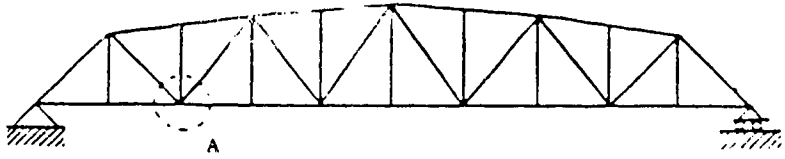
In CAN/CSA-S6-88 the factored shear resistance ( $V_r$ ) of gusset plate is determined by the following equation:

$$V_r = 0.50\phi A_g F_y \quad [1.1]$$

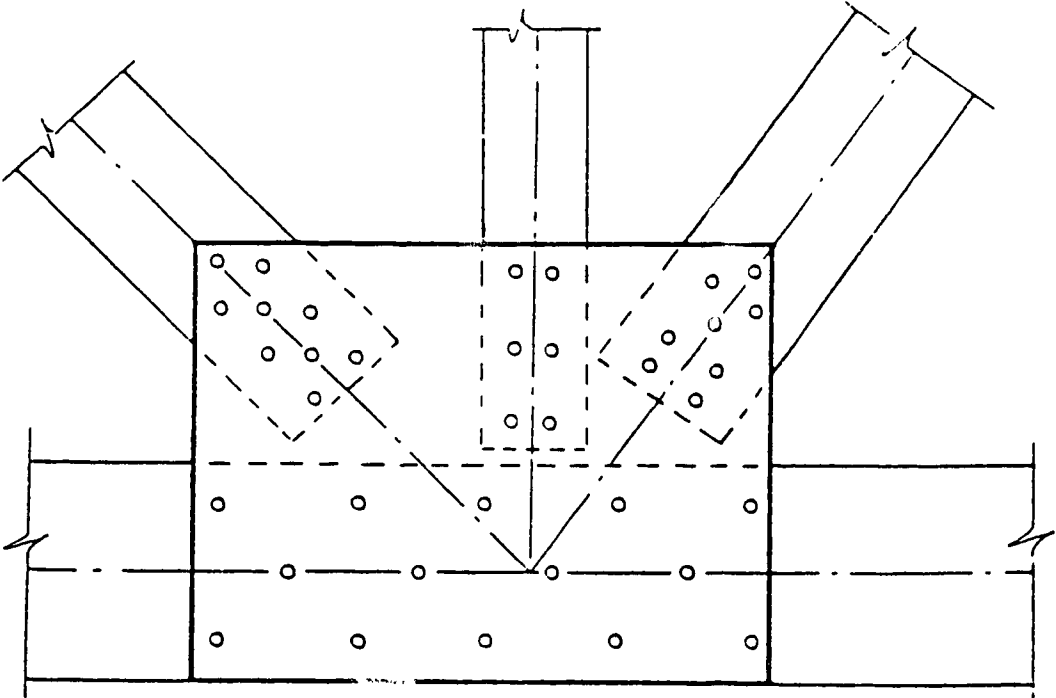
where  $\phi$  is a resistance factor,  $A_g$  is the gross area and  $F_y$  is the specified minimum yield strength of the material. The CAN/CSA-S6-88 standard also states that a gusset plate shall have ample thickness to resist shear, direct stress, and flexure at the weakest and most critical section. It also includes a provision to limit the ratio of the unsupported edge of the gusset plate to its thickness to  $945/\sqrt{F_y}$  in order to avoid local buckling of the gusset plate subjected to compression.

An alternative method proposed by Thornton (1984) to evaluate the buckling load of a gusset plate is to consider an imaginary fixed-fixed column strip of unit width below the Whitmore effective width in the gusset plate, as shown in Fig. 1.9. The buckling strength of the gusset plate is estimated to be the compressive resistance of an imaginary unit column strip. The length of the column strip is taken as the maximum of  $L_1$ ,  $L_2$  and  $L_3$ . Once the length of the column strip has been established, the compressive resistance of the column strip can be evaluated according to CAN/CSA-S16.1-M89. The effective length factor of 0.65 is recommended. It is assumed that the gusset plate will not buckle if the compressive resistance is greater than the compressive force on the Whitmore effective area. It should be noted that the Thornton method does not take into account the effects of

plate action, since a column buckling formula was employed. Besides, this method would not be appropriate if significant yielding occurs generally in the plate prior to buckling because the column buckling formula only considers the column strip underneath the effective width.



Truss Outline



Connection A

Fig. 1.1 Typical Gusset Plate Connection in a Warren Truss

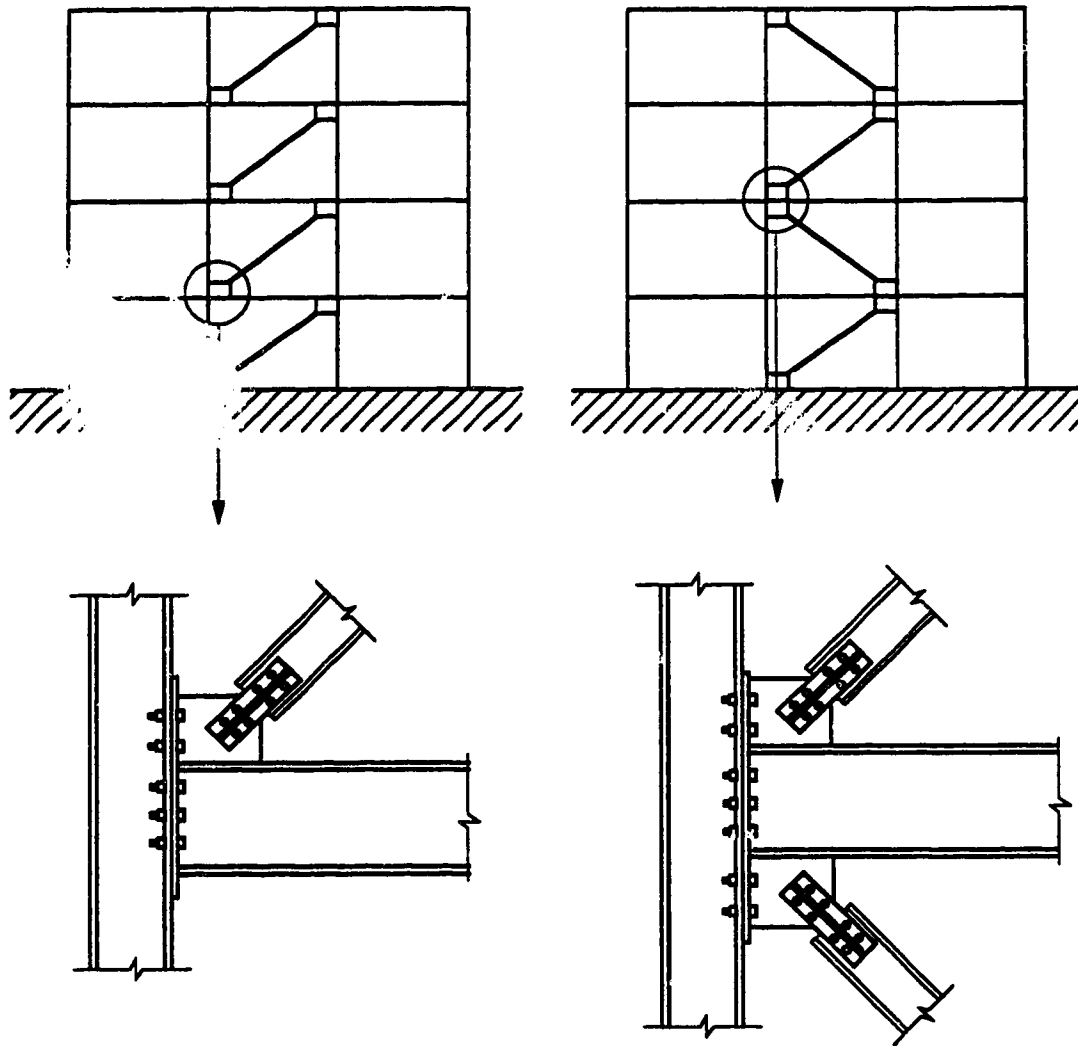


Fig. 1.2 Typical Braced Frames



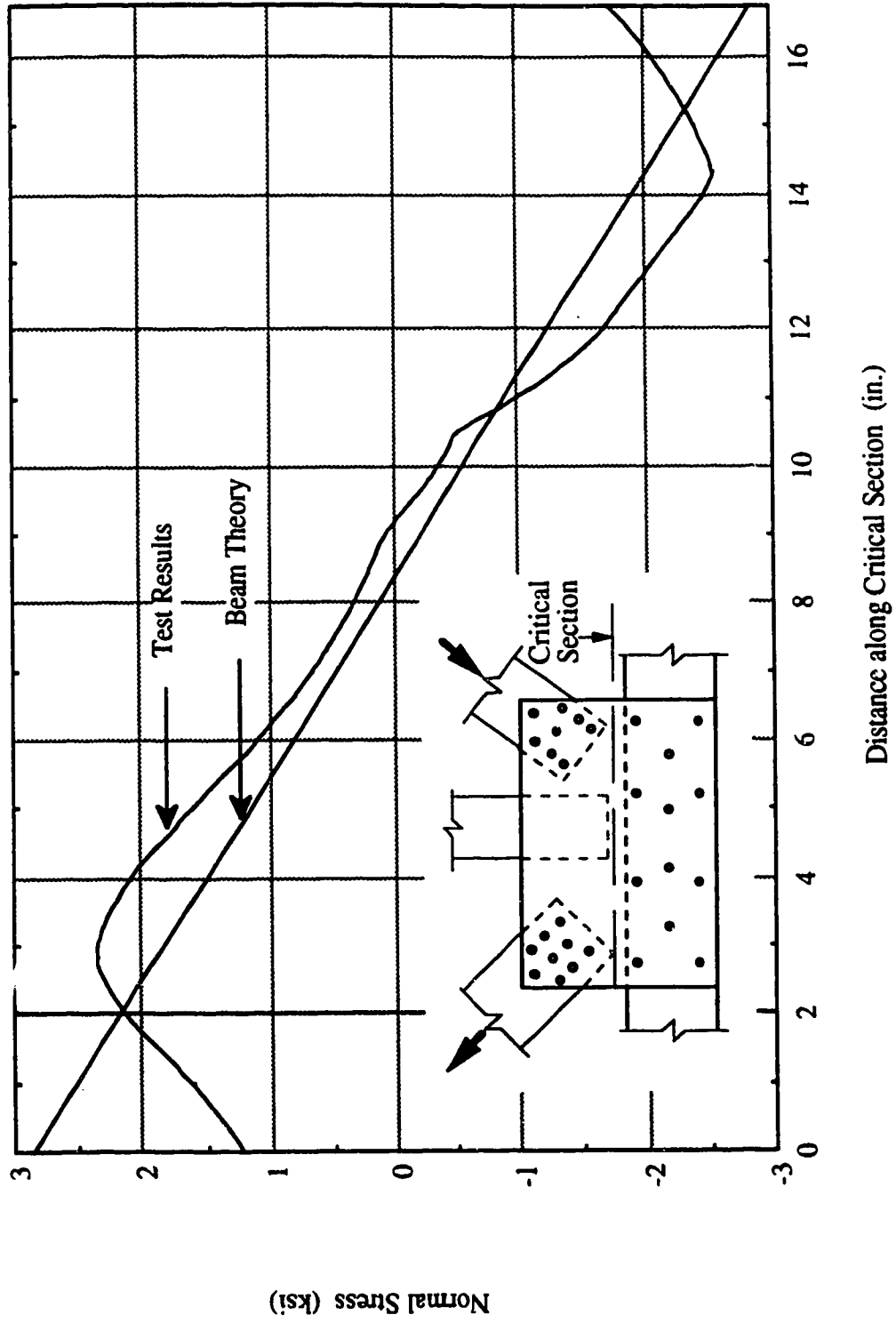


Fig. 1.3 Vertical Normal Stress Distribution Along the Critical Section

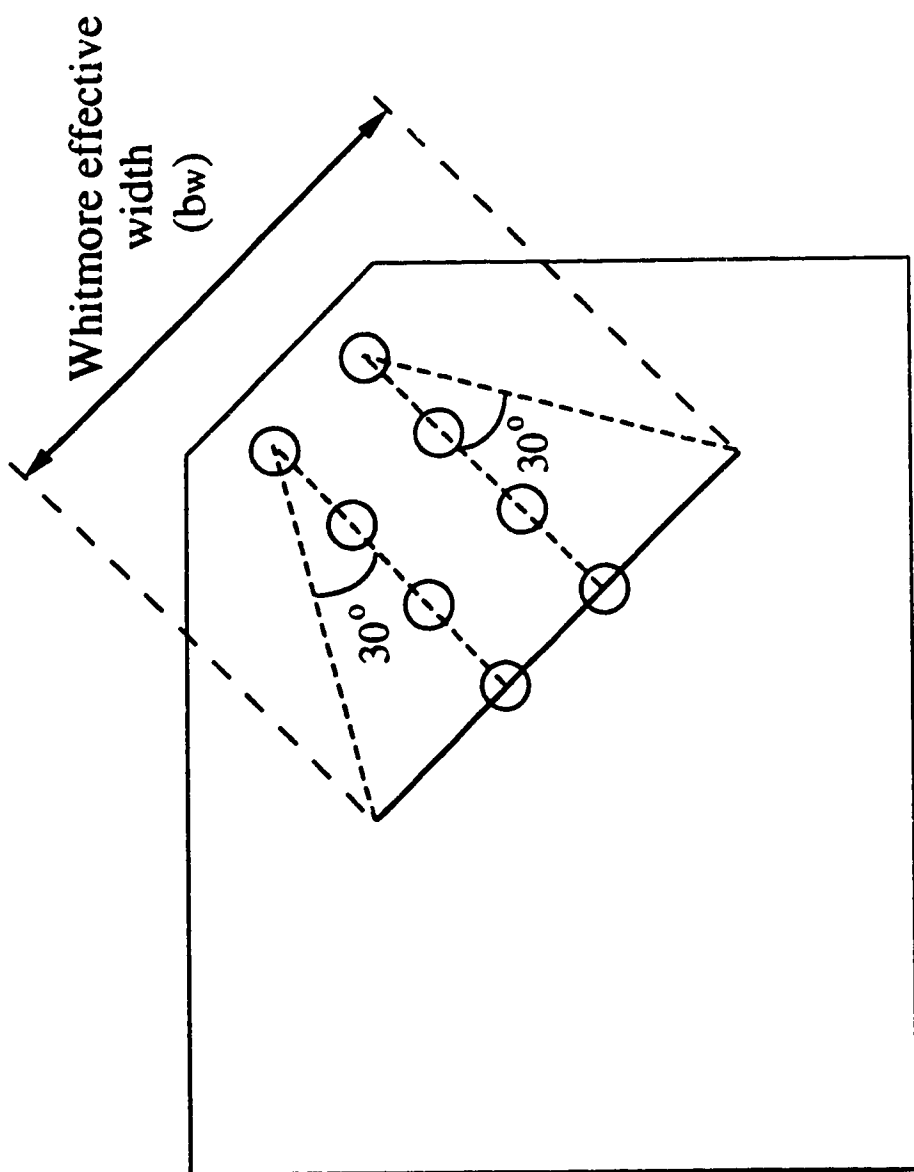
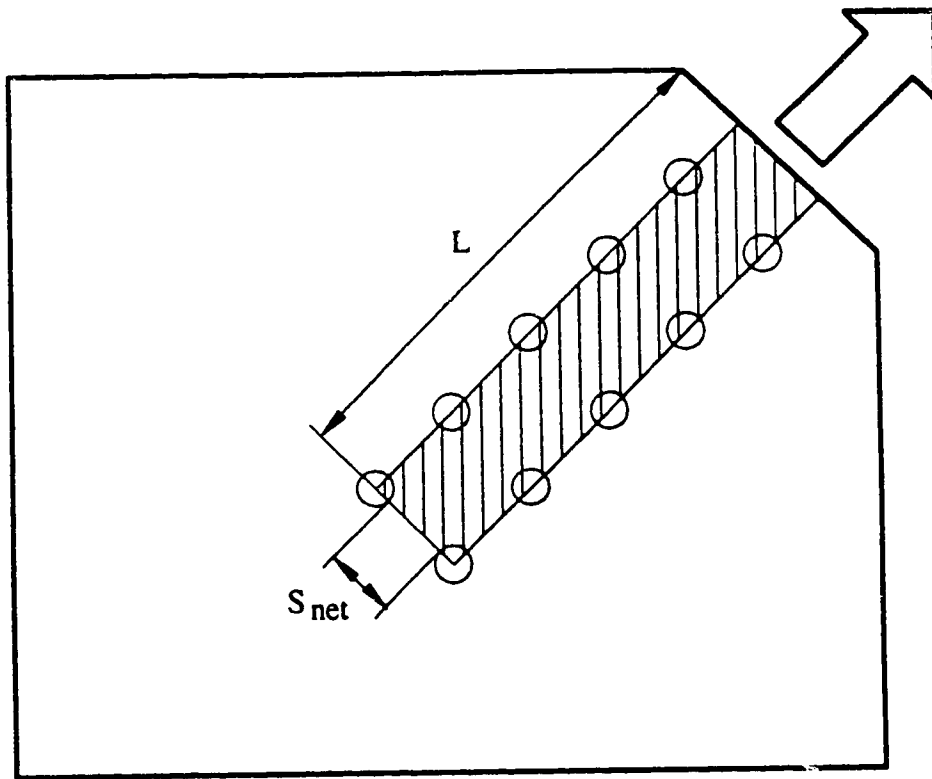


Fig. 1.4 Whitmore Effective Width Concept



**Ultimate Tear-out Resistance,  $R_n$  :**  
(Hardash and Bjorhovde, 1985)

$$R_n = F_u S_{net} t + 1.15 F_{eff} L t$$

**Fig. 1.5 Block Shear Tear-out Model**

Plate No. 1

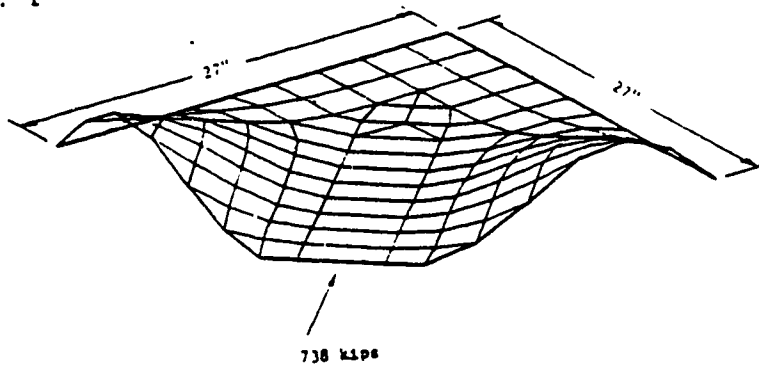


Plate No. 2

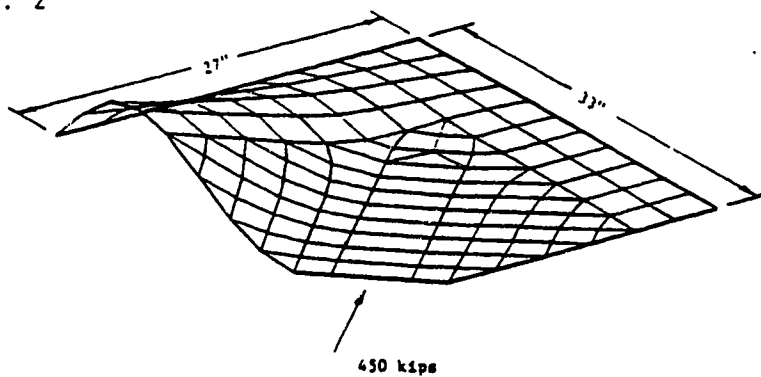
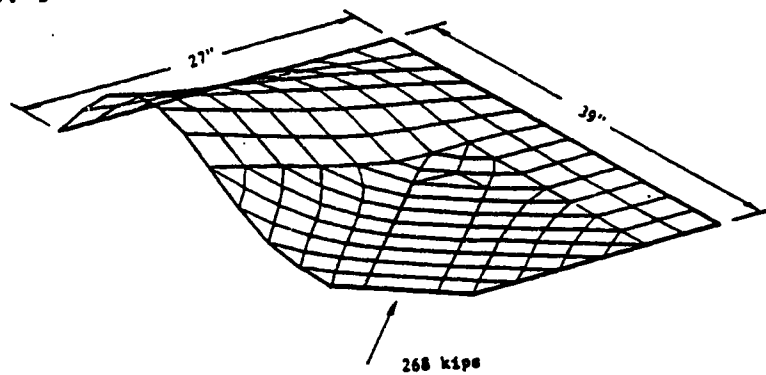


Plate No. 3



**Fig. 1.6 Typical Buckled Shapes for 45° Single Bracing Gusset**  
**(Williams and Richard 1986)**

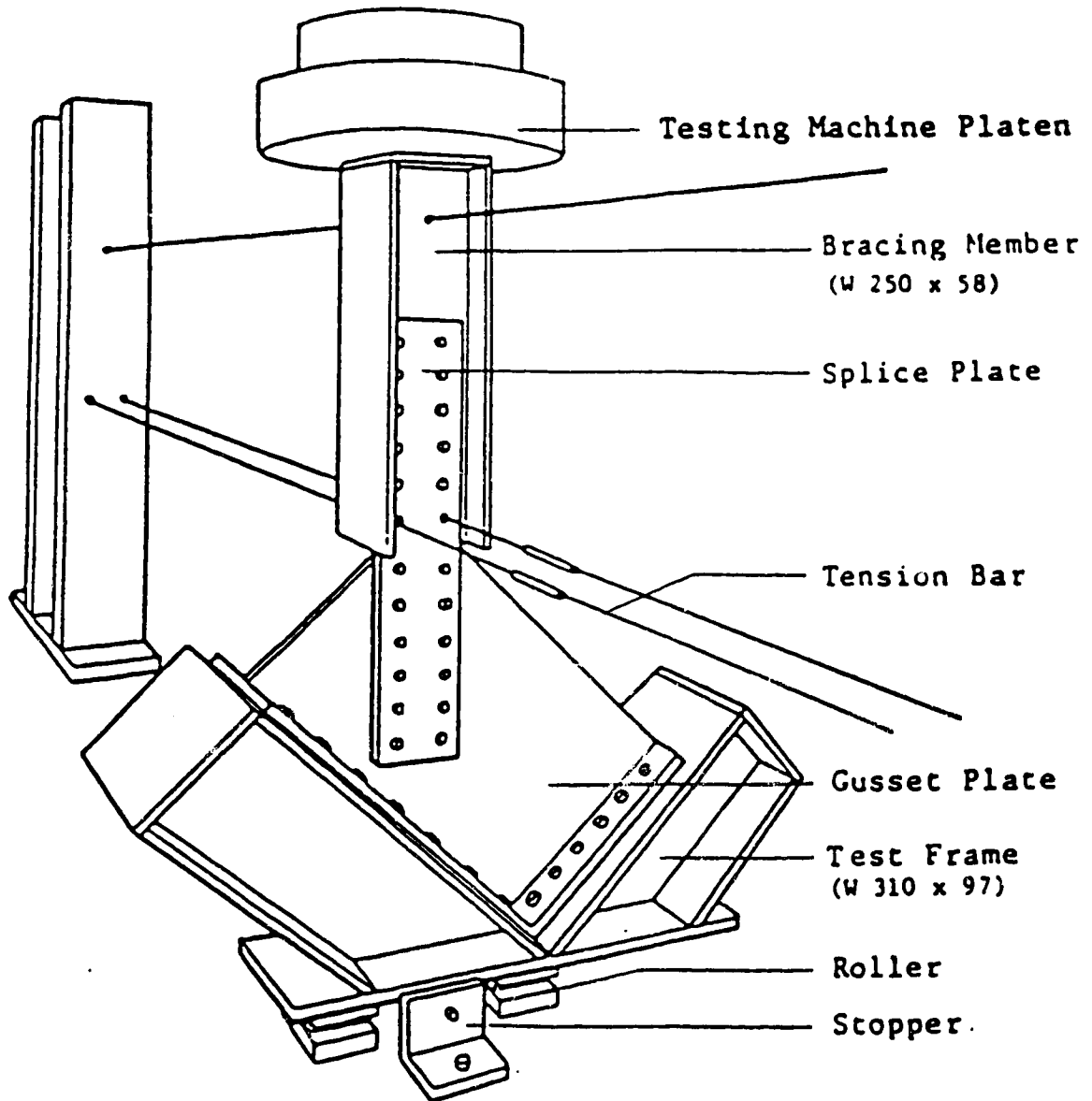


Fig. 1.7 Schematic Test Setup (Hu and Cheng 1987)

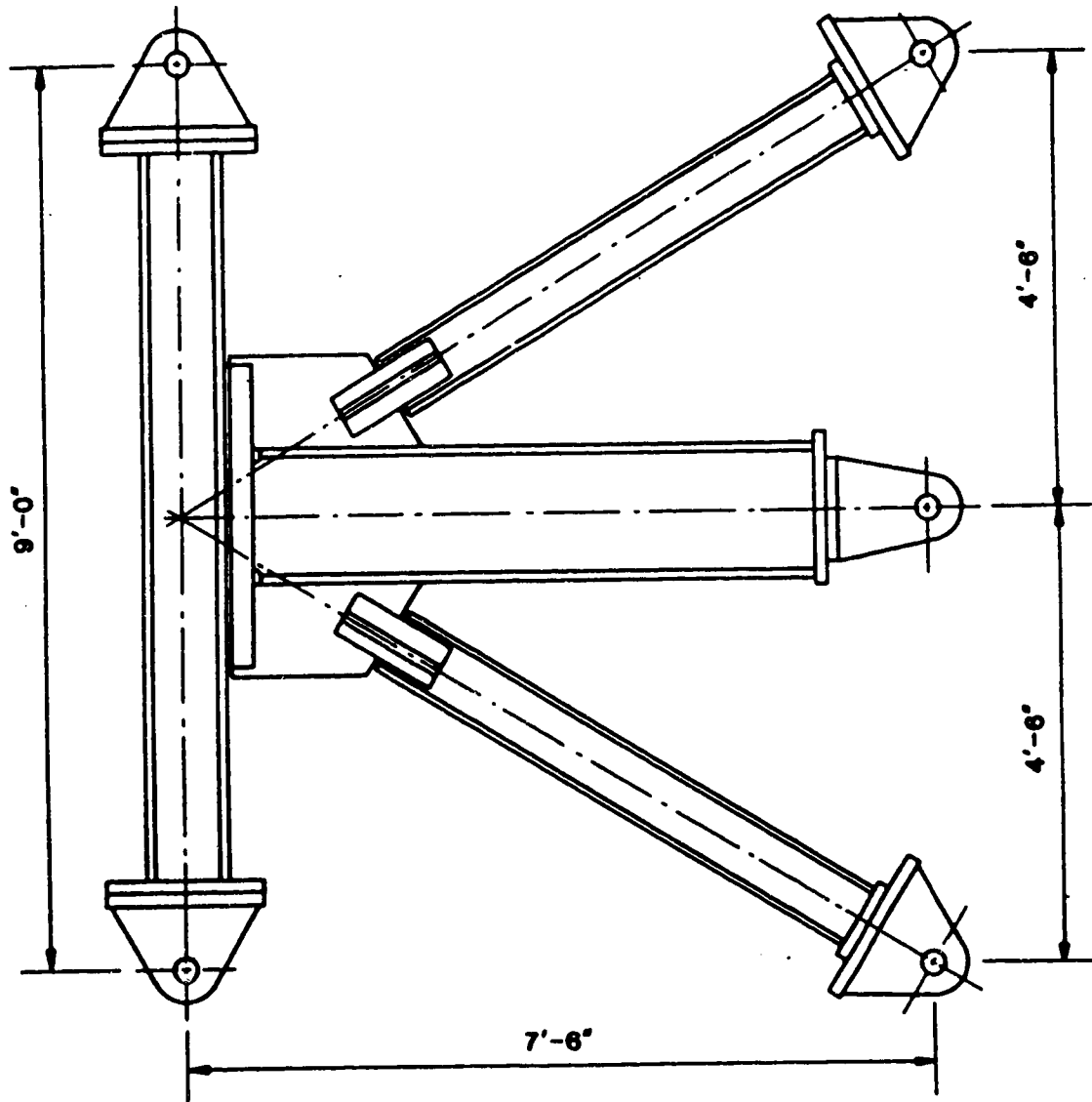


Fig. 1.8 Schematic Test Setup and Specimen Configuration (Gross 1990)

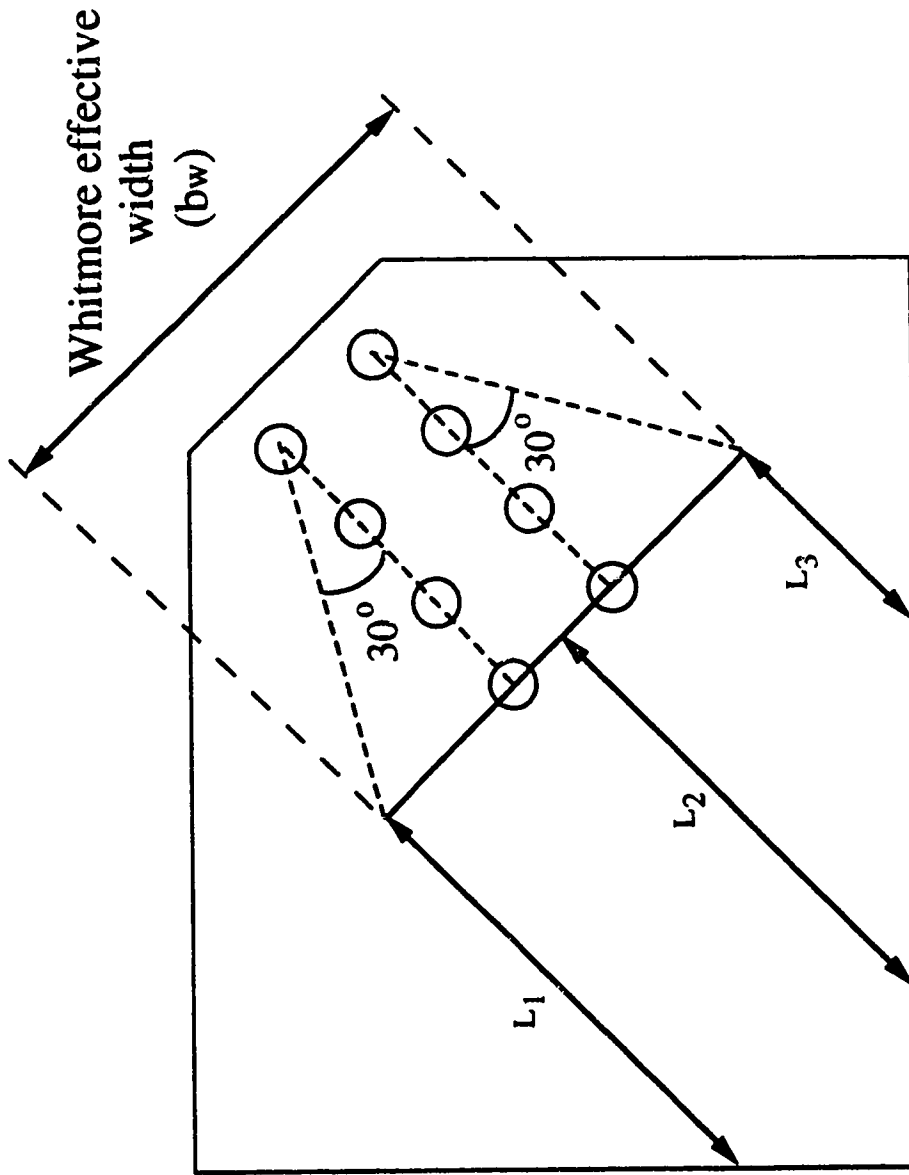


Fig. 1.9 Thornton Method

## **2. EXPERIMENTAL PROGRAM**

### **2.1 Introduction**

The design of a bracing system must consider the strength of the framing members, the diagonal bracing members and the gusset plate connections. If the applied load to the bracing system is such that compression exists in the diagonal bracing member, the stability of the gusset plate connection must also be investigated. In this case, the gusset plate may fail by buckling of the free edges, local buckling and/or crippling at the gusset plate area directly beneath the splice member. The ultimate compressive strength of the diagonal bracing member can readily be evaluated using CAN/CSA-S16.1-M89 specification. However, it is very difficult to evaluate the ultimate compressive strength of the gusset plate because of the complexity of the connection. When the ultimate compressive strength of the gusset plate is significantly lower than that of the diagonal bracing member, buckling of the gusset plate may occur prior to the stability failure of the bracing member. Hence, the bracing member may behave as a restraining member and provide rotational restraint to the gusset plate. It is assumed in this testing program that the bracing member provides infinite rotational restraint to the gusset plate connection and that the gusset plate fails before the ultimate strength of the bracing member is reached.

### **2.2 Scope**

The main purpose of this testing program was to examine the compressive behavior of gusset plate connections. In order to simulate the actual behavior of gusset plate connections, full-scale testing of diagonal bracing connection was employed. Because of the complexity of the problem, only one gusset plate configuration was chosen in the testing program, as shown in Fig. 2.1. A total of twenty-one tests were run on nineteen specimens in the entire experimental program. All the specimens were fabricated using CAN/CSA-G40.21-M92 300W steel. In general, the experimental program consisted of



two groups of specimens. The first group of specimens only considered the "isolated" compressive behavior of gusset plate connections. That is, the framing members to which the gusset plates were attached were excluded from the test parameters. The test variables included in this group were the gusset plate size and thickness, the brace angle, the out-of-plane restraint at the conjunction of gusset-to-splice, and the out-of-plane loading eccentricity. Two out-of-plane restraints were considered: namely, the "without-restraint" condition and the "with-restraint" condition. These two boundary conditions will be discussed in the section dealing with the of test setup. The out-of-plane loading eccentricity is produced by loading the gusset plate eccentrically with respect to its own plane. This happens frequently when the tubular bracing member has a slotted-in splice plate, as shown in Fig. 2.2. The actual configuration of these connections will be discussed in a later section. A 45° brace angle was used for all the specimens except for those which considered the brace angle as a test parameter.

The second group of specimens took into account the effects of the framing members on the compressive behavior of gusset plate connections. However, only the beam and column moments were considered. It was assumed that the axial force in the beam and column had negligible effects on the behavior of the gusset plate. The test variables in this group of specimens included the beam and column moment levels and gusset plate thickness. Based on some preliminary analytical studies of single and k-brace frames, the ratio of the column moment to the beam moment was chosen to be 0.5.

### **2.3 Specimen Description**

In general, there are five specimen designations used in the testing program: namely, GP, SP, AP, MP, and EP. The first letter of each designation represents the test variable for each type of specimen. These test variables are G-General, S-Size, A-Angle, M-Moment and E-Eccentricity.

For specimens which only considered the "isolated" compressive behavior of the gusset plate connection, two gusset plate sizes and three thicknesses were examined, as shown in Table 2.1. Drawings of the specimens are shown in Fig. 2.3. A similar plate aspect ratio of about 1.25 was maintained for both plate sizes of 500 x 400 and 850 x 700. As can be seen from Table 2.1, a relatively compact gusset plate section was selected for GP type specimens (500 x 400) to ensure that the specimens failed in the inelastic range. These specimens were employed to examine the general compressive behavior of the gusset plate connection particularly in the inelastic range. The GP type specimens and plate thickness tested in this program also represent practical gusset plate dimensions. For the SP type specimens, a larger plate size of 850 x 700 was used to investigate the size effect. However, only two plate thicknesses were considered (9.8 mm and 13.3 mm). For the specimen with out-of-plane loading eccentricity (EP type), only one gusset plate specimen (500 x 400 x 13.3) was fabricated. However, three tests were conducted with the same specimen by varying the type of splice member used to connect the specimen to the brace. Different types of splice members used with the EP type specimens will be discussed in the following section. The loading eccentricity of the specimens is shown in Table 2.1. A 45° brace angle was used for the GP, SP, MP and EP type specimens. For the AP type specimens, a brace angle of 30° was used. The gusset plate size and thicknesses used for the AP type specimens were identical to that of the GP type specimens. In addition, the effect of out-of-plane restraint conditions at the conjunction of gusset-to-splice was also examined for the GP and SP types specimens. Two restraint conditions were investigated: namely the "without-restraint" condition and the "with-restraint" condition. These restraint conditions will be discussed in Section 2.4 of Test Setup. To distinguish between these two restraint conditions, a letter R (restrained) was added to the specimen designation. For example, specimen GP1R implies same geometric configuration as specimen GP1 with restraint. For the SP type specimens, the same specimens were used to conduct the tests of

both restraint conditions since it was believed that the tests "without-restraint" would not have caused significant damage to the specimens.

For the specimens that incorporated the effects of beam and column moments, a specimen size of 500 x 400 was chosen with plate thicknesses varying from 6.5 mm to 13.3 mm as shown in Table 2.1. These specimens were designated as the MP type. The specimen shape was identical to the GP type specimens, as shown schematically in Fig. 2.3. As can be seen in Table 2.1, three 6.5 mm thick specimens were used to investigate the effects of moment levels. The applied beam and column moments to the specimens are also shown in Table 2.1. Two moment levels were investigated: namely, the beam moments of 250 kN·m and 375 kN·m. The ratio of the column moment to the beam moment was kept as 0.5 for all the tests. A 45° brace angle was used for the MP type specimens and only the "without-restraint" condition was examined.

The arrangements of the splice members for all the specimens are illustrated in Table 2.2. Two tee sections (WT125x22.5) and two 13.0 mm thick plates were used as the splice member for the GP, SP, MP and AP types specimens to ensure that the gusset plate failed before failure occurred in the splice member. These splice members are shown schematically in Fig. 2.4. This figure also illustrates the direction and orientation of the splice member which are important when examining the test results. For EP type specimens, the splice plate thickness (9.5 mm and 12.7 mm) and the type were varied. In particular, specimen EP3 was tested with a splice member that consisted of a tee-section (WT125 x 22.5) and a 9.5 mm plate. A schematic of the splice member is shown in Fig. 2.5. This splice member arrangement was employed to simulate the eccentricity produced by a tubular bracing member with a slotted-in splice plate, as shown in Fig. 2.2. Eight ASTM A325-M22 bolts were used to connect the splice member to the GP AP, MP and EP type specimens. For the SP type specimens, however, twelve M22 A325 bolts were used. All the bolted connections were installed by an air impact wrench using the

turn-of-nut method. All the gusset plates were directly welded onto the beam and column. After each test, the failed specimen was flame-cut and the surfaces of the beam and column were ground smooth before welding on the next specimen.

## **2.4 Test Setup**

### **2.4.1 General**

Two test setups were constructed for this testing program: namely, Scheme I and Scheme II, in order to incorporate all the test parameters mentioned above and facilitate the testing program. Scheme I of the test setup was used to perform tests on specimens which excluded the effects of the beam and column moments. On the other hand, Scheme II of the test setup was employed to conduct tests on specimens which included the effects of the beam and column moments. The specimens tested in Scheme I test setup were GP, SP, and EP type specimens. Although AP type specimens did not include the beam and column moments effect, the Scheme II test setup was used to facilitate the testing of AP type specimens. The MP type specimens were also tested with the Scheme II test setup since the main test parameter for this type of specimens was the effects of beam and column moments.

### **2.4.2 Scheme I**

The concept of this test setup was based on the work done by Hu and Cheng (1987). When gusset plate buckling occurred in a braced steel frame, the diagonal bracing member could sway out-of-plane as shown in Fig. 2.6a. This figure shows that the free edges of the gusset plate deform out-of-plane along with the diagonal member while the fixed edges of the plate remain in-plane due to the support from the steel frame. This deformation mode of the gusset plate can be simulated by allowing the steel frame instead of the diagonal bracing member to move out-of-plane, as shown in Fig. 2.6b. When comparing Figs. 2.6a and 2.6b, it can be seen that both arrangements produce the same out-of-plane

deformation mode of gusset plate. In order to simplify the test setup, therefore, the arrangement shown in Fig. 2.6b was used as the basis of designing the test frame.

The setup is shown schematically in Fig. 2.7 and a photograph of the test setup is shown in Fig. 2.8. The load was applied to the specimens by the MTS testing machine, and stroke control was used for all the tests. The vertical displacement of the specimen was also monitored by the MTS. As can be seen in Fig. 2.7, two W310 x 129 sections were used as the stub beam and column members, and the diagonal bracing member (W250 x 67) was fixed in place by four tension rods bolted to a set of columns located approximately four meters from the test frame. Sixteen ASTM A325-M22 bolts were used to connect the splice member to the diagonal bracing member. The stub beam and column were bolted to a distributing beam, which sat on three sets of rollers to allow out-of-plane movement. Two channel sections were also bolted to the distributing beam and supported on four sets of rollers to provide lateral stability for the test frame, as shown in Fig. 2.8. Stoppers were located at approximately 50 mm from both sides of the distributing beam to avoid sudden kicking out of the test frame.

As mentioned above, two out-of-plane restraint conditions were examined in the testing program: namely, the "without restraint" condition and the "with restraint" condition. For the "without-restraint" condition, the distributing beam was allowed to move out-of-plane while the diagonal bracing member was fixed in place by the tension rods. However, for the "with-restraint" condition, both the distributing beam and the diagonal bracing member were restrained from out-of-plane movement. Stoppers, which were located at about 50 mm from the distributing beam to prevent sudden kicking out of the test frame, were used to restrain the out-of-plane movement of the distributing beam by supporting a threaded rod which bore against the bottom flange of the distributing beam. The "with-restraint" condition was used only in the GP and SP type specimens.

### 2.4.3 Scheme II

The Scheme II test setup for the testing program must allow the application of beam and column moments and axial load in the bracing member in order for tests to be conducted on the MP type specimens, which include the effects of beam and column moments. To properly accommodate these requirements, a test frame and a loading system were designed based on the actual brace steel frame behavior shown previously in Fig. 2.6a. A schematic and a photograph of the test setup are shown in Figs. 2.9 and 2.10, respectively. This test setup was supported by a reaction frame that was bolted and pretensioned to the strong floor. As can be seen in Fig. 2.9, this test setup consisted of a W310x129 column welded on to a 16 mm thick base plate and a W530x101 beam section welded on to a 16 mm thick end plate. Matching bolt holes were pre-drilled in the end plate and the column flange. The end plate from the beam section was bolted to the column flange by twenty-six ASTM A325-M24 bolts. This complete assemblage was then bolted to the floor beam, and the floor beam was welded to two channel sections which were bolted to the strong floor to provide the reaction and lateral stability for the setup. A W200x86 section was used for the bracing member and the gusset plate specimen was welded to the beam flange and the end plate. It should be noted that, for the testing of AP type specimens, a different floor beam with a 15° (relative to horizontal) inclined flange was used for the setup in order to produce a 30° brace angle, as shown in Fig. 2.11.

It can be seen from Fig. 2.9 that this test setup allowed the bracing member to sway out-of-plane when buckling of the gusset plate occurred. To accomplish this behavior and still provide the axial load to the bracing member, a two-hydraulic ram system which could resist the secondary moment produced by the out-of-plane displacement of the gusset plate when buckling of the plate occurred was used. This two-hydraulic ram system is shown in Figs. 2.12 and 2.13. In order to employ this loading system, a W310 x 97 distributing beam was welded to the bracing member, as shown in Fig. 2.12, to receive the loads from

the 200 ton hydraulic rams which were 700 mm apart. This distance between the hydraulic rams provided the necessary moment arm for the loading system to resist the secondary moment. Diagonal stiffeners were also welded to the bracing member and to the ends of the distributing beam to strengthen the loading unit. The applied loads from the hydraulic rams were controlled by adjusting the oil pressure in each ram. Each hydraulic ram was controlled by a separate oil pressure supply from a control panel. Since the two hydraulic rams had to maintain equal stroke during testing to simulate the actual loading condition, a linear variable differential transformer (LVDT) was therefore attached to each hydraulic ram to control the amount of cylinder movement of the ram and the readings of the LVDTs were directly transferred to two voltmeters. A load cell was set underneath the hydraulic ram to monitor the apply load. A knife edge was used to properly align the point of load application, as shown in Fig. 2.12. Rollers were placed at the top of the hydraulic ram to allow the out-of-plane movement of the loading system. These rollers bore against the bottom flange of the supporting beam, which was bolted to the channel sections of the reaction frame, as shown in Fig. 2.9.

Lateral braces were also bolted to the distributing beam to provide lateral support to the loading system. The lateral braces with a roller at the end were supported by the flange of an I beam, which was bolted to the reaction frame as shown in Fig. 2.14. A piece of Teflon was placed in between the roller and the flange of the I-beam to allow vertical movement of the loading unit, as also shown in Fig. 2.14. This lateral bracing system was also stiffened by placing a piece of lumber in between the two lateral braces, and tension rods were then used to tighten the lateral braces against the lumber, such that the whole system could act as a single unit as illustrated in Fig. 2.14.

The beam and column moments were applied by the tension rods as shown in Fig. 2.9. Steel brackets were welded to the ends of the beam and column to provide support for the tension rod. A load cell was placed on the steel bracket and a bearing plate was put on the

other end of the load cell. The tension rod was then put through the load cell and the bearing plate and secured by a nut at the end. The other end of the tension rod was put through a hydraulic ram bearing against the end plate of a pedestal located away from the reaction frame, as shown in Fig. 2.9. Tension was developed in the rod when the cylinder of the hydraulic ram moved outward. The load cell, which sat in between the steel bracket and the bearing plate, recorded the applied load. Strain gauges located at 1000 mm from the ends of the beam and column were used to monitor the applied moments.

## **2.5 Instrumentation**

LVDT's were used to measure the out-of-plane deflection of the gusset plate free edges. LVDT's were also attached to the gusset plate underneath the splice member to monitor the out-of-plane movement at that region. This region was expected to be highly stressed, based on tests by Hu and Cheng (1987). The location of all the LVDTs for specimens GP, MP and SP types are shown schematically in Fig. 2.15. A slightly different arrangement of the LVDTs was used for the EP type specimens to better capture the importance of the test, as illustrated in Fig 2.16. This figure shows that more LVDTs were located on the splice members, which were expected to be the critical region for these specimens. The schematic of LVDT locations for the AP type specimens is shown in Fig. 2.17. In general, the arrangement of LVDT's for the AP type specimens was similar to that of the GP type specimens, except on the free edge of the short side due to a different brace angle. Two LVDT's were attached to the beam and column to record the out-of-plane displacement of the test frame. As shown in Fig. 2.18, the LVDT's attached to the gusset plate were mounted on a frame which was clamped to the beam and column. Hence, the LVDTs measured the out-of-plane displacement of the gusset plate relative to the test frame.

For the MP and AP type specimens, a cable transducer was also connected to the distributing beam, which was welded to the bracing member, to record the out-of-plane movement of the bracing member since the Scheme II test setup was used. The deflection



of the beam due to the applied load was monitored by connecting a brass wire to an LVDT which was located on a pedestal parallel to the tension rod. An identical arrangement of LVDT's was used for measuring the column deflection. Any vertical deformation of the specimen was recorded by an LVDT attached to the base of the splice member.

Strain gauges and rosettes were used to measure the strain distribution of the specimens and to monitor the level of applied beam and column moments for the MP type specimens. The location of strain gauges for the GP, SP, and EP type specimens are shown schematically in Fig. 2.19. Fig. 2.20 shows the location of strain gauges for the AP type specimens. All the strain gauges and rosettes were mounted on both sides of the specimen in order to confirm the readings and to detect bending behavior. Strain gauges were also placed at the mid-length of the free edges to capture strain bifurcation when buckling of the gusset plate occurred. Three rosettes were mounted 90 mm under the Whitmore critical section. However, for the EP type specimens, only the center rosette was mounted, since the critical location of these specimens was expected to be in the splice member. Hence, strain gauges were also mounted on the splice members of the EP type specimens as shown schematically in Fig. 2.21.

The location of strain gauges for the MP type specimens is shown schematically in Fig. 2.22. Again, strain gauges were placed at the mid-length of the free edges of the plate to detect strain bifurcation. To measure the effects of the beam and column moments on the gusset plate stress distribution, strain gauges were mounted perpendicular to the beam and column boundaries on the specimen, as illustrated in Fig. 2.22. Strain gauges were also mounted on the flanges of the bracing member to confirm the applied load.

A data acquisition system was used to collect all the test data and to record the MTS load and stroke. A x-y plotter was also used to record the MTS load versus stroke behavior during the tests for specimens tested with the Scheme I setup to monitor the loading process. However, for the specimens tested with Scheme II setup the readings of the apply

load and the lateral deflection of the specimens were manually fed into a computer after each load step to generate a current load deflection plot in order to monitor the loading process. Whitewash was applied to all the specimens to detect the yielding process.

## **2.6 Test Procedure**

For the GP type specimens, the tests with the "without-restraint" condition were first performed. If the failed specimen had excessive permanent deformation after the test of the "without-restraint" condition, this failed specimen would not be used again for the "with-restraint" condition test. In fact, a new specimen of the same type would be fabricated for the test of the "with-restraint" condition. However, for SP type specimens the same specimen was used for the tests of both the "without-restraint" and "with-restraint" conditions since it was expected the permanent deformation would not be significant for these specimens after the "without-restraint" condition test. Again, the SP type specimens were tested with the "without-restraint" condition first and after the test the failed specimens were straightened before performing the "with-restraint" condition test. Only the "without-restraint" condition tests were performed on the AP, MP and EP type specimens.

For the EP type specimens, only one gusset plate specimen (500 x 400 x 13.3) was used. The 9.5 mm thick splice plate was tested first, followed by the 13.0 mm thick splice plate, using the same gusset plate specimen. Again, any permanent deformation of the gusset plate after each test was corrected before performing the next test. Since it was expected that the tee-section splice member would produce a higher ultimate load than the splice plate (and therefore produced more permanent deformation on the gusset plate), the test with a tee-section as the splice member was conducted last.

In general, the loading process was the same for all the specimens except for those of the MP type which will be discussed below. An initial load was applied to the specimen to settle the test fixtures. At the initial loading stage, a predetermined load increment was

applied to the specimen and the specimen was allowed to stabilize during each load increment. When nonlinear load deflection was observed for the specimen, a smaller load increment was used to capture the nonlinearity. All the experimental observations during the test were recorded. In particular, the yield line pattern and process were recorded in detail to fully understand the load transfer mechanism from the bracing member to the beam and column through the gusset plate connection. The test was terminated when the ultimate load was reached and unloading of the specimen occurred, or the physical limit of the LVDT measuring the out-of-plane deflection was reached.

For the MP type specimens, the beam and column moments were applied in two or three increments; however, the moment ratio was always maintained at 0.5. In general, the maximum beam and column moments were applied at an axial load of approximately 25% of the Whitmore load of the specimens. Two moment levels were used in this test phase, as shown in Table 2.1. For the purpose of comparison, a 6.5 mm thick specimen was tested without beam and column moments. As mentioned previously, the level of moments was monitored by the strain gauges mounted on the beam and column flanges. A load was applied carefully to ensure that the stroke of the hydraulic rams was maintained equally by opening and closing the oil pressure valves. The stroke readings of the hydraulic rams which were measured by LVDT's directly connected to a voltmeter were observed closely. The beam and column moments were regularly checked and adjusted to maintain the maximum values. After applying the maximum moments, axial load was increased incrementally by a predetermined amount. The specimen was allowed to stabilize after each load increment. Again, when the nonlinear load deflection was observed for the specimen, a smaller load increment was used to capture the nonlinearity. All the experimental observations were recorded especially the yielding process and pattern.

## **2.7 Presentation of Test Results**

The test results of each specimen type will be presented separately in the following chapters. The test results of the GP type specimens are presented first, followed by the SP, AP, MP and finally, the EP type specimens (chapters 3-7). Each chapter contains the load versus deflection curves, the load versus strain gauge readings curves and the out-of-plane deflected shapes of the free edges and the centerline of the specimens. Chapter 8 presents a discussion and comparison of the test results. Comparisons with the predictions by the Whitmore and Thornton methods are also included.

Table 2.1. Specimen Description

Specimen Designation	Plate Size (mm x mm)	Plate Thickness (mm)	Loading Eccentricity (mm)	Beam Moment Mb (kN·m)	Column Moment Mc (kN·m)	Brace Angle
GP1	500 x 400	13.3	-	-	-	45°
GP2	500 x 400	9.8	-	-	-	45°
GP3	500 x 400	6.5	-	-	-	45°
GP1R	500 x 400	13.3	-	-	-	45°
GP2R	500 x 400	9.8	-	-	-	45°
GP3R	500 x 400	6.5	-	-	-	45°
SP1	850 x 700	13.3	-	-	-	45°
SP2	850 x 700	9.8	-	-	-	45°
AP1	500 x 400	13.3	-	-	-	30°
AP2	500 x 400	9.8	-	-	-	30°
AP3	500 x 400	6.5	-	-	-	30°
MP1	500 x 400	13.3	-	250	125	45°
MP2	500 x 400	9.8	-	250	125	45°
MP3	500 x 400	6.5	-	250	125	45°
MP3A	500 x 400	6.5	-	375	187.5	45°
MP3B	500 x 400	6.5	-	0	0	45°
EP1	500 x 400	13.3	11.4	-	-	45°
EP2	500 x 400	13.3	13.2	-	-	45°
EP3	500 x 400	13.3	53.0	-	-	45°

Table 2.2. Types of Splicing Members

Specimen Designation	Types of Splicing Member
GP Type	2 x WT 125 x 22.5 2 x Plate 870 x 148 x 13.0
SP Type	2 x WT 125 x 22.5 2 x Plate 870 x 148 x 13.0
AP Type	2 x WT 125 x 22.5 2 x Plate 870 x 148 x 13.0
MP Type	2 x WT 125 x 22.5 2 x Plate 870 x 148 x 13.0
EP1	Plate 870 x 148 x 9.5
EP2	Plate 870 x 148 x 13.0
EP3	WT 125 x 22.5 Plate 870 x 148 x 9.5

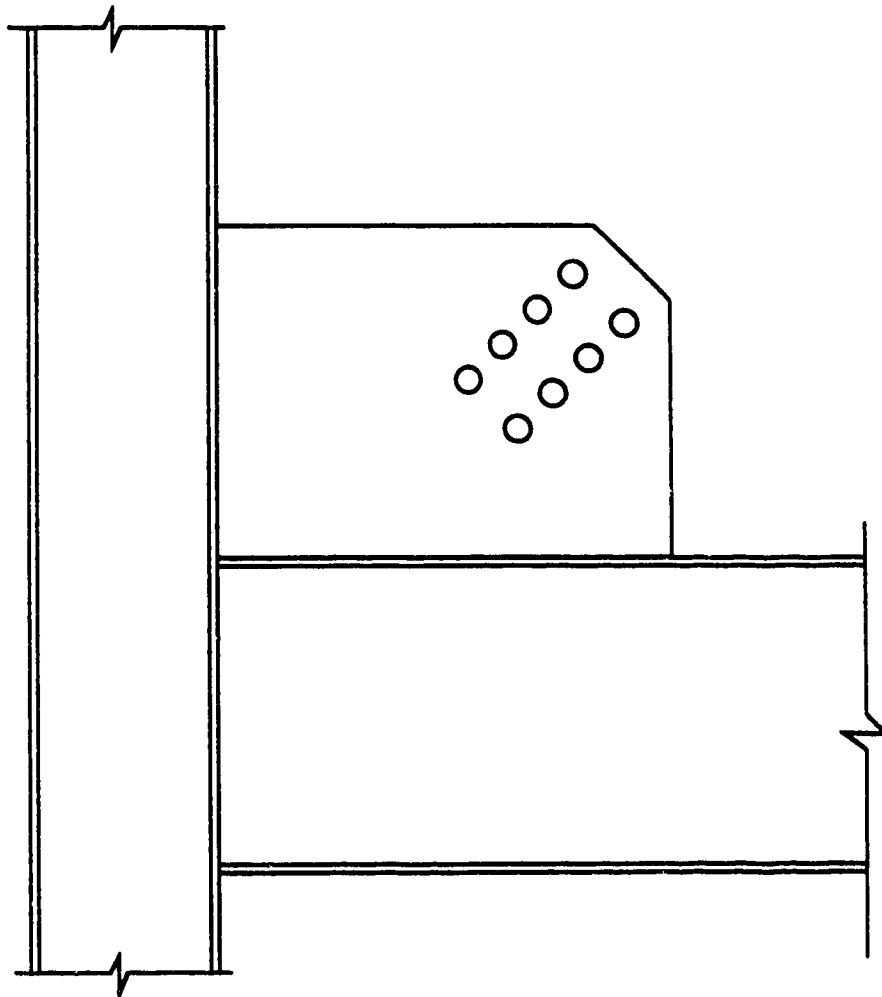


Fig. 2.1 Typical Gusset Plate Configuration

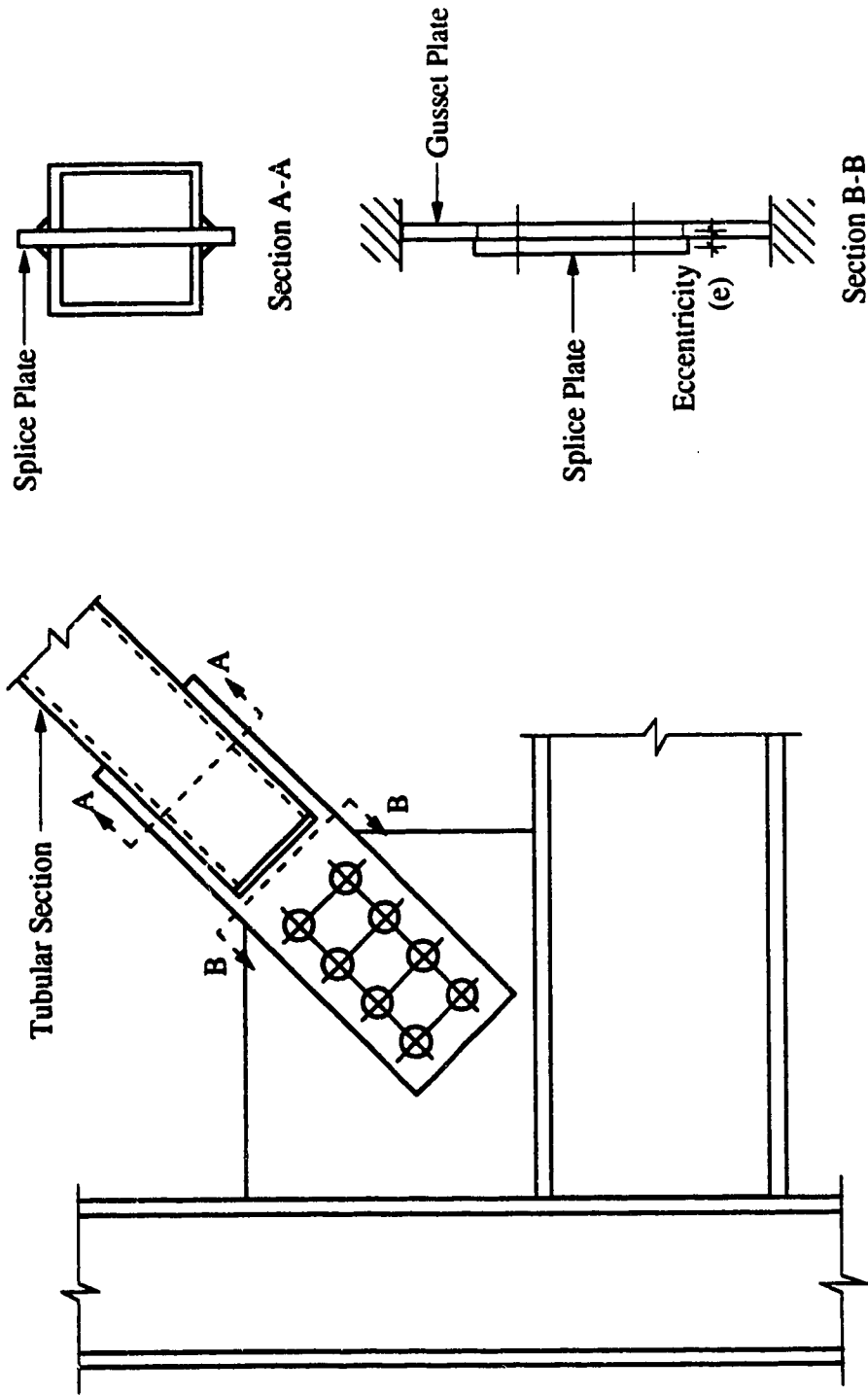


Fig. 2.2 Gusset Plate Connection of Tubular Section Bracing



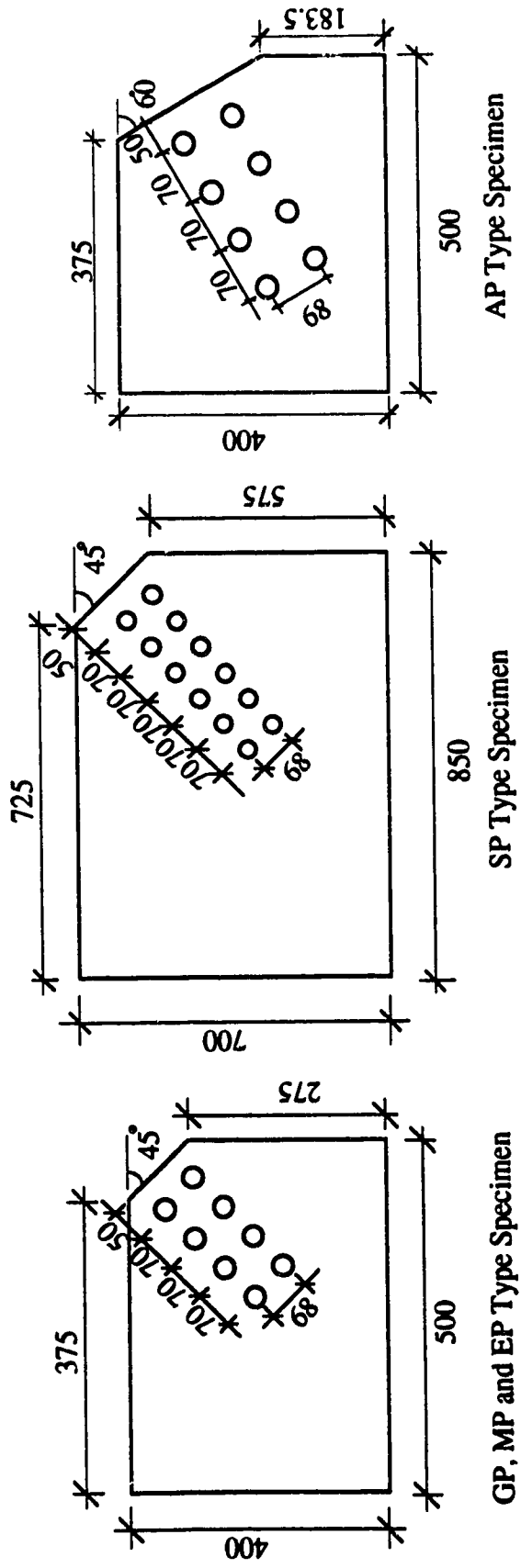


Fig. 2.3 Schematic of Test Specimens

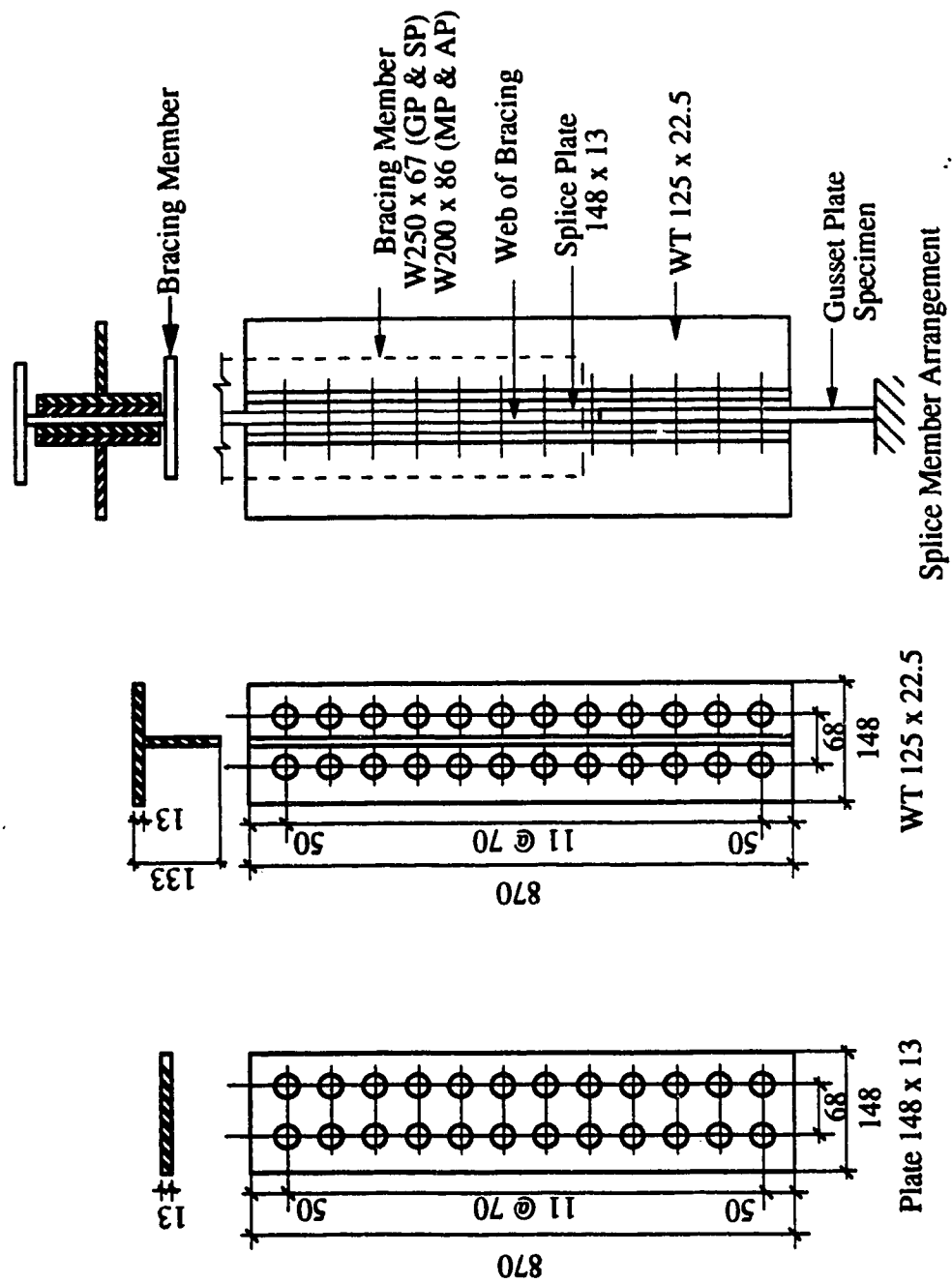


Fig. 2.4 Splice Members and Splicing Arrangement for GP, SP, MP and AP Type Specimens

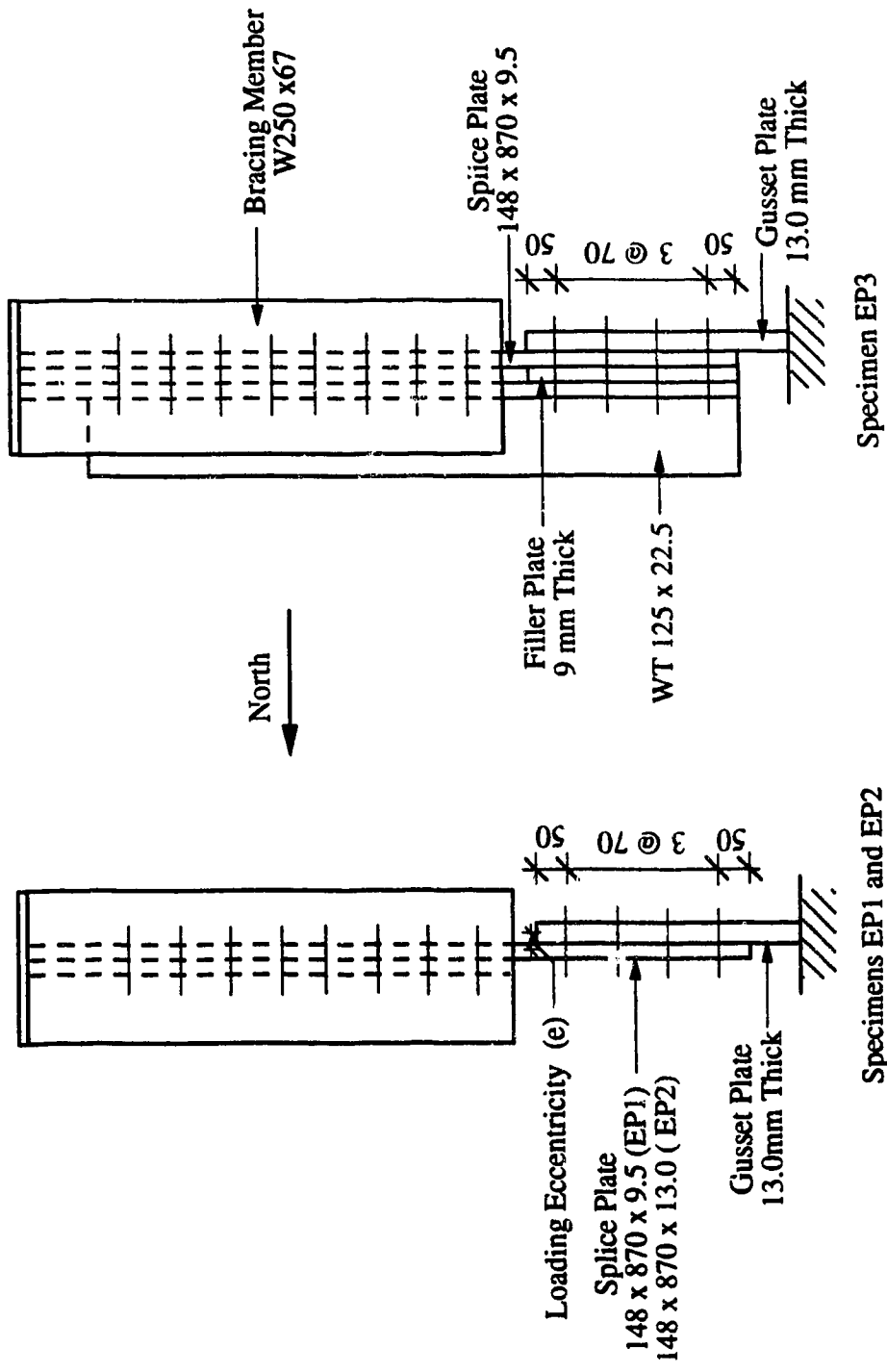
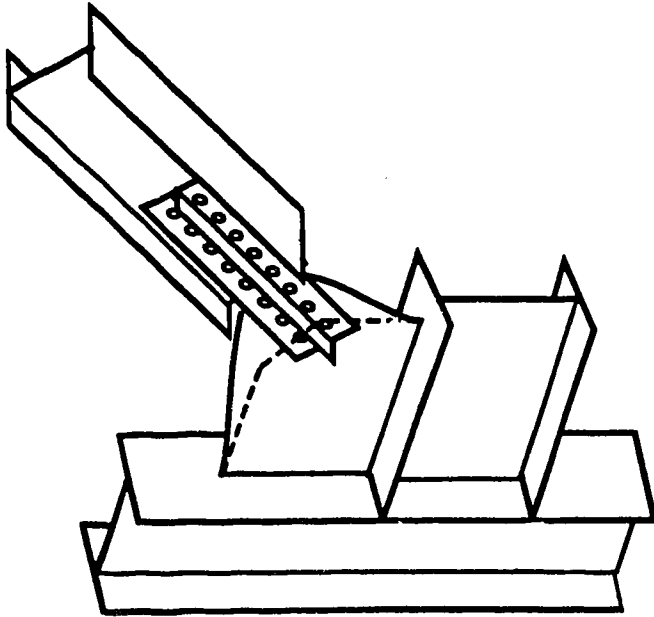
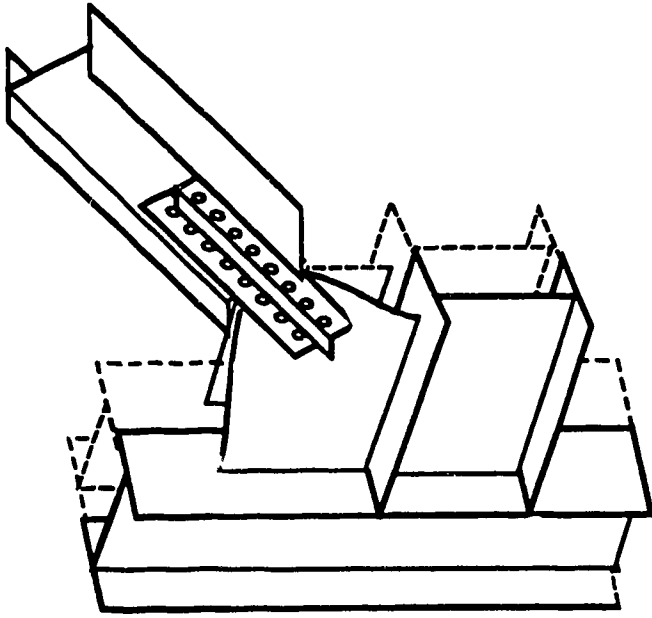


Fig. 2.5 Splice Member Arrangement for EP Type Specimens



**Fig. 2.6b Test Frame Behavior: The Beam and  
Column and Gusset Plate Fixed Edges  
Deformed Out-of-Plane during Buckling**

**Fig. 2.6a Actual Braced Frame Behavior: Bracing  
Member and Gusset Plate Free Edges  
Deformed Out-of-Plane during Buckling**

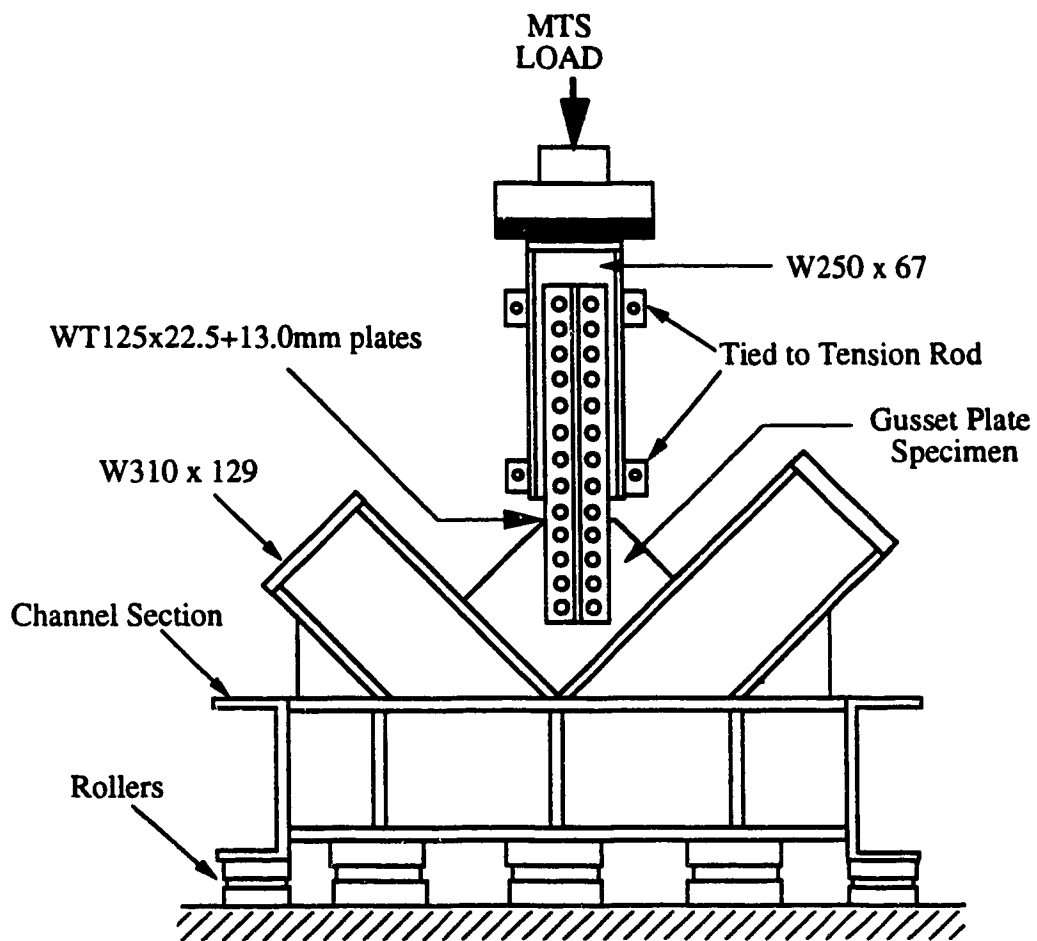
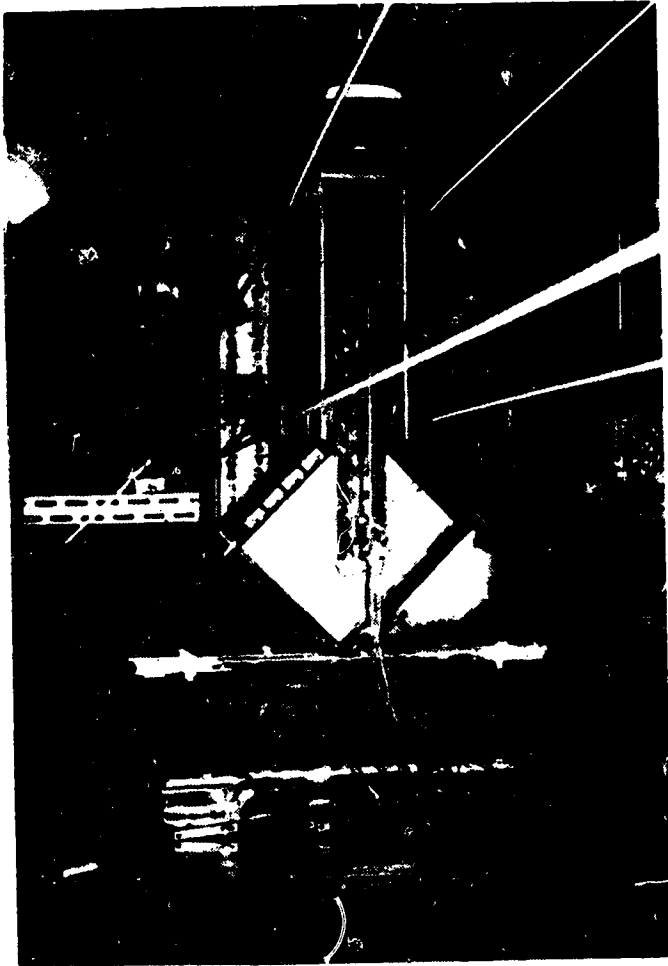


Fig. 2.7 Schematic of Test Setup for Scheme I



**Fig. 2.8** Picture of Scheme I Test Setup

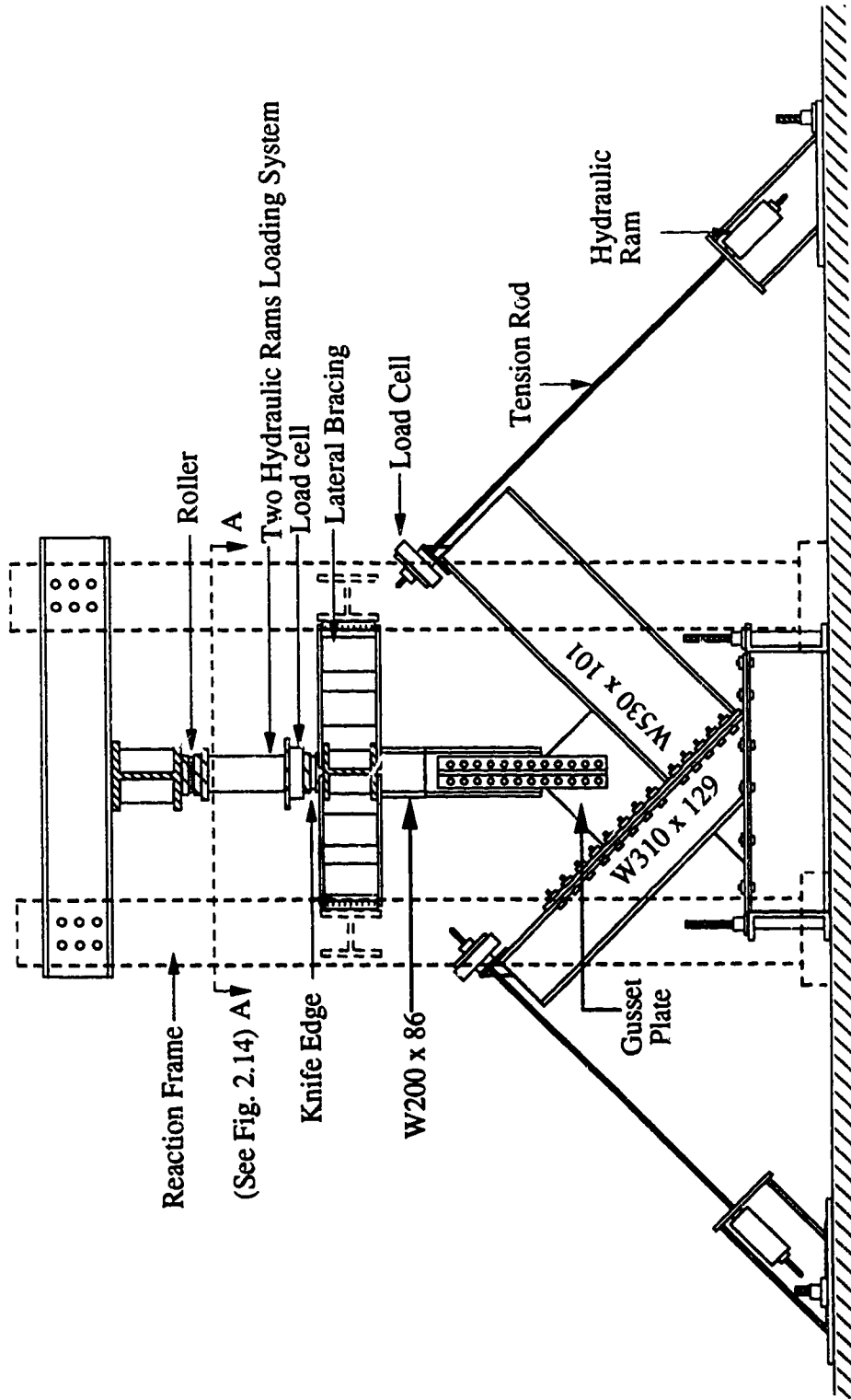
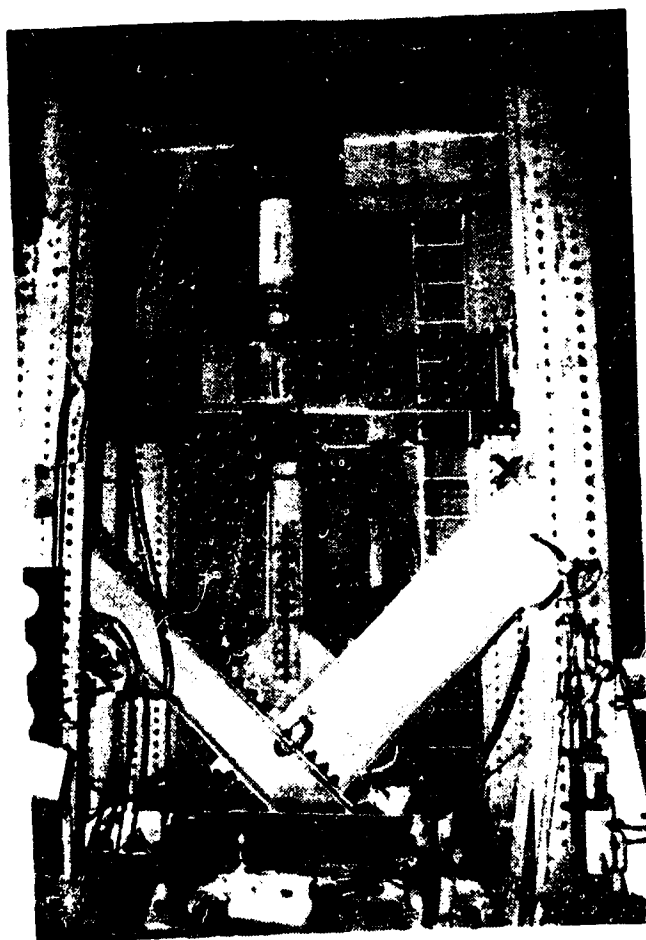


Fig. 2.9 Schematic of Test Setup for Scheme II



**Fig. 2.10** Picture of Scheme II Test Setup





**Fig. 2.11 Picture of Test Setup for AP Type Specimens**

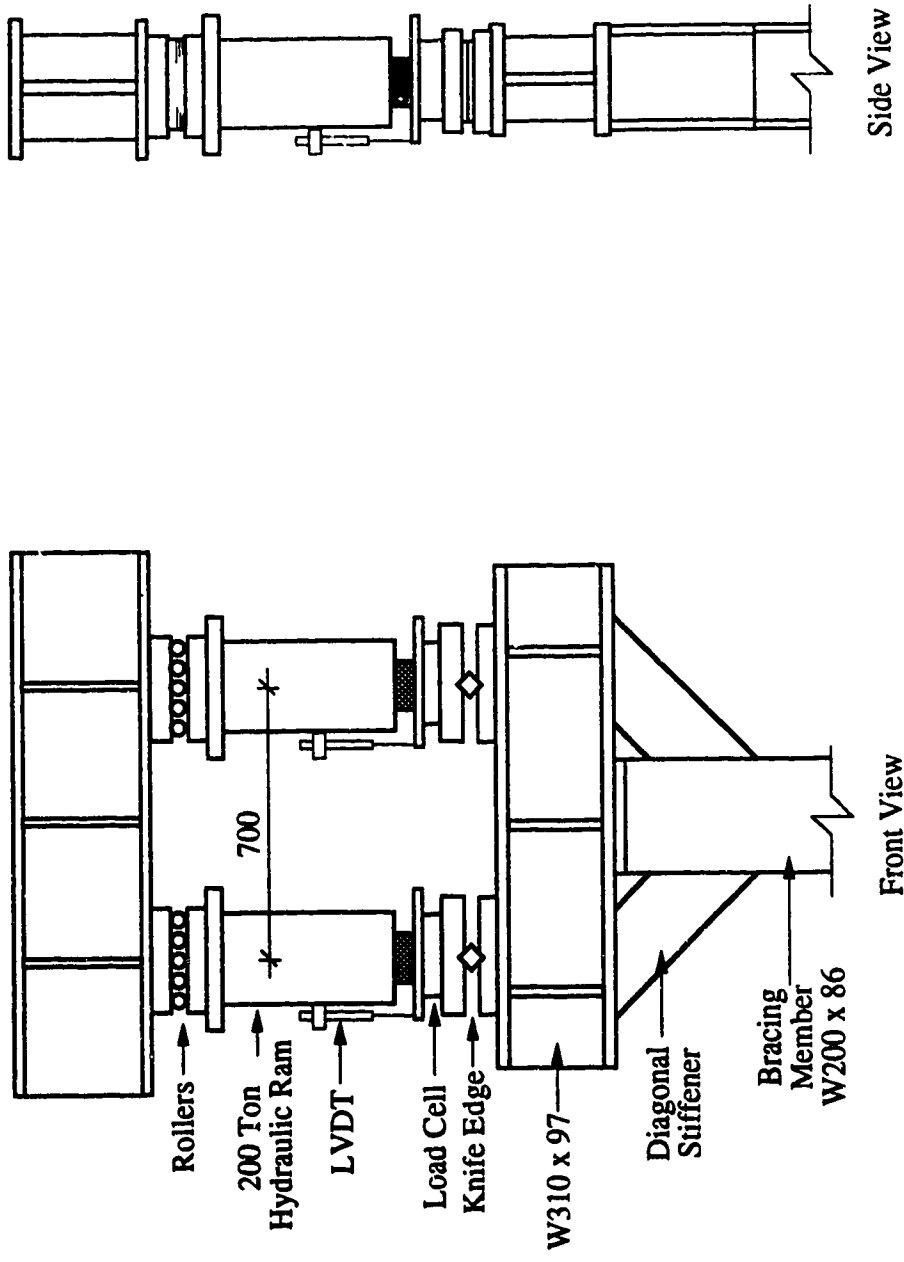


Fig.2.12 Schematic of Loading System

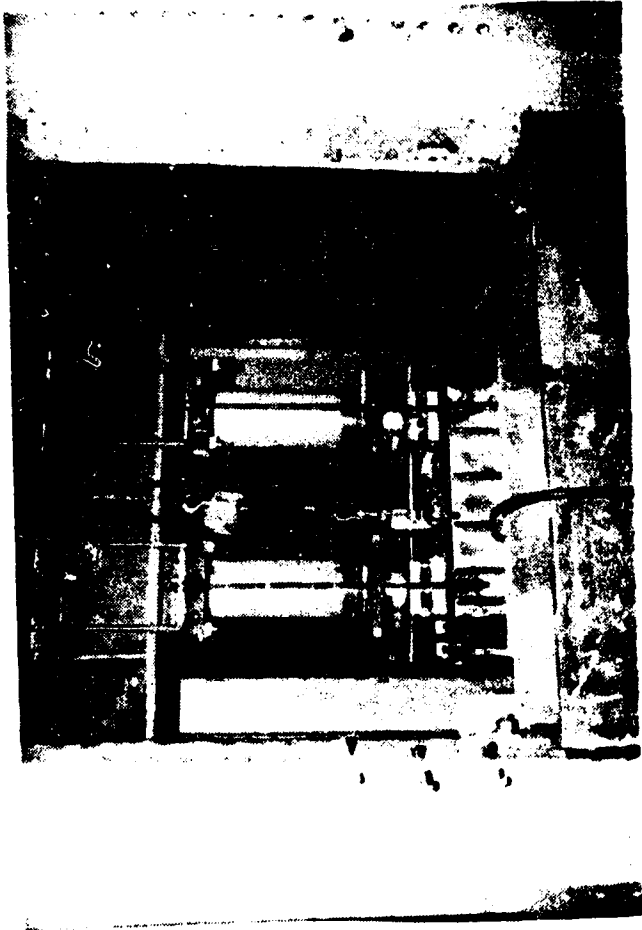
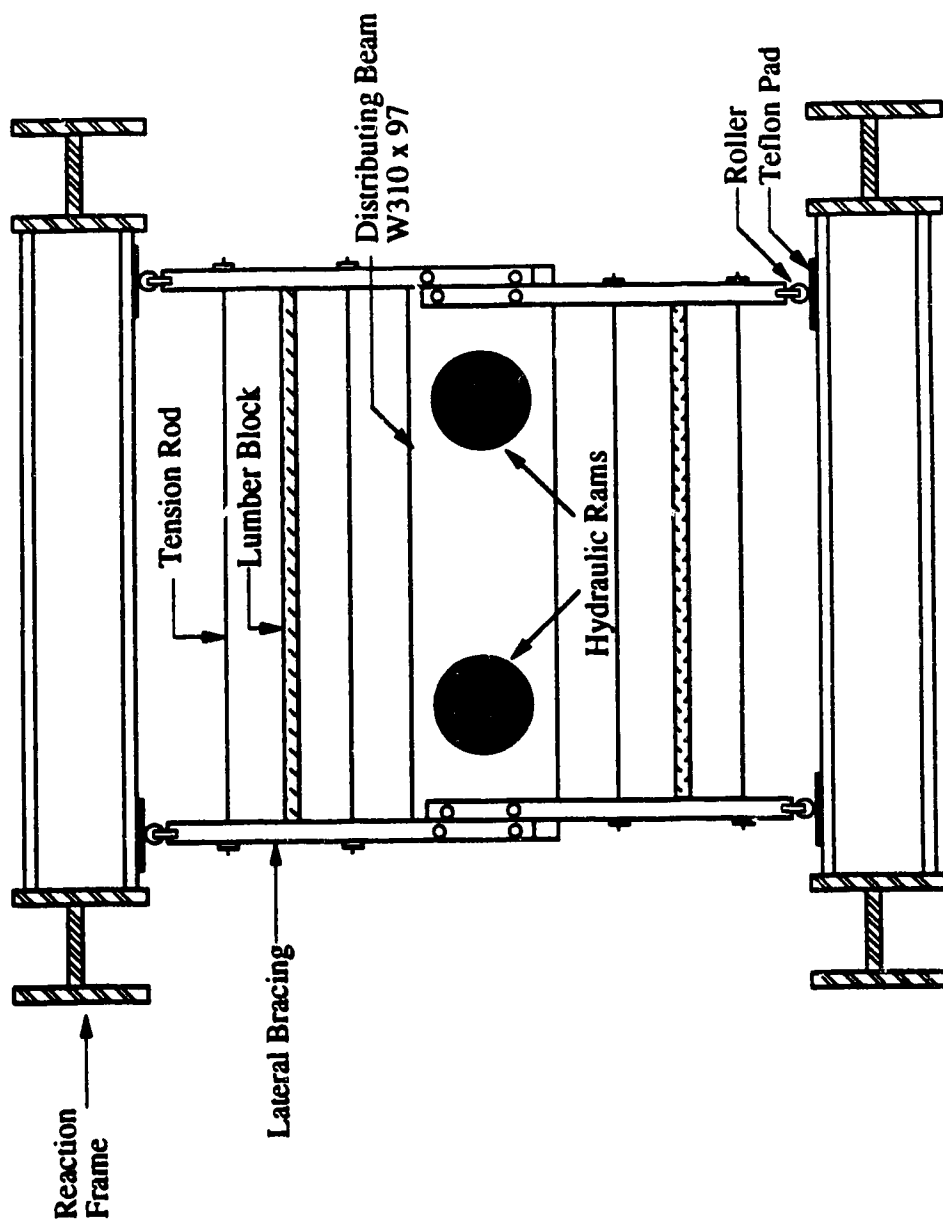


Fig. 2.13 Picture of Loading System



Section A-A of Fig. 2.9

Fig. 2.14 Schematic of Lateral Bracing for the Loading Unit

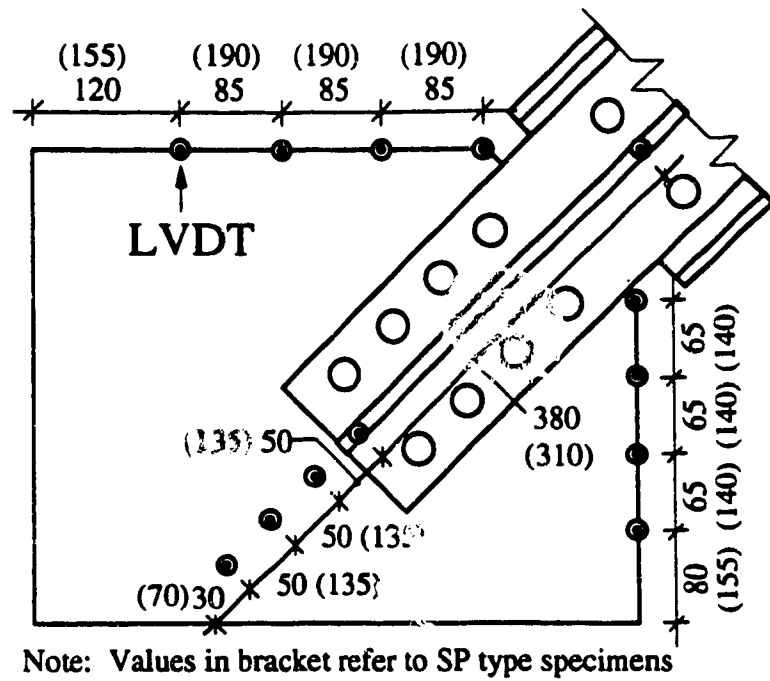


Fig. 2.15 Schematic of LVDT Locations for GP, SP and MP Type Specimens

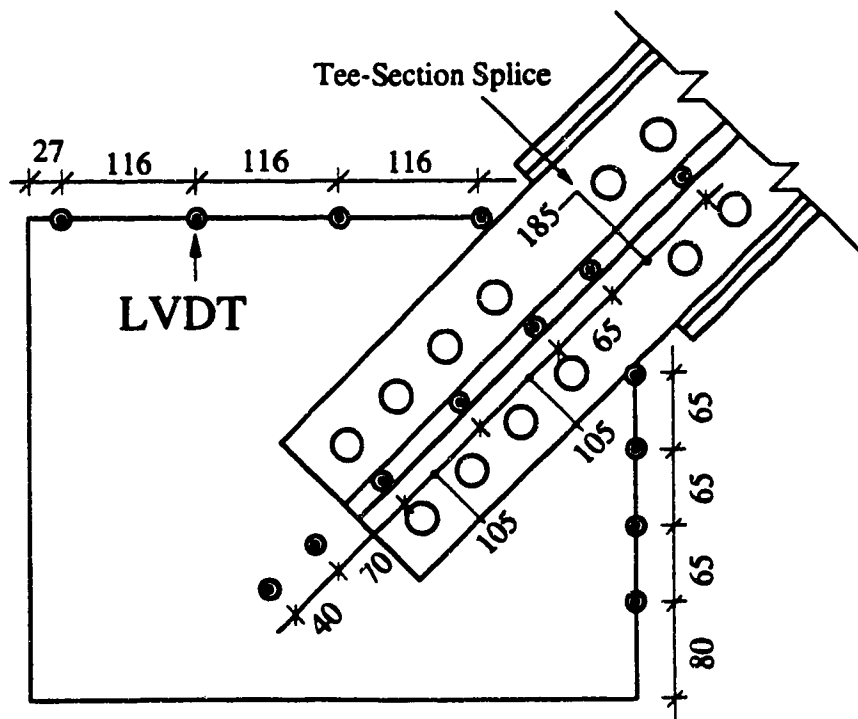


Fig. 2.16 Schematic of LVDT Location for EP Type Specimens

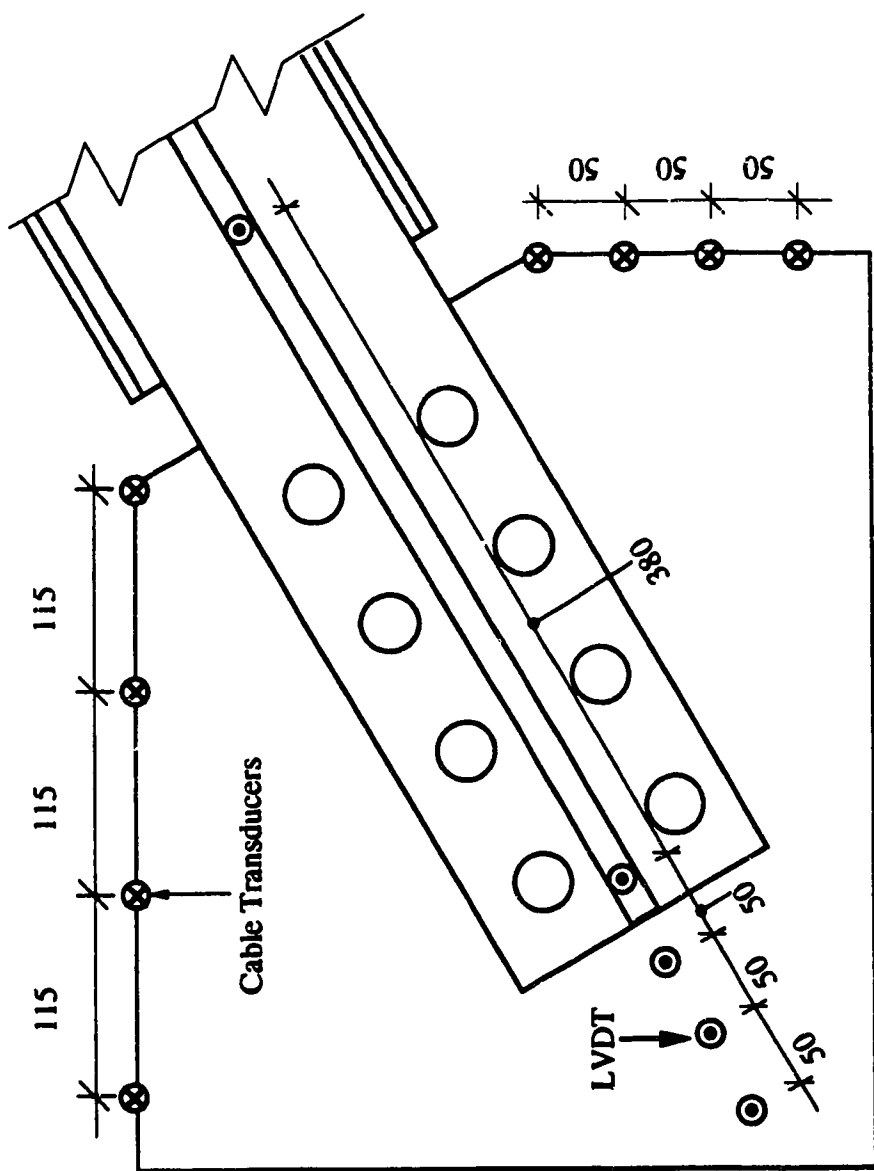


Fig. 2.17 Schematic of Cable Transducers and LVDTs Location for AP Type Specimens



Fig. 2.18b Close-up of LVDTs on Short Free Edge of Specimen

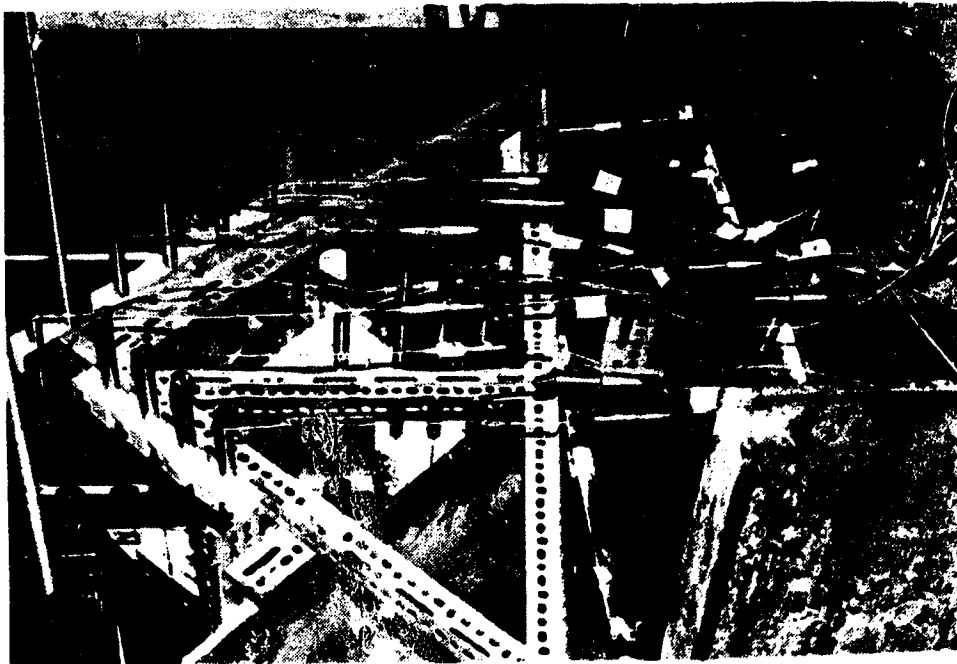


Fig. 2.18a LVDTs Arrangement on Supporting Frame

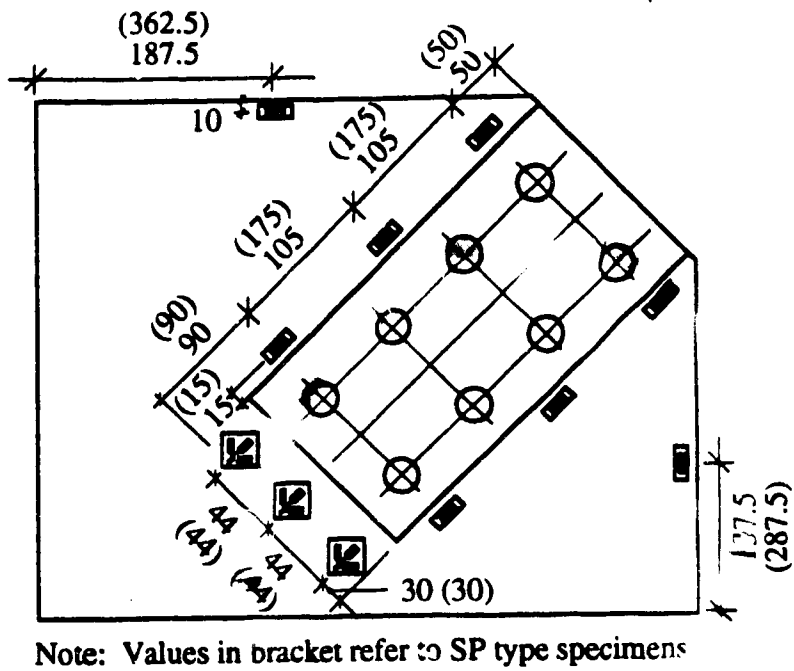


Fig. 2.19 Location of Strain Gauges for GP, SP and FR Types Specimens

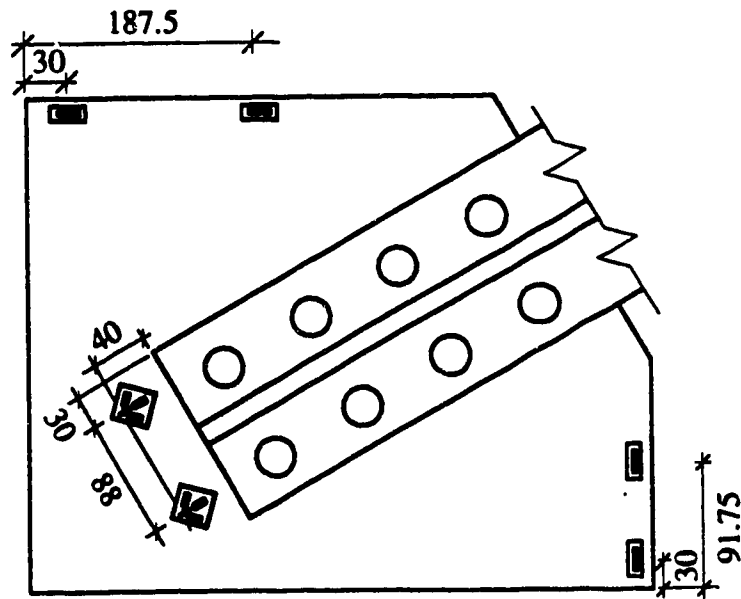


Fig. 2.20 Location of Strain Gauges for AP Type Specimens



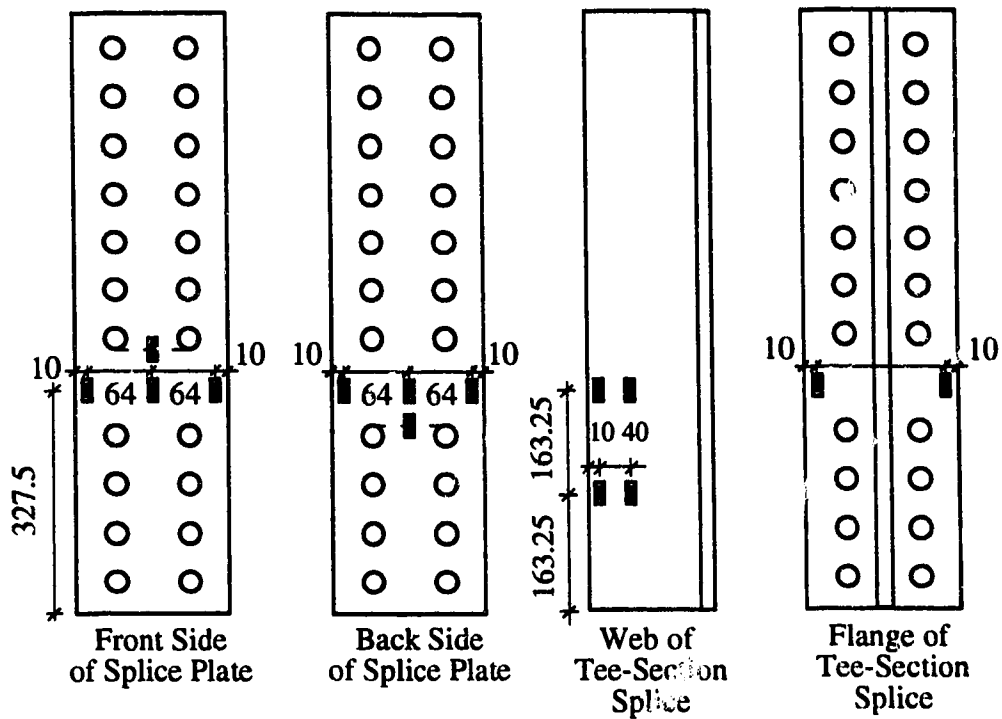


Fig. 2.21 Location of Strain Gauges of Splice Member for EP Type Specimens

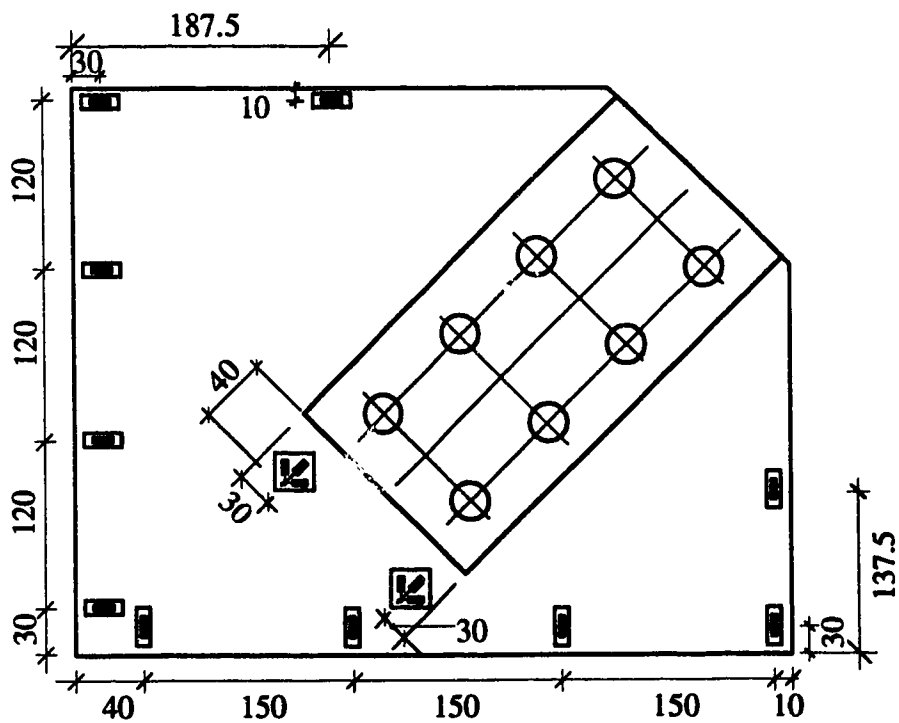


Fig. 2.22 Location of Strain Gauges for MP Type Specimens

### **3. TEST RESULTS OF GP TYPE SPECIMENS**

#### **3.1 General**

The GP type specimens were employed to examine the general behavior of gusset plate connections subject to compression in the inelastic range. Three plate thicknesses were tested and two out-of-plane restraint conditions at the base of the test frame were examined. The test results of the GP type specimens are summarized in Table 3.1. The Whitmore load, based on the material static yield strength, and the Thornton load, based on an effective length factor,  $k=0.65$ , are also included in the table for comparison. It should be noted that when evaluating the unsupported length of the column strip for the Thornton load, the maximum distance measured from the end of the splicing member to the beam and column boundary was used instead of the distance measured from the last row of bolts since it was believed that the splicing member (tee-sections and plates) should provide sufficient support to the column strip. In general, the test results show that the ultimate load of the specimens increased with an increasing plate thickness. However, it can be seen from the table that providing out-of-plane restraint at the base of the test frame did not affect the ultimate loads of the specimens significantly. In addition, both the Whitmore method and the Thornton method provided conservative estimates of the strength of the specimens.

Since the same heats of each steel plate thickness were used for all types of specimens (GP,SP,AP,MP and EP) with the same thickness, the material properties of the specimens will thus only be discussed once in this chapter. The material properties of the tested coupons are presented in Table 3.2 for each specimen plate thickness. The values shown in the table are averages of four coupons with two coupons tested in each orthogonal direction. The coupon test results showed that similar material properties were recorded for coupons in both orthogonal directions. Complete stress-strain curves were also recorded to provide the material models for later numerical analyses. However, it should be noted that

average values were used to produce these curves. A typical stress-strain curve for a plate thickness of 9.8 mm is shown Fig. 3.1.

### **3.2 Without Out-of-Plane Restraint at the Base of Test Frame**

#### **3.2.1 Behavior of Load versus In-Plane Deformation**

All the specimens failed by sway buckling with the stub beam and column test frame deflected out-of-plane. The in-plane behavior of the specimens is best illustrated by examining the curves of the load versus the vertical displacement of the loading head as shown in Figs. 3.2 to 3.4. These curves show that linear behavior existed in the early loading stage for specimens GP1 and GP2 except in the initial stage when settling of the test fixtures took place. However, for specimen GP3 relatively linear behavior was observed from the beginning of loading until the ultimate load of the specimen was reached. This probably indicates that specimen GP3 did not experience a lot of yielding prior to failure occurring. The load levels at which the curves of load versus vertical displacement turned nonlinear for specimens GP1 and GP2 correspond very well to the yield load predicted by the Whitmore method, as shown in Figs. 3.2 and 3.3. Once the nonlinear behavior began, the curves turned gradually until the ultimate load of the specimen was reached. It should also be noted that the vertical displacement of the specimens only increased slightly after bifurcation occurred.

#### **3.2.2 Behavior of Load versus Out-of-Plane Displacement of Test Frame**

The load versus out-of-plane displacement of the test frame curves for the specimens are shown in Figs 3.5 to 3.7. These curves indicate that an initial imperfection existed in the specimens since out-of-plane displacement of the test frame was recorded from the beginning of loading. Figures 3.5 to 3.7 show that nonlinear load displacement behavior was observed for all the specimens prior to when the ultimate load was reached. It can also

be seen from the figures that the lateral displacement of the test frame increased significantly after the ultimate load was reached. The final lateral displacement of the test frame ranges from 6 mm to 12 mm, depending on the specimens. It was also observed that no sudden decrease in the load carrying capacity of the specimens was recorded after reaching the ultimate load.

### **3.2.3 Strain Gauge Results**

The strain readings from the strain gauges mounted at the mid-length of the gusset plate long free edges were plotted against the applied load, as shown in Figs 3.8 to 3.10. These plots show that the longitudinal strains at the mid-length of the long free edge increased linearly with respect to the applied load until strain bifurcation occurred at the ultimate load, except with specimen GP1, which showed a slight strain reversal at about 75 percent of the ultimate load. In addition, that the strain readings from both sides of the gusset plate were only slightly different indicated that only a small amount of out-of-plane bending of the plate at the long free edge had occurred prior to when the ultimate load of the specimens was reached. The curves of load versus longitudinal strains at mid-length of the short free edges of the specimens are shown in Figs. 3.11 to 3.13. It can be seen from the figures for specimens GP1 and GP2 that linear behavior was observed until a load level (below the ultimate load) at which strain reversal of the specimens at the short free edge occurred. For specimen GP2, the strain reversal process continued until strain bifurcation occurred. An increase in longitudinal compressive strain was observed, however, at the short free edge for specimen GP1 prior to strain bifurcation. The strain reversal process occurring at the free edges in these specimens may be attributed to the in-plane bending of the free edges caused by the extensive yielding of the gusset plate area underneath the splice member. Although linear load versus strain behavior was noticed for specimen GP3, the different strain readings that were recorded from both sides of the specimen from the beginning of loading indicated that bending at the short side free edge of the plate had occurred. It

should be noted that all the longitudinal strain readings recorded from the free edges were within the elastic range prior to buckling. The rosette readings recorded from the plate area underneath the splice member were also examined. It was found that the rosette strain readings corresponded very well to the prediction by the Whitmore method. The direction of principal strains occurred at an angle of approximately  $40^\circ$  from the horizontal. Since the brace angle for these specimens was  $45^\circ$ , it can be seen that the direction of the principal strains at the rosettes almost aligned with the loading angle.

#### **3.2.4 Yielding Behavior of Specimens**

During the tests, extensive yielding was observed for specimens GP1 and GP2. However, specimen GP3 only showed moderate yielding at the gusset plate area underneath the splice member. To illustrate the load transfer mechanism from the splice member to the beam and column support boundary through the gusset plate specimen, the yielding pattern and process of the specimens were recorded during tests. A schematic of the yielding pattern at various load levels for specimen GP1 is shown in Fig. 3.14 and a photograph of the failed specimen are shown in Fig. 3.15. A yielding process similar to that of GP1 was observed for specimen GP2. As can be seen in Fig. 3.14, yield lines were first noticed at the gusset plate area underneath the splice member. These yield lines were oriented at an angle of approximately  $45^\circ$  to the horizontal. Subsequently, the yielding at this region progressed towards the beam and column boundary and the yield lines developed were parallel to the boundary (Fig. 3.14b). As loading continued, horizontal yield lines were also observed in the area about the two sides of the splice member (Fig. 3.14d). Finally, as the applied load approached the ultimate load yield lines were developed at the free edges and extensive yielding was observed for the entire gusset plate area. The yield lines observed at the free edges were probably caused by plate out-of-plane bending when buckling occurred. It should also be noted that the final yielding pattern of the specimens indicated that a mechanism was formed for specimens GP1 and GP2. Plastic hinges were observed at the

mid-length of the free edges and underneath the splice member extending to the beam and column boundary as shown in Fig. 3.15.

Based on the above yielding pattern, it can be seen that the loading mechanism of these specimens can be described as follows. As predicted by the Whitmore method, the gusset plate area underneath the line that passes through the last row of bolts was stressed significantly. Hence, at a load level close to the yield load, as estimated by the Whitmore method, yield lines parallel to the beam and column boundary were observed in the area underneath the splice member. As the applied load increased, the yielding in this area progressed. When extensive yielding in this area had developed, the load was redistributed to the gusset plate area on the two sides of the splice member. Hence, compressive yield lines were also formed in this area as the load increased. The yielding extended towards the remaining part of the gusset plate when the applied load increased. The in-plane stiffness of the gusset plate deteriorated as yielding continued. Plastic bifurcation buckling of the gusset plate occurred when the in-plane stiffness decreased to a certain level.

### **3.2.5 Out-of-Plane Deflected Shapes of Free Edges and Along Centerline of Splicing Member**

The out-of-plane deflected shapes of the free edges of the specimens and along the centerline of the splice member to the beam and column boundary are shown in Fig. 3.16, and a photograph of the deflected shape along the long free edge for specimen GP1 is shown in Fig. 3.17. These deflected shapes were normalized by the maximum displacement occurring in each specimen. In general, the deflected shapes resembled the buckled shape of a fixed-guided column. However, for specimen GP3 local deformation of the gusset plate was observed underneath the splice member, as shown in Fig. 3.16. The figure also shows that a small movement of the splice member at the tension rod restraint location was recorded. When the gusset plate deformed out-of-plane, the splice

member would transfer a shear force induced by the secondary moment to the bracing member. Since the brace member was restrained by the tension rods which were attached to the supports mounted on the flanges of the brace member, the shear force caused local bending of the web of the brace member about the tension rod supports. This slight bending of the web was also observed in the tests. A slight twisting of the splice member was also recorded when buckling occurred due to the unsymmetrical plate geometry.

### **3.3 With Out-of-Plane Restraint at the Base of Test Frame**

#### **3.3.1 Behavior of Load versus In-Plane Deformation**

The general failure mode of the specimens was plate local buckling. Depending on the specimens, plate local buckling could occur at the specimens' free edges and the plate area underneath the splice member. Figures 3.18 to 3.20 illustrate the load versus vertical in-plane displacement of the loading head. Similar in-plane stiffnesses as without out-of-plane restraint (Figs. 3.2-3.4) were observed. Again, nonlinear behavior was observed for all the specimens at the beginning of loading due to the settling of the test fixtures. Subsequently, linear behavior was observed until the specimens reached the yield load estimated by the Whitmore effective width method as shown in the figures. From then on, the curves gradually turned to the ultimate load, followed by moderate unloading. It should be noted that strain gauges were not used in these specimens since it was believed that the strain gauge results from the tests of the specimens without restraint would provide sufficient information on the stress and strain distribution for gusset plates subject to compression.

#### **3.3.2 Behavior of Load versus Out-of-Plane Displacement at Mid-Length of Long Free Edge**

The load versus out-of-plane displacement at the mid-length of the long free edges is shown in Figs. 3.21 to 3.23. It can be seen from the figures that relatively small lateral

deflection at mid-length of the long free edge was recorded until the applied load approached the ultimate load. It was also observed that the load carrying capacity of the specimens did not decrease significantly after reaching the ultimate load. The final lateral displacement of the specimens ranged from 9 mm to 20 mm.

### **3.3.3 Yielding Behavior of Specimens**

During the tests, extensive yielding was observed for specimens GP1R and GP2R. For specimen GP3R, however, very slight yield lines were recorded when the plate had almost reached the buckling load. This yielding progressed moderately at the plate area underneath the splice member as load increased to the ultimate. In general, the yielding process for specimens GP1R and GP2R tested with restraint at the base of the test frame was similar to that of specimens tested without restraint. Initial yielding was observed at the plate area underneath the splice member at a load level close to the yield load predicted by the Whitmore method. Again, yielding continued to progress in this area as the load increased. When the applied load increased to a certain level, yield lines were observed in the area about both sides of the splice member. Finally, yield lines were also developed at the free edges when buckling occurred.

### **3.3.4 Out-of-Plane Deflected Shapes of Free Edges and along Centerline of Splicing Member**

The out-of-plane deflected shapes of the free edges and along the centerline of the splice member for all the specimens are shown in Fig. 3.24. Again, these deflected shapes were normalized by the maximum displacement occurring in each specimen. It can be seen from these figures that considerable movement was recorded at the tension rod restraint location due to local bending of the web of the bracing member about the tension rod support. In general, however, the deflected shapes of the free edges resembled the buckled shapes of a



column fixed at one end and supported by a lateral spring at the other end. The maximum displacement of the specimens occurred at about the mid-length of the long free edge. The displacement along the centerline of the splice member was small relative to that of the long free edge, but varied depending on the specimen.

Table 3.1 Test Results of GP Type Specimens

Specimen Designation	Plate Size (mm x mm x mm)	Ultimate Load (kN)	Whitmore Load $P_w$ (kN)	Thornton Load $P_t$ $k = 0.65$ (kN)
GP1	500 x 400 x 13.3	1956	1216	1142
GP2	500 x 400 x 9.8	1356	930	828
GP3	500 x 400 x 6.5	742	555	439
GP1R	500 x 400 x 13.3	2057	1216	1142
GP2R	500 x 400 x 9.8	1487	930	828
GP3R	500 x 400 x 6.5	790	555	439

Table 3.2 Material Properties

Material	Static Yield Strength (MPa)	Ultimate Strength (MPa)	Modulus of Elasticity (MPa)
13.3 mm Gusset Plate	295	501	207 600
9.8 mm Gusset Plate	305	465	210 200
6.5 mm Gusset Plate	275	467	196 000
13.0 mm Splice Plate	285	510	199 960
9.5 mm Splice Plate	435	540	201 500
13.0 mm Flange of Tee-Section Splice Member	284	503	197 800

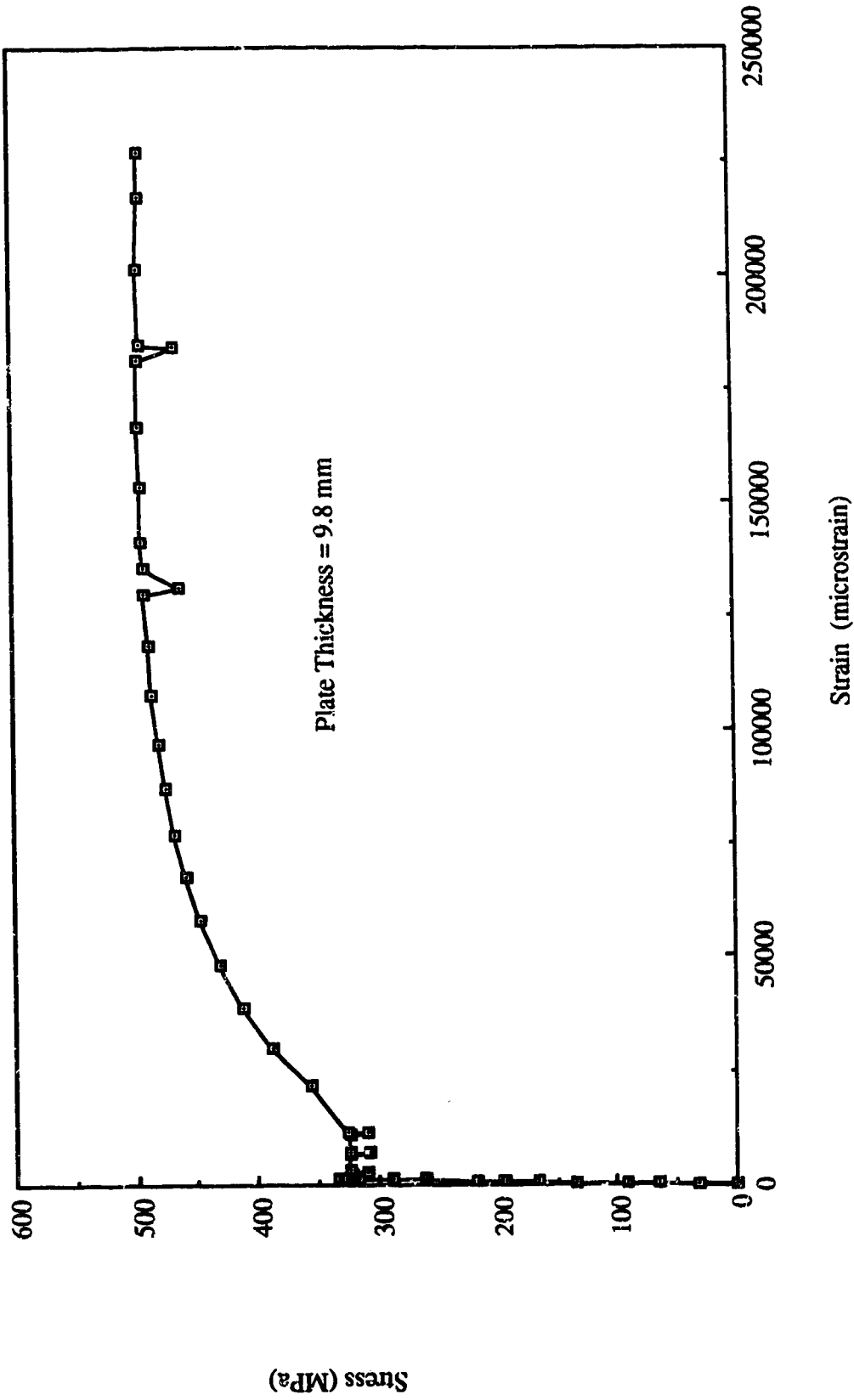


Fig. 3.1 Stress Strain Curve for 9.8 mm Thick Specimen

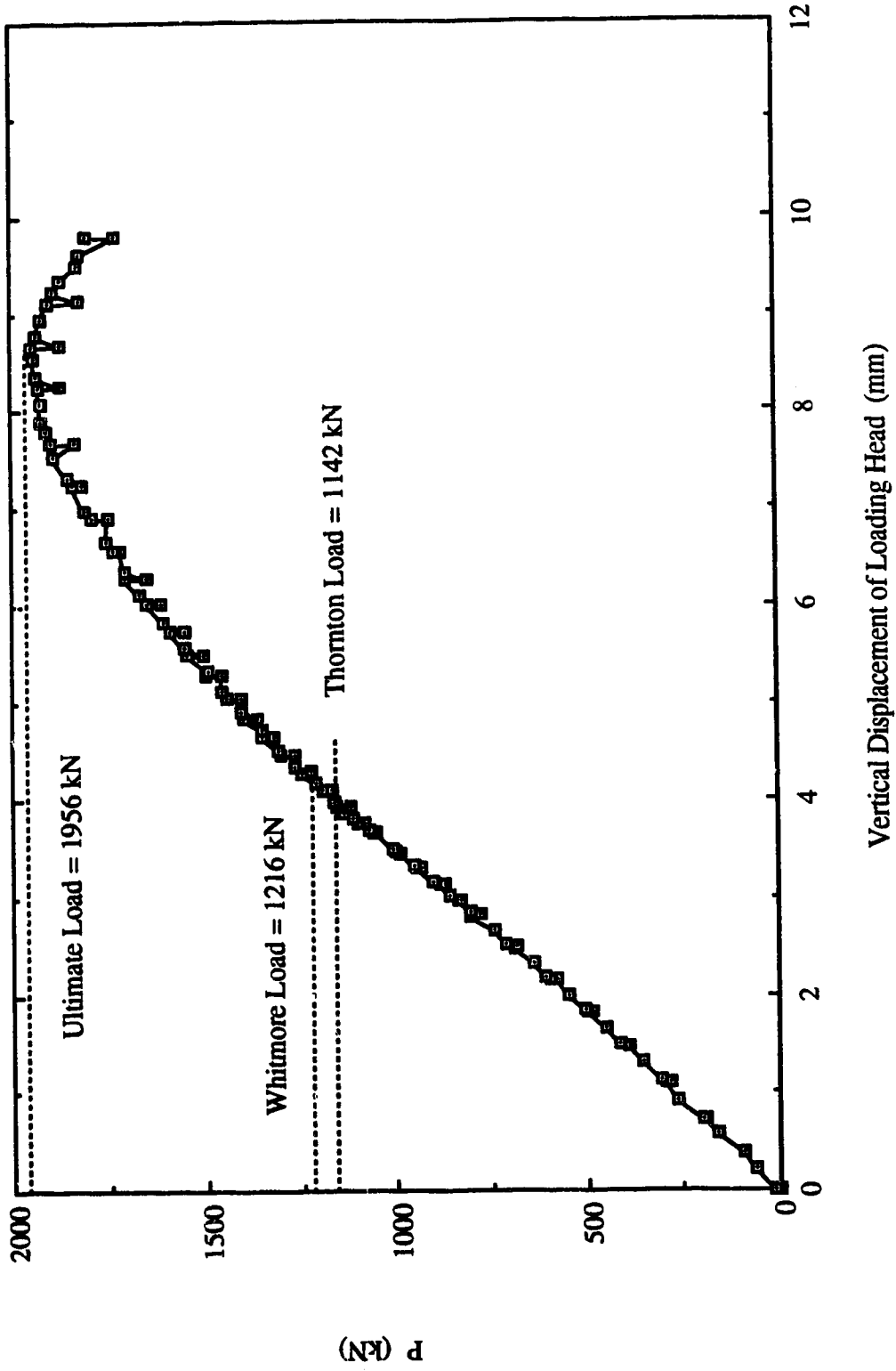


Fig. 3.2 Load vs. Vertical Displacement of Loading Head for Specimen GP1

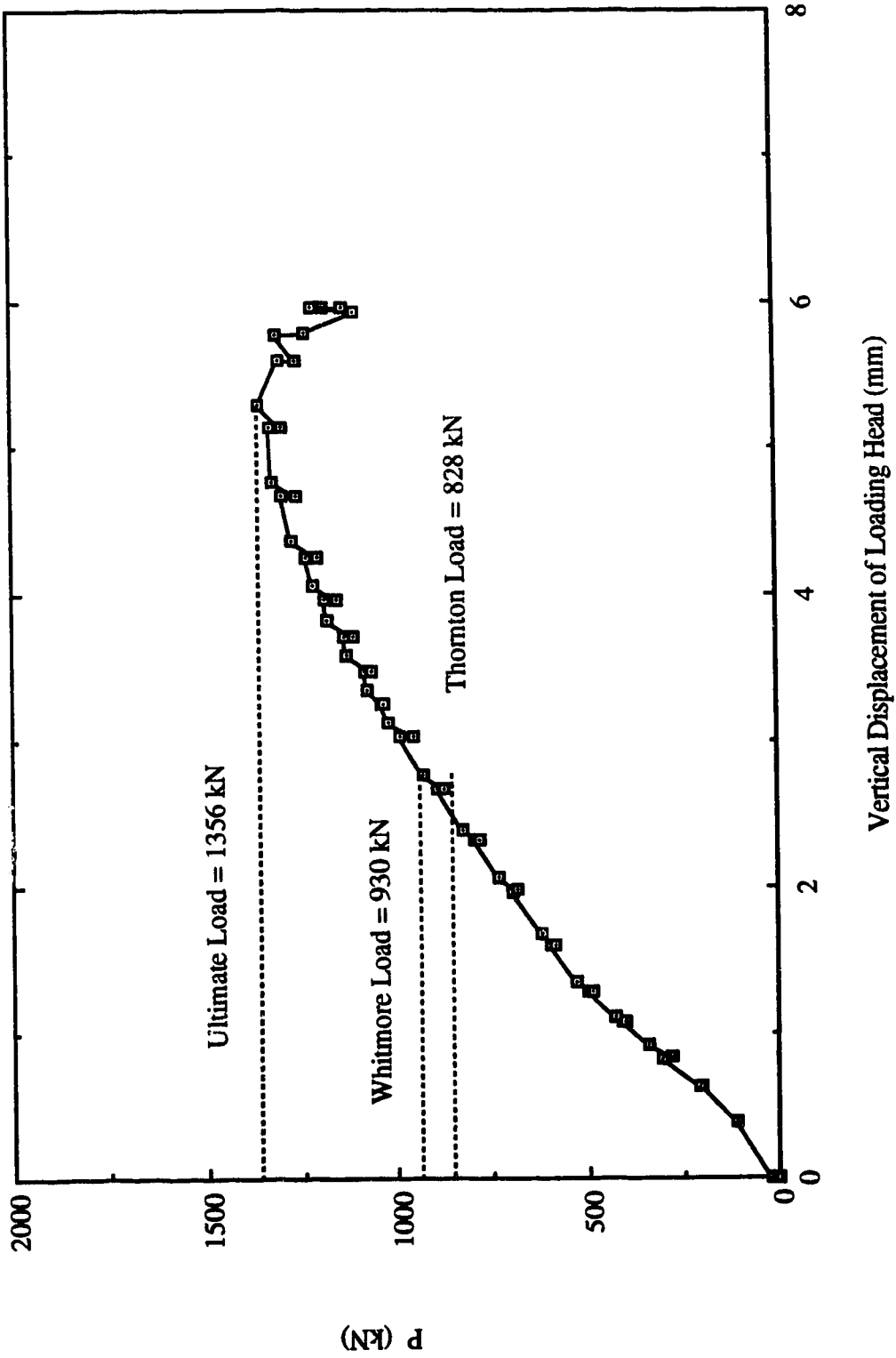


Fig. 3.3 Load vs. Vertical Displacement of Loading Head for Specimen GP2

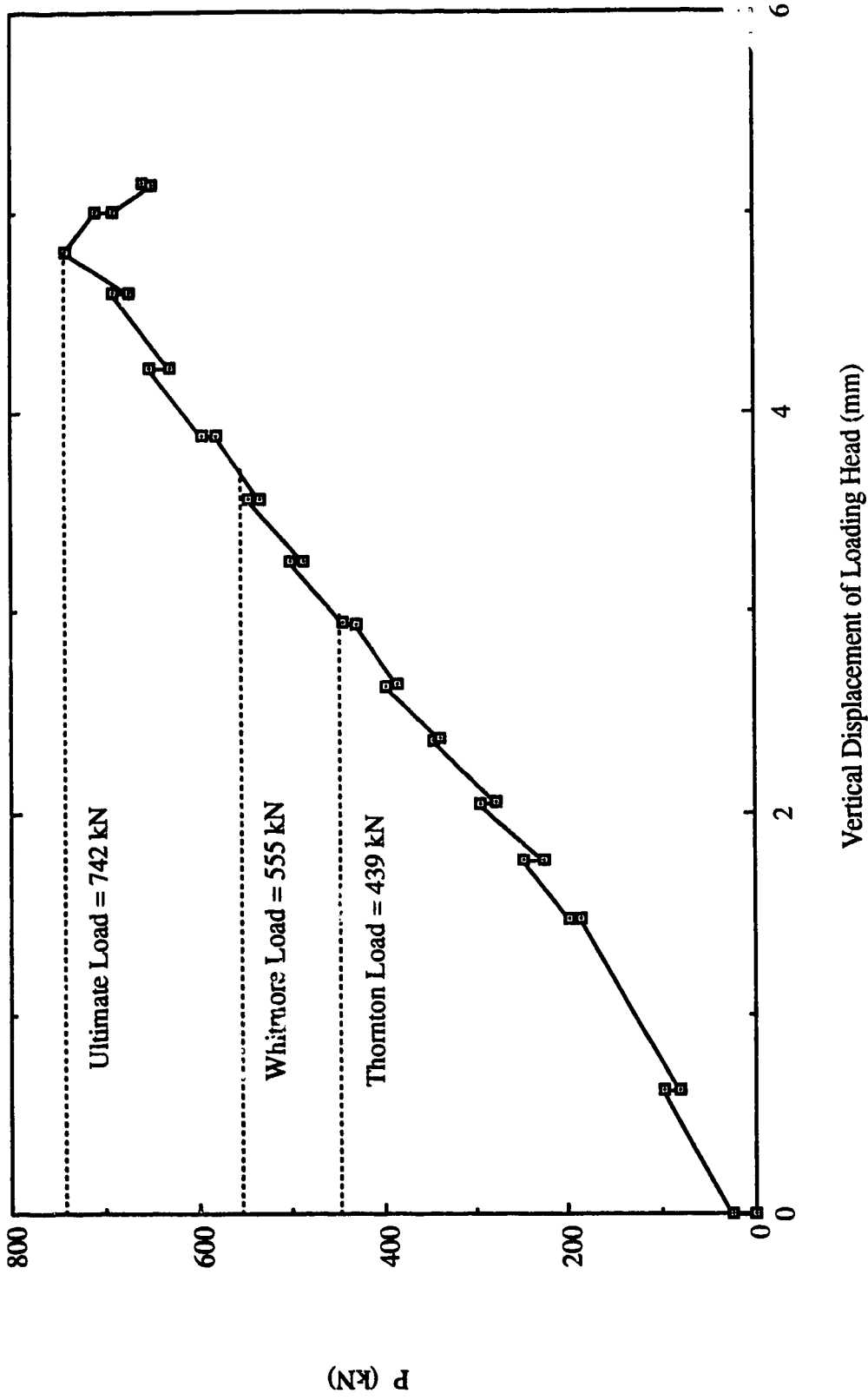


Fig. 3.4 Load vs. Vertical Displacement of Loading Head for Specimen GP3

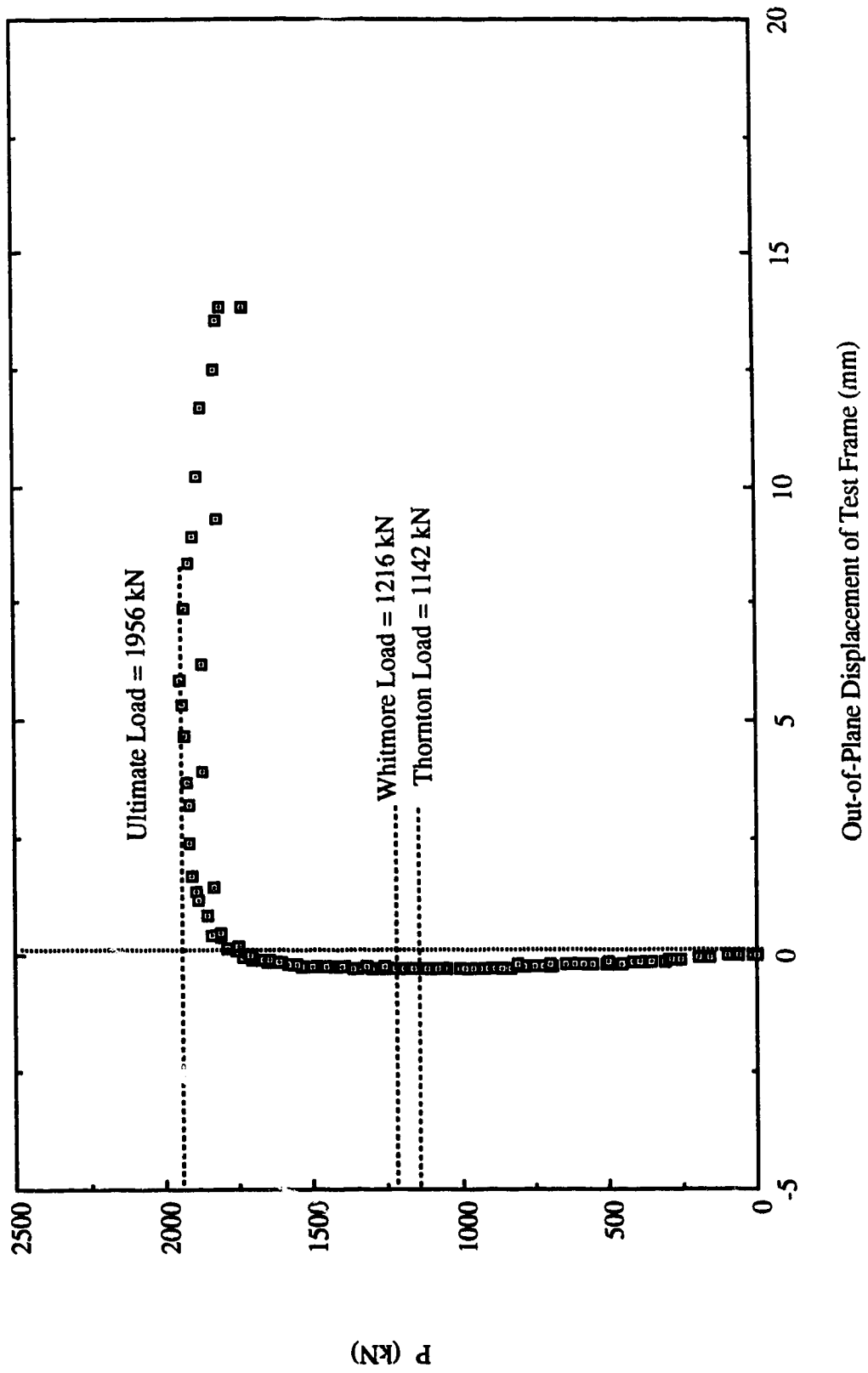
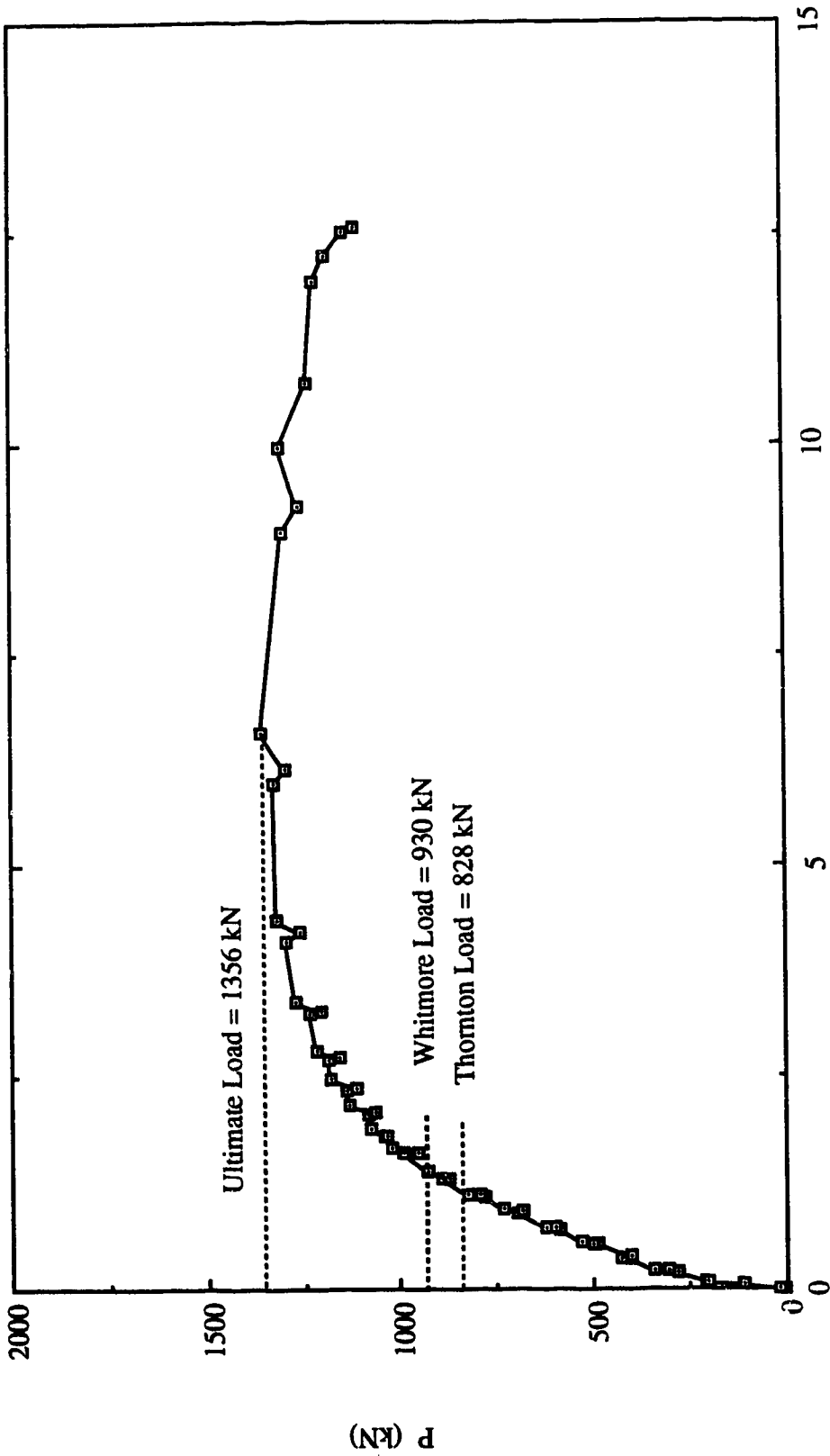


Fig. 3.5 Load vs. Out-of-Plane Displacement of Test Frame for Specimen GP1



Out-of-Plane Displacement of Test Frame (mm)

Fig. 3.6 Load vs. Out-of-Plane Displacement of Test Frame for Specimen GP2



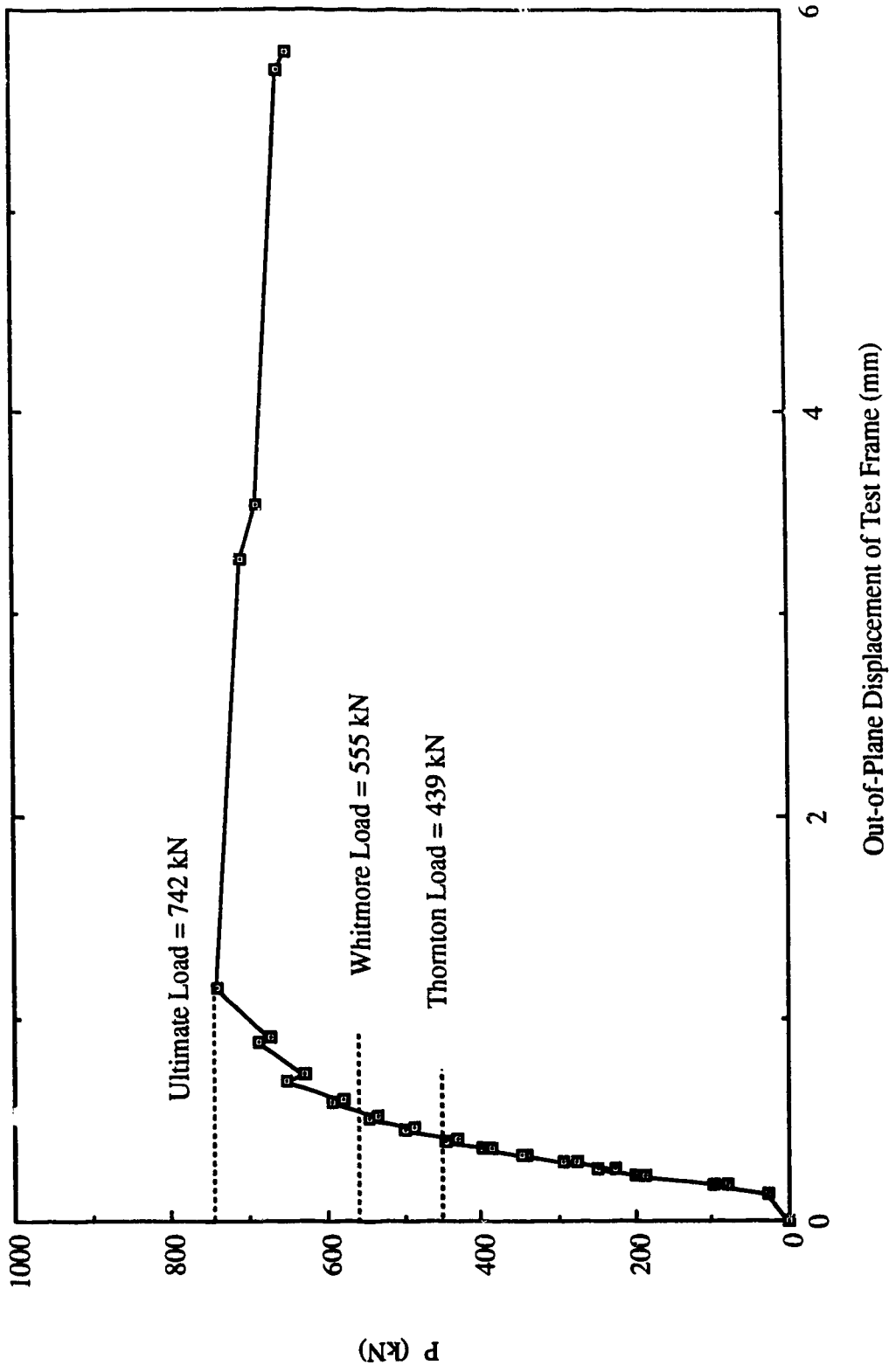


Fig. 3.7 Load vs. Out-of-Plane Displacement of Test Frame for Specimen GP3

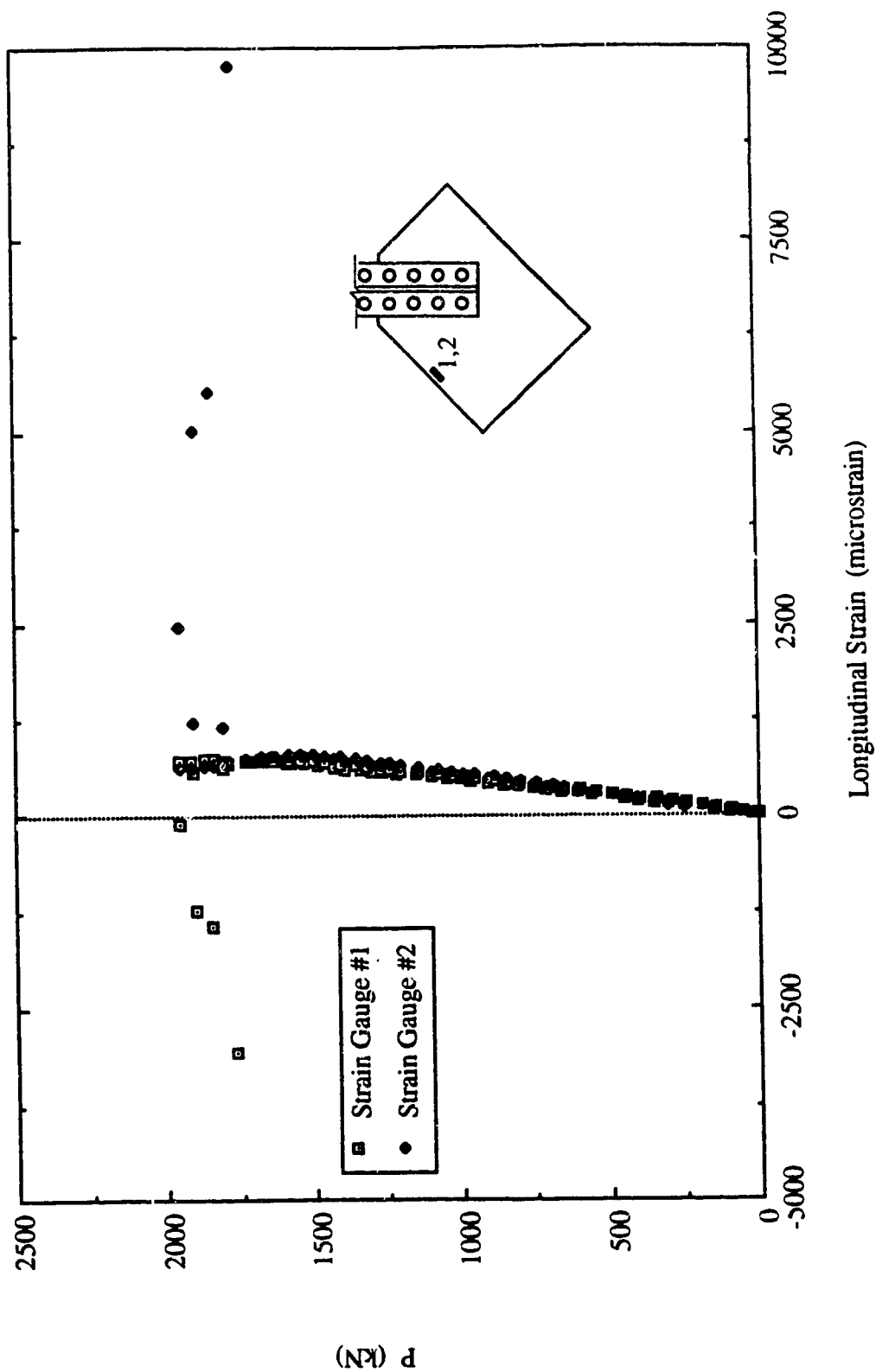


Fig. 3.8 Load vs. Strain Gauge Readings at Mid-Length of Long Free Edge for Specimen GPI

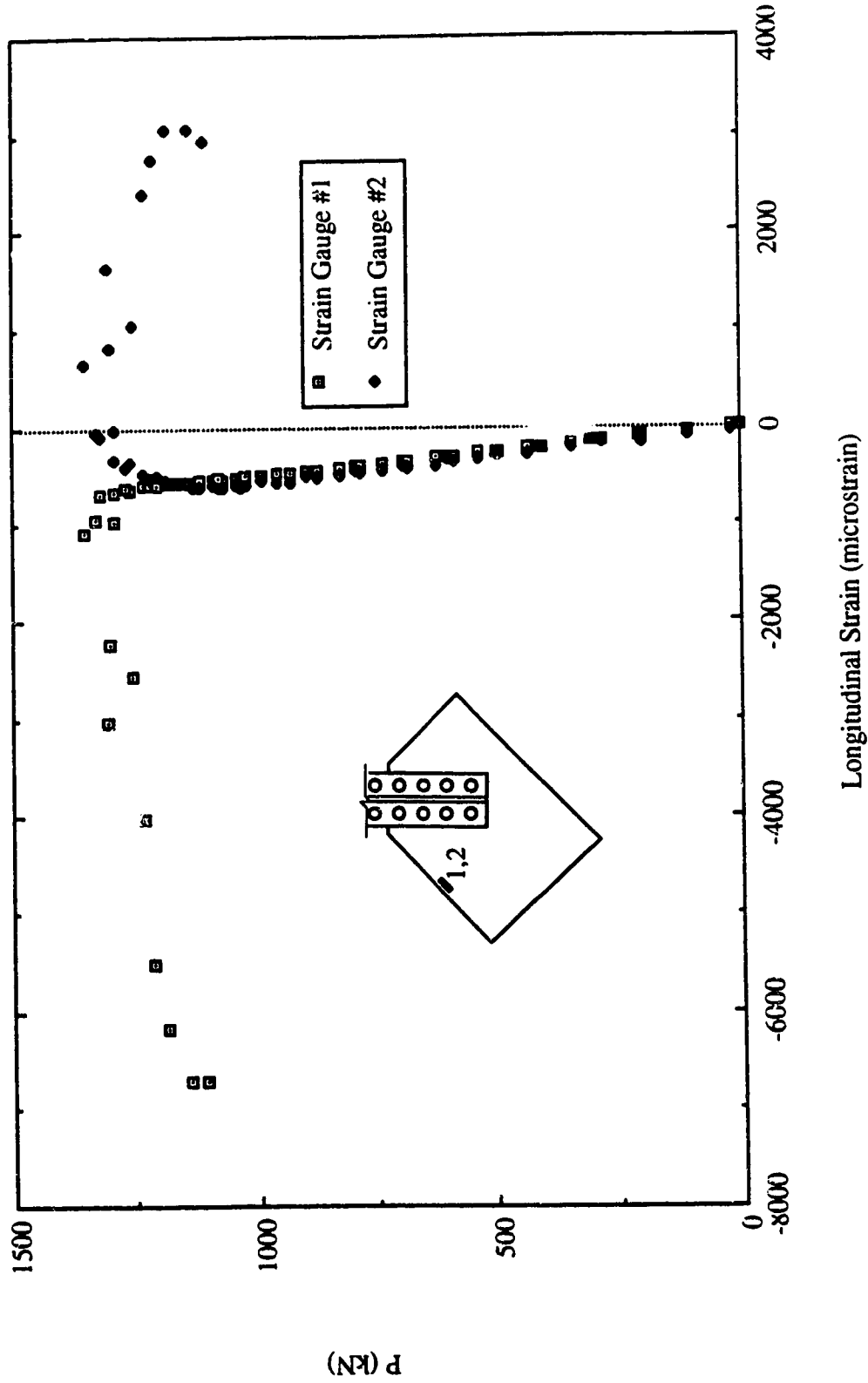


Fig. 3.9 Load vs. Strain Gauge Readings at Mid-Length of Long Free Edge for Specimen GP2

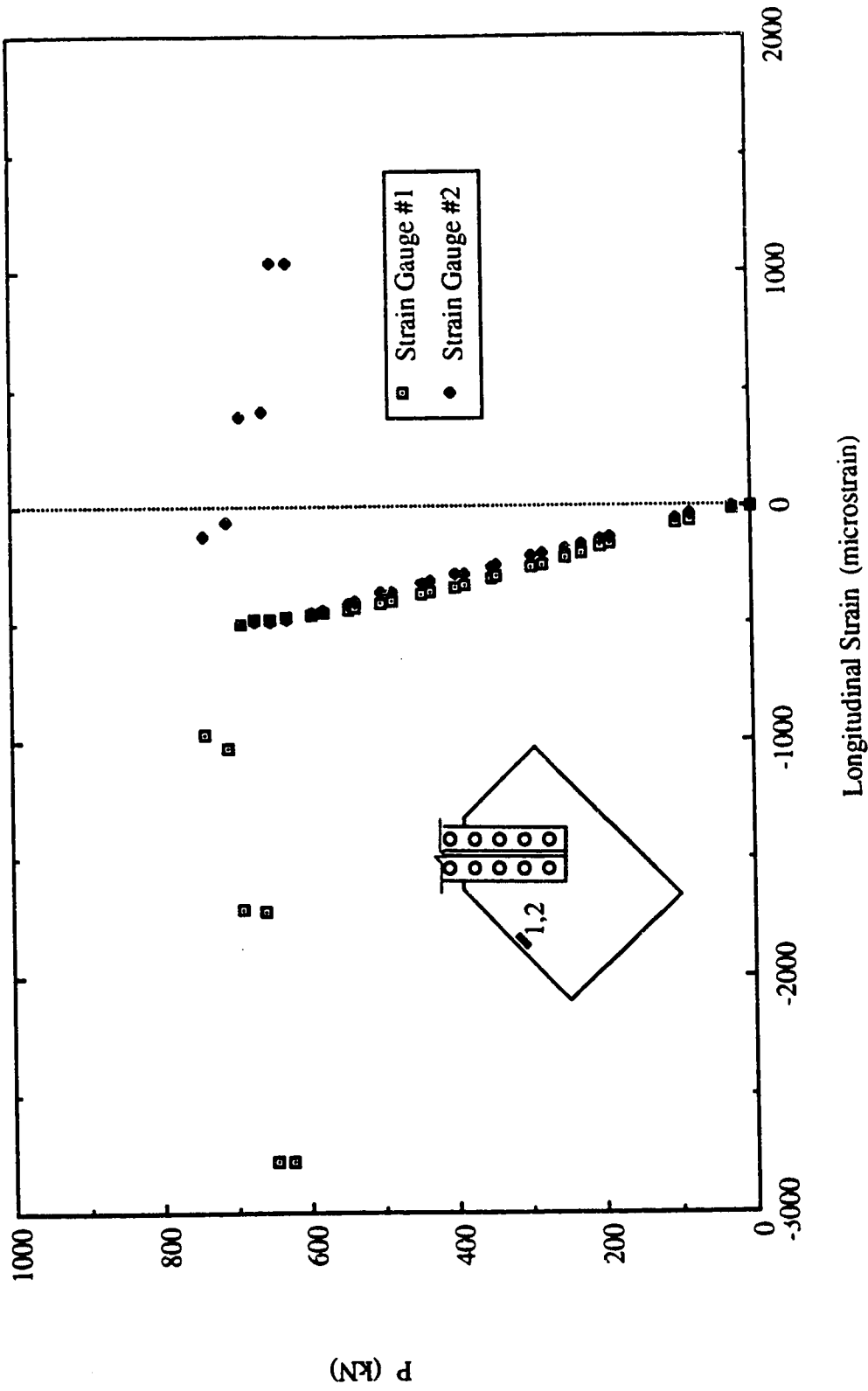


Fig. 3.10 Load vs. Strain Gauge Readings at Mid-Length of Long Free Edge for Specimen GP3

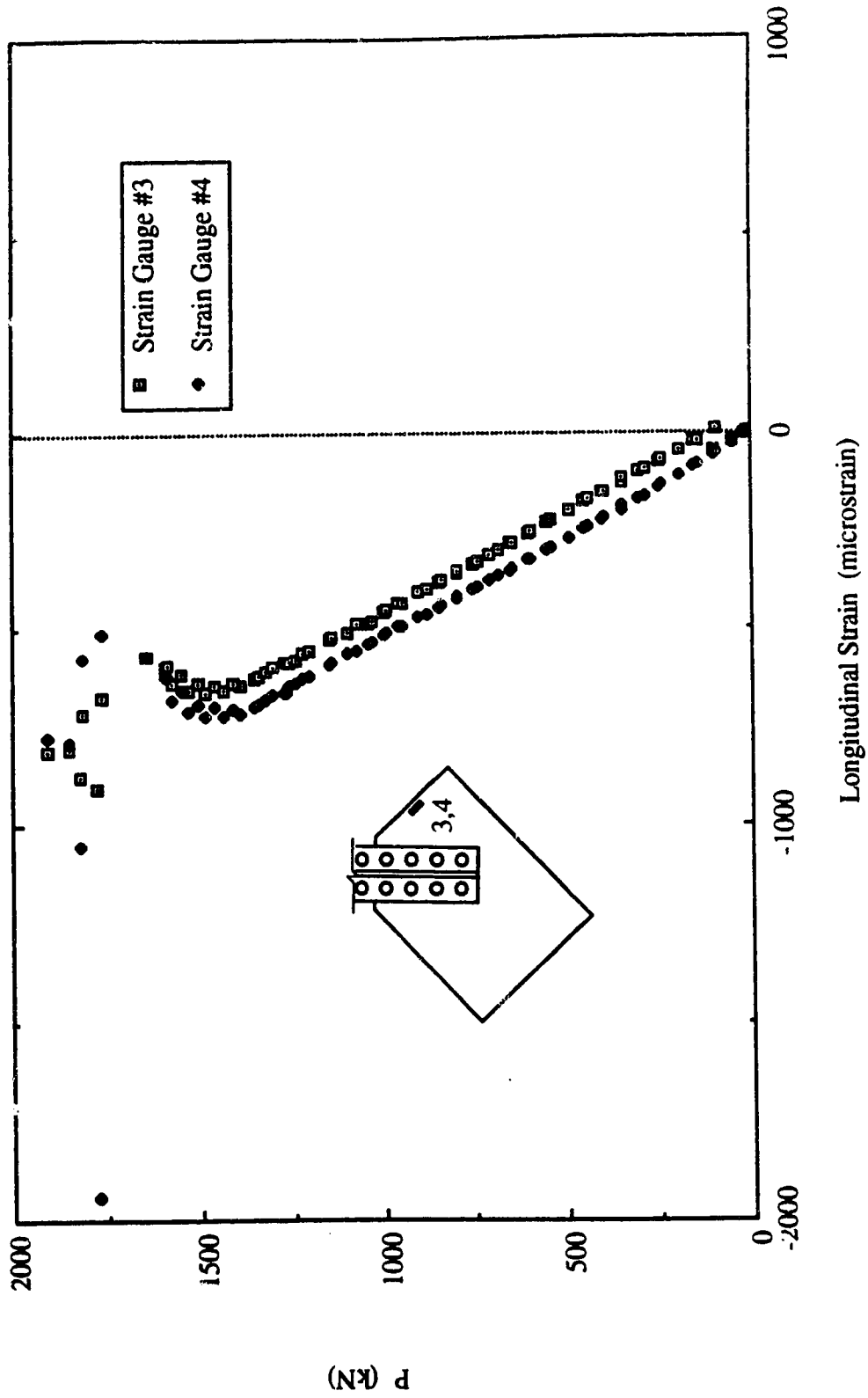


Fig. 3.11 Load vs. Strain Gauge Readings at Mid-Length of Short Free Edge for Specimen GPI

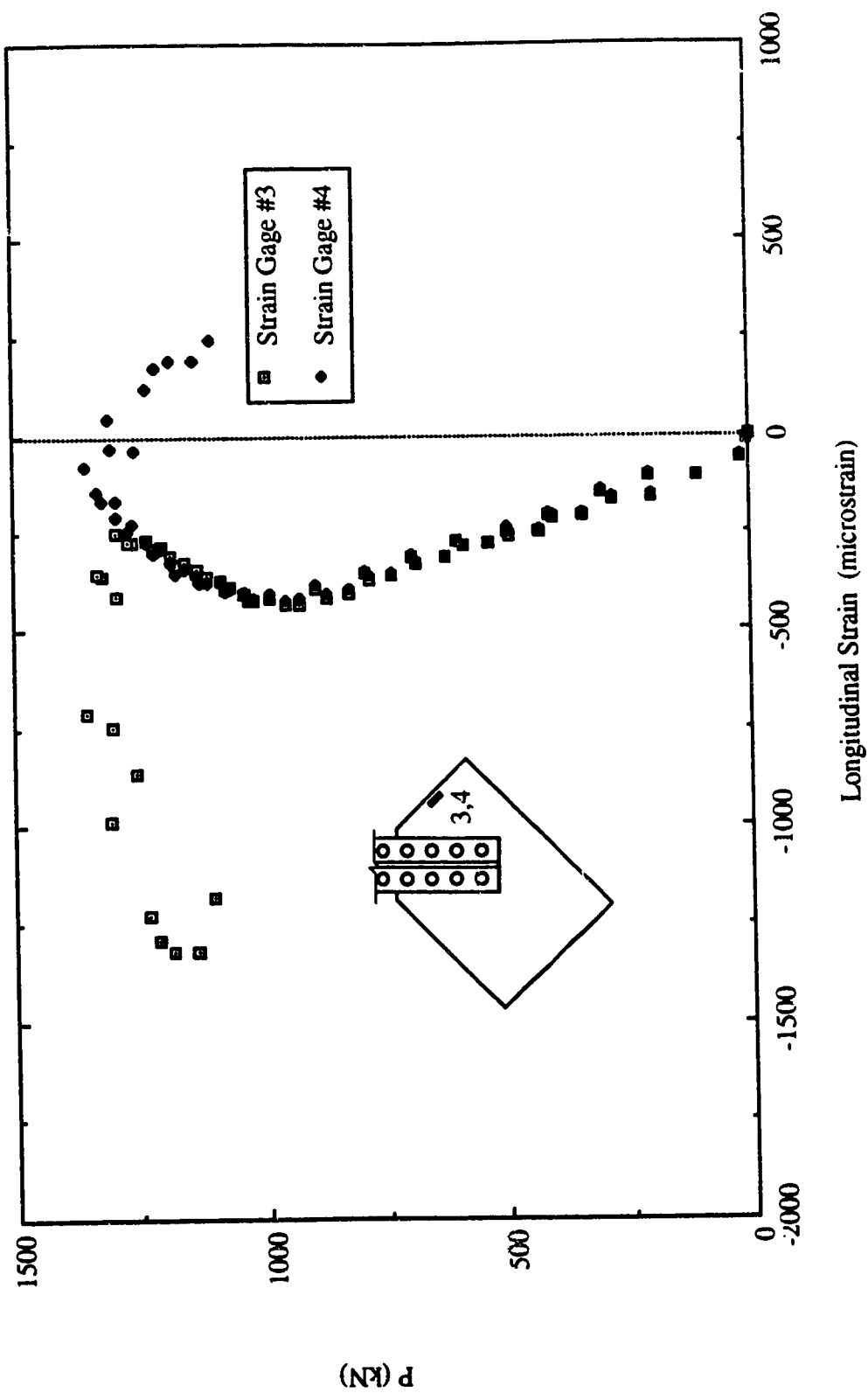


Fig. 3.12 Load vs. Strain Gauge Readings at Mid-Length of Short Free Edge for Specimen GP2

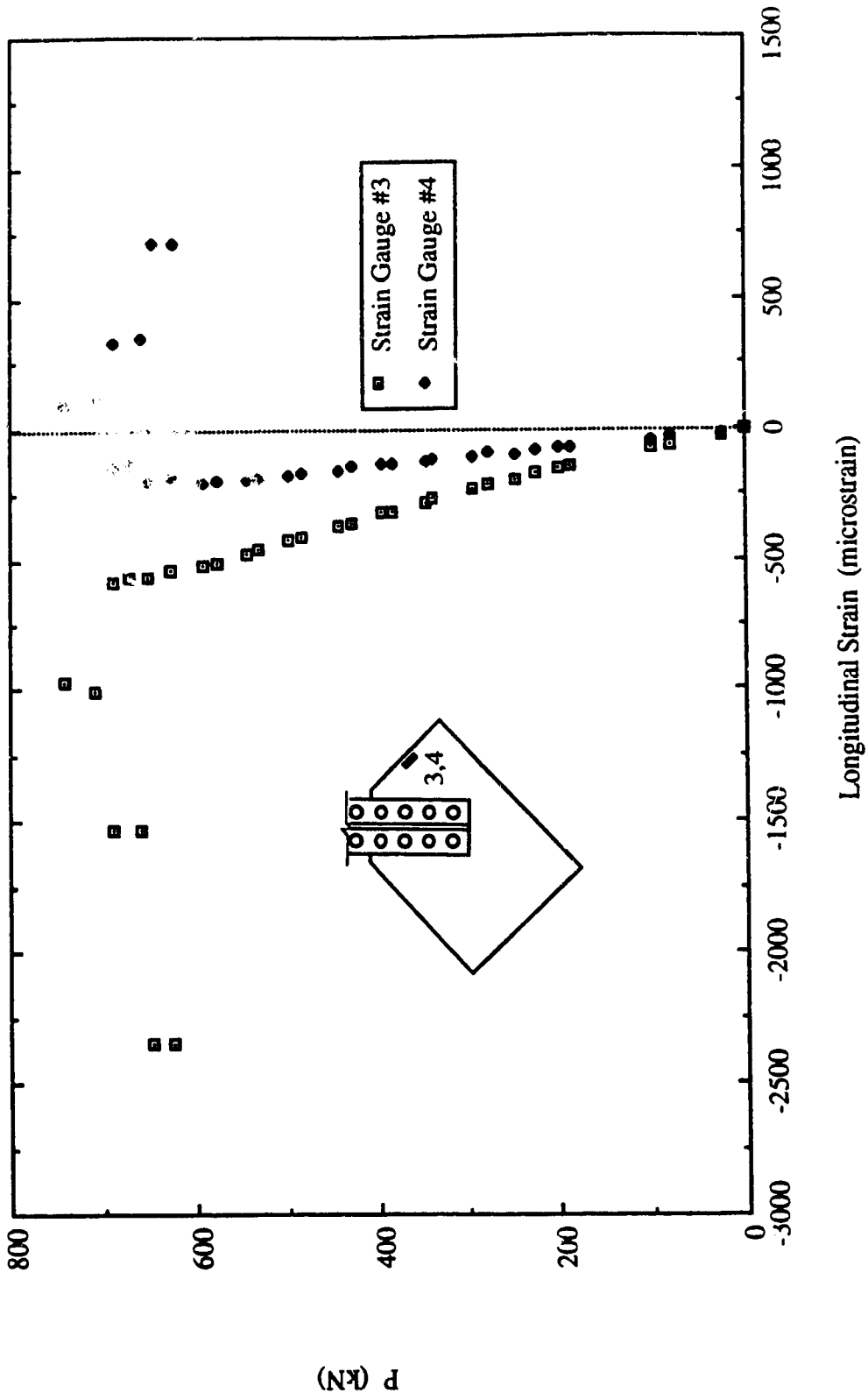


Fig. 3.13 Load vs. Strain Gauge Readings at Mid-Length of Short Free Edge for Specimen GP3

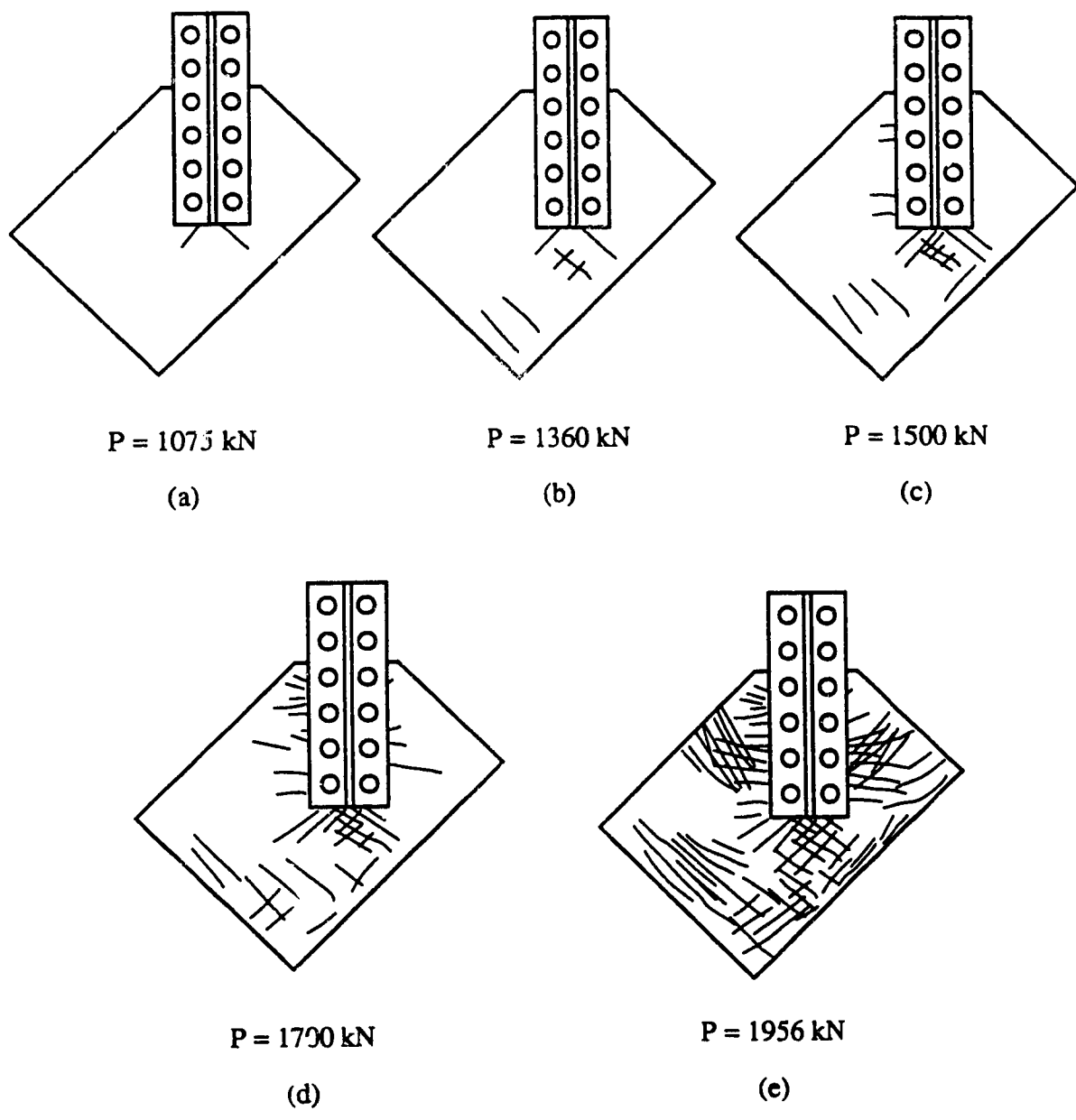


Fig. 3.14 Schematic of Yielding Process for Specimen GP1





**Fig. 3.15** Picture of Failed Specimen GP1

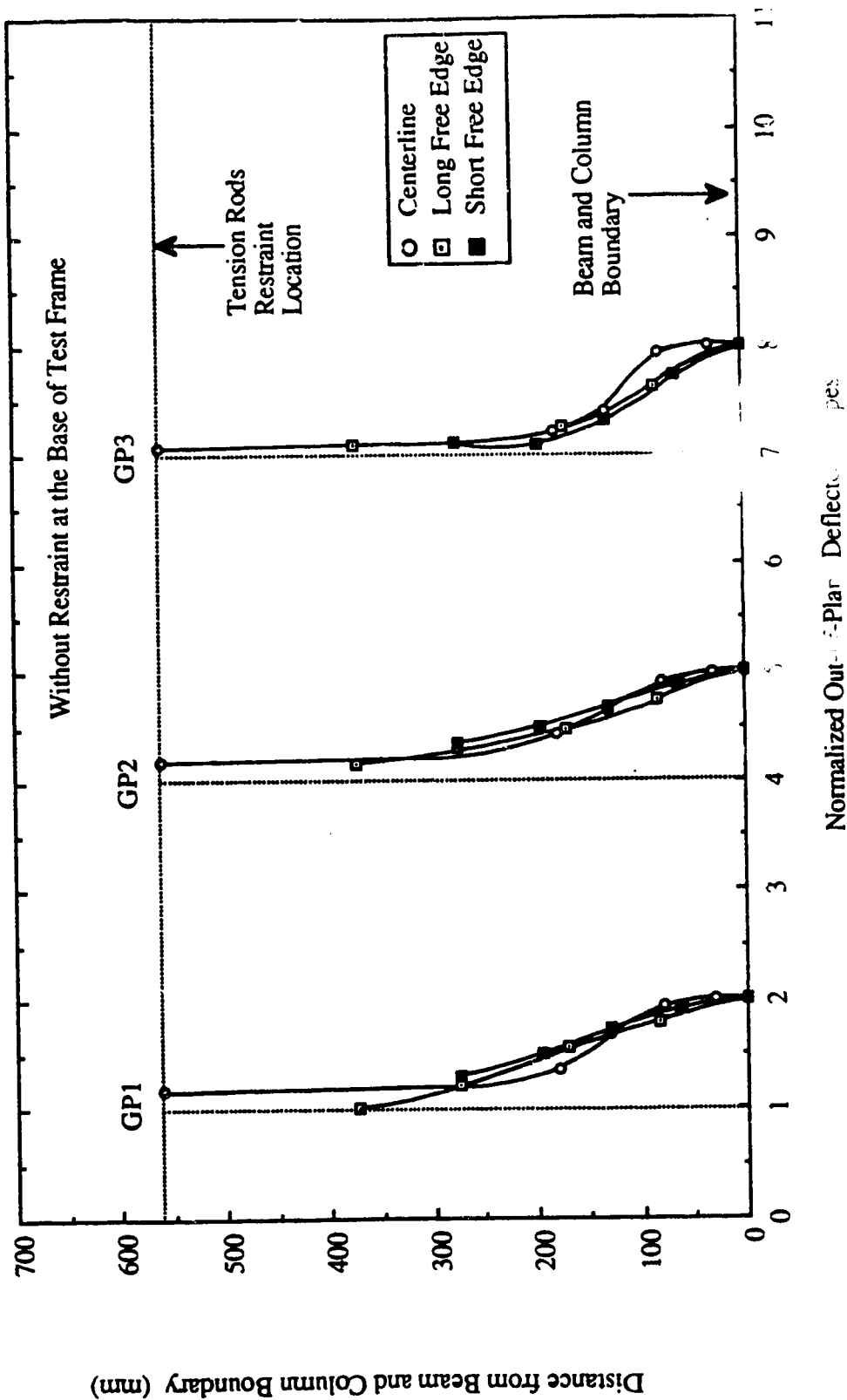
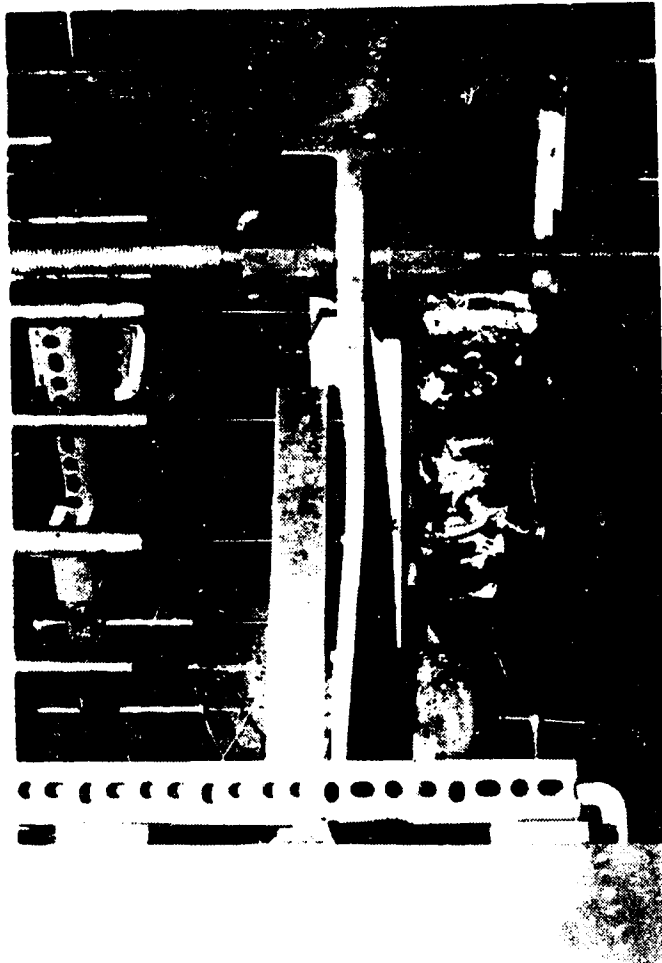


Fig. 3.16 Out-of-Plane Deflected Shape at Free Edges and Along Centerline of Splice for GP Type Specimens



**Fig. 3.17** Picture of Out-of-Plane Deflected Shapes at Long Free Edge for Specimen GP1

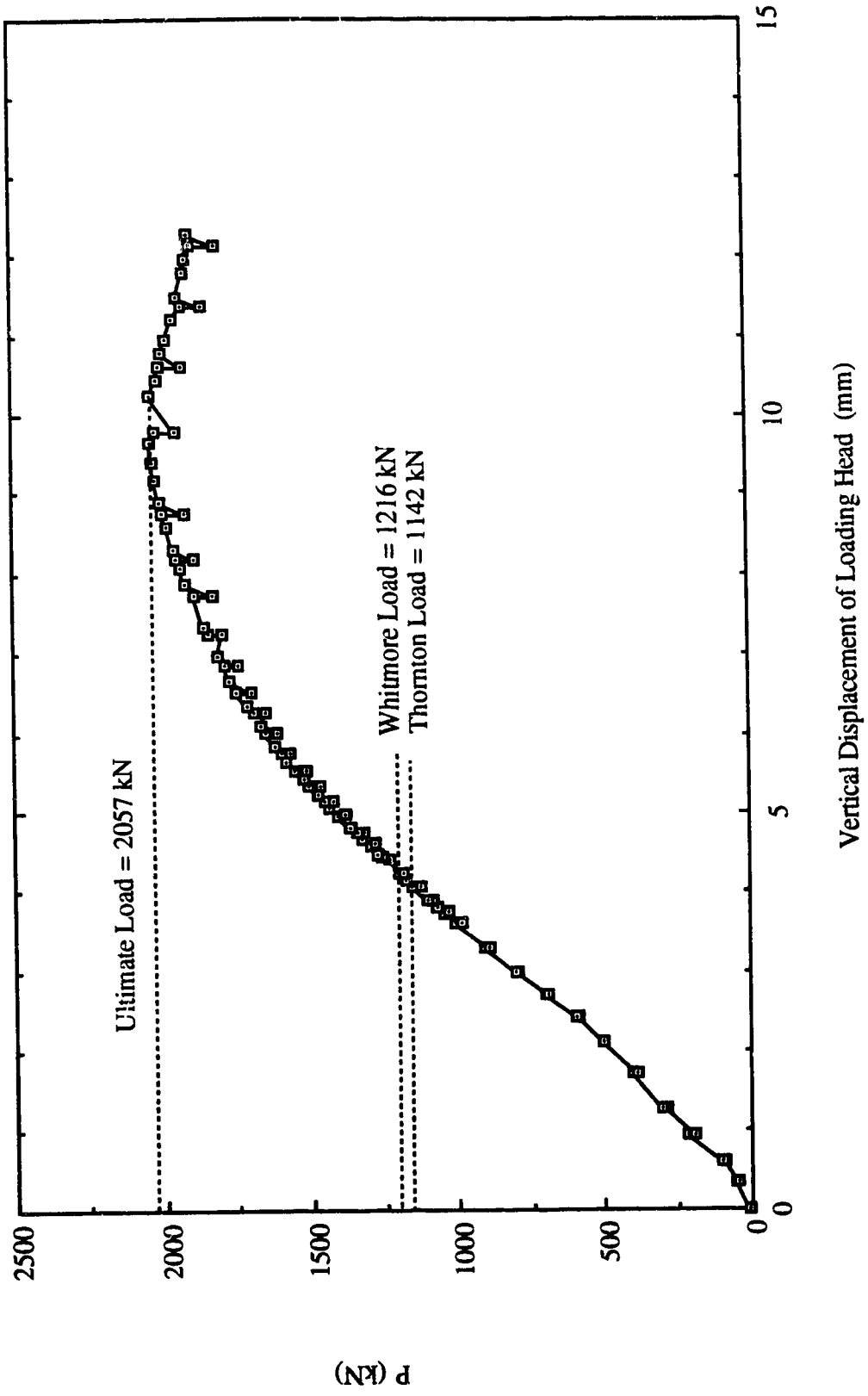


Fig. 3.18 Load vs. Vertical Displacement of Loading Head for Specimen GP1R

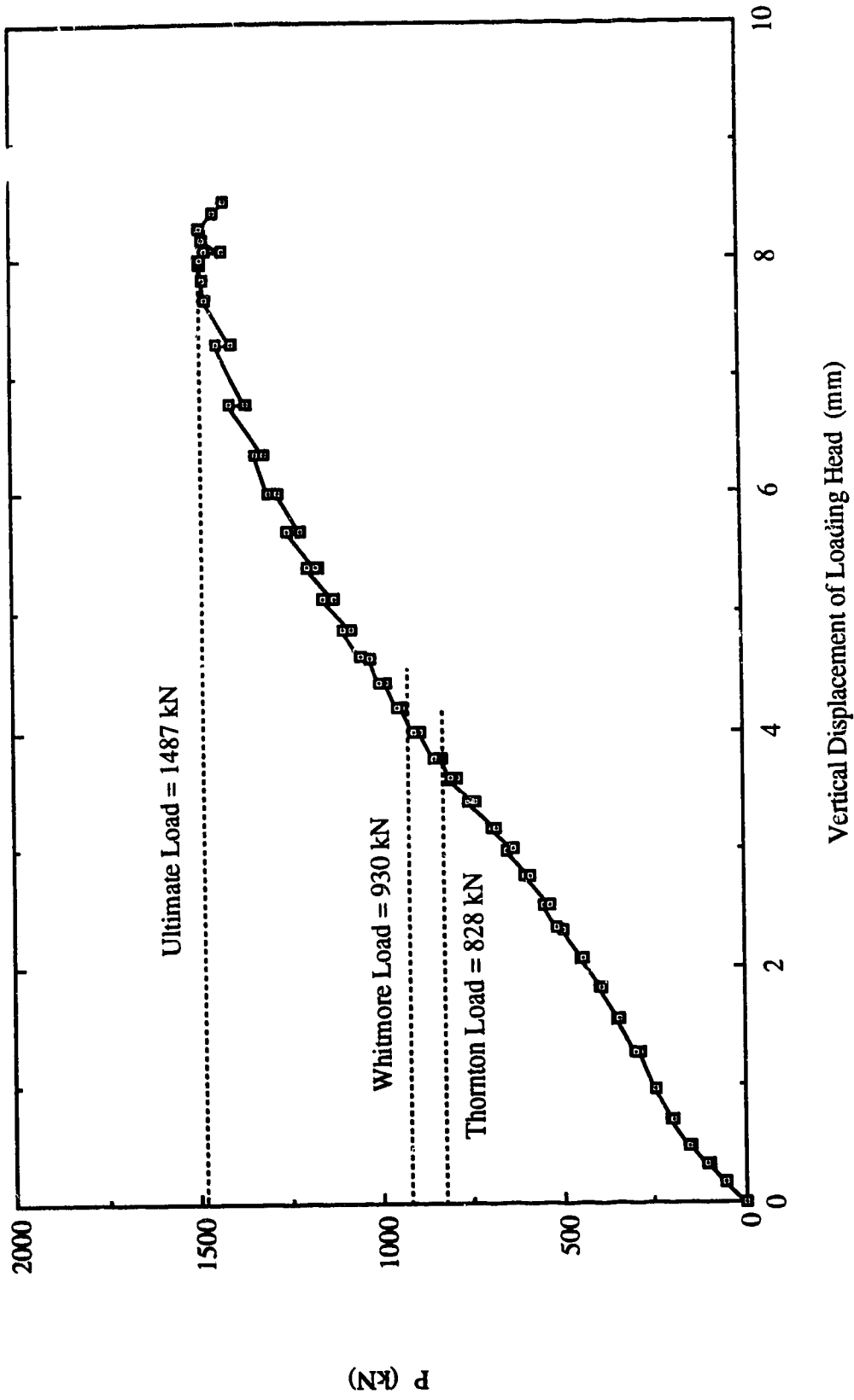


Fig. 3.19 Load vs. Vertical Displacement of Loading Head for Specimen GP2R

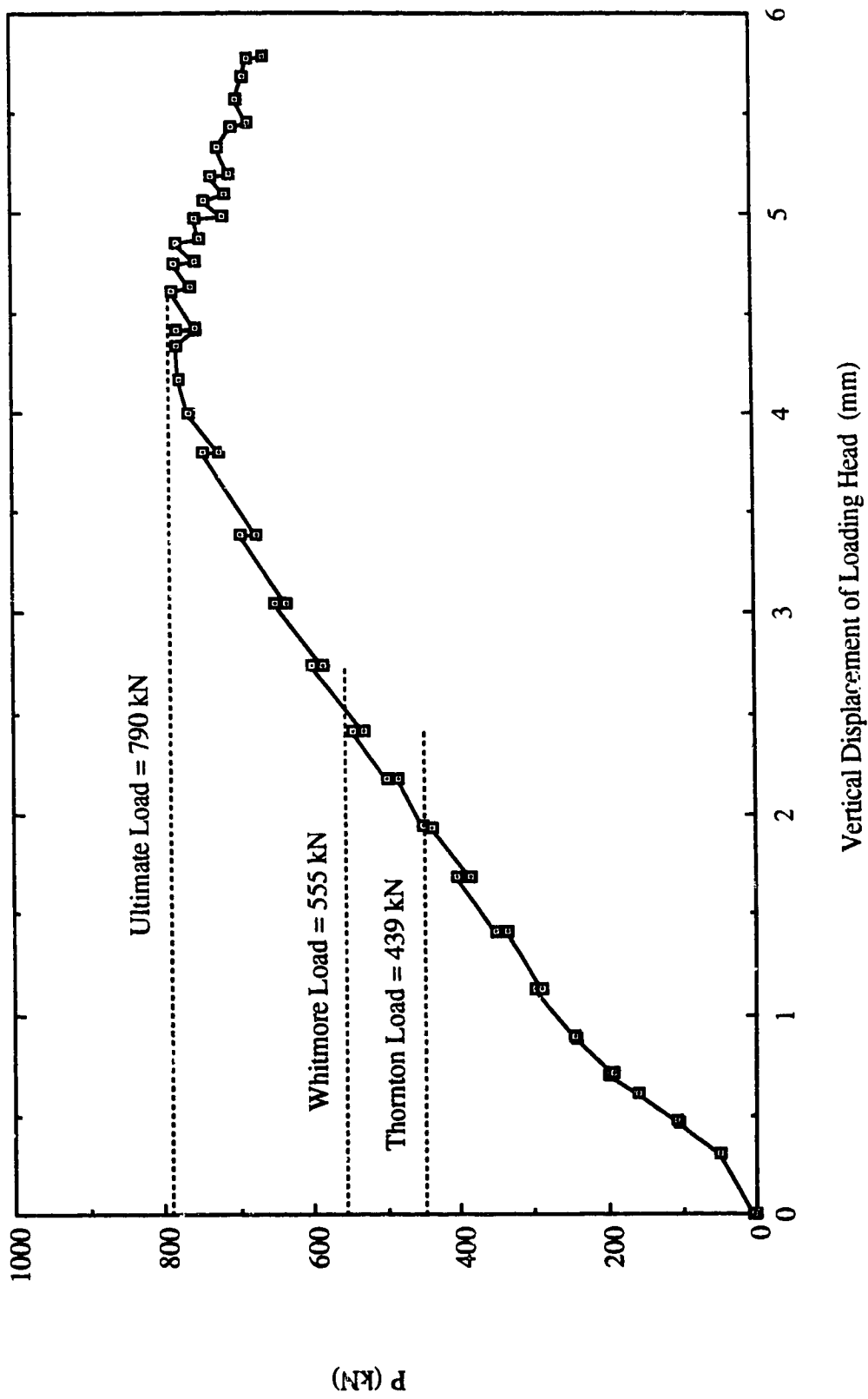
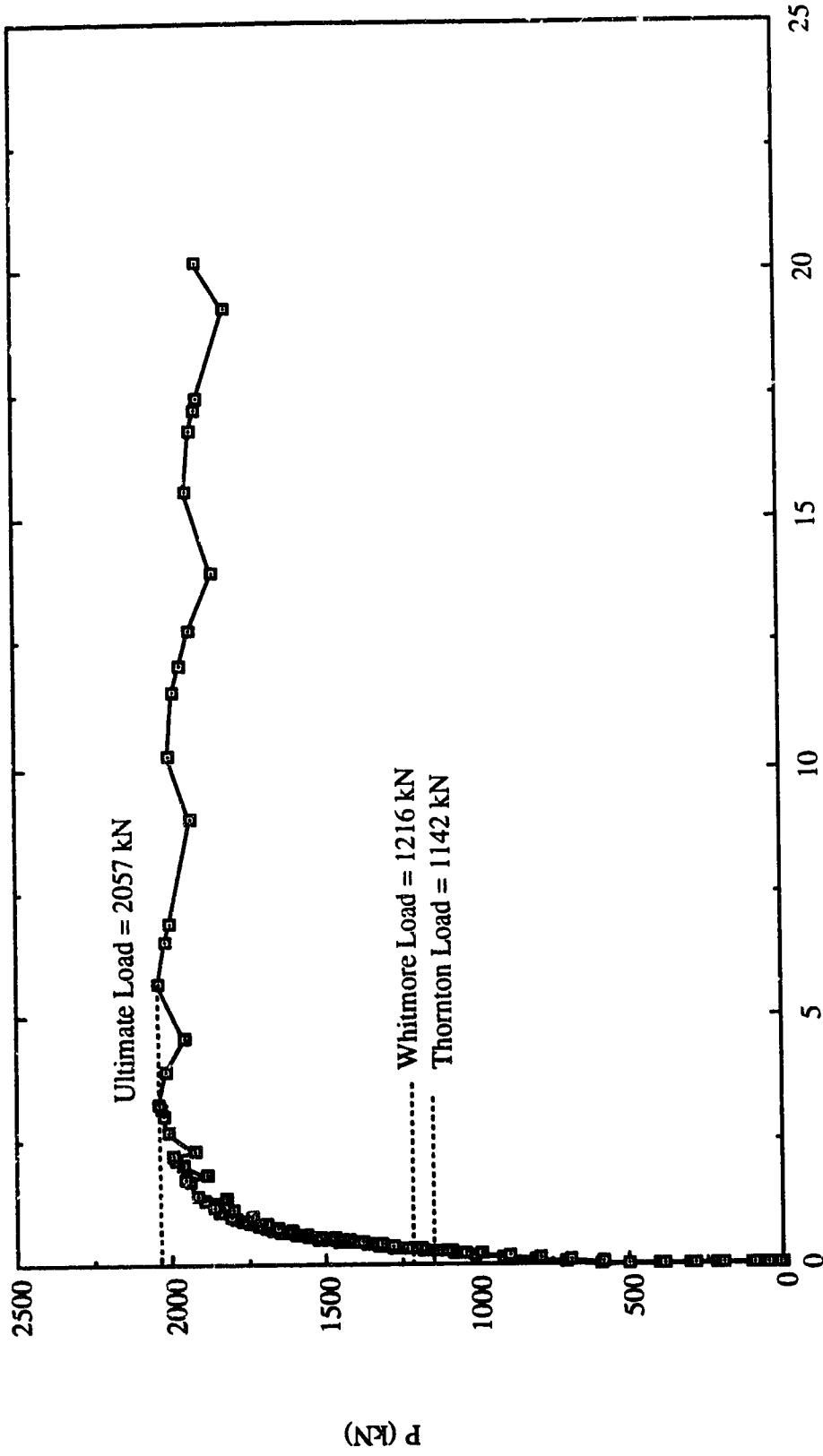


Fig. 3.20 Load vs. Vertical Displacement of Loading Head for Specimen GP3R



Out-of-Plane Displacement at Mid-Length of Long Free Edge (mm)

Fig. 3.21 Load vs. Out-of-Plane Displacement at Mid-Length of Long Free Edge for Specimen GP1R

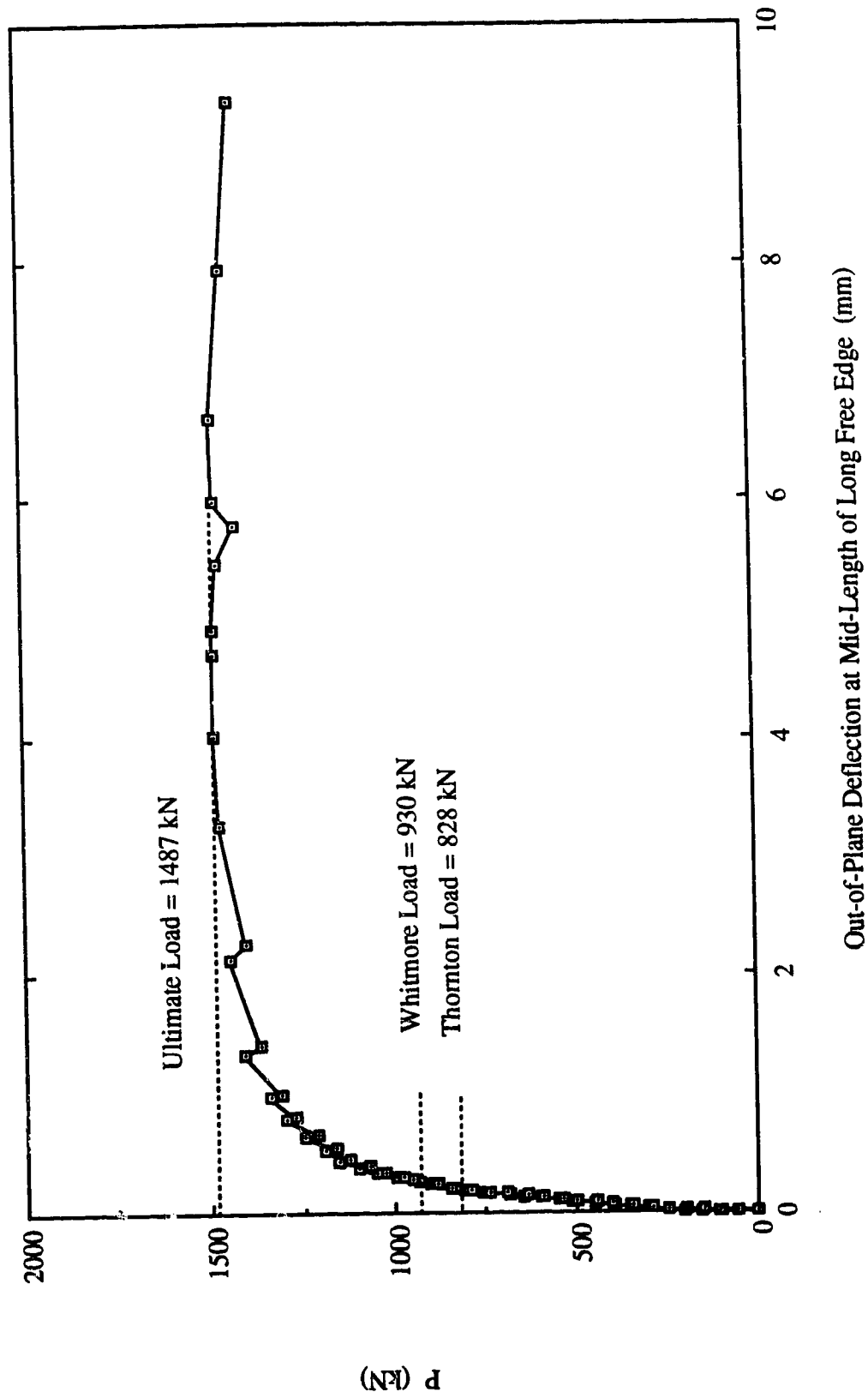


Fig. 3.22 Load vs. Out-of-Plane Displacement at Mid-Length of Long Free Edge for Specimen GP2R



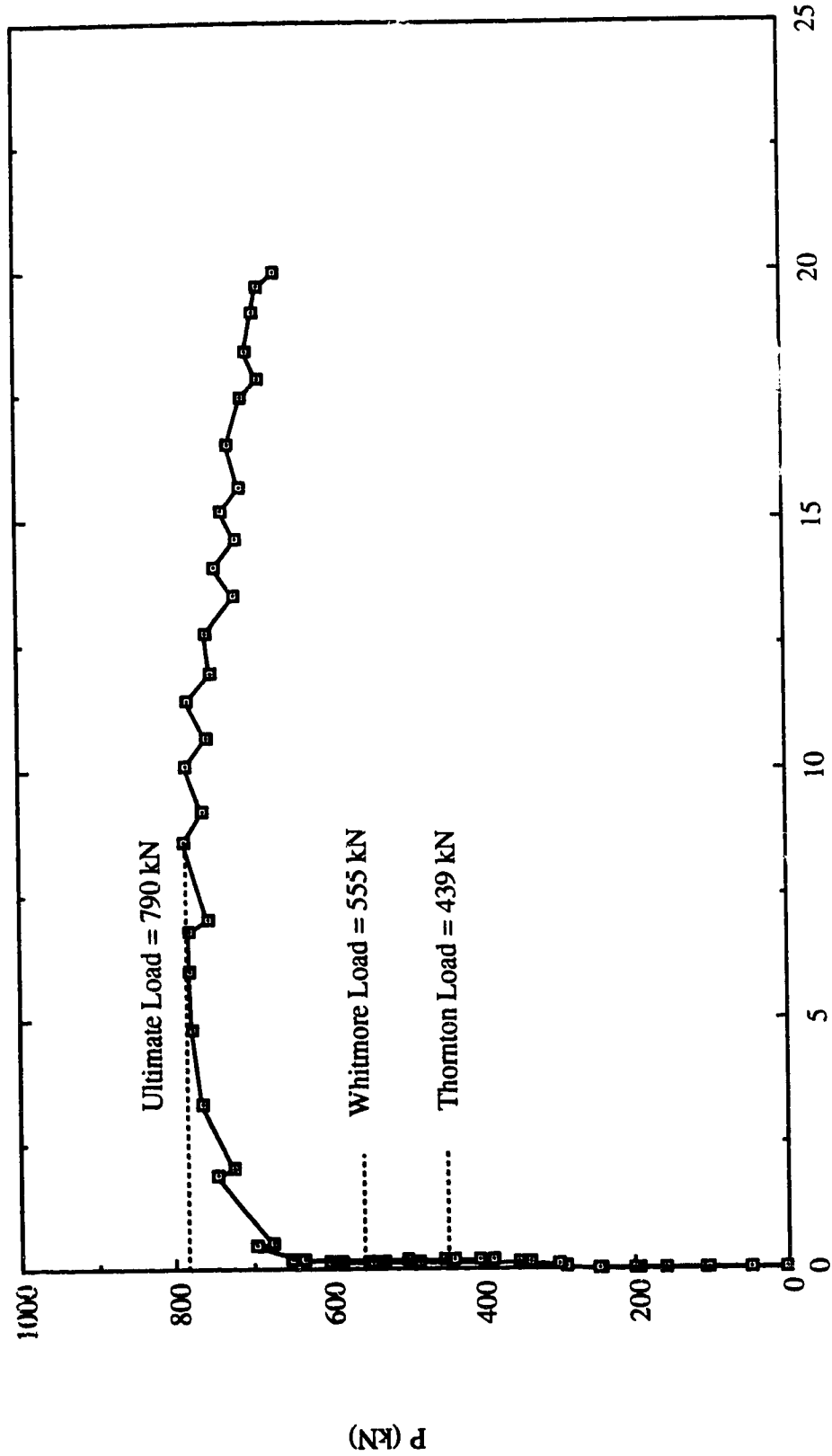


Fig. 3.23 Load vs. Out-of-Plane Displacement at Mid-Length of Long Free Edge for Specimen GP3R

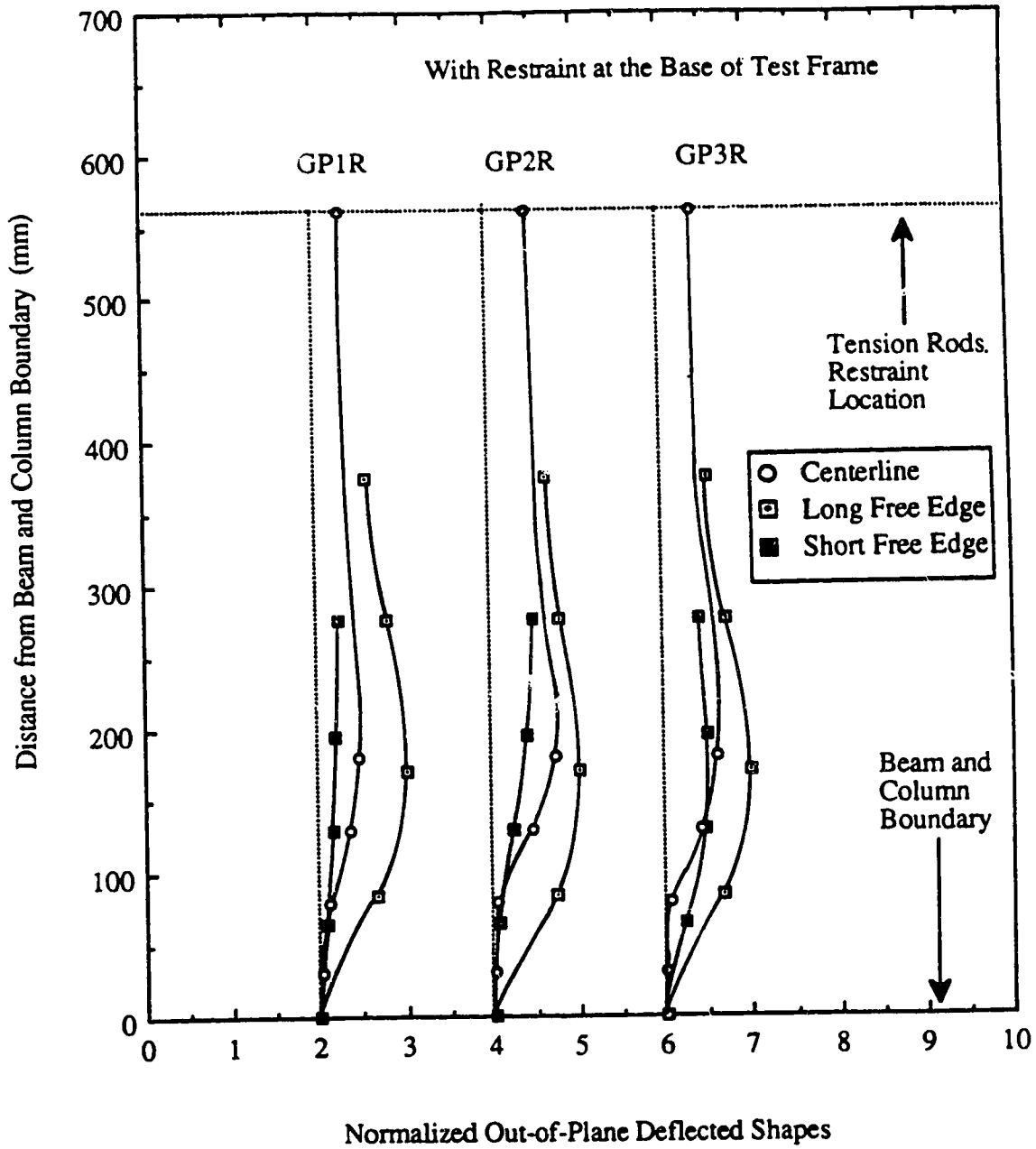


Fig. 3.24 Out-of-Plane Deflected Shapes at Free Edges and Along Centerline of Splice for GP Type Specimens - With Restraint

## **4. TEST RESULTS OF SP TYPE SPECIMENS**

### **4.1 General**

The SP type specimens were used to examine the effects of gusset plate size on the compressive behavior of the connection, and two specimens were tested with plate thickness of 13.3 mm and 9.8 mm. Again, the out-of-plane restraint at the base of the test frame was also included as a test variable in testing these specimens. The test results of the SP type specimens are summarized in Table 4.1. It can be seen from the table that the ultimate load of the specimens increased with increasing plate thickness. The test results also show that an appreciable increase in the ultimate load was recorded for specimen SP1 when out-of-plane restraint was applied to the base of the test frame. In addition, for specimen SP2, a significant increase in the ultimate load due to the out-of-plane restraint was observed, as shown in Table 4.1. The predictions by both the Whitmore method and the Thornton method are also included in the table. In general, it can be seen that the Whitmore method overestimated the strength of the specimens for both restraint conditions, except for the case of specimen SP2 with restraint. On the other hand, the Thornton method provided conservative estimates of the strength of specimens.

### **4.2 Without Out-of-Plane Restraint at Base of Test Frame**

#### **4.2.1 Behavior of Load versus In-Plane Deformation**

The failure mode for both specimens SP1 and SP2 was sway buckling of the connection. The curves of load versus the vertical displacement of the loading head are illustrated in Figs. 4.1 and 4.2. It can be seen from these figures that both specimens were not able to reach the yield load level estimated by the Whitmore's method. However, the ultimate load of the thick specimen (SP1-13.3 mm) reached about 87 percent of the corresponding Whitmore load. On the other hand, the thin specimen (SP2-9.8 mm) only reached about 71 percent of the corresponding Whitmore load. A linear load deflection behavior was

observed until the applied load was close to the ultimate load at which significant out-of-plane displacement had occurred. In particular, the load deflection curve for specimen SP2 was linear until it reached the ultimate load. The vertical displacement of the loading head only increased slightly after the specimens buckled.

#### **4.2.2 Behavior of Load versus Out-of-Plane Displacement of Test Frame**

The out-of-plane displacement of the test frame was recorded for both specimens from the beginning of loading due to the presence of initial imperfections. These imperfections were caused by the initial out-of-straightness of the plate and the welding procedure. The curves of load versus the out-of-plane displacement of the test frame are shown in Figs. 4.3 and 4.4. For specimen SP1, the load deflection curve gradually increased until the applied load reached approximately 1400 kN, at which a significant out-of-plane displacement was observed. The displacement continued to increase with a slight increase in the applied load. At a displacement of about 16 mm, a significant increase in stiffness of the connection was observed. This increase in stiffness was probably caused by local bending of the gusset plate underneath the splice member, and this will be discussed later when the strain gauges readings are examined. The ultimate load of the specimen was reached at 1606 kN, with a deflection of about 17.5 mm. For specimen SP2, the load versus out-of-plane displacement curve gradually increased until the buckling of the specimen occurred. The ultimate load of the specimen was reached at 1010 kN with a displacement of about 17.5 mm. The final displacement of the test frame was approximately 24.5 mm, and the applied load was maintained very close to the ultimate load of the specimen.

#### **4.2.3 Strain Gauge Results**

The curves of load versus strains are shown in Figs. 4.5 to 4.10. It can be seen from the plots for strain readings recorded at the mid-length of the free edges (Figs. 4.5, 4.6, 4.7,

and 4.8) that bending of the plate occurred from the beginning of loading. Again, this was mainly caused by the initial imperfections of the plate and hence the misalignment of the loading head. Nonetheless, these plots indicated the occurrence of strain bifurcation when the specimens buckled. It should also be noted that the strain readings for the specimens were within the elastic range prior to reaching the ultimate load. As mentioned above, a change in the bending direction of the plate underneath the splice member was observed at a load level of about 1400 kN for specimen SP1. This phenomenon can be shown by the plot of load versus rosette strain readings at a load level close to the ultimate for specimen SP1, as illustrated in Fig. 4.9. This figure illustrates that the strain reversal existed at a load level of about 1380 kN at which point a change of the bending direction of the plate underneath the splice member had occurred. As the out-of-plane displacement of the test frame increased from this load level, the compressive strain at rosette gauge #22 decreased, while increasing compressive strains were recorded at rosette gauge #21 as shown in Fig. 4.9. At a load level of about 1506 kN, the compressive strain at rosette gauge #22 increased because of the local bending of the plate underneath the splice member, and a significant increase in the compressive strain at rosette gauge #21 was also observed. This local bending behavior of the plate might attribute to the increase in the out-of-plane stiffness of the specimen at this load level. The applied load continued to increase with the increasing compressive strain at rosette gauge #22 until the ultimate load was reached.

#### **4.2.4 Yielding Behavior of Specimens**

In general, only moderate yielding was observed for the SP type specimens. For specimen SP1, the yielding was first observed close to the corner of the beam and column boundary at a load level of about 1200 kN. As load increased to approximately 1550 kN, yield lines were observed in the area about the two sides of the splice member and also underneath the splice member. When the applied load approached the ultimate level, the yielding at the corner of the beam and column boundary increased. Finally, at the ultimate yield lines

were observed on the specimen along the beam and column boundary, as shown in Fig. 4.11. For specimen SP2, yield lines were first detected in the area about the two sides of the splice member when the applied load was approximately 900 kN. As the load increased, yielding was also observed near the beam and column boundary. Again, yield lines were detected along the beam and column boundary at the ultimate load level.

#### **4.2.5 Out-of-Plane Deflected Shapes of Free Edges and along Centerline of Splicing Member**

The out-of-plane deflected shapes for the specimens are shown in Fig. 4.12. In general, it can be seen from this figure that the deflected shapes resembled the buckled shapes of a fixed-guided column, except for the deflected shapes of the long free edge of specimen SP2. This different deflected shape was caused by the initial out-of-straightness of the free edge. In fact, significant warping of the specimen was observed after the plate was first welded to the beam and column. Hence, to correct the imperfection, the specimen was cut from the beam and column and welded back on. However, some noticeable imperfections still existed after re-welding. For specimen SP1, the LVDT's readings at the early stage of loading indicated that the deflected shape along the centerline of the splice member was similar to that of the long free edge of specimen SP2. However, as the applied load increased close to the ultimate load, the deflected shape shifted to the fixed-guided mode.

### **4.3 With Out-of-Plane Restraint at Base of Test Frame**

#### **4.3.1 General**

It was mentioned in the previous chapter that the same SP type specimens were used in conducting tests of both out-of-plane restraint conditions at the base of the test frame. As expected, permanent deformation existed in the failed specimens after the tests performed without a restraint condition. Therefore, in order to correct the imperfection, lateral force

was applied to the beam and column to push the failed specimen back to its original position. Unfortunately, appreciable imperfection still existed in the specimens after this remedial measure.

#### **4.3.2 Behavior of Load versus In-Plane Deformation**

The curves of load versus vertical displacement of the loading head are illustrated in Figs. 4.13 and 4.14. An initial nonlinearity of load deflection curves existed due to settling of the test fixtures. Subsequently, linear behavior was observed until the applied load approached the ultimate load. In particular, the applied load increased gradually to the ultimate load for specimen SP1. On the other hand, a relatively rapid increase to the ultimate load was observed for specimen SP2. It can be seen from the figures that after reaching the ultimate load, the applied load decreased with increasing vertical deflection.

#### **4.3.3 Behavior of Load versus Out-of-Plane Displacement at Mid-Length of Long Free Edge**

The curves of load versus the out-of-plane displacement at mid-length of the long free edge are shown in Figs. 4.15 and 4.16. For both specimens, a nonlinear load deflection behavior was observed at the beginning of loading. This was mainly caused by the initial imperfection induced after the previous testing of the specimens as mentioned above. In addition, the curve for specimen SP2 indicated that the long free edge at mid-length originally deformed eastward. However, when loading continued, the deformation gradually moved westward until buckling occurred, at which the plate deformed towards the east again. This behavior was probably because of the local bending of the specimen at the mid-length of the long free edge caused by the imperfection. When the specimen reached the ultimate load, the connection buckled eastward, which forced the long free edge to deform in the same direction.

#### **4.3.4 Yielding Behavior of Specimens**

Since these two specimens were tested previously, only any additional yielding observed in the tests with restraint at the conjunction of the gusset-to-splice will be discussed. For both specimens, the yield lines were recorded at the gusset plate near the corner of the splice member, as shown in Figs. 4.17 and 4.18. Local out-of-plane deflection of the specimens was also observed underneath the splice member. In addition, yield lines were recorded at the mid-length of the free edges. These yield lines originated from the gusset plate area near the corner of the splice member and extended towards the mid-length of the free edges, as shown in Fig. 4.19.

#### **4.3.5 Out-of-Plane Deflected Shapes of Free Edges and along Centerline of Splicing Member**

The normalized out-of-plane displacement for the free edges and along the centerline of the splice member for both specimens is shown in Fig. 4.20. Again, it can be seen from the figure that out-of-plane movement at the conjunction of the gusset-to-splice was recorded. Similar to GP type specimens, this displacement was caused by the bending of the web of the bracing about the tension rod supports. Nonetheless, these figures show the effects of out-of-plane restraint on the buckled shapes of the specimens. It should also be noted that the maximum out-of-plane displacement for both specimens occurred at the long free edge.



Table 4.1 Test Results of SP Type Specimens

Specimen Designation	Plate Size (mm x mm x mm)	Ultimate Load Without Restraint (kN)	Ultimate Load With Restraint (kN)	Whitmore Load $P_w$ (kN)	Thornton Load $P_t$ $k=0.65$ (kN)
SP1	850 x 700 x 13.3	1606	1760	1852	1228
SP2	850 x 700 x 9.8	1010	1477	1416	640

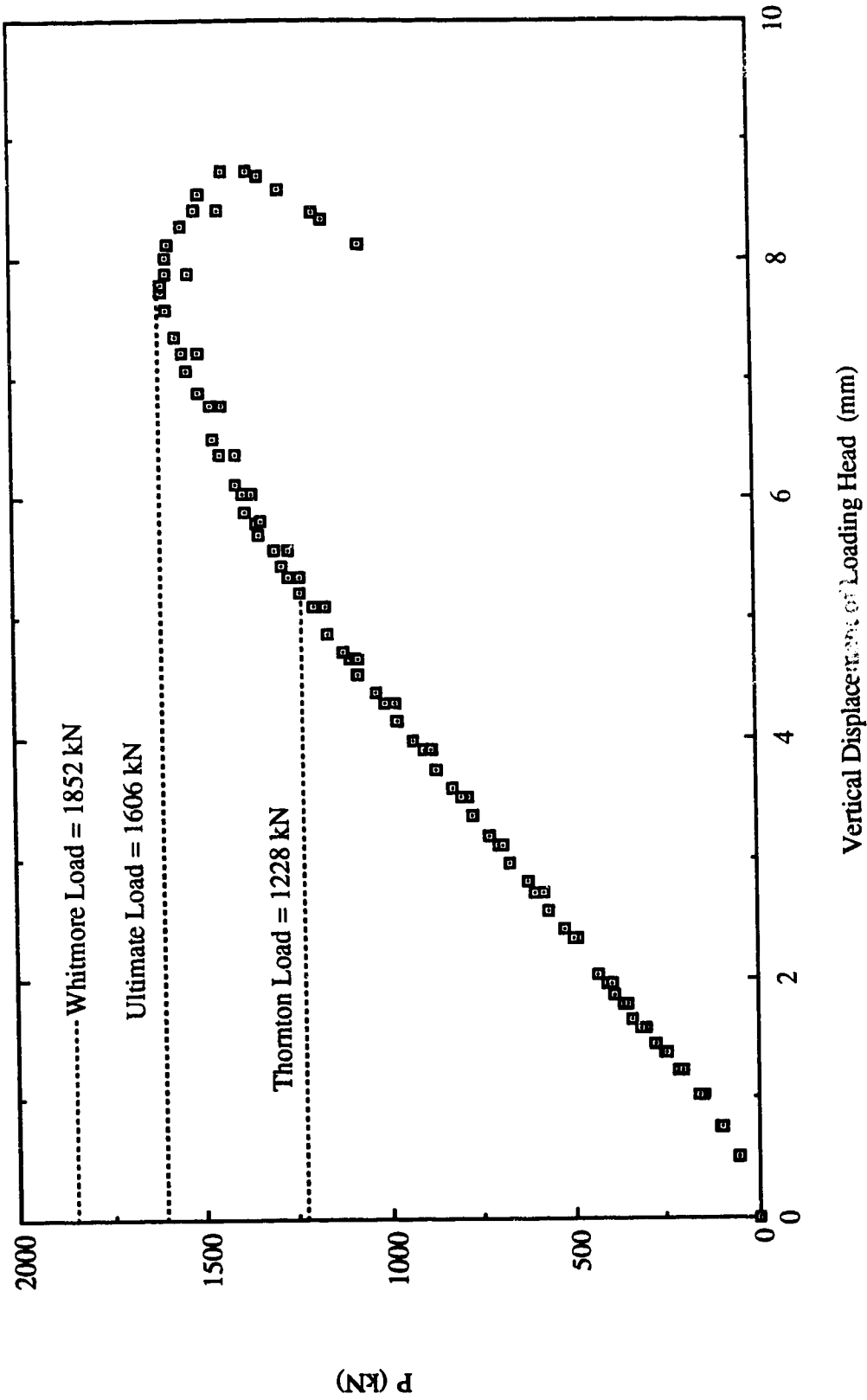


Fig. 4.1 Load vs. Vertical Displacement of Loading Head for Specimen SP1 - Without Restraint

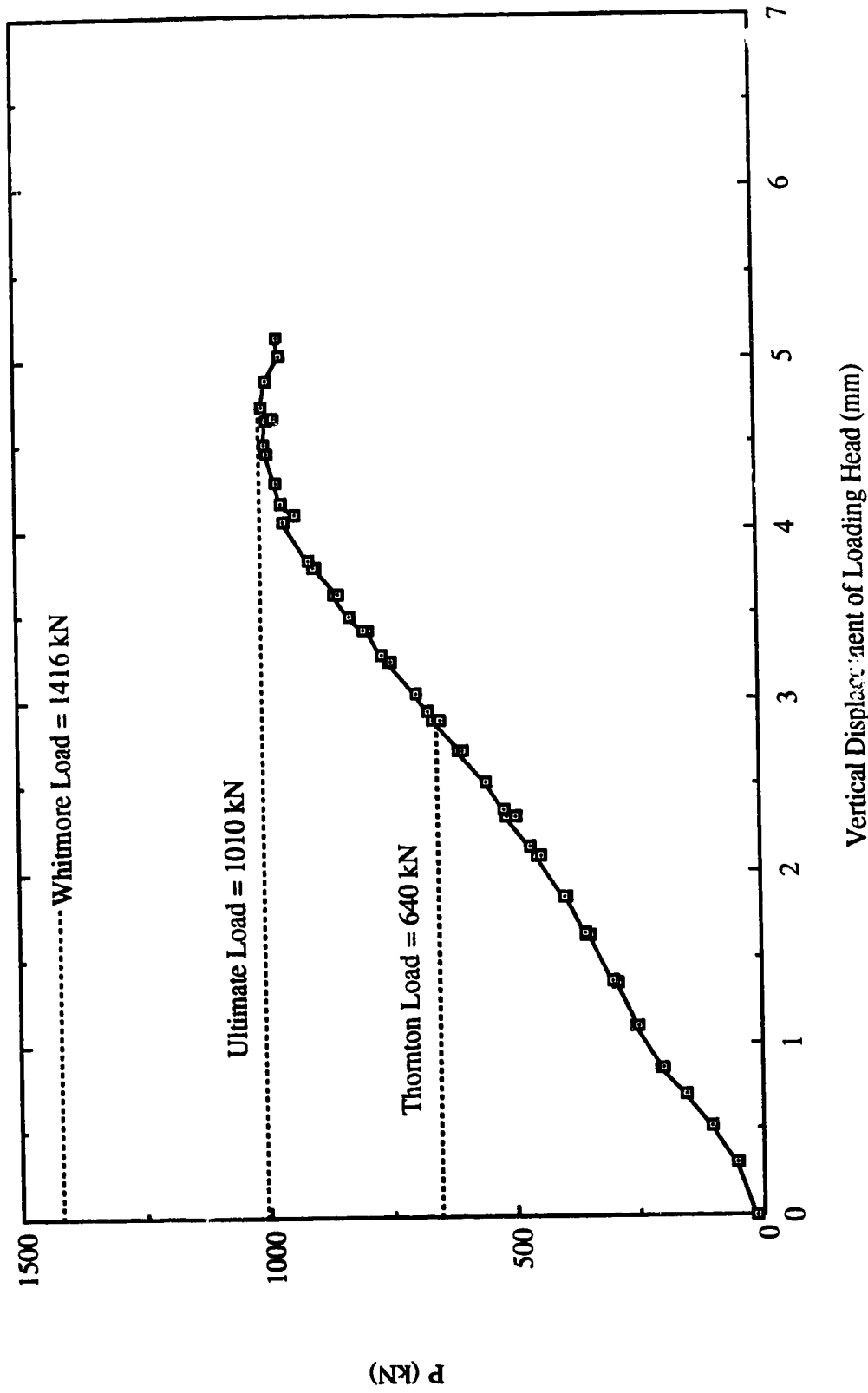


Fig. 4.2 Load vs. Vertical Displacement of Loading Head for Specimen SP2 - Without Restraint

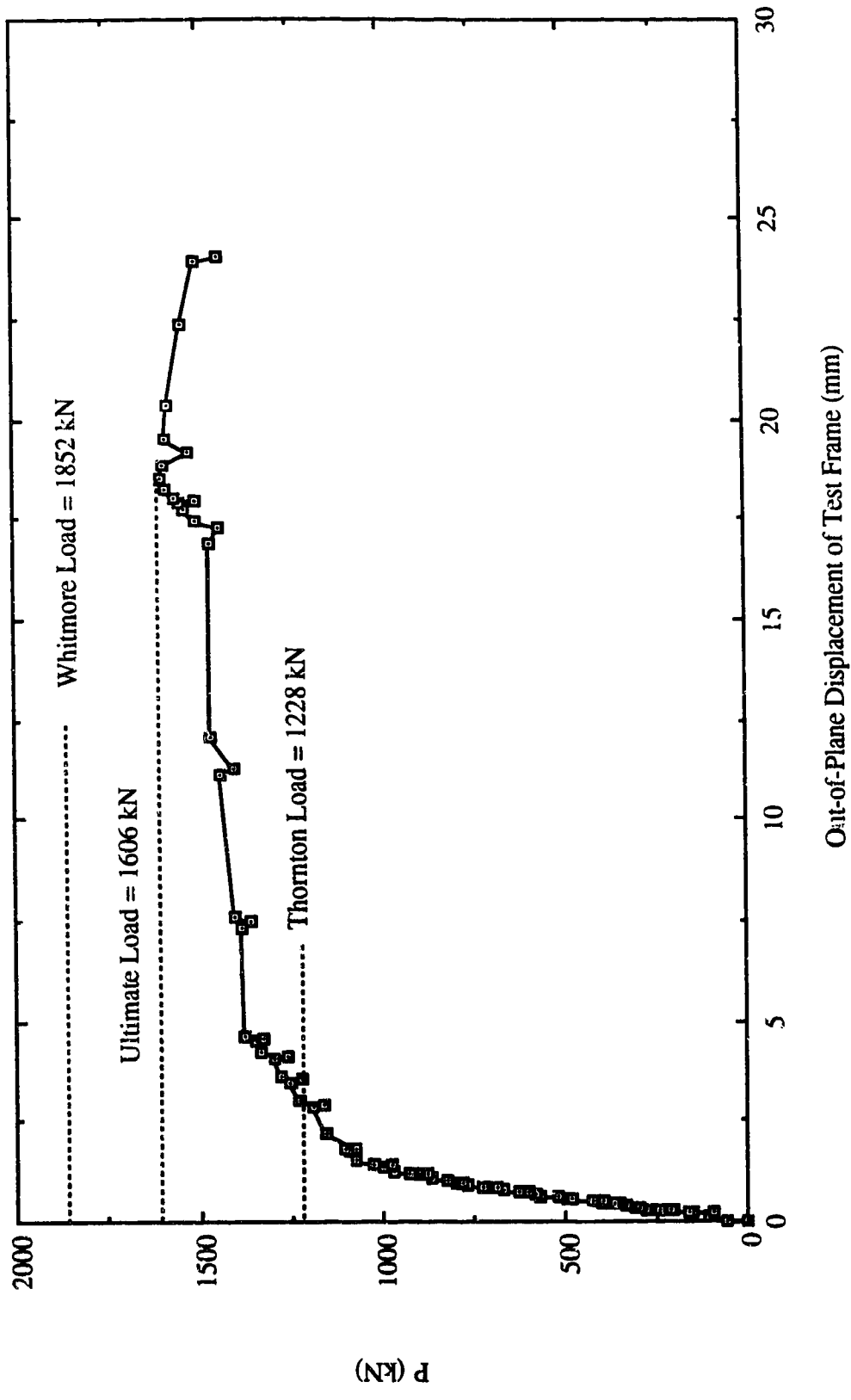


Fig. 4.3 Load vs. Out-of-Plane Displacement of Test Frame for Specimen SP1 - Without Restraint

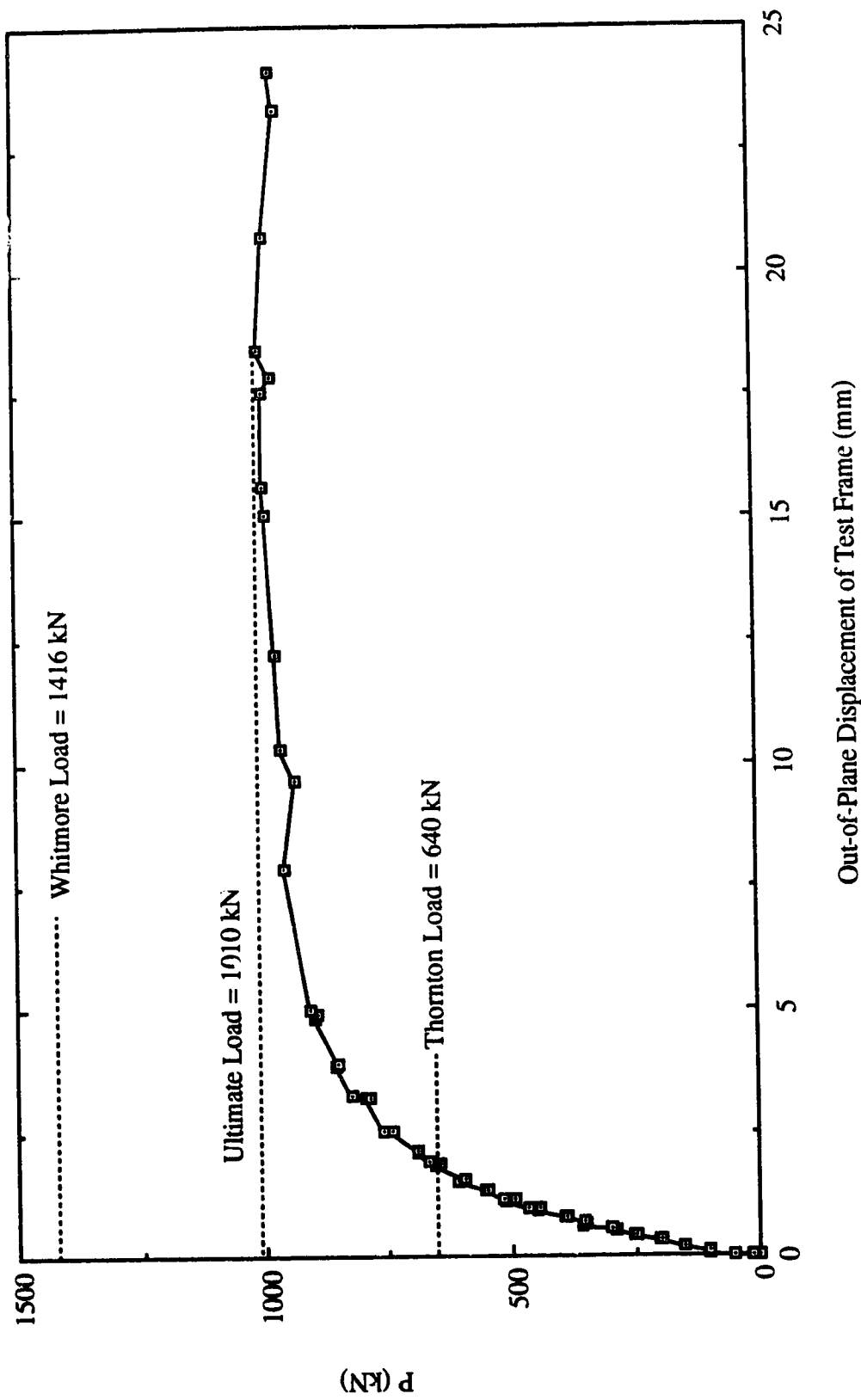


Fig. 4.4 Load vs. Out-of-Plane Displacement of Test Frame for Specimen SP2 - Without Restraint

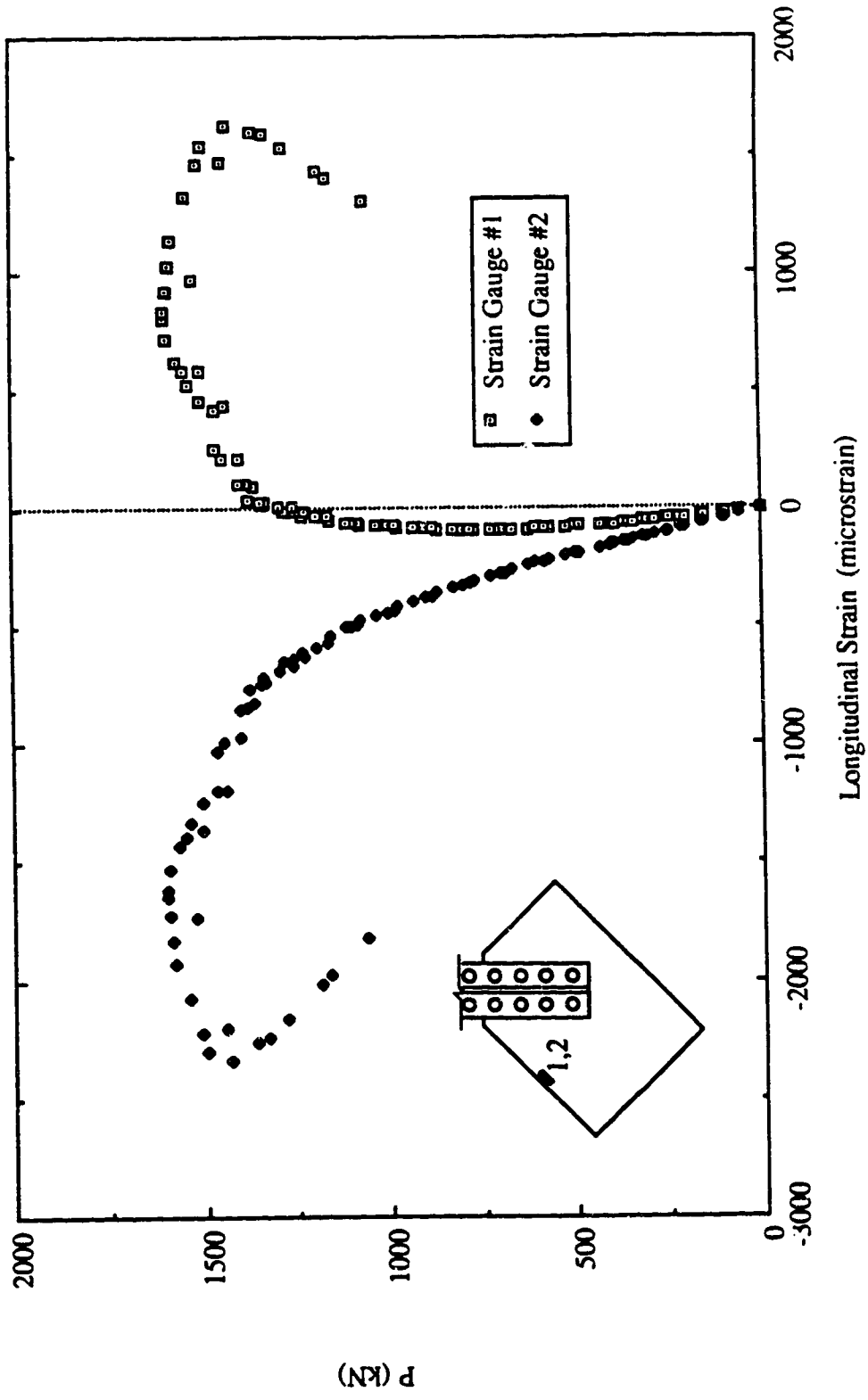


Fig. 4.5 Load vs. Strain Gauge Readings at Mid-Length of Long Free Edge for Specimen SP1 - Without Restraint

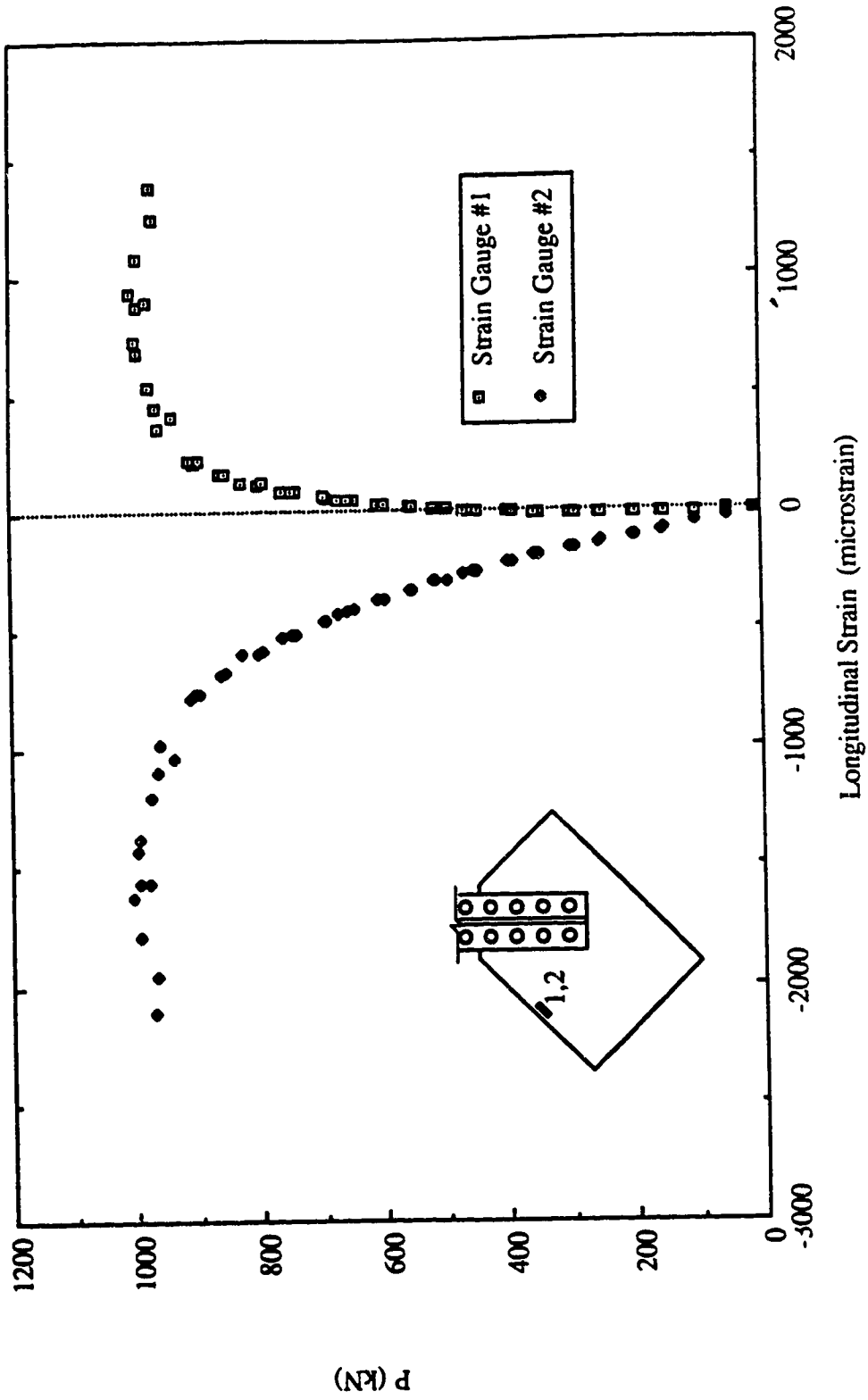


Fig. 4.6 Load vs. Strain Gauge Readings at Mid-Length of Long Free Edge for Specimen SP2 - Without Restraint

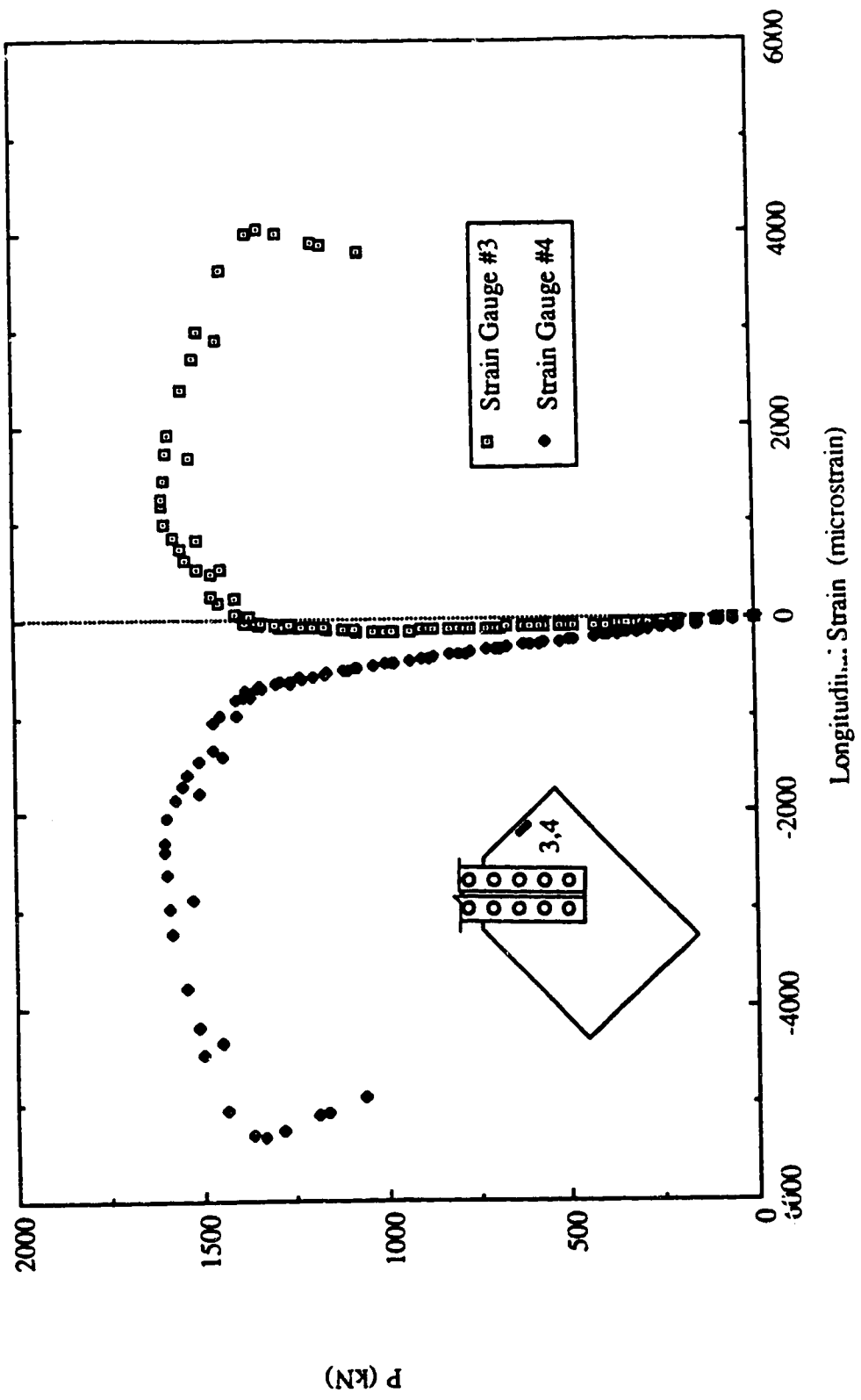


Fig. 4.7 Load vs. Strain Gauge Readings at Mid-Length of Short Free Edge for Specimen SP1 - Without Restraint



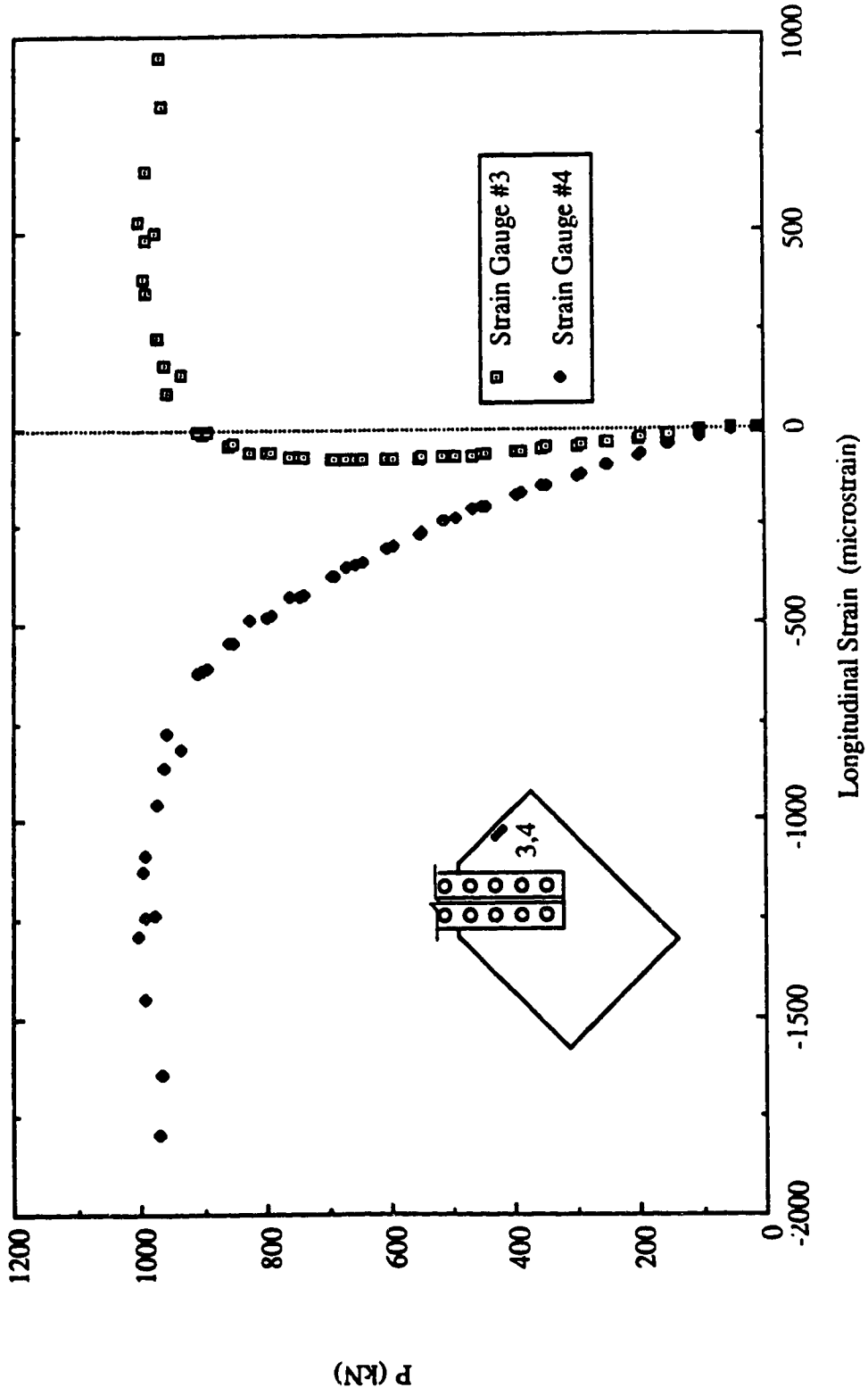


Fig. 4.8 Load vs. Strain Gauge Readings at Mid-Length of Short Free Edge for Specimen SP2 - Without Restraint

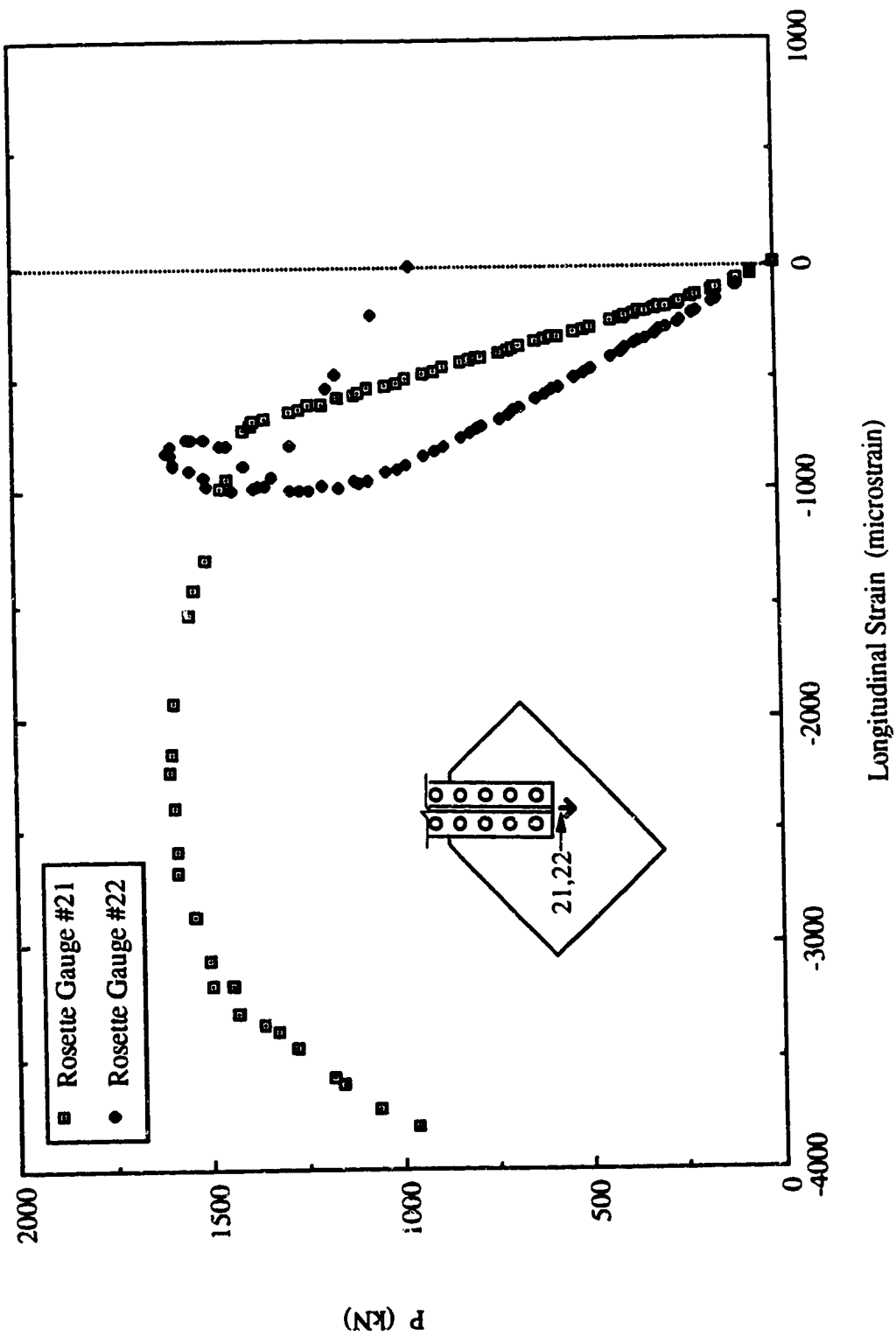


Fig. 4.9 Load vs. Strain Readings at Rosette Location for Specimen SP1 - Without Restraint

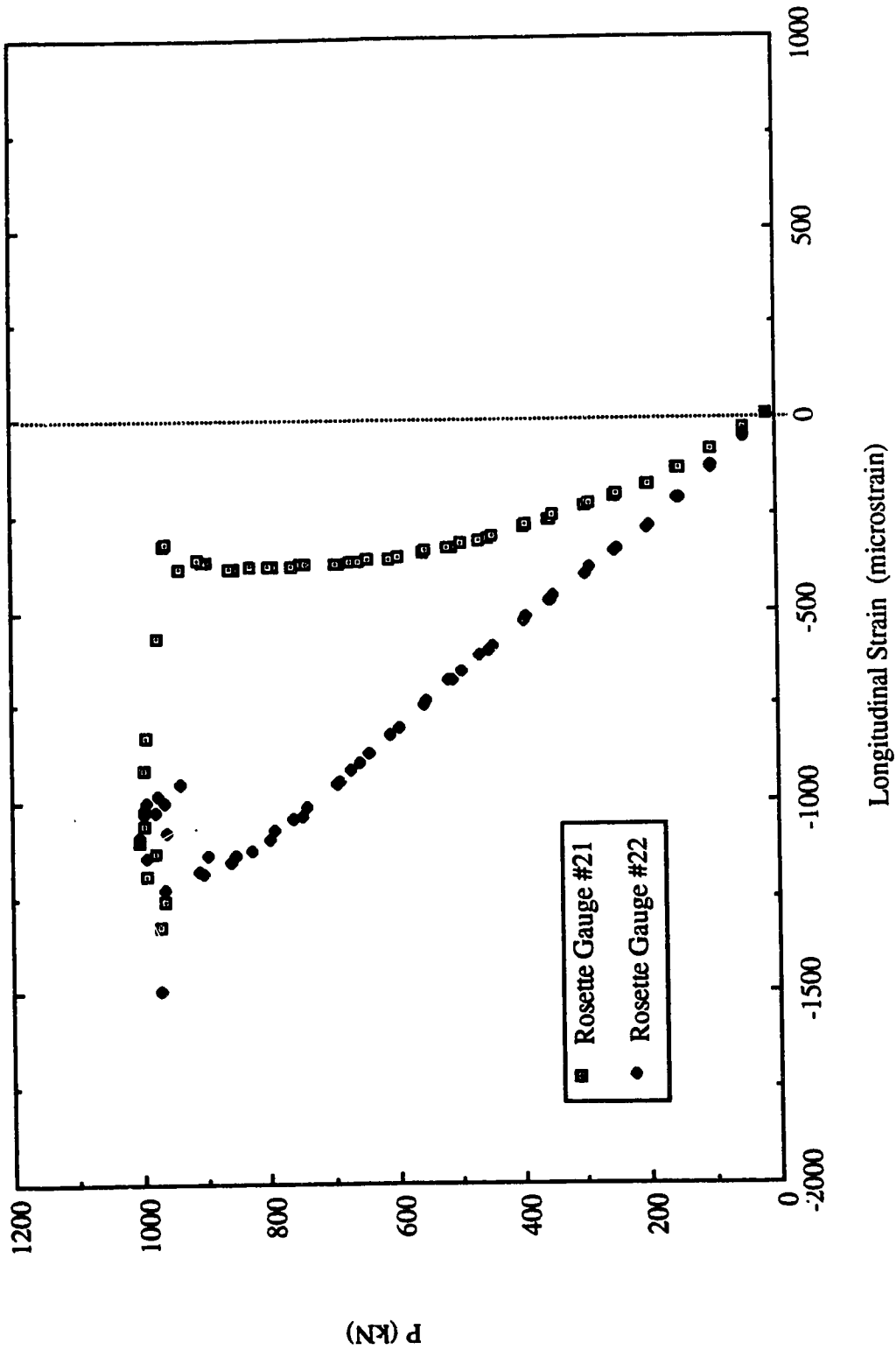


Fig. 4.10 Load vs. Strain Readings at Rosette Location for Specimen SP2 - Without Restraint



**Fig. 4.11** Picture of Failed Specimen SP1

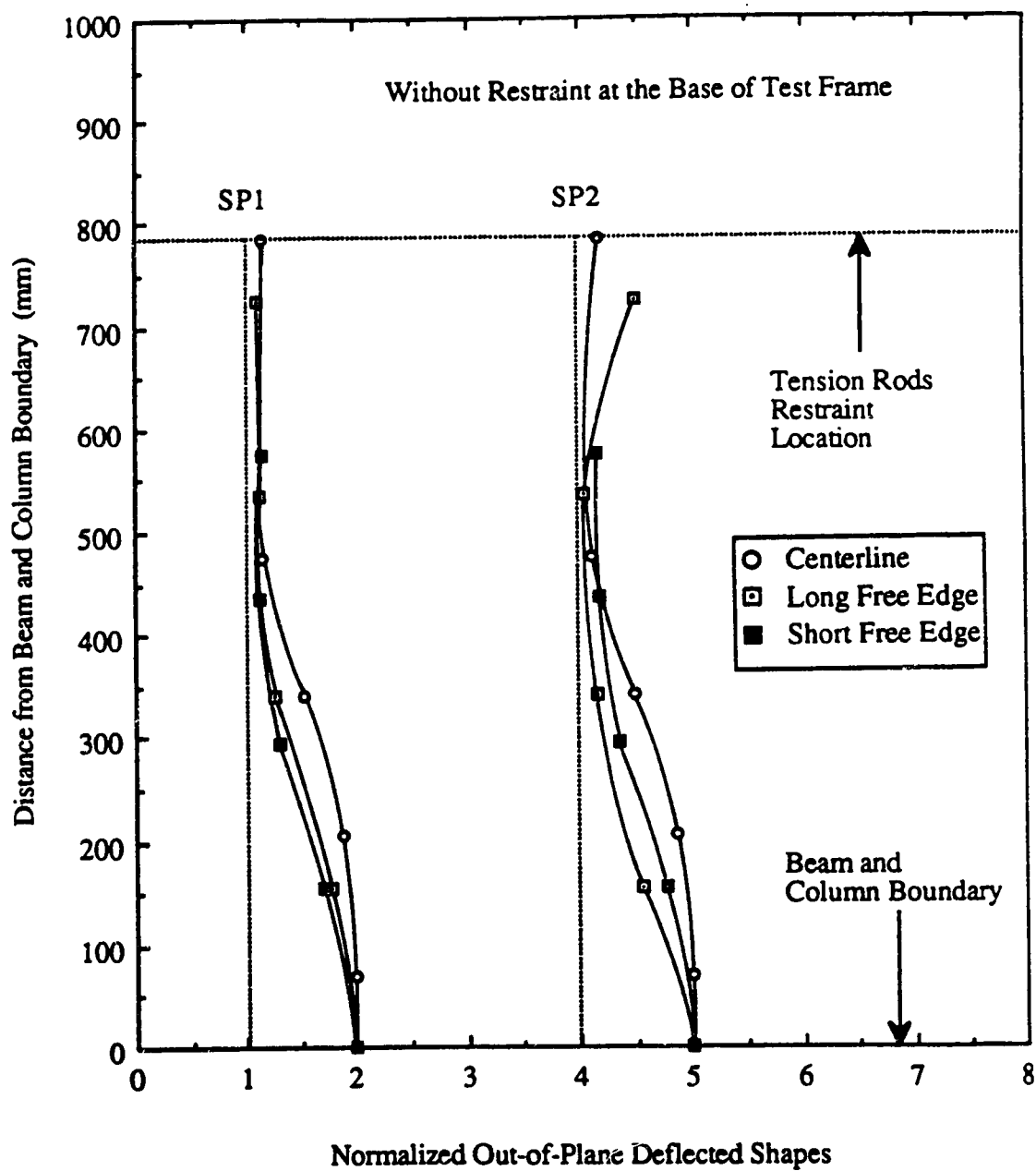


Fig. 4.12 Out-of-Plane Deflected Shapes at Free Edges and Along the Centerline of Splice for SP Type Specimens - Without Restraint

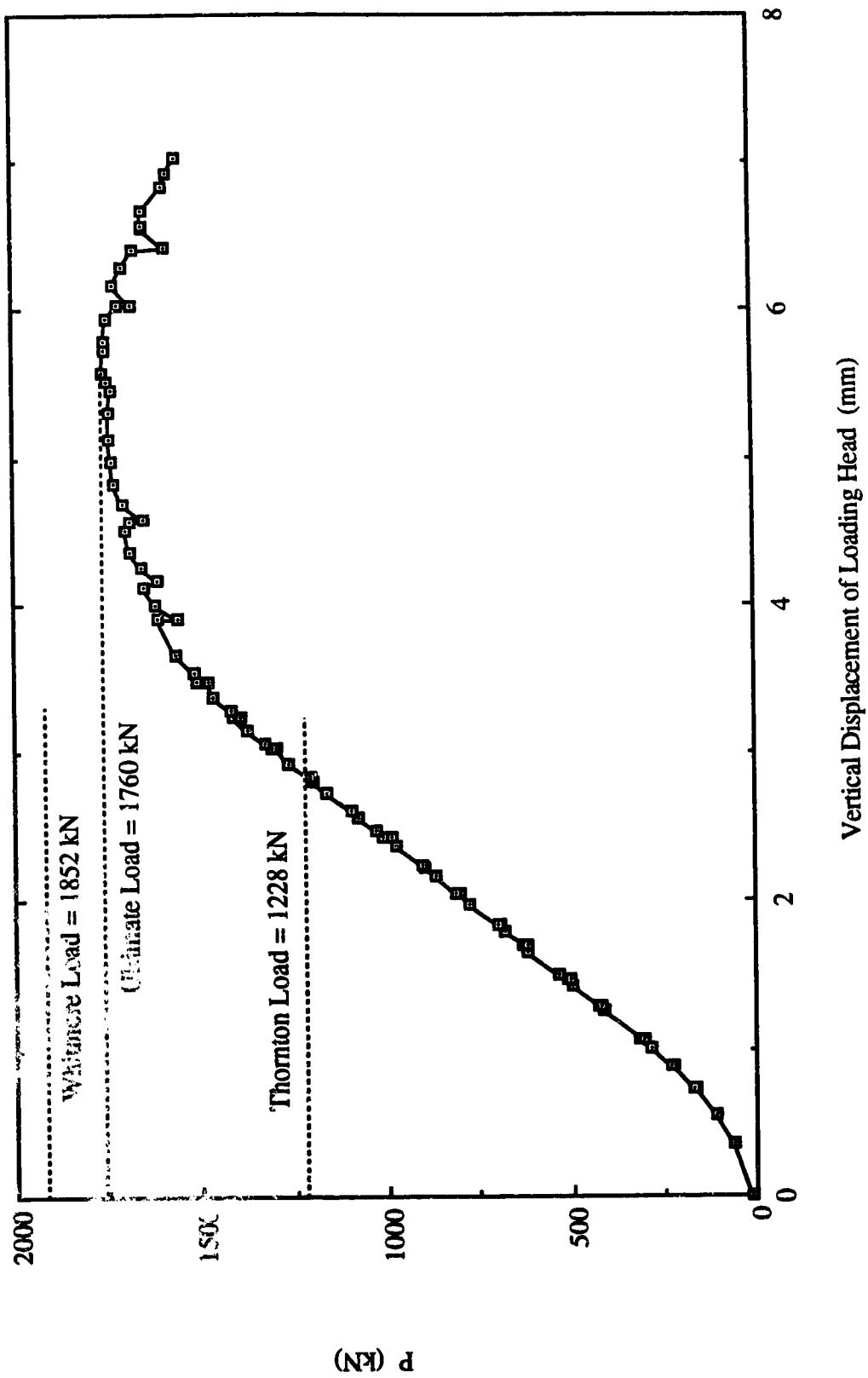


Fig. 4.13 Load vs. Vertical Displacement of Loading Head for Specimen SP1 - With Restraint

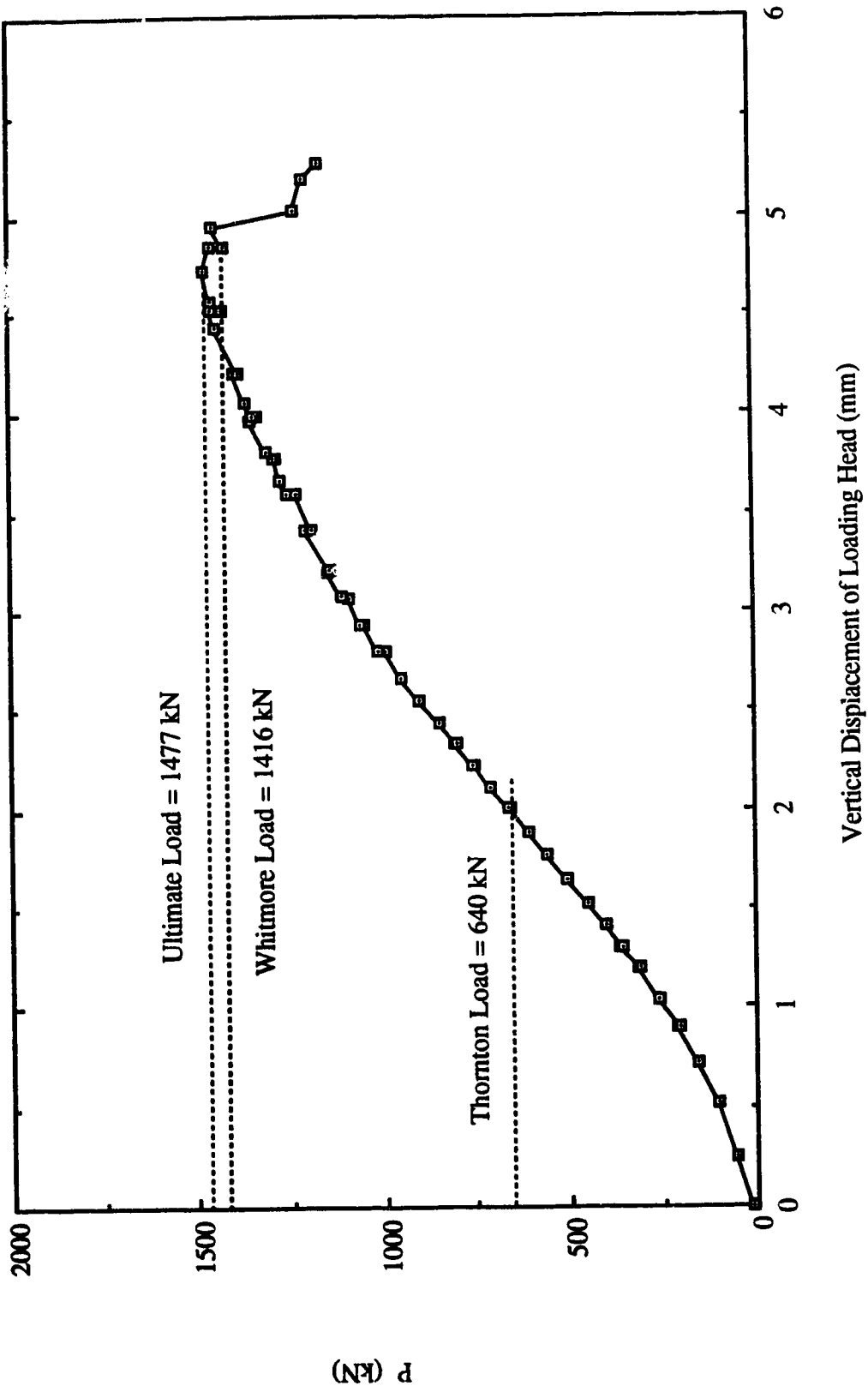


Fig. 4.14 Load vs. Vertical Displacement of Loading Head for Specimen SP2 - With Restraint

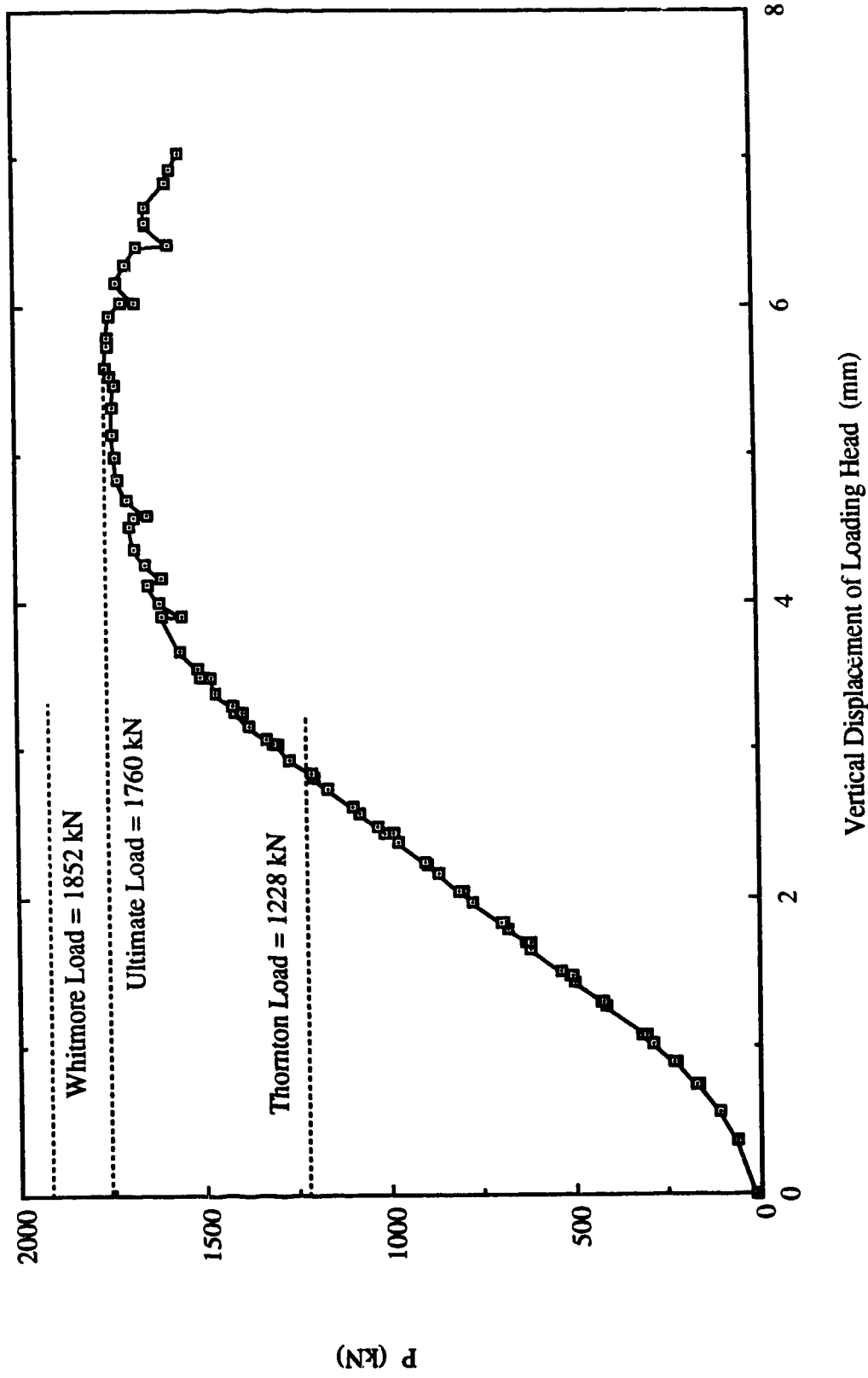


Fig. 4.15 Load vs. Out-of-Plane Displacement at Mid-Length of Long Free Edge for Specimen SP1 - With Restraint



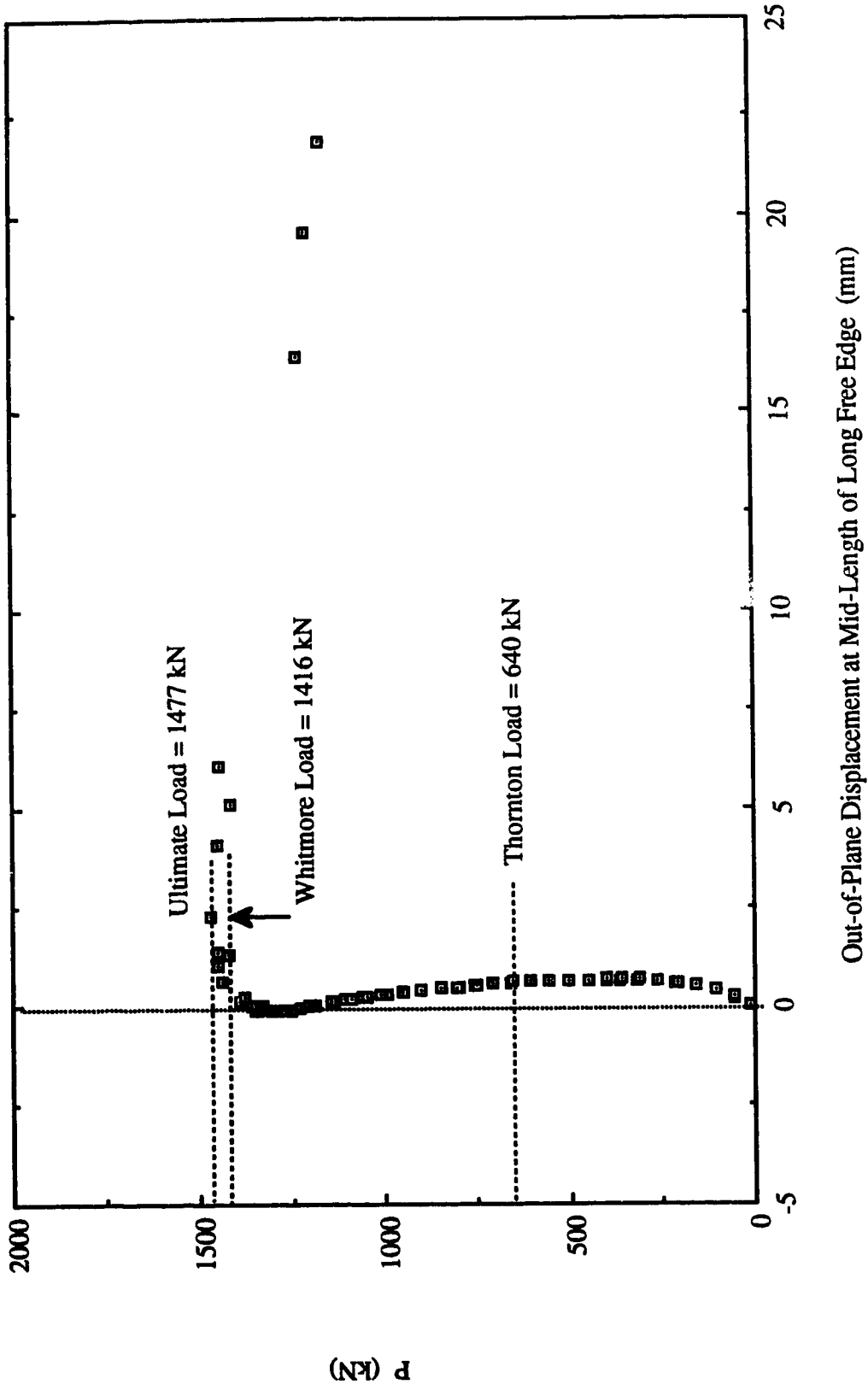
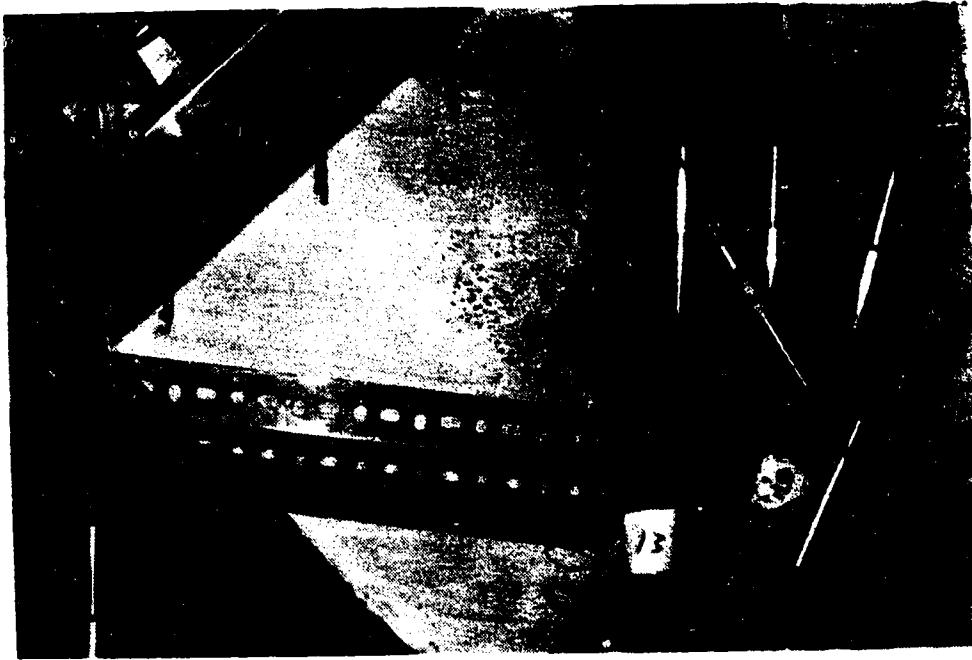
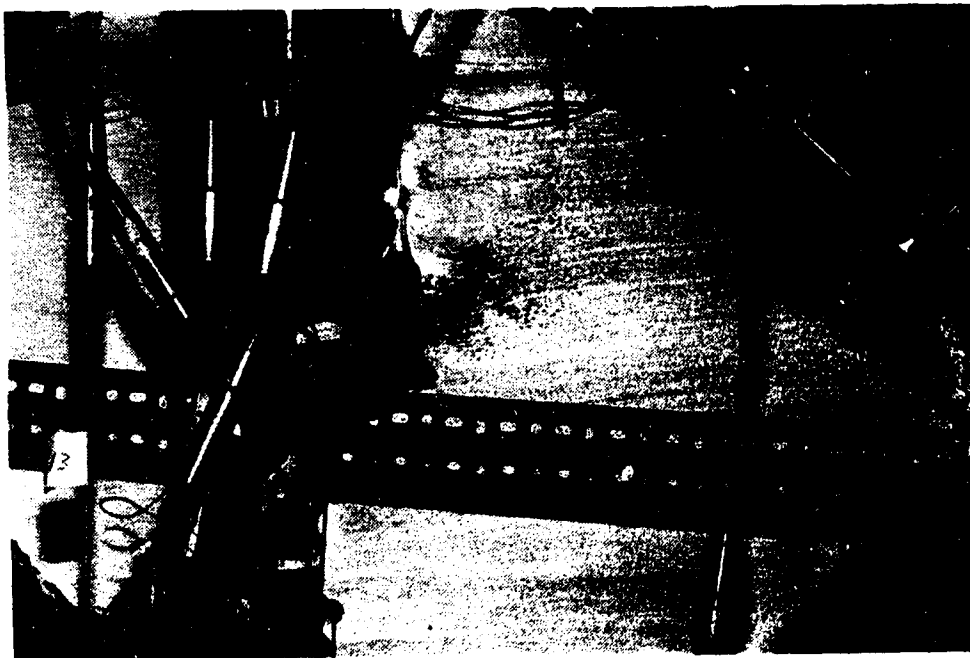


Fig. 4.16 Load vs. Out-of-Plane Displacement at Mid-Length of Long Free Edge for Specimen SP2 - With Restraint



**Fig. 4.17 Yield Lines Observed Near South Corner of Splice for Specimen SP1 - With Restraint**



**Fig. 4.18 Yield Lines Observed Near North Corner of Splice for Specimen SP1 - With Restraint**

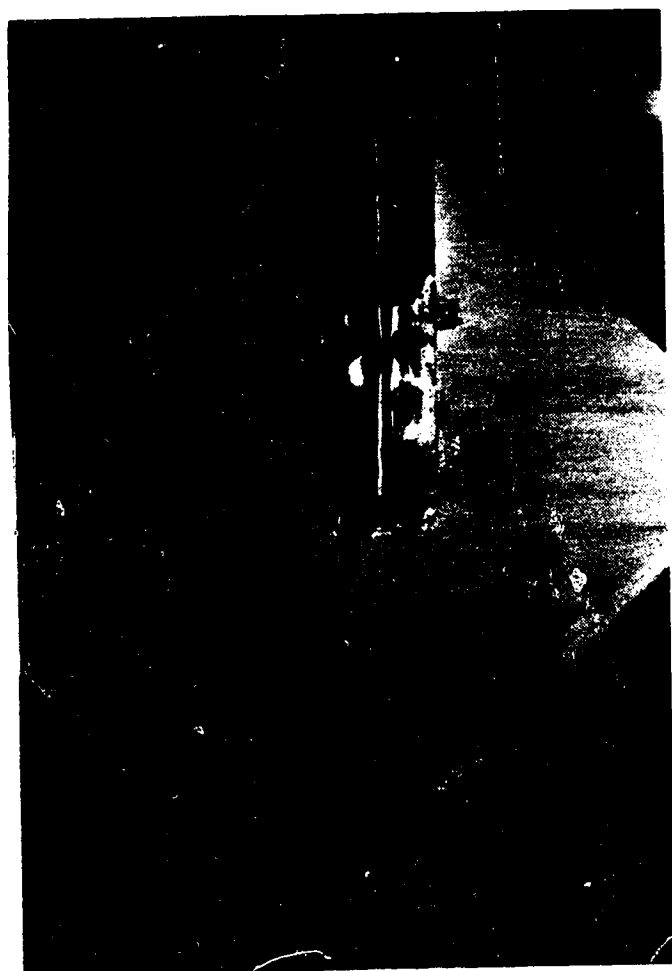


**Fig. 4.19 Yield Lines for Specimen SP1 - With Restraint**

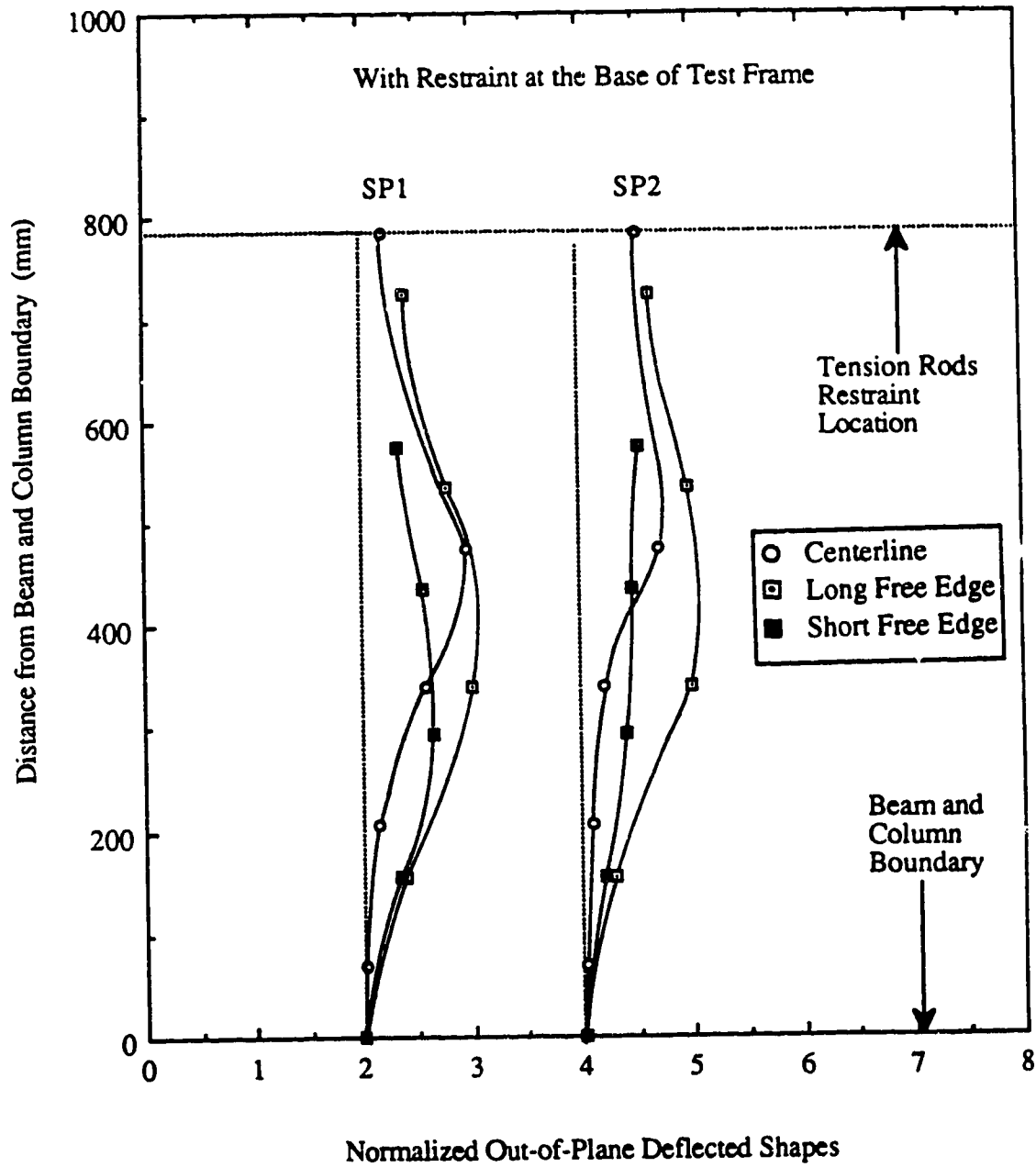


Fig. 4.20 Out-of-Plane Deflected Shapes at Free Edges and Along Centerline of Splice for SP Type Specimens - With Restraint

## **5. TEST RESULTS OF AP TYPE SPECIMENS**

### **5.1 General**

The AP set of specimens was employed to study the effects of the brace angle on the behavior and ultimate load of the gusset plate connections. The same plate geometry as that of the GP type specimens was used for the AP type specimens. It should be noted that the scheme II test setup was employed to perform the tests. A 30° brace angle was chosen for the AP type specimens, such that comparison could be made with the GP type specimen, which has a 45° brace angle. Three gusset plate thicknesses with a similar splice member as that of the GP specimens were tested. The test results of the AP type specimens are shown in Table 5.1. The failure mode of the specimens was sway buckling with the bracing member deflected out-of-plane.

### **5.2 Behavior of Load versus In-Plane Deformation**

As described in the previous chapter, an LVDT was attached to the bottom of the splice member to record the vertical deformation of the specimen. However, for specimens AP1 and AP3, this LVDT did not function properly during testing. Nonetheless, testing for these two specimens was continued since the applied load was significantly high when the LVDT malfunctioned. On the other hand, the LVDT performed normally during the testing of specimen AP2. Therefore, for specimens AP1 and AP3, readings recorded from the LVDT's attached to the hydraulic rams to measure the vertical stroke were used to examine the behavior of load versus vertical deformation of the specimen. However, it should be noted that the measurements of the LVDT's also included the elastic deflections of the reaction beam and channels.

The curves of load versus vertical stroke of the hydraulic rams are illustrated in Figs. 5.1 to 5.3. As can be seen from the figures, the strokes from both hydraulic rams were

maintained quite close to each other except at the final stage of loading. Fig. 5.1 shows that a bolt slip occurred at load levels of about 1000 kN and 1350 kN. However, no bolt slip was recorded for specimens AP2 and AP3. In general, a nonlinear load deflection behavior was observed for the specimens at the initial loading stage due to the settling of the test fixtures. Subsequently, a linear load deflection was observed for the specimens until the applied load reached the corresponding Whitmore load level, at which point nonlinear behavior began as shown in the figures. After reaching the ultimate load, a drop in the applied load without a significant increase in the strokes was observed. For specimens AP2 and AP3, the rate of unloading decreased as the strokes increased. The curve of load versus in plane deformation measured at the end of splice by an LVDT for specimen AP2 is shown in Fig. 5.4. The curve shows that, except in the early loading stage the load deflection behavior was linear until the applied load reached the Whitmore load level at 930 kN. From then on nonlinear behavior was observed until ultimate load was reached. When comparing Figs. 5.2 to 5.4, it can be seen that about 7 mm of elastic deflection of the reaction beams was recorded. However, the general behavior of these two curves was quite similar.

### **5.3 Behavior of Load versus Out-of-Plane Displacement**

The curves of load versus the out-of-plane displacement of the gusset plate at the conjunction of gusset-to-splice are shown in Figs. 5.5 to 5.7. As can be seen from Fig. 5.5, a discontinuity of the load deflection curve was observed for specimen AP1. This discontinuity was caused by a sudden vibration which occurred during the bolt slip. The recorded bolt slip has been discussed in the previous section. In general, a linear load deflection behavior was observed for the specimens until the applied load was close to the ultimate load. Both specimens AP1 and AP2 were able to maintain the load level close to the ultimate load after buckling occurred, except for specimen AP3, which showed an appreciable decrease in the ultimate load. This may be because specimen AP3 had a

relatively low bending rigidity compared to specimens AP1 and AP2. Hence, when buckling occurred, the yielding of specimen AP3 progressed rapidly and the applied load therefore dropped quickly after the specimen reached the ultimate load. The final out-of-plane displacement for all the specimens was approximately 25 mm, which is the physical limit of the measuring LVDT.

#### **5.4 Strain Gauge Results**

The strain readings at the mid-length of the free edges and the area underneath the splice member were examined. Again, strain readings at the free edges indicated that elastic strain distribution occurred in the vicinity of the free edges prior to when the ultimate load was reached. The curves of load versus strain at the mid-length of the long free edge are shown in Figs. 5.8 to 5.10. These figures show that a linear behavior was observed until the applied load was close to the ultimate load. As can be seen from the figures, strain readings from both sides of the specimen were similar at the early loading stage. However, as load increased, these strain readings deviated from each other. When the load increased to the ultimate load level, strain bifurcation occurred, as illustrated by the figures. Strain readings at the short free edge show that compressive strains were recorded in the initial stage of loading. However, as loading progressed, unloading was observed in the vicinity of the short free edge, and eventually, tensile strains were recorded as illustrated typically in Fig. 5.11 for specimen AP3. This unloading behavior was probably caused by the in-plane bending of the plate. Since these specimens were tested with a brace angle of  $30^\circ$ , the horizontal component of the applied load might be significant in causing this in-plane bending behavior. The curves of load versus strain recorded at the center gauges of the rosette are shown in Figs. 5.12 to 5.14. These two gauges recorded the strain readings from both sides of the plate. It can be seen from these figures that the out-of-plane bending of the plate, which was probably due to the initial imperfection, occurred at an early stage

of loading. In particular, specimen AP3 showed nonlinear behavior from the beginning of loading.

### **5.5 Yielding Behavior of Specimens**

The general yield pattern of the AP type specimens was similar to that of the GP type specimens. However, for the AP type specimens, the yield lines were first observed close to the beam and column boundary. For specimen AP1, the yield lines underneath the splice member were recorded at about 58 percent of the ultimate load. Again, as loading progressed, the yielding was spread about the two sides of the splice member. However, only moderate yielding was observed about the side of the splice member close to the long free edge. On the other hand, significant yielding was recorded about the other side of the splice member near the short side free edge. Extensive yielding was observed underneath the splice member, and yielding about the side of the splice member close to the short free edge progressed significantly at a load level of approximately 85 percent of the ultimate load. The failed specimen AP1, which indicated severe yielding occurred in the area of the short side free edge, is shown in Fig. 5.15. Figure 5.16 illustrates the other side of the failed specimen AP1, which showed the severity of the yielding. The yield lines similar to that of GP type specimens were also observed along the beam and column boundary and at the mid-length of the long free edge of the failed specimens, as shown typically in Figs. 5.15 and 5.16.

The yielding process and pattern for specimen AP2 were similar to that of specimen AP1. However, yielding underneath the splice member was detected at about 45 percent of the ultimate load. Again, extensive yielding was recorded in the area of the short side free edge. The failed specimen AP2 also indicated that severe yielding occurred in the area underneath the splice member. Figures 5.17 and 5.18 illustrate the failed specimen of AP2 with the presence of the yield line mechanism along the beam and column boundary and at



the mid-length of the long free edge. For specimen AP3, the flaking of whitewash underneath the splice member was observed at a load level of about 80 percent of the ultimate load. Again, as the load increased yielding occurred about the two sides of the splice member. The failed specimen indicated that only moderate yielding existed underneath the splice member when it was compared to that of specimens AP1 and AP2. However, extensive yielding similar to that of specimens AP1 and AP2 in the area of the short free edge was recorded for specimen AP3. Again, yield lines developed along the beam and column boundary and at the mid-length of the long free edge.

#### **5.6 Out-of-Plane Deflected Shapes of Free Edges and along Centerline of Splicing Member**

The normalized out-of-plane deflected shapes of the specimens are shown in Fig. 5.19. It can be seen from the figure that the maximum deflection occurred at the long free edge. In general, the deflected shapes resembled the buckled shape of a fixed-guided column. The deflected shapes for specimens AP1 and AP2 indicated that significant rotation occurred at the beam and column boundary due to severe yielding. The deflected shape of the long free edge for specimen AP3 also showed a slight local bending near the mid-length. A picture of the out-of-plane deflected shape along the long free edge of specimen AP2 is shown in Fig. 5.20.

Table 5.1 Test Results of AP Type Specimens

Specimen Designation	Plate Size (mm x mm x mm)	Ultimate Load (kN)	Whitmore Load $P_w$ (kN)	Thornton Load $P_t$ $k = 0.65$ (kN)
AP1	500 x 400 x 13.3	1720	1216	1119
AP2	500 x 400 x 9.8	1210	930	801
AP3	500 x 400 x 6.5	728	555	404

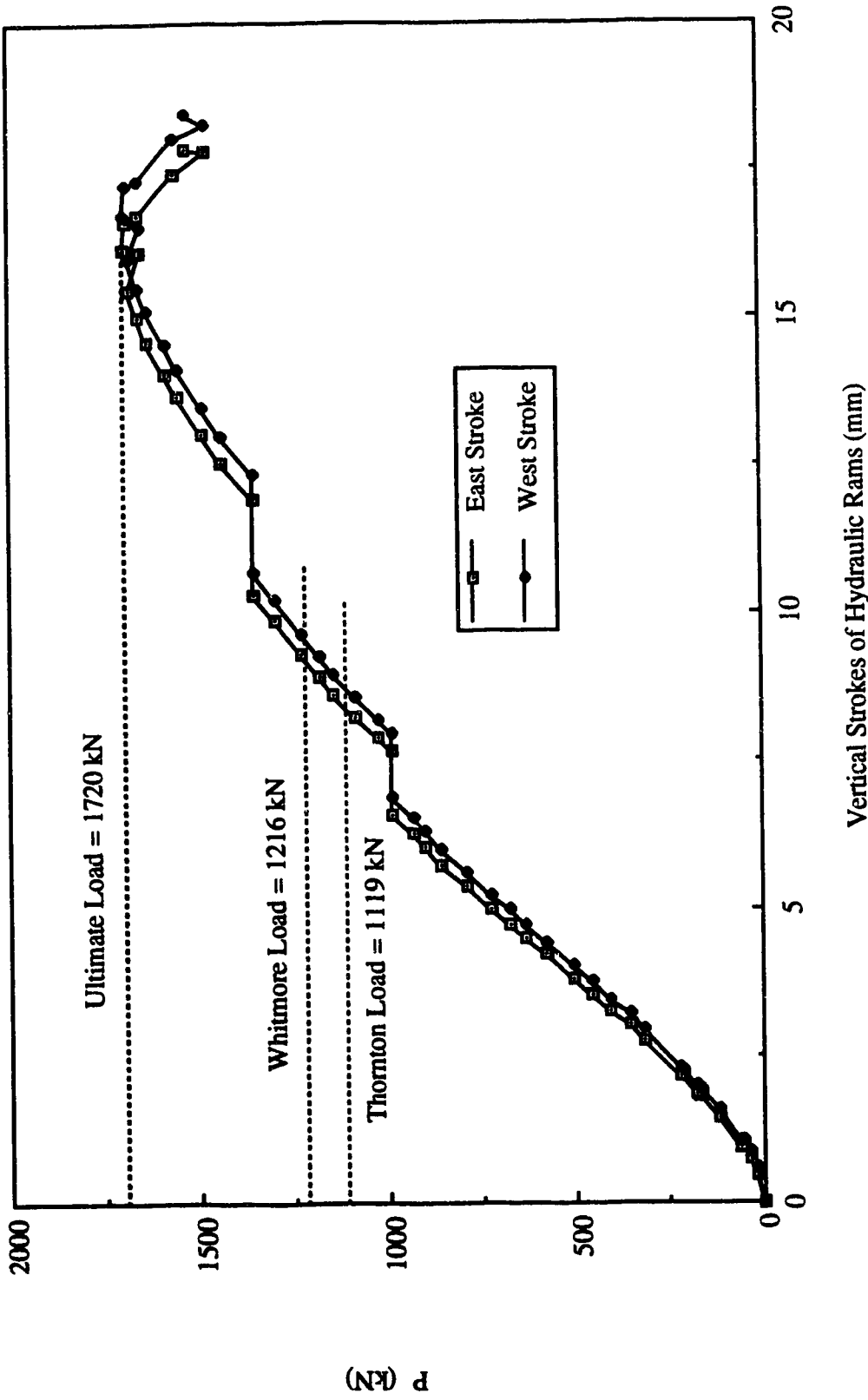


Fig. 5.1 Load vs. Vertical Strokes of Hydraulic Rams for Specimen AP1

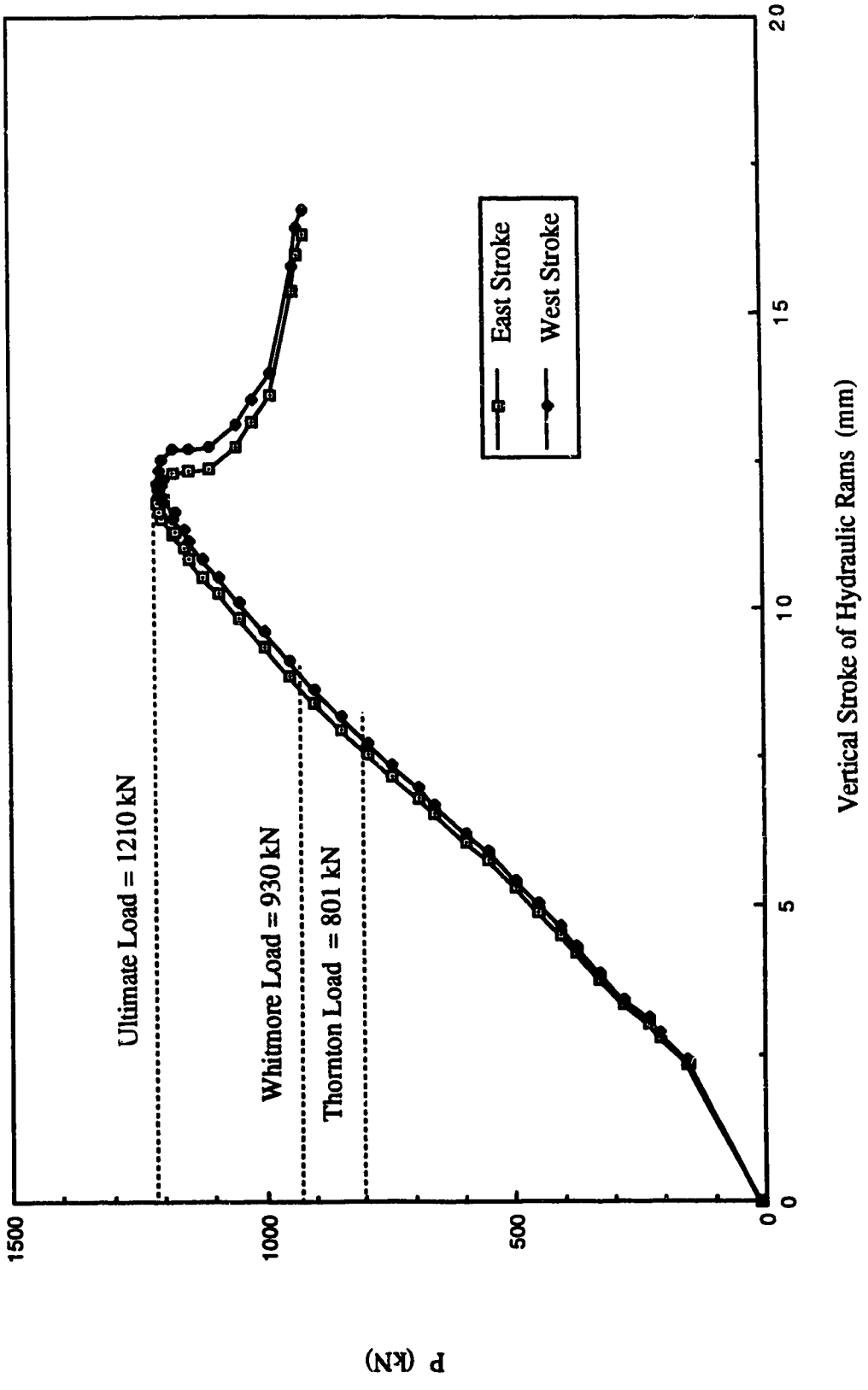


Fig. 5.2 Load vs. Vertical Strokes of Hydraulic Rams for Specimen AP2

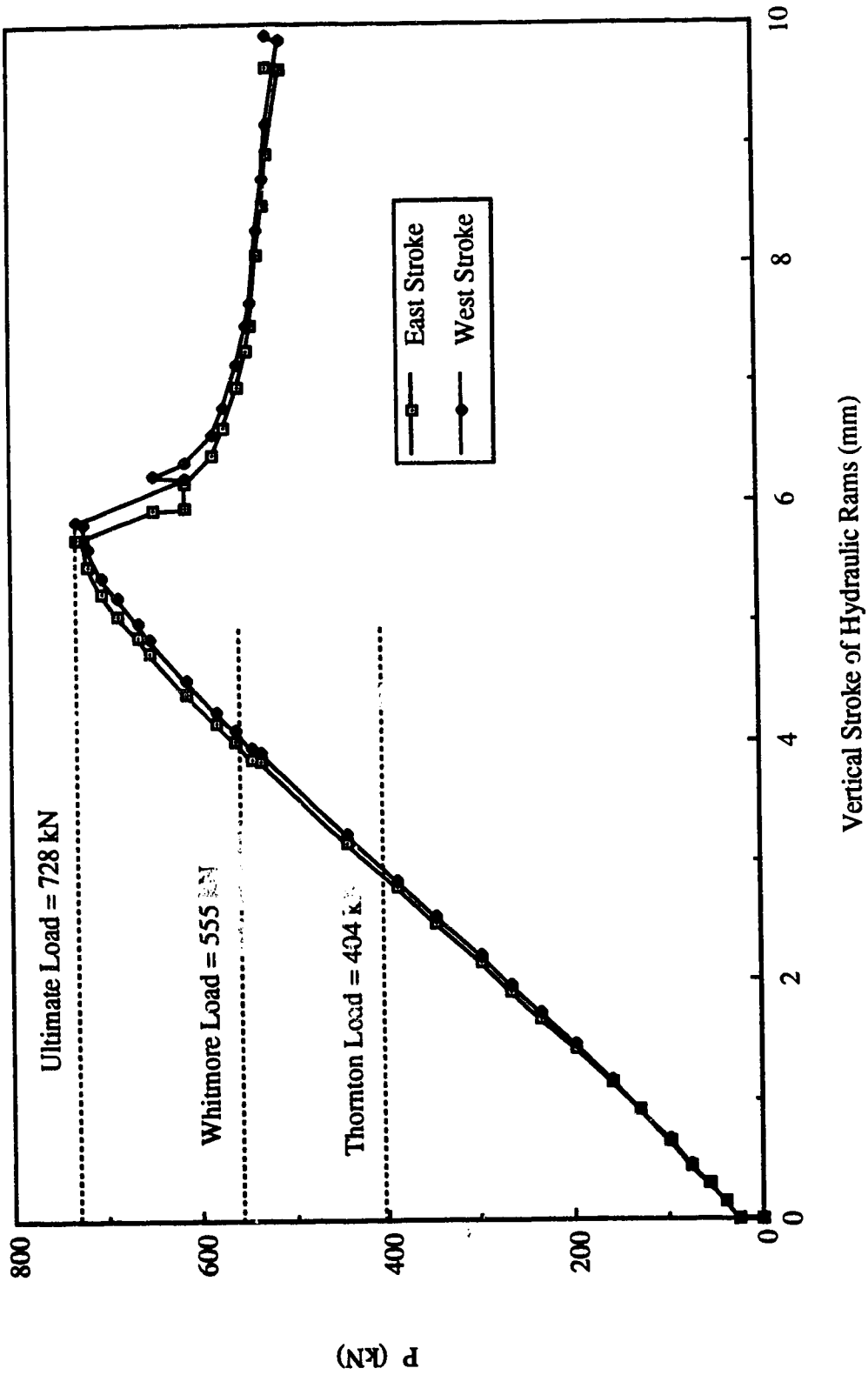
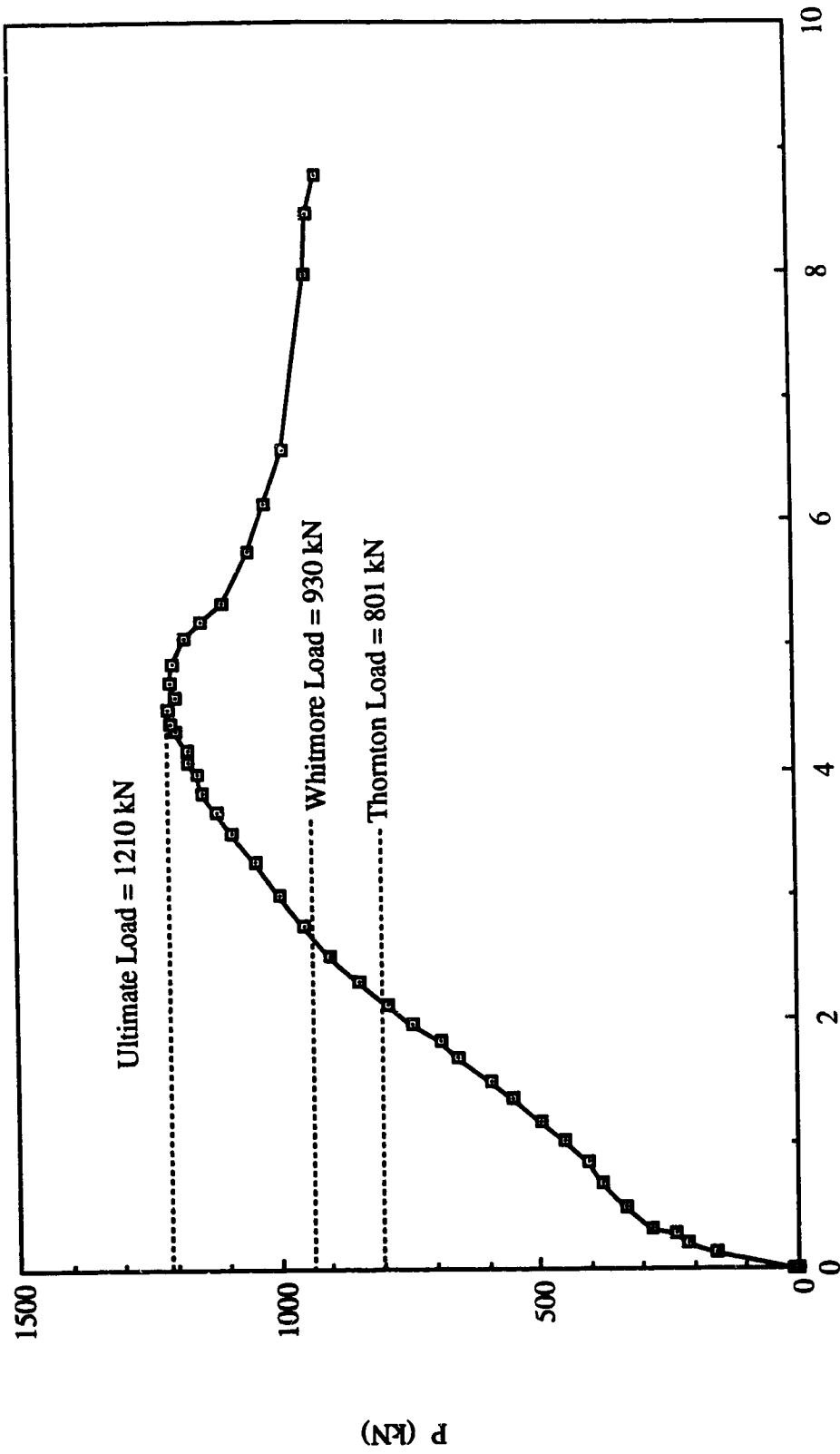
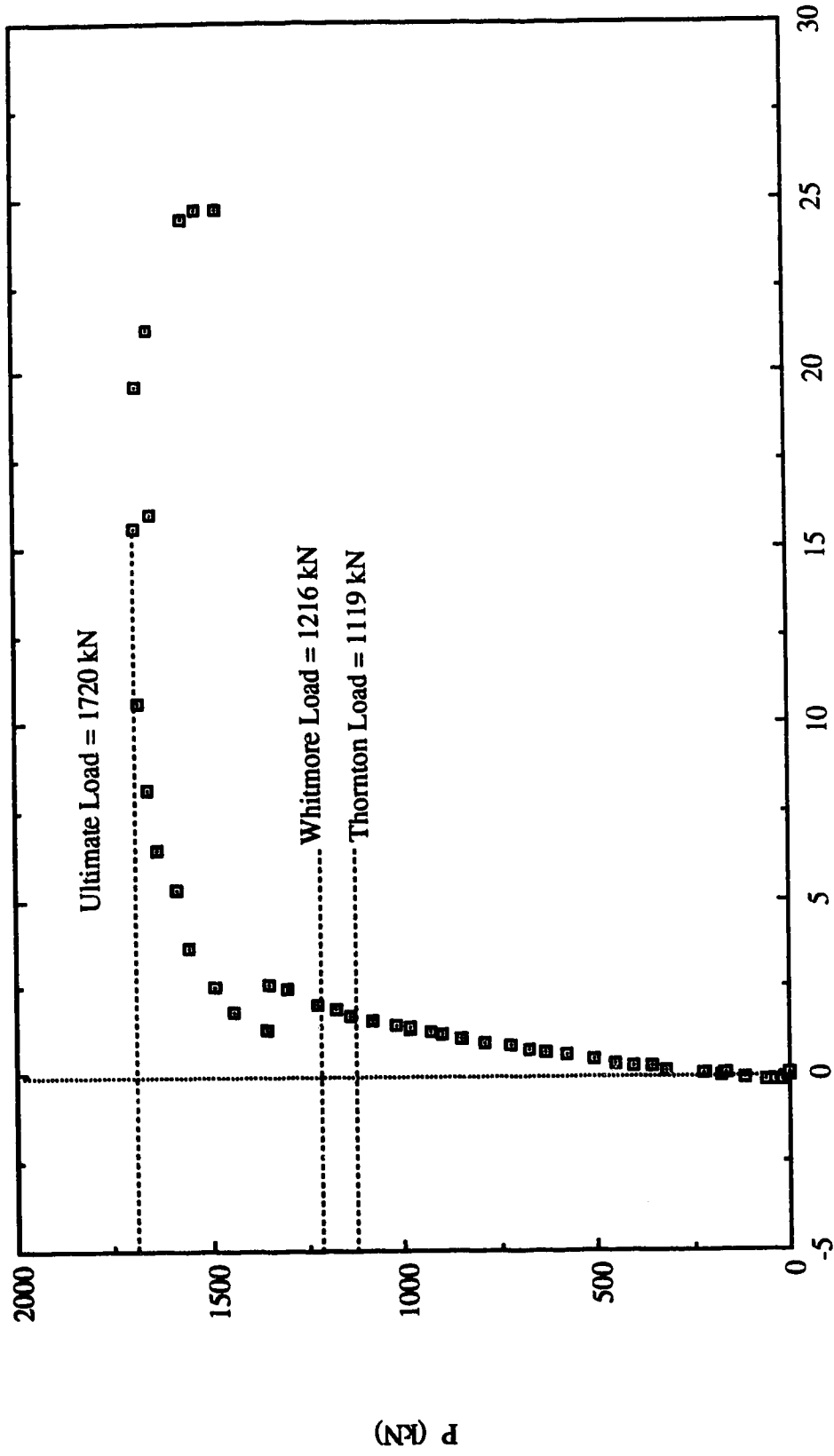


Fig. 5.3 Load vs. Vertical Stroke of Hydraulic Rams for Specimen AP3



Vertical Deformation of Specimen Measured at End of Splice (mm)  
 Fig. 5.4 Load vs. In-Plane Deformation Measured at End of Splice for Specimen AP2



Out-of-Plane Displacement at Conjunction of Gusset-to-Splice (mm)

Fig. 5.5 Load vs. Out-of-Plane Displacement at Conjunction of Gusset-to-Splice for Specimen AP1

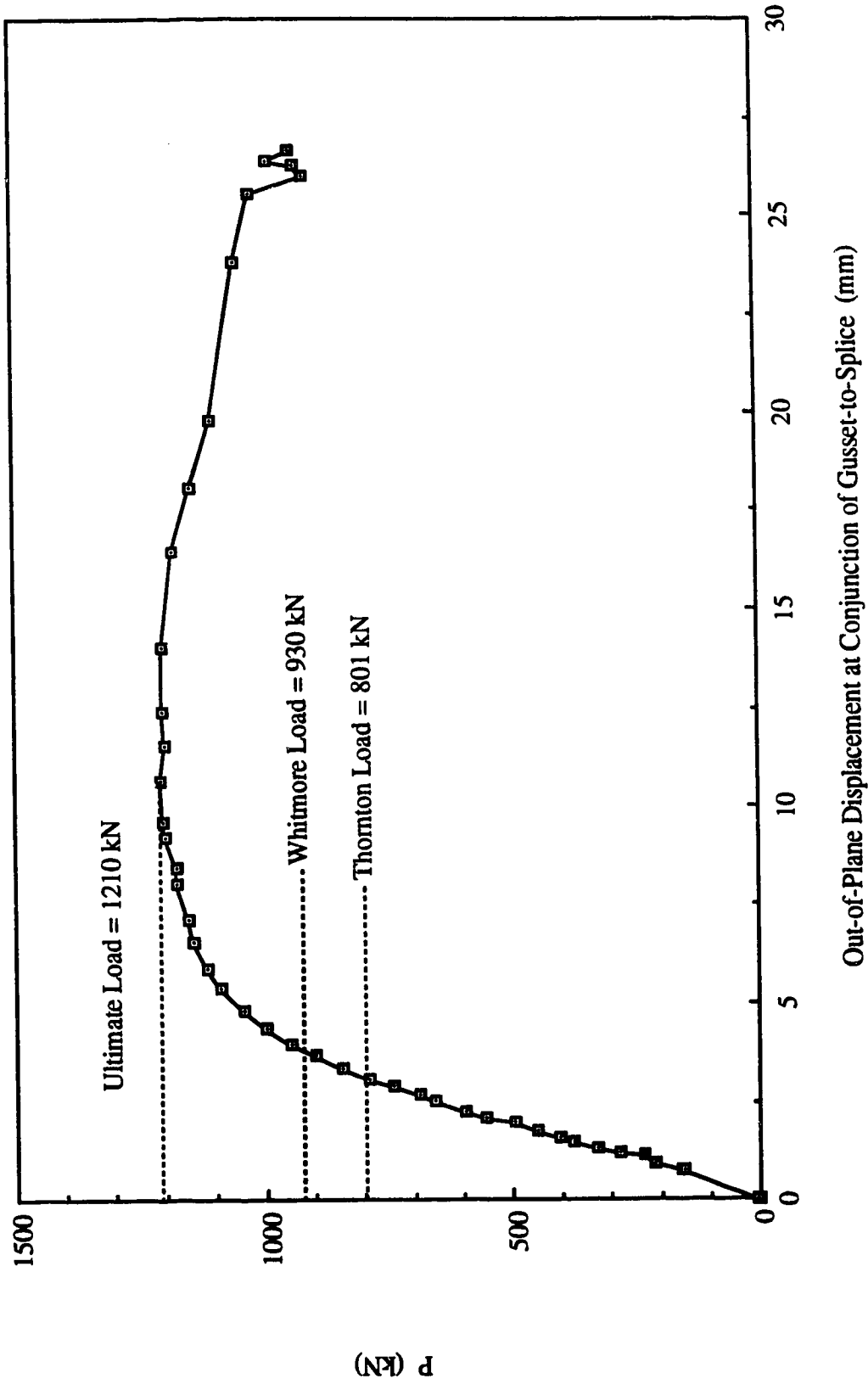
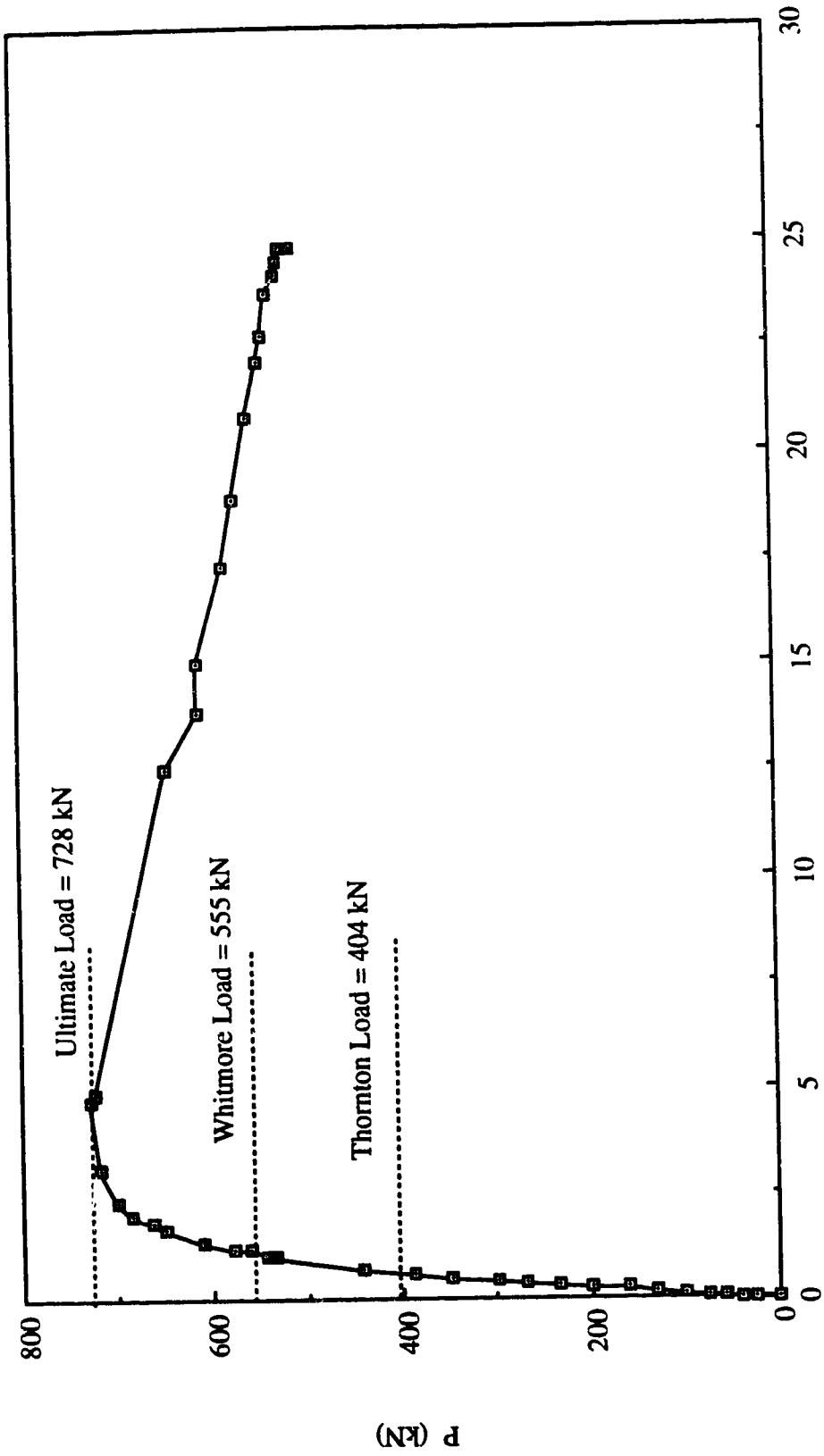


Fig. 5.6 Load vs. Out-of-Plane Displacement at Conjunction of Gusset-to-Splice for Specimen AP2





Out-of-Plane Displacement at Conjunction of Gusset-to-Splice (mm)

Fig. 5.7 Load vs. Out-of-Plane Displacement at Conjunction of Gusset-to-Splice for Specimen AP3

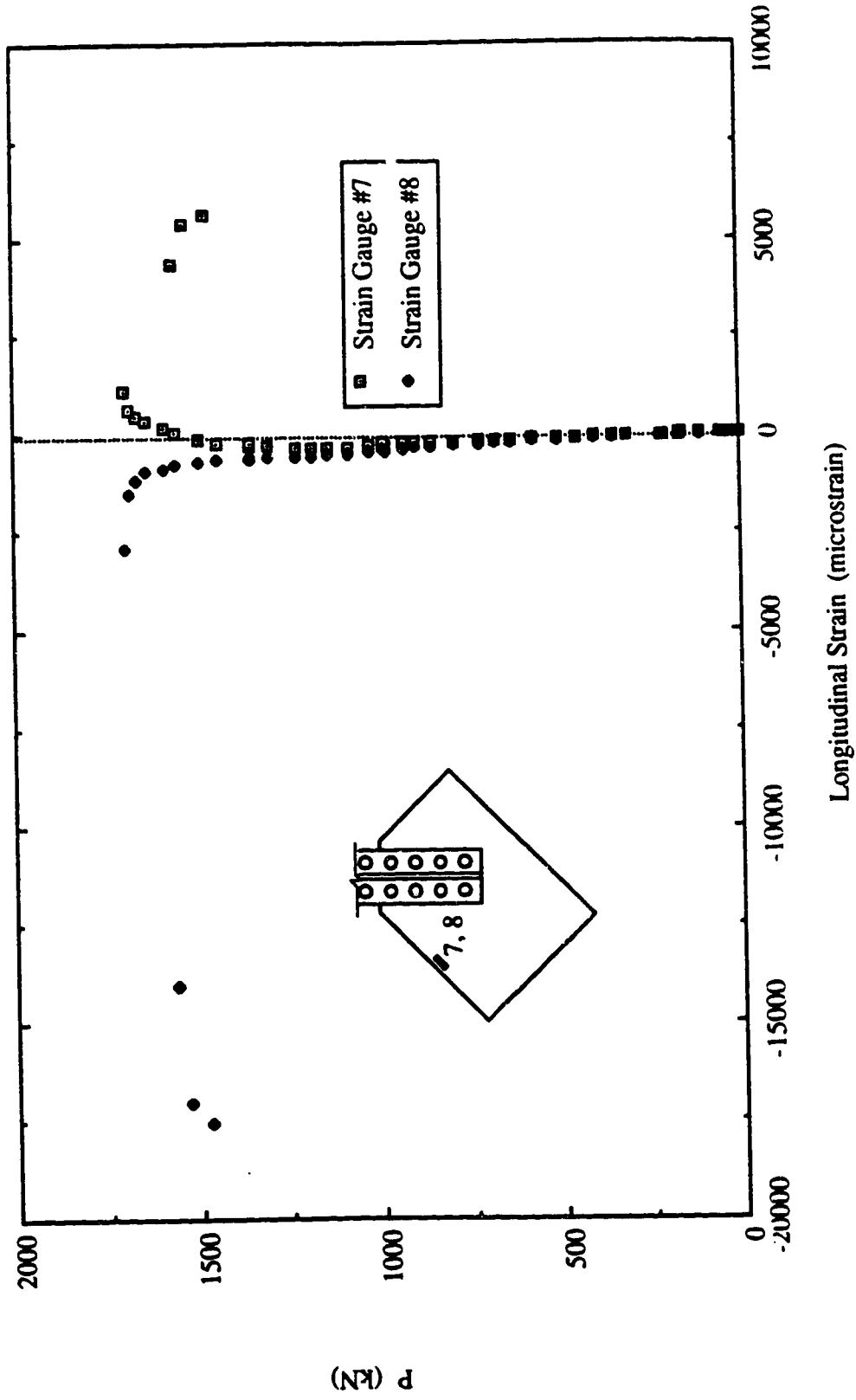


Fig. 5.8 Load vs. Strain Gauge Readings at Mid-Length of Long Free Edge for Specimen AP1

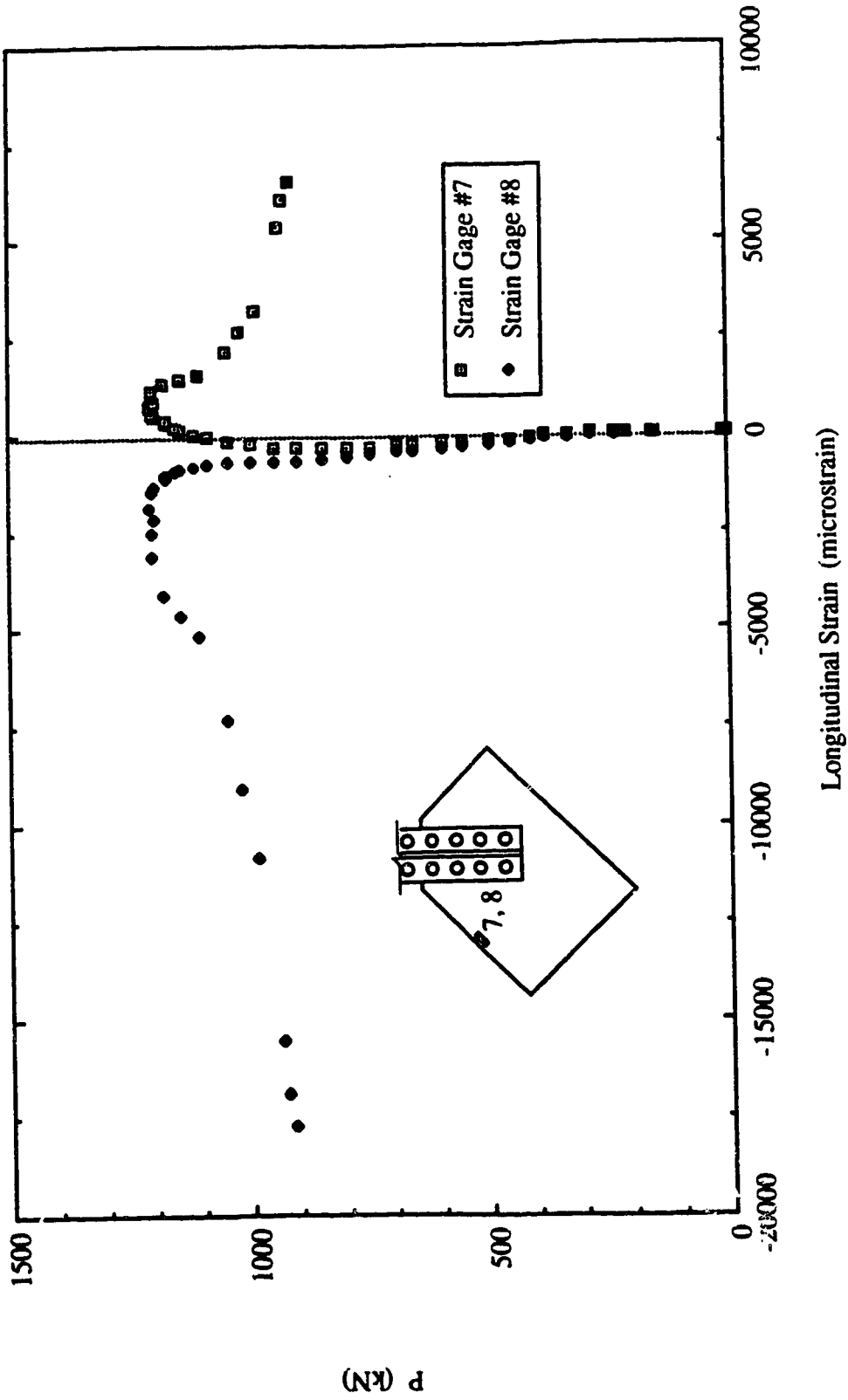


Fig. 5.9 Load vs. Strain Gauge Readings at Mid-length of Long Free Edge for Specimen AP2

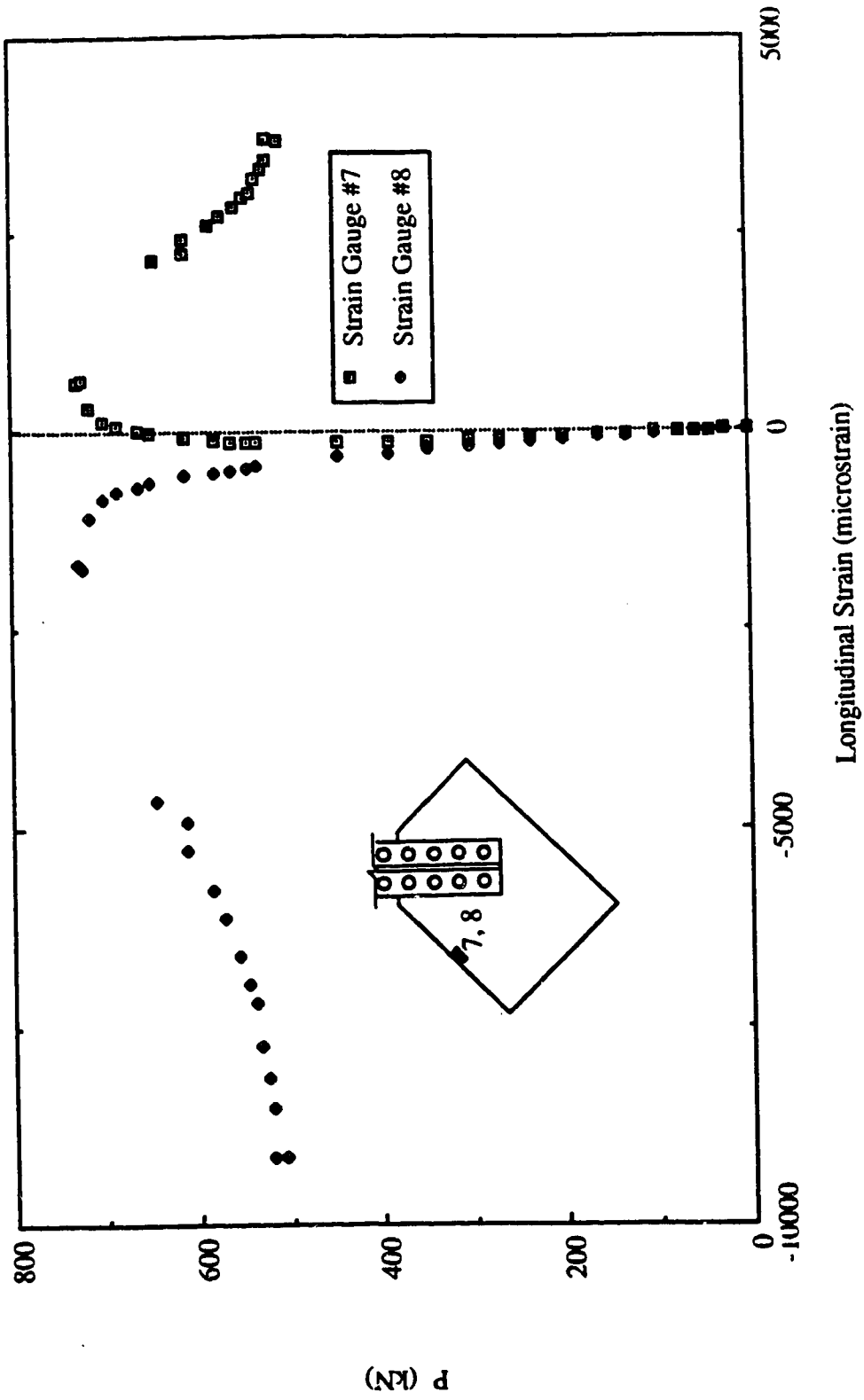


Fig. 5.10 Load vs. Strain Gauge Readings at Mid-Length of Long Free Edge for Specimen AP3

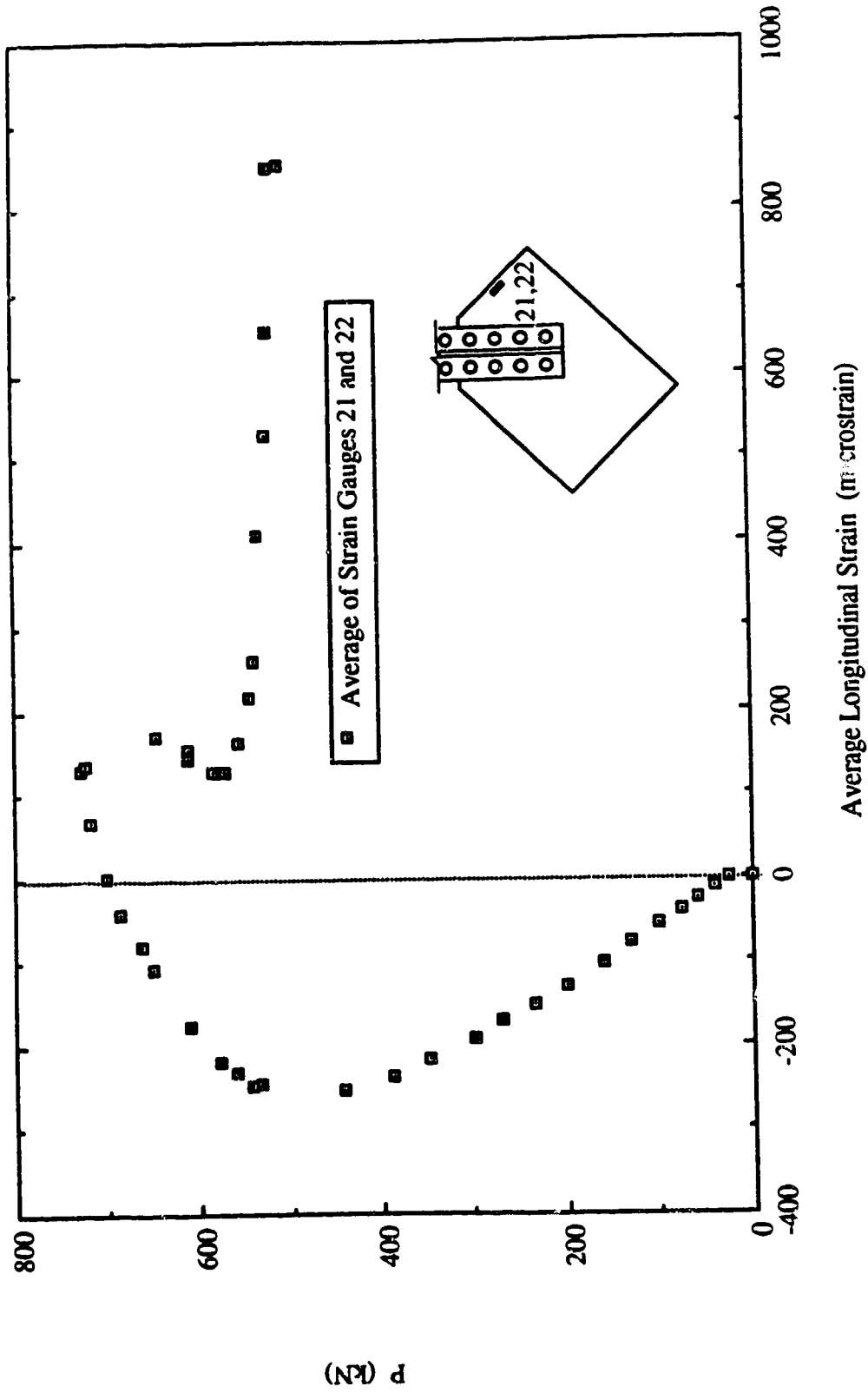


Fig. 5.11 Load vs. Average Strain Gauge Readings at Mid-Length of Short Free Edge for Specimen AP3

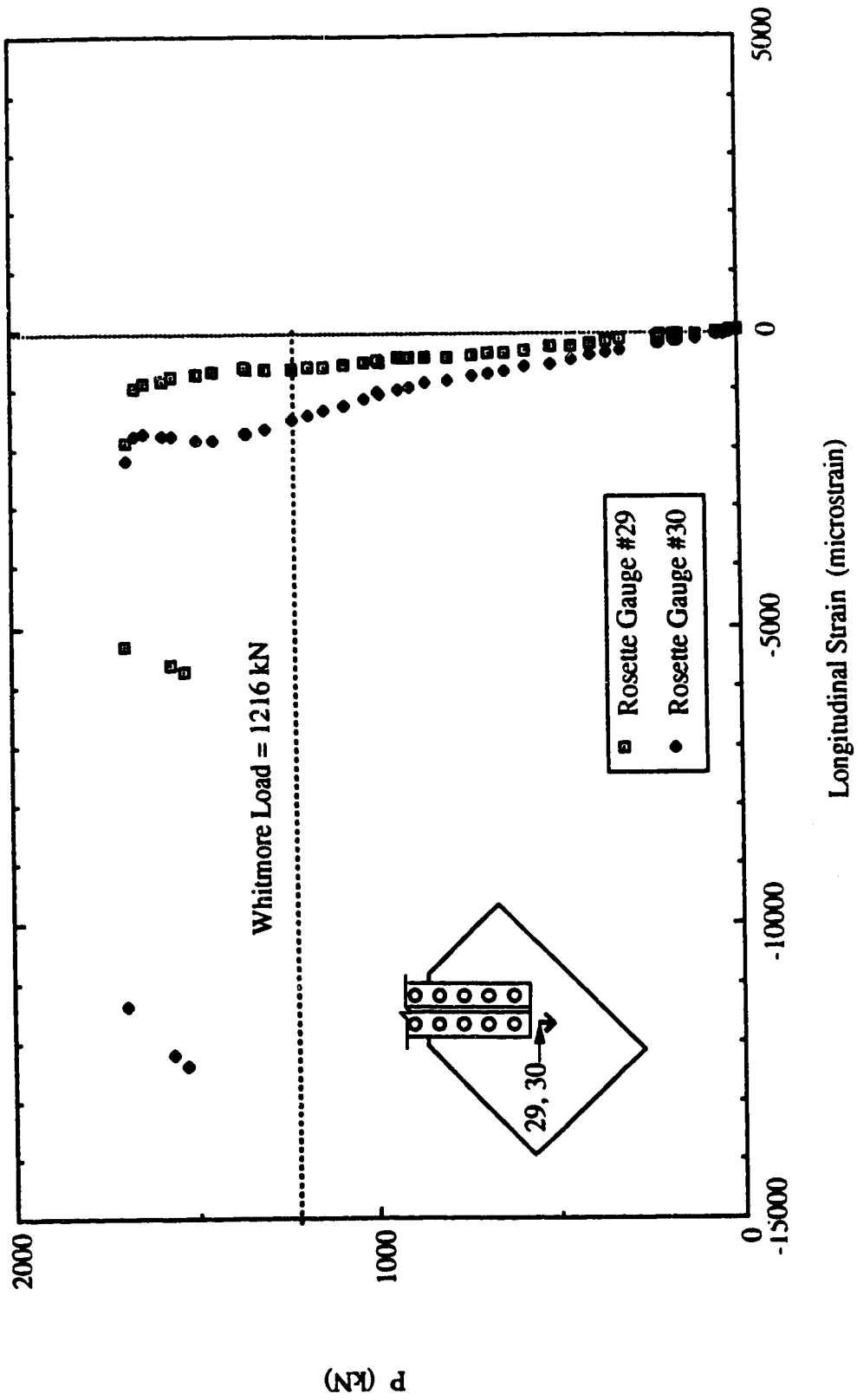


Fig. 5.12 Load vs. Rosette Gauge Readings for Specimen AP1

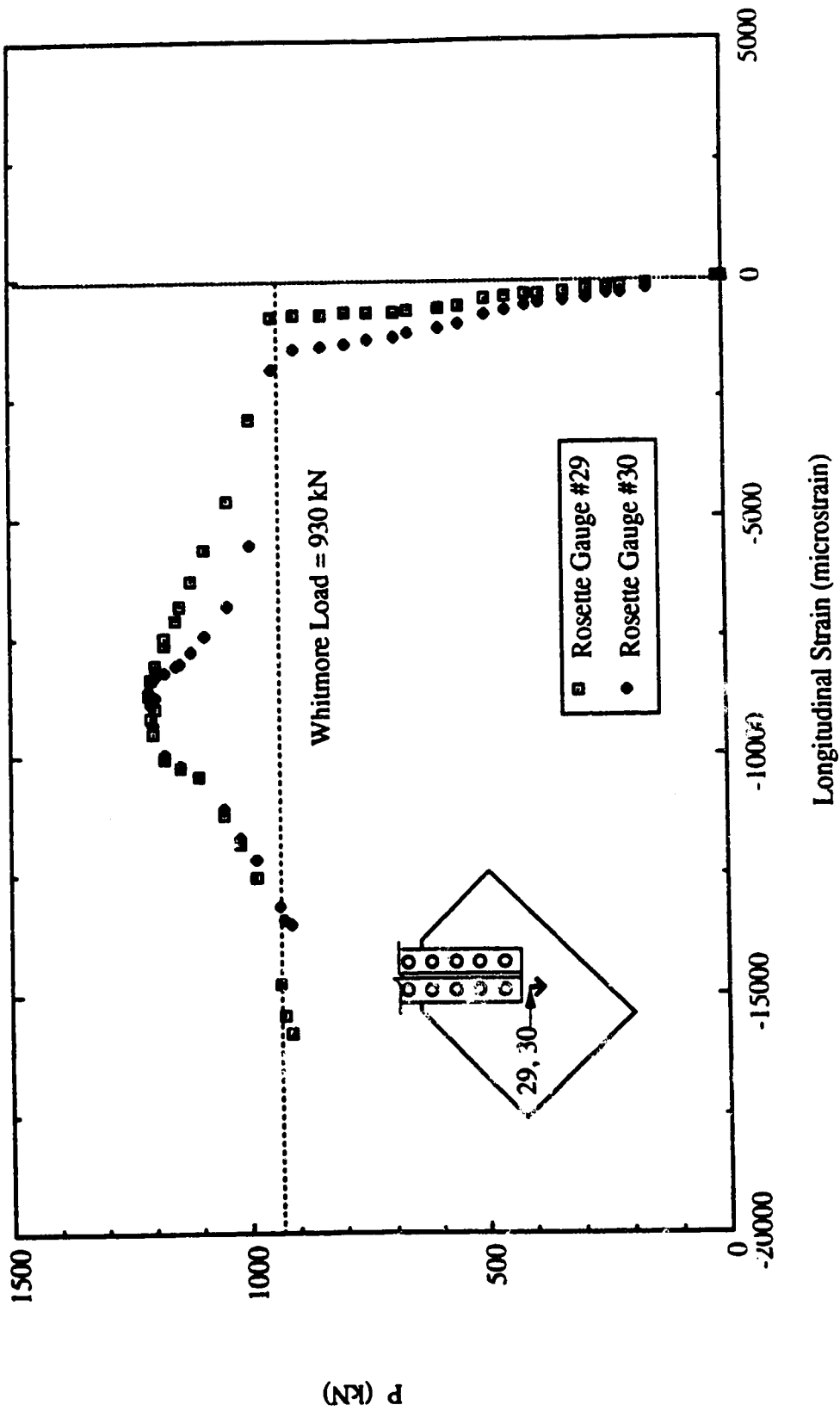


Fig. 5.13 Load vs. Rosette Gauge Readings for Specimen AP2

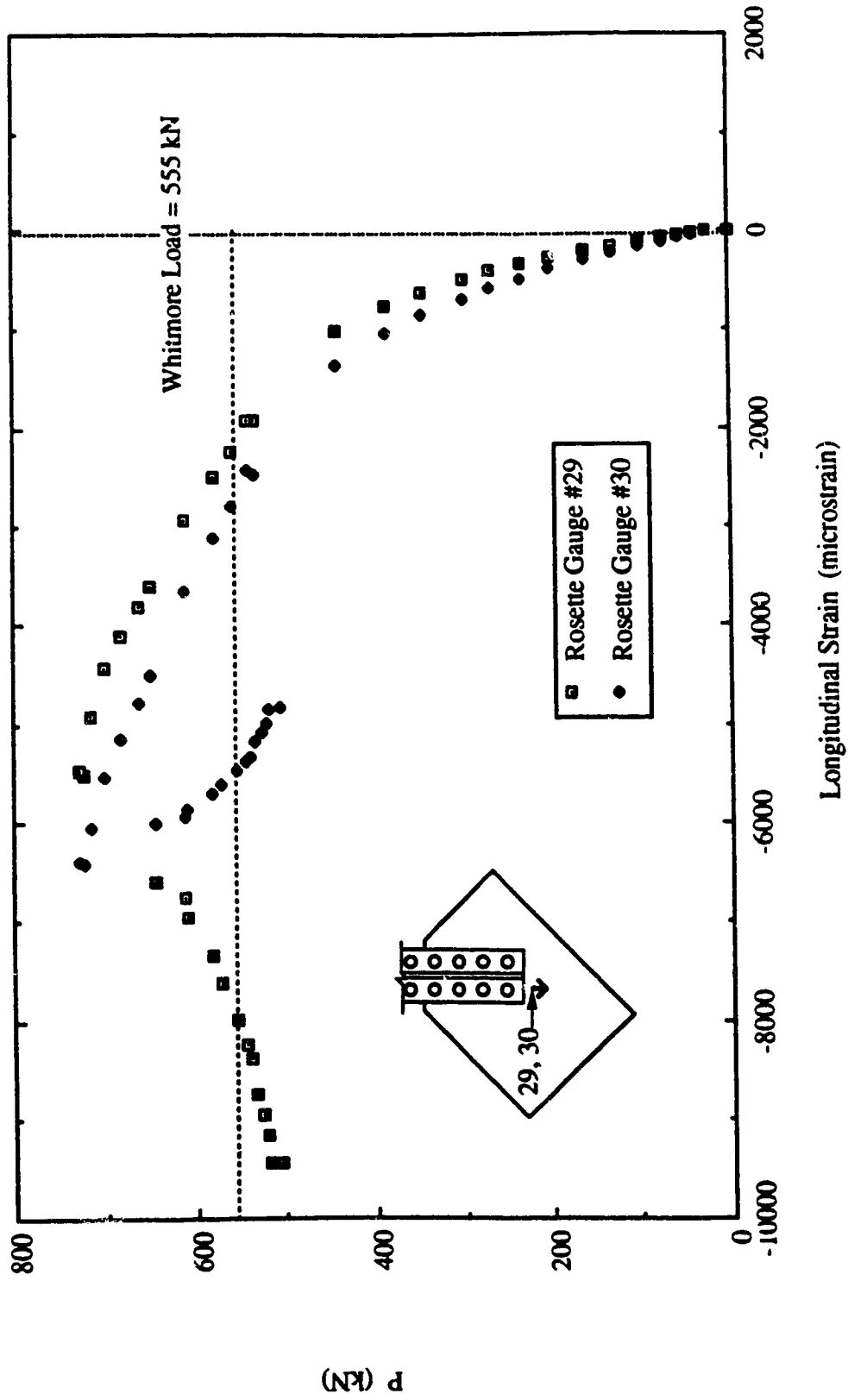
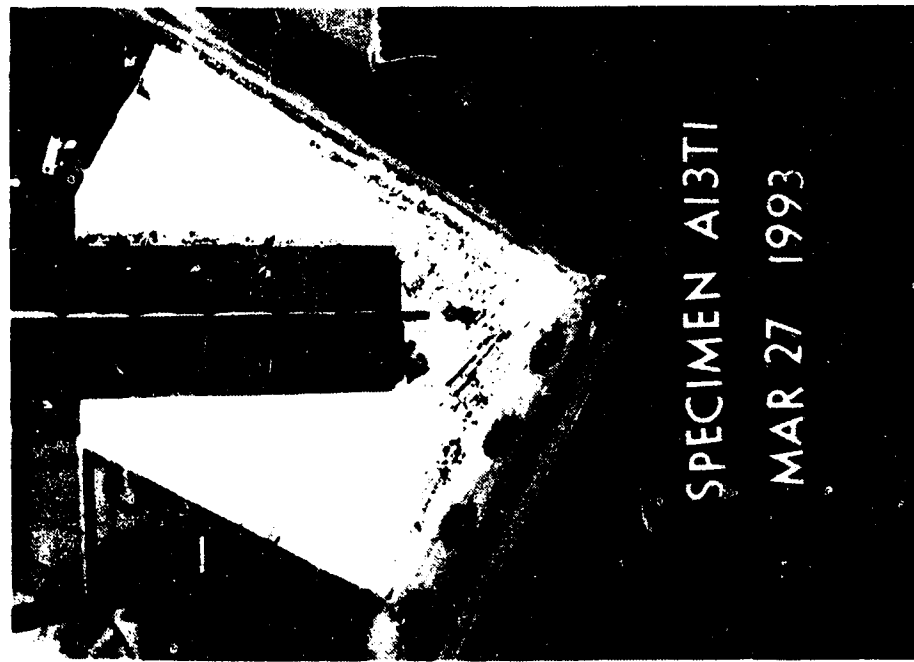


Fig. 5.14 Load vs. Rosette Gauge Readings for Specimen AP3





**Fig. 5.15 Yielding at West Side of Failed Specimen API**



**Fig. 5.16 Yielding at East Side of Failed Specimen API**

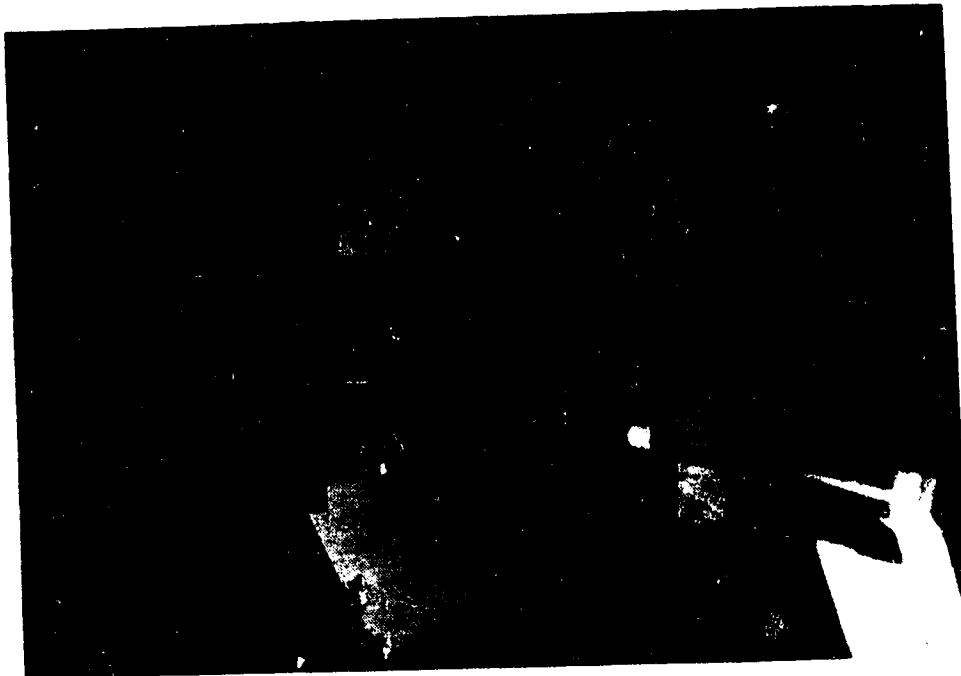


Fig. 5.18 Yielding at East Side of Failed Specimen AP2

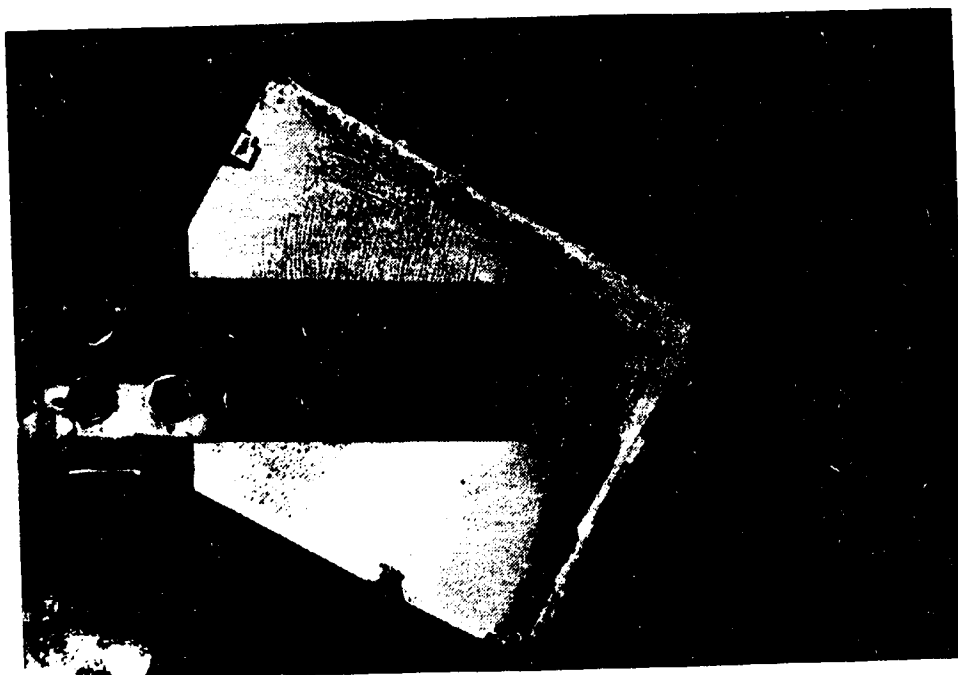


Fig. 5.17 Yielding at West Side of Failed Specimen AP2

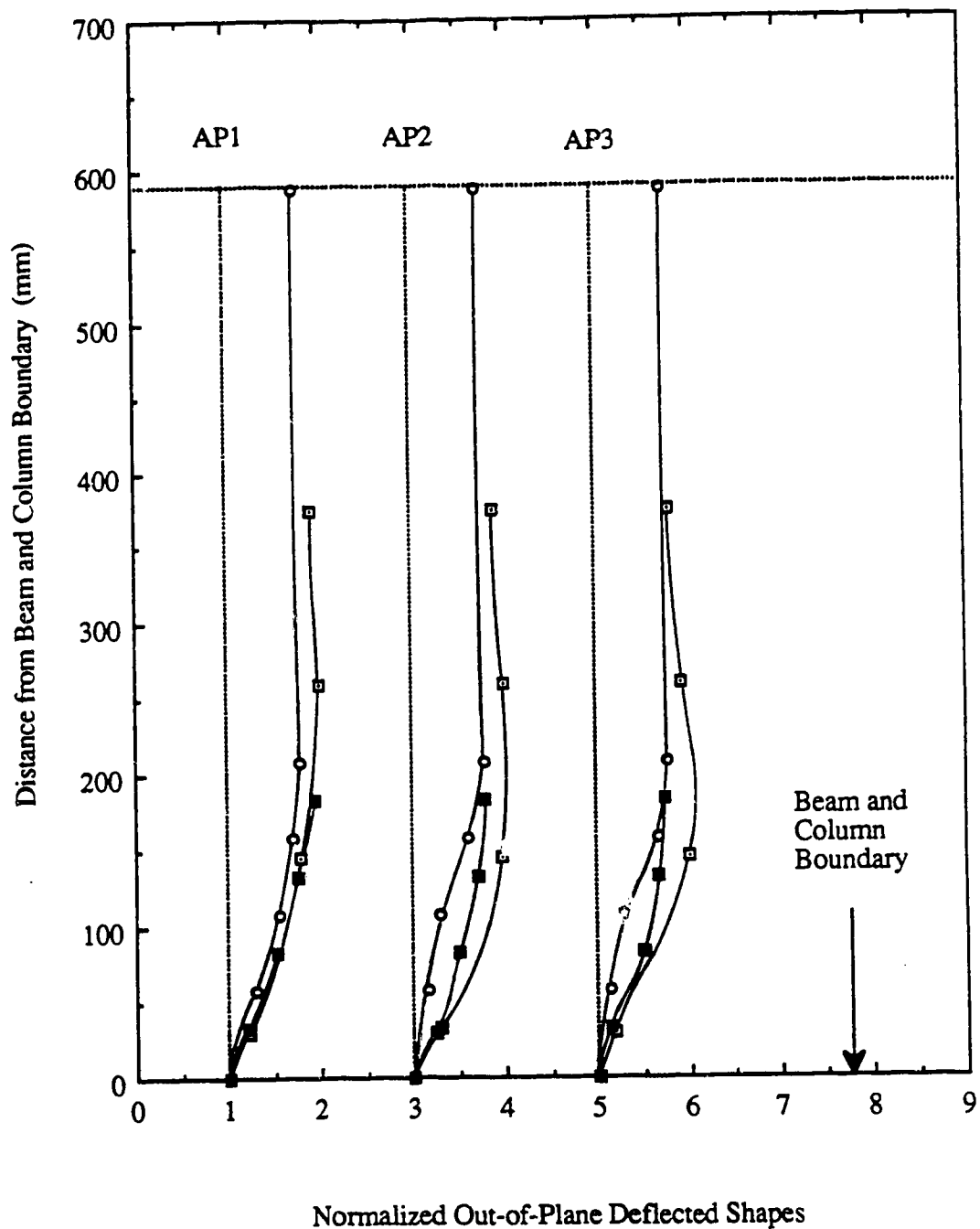
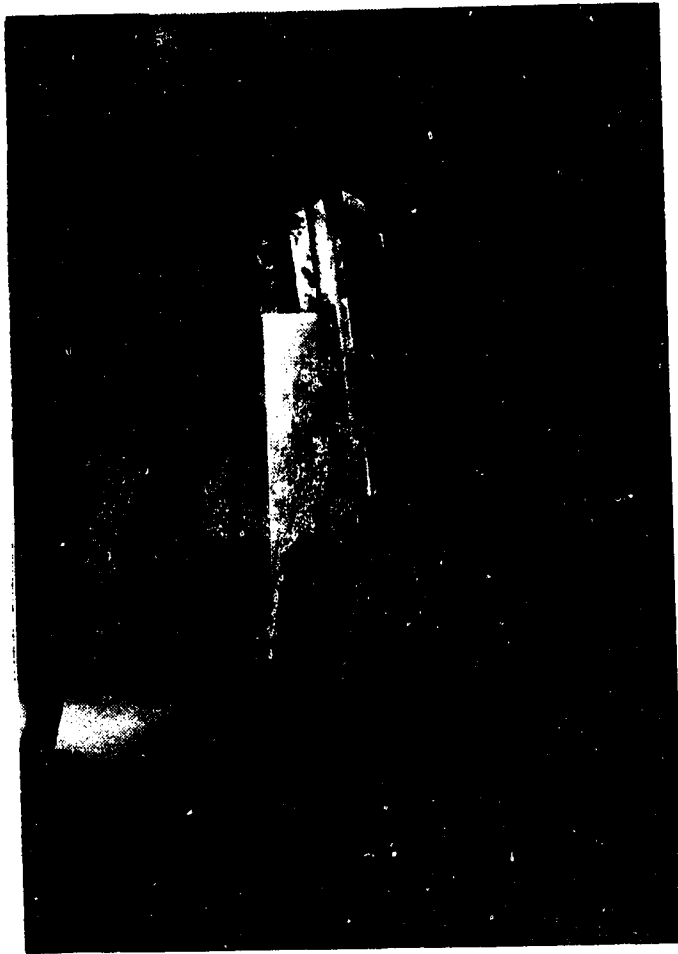


Fig. 5.19 Out-of-Deflected Shapes at Free Edges and Along Centerline of Splice for AP Type Specimens



**Fig. 5.20** Picture of Out-of-Plane Deflected Shapes at Long Free Edge for Specimen AP2

## **6. TEST RESULTS OF MP TYPE SPECIMENS**

### **6.1 General**

The test results of the GP, SP and AP types specimens described previously only concerned the compressive behavior of the gusset plate connection without the effects of beam and column moments. However, the delivery of compression to the gusset plate must involve the beam and column moments, shears and axial force. The MP type specimens were used in order to investigate the effects of the beam and column moments on the compressive behavior and ultimate strength of the gusset plate specimens. To study the effects of the beam and column moments, a specimen size and geometry similar to that of the GP type specimens were used for the MP type specimens. It will be recalled that the beam and column moments used for specimens MP1, MP2 and MP3 were 250 kN·m and 125 kN·m respectively. For specimen MP3A, higher beam and column moments of 375 kN·m and 187.5 kN·m were applied. Finally, specimen MP3B was tested without beam and column moment. The test results of the MP type specimens are summarized in Table 6.1. Again, the failure mode of specimens was the sway buckling of the connection.

### **6.2 Behavior of Load versus In-Plane Deformation**

The curves of load versus in-plane vertical deformation of the specimen and load versus vertical displacement of the hydraulic rams are shown in Figs. 6.1 to 6.10. It should be noted that the vertical deformation of the specimen was recorded by an LVDT attached to the end of the splice member. For specimen MP1, the curve of in-plane deformation illustrated the occurrence of bolt slips during testing. The first bolt slip was recorded at a load level of about 700 kN, when a drop in applied load accompanied by an increase in vertical displacement was observed. However, for the curve of vertical displacement of the hydraulic rams a bolt slip occurred without a significant increase in vertical displacement. This was because there was a decrease in the applied load during the bolt slip; therefore, the

elastic deflection of the reaction beam was also decreased. Hence, the LVDT's attached to the hydraulic rams (supported by the reaction beam) moved downward during the bolt slip, while the core of the LVDTs still recorded the vertical displacement caused by the bolt slip. These two movements thus counteracted each other. Therefore, the LVDT's readings did not show a significant vertical displacement during this bolt slip. Bolts slips were again recorded as loading continued; however, both curves showed a similar vertical movement during these slips, since there was a negligible decrease in the applied load when the bolt slips occurred. The curve of in-plane deformation of the specimen also showed that the specimen started to behave nonlinearly at an applied load of about 1000 kN. When the applied load reached about 1600 kN, another bolt slip with a decrease in the applied load level was observed. As loading continued, the curve gradually turned to the ultimate load level. The unloading path of the specimen was not recorded since the out-of-plane displacement had already reached the physical limit of the measuring device. The curve for the vertical displacement of the hydraulic rams shows that an almost identical vertical movement was recorded for both rams during testing, and this was the objective of the loading system as mentioned in Chapter 2. It was also observed that the vertical displacement of the hydraulic rams was higher than the in-plane deformation of the specimen due to the elastic deflection of the reaction beam.

For specimen MP2, the nonlinear load deflection behavior of the load versus vertical displacement of the hydraulic ram and in-plane vertical deformation of the specimen were observed at a load level of about 500 kN, as shown in Figs 6.3 and 6.4. Figure 6.4 shows that the in-plane stiffness of specimen MP2 decreased rapidly, followed by the initial stage of nonlinearity. However, the in-plane stiffness was maintained once the applied load was increased to about 750 kN, at which an almost constant in-plane stiffness was observed until the specimen reached the ultimate load. Subsequently, a gradual unloading path was observed, and the specimen appeared to stabilize at a lower load level of about 900 kN. A similar behavior was observed for the curve of the load versus vertical displacement of

hydraulic rams. However, the degree of nonlinearity of the load deflection curve was less than that of the vertical displacement of the specimen due to the presence of the elastic deflection of the reaction beam.

In general, the behavior of the load versus vertical displacement of the hydraulic ram and the in-plane deformation of the specimen was similar for specimens MP3, MP3A and MP3B. However, the in-plane stiffness for specimen MP3B prior to its reaching the ultimate was relatively higher than that of specimens MP3 and MP3A. It was also observed that the in-plane stiffness for specimen MP3 was higher than that of specimen MP3A. This behavior was probably due to the effects of beam and column moments, and will be discussed in Chapter 8. The curves of load versus in-plane vertical deformation of the specimens show that nonlinear load deflection behavior for specimens MP3 and MP3A occurred at about 50 percent of the corresponding ultimate loads, as shown in Figs. 6.6 and 6.8. For specimen MP3B nonlinear behavior was observed at about 70 percent of the ultimate load, as illustrated in Fig. 6.10. Again, as loading continued, the curves gradually turned to the corresponding ultimate load levels. However, for specimen MP3A, a bolt slip was recorded at a load level of about 760 kN and the applied load dropped to approximately 710 kN before reaching the ultimate load level. A gradual unloading path was observed for the specimens, and these curves show that the specimens appeared to stabilize at a load level of about 450 kN.

### **6.3 Behavior of Load versus Out-of-Plane Displacement**

The curves of load versus out-of-plane displacement at the conjunction of gusset-to-splice for the specimens are shown in Figs. 6.11 to 6.15. For specimen MP1, a relatively linear load deflection behavior was observed until the applied load reached approximately 1000 kN. It should also be noted that the displacement at the early loading stage was relatively small, probably because of the effects of the beam and column moment. When the applied

load reached about 1650 kN, a sudden drop in load to approximately 1450 kN was recorded. Subsequently, the applied load increased again, back to the load level of about 1600 kN without a significant increase in out-of-plane displacement. From then on, the applied load increased with increasing displacement until the load reached an ultimate load of 1933 kN with a displacement of about 11mm. After reaching the ultimate load, the specimen unloaded gradually without a significant decrease in the applied load, as shown in Fig. 6.11. When the load deflection curve in the early loading stage is examined closely, it can be seen that drops in the applied load due to bolt slips were recorded, as has already been discussed in the previous section.

For specimens MP2 and MP3, the load deflection behavior was quite similar, as shown in Figs. 6.12 and 6.13. Linear load deflection behavior was observed until the applied load reached approximately 40 percent and 50 percent of the ultimate loads for specimens MP2 and MP3 respectively. However, the out-of-plane stiffness of both specimens only reduced slightly as loading continued until the specimens reached the ultimate loads. It should also be noted that the out-of-plane displacement of the specimens recorded prior to buckling was relatively small, as shown in the figures. The recorded displacement at the ultimate load for both specimens was about 3 mm. A gradual unloading behavior was also observed for both specimens. However, for specimen MP2, the rate of unloading was lesser than that of specimen MP3.

The curve of load versus out-of-plane displacement for specimen MP3A shows a slightly different behavior from that of specimen MP3 as shown in Fig. 6.14. In general, a negligible out-of-plane displacement was recorded for this specimen prior to its reaching the ultimate load. As can be seen from the figure, the specimen originally deformed towards the east. However, a sudden change in displacement direction at load step #7 was observed. This opposite movement of the specimen was due to the application of the full values of the beam and column moment (375 kN·m and 186.5 kN·m, respectively) at that



load step. As loading continued, only a very slight increase in the out-of-plane westward displacement was observed. When the applied load reached the ultimate load of 819 kN, bifurcation occurred with the specimen deformed towards the west. Since the buckling phenomenon occurred rapidly, therefore, it was unable to record readings between the ultimate load and the next load level which had a displacement of 15 mm. However, it can still be seen that the unloading process for the specimen was quite gradual.

For specimen MP3B, which excluded the beam and column moments, the curve of load versus out-of-plane displacement was similar to that of specimen MP3, as shown in Fig. 6.15. The curve was relatively linear up to 700 kN. Then the curve slowly turned to the ultimate load of 821 kN. Again, it was unable to record successive readings after the ultimate load until the applied load reached a lower level. However, a gradual unloading process was observed for the specimen. It should be noted that all the MP type specimens with a plate thickness of 6.5 mm reached approximately the same load level of 450 kN at the final load step, regardless of the level of the applied beam and column moments.

#### **6.4 Strain Gauge Results**

The in-plane stress distribution of the specimen was affected by the beam and column moments as observed from the strain gauges readings. For specimen MP1, yielding was first observed at the rosette close to the beam boundary at an applied load of about 770 kN. However, the yield load predicted by the Whitmore method was approximately 1200 kN. This early yielding of the specimen may be attributed to the effects of the beam and column moment. A similar behavior was also observed for the other MP type specimens. In particular, for specimen MP2 and MP3, yielding at the rosette occurred at an applied load of about 55 and 30 percent of the corresponding yield loads predicted by the Whitmore method. It should be noted that for specimens MP1, MP2, and MP3, full values of the beam and column moments had already been applied to the specimens when the test yield

loads were recorded. However, specimen MP3A, which was subject to higher beam and column moment (  $M_b=375$  kN·m,  $M_c=186.5$  kN·m ), showed a yielding at the rosette when the applied load was maintained at about 100 kN and the applied beam and column moments were increased from 50 percent to the full values.

The curves of load versus strains recorded at the mid-length and the fixed end of the free edges are shown in Figs.6.16 to 6.31. In general, the plots of load versus longitudinal strains at the mid-length of the free edges show that the strain readings in the elastic range were recorded prior to their reaching the ultimate load of the specimens. Furthermore, similar strain readings were recorded from both sides of the specimens before strain bifurcation occurred at ultimate load levels, except for specimen MP1. For specimen MP1, strain reversal was observed at the long free edge as shown in Fig. 6.16, and the strain readings from both sides of the specimen at the short free edge deviated at an early loading stage, as illustrated in Fig. 6.24. The strain readings recorded at the fixed ends of the free edges showed that tension existed in that vicinity. In particular, specimens MP3 and MP3A showed tensile yielding at the fixed ends of the free edges when the full values of the beam and column moments were applied, as shown in Figs. 6.29 and 6.31 respectively. As loading continued, tensile strain recorded at the fixed ends of the free edges increased slightly until strain bifurcation occurred at the ultimate loads. It should also be noted that strain gauges located at the fixed end of the free edges were mounted 30 mm away from the boundary. Hence, it is believed that tensile yielding should have occurred right at the fixed end of free edges before it was even detected by the strain gauges. In addition, the vicinity of the fixed end of the free edges was also a stress concentration area, due to abrupt change of geometry.

To investigate the effects of the beam and column moments on the in-plane stress distribution of the specimen, the strain readings along the beam and column boundary were examined. A plot of strain readings along the beam and column boundary at three levels

( 1/3, 2/3, and full values ) of the applied beam and column moments for specimen MP1 is shown in Fig. 6.32. The strain readings shown in the figure had already excluded the effects of the axial load. It can be seen from the figure that a high stress gradient existed along the beam and column boundary, especially along the beam boundary, in the vicinity of the short free edge. In general, tensile strains were observed along the column boundary. However, compressive strains were recorded near the mid-length of the beam boundary, as shown in the figure. The reduced strain readings at the rosettes indicated that the applied beam and column moments induced compressive strains in the plate area underneath the splice member. Hence, early yielding at that region was recorded for the MP type specimens.

### **6.5 Yielding Behavior of Specimens**

The yielding process and pattern for the MP type specimens were only slightly different from those of the GP type specimens, except for specimen MP3B, which behaved similarly to specimen GP3. In general, yield lines were first observed near the beam boundary. These yield lines were almost parallel to it. Yielding underneath the splice member was then recorded. As loading continued, yielding underneath the splice member progressed and yield lines were also recorded about the two sides of the splice member. In particular, for specimens MP1, MP2 and MP3A, extensive yielding of the specimens was observed prior to buckling. However, for specimen MP3 moderate yielding was observed underneath the splice member. After buckling occurred, yield lines were also formed at the mid-length of the long free edge and along the beam and column boundary. A picture of the failed specimen MP1, shown in Fig. 6.33, illustrates the extent of the yielding and also the location of the yield line mechanism. When the failed specimen MP3 was examined, a fracture from the weld at the fixed end of the short free edge was observed. Hence, for specimens MP3A and MP3B, a larger weld size was used to prevent fracture at that location.

### **6.6 Out-of-Plane Deflected Shapes of Free Edges and Along Centerline of Splicing Member**

The normalized out-of-plane deflected shapes of the MP type specimens are shown in Fig. 6.34. In general, the out-of-plane deflected shapes of the specimens resembled the buckled shape of a fixed-pinned column. The figure shows that the end of the free edges attached to the beam and column boundary exhibited quite a significant rotation. This is probably due to the tensile yielding caused by the beam and column moments. Pictures of the deflected shapes of the free edges for specimen MP3A are shown in Fig.6.35 to illustrate the amount of rotation which existed at the ends. It can be seen from these pictures that the lower end of the free edges was almost in a straight position, indicating that the lower end rotated as a rigid body.

Table 6.1 Test Results of MP Type Specimens

Specimen Designation	Plate Size (mm x mm x mm)	Beam Moment $M_b$ (kN·m)	Column Moment $M_c$ (kN·m)	Ultimate Load $P$ (kN)	Whitmore Load $P_w$ (kN)	Thornton Load $P_t$ $k = 0.65$ (kN)
MP1	500 x 400 x 13.3	250	125	1933	1216	1142
MP2	500 x 400 x 9.8	250	125	1316	930	828
MP3	500 x 400 x 6.5	250	125	721	555	459
MP3A	500 x 400 x 6.5	375	187.5	819	555	459
MP3B	500 x 400 x 6.5	0	0	821	555	459

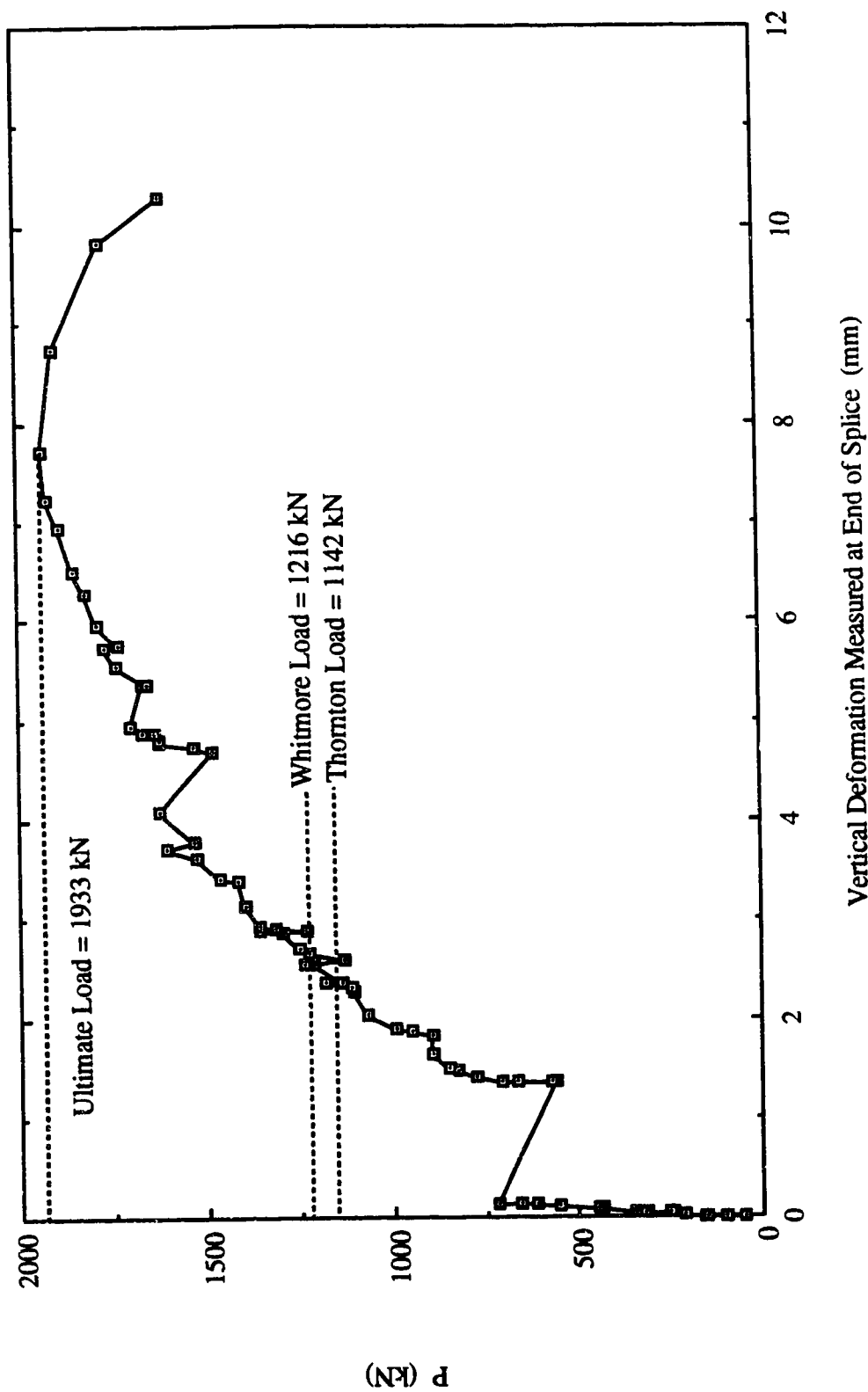


Fig. 6.1 Load vs. In-Plane Deformation Measured at End of Splice for Specimen MP1

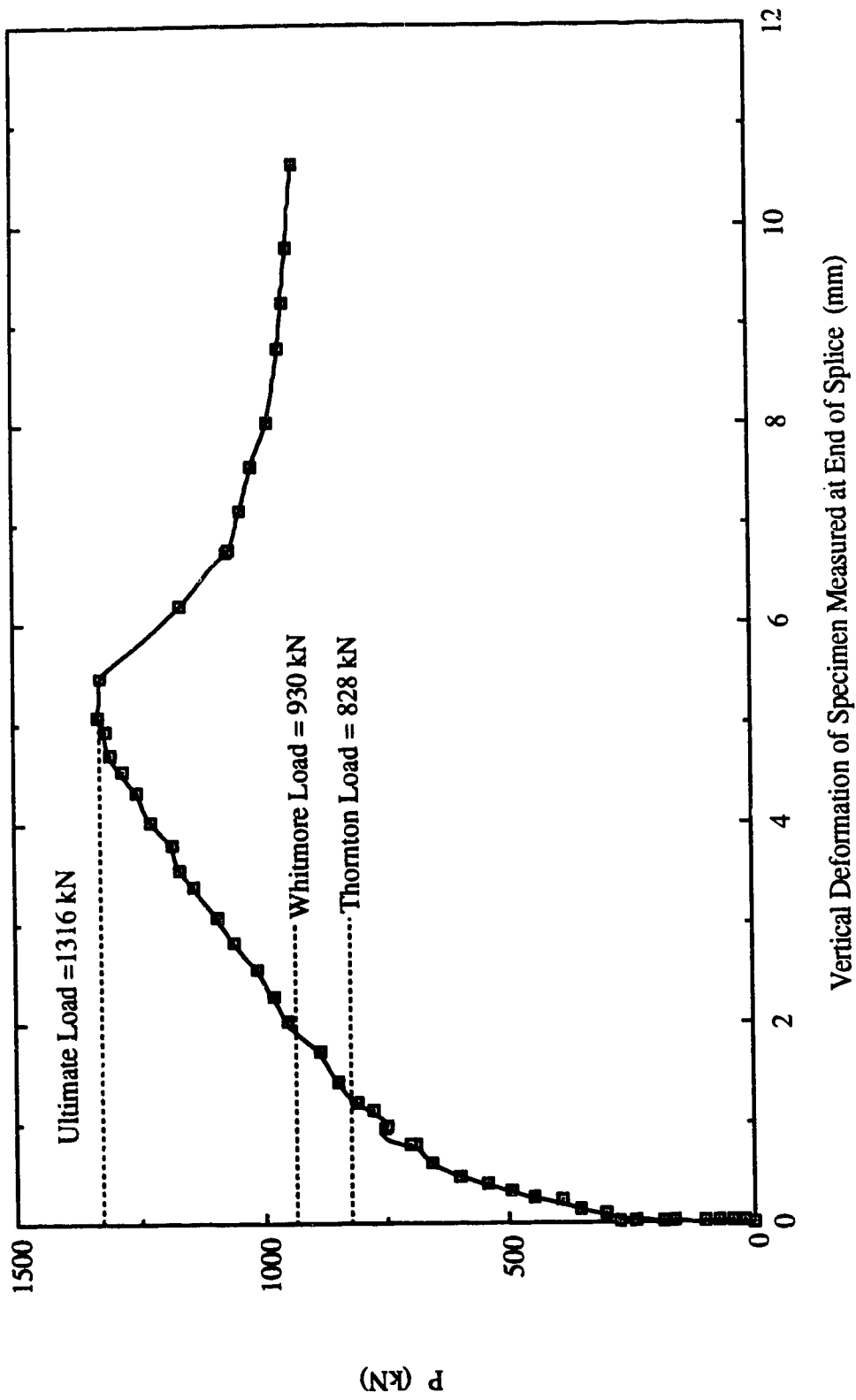
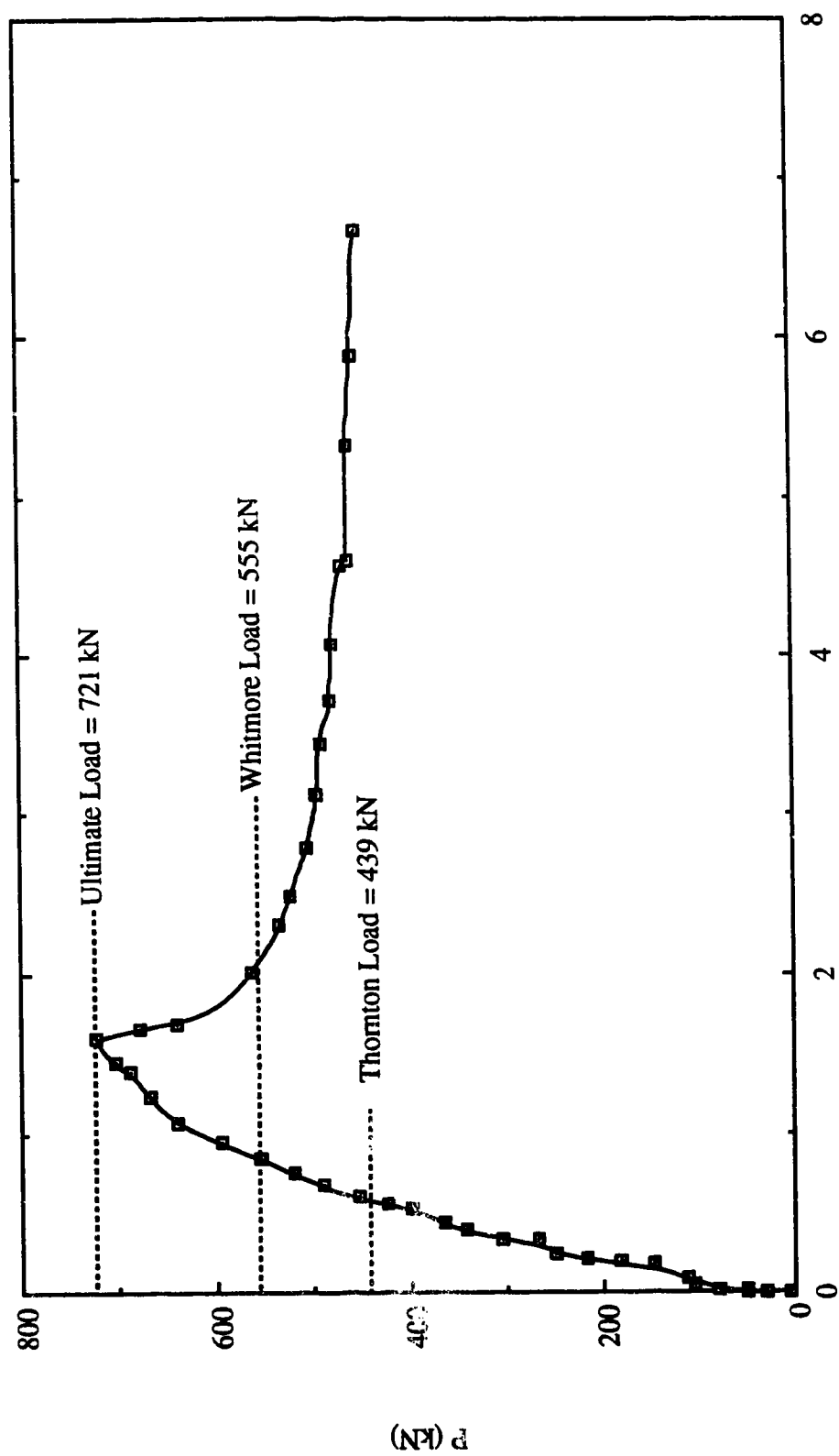


Fig. 6.2 Load vs. In-Plane Deformation Measured at End of Splice for Specimen MP2



Vertical Deformation of Specimen Measured at End of Splice (mm)

Fig. 6.3 Load vs. In-Plane Deformation Measured at End of Splice for Specimen MP3



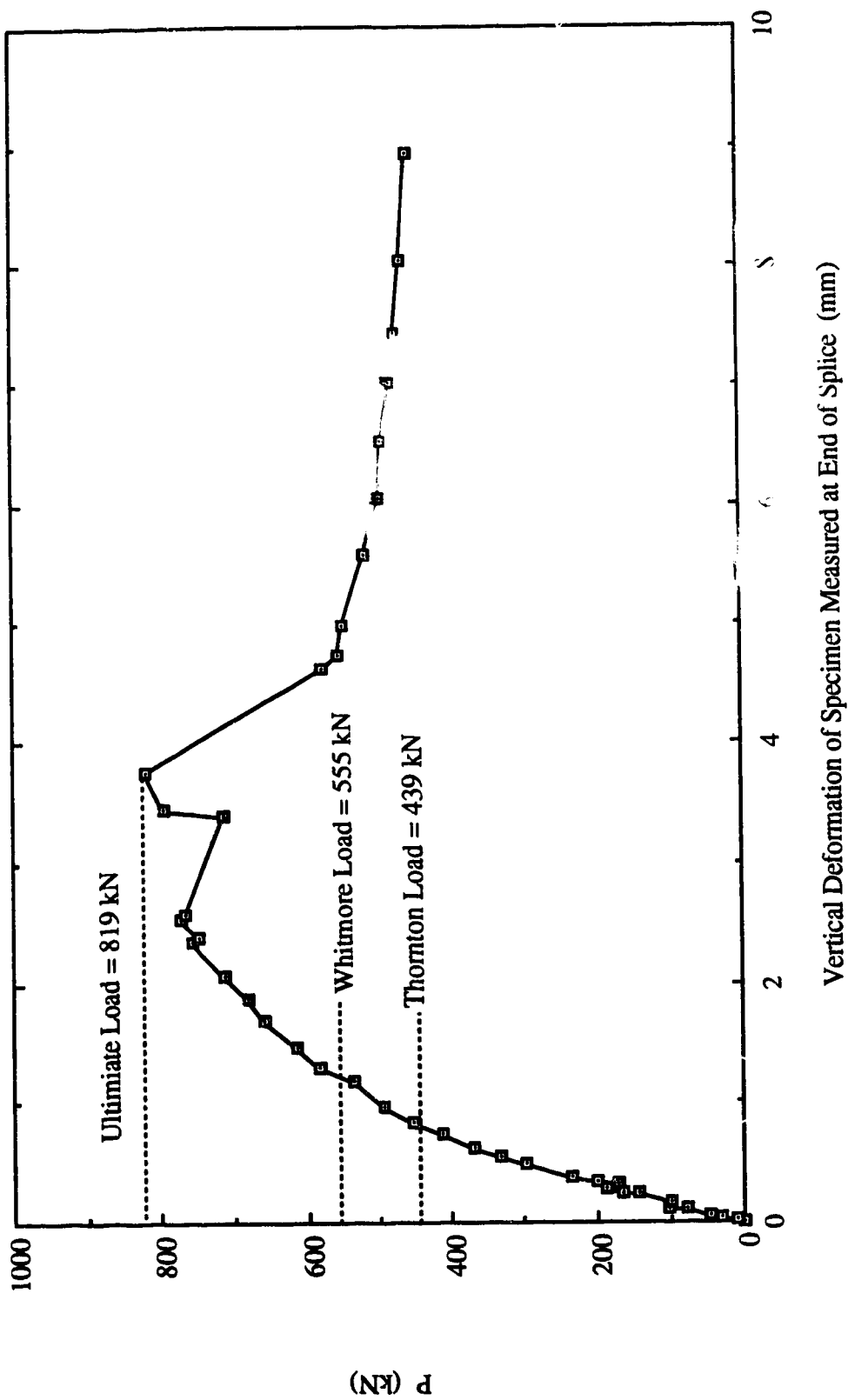
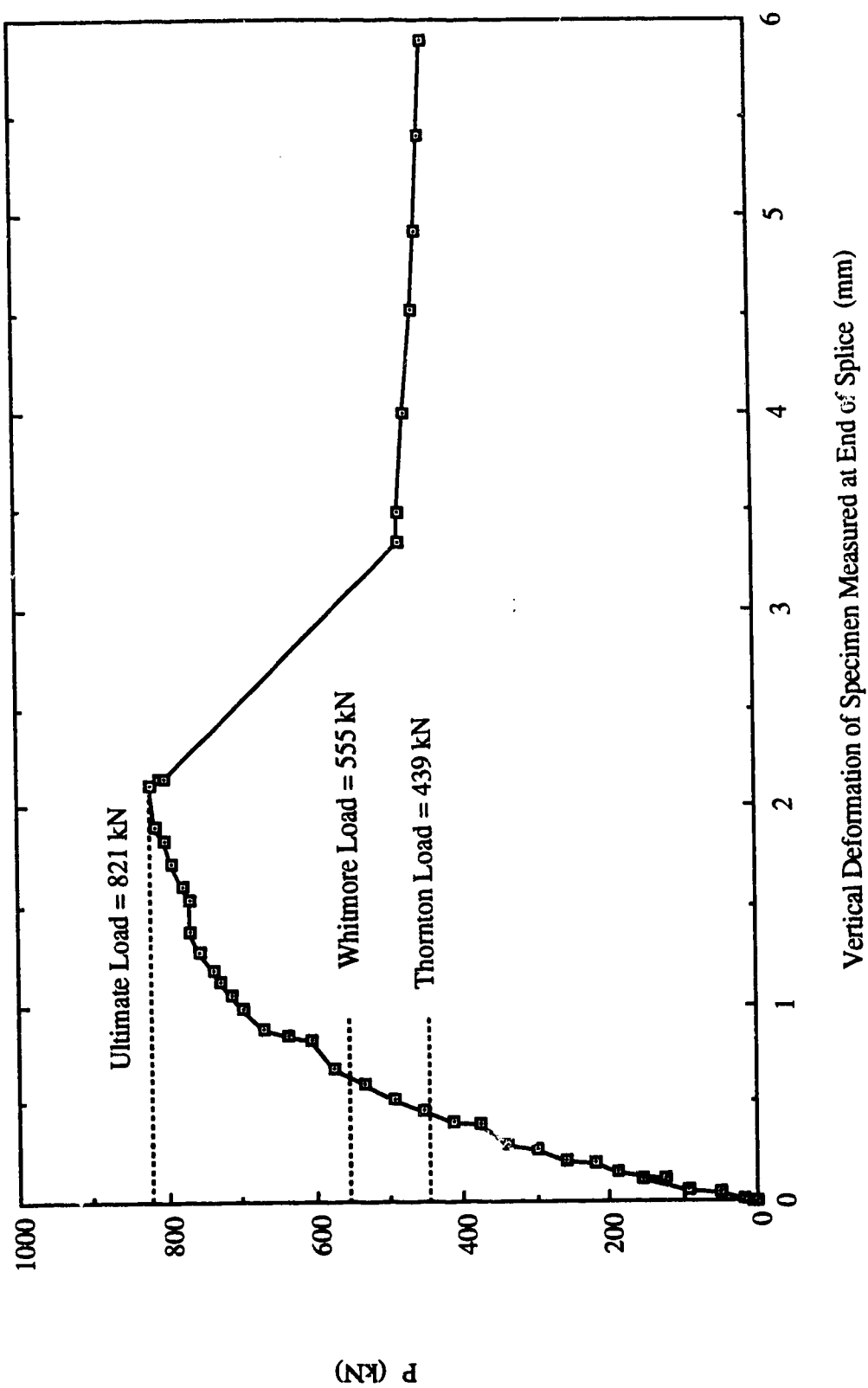


Fig. 6.4 Load vs. In-Plane Deformation Measured at End of Splice for Specimen MP3A



Vertical Deformation of Specimen Measured at End of Splice (mm)

Fig. 6.5 Load vs. In-Plane Deformation Measured at End of Splice for Specimen MP3B

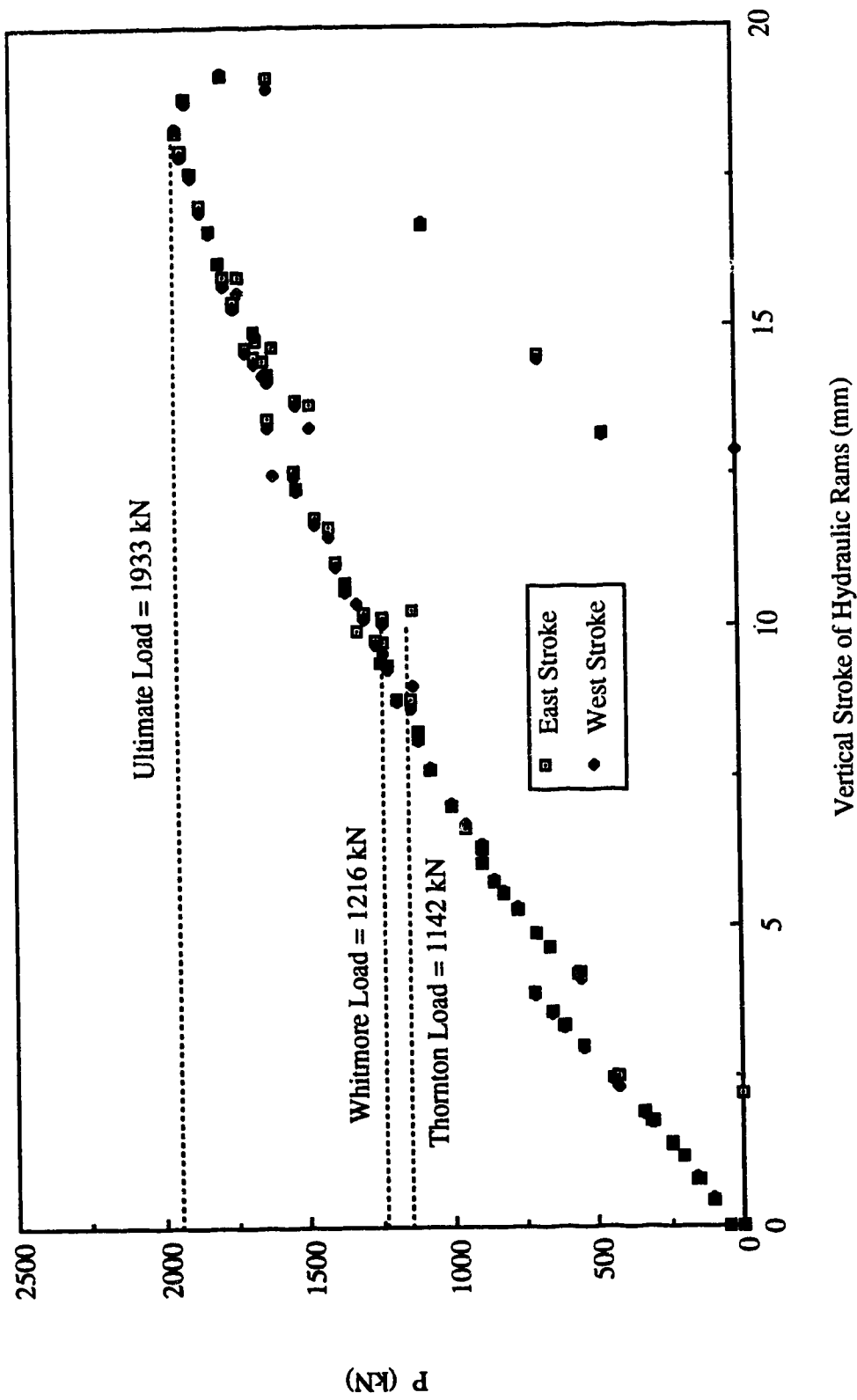


Fig. 6.6 Load vs. Vertical Strokes of Hydraulic Rams for Specimen MP1

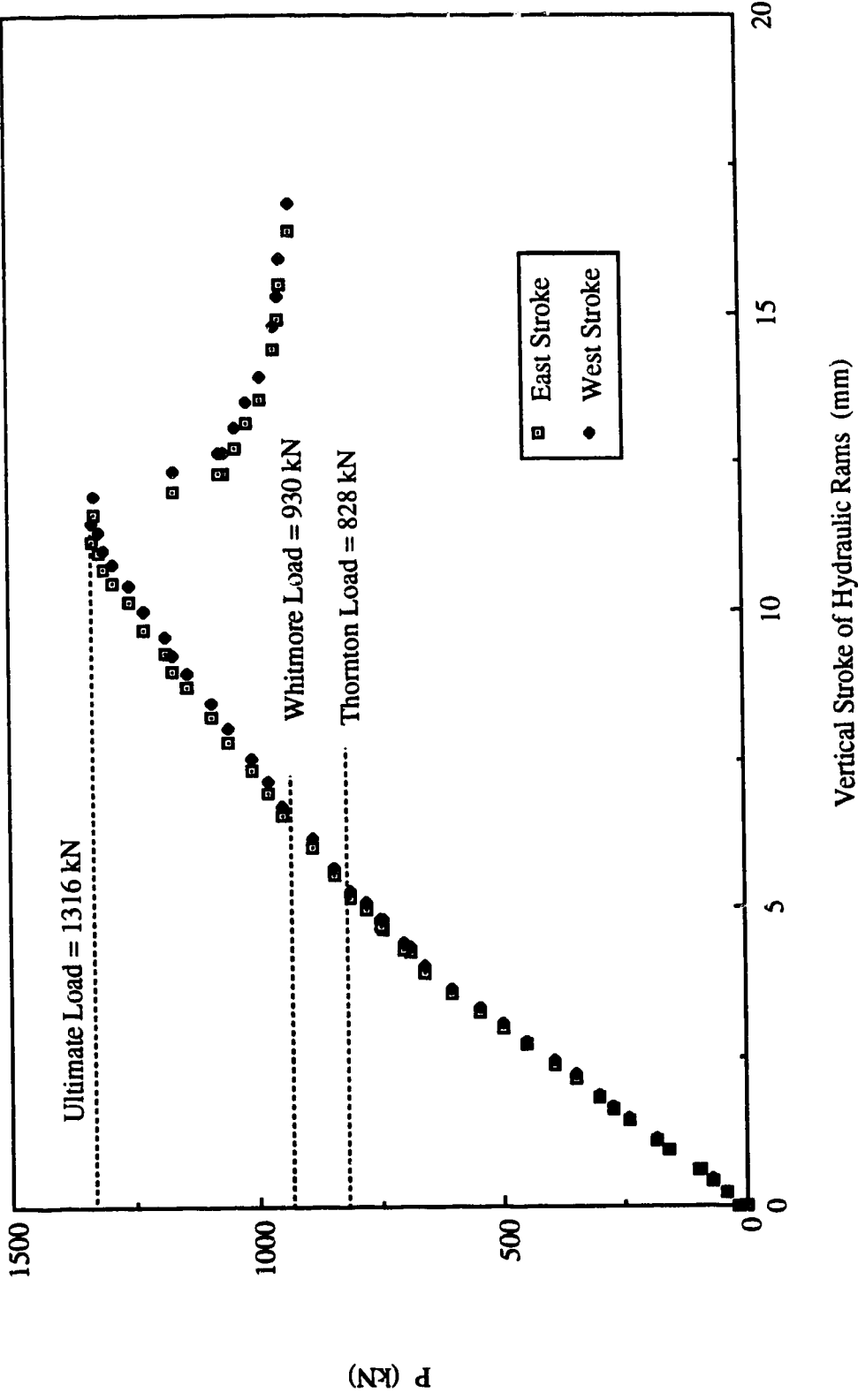


Fig. 6.7 Load vs. Vertical Strokes of Hydraulic Rams for Specimen MP2

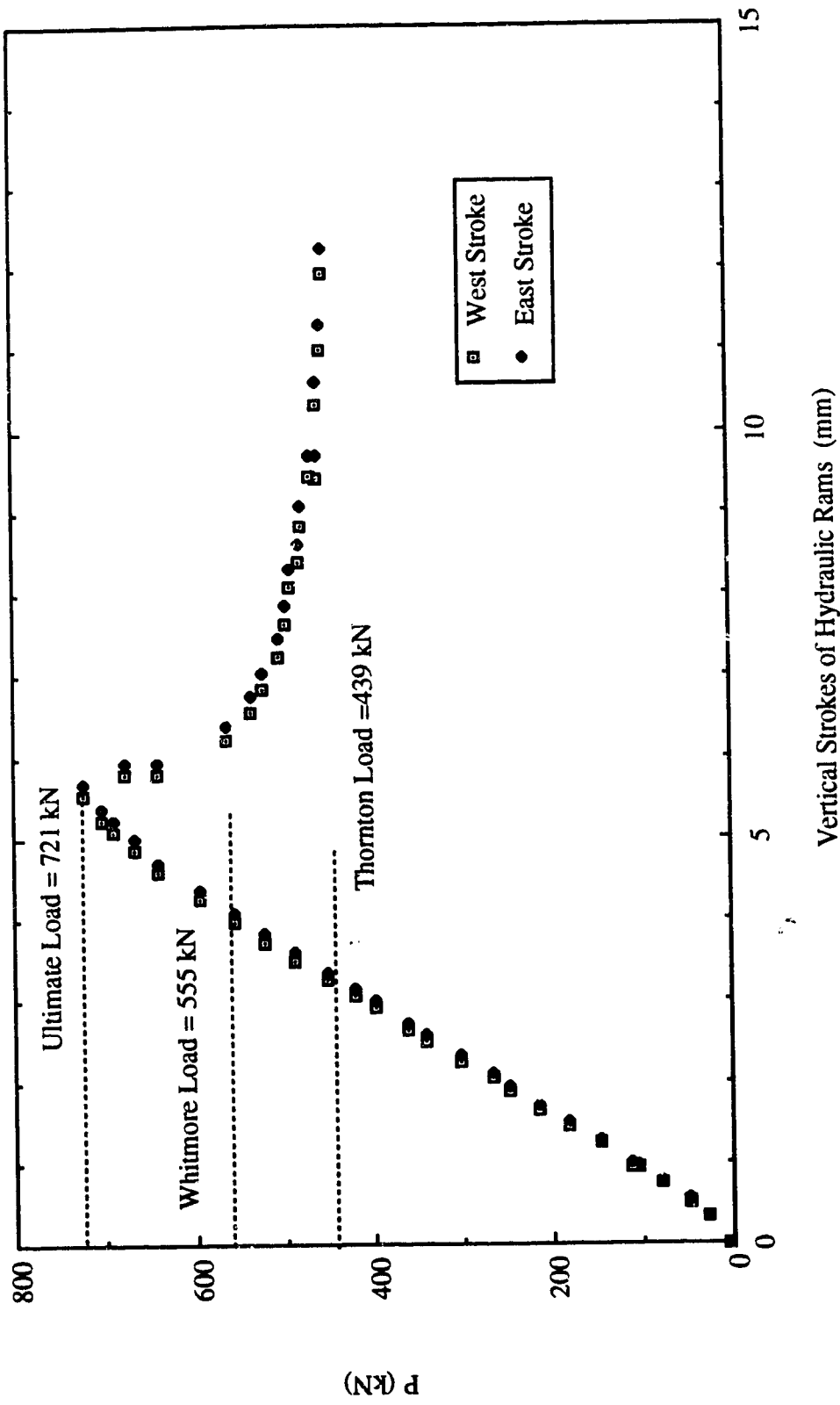


Fig. 6.8 Load vs. Vertical Strokes of Hydraulic Rams for Specimen MP3

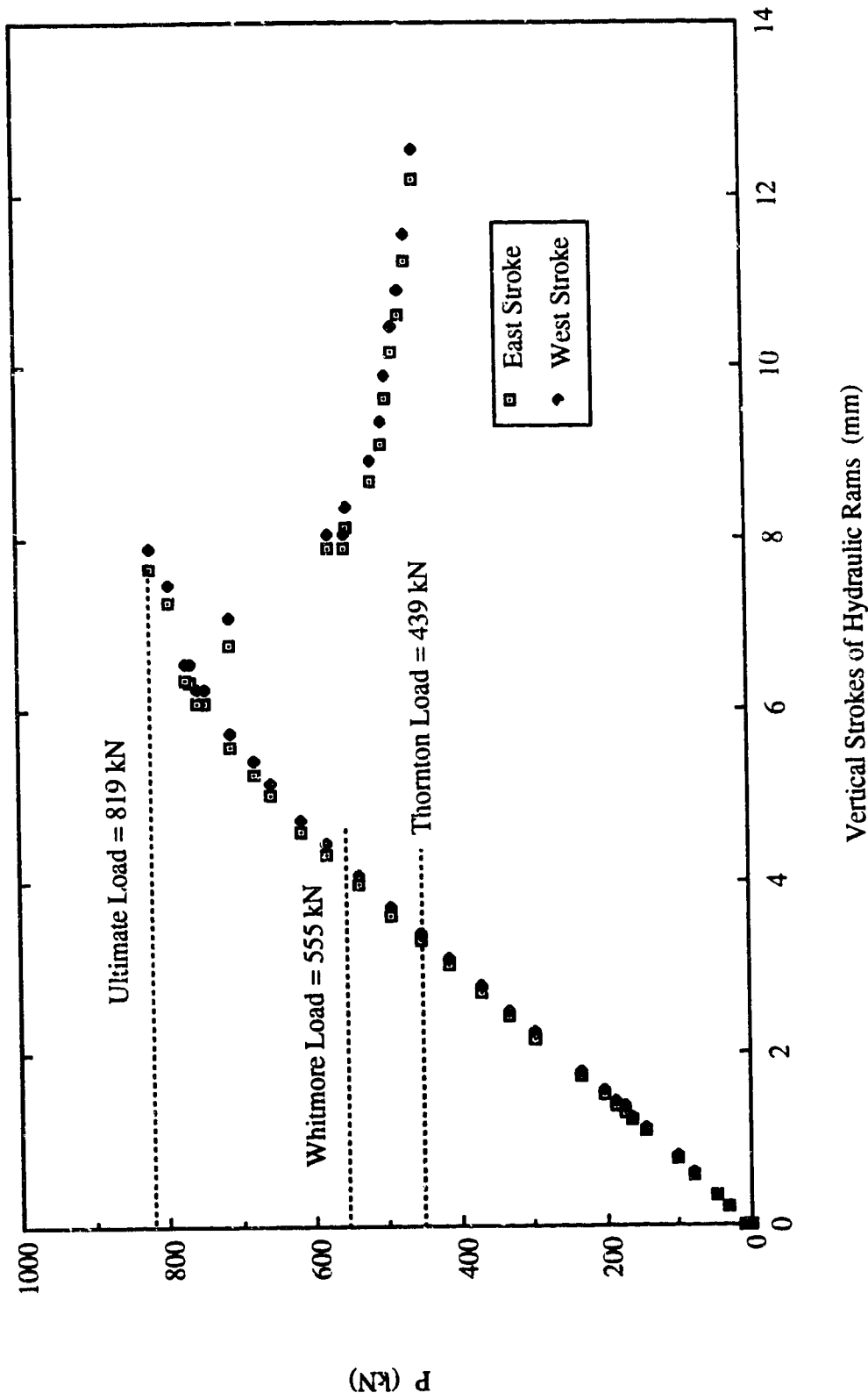


Fig. 6.9 Load vs. Vertical Strokes of Hydraulic Rams for Specimen MP3A

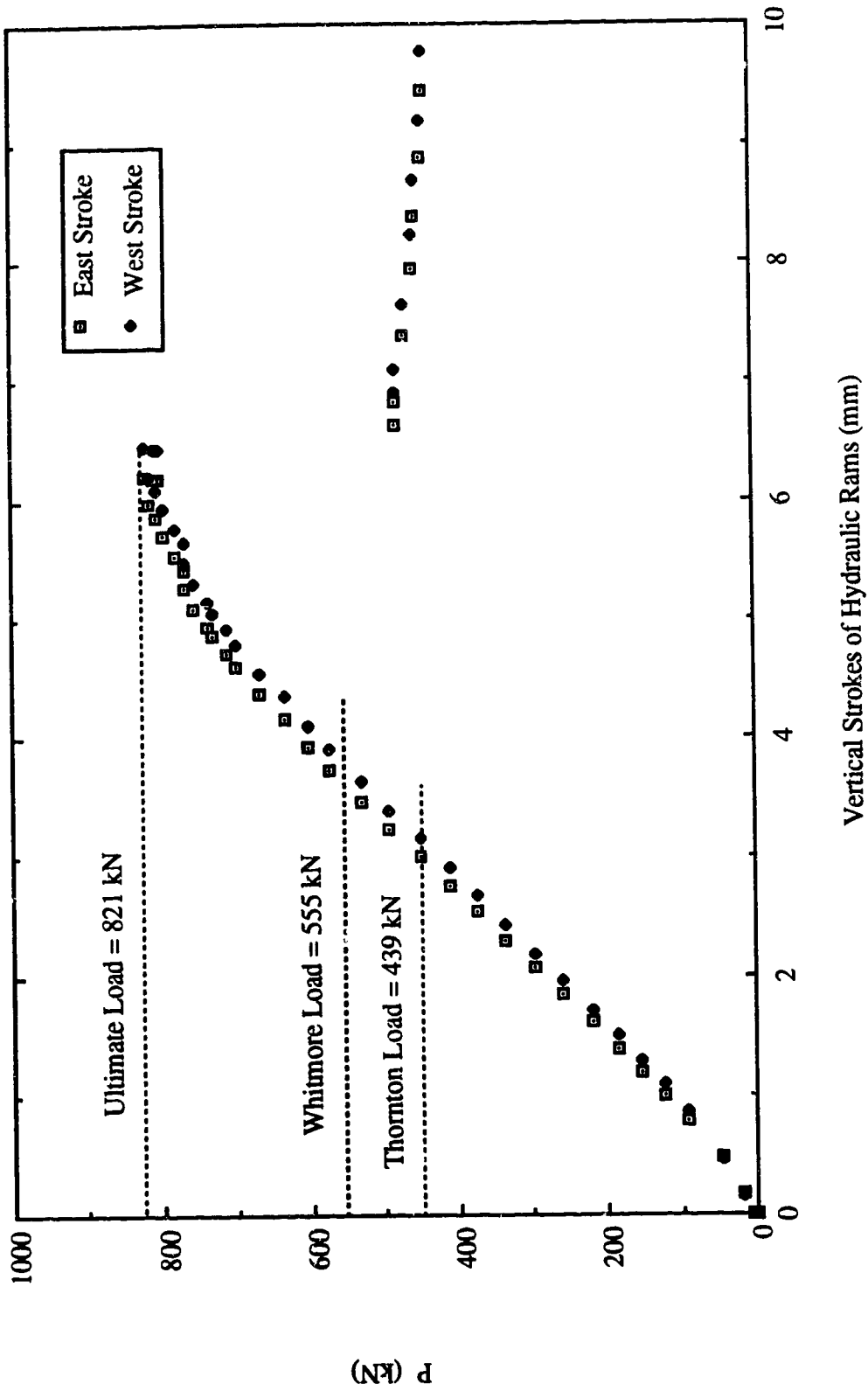


Fig. 6.10 Load vs. Vertical Strokes of Hydraulic Rams for Specimen MP3B

7

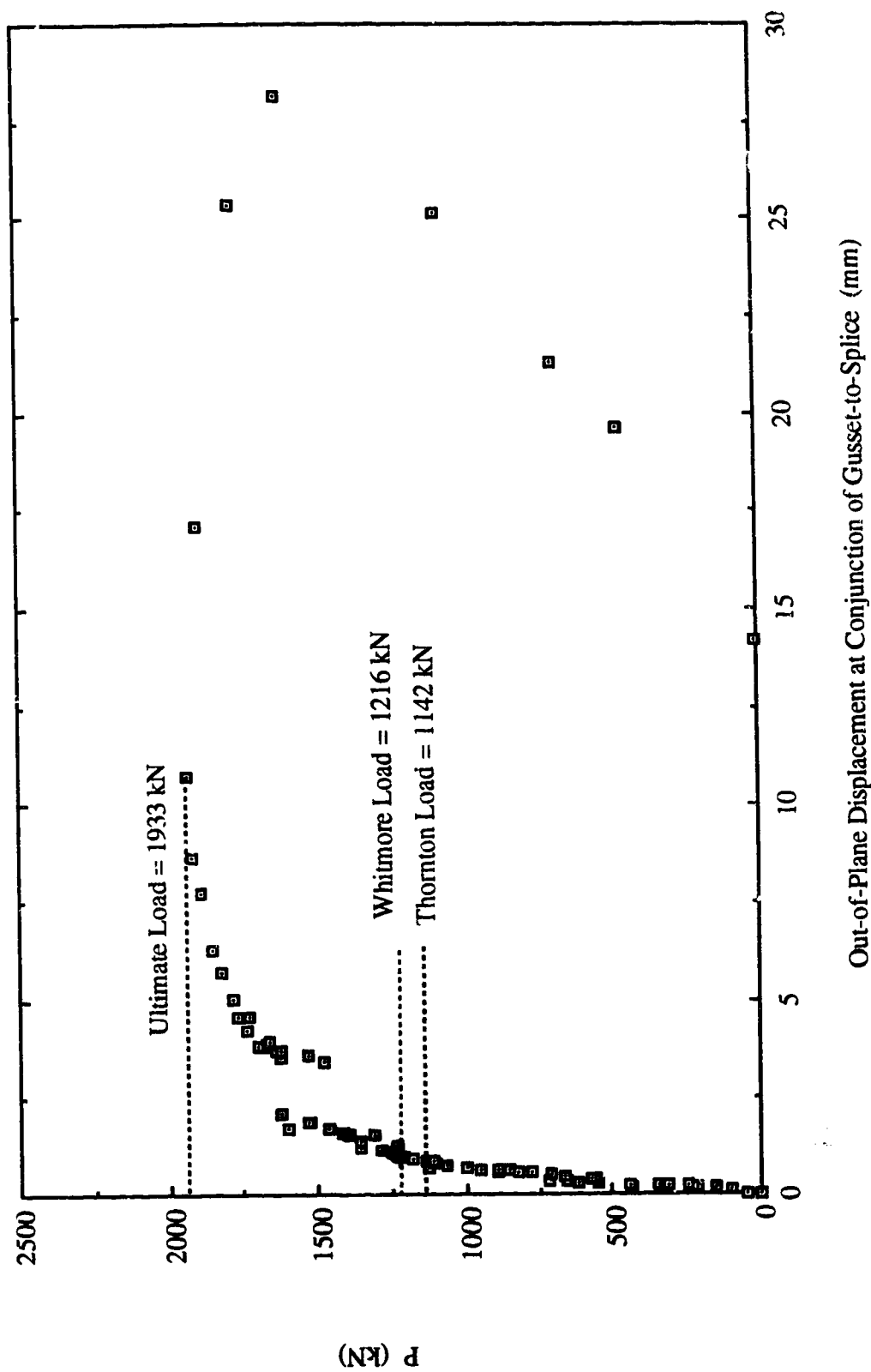


Fig. 6.11 Load vs. Out-of-Plane Displacement at Conjunction of Gusset-to-Splice for Specimen MP1



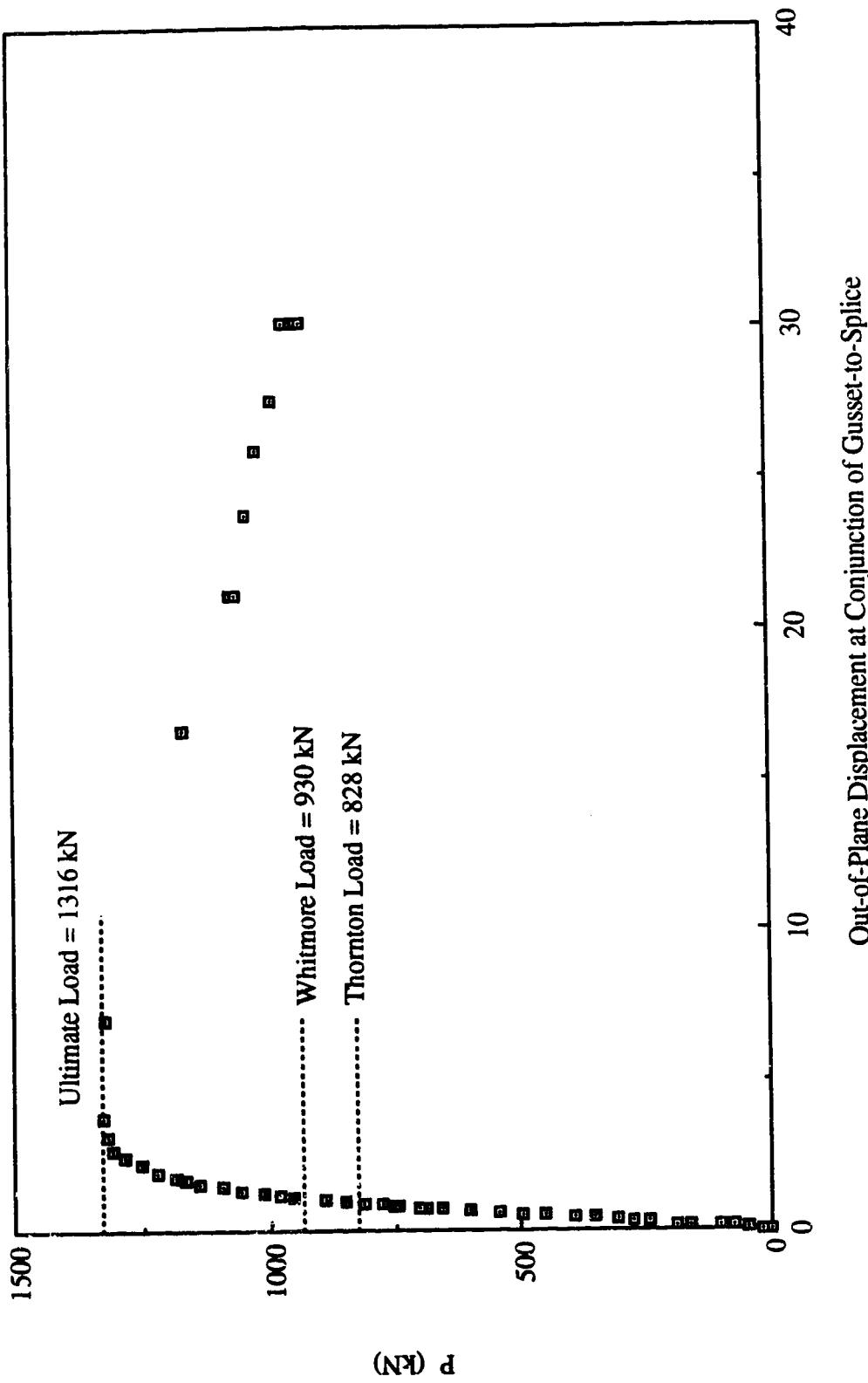


Fig. 6.12 Load vs. Out-of-Plane Displacement at Conjunction of Gusset-to-Splice for Specimen MP2

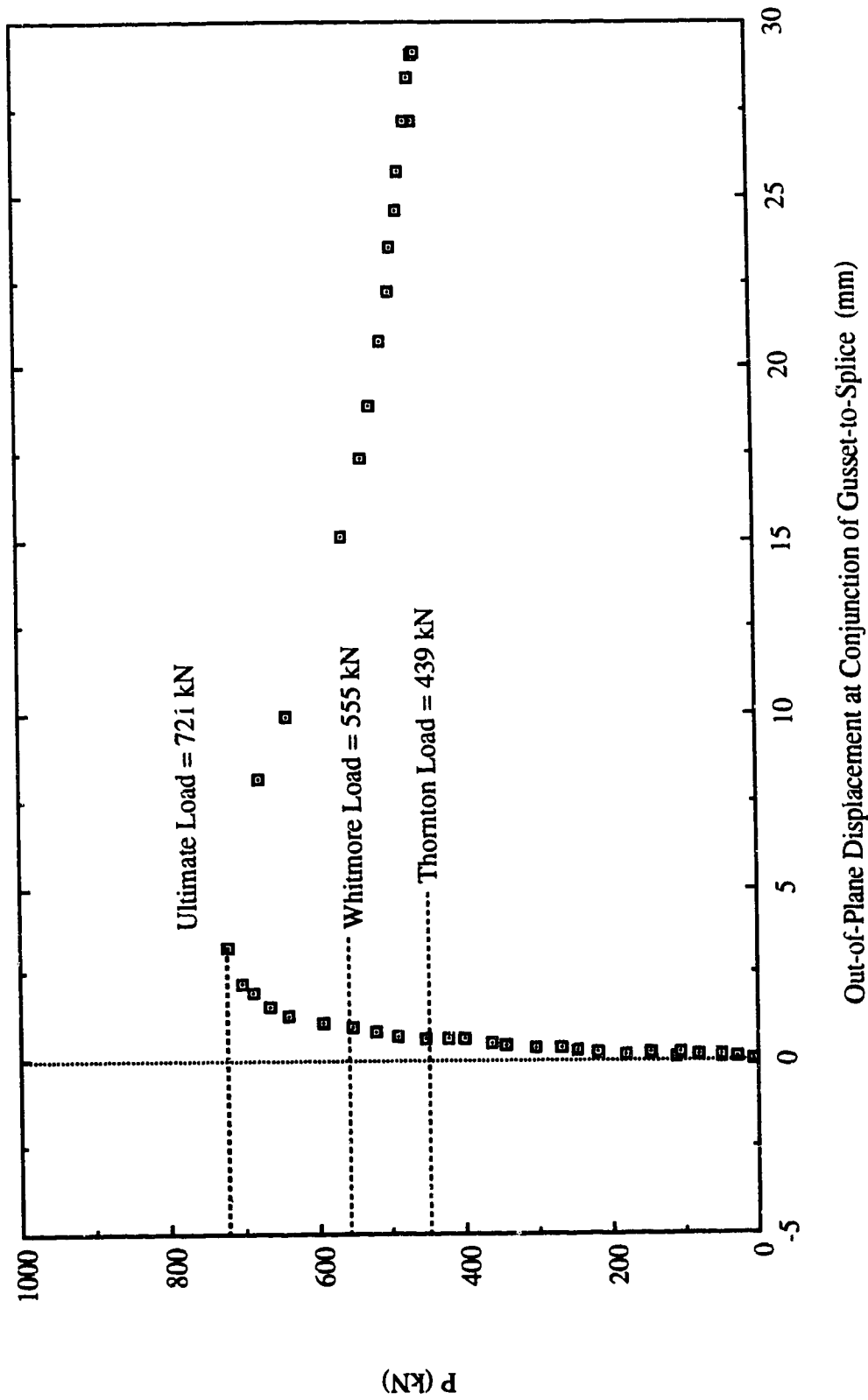


Fig. 6.13 Load vs. Out-of-Plane Displacement at Conjunction of Gusset-to-Splice for Specimen MP3

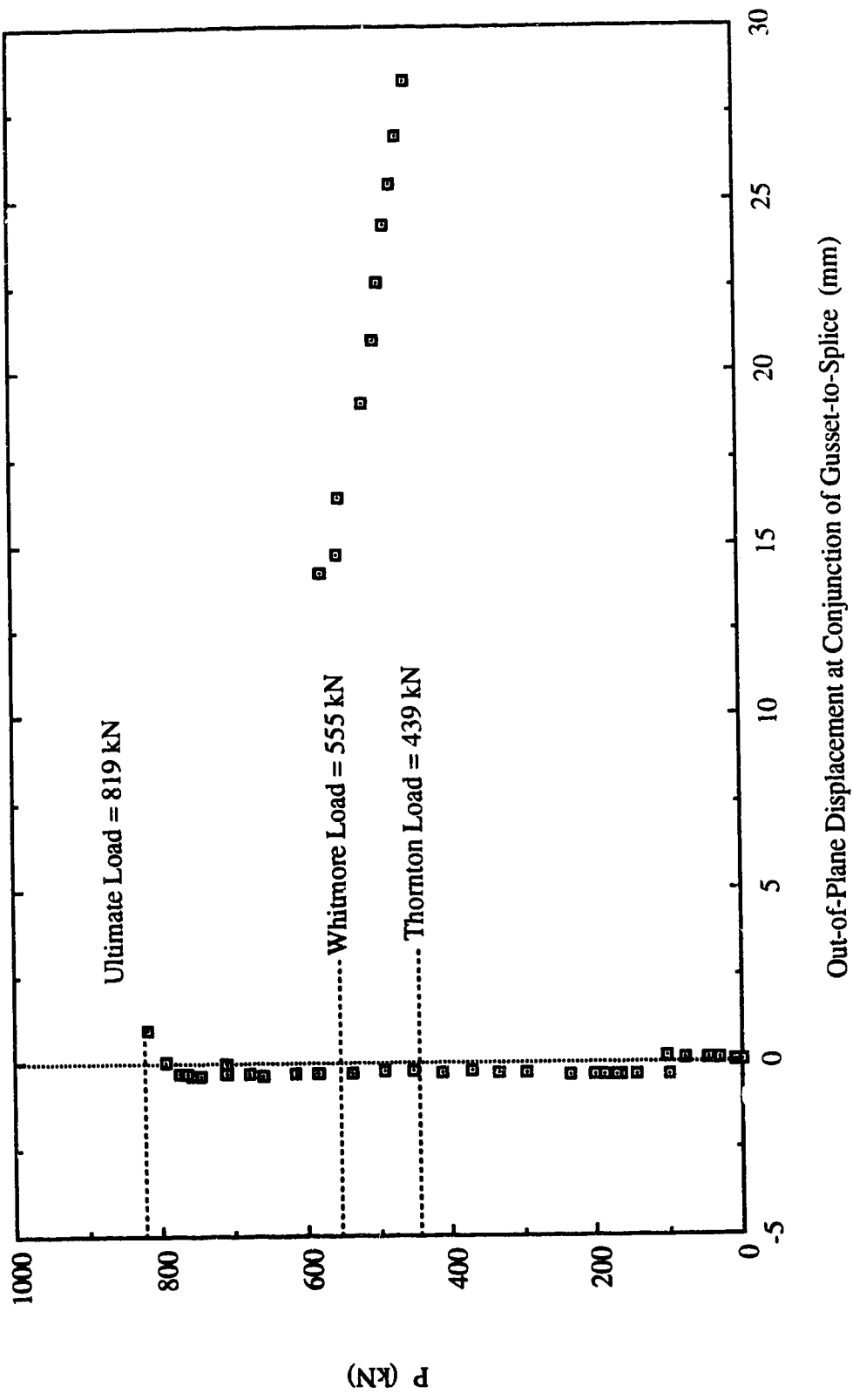
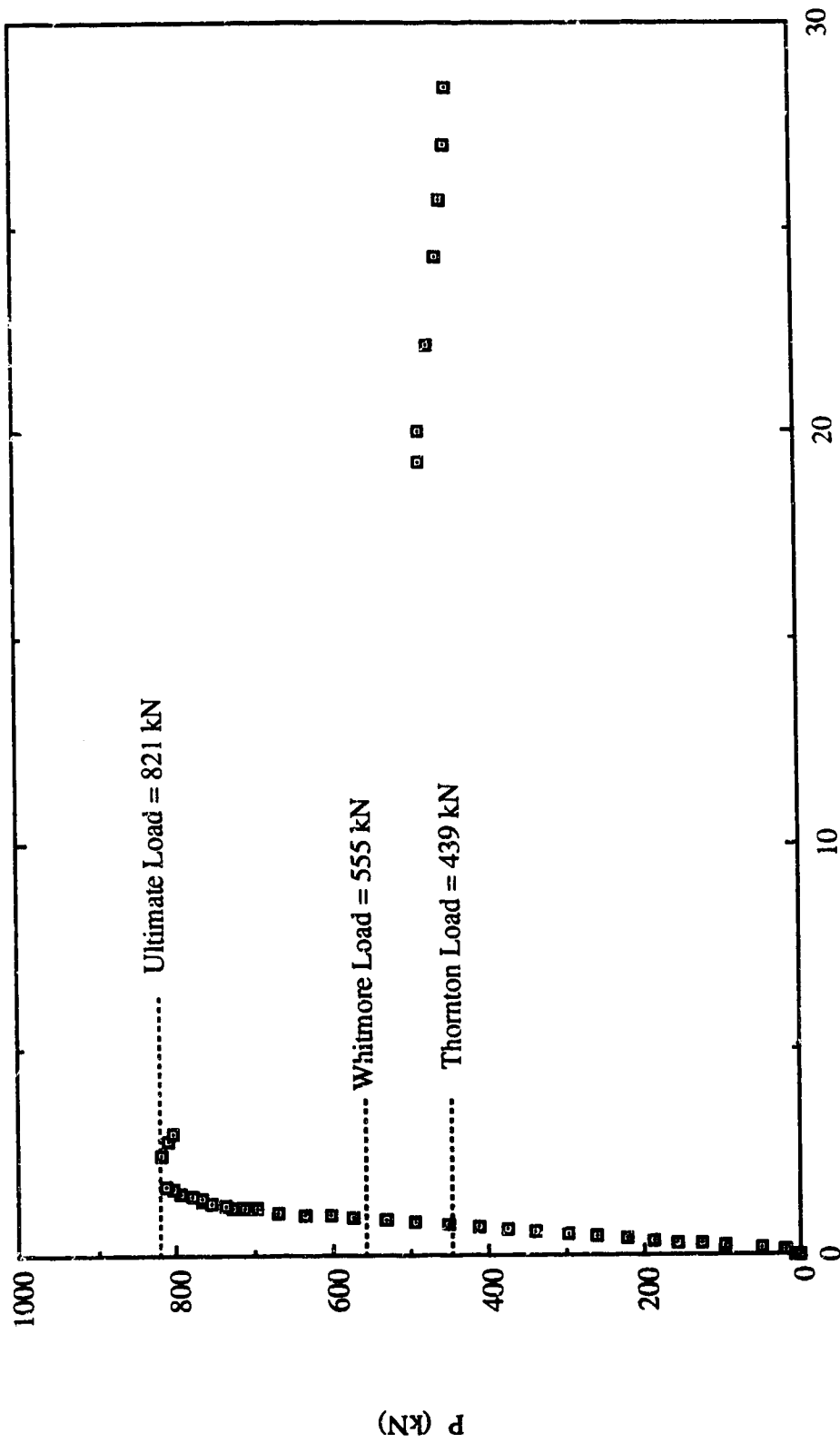


Fig. 6.14 Load vs. Out-of-Plane Displacement at Conjunction of Gusset-to-Splice for Specimen MP3A



Out-of-Displacement at Conjunction of Gusset-to-Splice (mm)

Fig. 6.15 Load vs. Out-of-Plane Displacement at Conjunction of Gusset-to-Splice for Specimen MP3B

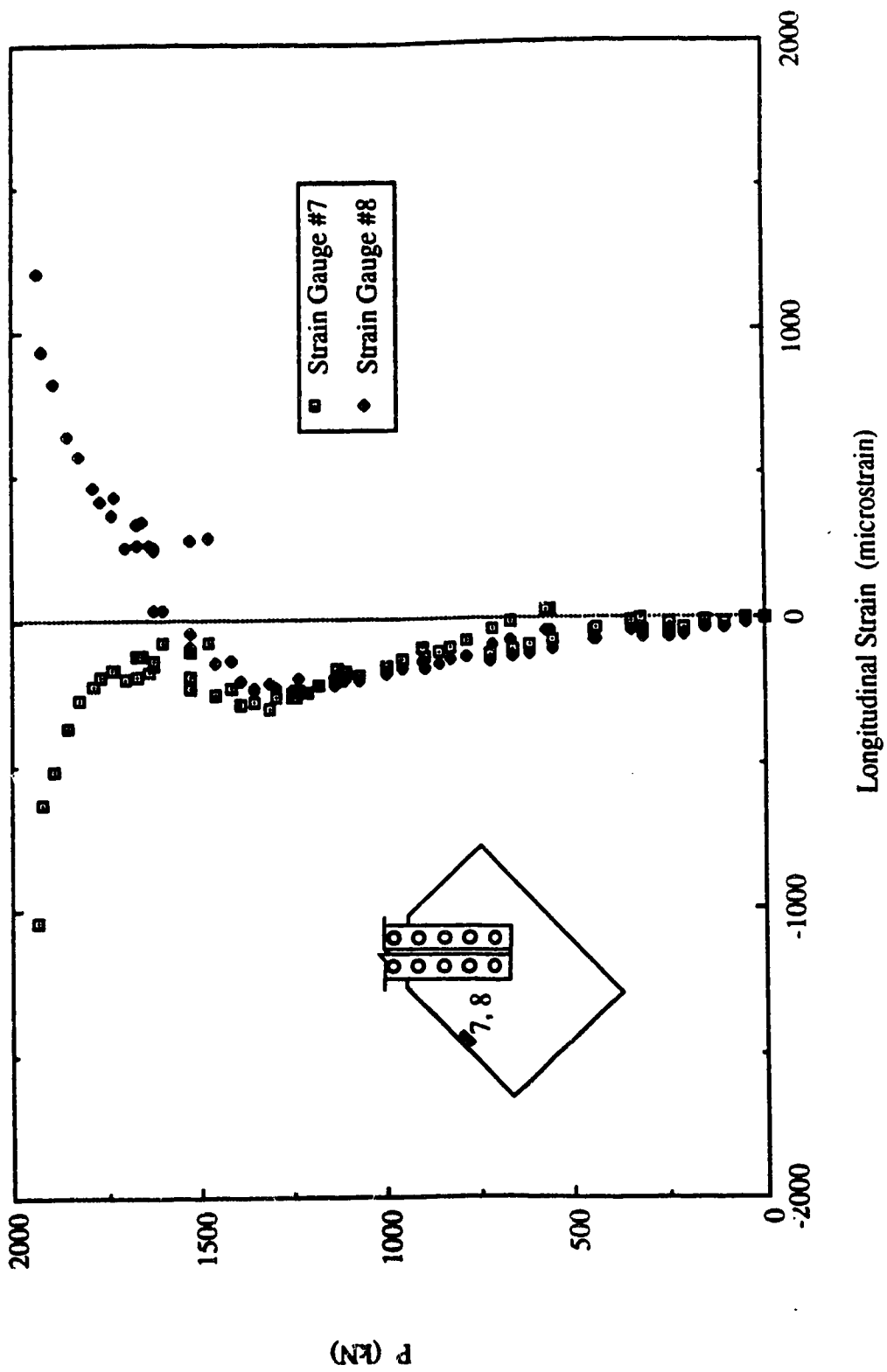


Fig. 6.16 Load vs. Strain Gauge Readings at Mid-Length of Long Free Edge for Specimen MP1

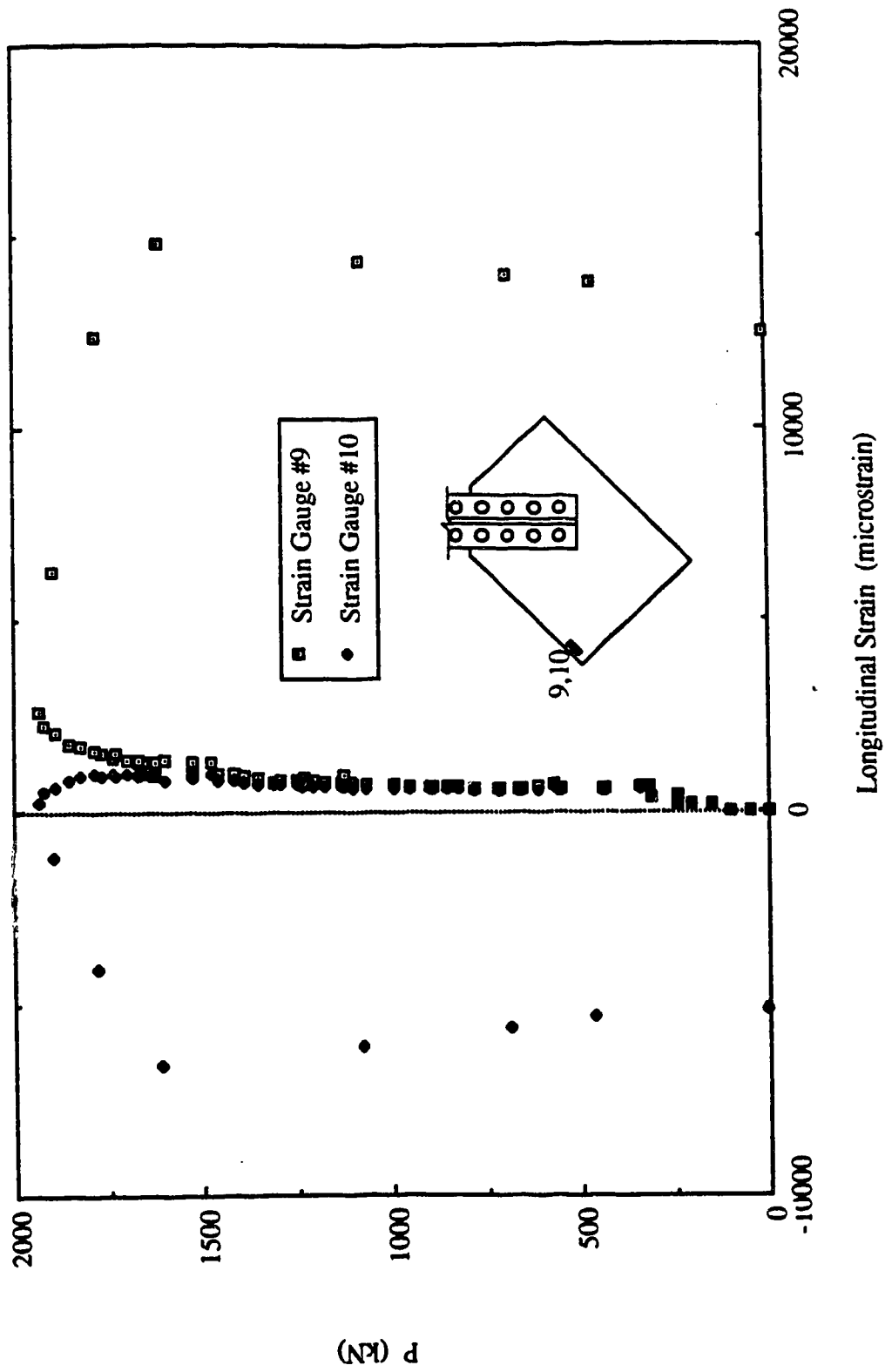


Fig. 6.17 Load vs. Strain Gauge Readings at End of Long Free Edge for Specimen MPI

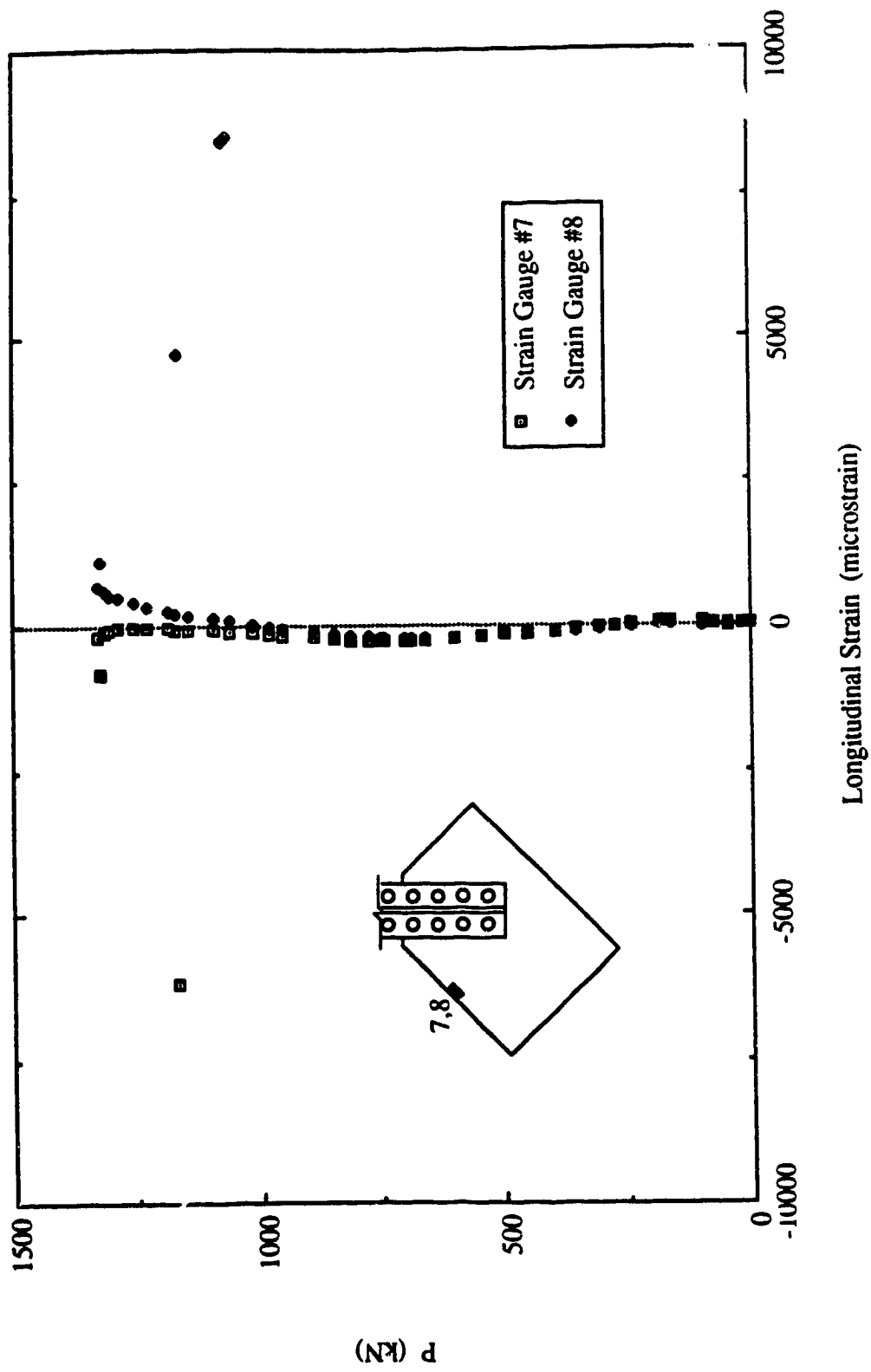


Fig. 6.18 Load vs. Strain Gauge Readings at Mid-Length of Long Free Edge for Specimen MP2

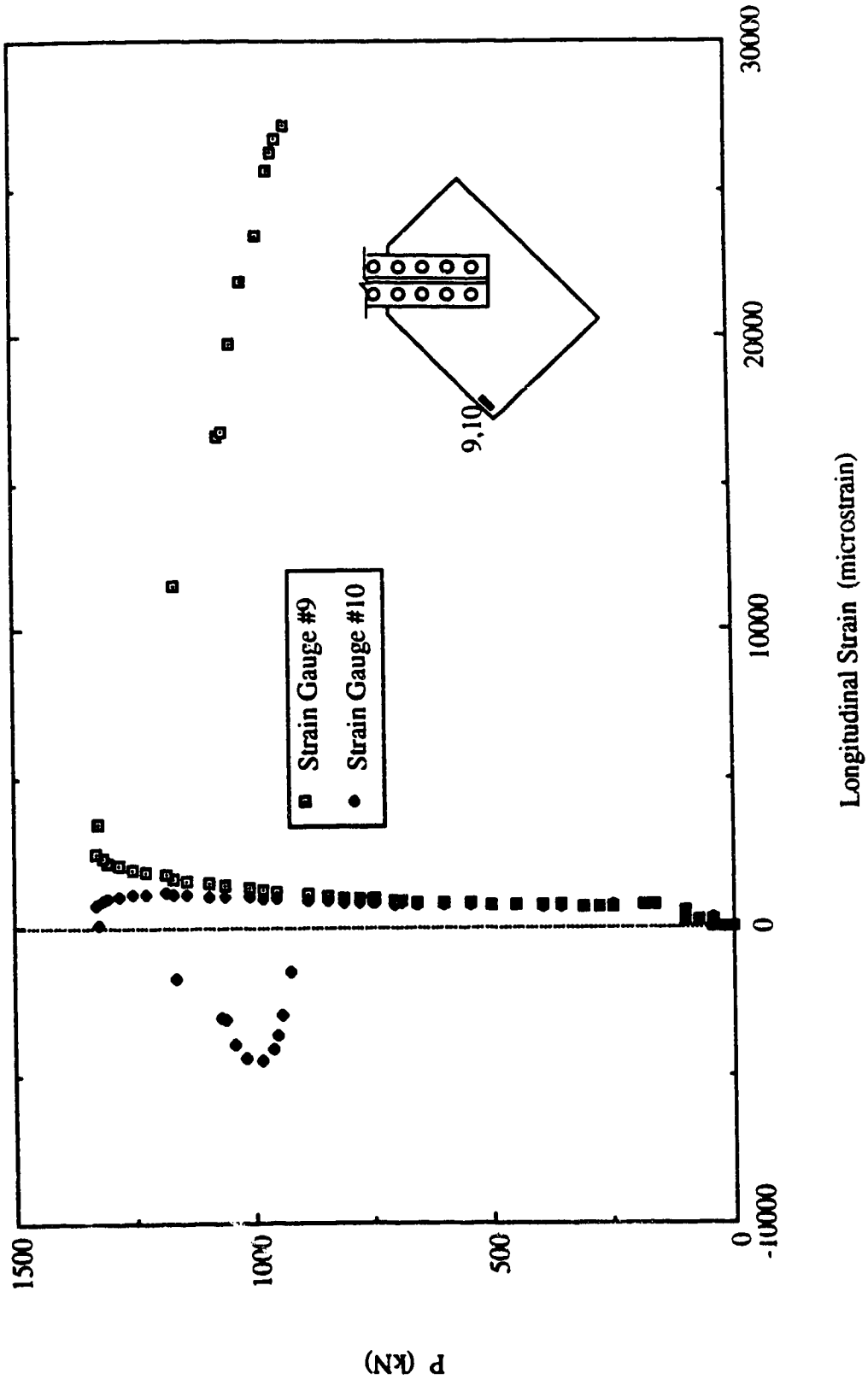


Fig. 6.19 Load vs. Strain Gauge Readings at End of Long Free Edge for Specimen MP2



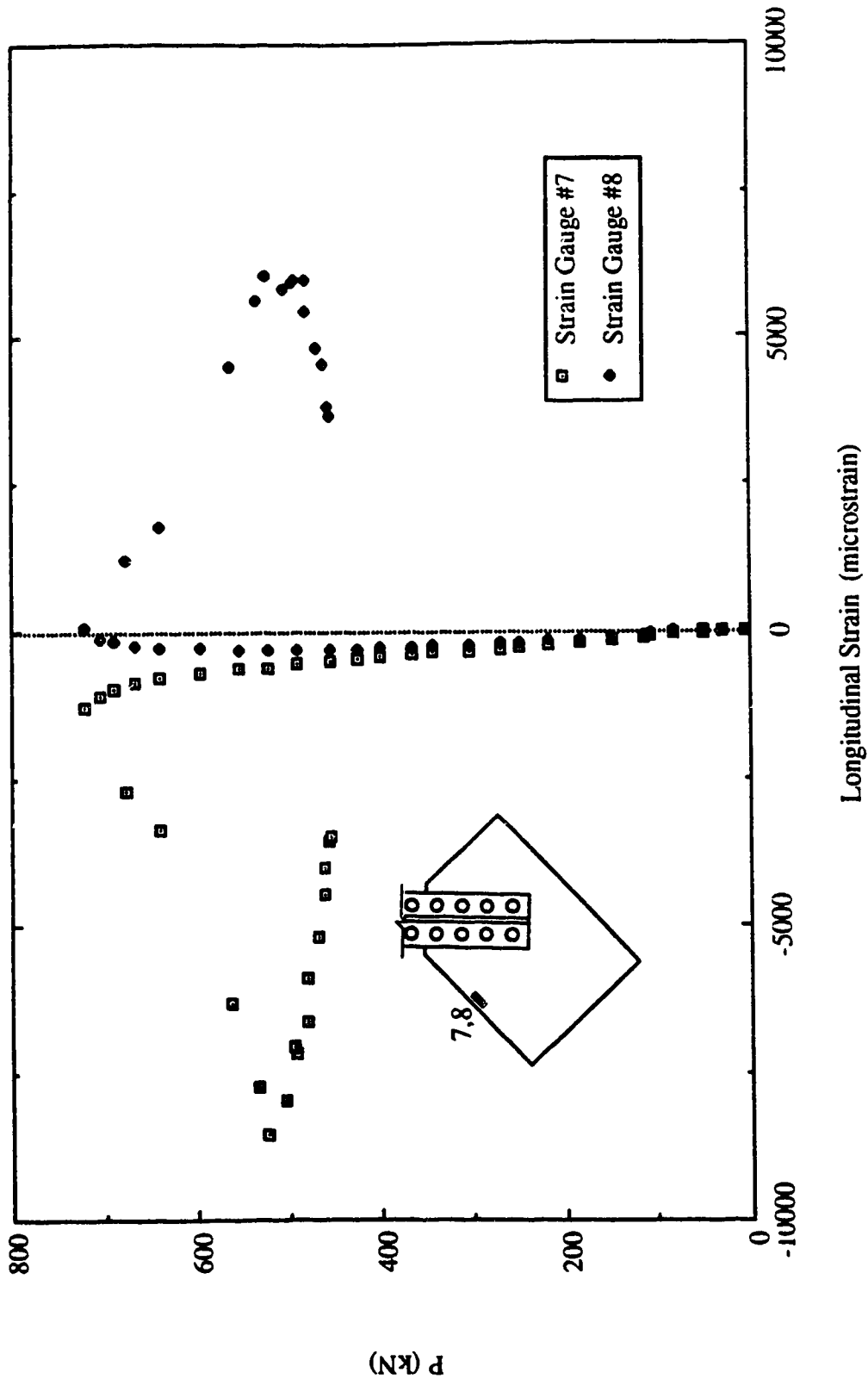


Fig. 6.20 Load vs. Strain Gauge Readings at Mid-Length of Long Free Edge for Specimen MP3

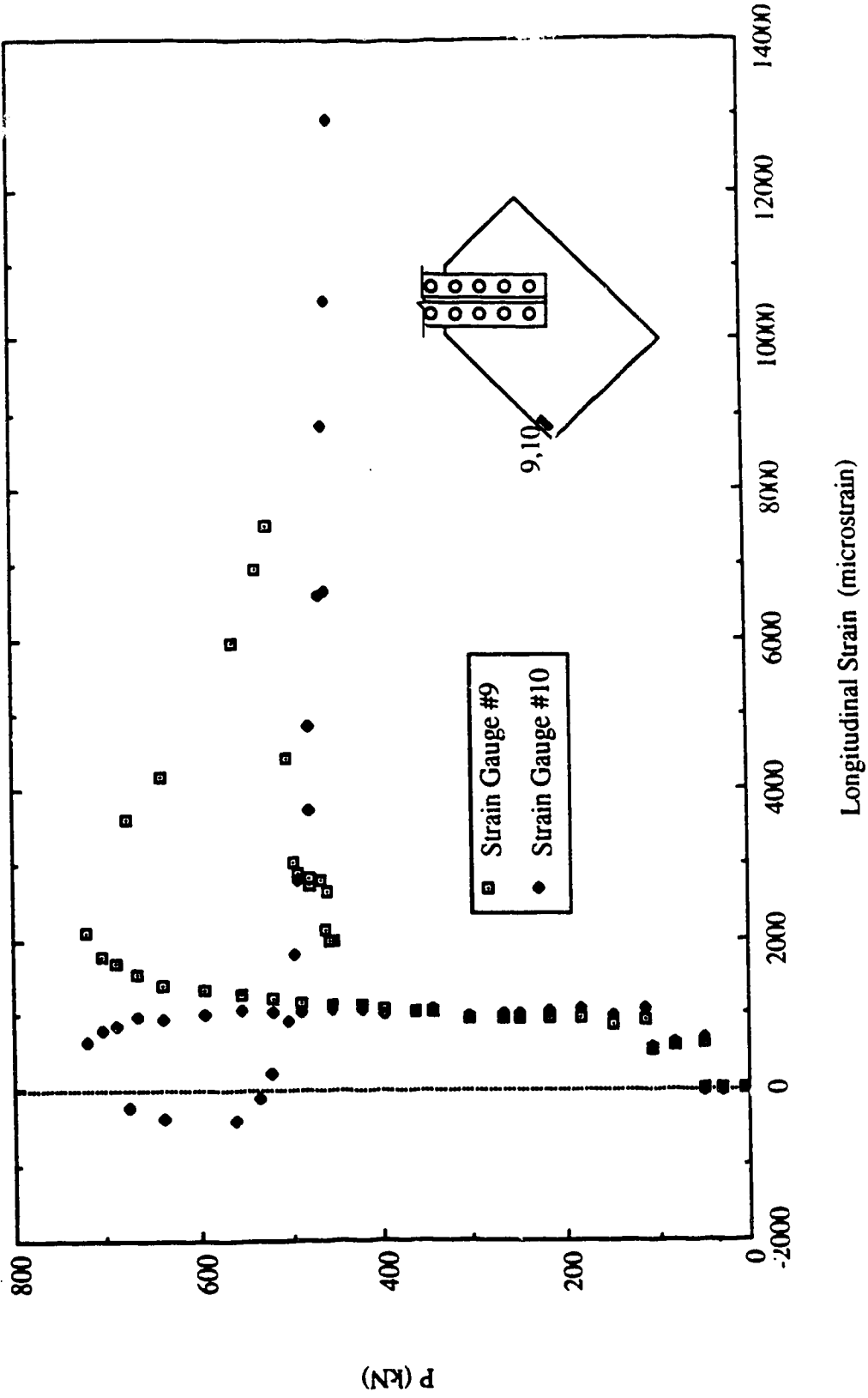


Fig. 6.21 Load vs. Strain Gauge Readings at End of Long Free Edge for Specimen MP3

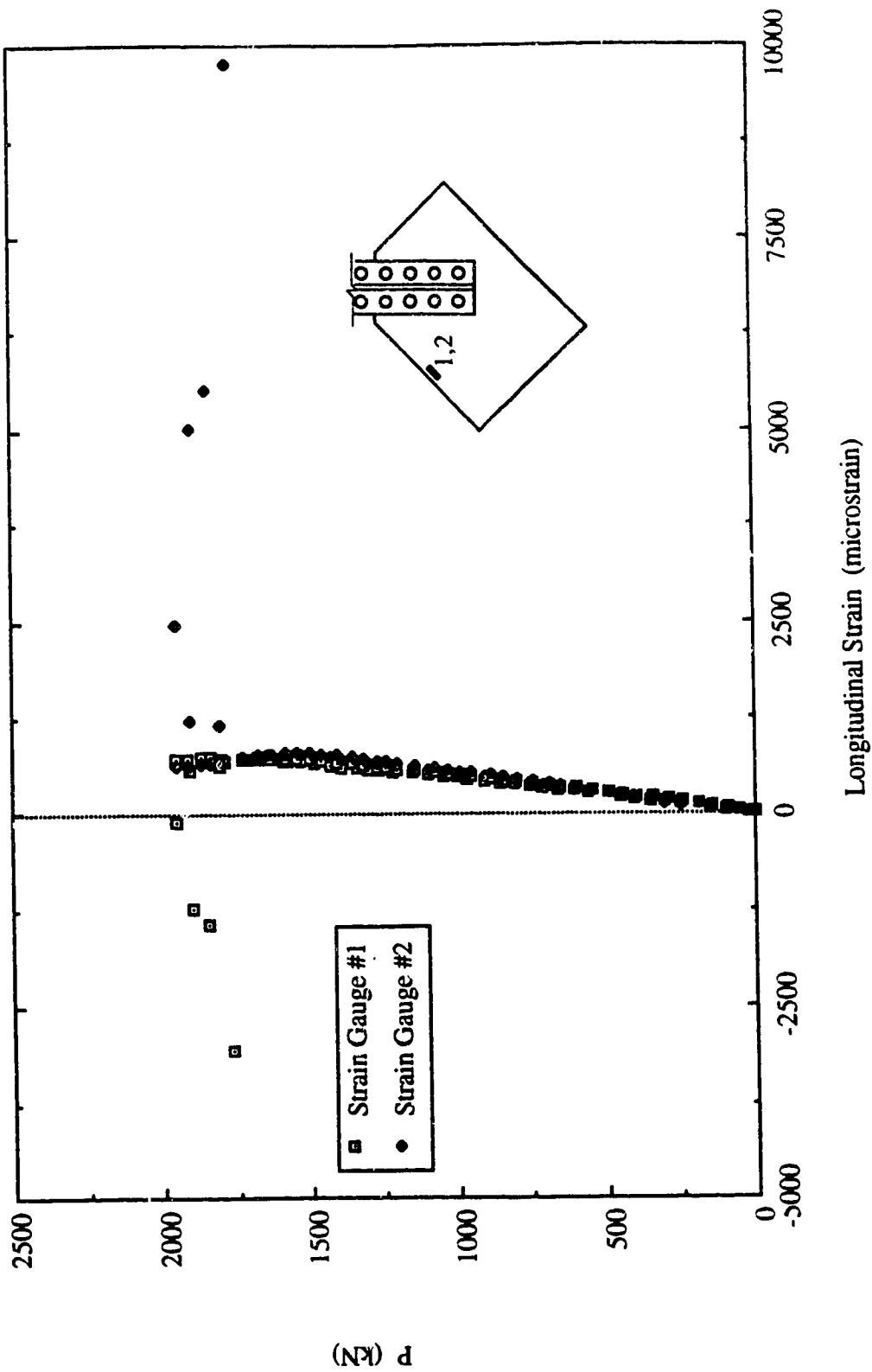


Fig. 3.8 Load vs. Strain Gauge Readings at Mid-Length of Long Free Edge for Specimen GP1

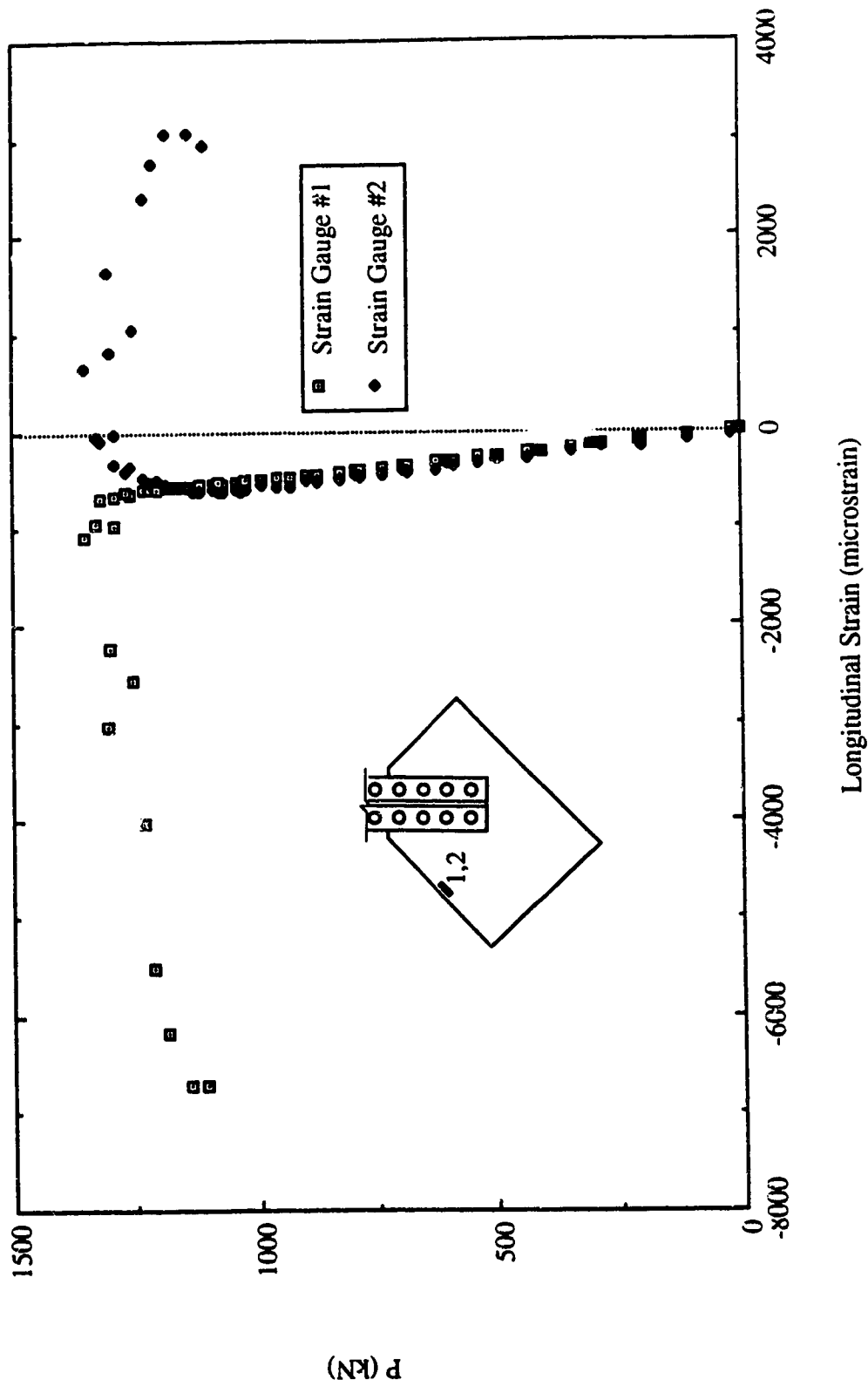


Fig. 3.9 Load vs. Strain Gauge Readings at Mid-Length of Long Free Edge for Specimen GP2

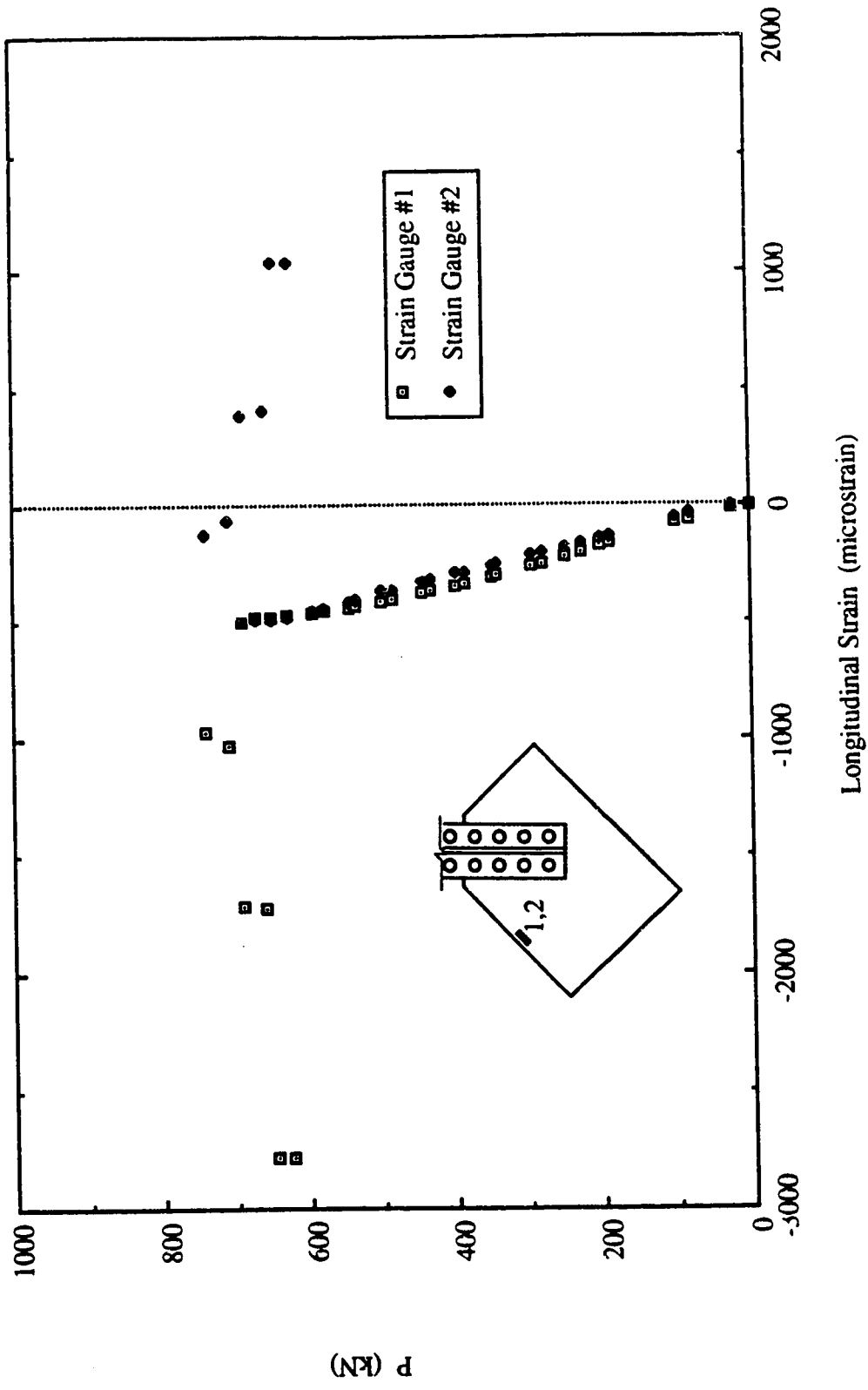


Fig. 3.10 Load vs. Strain Gauge Readings at Mid-Length of Long Free Edge for Specimen GP3

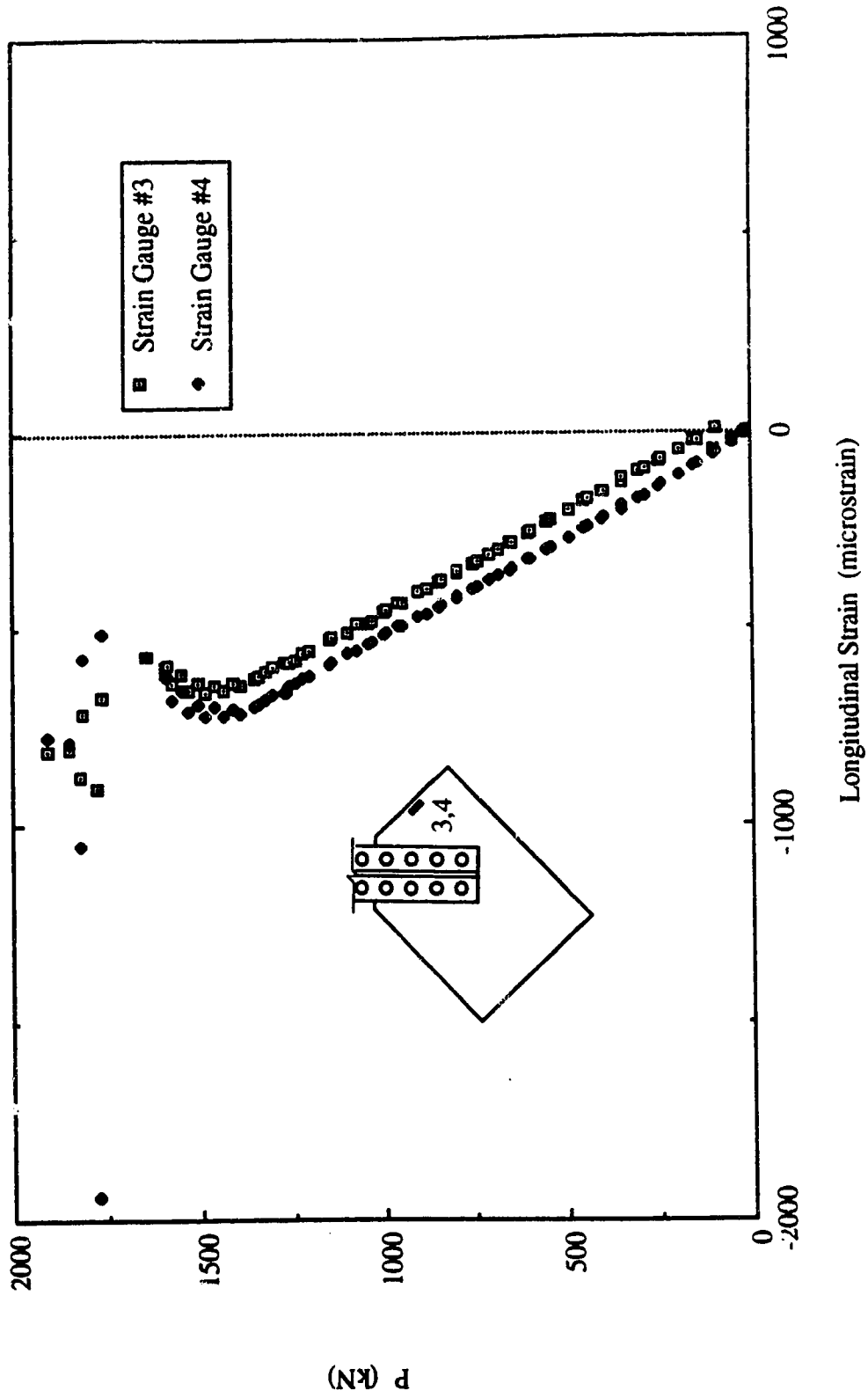


Fig. 3.11 Load vs. Strain Gauge Readings at Mid-Length of Short Free Edge for Specimen GPI

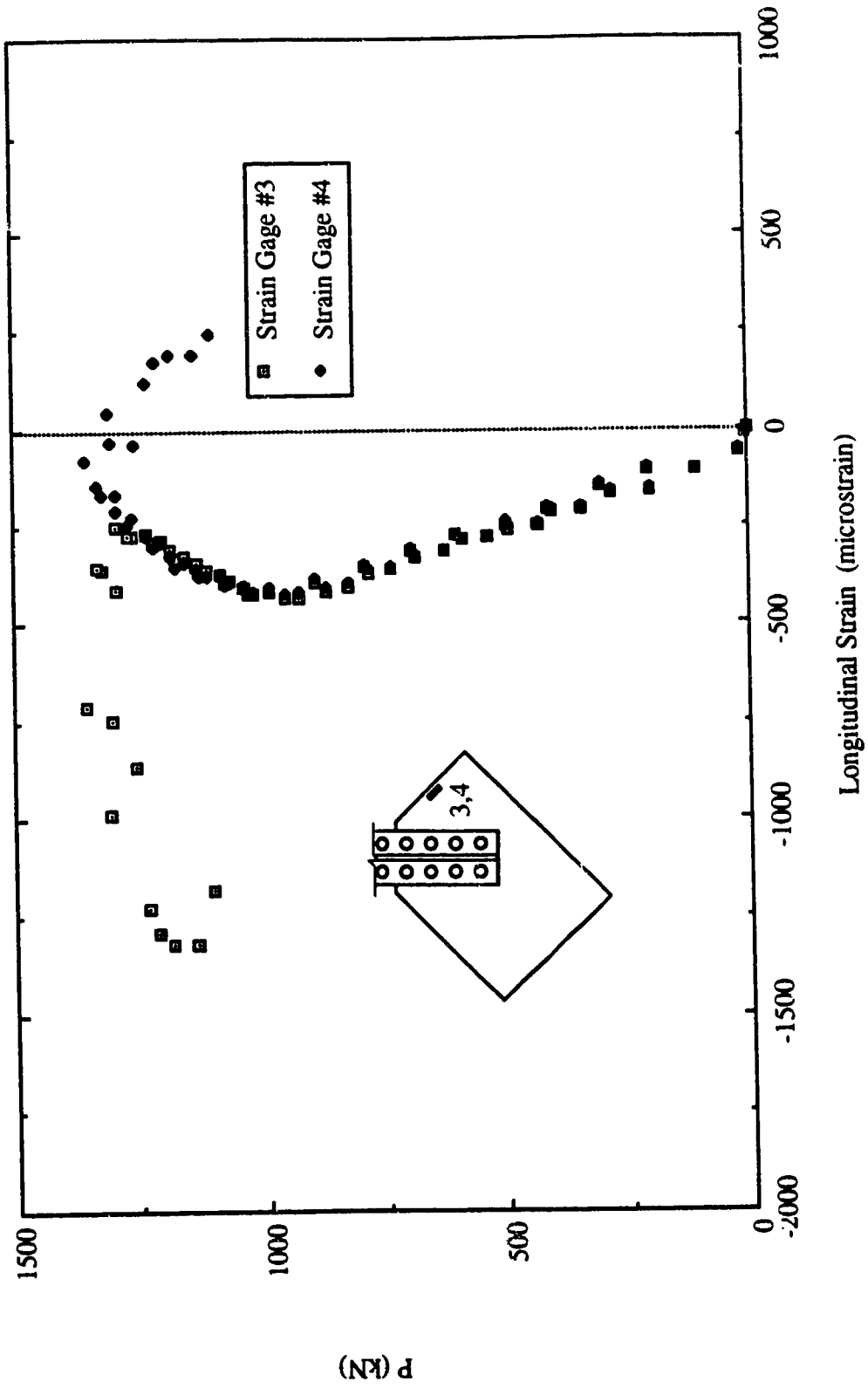


Fig. 3.12 Load vs. Strain Gauge Readings at Mid-Length of Short Free Edge for Specimen GP2

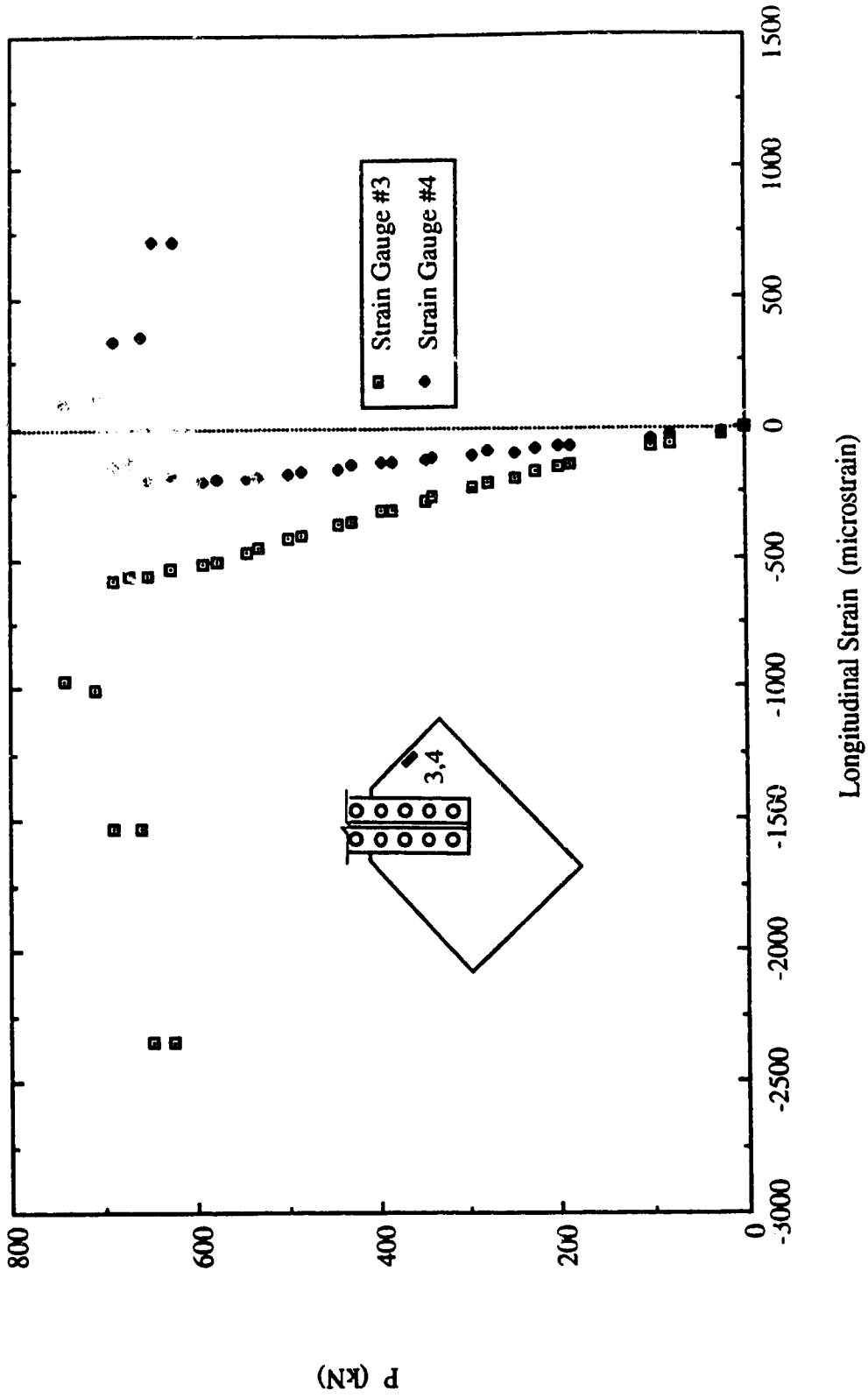


Fig. 3.13 Load vs. Strain Gauge Readings at Mid-Length of Short Free Edge for Specimen GP3



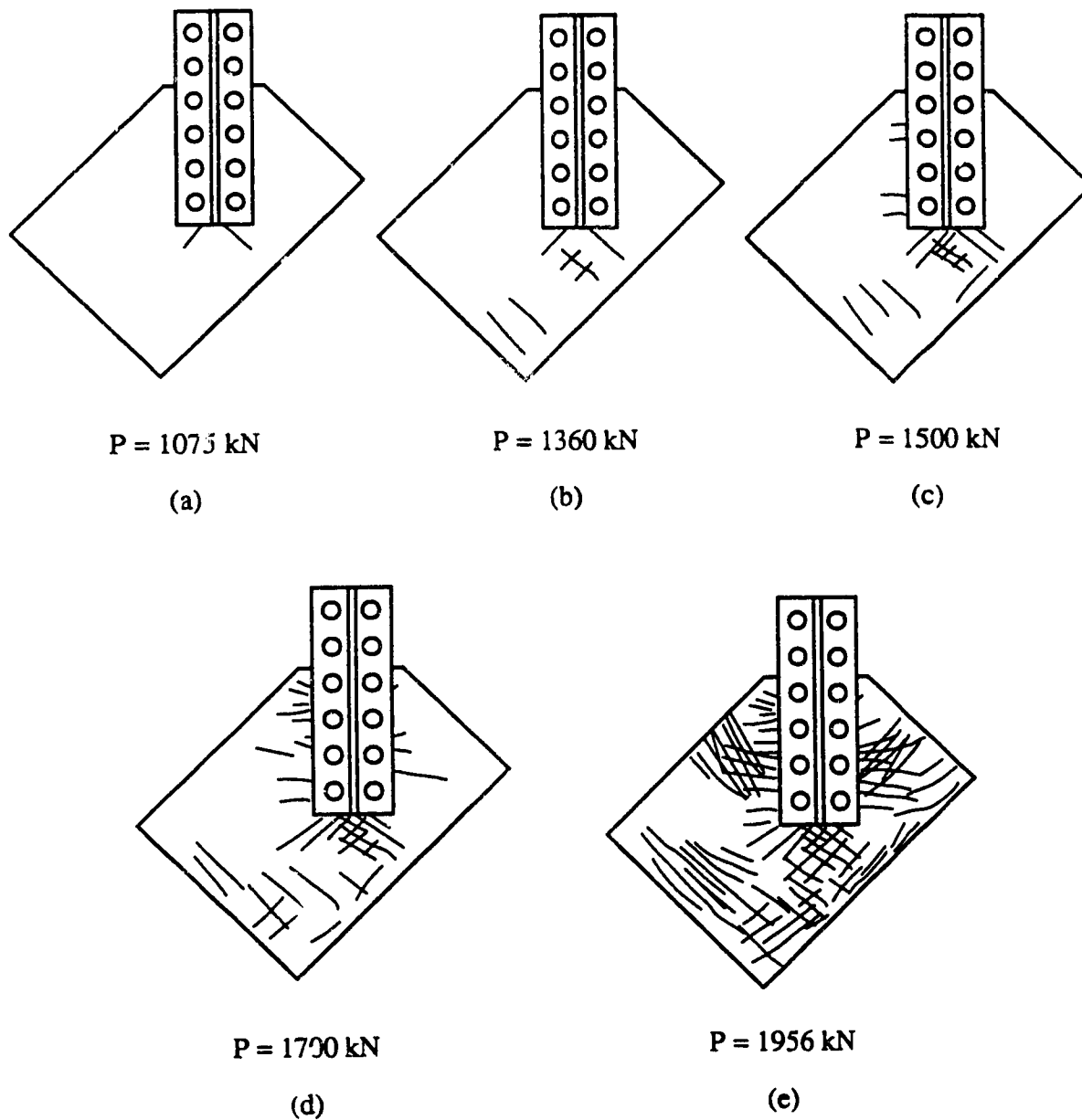


Fig. 3.14 Schematic of Yielding Process for Specimen GP1



**Fig. 3.15** Picture of Failed Specimen GP1

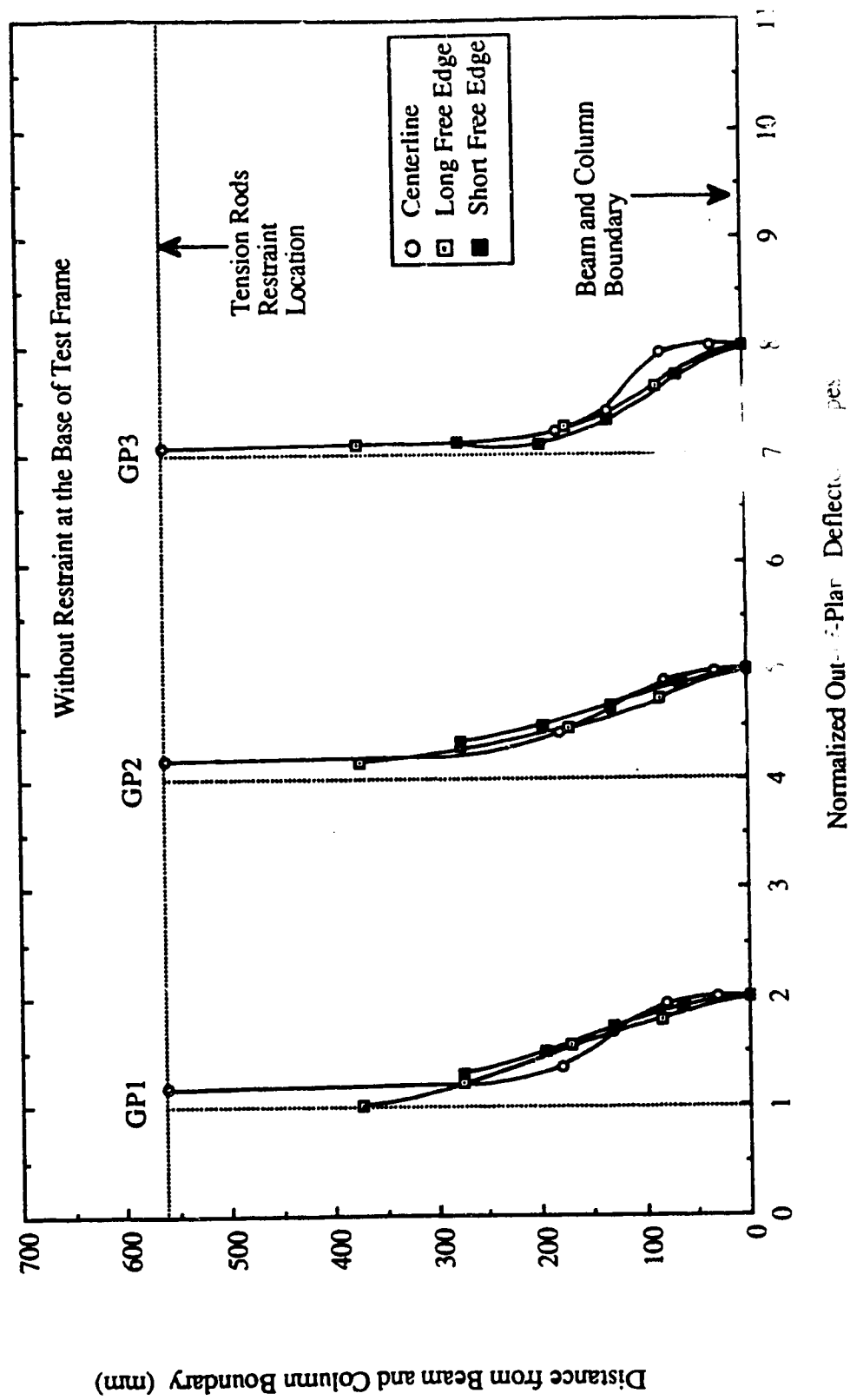
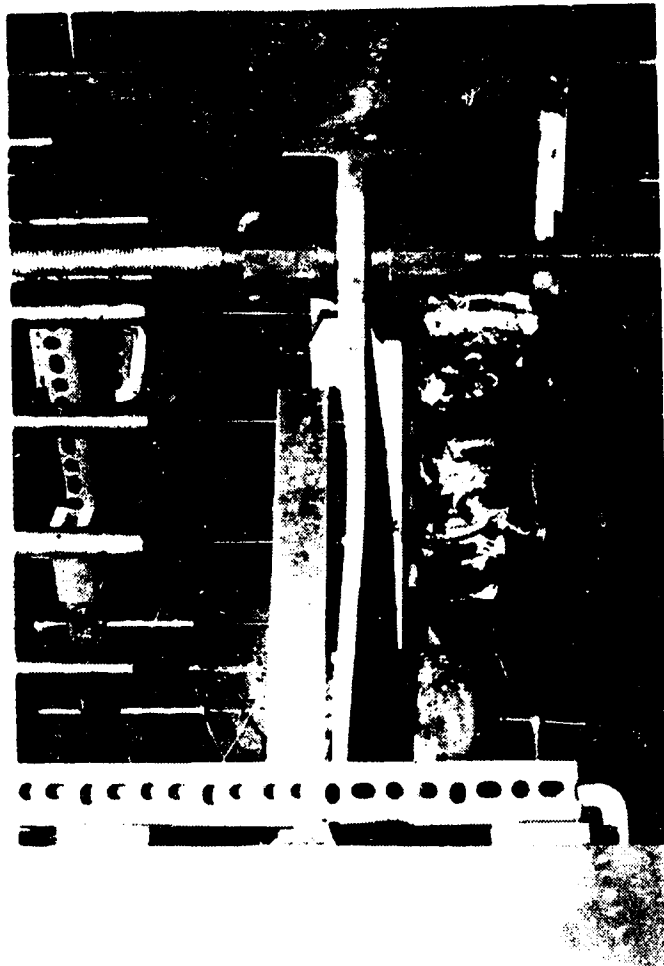


Fig. 3.16 Out-of-Plane Deflected Shapes at Free Edges and Along Centerline of Splice for GP Type Specimens



**Fig. 3.17** Picture of Out-of-Plane Deflected Shapes at Long Free Edge for Specimen GP1

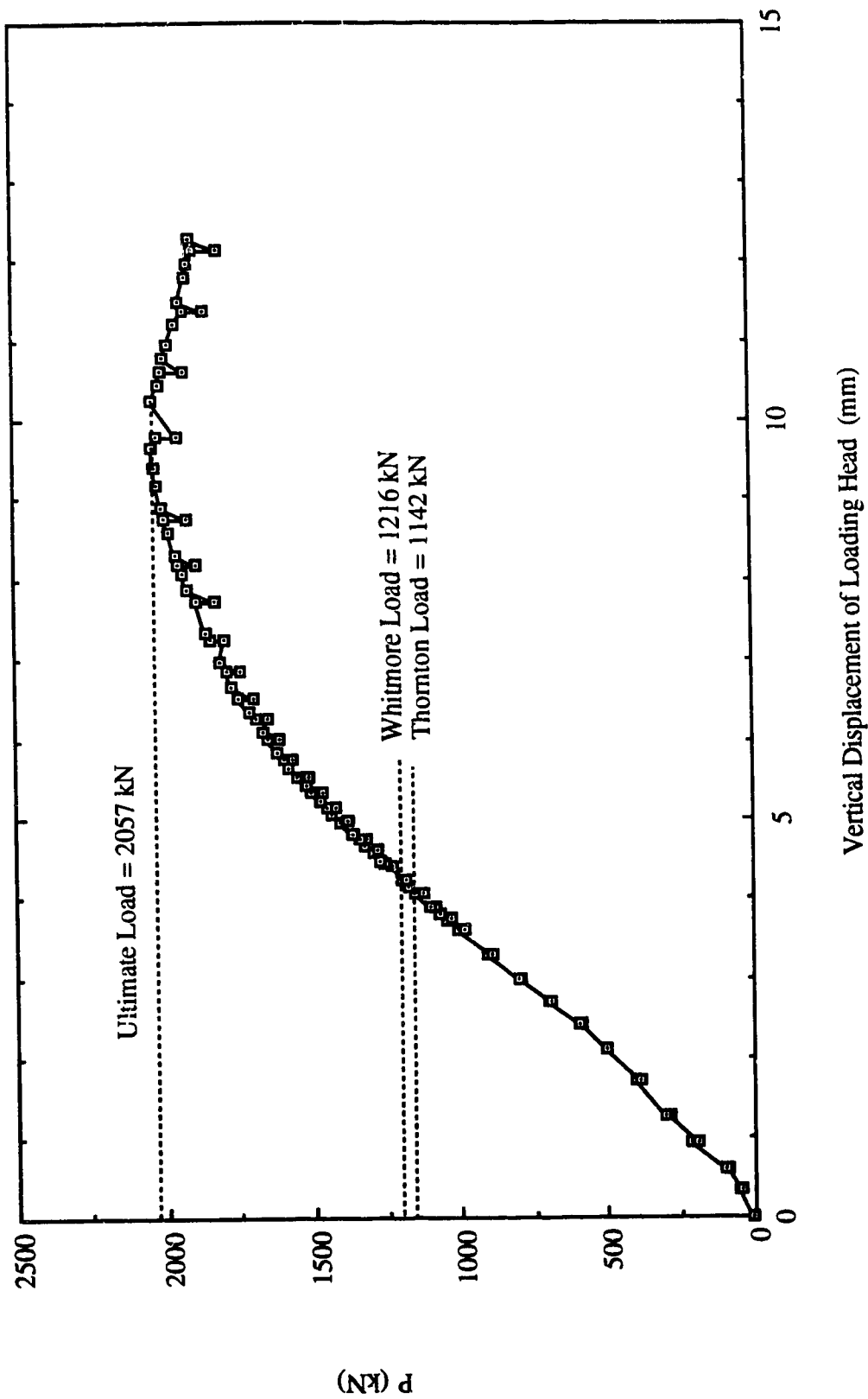


Fig. 3.18 Load vs. Vertical Displacement of Loading Head for Specimen GPIR

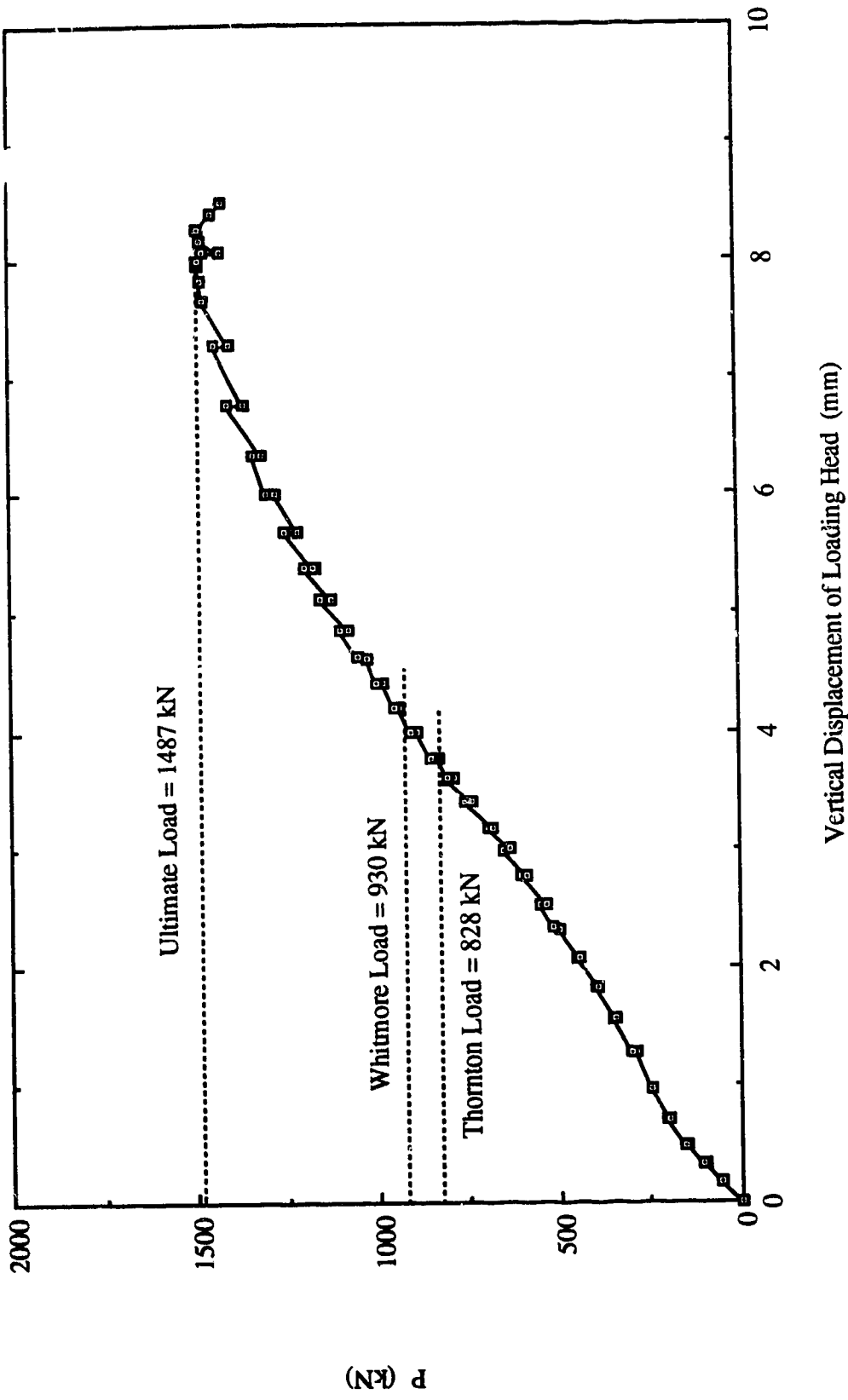


Fig. 3.19 Load vs. Vertical Displacement of Loading Head for Specimen GP2R

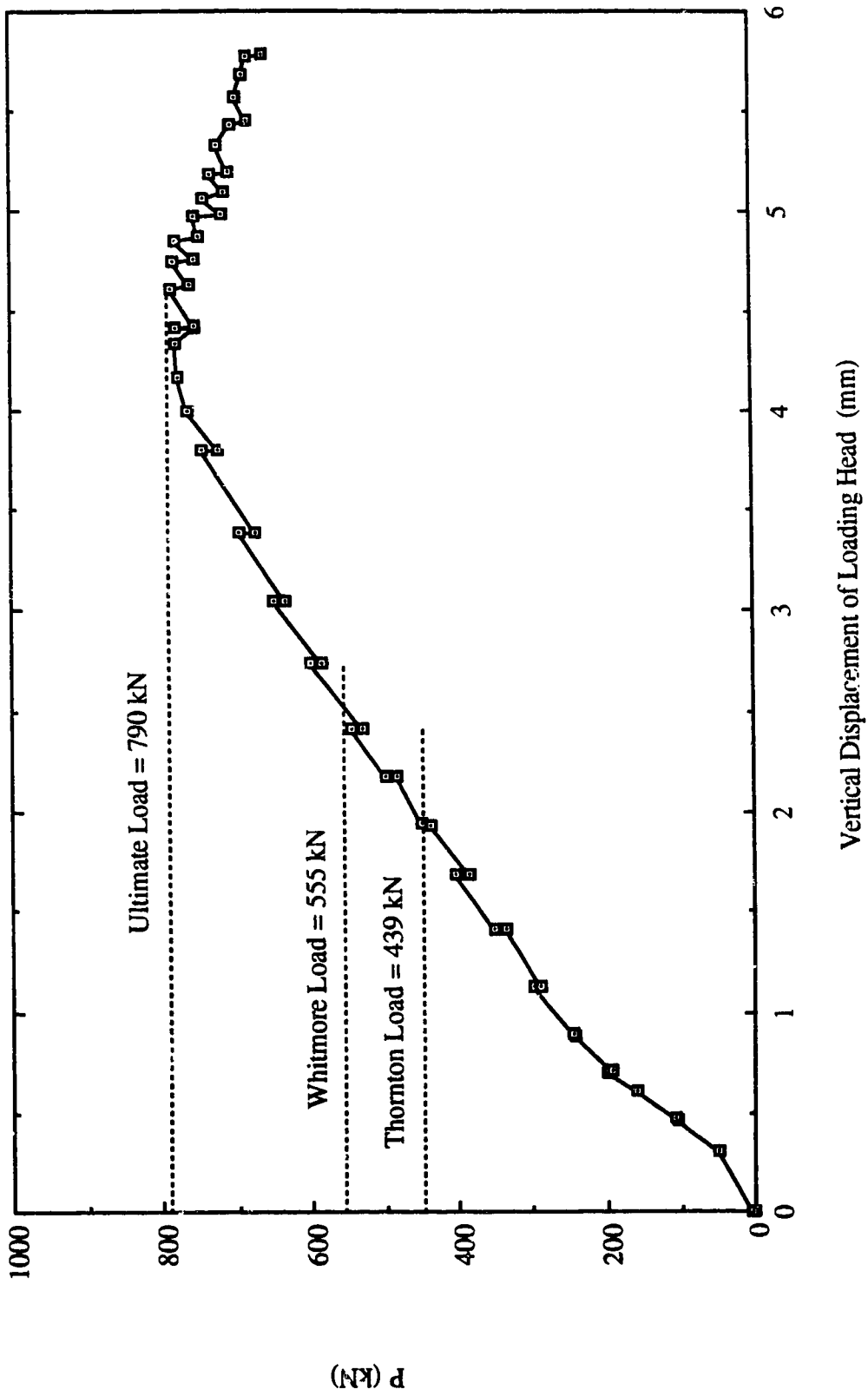
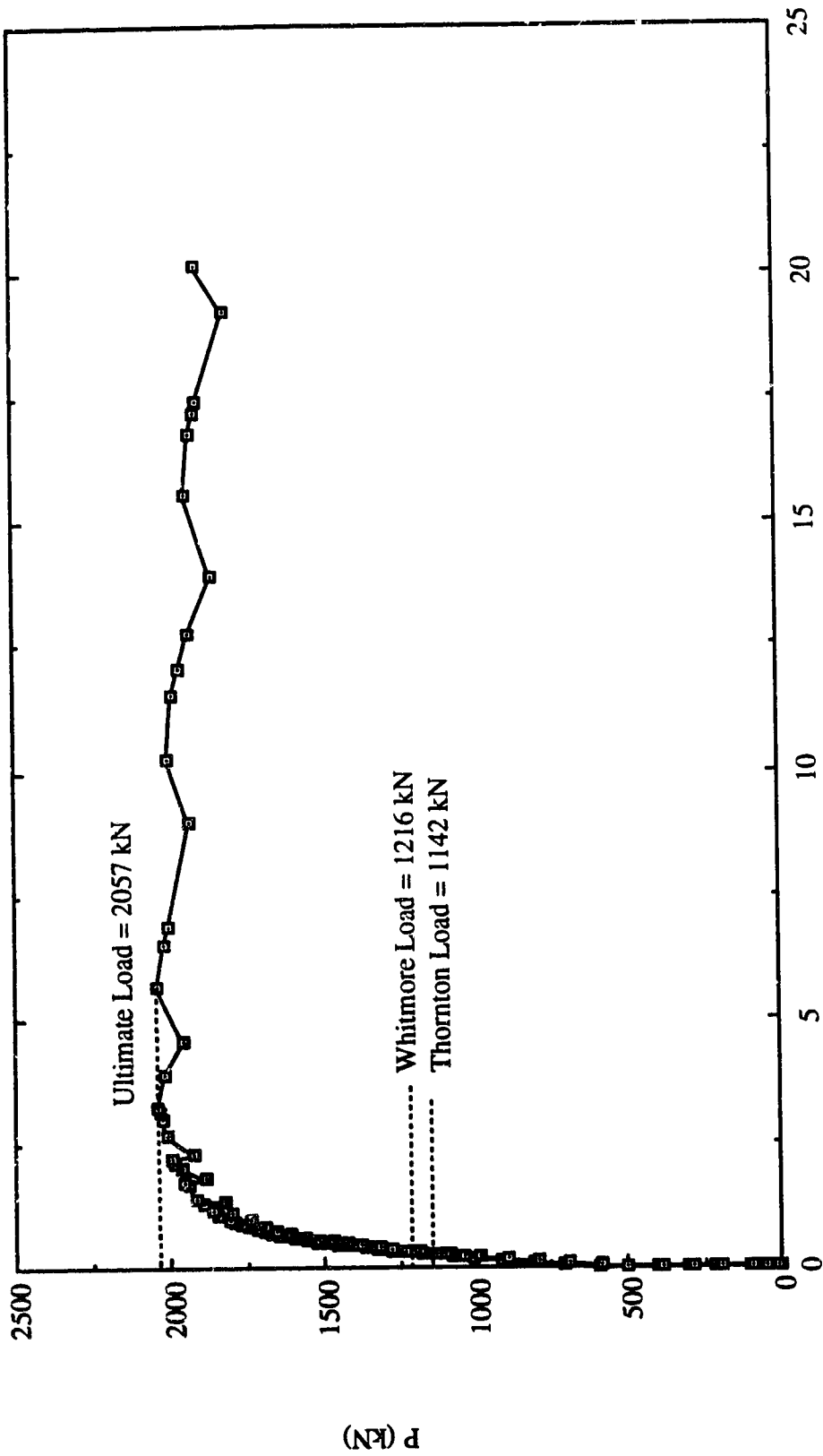


Fig. 3.20 Load vs. Vertical Displacement of Loading Head for Specimen GP3R



Out-of-Plane Displacement at Mid-Length of Long Free Edge (mm)

Fig. 3.21 Load vs. Out-of-Plane Displacement at Mid-Length of Long Free Edge for Specimen GP1R



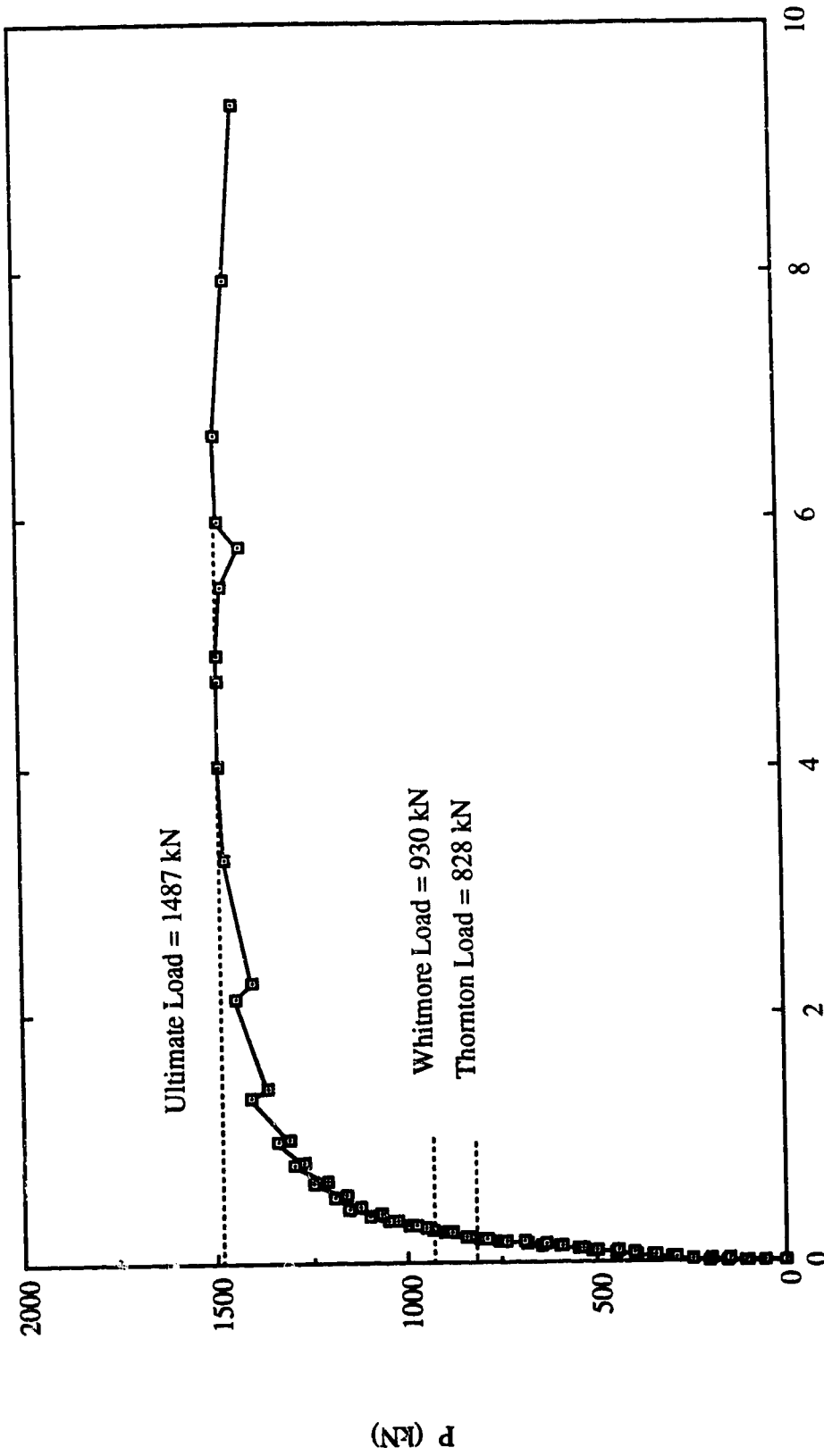


Fig. 3.22 Load vs. Out-of-Plane Displacement at Mid-Length of Long Free Edge for Specimen GP2R

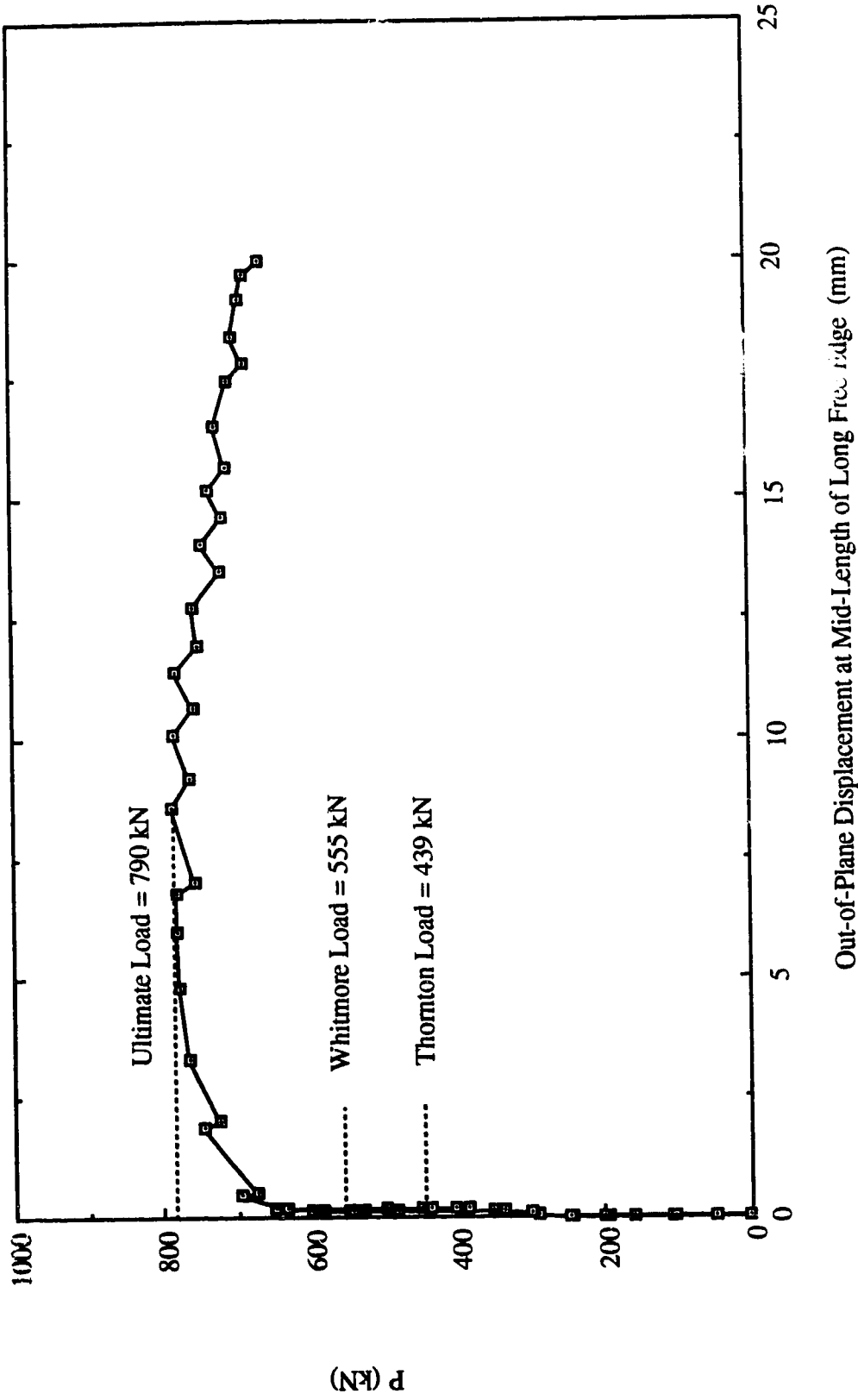


Fig. 3.23 Load vs. Out-of-Plane Displacement at Mid-Length of Long Free Edge for Specimen GP3R

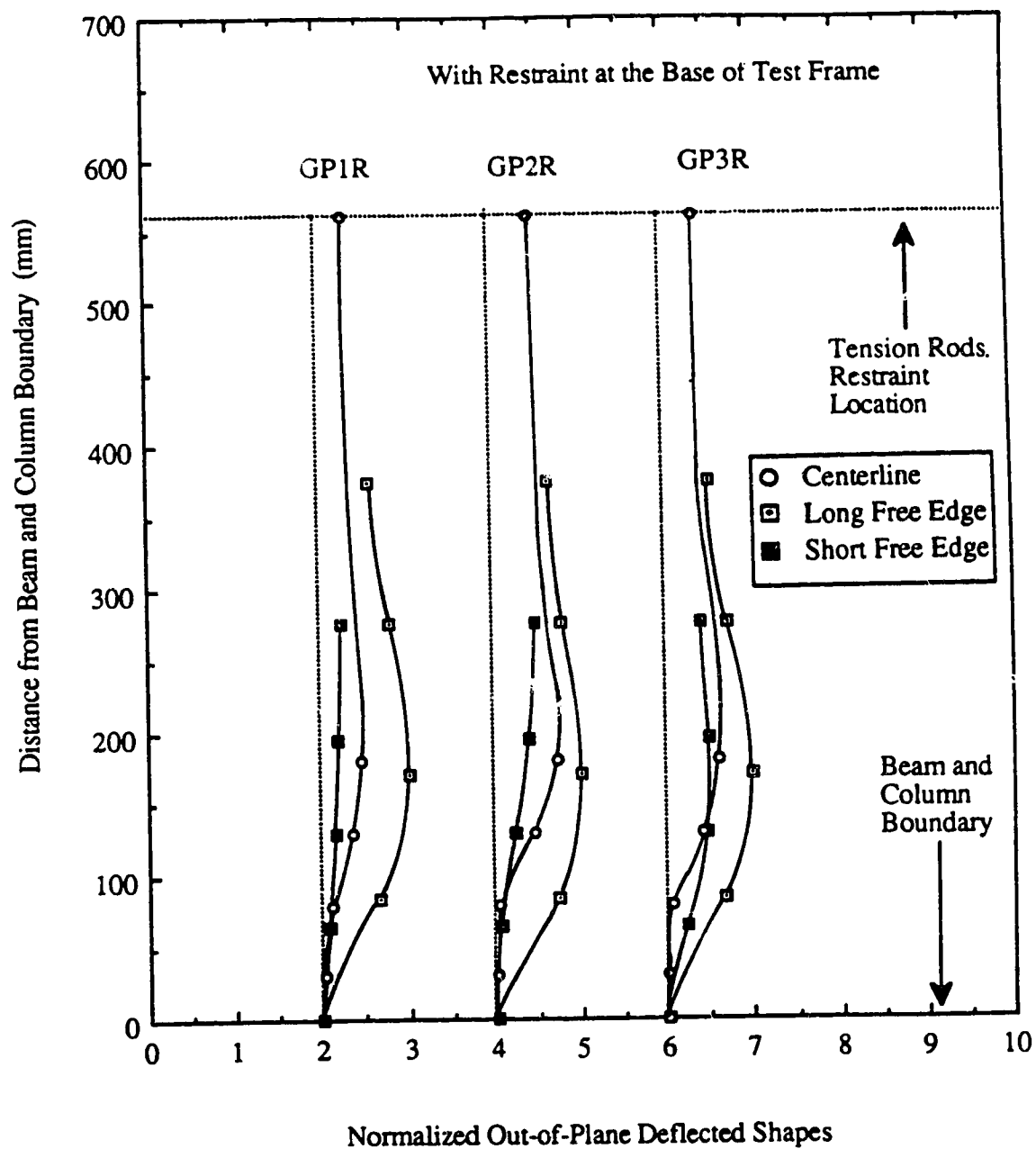


Fig. 3.24 Out-of-Plane Deflected Shapes at Free Edges and Along Centerline of Splice for GP Type Specimens - With Restraint

## **4. TEST RESULTS OF SP TYPE SPECIMENS**

### **4.1 General**

The SP type specimens were used to examine the effects of gusset plate size on the compressive behavior of the connection, and two specimens were tested with plate thickness of 13.3 mm and 9.8 mm. Again, the out-of-plane restraint at the base of the test frame was also included as a test variable in testing these specimens. The test results of the SP type specimens are summarized in Table 4.1. It can be seen from the table that the ultimate load of the specimens increased with increasing plate thickness. The test results also show that an appreciable increase in the ultimate load was recorded for specimen SP1 when out-of-plane restraint was applied to the base of the test frame. In addition, for specimen SP2, a significant increase in the ultimate load due to the out-of-plane restraint was observed, as shown in Table 4.1. The predictions by both the Whitmore method and the Thornton method are also included in the table. In general, it can be seen that the Whitmore method overestimated the strength of the specimens for both restraint conditions, except for the case of specimen SP2 with restraint. On the other hand, the Thornton method provided conservative estimates of the strength of specimens.

### **4.2 Without Out-of-Plane Restraint at Base of Test Frame**

#### **4.2.1 Behavior of Load versus In-Plane Deformation**

The failure mode for both specimens SP1 and SP2 was sway buckling of the connection. The curves of load versus the vertical displacement of the loading head are illustrated in Figs. 4.1 and 4.2. It can be seen from these figures that both specimens were not able to reach the yield load level estimated by the Whitmore's method. However, the ultimate load of the thick specimen (SP1-13.3 mm) reached about 87 percent of the corresponding Whitmore load. On the other hand, the thin specimen (SP2-9.8 mm) only reached about 71 percent of the corresponding Whitmore load. A linear load deflection behavior was

observed until the applied load was close to the ultimate load at which significant out-of-plane displacement had occurred. In particular, the load deflection curve for specimen SP2 was linear until it reached the ultimate load. The vertical displacement of the loading head only increased slightly after the specimens buckled.

#### **4.2.2 Behavior of Load versus Out-of-Plane Displacement of Test Frame**

The out-of-plane displacement of the test frame was recorded for both specimens from the beginning of loading due to the presence of initial imperfections. These imperfections were caused by the initial out-of-straightness of the plate and the welding procedure. The curves of load versus the out-of-plane displacement of the test frame are shown in Figs. 4.3 and 4.4. For specimen SP1, the load deflection curve gradually increased until the applied load reached approximately 1400 kN, at which a significant out-of-plane displacement was observed. The displacement continued to increase with a slight increase in the applied load. At a displacement of about 16 mm, a significant increase in stiffness of the connection was observed. This increase in stiffness was probably caused by local bending of the gusset plate underneath the splice member, and this will be discussed later when the strain gauge readings are examined. The ultimate load of the specimen was reached at 1606 kN, with a deflection of about 17.5 mm. For specimen SP2, the load versus out-of-plane displacement curve gradually increased until the buckling of the specimen occurred. The ultimate load of the specimen was reached at 1010 kN with a displacement of about 17.5 mm. The final displacement of the test frame was approximately 24.5 mm, and the applied load was maintained very close to the ultimate load of the specimen.

#### **4.2.3 Strain Gauge Results**

The curves of load versus strains are shown in Figs. 4.5 to 4.10. It can be seen from the plots for strain readings recorded at the mid-length of the free edges (Figs. 4.5, 4.6, 4.7,

and 4.8) that bending of the plate occurred from the beginning of loading. Again, this was mainly caused by the initial imperfections of the plate and hence the misalignment of the loading head. Nonetheless, these plots indicated the occurrence of strain bifurcation when the specimens buckled. It should also be noted that the strain readings for the specimens were within the elastic range prior to reaching the ultimate load. As mentioned above, a change in the bending direction of the plate underneath the splice member was observed at a load level of about 1400 kN for specimen SP1. This phenomenon can be shown by the plot of load versus rosette strain readings at a load level close to the ultimate for specimen SP1, as illustrated in Fig. 4.9. This figure illustrates that the strain reversal existed at a load level of about 1380 kN at which point a change of the bending direction of the plate underneath the splice member had occurred. As the out-of-plane displacement of the test frame increased from this load level, the compressive strain at rosette gauge #22 decreased, while increasing compressive strains were recorded at rosette gauge #21 as shown in Fig. 4.9. At a load level of about 1506 kN, the compressive strain at rosette gauge #22 increased because of the local bending of the plate underneath the splice member, and a significant increase in the compressive strain at rosette gauge #21 was also observed. This local bending behavior of the plate might attribute to the increase in the out-of-plane stiffness of the specimen at this load level. The applied load continued to increase with the increasing compressive strain at rosette gauge #22 until the ultimate load was reached.

#### **4.2.4 Yielding Behavior of Specimens**

In general, only moderate yielding was observed for the SP type specimens. For specimen SP1, the yielding was first observed close to the corner of the beam and column boundary at a load level of about 1200 kN. As load increased to approximately 1550 kN, yield lines were observed in the area about the two sides of the splice member and also underneath the splice member. When the applied load approached the ultimate level, the yielding at the corner of the beam and column boundary increased. Finally, at the ultimate yield lines

were observed on the specimen along the beam and column boundary, as shown in Fig. 4.11. For specimen SP2, yield lines were first detected in the area about the two sides of the splice member when the applied load was approximately 900 kN. As the load increased, yielding was also observed near the beam and column boundary. Again, yield lines were detected along the beam and column boundary at the ultimate load level.

#### **4.2.5 Out-of-Plane Deflected Shapes of Free Edges and along Centerline of Splicing Member**

The out-of-plane deflected shapes for the specimens are shown in Fig. 4.12. In general, it can be seen from this figure that the deflected shapes resembled the buckled shapes of a fixed-guided column, except for the deflected shapes of the long free edge of specimen SP2. This different deflected shape was caused by the initial out-of-straightness of the free edge. In fact, significant warping of the specimen was observed after the plate was first welded to the beam and column. Hence, to correct the imperfection, the specimen was cut from the beam and column and welded back on. However, some noticeable imperfections still existed after re-welding. For specimen SP1, the LVDT's readings at the early stage of loading indicated that the deflected shape along the centerline of the splice member was similar to that of the long free edge of specimen SP2. However, as the applied load increased close to the ultimate load, the deflected shape shifted to the fixed-guided mode.

### **4.3 With Out-of-Plane Restraint at Base of Test Frame**

#### **4.3.1 General**

It was mentioned in the previous chapter that the same SP type specimens were used in conducting tests of both out-of-plane restraint conditions at the base of the test frame. As expected, permanent deformation existed in the failed specimens after the tests performed without a restraint condition. Therefore, in order to correct the imperfection, lateral force

was applied to the beam and column to push the failed specimen back to its original position. Unfortunately, appreciable imperfection still existed in the specimens after this remedial measure.

#### **4.3.2 Behavior of Load versus In-Plane Deformation**

The curves of load versus vertical displacement of the loading head are illustrated in Figs. 4.13 and 4.14. An initial nonlinearity of load deflection curves existed due to settling of the test fixtures. Subsequently, linear behavior was observed until the applied load approached the ultimate load. In particular, the applied load increased gradually to the ultimate load for specimen SP1. On the other hand, a relatively rapid increase to the ultimate load was observed for specimen SP2. It can be seen from the figures that after reaching the ultimate load, the applied load decreased with increasing vertical deflection.

#### **4.3.3 Behavior of Load versus Out-of-Plane Displacement at Mid-Length of Long Free Edge**

The curves of load versus the out-of-plane displacement at mid-length of the long free edge are shown in Figs. 4.15 and 4.16. For both specimens, a nonlinear load deflection behavior was observed at the beginning of loading. This was mainly caused by the initial imperfection induced after the previous testing of the specimens as mentioned above. In addition, the curve for specimen SP2 indicated that the long free edge at mid-length originally deformed eastward. However, when loading continued, the deformation gradually moved westward until buckling occurred, at which the plate deformed towards the east again. This behavior was probably because of the local bending of the specimen at the mid-length of the long free edge caused by the imperfection. When the specimen reached the ultimate load, the connection buckled eastward, which forced the long free edge to deform in the same direction.



#### **4.3.4 Yielding Behavior of Specimens**

Since these two specimens were tested previously, only any additional yielding observed in the tests with restraint at the conjunction of the gusset-to-splice will be discussed. For both specimens, the yield lines were recorded at the gusset plate near the corner of the splice member, as shown in Figs. 4.17 and 4.18. Local out-of-plane deflection of the specimens was also observed underneath the splice member. In addition, yield lines were recorded at the mid-length of the free edges. These yield lines originated from the gusset plate area near the corner of the splice member and extended towards the mid-length of the free edges, as shown in Fig. 4.19.

#### **4.3.5 Out-of-Plane Deflected Shapes of Free Edges and along Centerline of Splicing Member**

The normalized out-of-plane displacement for the free edges and along the centerline of the splice member for both specimens is shown in Fig. 4.20. Again, it can be seen from the figure that out-of-plane movement at the conjunction of the gusset-to-splice was recorded. Similar to GP type specimens, this displacement was caused by the bending of the web of the bracing about the tension rod supports. Nonetheless, these figures show the effects of out-of-plane restraint on the buckled shapes of the specimens. It should also be noted that the maximum out-of-plane displacement for both specimens occurred at the long free edge.

Table 4.1 Test Results of SP Type Specimens

Specimen Designation	Plate Size (mm x mm x mm)	Ultimate Load Without Restraint (kN)	Ultimate Load With Restraint (kN)	Whitmore Load $P_w$ (kN)	Thornton Load $P_t$ $k=0.65$ (kN)
SP1	850 x 700 x 13.3	1606	1760	1852	1228
SP2	850 x 700 x 9.8	1010	1477	1416	640

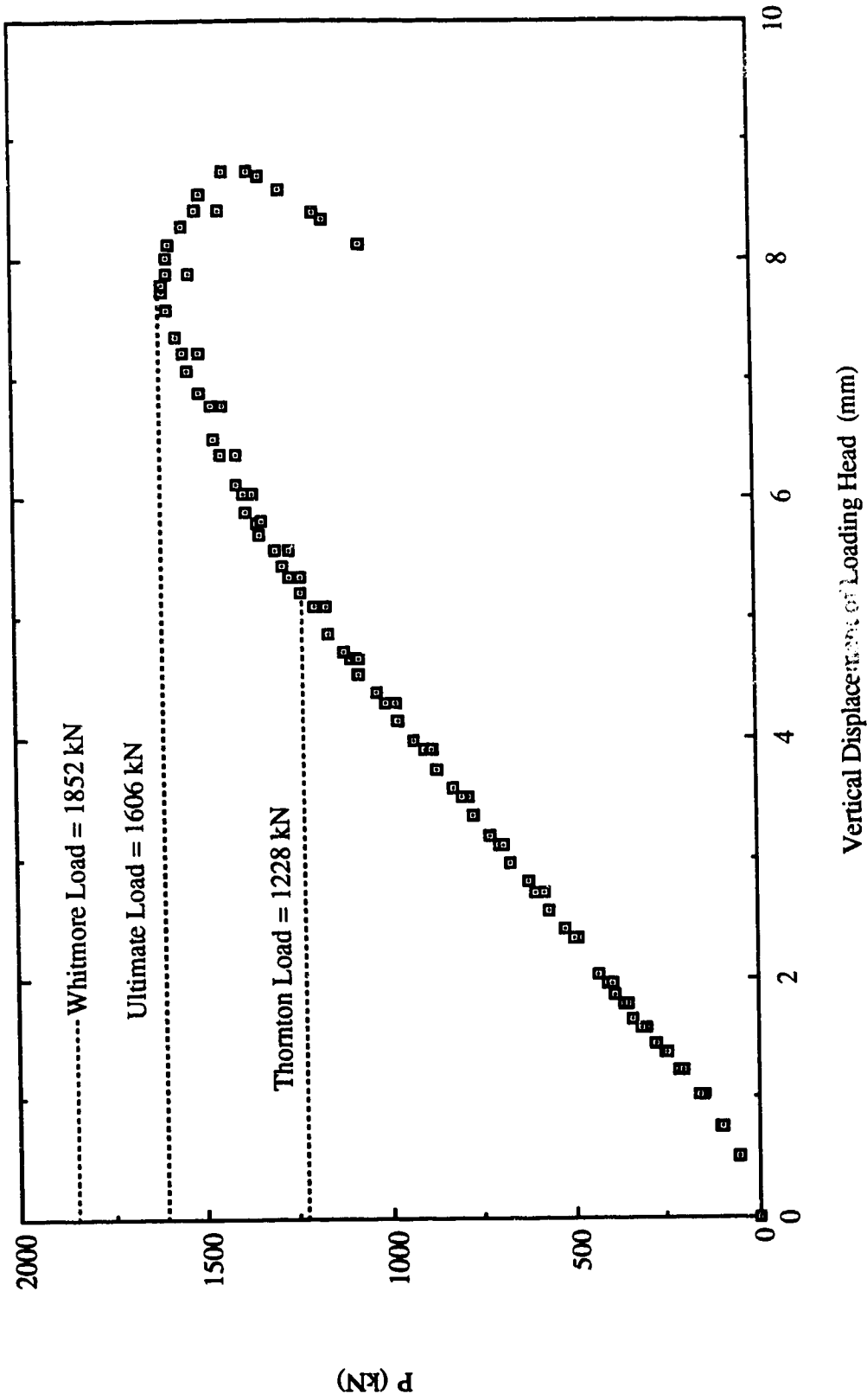


Fig. 4.1 Load vs. Vertical Displacement of Loading Head for Specimen SP1 - Without Restraint

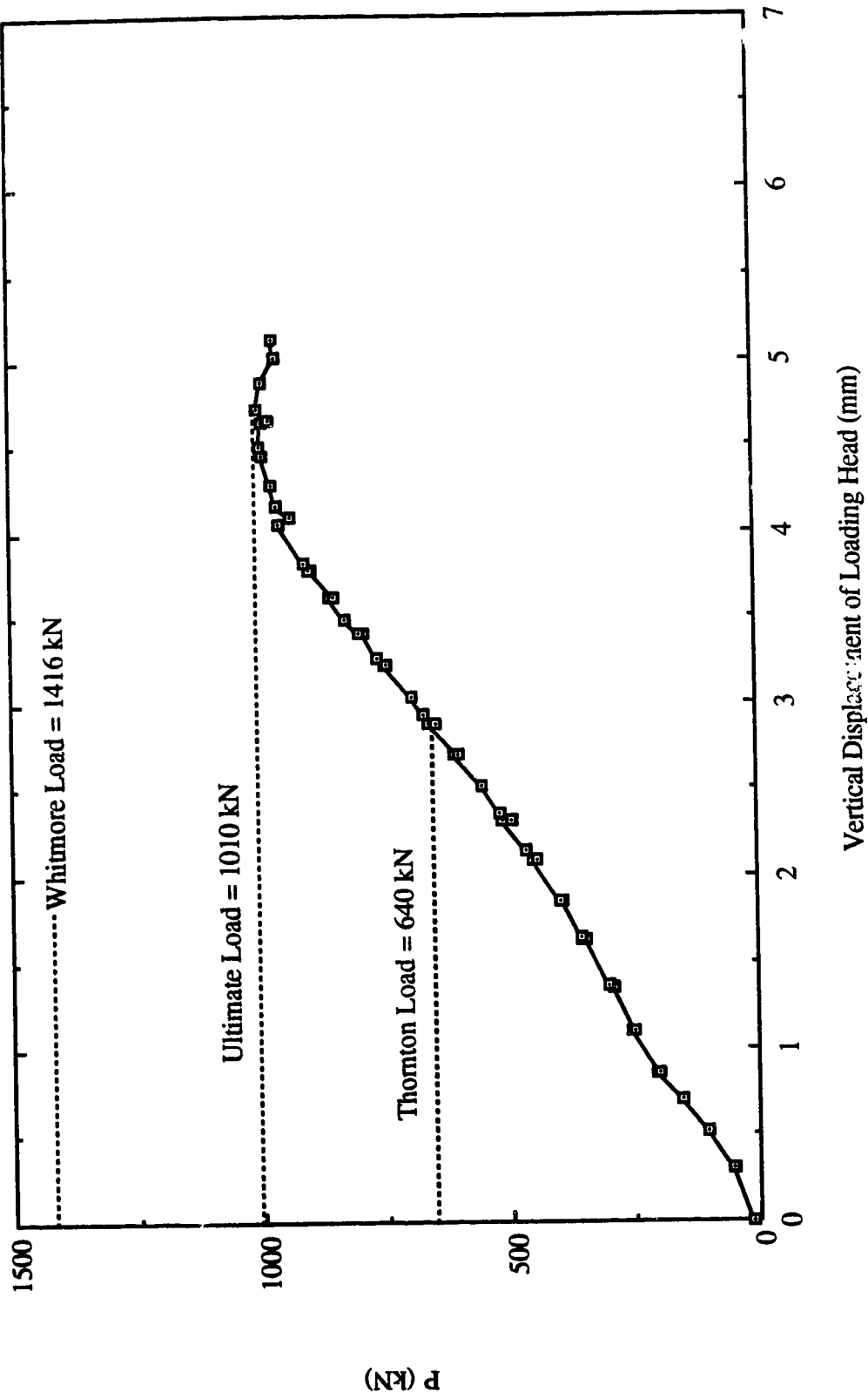


Fig. 4.2 Load vs. Vertical Displacement of Loading Head for Specimen SP2 - Without Restraint

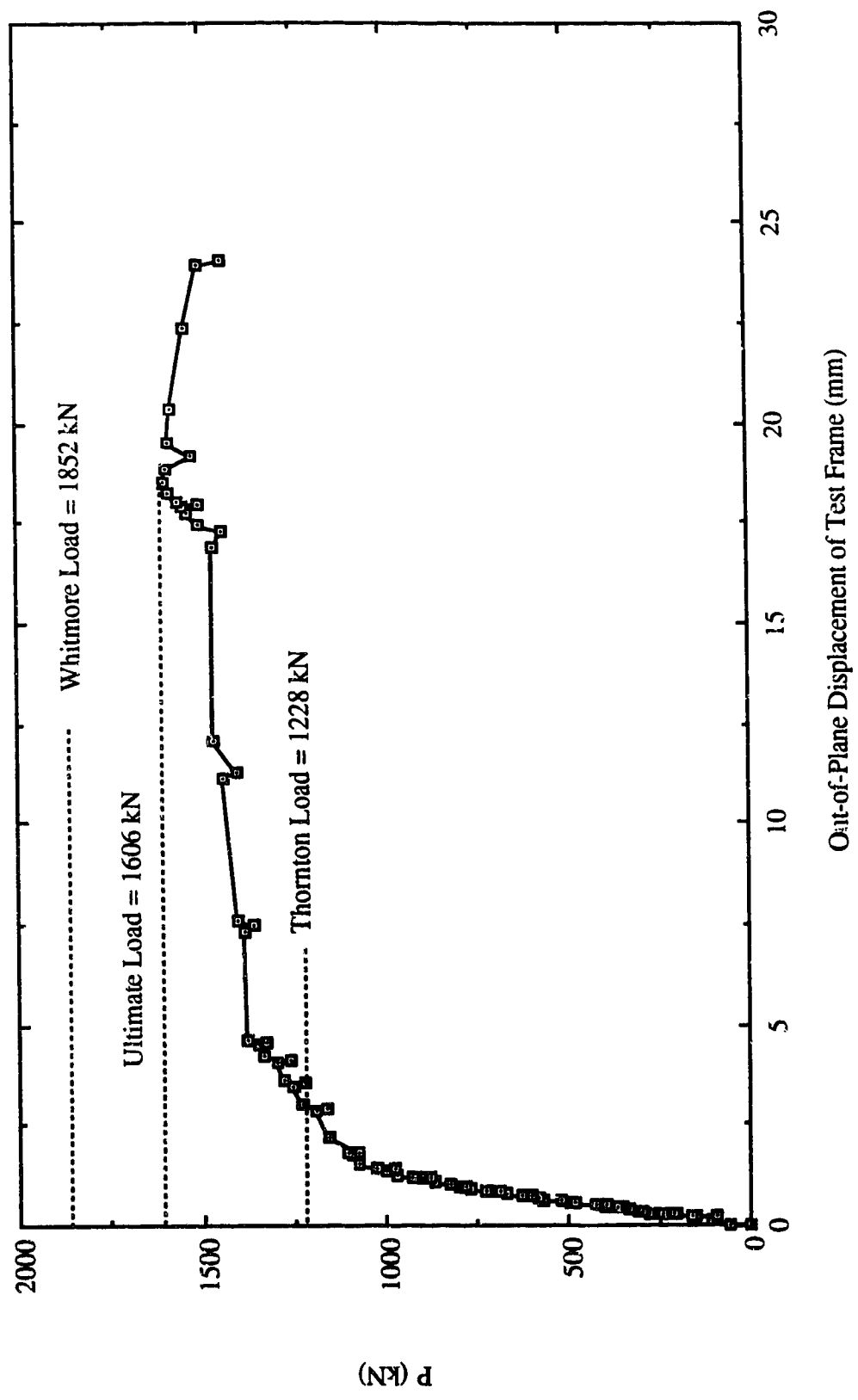


Fig. 4.3 Load vs. Out-of-Plane Displacement of Test Frame for Specimen SP1 - Without Restraint

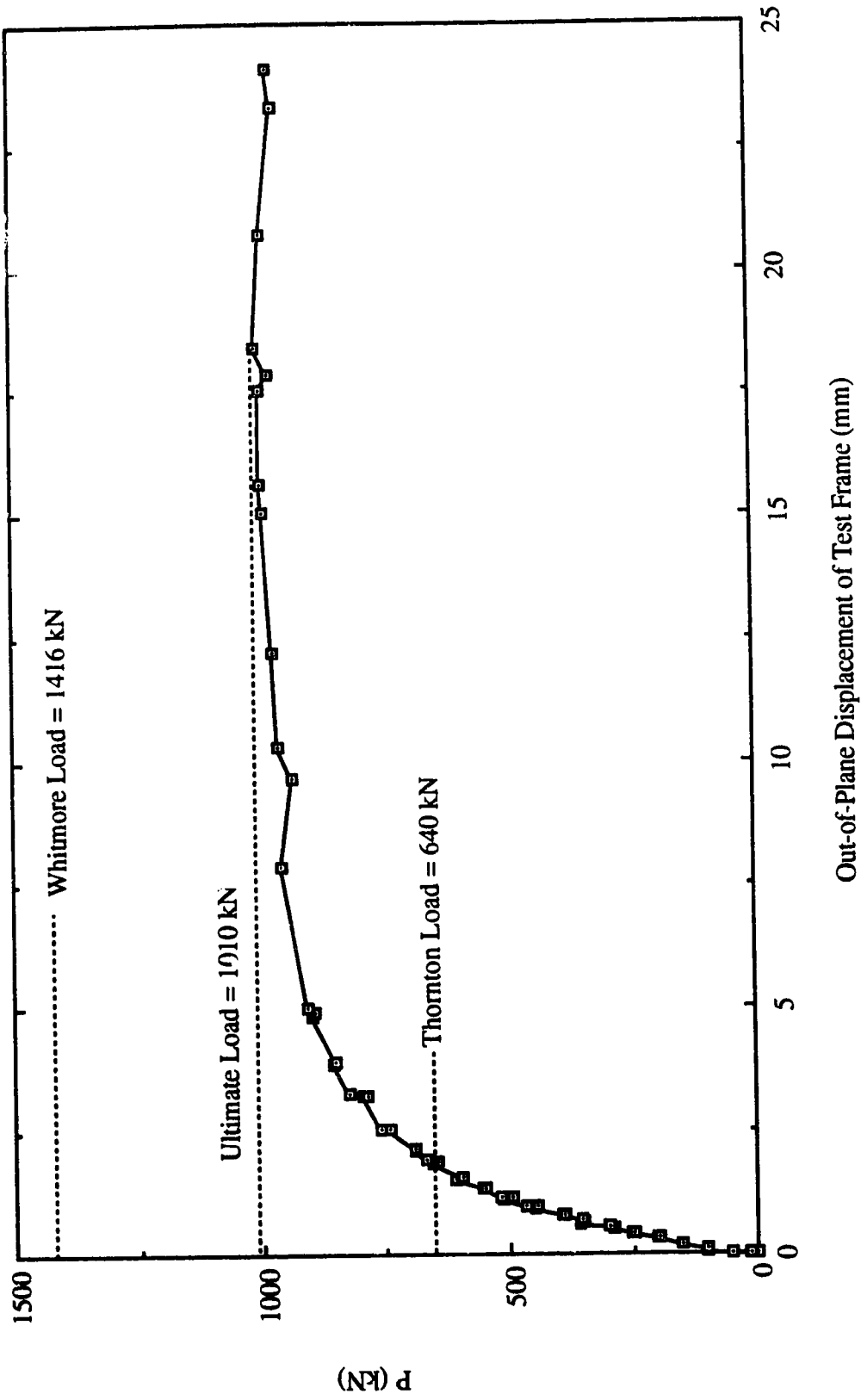


Fig. 4.4 Load vs. Out-of-Plane Displacement of Test Frame for Specimen SP2 - Without Restraint

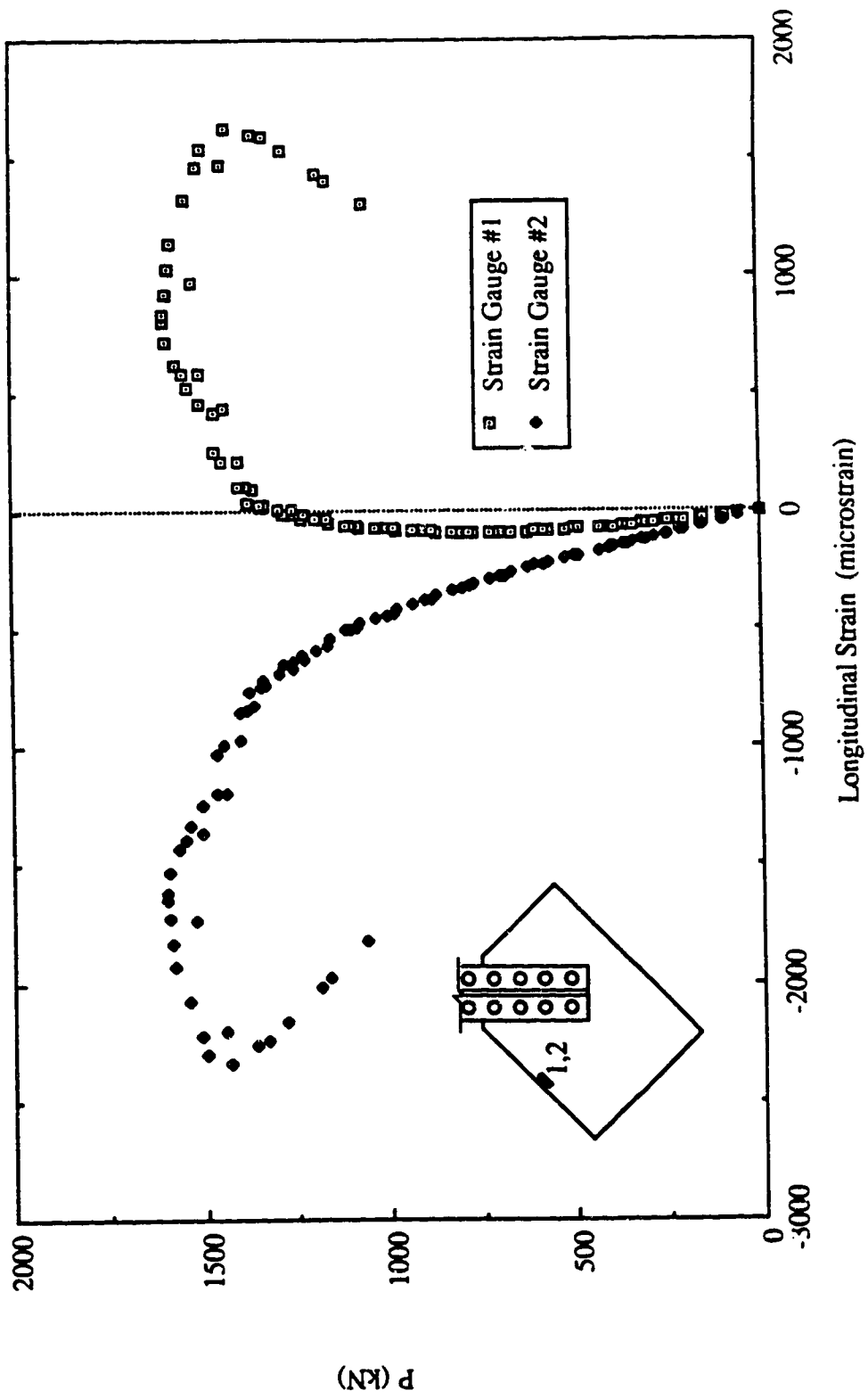


Fig. 4.5 Load vs. Strain Gauge Readings at Mid-Length of Long Free Edge for Specimen SP1 - Without Restraint

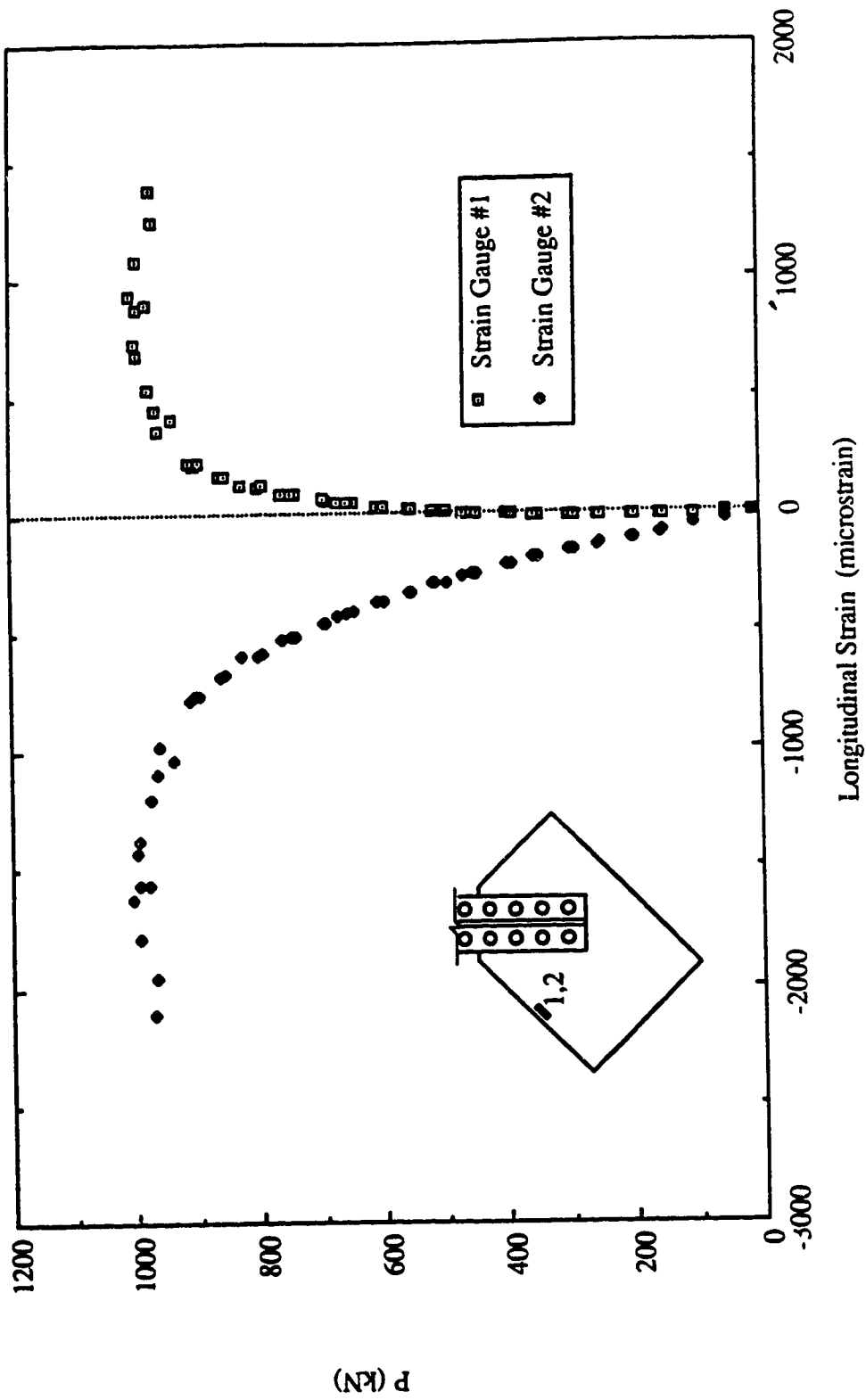


Fig. 4.6 Load vs. Strain Gauge Readings at Mid-Length of Long Free Edge for Specimen SP2 - Without Restraint



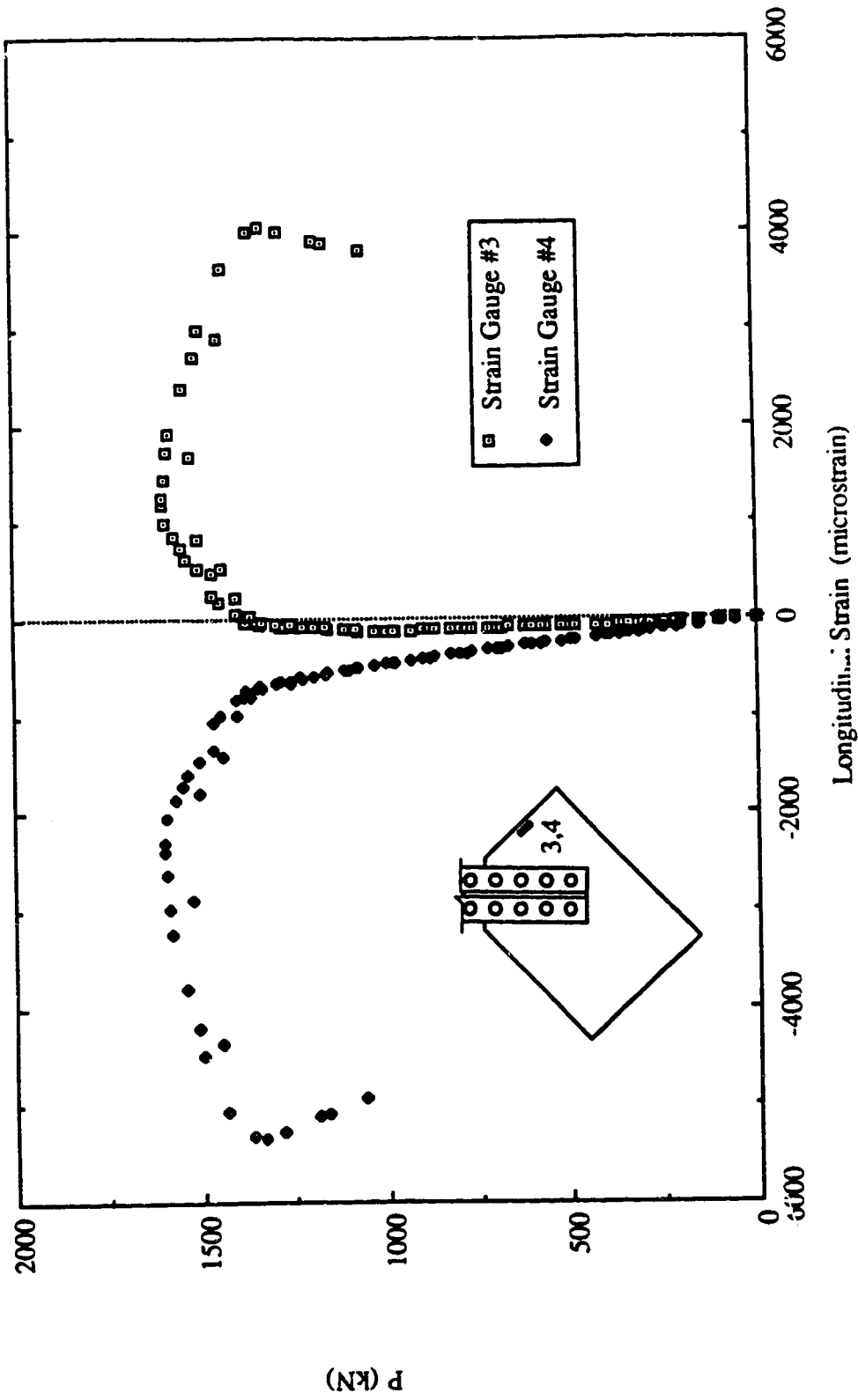


Fig. 4.7 Load vs. Strain Gauge Readings at Mid-Length of Short Free Edge for Specimen SP1 - Without Restraint

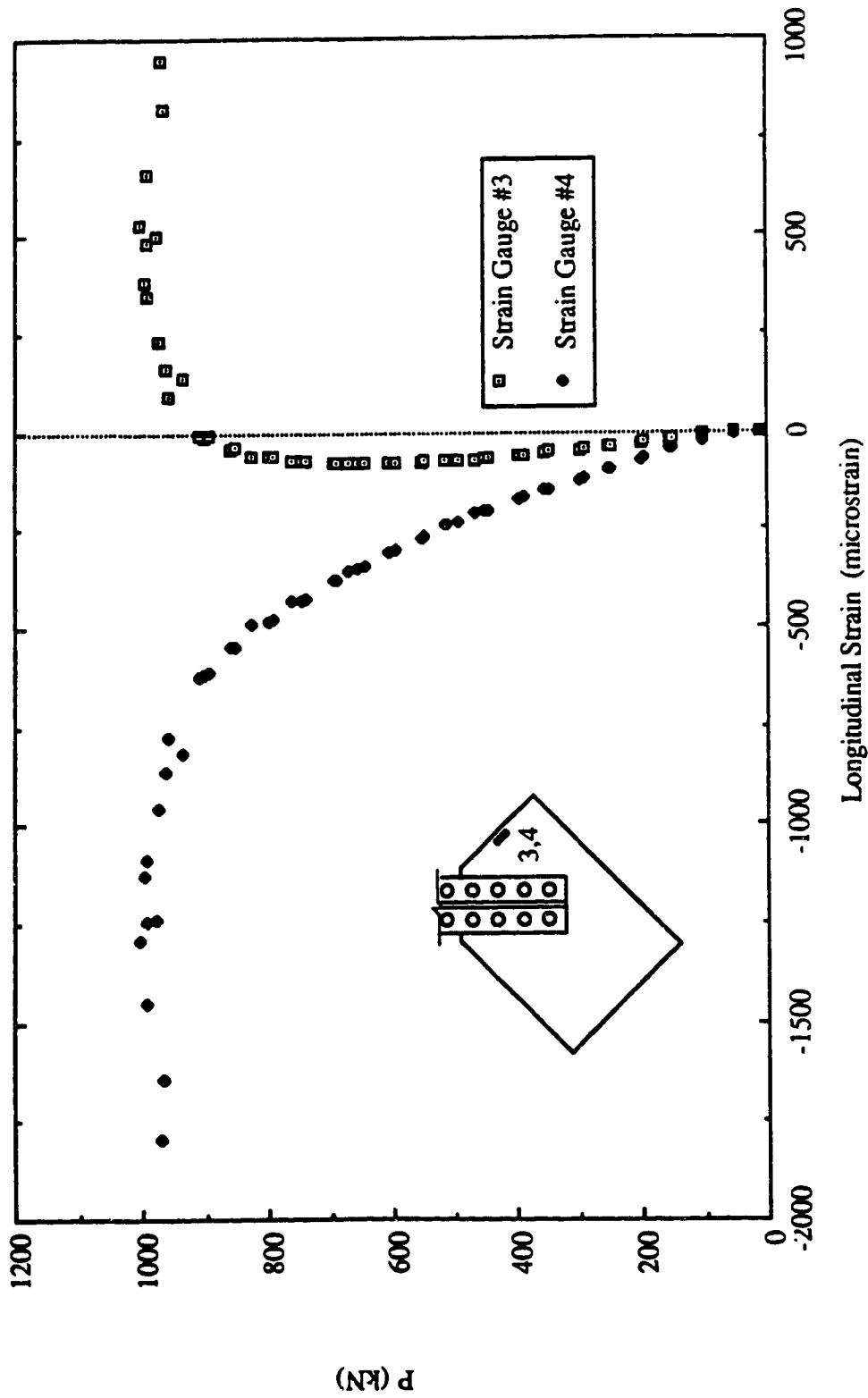


Fig. 4.8 Load vs. Strain Gauge Readings at Mid-Length of Short Free Edge for Specimen SP2 - Without Restraint

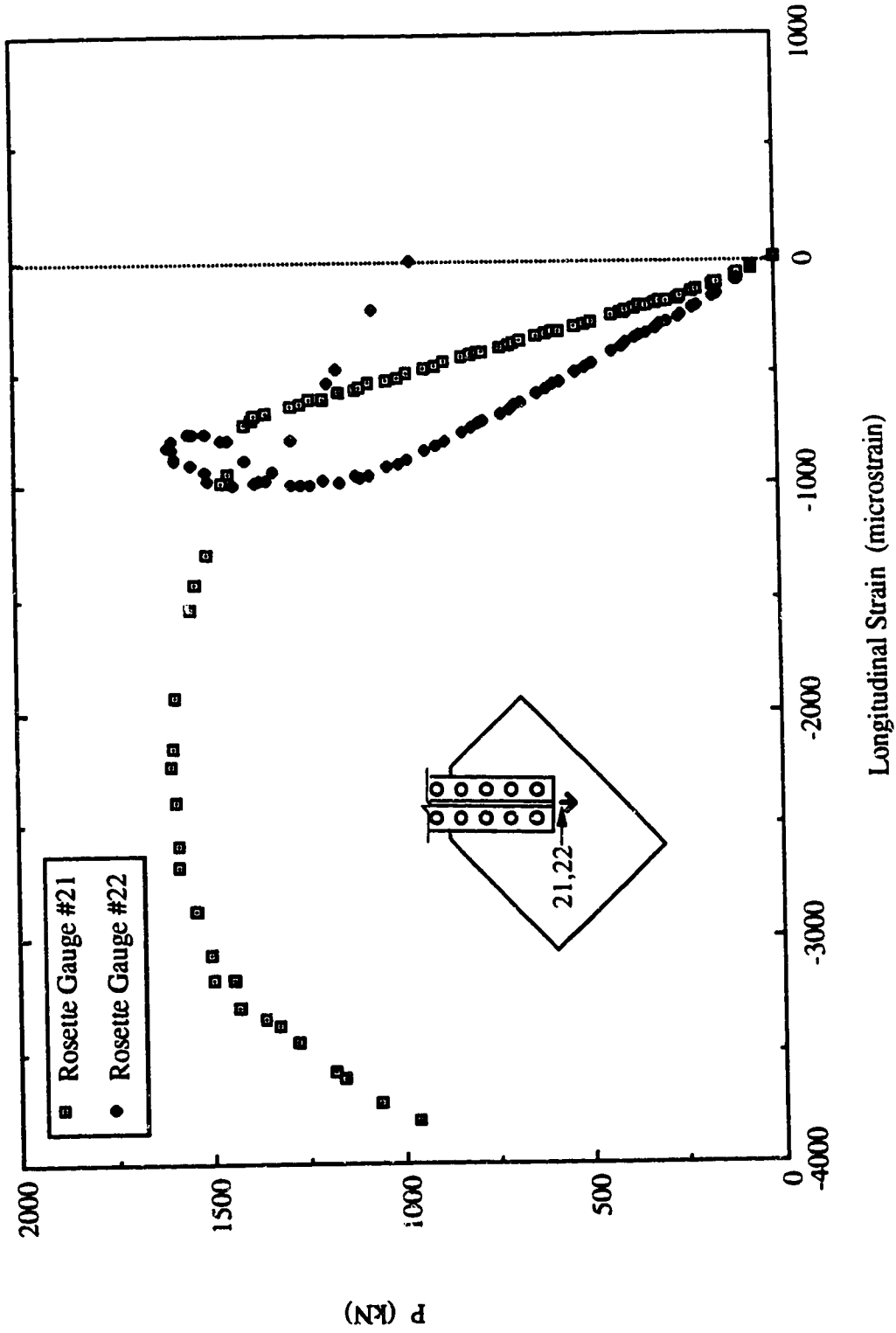


Fig. 4.9 Load vs. Strain Readings at Rosette Location for Specimen SP1 - Without Restraint

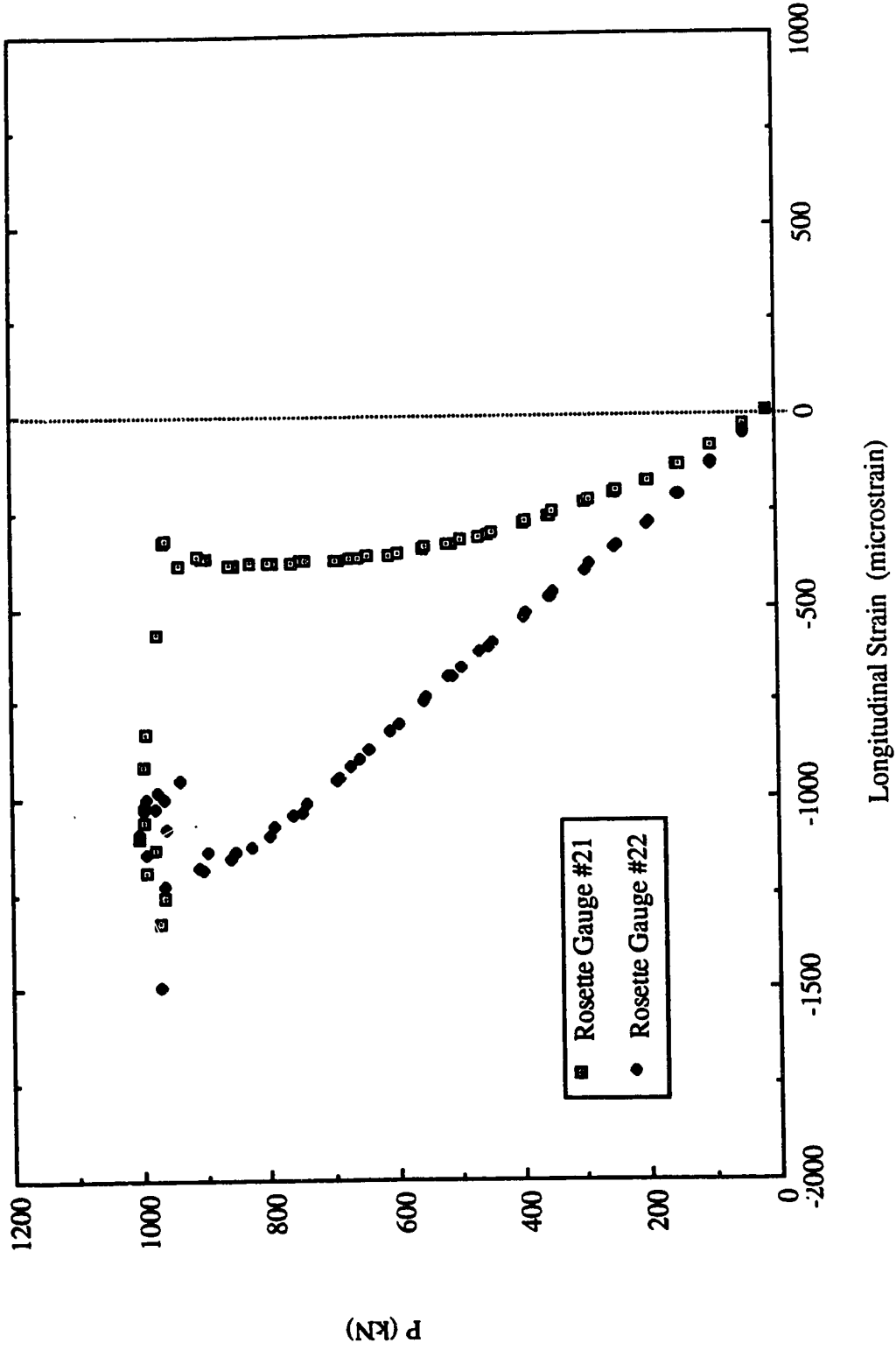


Fig. 4.10 Load vs. Strain Readings at Rosette Location for Specimen SP2 - Without Restraint



**Fig. 4.11 Picture of Failed Specimen SP1**

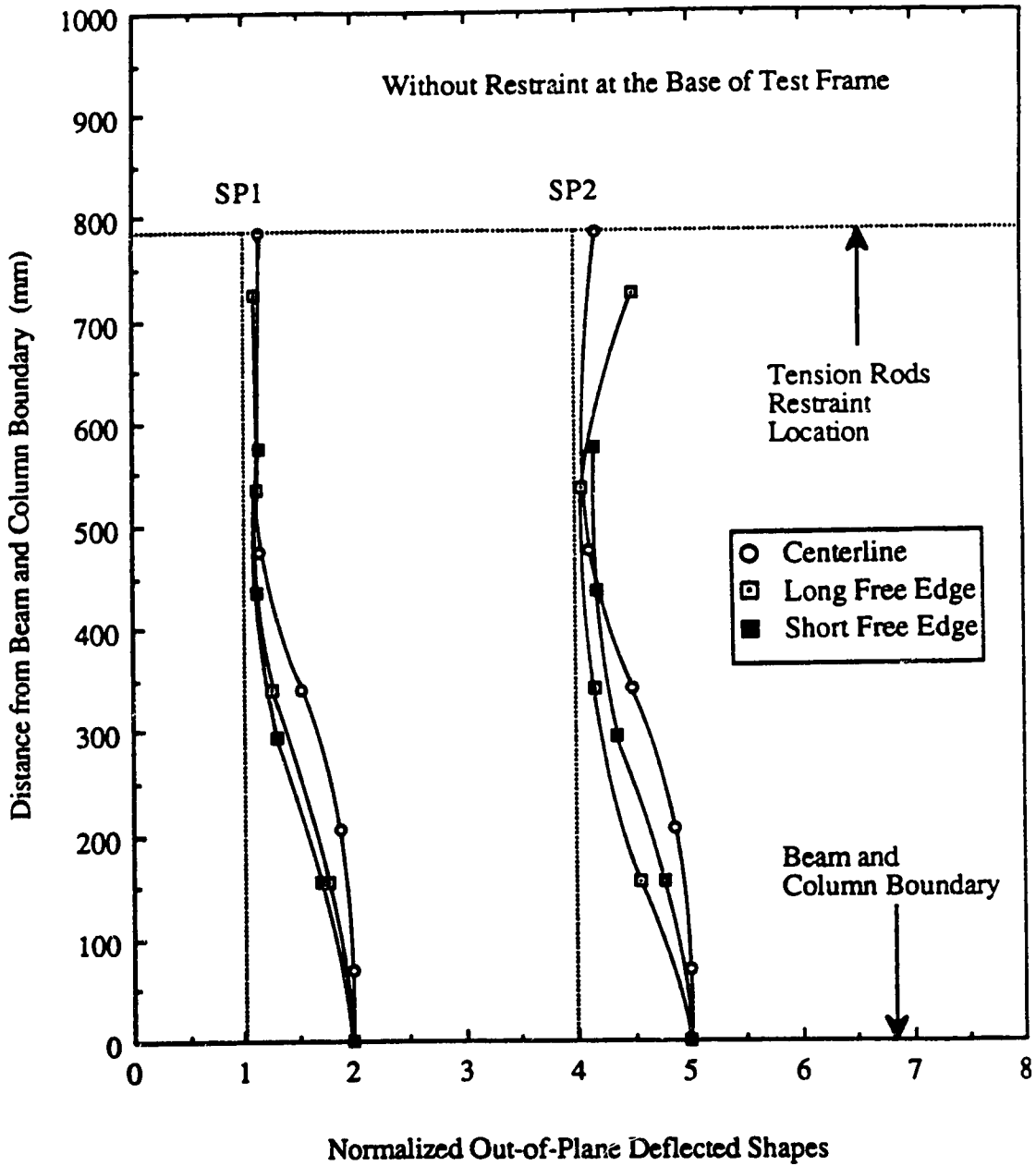


Fig. 4.12 Out-of-Plane Deflected Shapes at Free Edges and Along the Centerline of Splice for SP Type Specimens - Without Restraint

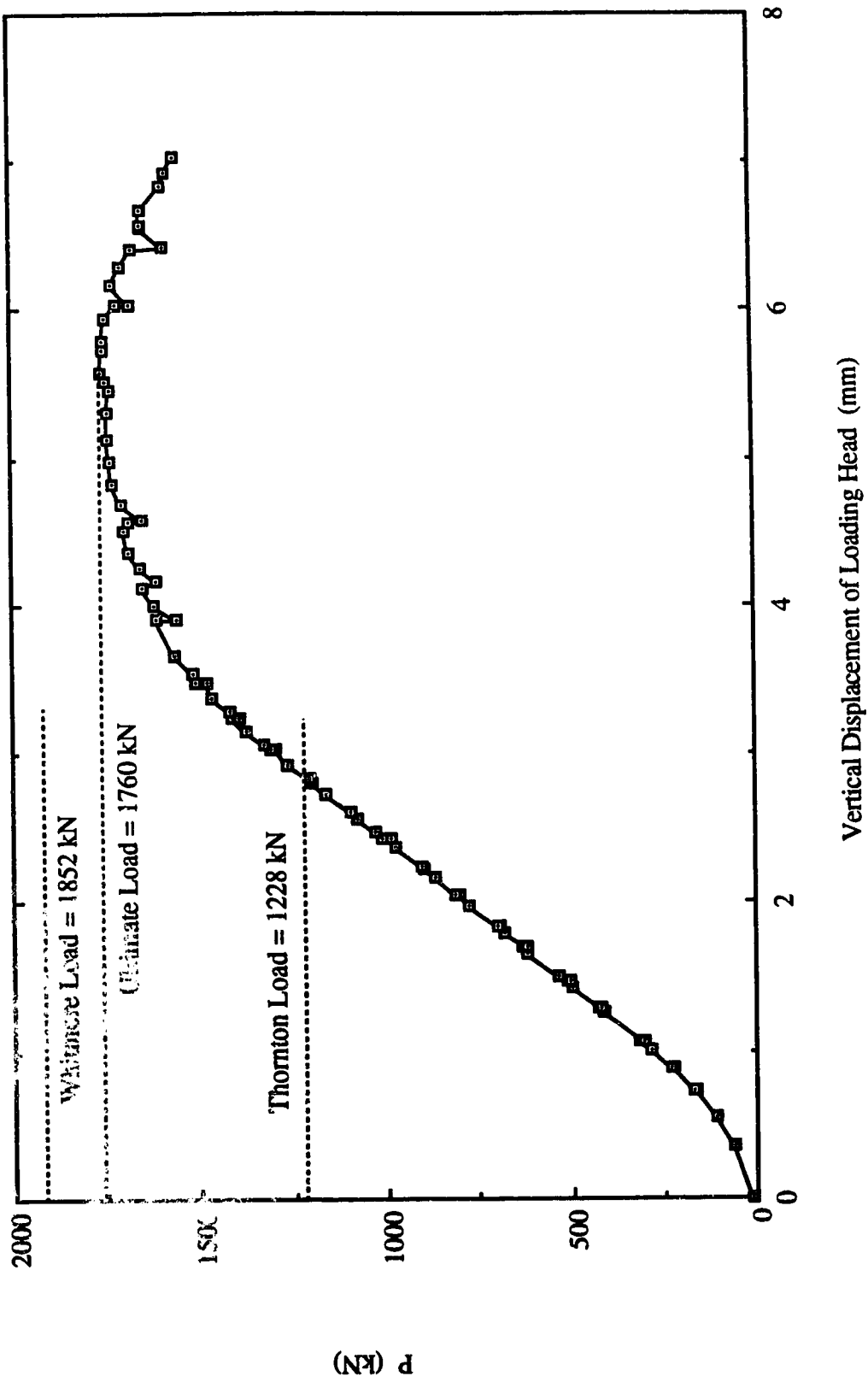


Fig. 4.13 Load vs. Vertical Displacement of Loading Head for Specimen SP1 - With Restraint

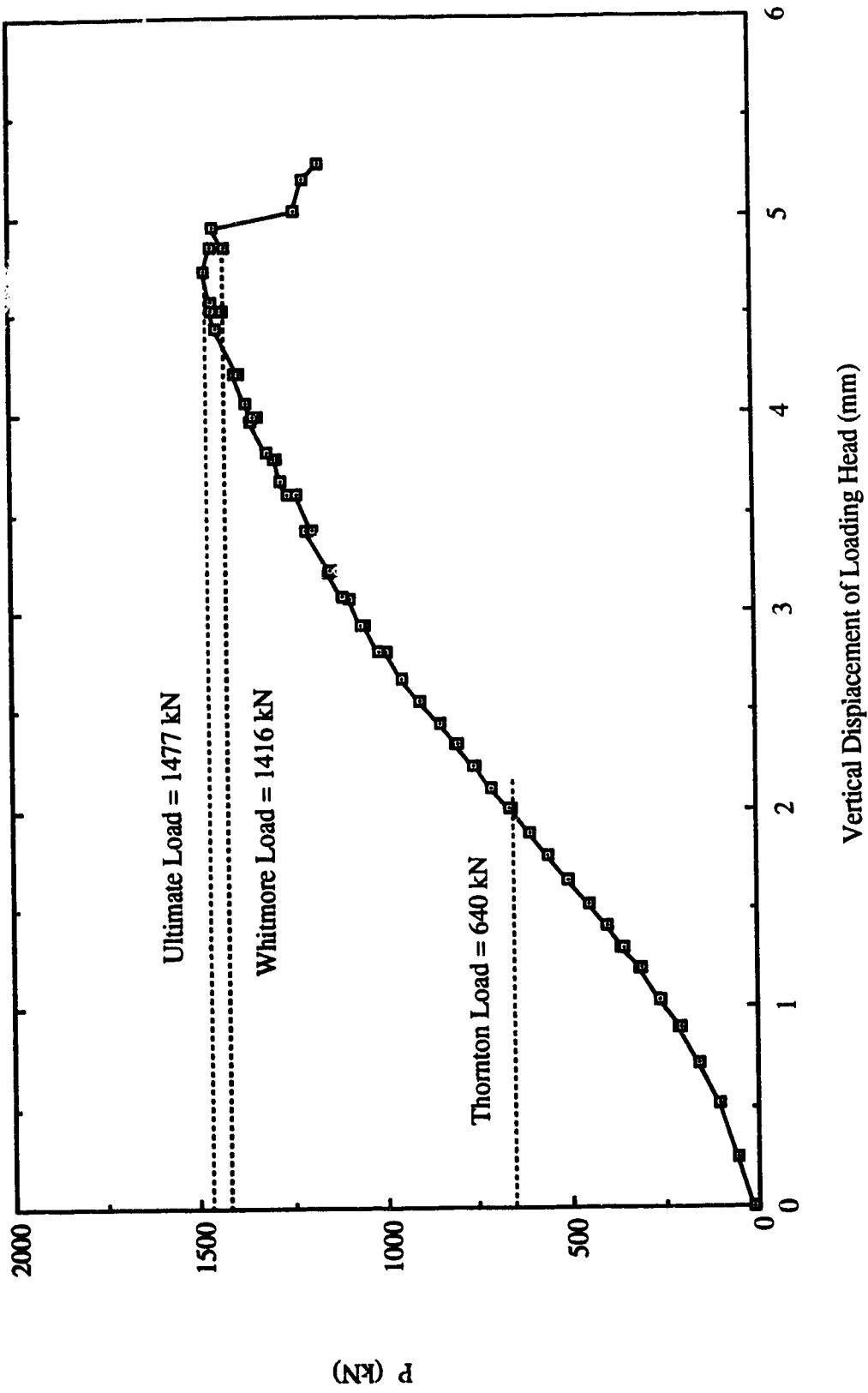


Fig. 4.14 Load vs. Vertical Displacement of Loading Head for Specimen SP2 - With Restraint



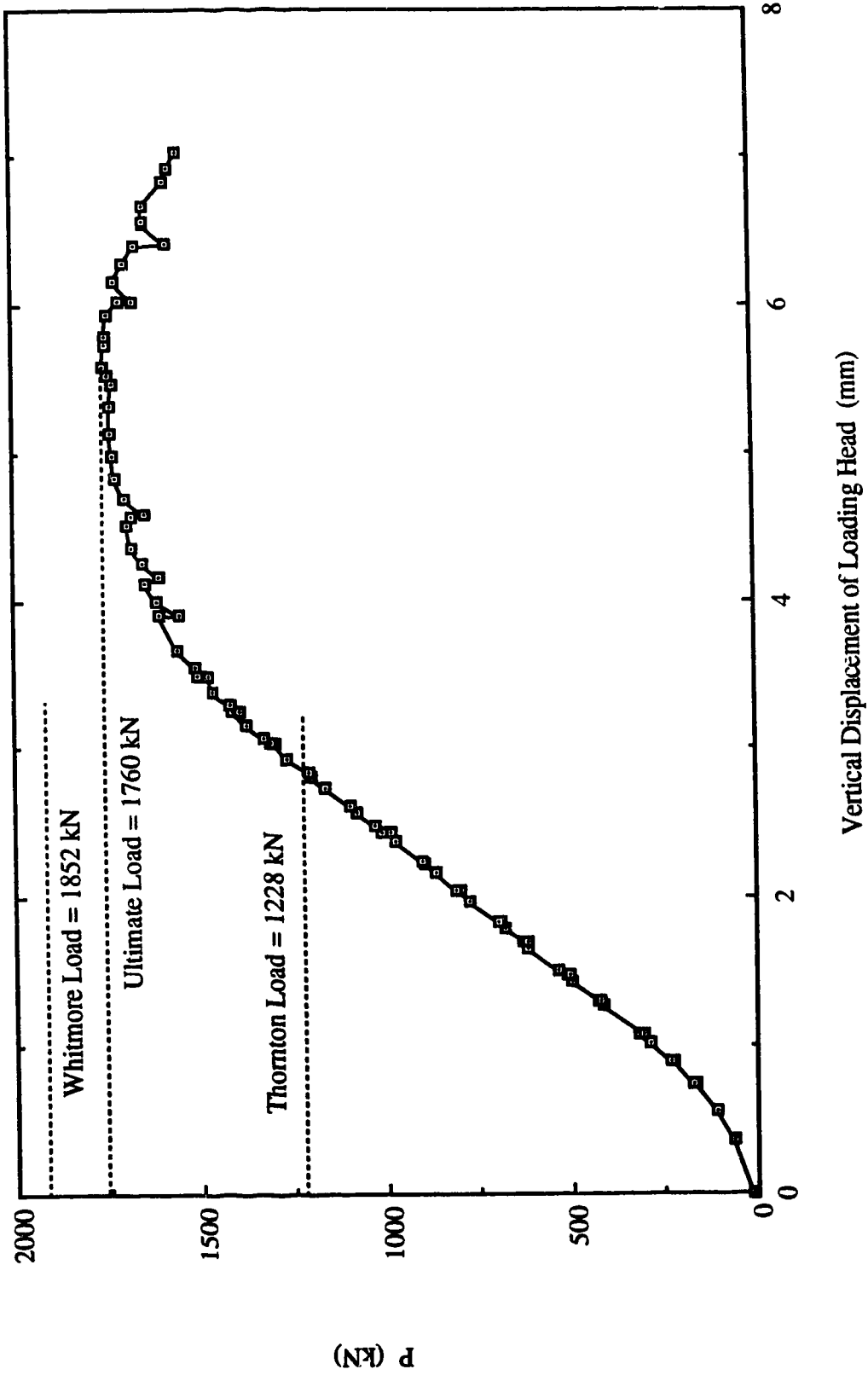


Fig. 4.15 Load vs. Out-of-Plane Displacement at Mid-Length of Long Free Edge for Specimen SPI - With Restraint

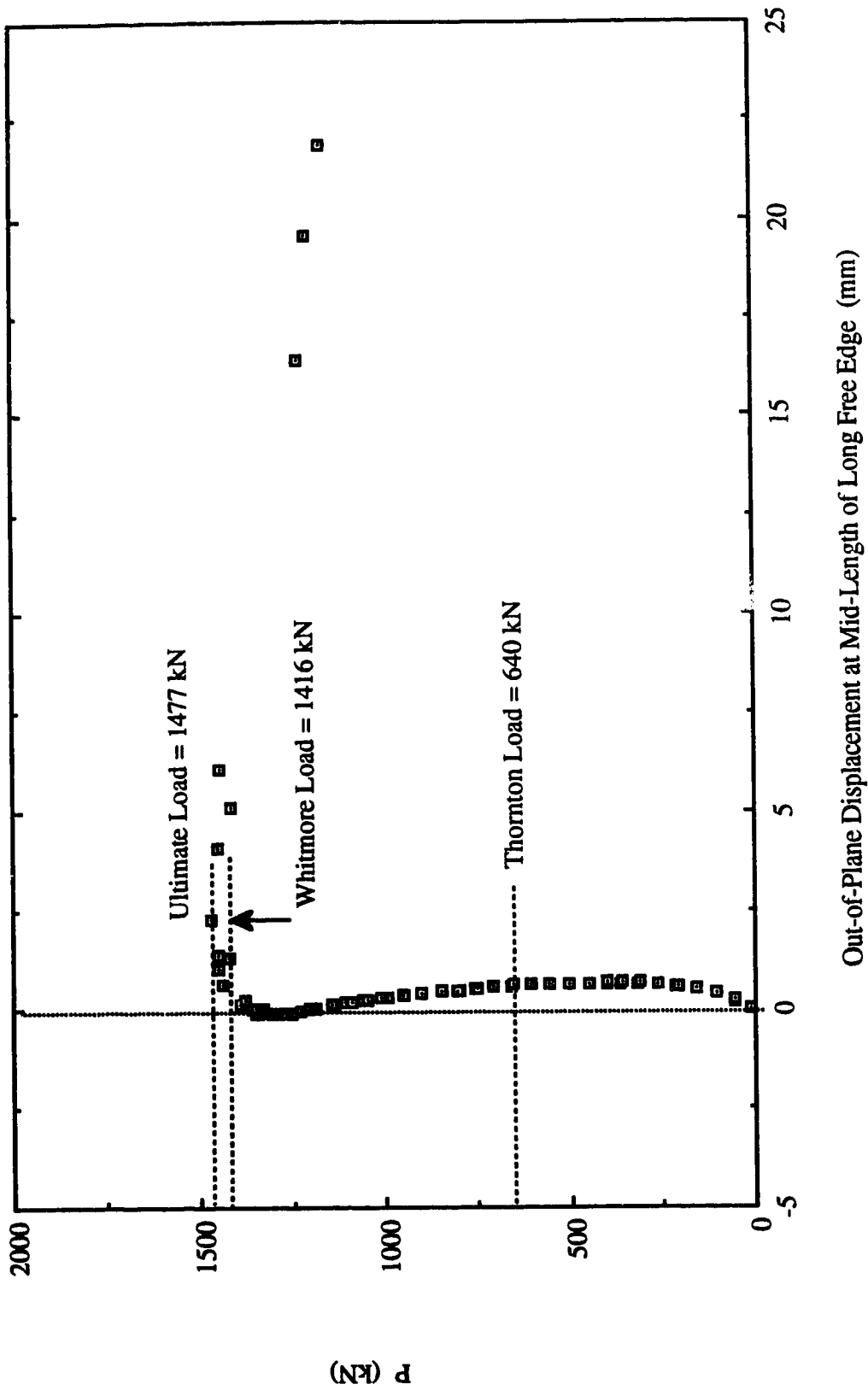
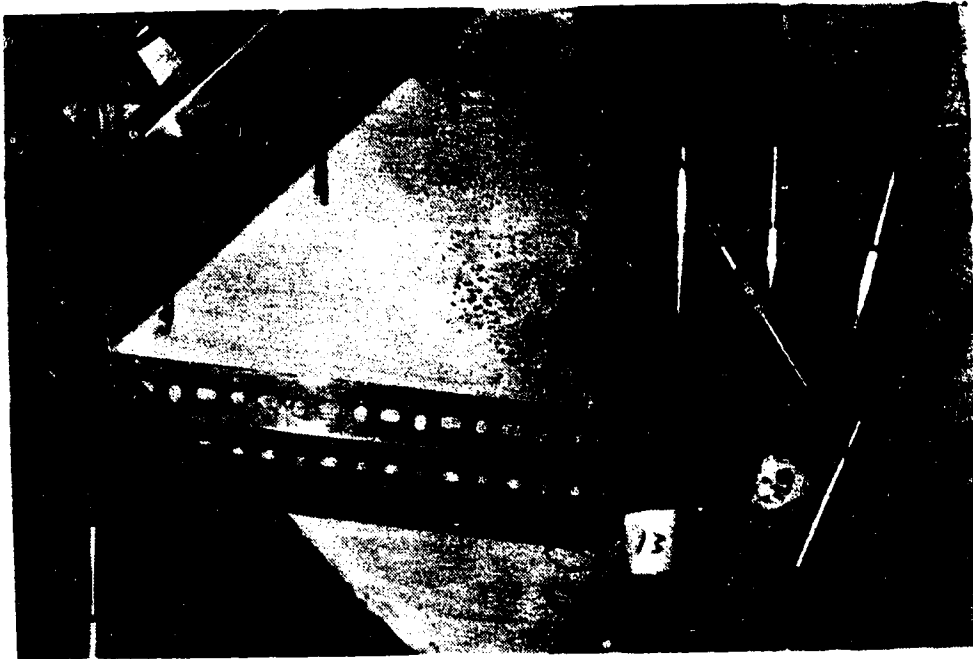
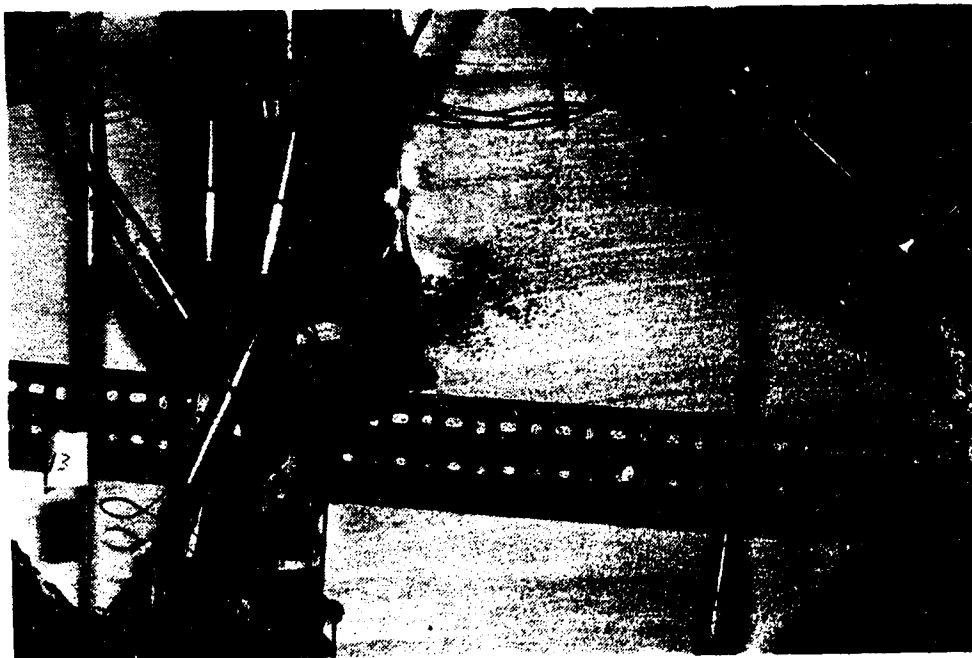


Fig. 4.16 Load vs. Out-of-Plane Displacement at Mid-Length of Long Free Edge for Specimen SP2 - With Restraint



**Fig. 4.17 Yield Lines Observed Near South Corner of Splice for Specimen SP1 - With Restraint**



**Fig. 4.18 Yield Lines Observed Near North Corner of Splice for Specimen SP1 - With Restraint**

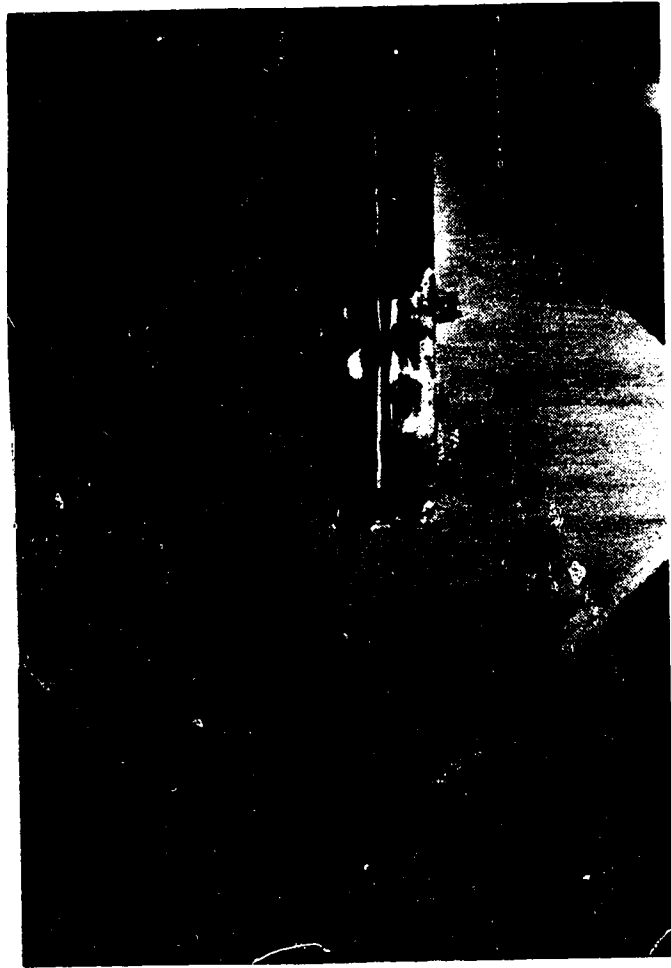


**Fig. 4.19 Yield Lines for Specimen SP1 - With Restraint**

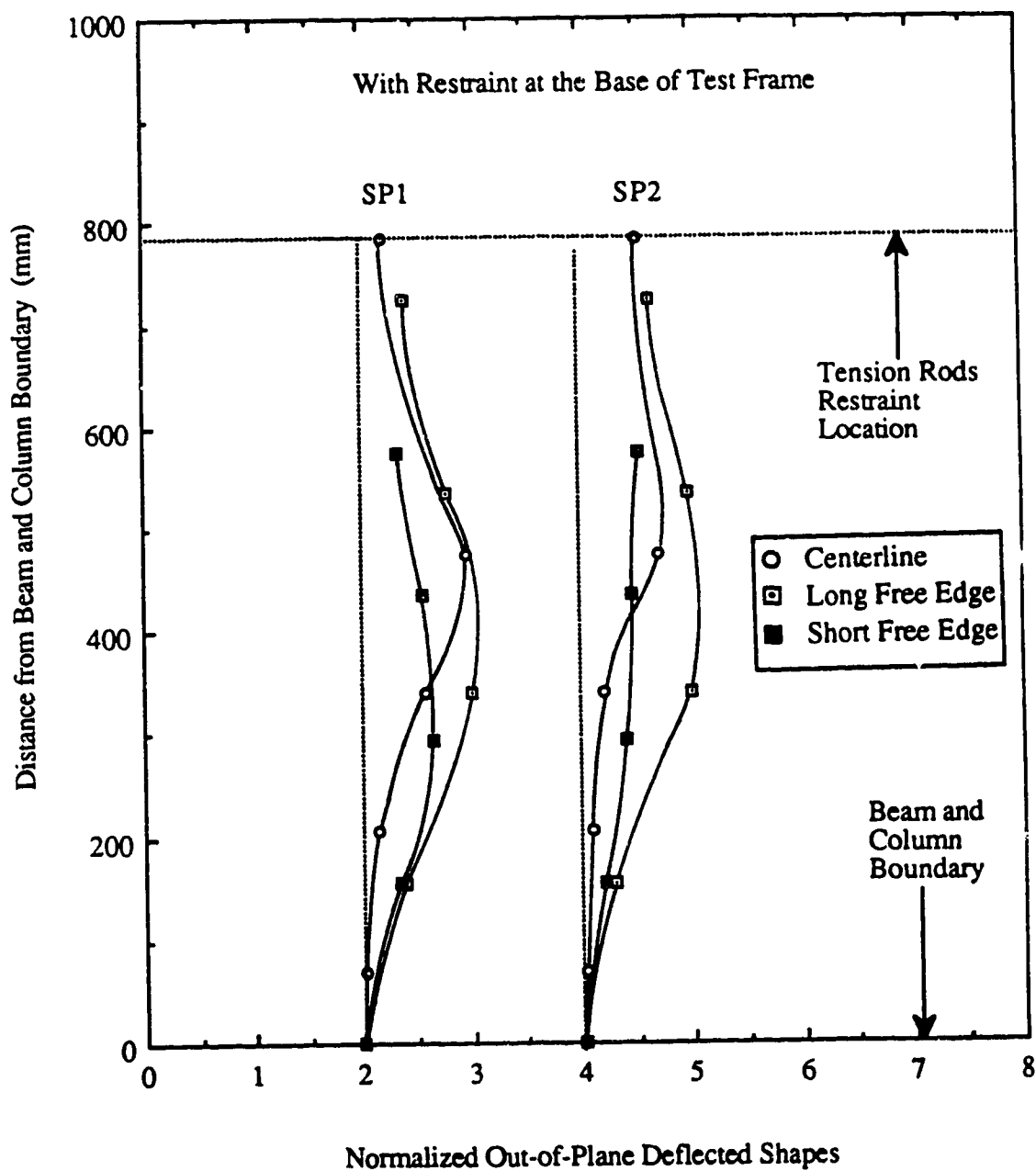


Fig. 4.20 Out-of-Plane Deflected Shapes at Free Edges and Along Centerline of Splice for SP Type Specimens - With Restraint

## **5. TEST RESULTS OF AP TYPE SPECIMENS**

### **5.1 General**

The AP set of specimens was employed to study the effects of the brace angle on the behavior and ultimate load of the gusset plate connections. The same plate geometry as that of the GP type specimens was used for the AP type specimens. It should be noted that the scheme II test setup was employed to perform the tests. A 30° brace angle was chosen for the AP type specimens, such that comparison could be made with the GP type specimen, which has a 45° brace angle. Three gusset plate thicknesses with a similar splice member as that of the GP specimens were tested. The test results of the AP type specimens are shown in Table 5.1. The failure mode of the specimens was sway buckling with the bracing member deflected out-of-plane.

### **5.2 Behavior of Load versus In-Plane Deformation**

As described in the previous chapter, an LVDT was attached to the bottom of the splice member to record the vertical deformation of the specimen. However, for specimens AP1 and AP3, this LVDT did not function properly during testing. Nonetheless, testing for these two specimens was continued since the applied load was significantly high when the LVDT malfunctioned. On the other hand, the LVDT performed normally during the testing of specimen AP2. Therefore, for specimens AP1 and AP3, readings recorded from the LVDT's attached to the hydraulic rams to measure the vertical stroke were used to examine the behavior of load versus vertical deformation of the specimen. However, it should be noted that the measurements of the LVDT's also included the elastic deflections of the reaction beam and channels.

The curves of load versus vertical stroke of the hydraulic rams are illustrated in Figs. 5.1 to 5.3. As can be seen from the figures, the strokes from both hydraulic rams were

maintained quite close to each other except at the final stage of loading. Fig. 5.1 shows that a bolt slip occurred at load levels of about 1000 kN and 1350 kN. However, no bolt slip was recorded for specimens AP2 and AP3. In general, a nonlinear load deflection behavior was observed for the specimens at the initial loading stage due to the settling of the test fixtures. Subsequently, a linear load deflection was observed for the specimens until the applied load reached the corresponding Whitmore load level, at which point nonlinear behavior began as shown in the figures. After reaching the ultimate load, a drop in the applied load without a significant increase in the strokes was observed. For specimens AP2 and AP3, the rate of unloading decreased as the strokes increased. The curve of load versus in plane deformation measured at the end of splice by an LVDT for specimen AP2 is shown in Fig. 5.4. The curve shows that, except in the early loading stage the load deflection behavior was linear until the applied load reached the Whitmore load level at 930 kN. From then on nonlinear behavior was observed until ultimate load was reached. When comparing Figs. 5.2 to 5.4, it can be seen that about 7 mm of elastic deflection of the reaction beams was recorded. However, the general behavior of these two curves was quite similar.

### **5.3 Behavior of Load versus Out-of-Plane Displacement**

The curves of load versus the out-of-plane displacement of the gusset plate at the conjunction of gusset-to-splice are shown in Figs. 5.5 to 5.7. As can be seen from Fig. 5.5, a discontinuity of the load deflection curve was observed for specimen AP1. This discontinuity was caused by a sudden vibration which occurred during the bolt slip. The recorded bolt slip has been discussed in the previous section. In general, a linear load deflection behavior was observed for the specimens until the applied load was close to the ultimate load. Both specimens AP1 and AP2 were able to maintain the load level close to the ultimate load after buckling occurred, except for specimen AP3, which showed an appreciable decrease in the ultimate load. This may be because specimen AP3 had a

relatively low bending rigidity compared to specimens AP1 and AP2. Hence, when buckling occurred, the yielding of specimen AP3 progressed rapidly and the applied load therefore dropped quickly after the specimen reached the ultimate load. The final out-of-plane displacement for all the specimens was approximately 25 mm, which is the physical limit of the measuring LVDT.

#### **5.4 Strain Gauge Results**

The strain readings at the mid-length of the free edges and the area underneath the splice member were examined. Again, strain readings at the free edges indicated that elastic strain distribution occurred in the vicinity of the free edges prior to when the ultimate load was reached. The curves of load versus strain at the mid-length of the long free edge are shown in Figs. 5.8 to 5.10. These figures show that a linear behavior was observed until the applied load was close to the ultimate load. As can be seen from the figures, strain readings from both sides of the specimen were similar at the early loading stage. However, as load increased, these strain readings deviated from each other. When the load increased to the ultimate load level, strain bifurcation occurred, as illustrated by the figures. Strain readings at the short free edge show that compressive strains were recorded in the initial stage of loading. However, as loading progressed, unloading was observed in the vicinity of the short free edge, and eventually, tensile strains were recorded as illustrated typically in Fig. 5.11 for specimen AP3. This unloading behavior was probably caused by the in-plane bending of the plate. Since these specimens were tested with a brace angle of  $30^\circ$ , the horizontal component of the applied load might be significant in causing this in-plane bending behavior. The curves of load versus strain recorded at the center gauges of the rosette are shown in Figs. 5.12 to 5.14. These two gauges recorded the strain readings from both sides of the plate. It can be seen from these figures that the out-of-plane bending of the plate, which was probably due to the initial imperfection, occurred at an early stage



of loading. In particular, specimen AP3 showed nonlinear behavior from the beginning of loading.

### **5.5 Yielding Behavior of Specimens**

The general yield pattern of the AP type specimens was similar to that of the GP type specimens. However, for the AP type specimens, the yield lines were first observed close to the beam and column boundary. For specimen AP1, the yield lines underneath the splice member were recorded at about 58 percent of the ultimate load. Again, as loading progressed, the yielding was spread about the two sides of the splice member. However, only moderate yielding was observed about the side of the splice member close to the long free edge. On the other hand, significant yielding was recorded about the other side of the splice member near the short side free edge. Extensive yielding was observed underneath the splice member, and yielding about the side of the splice member close to the short free edge progressed significantly at a load level of approximately 85 percent of the ultimate load. The failed specimen AP1, which indicated severe yielding occurred in the area of the short side free edge, is shown in Fig. 5.15. Figure 5.16 illustrates the other side of the failed specimen AP1, which showed the severity of the yielding. The yield lines similar to that of GP type specimens were also observed along the beam and column boundary and at the mid-length of the long free edge of the failed specimens, as shown typically in Figs. 5.15 and 5.16.

The yielding process and pattern for specimen AP2 were similar to that of specimen AP1. However, yielding underneath the splice member was detected at about 45 percent of the ultimate load. Again, extensive yielding was recorded in the area of the short side free edge. The failed specimen AP2 also indicated that severe yielding occurred in the area underneath the splice member. Figures 5.17 and 5.18 illustrate the failed specimen of AP2 with the presence of the yield line mechanism along the beam and column boundary and at

the mid-length of the long free edge. For specimen AP3, the flaking of whitewash underneath the splice member was observed at a load level of about 80 percent of the ultimate load. Again, as the load increased yielding occurred about the two sides of the splice member. The failed specimen indicated that only moderate yielding existed underneath the splice member when it was compared to that of specimens AP1 and AP2. However, extensive yielding similar to that of specimens AP1 and AP2 in the area of the short free edge was recorded for specimen AP3. Again, yield lines developed along the beam and column boundary and at the mid-length of the long free edge.

#### **5.6 Out-of-Plane Deflected Shapes of Free Edges and along Centerline of Splicing Member**

The normalized out-of-plane deflected shapes of the specimens are shown in Fig. 5.19. It can be seen from the figure that the maximum deflection occurred at the long free edge. In general, the deflected shapes resembled the buckled shape of a fixed-guided column. The deflected shapes for specimens AP1 and AP2 indicated that significant rotation occurred at the beam and column boundary due to severe yielding. The deflected shape of the long free edge for specimen AP3 also showed a slight local bending near the mid-length. A picture of the out-of-plane deflected shape along the long free edge of specimen AP2 is shown in Fig. 5.20.

Table 5.1 Test Results of AP Type Specimens

Specimen Designation	Plate Size (mm x mm x mm)	Ultimate Load (kN)	Whitmore Load $P_w$ (kN)	Thornton Load $P_t$ $k = 0.65$ (kN)
AP1	500 x 400 x 13.3	1720	1216	1119
AP2	500 x 400 x 9.8	1210	930	801
AP3	500 x 400 x 6.5	728	555	404

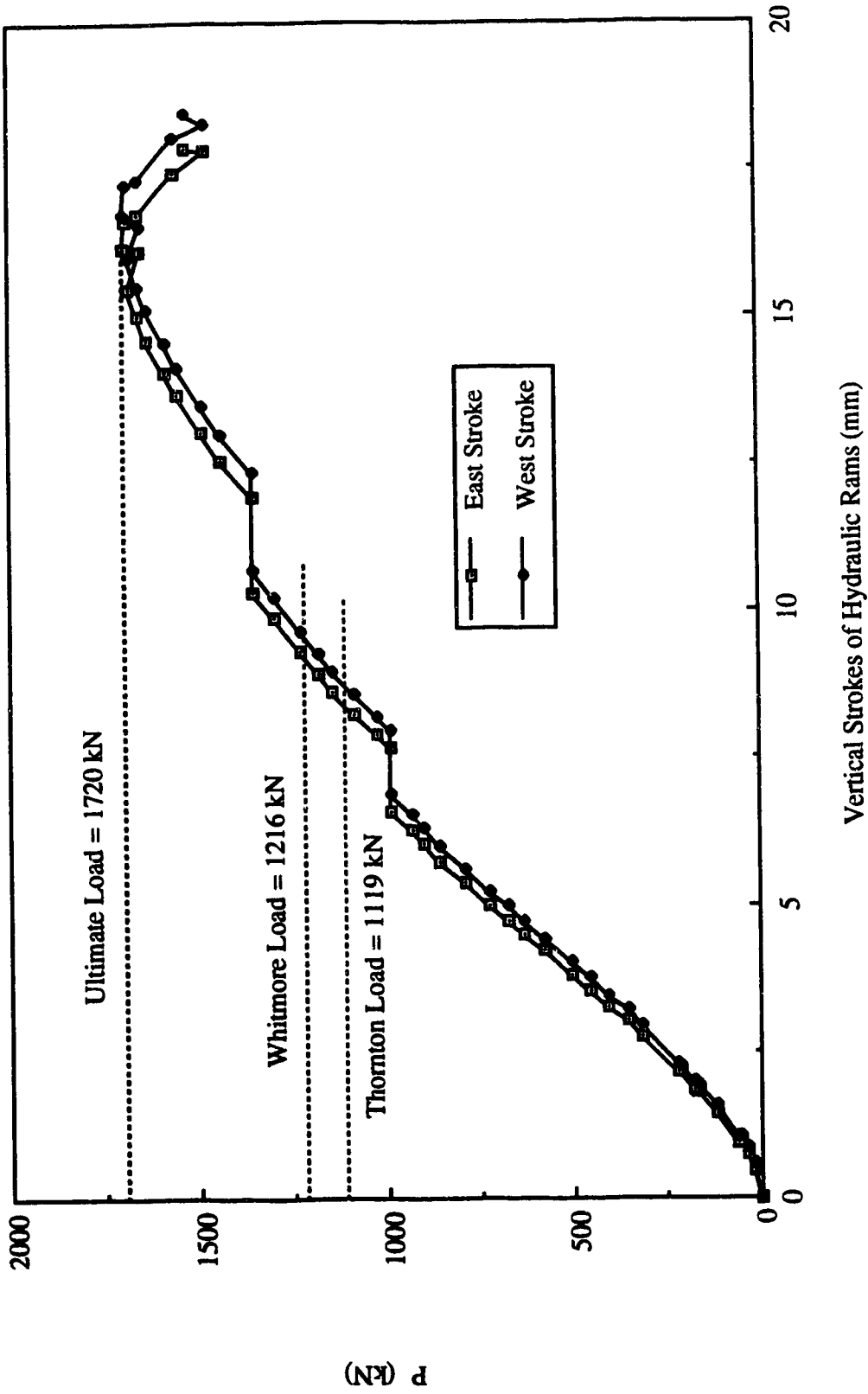


Fig. 5.1 Load vs. Vertical Strokes of Hydraulic Rams for Specimen AP1

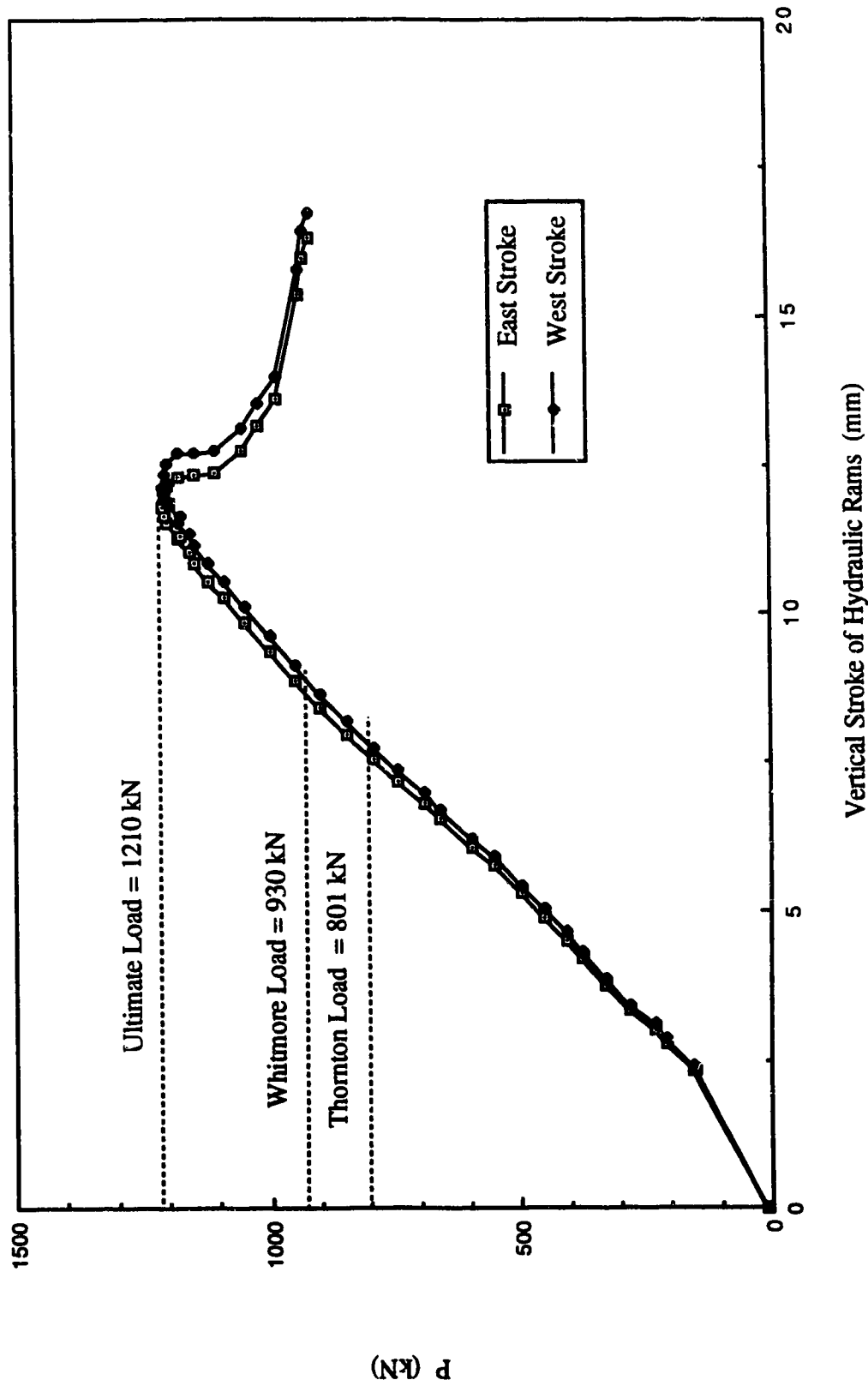


Fig. 5.2 Load vs. Vertical Strokes of Hydraulic Rams for Specimen AP2

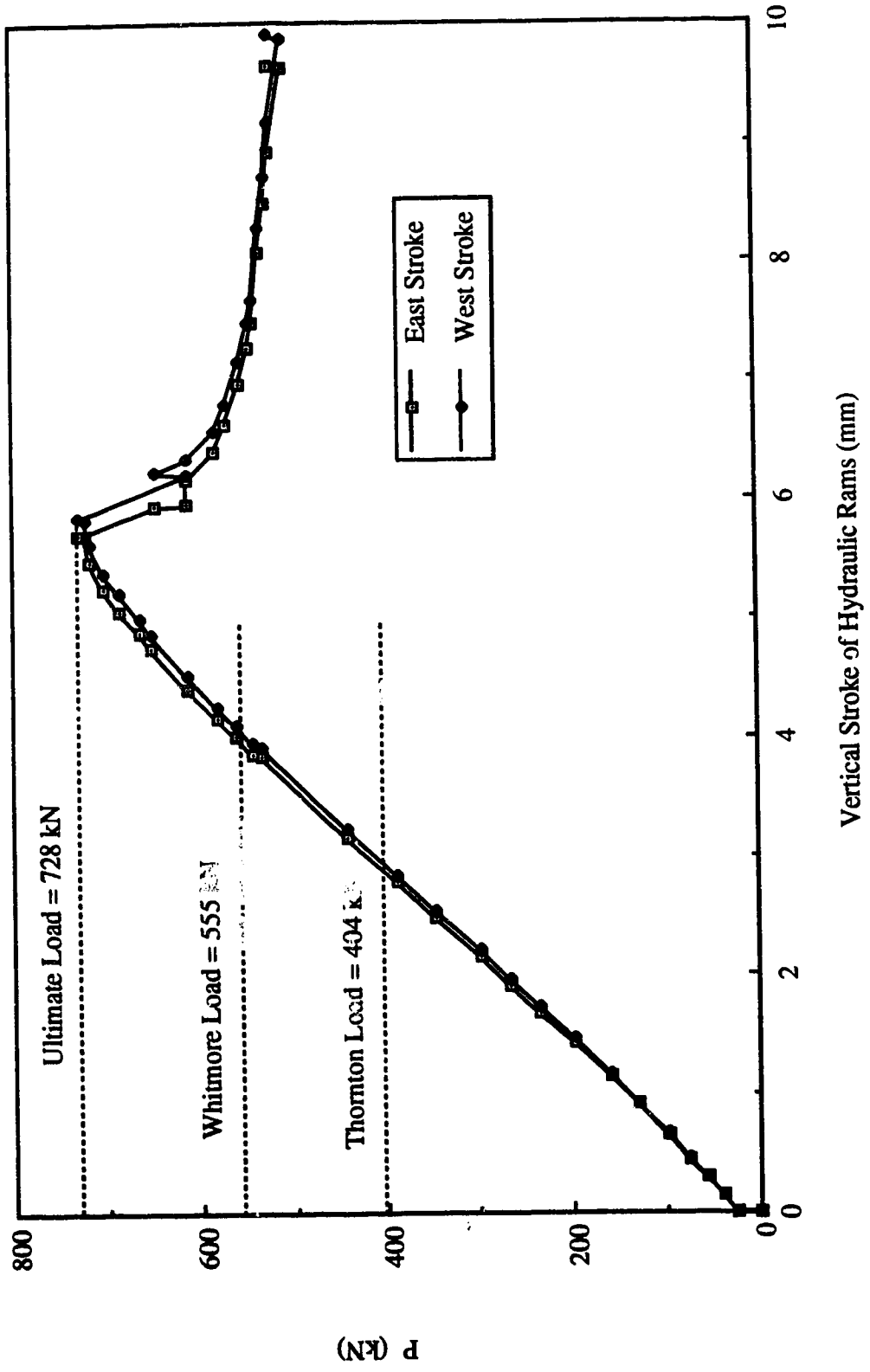


Fig. 5.3 Load vs. Vertical Stroke of Hydraulic Rams for Specimen AP3

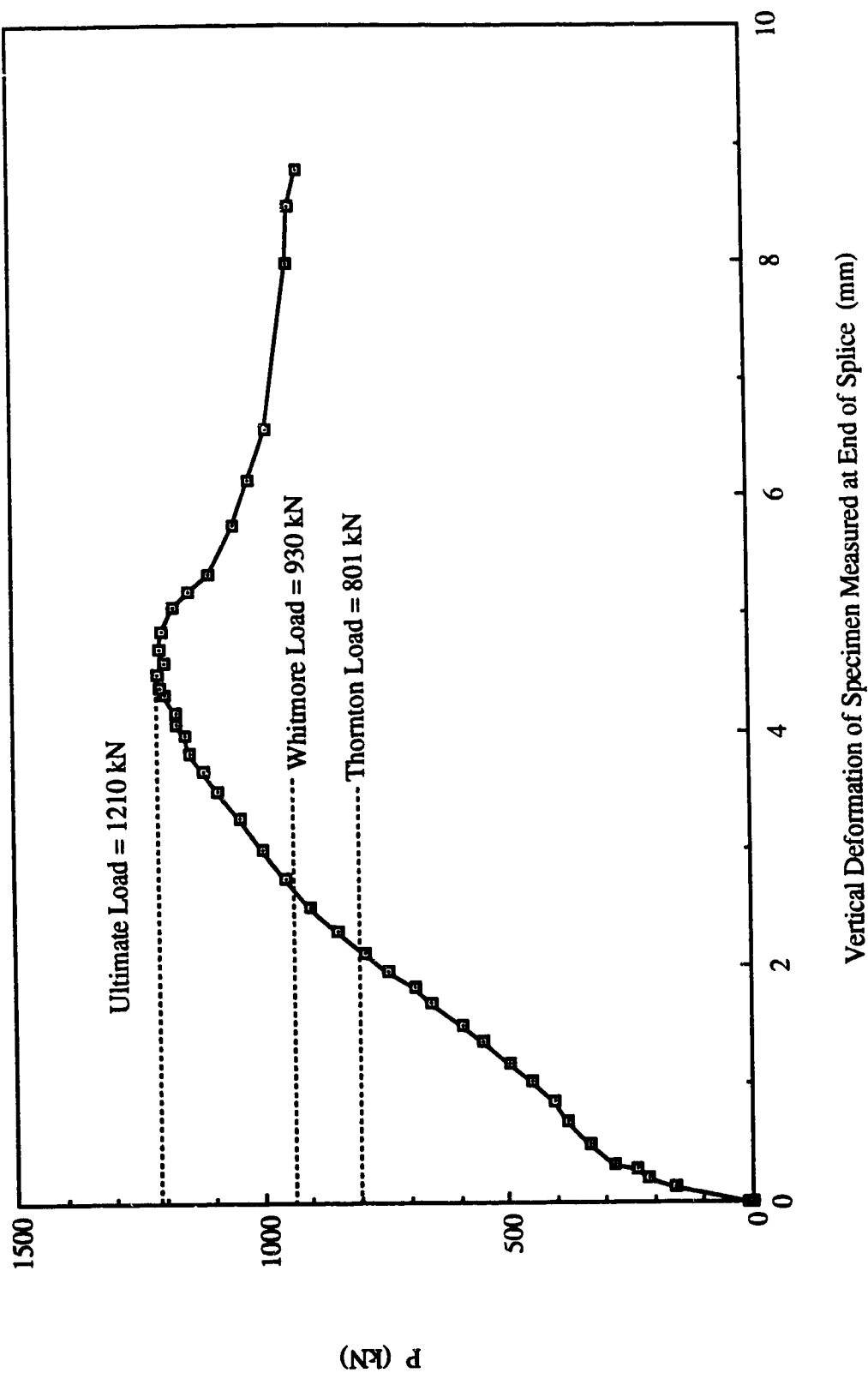
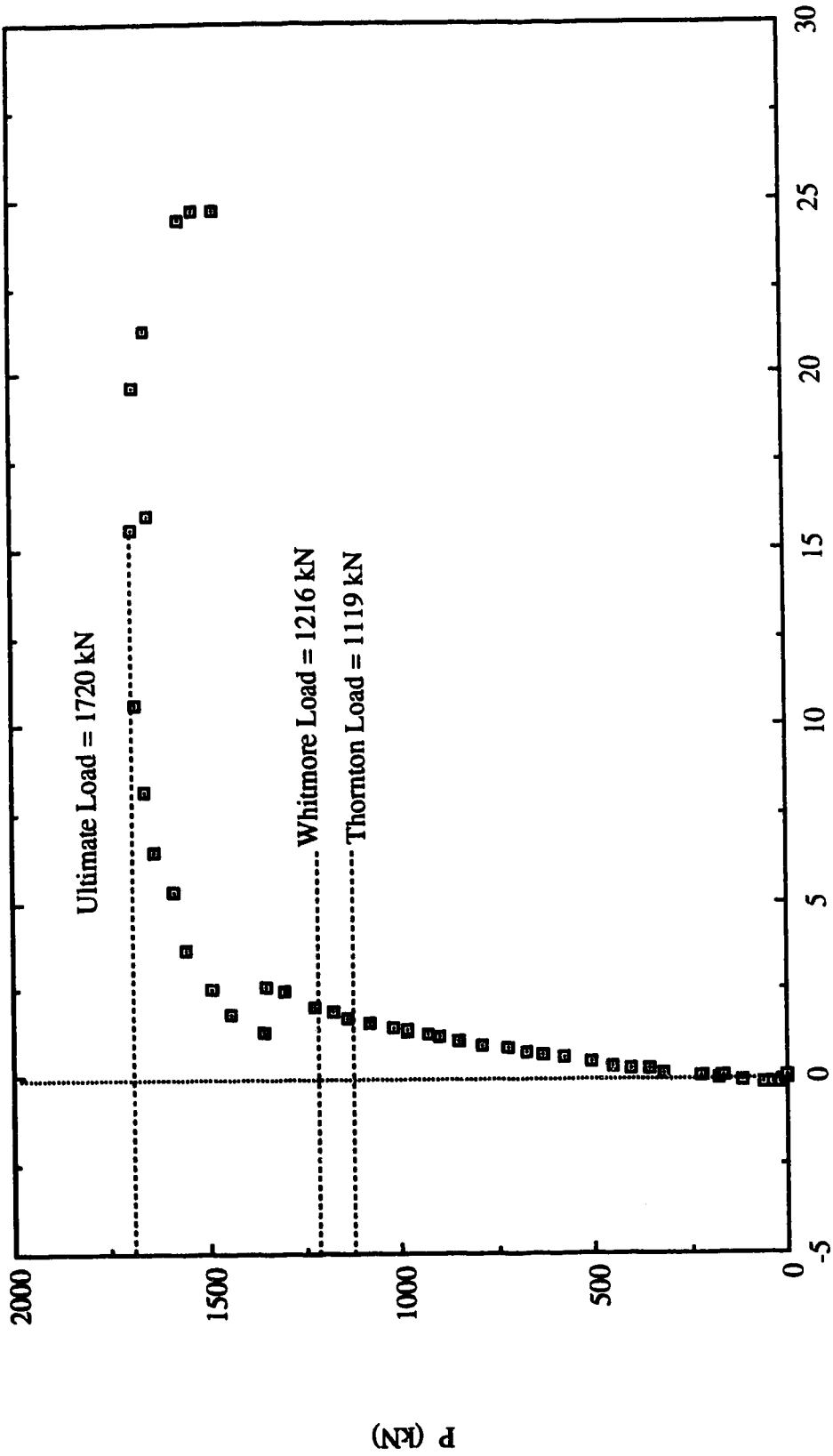


Fig. 5.4 Load vs. In-Plane Deformation Measured at End of Splice for Specimen AP2



Out-of-Plane Displacement at Conjunction of Gusset-to-Splice (mm)

Fig. 5.5 Load vs. Out-of-Plane Displacement at Conjunction of Gusset-to-Splice for Specimen API



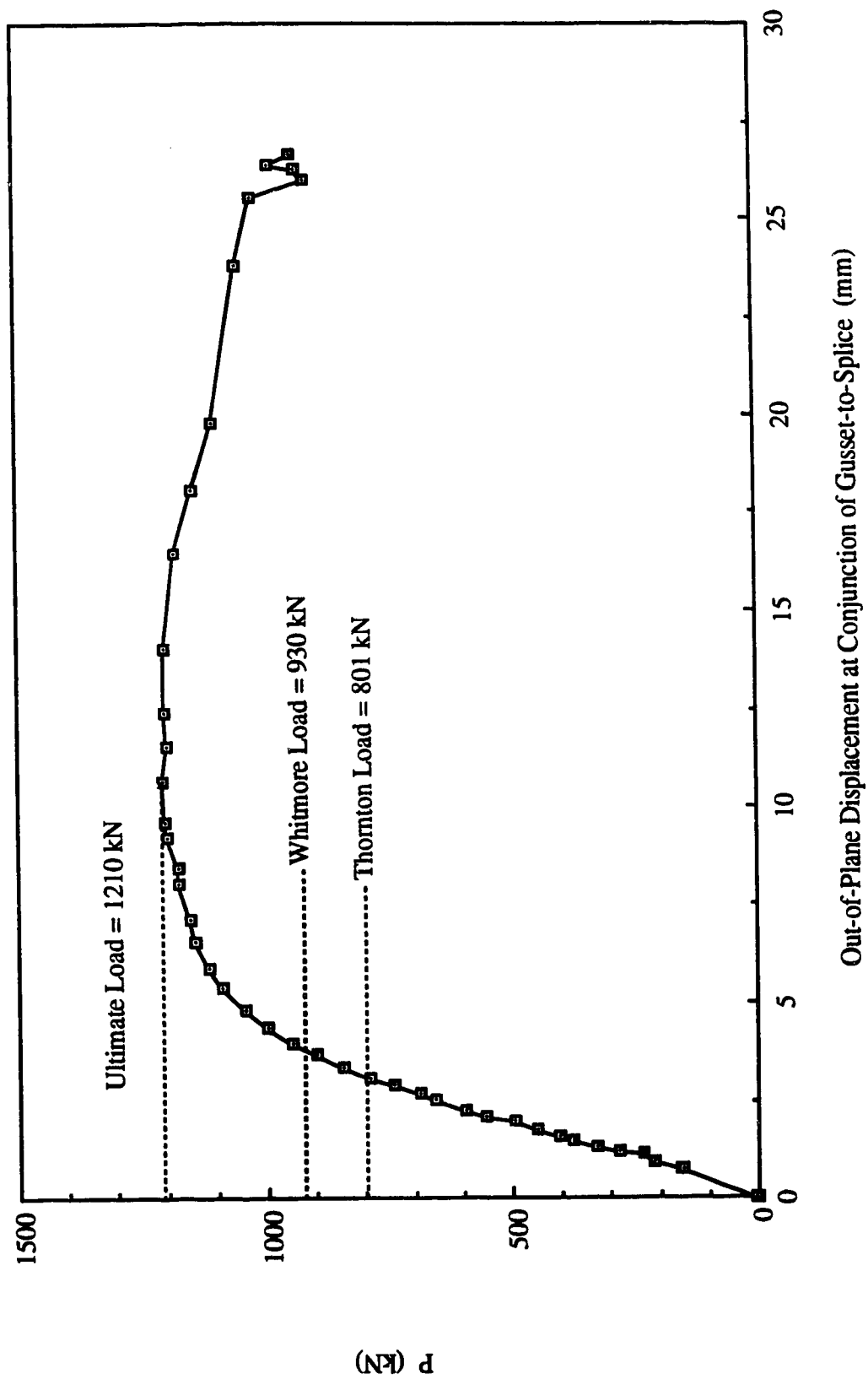
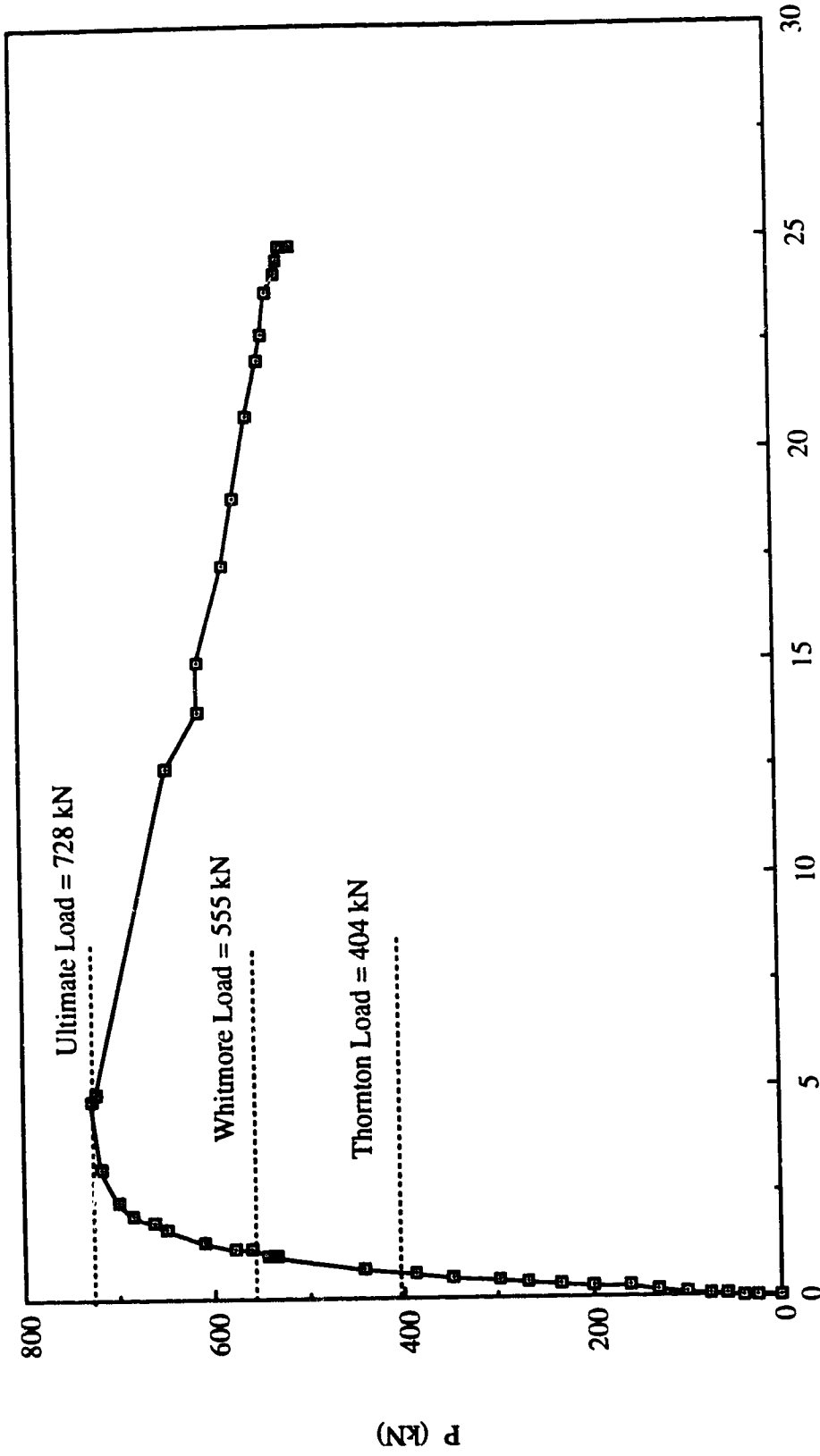


Fig. 5.6 Load vs. Out-of-Plane Displacement at Conjunction of Gusset-to-Splice for Specimen AP2



Out-of-Plane Displacement at Conjunction of Gusset-to-Splice (mm)

Fig. 5.7 Load vs. Out-of-Plane Displacement at Conjunction of Gusset-to-Splice for Specimen AP3

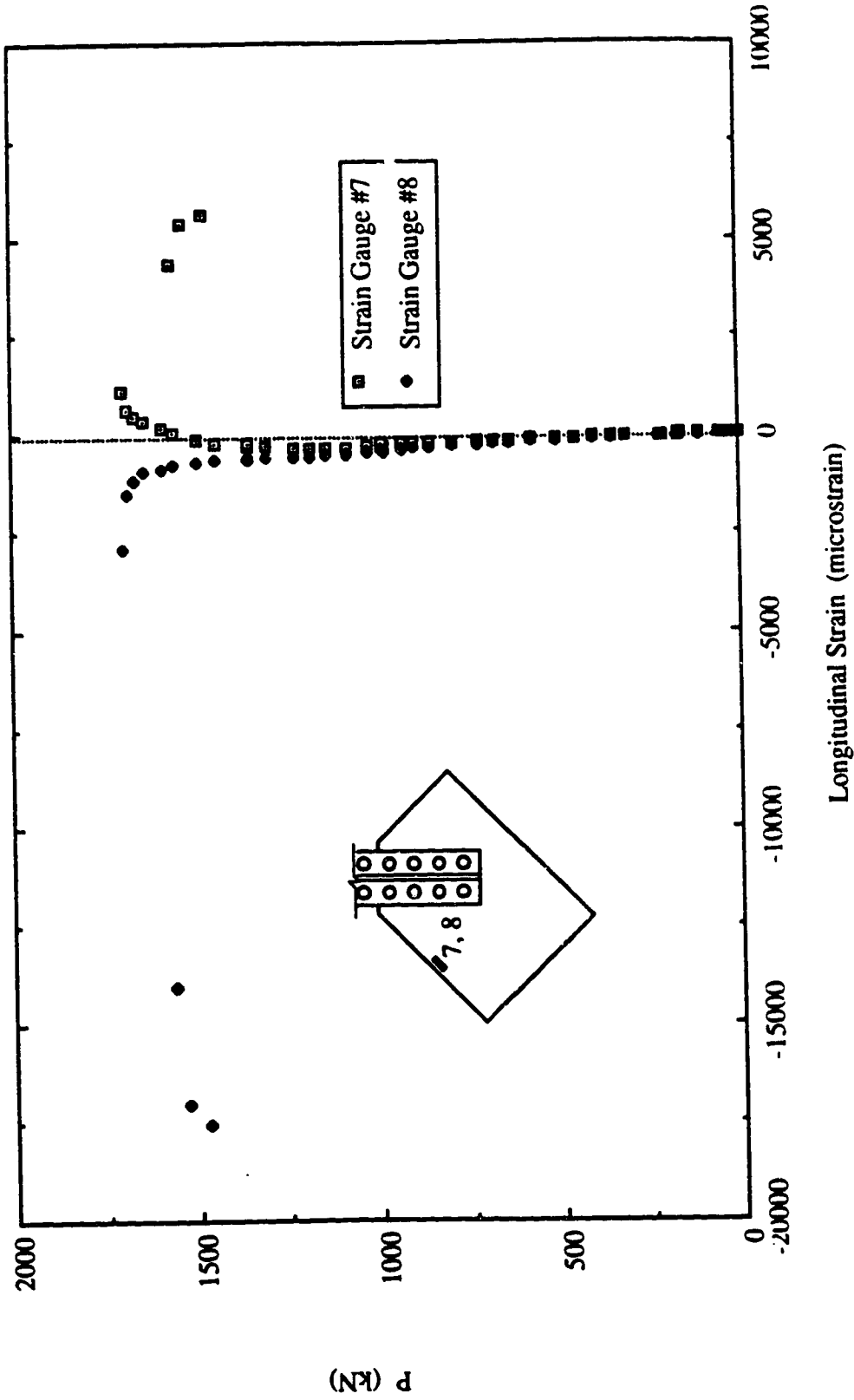


Fig. 5.8 Load vs. Strain Gauge Readings at Mid-Length of Long Free Edge for Specimen AP1

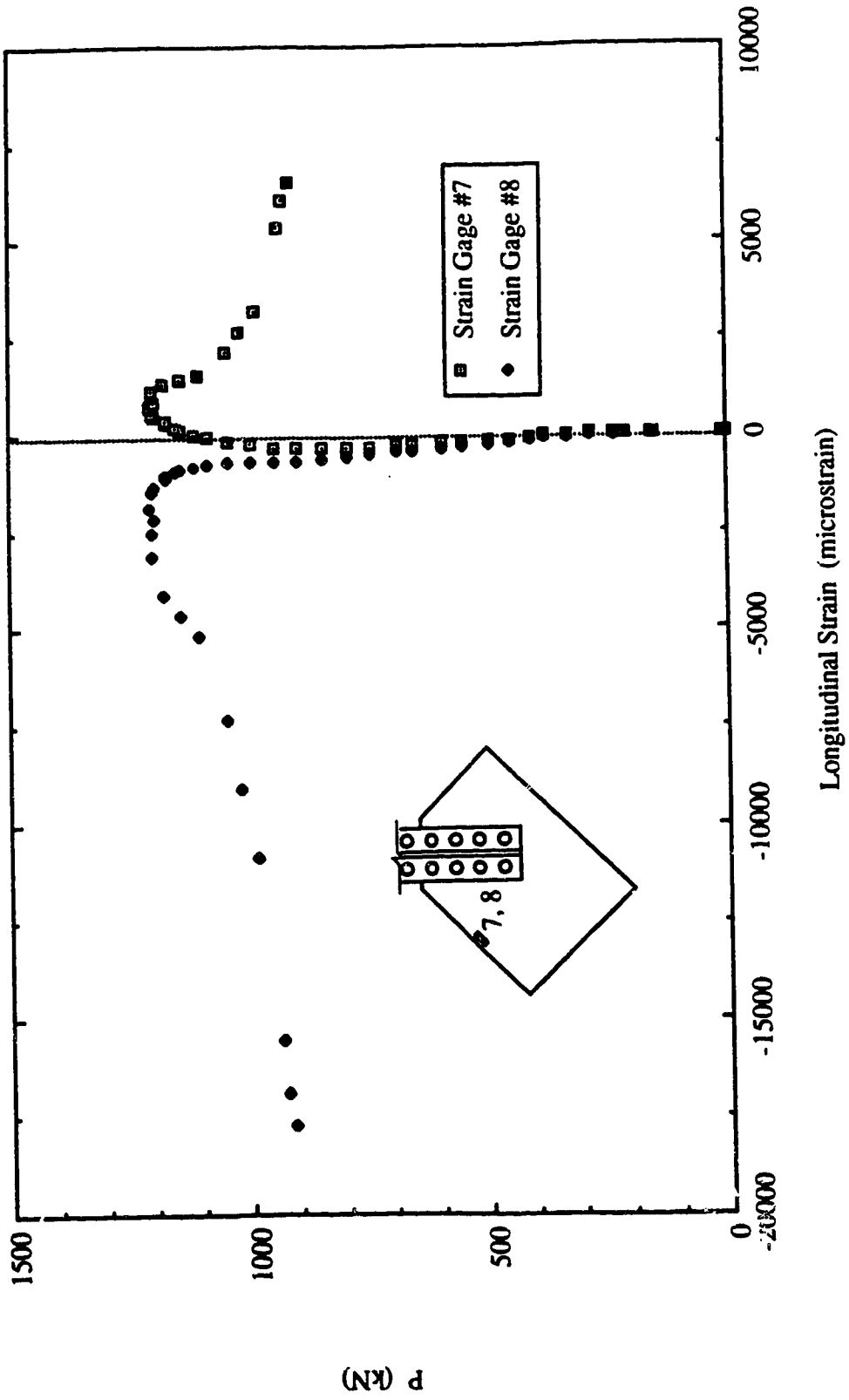


Fig. 5.9 Load vs. Strain Gauge Readings at Mid-length of Long Free Edge for Specimen AP2

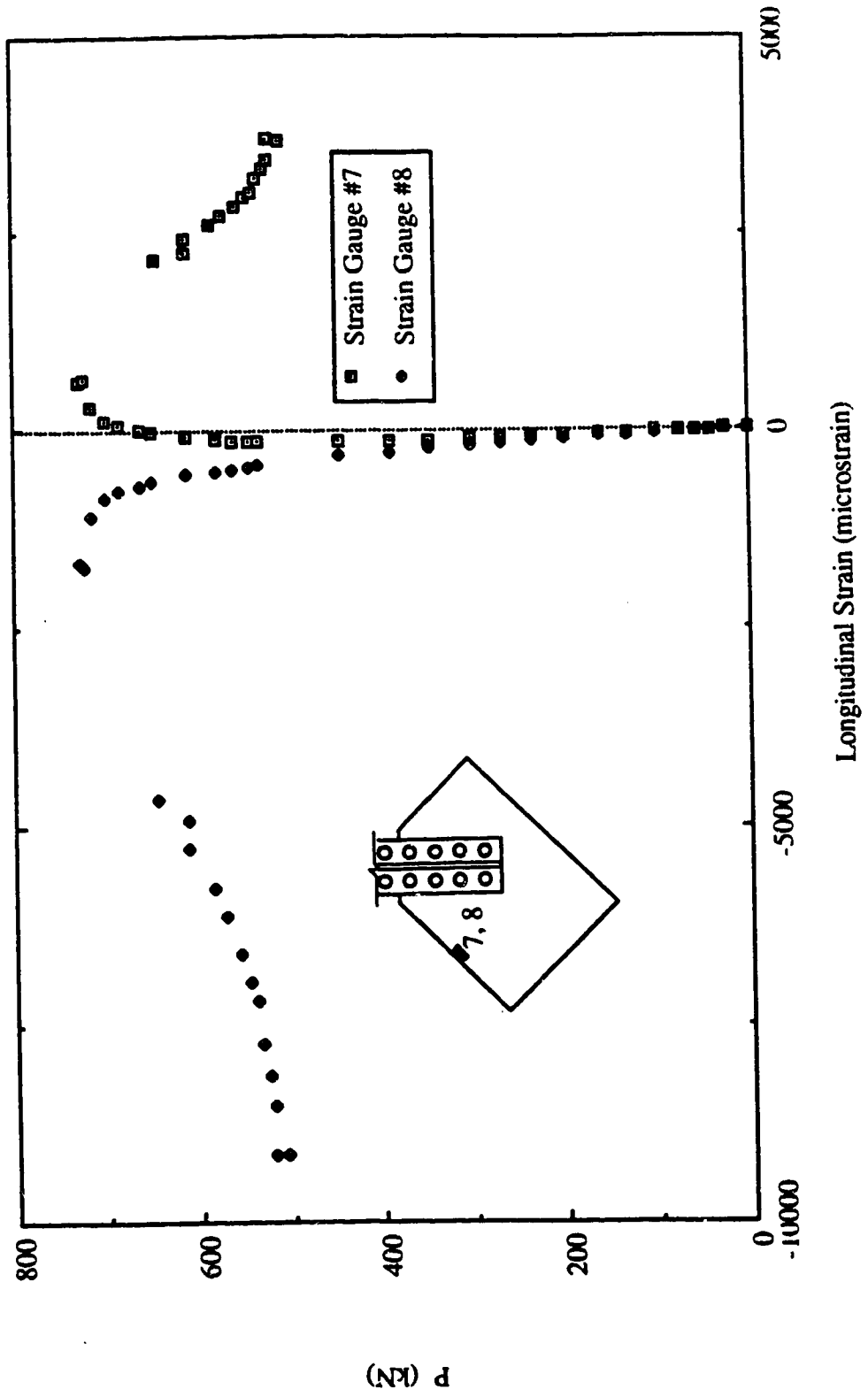


Fig. 5.10 Load vs. Strain Gauge Readings at Mid-Length of Long Free Edge for Specimen AP3

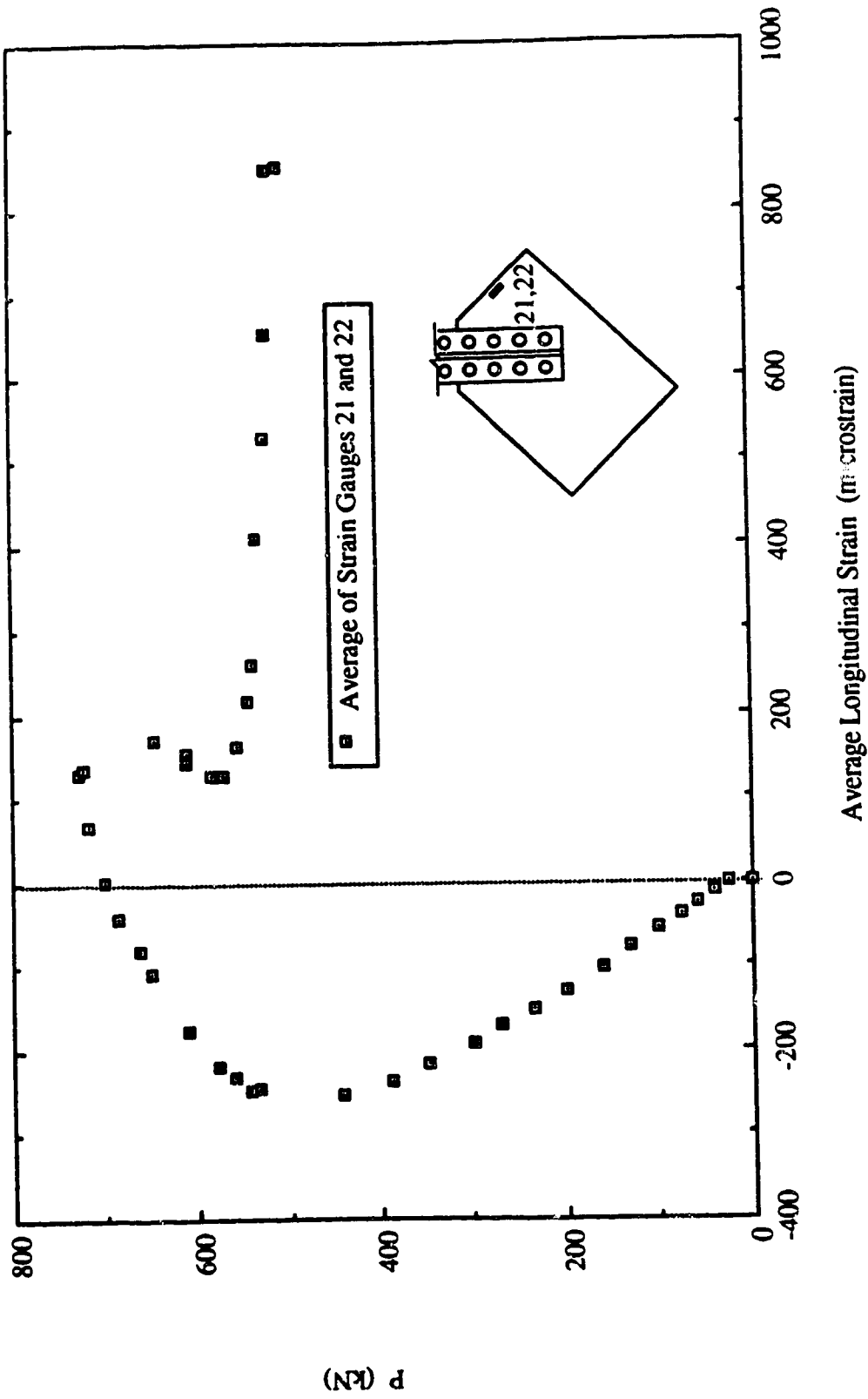


Fig. 5.11 Load vs. Average Strain Gauge Readings at Mid-Length of Short Free Edge for Specimen AP3

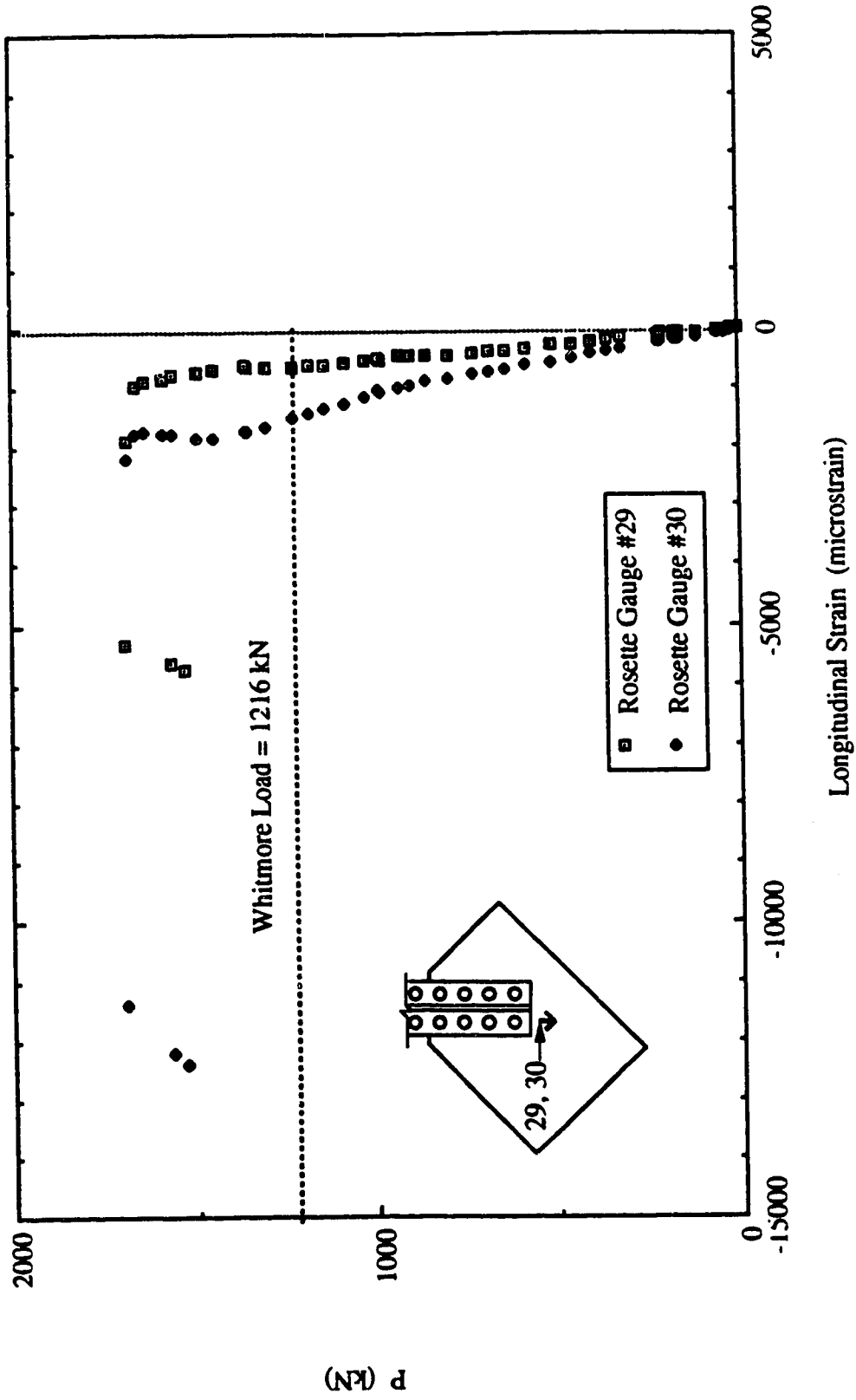


Fig. 5.12 Load vs. Rosette Gauge Readings for Specimen API

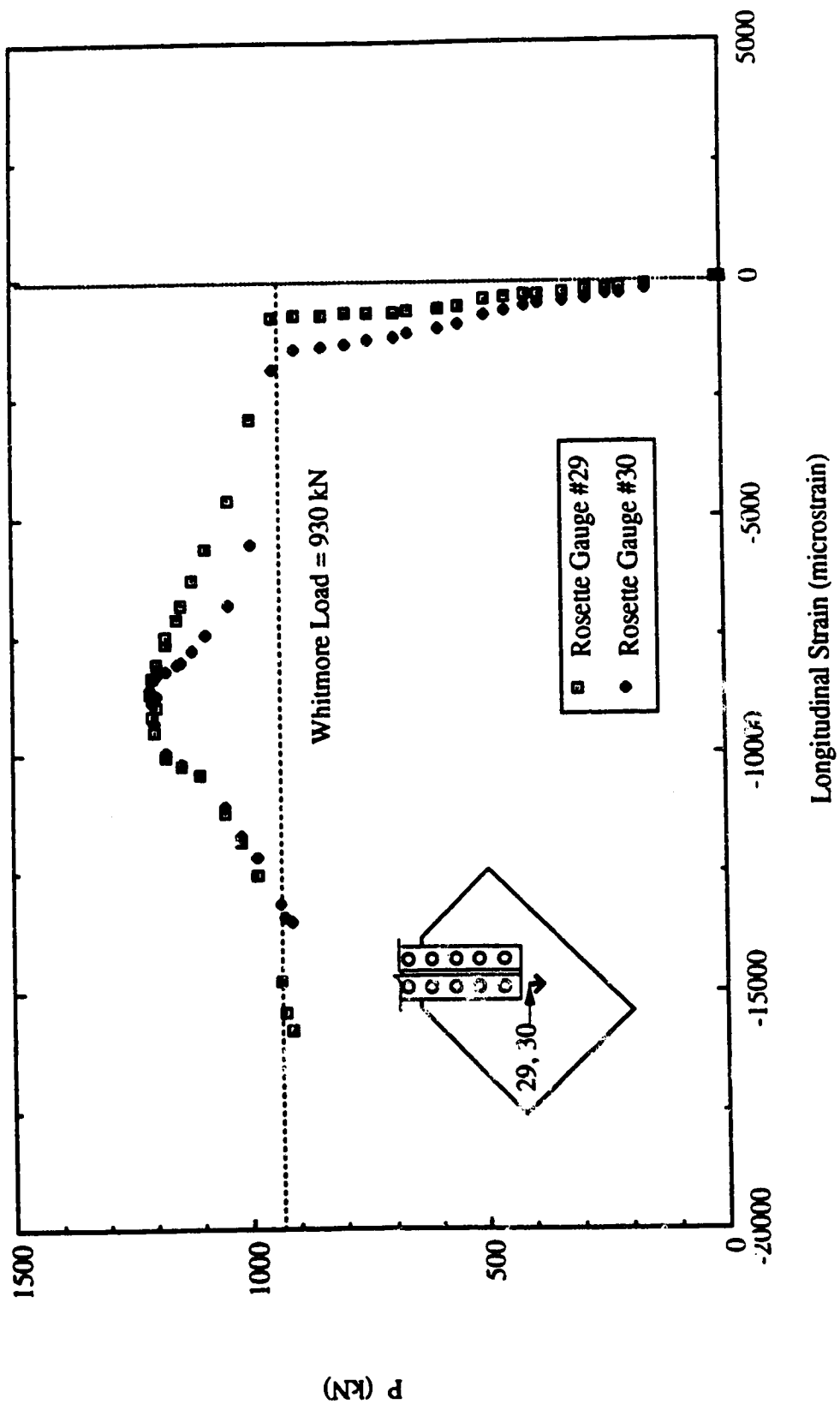


Fig. 5.13 Load vs. Rosette Gauge Readings for Specimen AP2



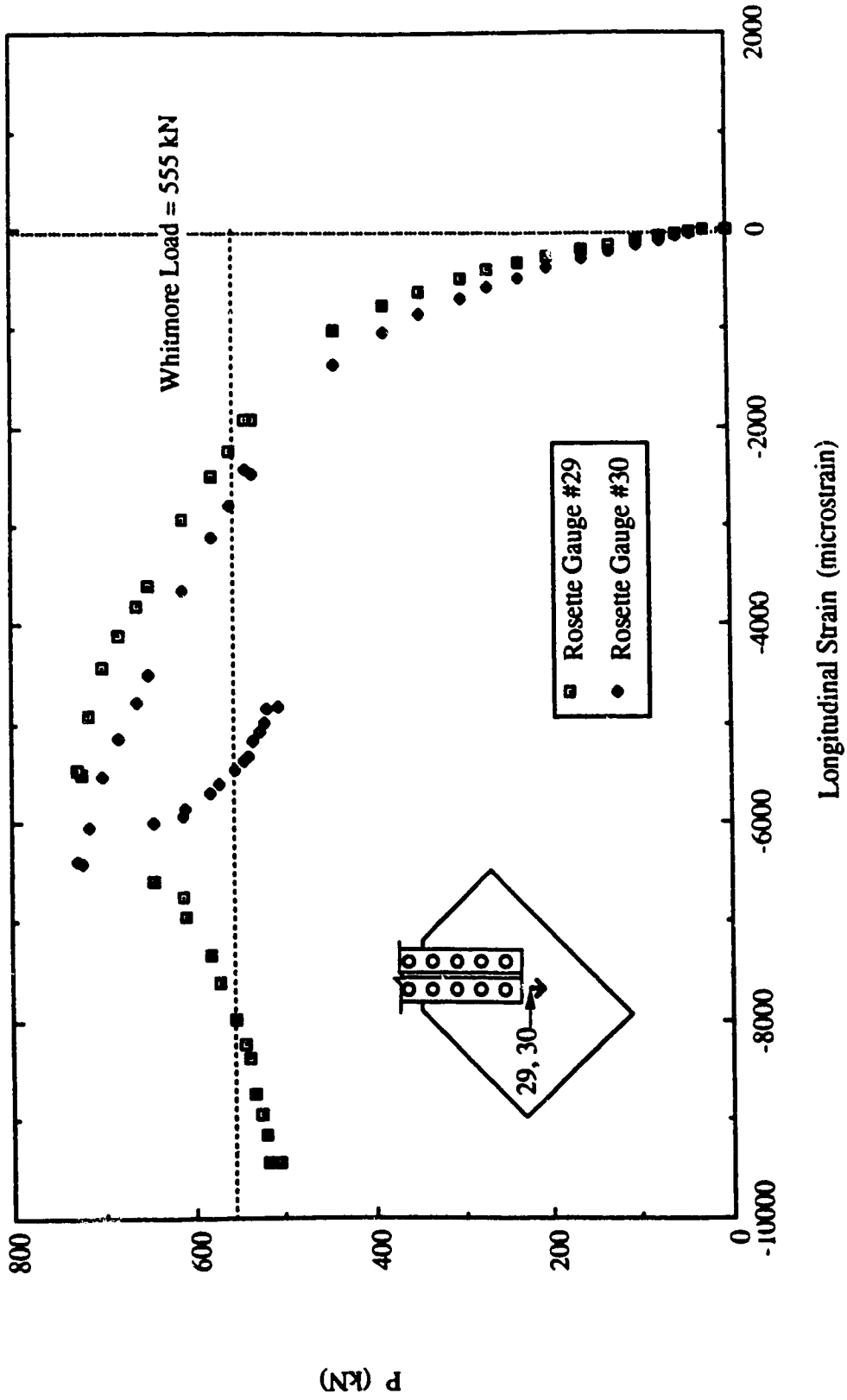


Fig. 5.14 Load vs. Rosette Gauge Readings for Specimen AP3



Fig. 5.15 Yielding at West Side of Failed Specimen API

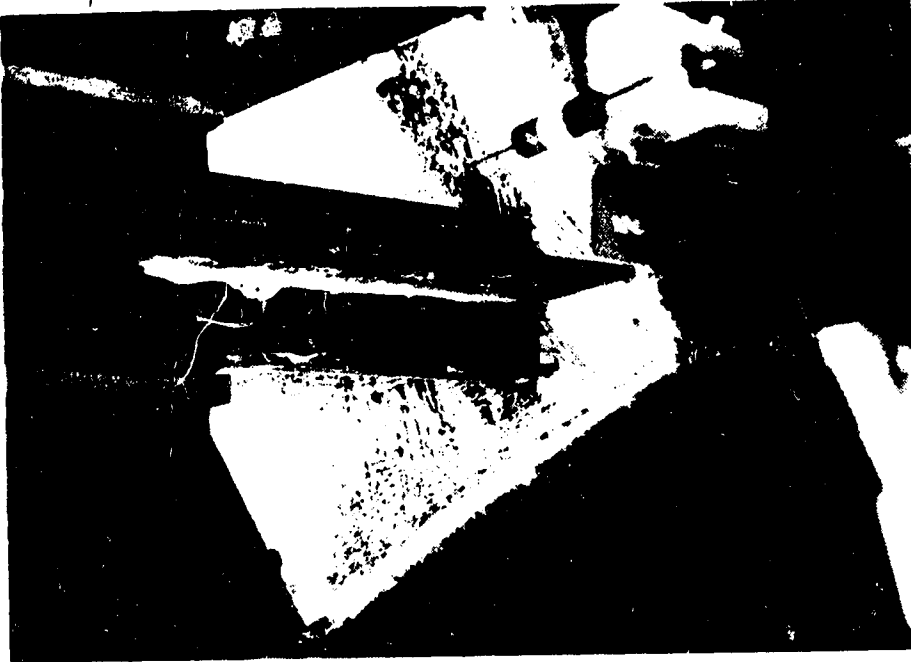


Fig. 5.16 Yielding at East Side of Failed Specimen API

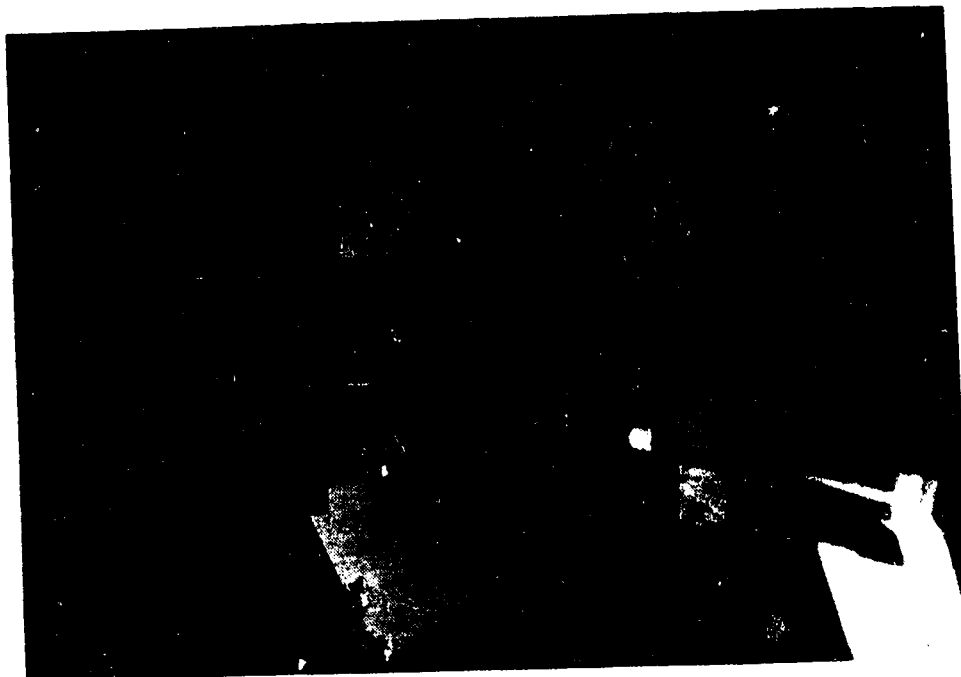


Fig. 5.18 Yielding at East Side of Failed Specimen AP2

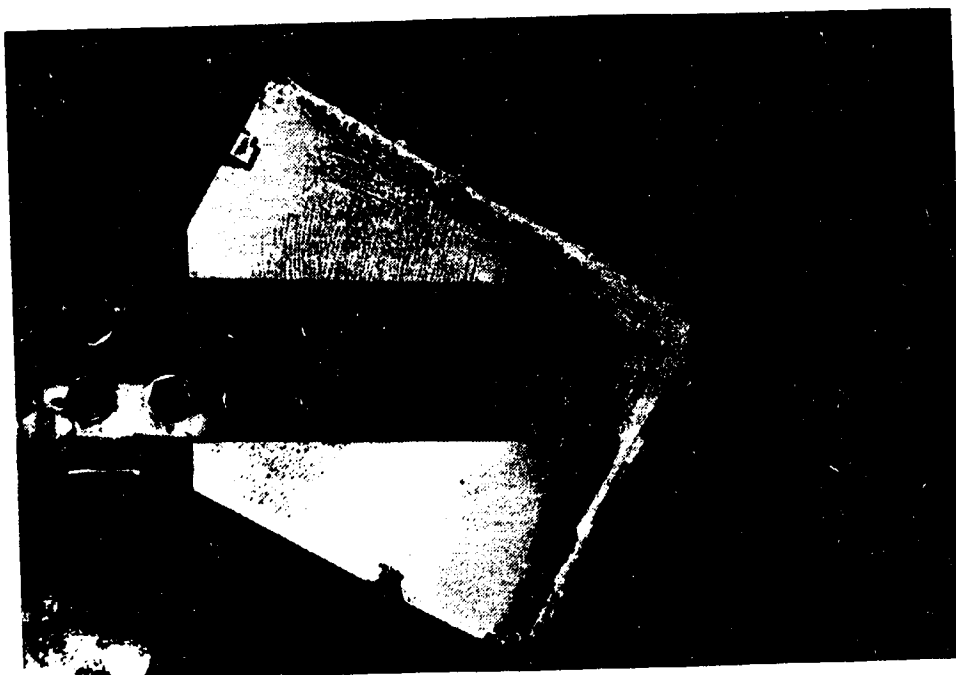


Fig. 5.17 Yielding at West Side of Failed Specimen AP2

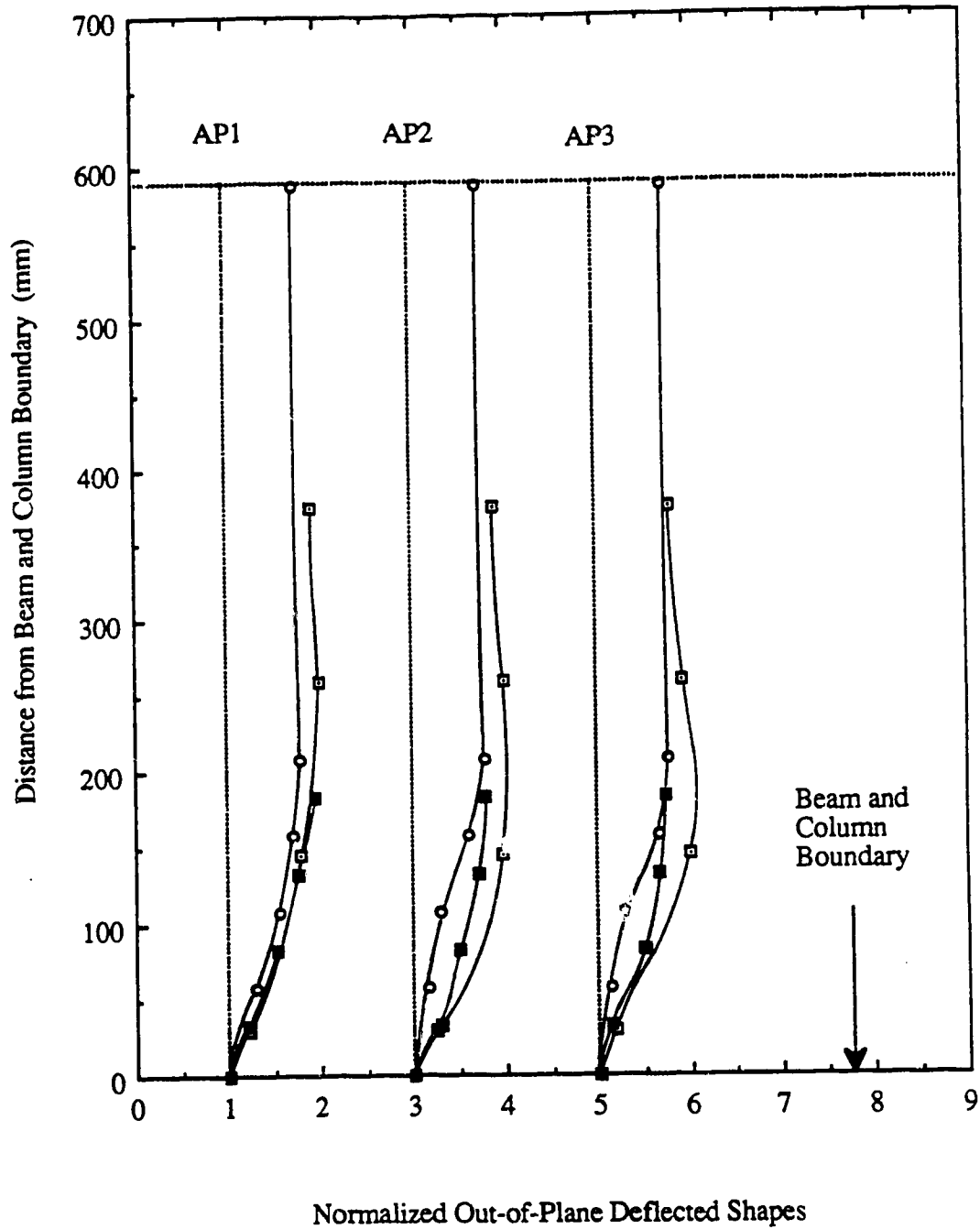
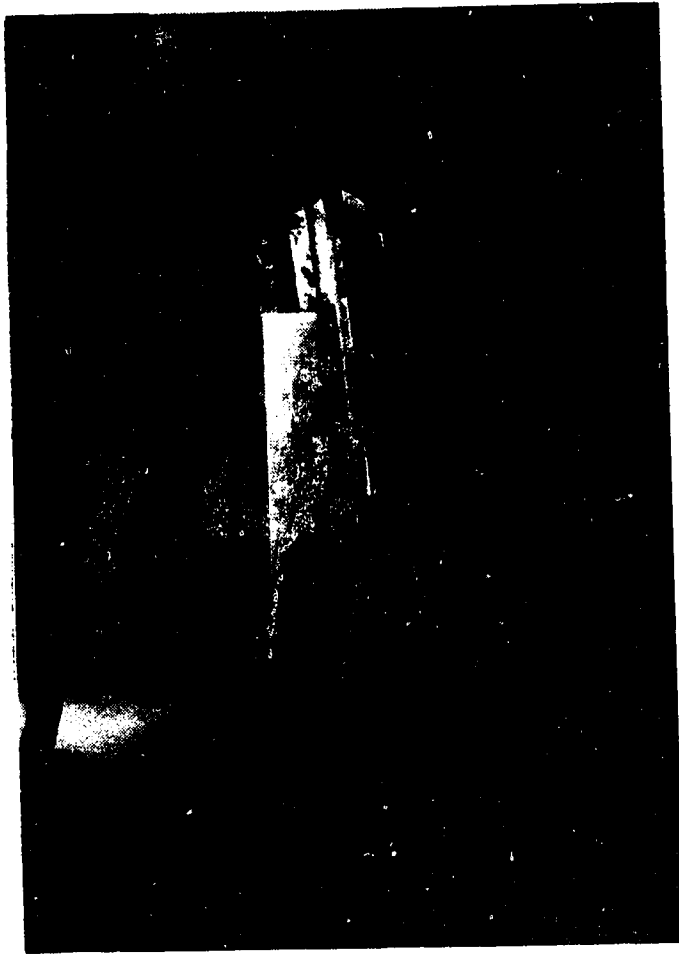


Fig. 5.19 Out-of-Plane Deflected Shapes at Free Edges and Along Centerline of Splice for AP Type Specimens



**Fig. 5.20** Picture of Out-of-Plane Deflected Shapes at Long Free Edge for Specimen AP2

## **6. TEST RESULTS OF MP TYPE SPECIMENS**

### **6.1 General**

The test results of the GP, SP and AP types specimens described previously only concerned the compressive behavior of the gusset plate connection without the effects of beam and column moments. However, the delivery of compression to the gusset plate must involve the beam and column moments, shears and axial force. The MP type specimens were used in order to investigate the effects of the beam and column moments on the compressive behavior and ultimate strength of the gusset plate specimens. To study the effects of the beam and column moments, a specimen size and geometry similar to that of the GP type specimens were used for the MP type specimens. It will be recalled that the beam and column moments used for specimens MP1, MP2 and MP3 were 250 kN·m and 125 kN·m respectively. For specimen MP3A, higher beam and column moments of 375 kN·m and 187.5 kN·m were applied. Finally, specimen MP3B was tested without beam and column moment. The test results of the MP type specimens are summarized in Table 6.1. Again, the failure mode of specimens was the sway buckling of the connection.

### **6.2 Behavior of Load versus In-Plane Deformation**

The curves of load versus in-plane vertical deformation of the specimen and load versus vertical displacement of the hydraulic rams are shown in Figs. 6.1 to 6.10. It should be noted that the vertical deformation of the specimen was recorded by an LVDT attached to the end of the splice member. For specimen MP1, the curve of in-plane deformation illustrated the occurrence of bolt slips during testing. The first bolt slip was recorded at a load level of about 700 kN, when a drop in applied load accompanied by an increase in vertical displacement was observed. However, for the curve of vertical displacement of the hydraulic rams a bolt slip occurred without a significant increase in vertical displacement. This was because there was a decrease in the applied load during the bolt slip; therefore, the

elastic deflection of the reaction beam was also decreased. Hence, the LVDT's attached to the hydraulic rams (supported by the reaction beam) moved downward during the bolt slip, while the core of the LVDTs still recorded the vertical displacement caused by the bolt slip. These two movements thus counteracted each other. Therefore, the LVDT's readings did not show a significant vertical displacement during this bolt slip. Bolts slips were again recorded as loading continued; however, both curves showed a similar vertical movement during these slips, since there was a negligible decrease in the applied load when the bolt slips occurred. The curve of in-plane deformation of the specimen also showed that the specimen started to behave nonlinearly at an applied load of about 1000 kN. When the applied load reached about 1600 kN, another bolt slip with a decrease in the applied load level was observed. As loading continued, the curve gradually turned to the ultimate load level. The unloading path of the specimen was not recorded since the out-of-plane displacement had already reached the physical limit of the measuring device. The curve for the vertical displacement of the hydraulic rams shows that an almost identical vertical movement was recorded for both rams during testing, and this was the objective of the loading system as mentioned in Chapter 2. It was also observed that the vertical displacement of the hydraulic rams was higher than the in-plane deformation of the specimen due to the elastic deflection of the reaction beam.

For specimen MP2, the nonlinear load deflection behavior of the load versus vertical displacement of the hydraulic ram and in-plane vertical deformation of the specimen were observed at a load level of about 500 kN, as shown in Figs 6.3 and 6.4. Figure 6.4 shows that the in-plane stiffness of specimen MP2 decreased rapidly, followed by the initial stage of nonlinearity. However, the in-plane stiffness was maintained once the applied load was increased to about 750 kN, at which an almost constant in-plane stiffness was observed until the specimen reached the ultimate load. Subsequently, a gradual unloading path was observed, and the specimen appeared to stabilize at a lower load level of about 900 kN. A similar behavior was observed for the curve of the load versus vertical displacement of

hydraulic rams. However, the degree of nonlinearity of the load deflection curve was less than that of the vertical displacement of the specimen due to the presence of the elastic deflection of the reaction beam.

In general, the behavior of the load versus vertical displacement of the hydraulic ram and the in-plane deformation of the specimen was similar for specimens MP3, MP3A and MP3B. However, the in-plane stiffness for specimen MP3B prior to its reaching the ultimate was relatively higher than that of specimens MP3 and MP3A. It was also observed that the in-plane stiffness for specimen MP3 was higher than that of specimen MP3A. This behavior was probably due to the effects of beam and column moments, and will be discussed in Chapter 8. The curves of load versus in-plane vertical deformation of the specimens show that nonlinear load deflection behavior for specimens MP3 and MP3A occurred at about 50 percent of the corresponding ultimate loads, as shown in Figs. 6.6 and 6.8. For specimen MP3B nonlinear behavior was observed at about 70 percent of the ultimate load, as illustrated in Fig.6.10. Again, as loading continued, the curves gradually turned to the corresponding ultimate load levels. However, for specimen MP3A, a bolt slip was recorded at a load level of about 760 kN and the applied load dropped to approximately 710 kN before reaching the ultimate load level. A gradual unloading path was observed for the specimens, and these curves show that the specimens appeared to stabilize at a load level of about 450 kN.

### **6.3 Behavior of Load versus Out-of-Plane Displacement**

The curves of load versus out-of-plane displacement at the conjunction of gusset-to-splice for the specimens are shown in Figs. 6.11 to 6.15. For specimen MP1, a relatively linear load deflection behavior was observed until the applied load reached approximately 1000 kN. It should also be noted that the displacement at the early loading stage was relatively small, probably because of the effects of the beam and column moment. When the applied



load reached about 1650 kN, a sudden drop in load to approximately 1450 kN was recorded. Subsequently, the applied load increased again, back to the load level of about 1600 kN without a significant increase in out-of-plane displacement. From then on, the applied load increased with increasing displacement until the load reached an ultimate load of 1933 kN with a displacement of about 11mm. After reaching the ultimate load, the specimen unloaded gradually without a significant decrease in the applied load, as shown in Fig. 6.11. When the load deflection curve in the early loading stage is examined closely, it can be seen that drops in the applied load due to bolt slips were recorded, as has already been discussed in the previous section.

For specimens MP2 and MP3, the load deflection behavior was quite similar, as shown in Figs. 6.12 and 6.13. Linear load deflection behavior was observed until the applied load reached approximately 40 percent and 50 percent of the ultimate loads for specimens MP2 and MP3 respectively. However, the out-of-plane stiffness of both specimens only reduced slightly as loading continued until the specimens reached the ultimate loads. It should also be noted that the out-of-plane displacement of the specimens recorded prior to buckling was relatively small, as shown in the figures. The recorded displacement at the ultimate load for both specimens was about 3 mm. A gradual unloading behavior was also observed for both specimens. However, for specimen MP2, the rate of unloading was lesser than that of specimen MP3.

The curve of load versus out-of-plane displacement for specimen MP3A shows a slightly different behavior from that of specimen MP3 as shown in Fig. 6.14. In general, a negligible out-of-plane displacement was recorded for this specimen prior to its reaching the ultimate load. As can be seen from the figure, the specimen originally deformed towards the east. However, a sudden change in displacement direction at load step #7 was observed. This opposite movement of the specimen was due to the application of the full values of the beam and column moment (375 kN·m and 186.5 kN·m, respectively) at that

load step. As loading continued, only a very slight increase in the out-of-plane westward displacement was observed. When the applied load reached the ultimate load of 819 kN, bifurcation occurred with the specimen deformed towards the west. Since the buckling phenomenon occurred rapidly, therefore, it was unable to record readings between the ultimate load and the next load level which had a displacement of 15 mm. However, it can still be seen that the unloading process for the specimen was quite gradual.

For specimen MP3B, which excluded the beam and column moments, the curve of load versus out-of-plane displacement was similar to that of specimen MP3, as shown in Fig. 6.15. The curve was relatively linear up to 700 kN. Then the curve slowly turned to the ultimate load of 821 kN. Again, it was unable to record successive readings after the ultimate load until the applied load reached a lower level. However, a gradual unloading process was observed for the specimen. It should be noted that all the MP type specimens with a plate thickness of 6.5 mm reached approximately the same load level of 450 kN at the final load step, regardless of the level of the applied beam and column moments.

#### **6.4 Strain Gauge Results**

The in-plane stress distribution of the specimen was affected by the beam and column moments as observed from the strain gauges readings. For specimen MP1, yielding was first observed at the rosette close to the beam boundary at an applied load of about 770 kN. However, the yield load predicted by the Whitmore method was approximately 1200 kN. This early yielding of the specimen may be attributed to the effects of the beam and column moment. A similar behavior was also observed for the other MP type specimens. In particular, for specimen MP2 and MP3, yielding at the rosette occurred at an applied load of about 55 and 30 percent of the corresponding yield loads predicted by the Whitmore method. It should be noted that for specimens MP1, MP2, and MP3, full values of the beam and column moments had already been applied to the specimens when the test yield

loads were recorded. However, specimen MP3A, which was subject to higher beam and column moment (  $M_b=375 \text{ kN}\cdot\text{m}$ ,  $M_c=186.5 \text{ kN}\cdot\text{m}$  ), showed a yielding at the rosette when the applied load was maintained at about 100 kN and the applied beam and column moments were increased from 50 percent to the full values.

The curves of load versus strains recorded at the mid-length and the fixed end of the free edges are shown in Figs.6.16 to 6.31. In general, the plots of load versus longitudinal strains at the mid-length of the free edges show that the strain readings in the elastic range were recorded prior to their reaching the ultimate load of the specimens. Furthermore, similar strain readings were recorded from both sides of the specimens before strain bifurcation occurred at ultimate load levels, except for specimen MP1. For specimen MP1, strain reversal was observed at the long free edge as shown in Fig. 6.16, and the strain readings from both sides of the specimen at the short free edge deviated at an early loading stage, as illustrated in Fig. 6.24. The strain readings recorded at the fixed ends of the free edges showed that tension existed in that vicinity. In particular, specimens MP3 and MP3A showed tensile yielding at the fixed ends of the free edges when the full values of the beam and column moments were applied, as shown in Figs. 6.29 and 6.31 respectively. As loading continued, tensile strain recorded at the fixed ends of the free edges increased slightly until strain bifurcation occurred at the ultimate loads. It should also be noted that strain gauges located at the fixed end of the free edges were mounted 30 mm away from the boundary. Hence, it is believed that tensile yielding should have occurred right at the fixed end of free edges before it was even detected by the strain gauges. In addition, the vicinity of the fixed end of the free edges was also a stress concentration area, due to abrupt change of geometry.

To investigate the effects of the beam and column moments on the in-plane stress distribution of the specimen, the strain readings along the beam and column boundary were examined. A plot of strain readings along the beam and column boundary at three levels

( 1/3, 2/3, and full values ) of the applied beam and column moments for specimen MP1 is shown in Fig. 6.32. The strain readings shown in the figure had already excluded the effects of the axial load. It can be seen from the figure that a high stress gradient existed along the beam and column boundary, especially along the beam boundary, in the vicinity of the short free edge. In general, tensile strains were observed along the column boundary. However, compressive strains were recorded near the mid-length of the beam boundary, as shown in the figure. The reduced strain readings at the rosettes indicated that the applied beam and column moments induced compressive strains in the plate area underneath the splice member. Hence, early yielding at that region was recorded for the MP type specimens.

### **6.5 Yielding Behavior of Specimens**

The yielding process and pattern for the MP type specimens were only slightly different from those of the GP type specimens, except for specimen MP3B, which behaved similarly to specimen GP3. In general, yield lines were first observed near the beam boundary. These yield lines were almost parallel to it. Yielding underneath the splice member was then recorded. As loading continued, yielding underneath the splice member progressed and yield lines were also recorded about the two sides of the splice member. In particular, for specimens MP1, MP2 and MP3A, extensive yielding of the specimens was observed prior to buckling. However, for specimen MP3 moderate yielding was observed underneath the splice member. After buckling occurred, yield lines were also formed at the mid-length of the long free edge and along the beam and column boundary. A picture of the failed specimen MP1, shown in Fig. 6.33, illustrates the extent of the yielding and also the location of the yield line mechanism. When the failed specimen MP3 was examined, a fracture from the weld at the fixed end of the short free edge was observed. Hence, for specimens MP3A and MP3B, a larger weld size was used to prevent fracture at that location.

### **6.6 Out-of-Plane Deflected Shapes of Free Edges and Along Centerline of Splicing Member**

The normalized out-of-plane deflected shapes of the MP type specimens are shown in Fig. 6.34. In general, the out-of-plane deflected shapes of the specimens resembled the buckled shape of a fixed-pinned column. The figure shows that the end of the free edges attached to the beam and column boundary exhibited quite a significant rotation. This is probably due to the tensile yielding caused by the beam and column moments. Pictures of the deflected shapes of the free edges for specimen MP3A are shown in Fig.6.35 to illustrate the amount of rotation which existed at the ends. It can be seen from these pictures that the lower end of the free edges was almost in a straight position, indicating that the lower end rotated as a rigid body.

Table 6.1 Test Results of MP Type Specimens

Specimen Designation	Plate Size (mm x mm x mm)	Beam Moment M <sub>b</sub> (kN.m)	Column Moment M <sub>c</sub> (kN.m)	Ultimate Load P (kN)	Whitmore Load P <sub>w</sub> (kN)	Thornton Load P <sub>t</sub> k = 0.65 (kN)
MP1	500 x 400 x 13.3	250	125	1933	1216	1142
MP2	500 x 400 x 9.8	250	125	1316	930	828
MP3	500 x 400 x 6.5	250	125	721	555	459
MP3A	500 x 400 x 6.5	375	187.5	819	555	459
MP3B	500 x 400 x 6.5	0	0	821	555	459

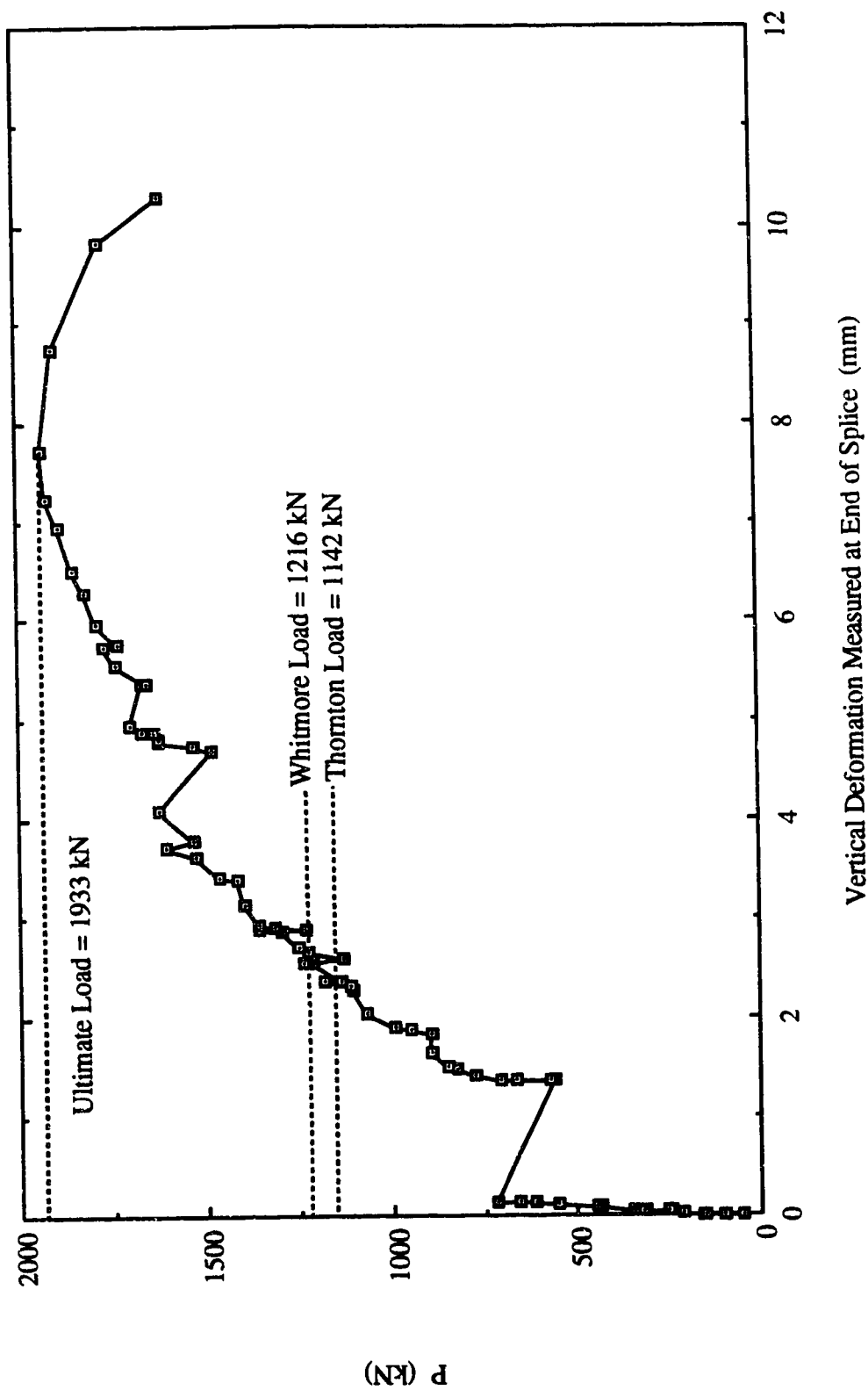


Fig. 6.1 Load vs. In-Plane Deformation Measured at End of Splice for Specimen MP1

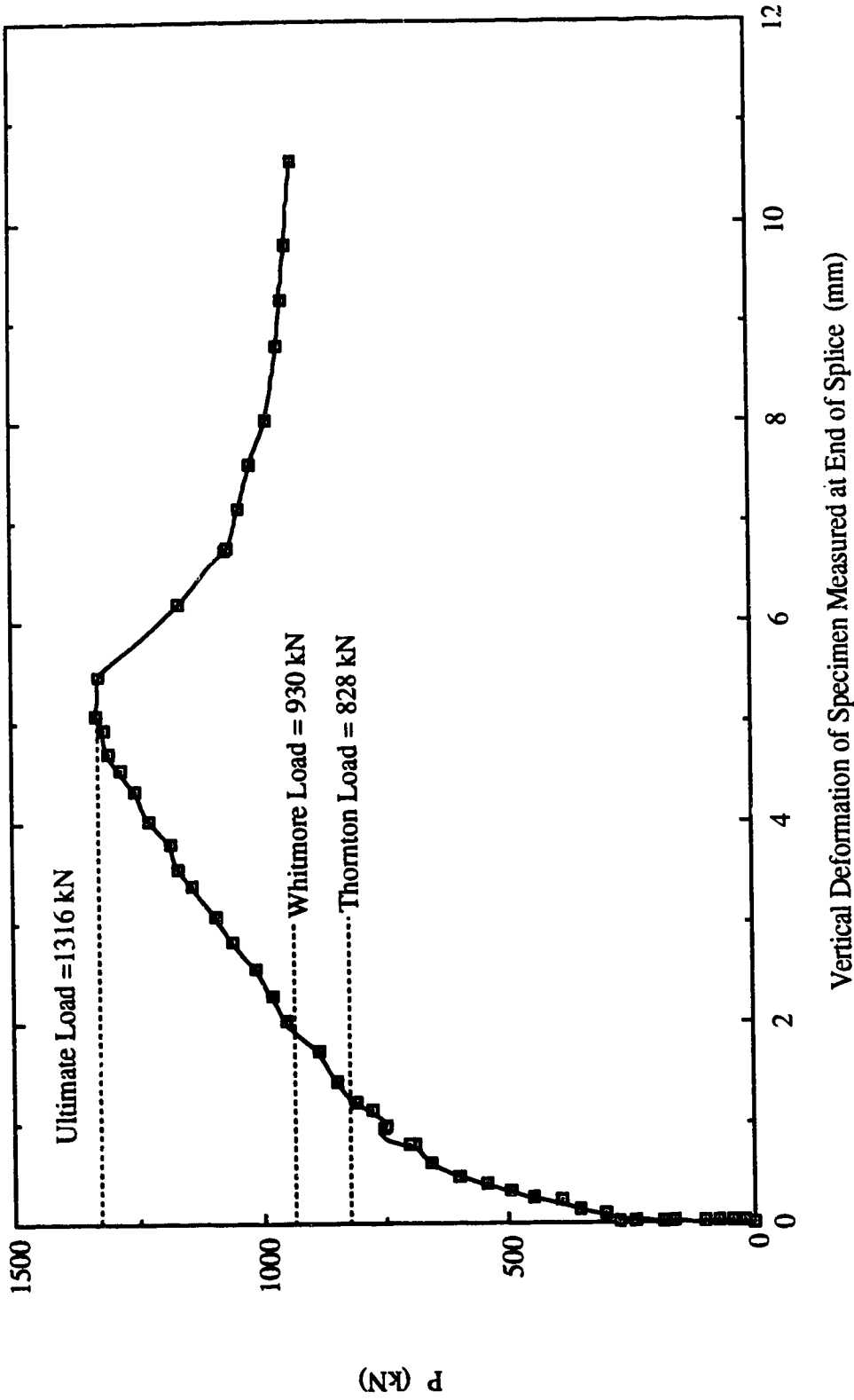
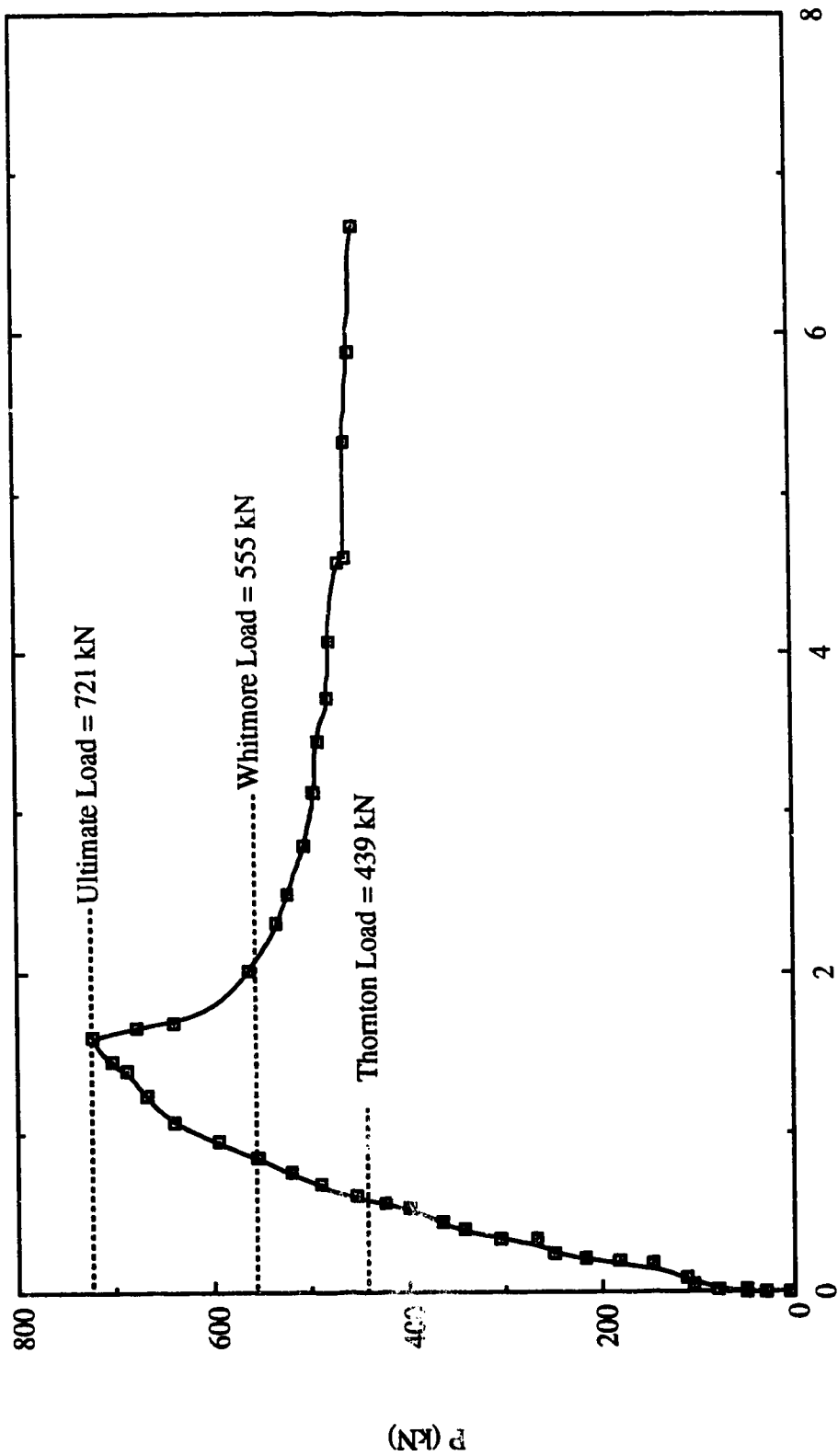


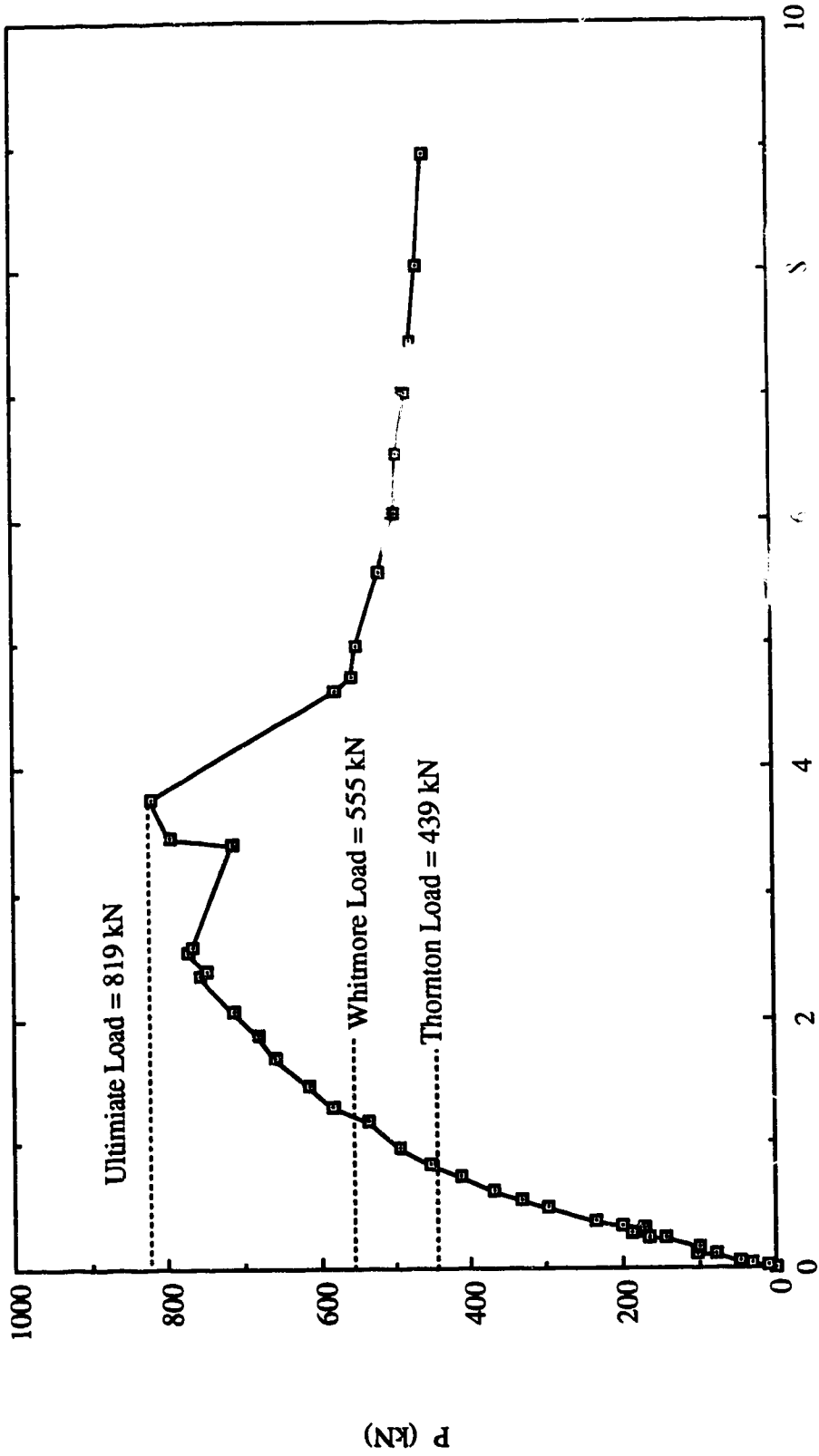
Fig. 6.2 Load vs. In-Plane Deformation Measured at End of Splice for Specimen MP2





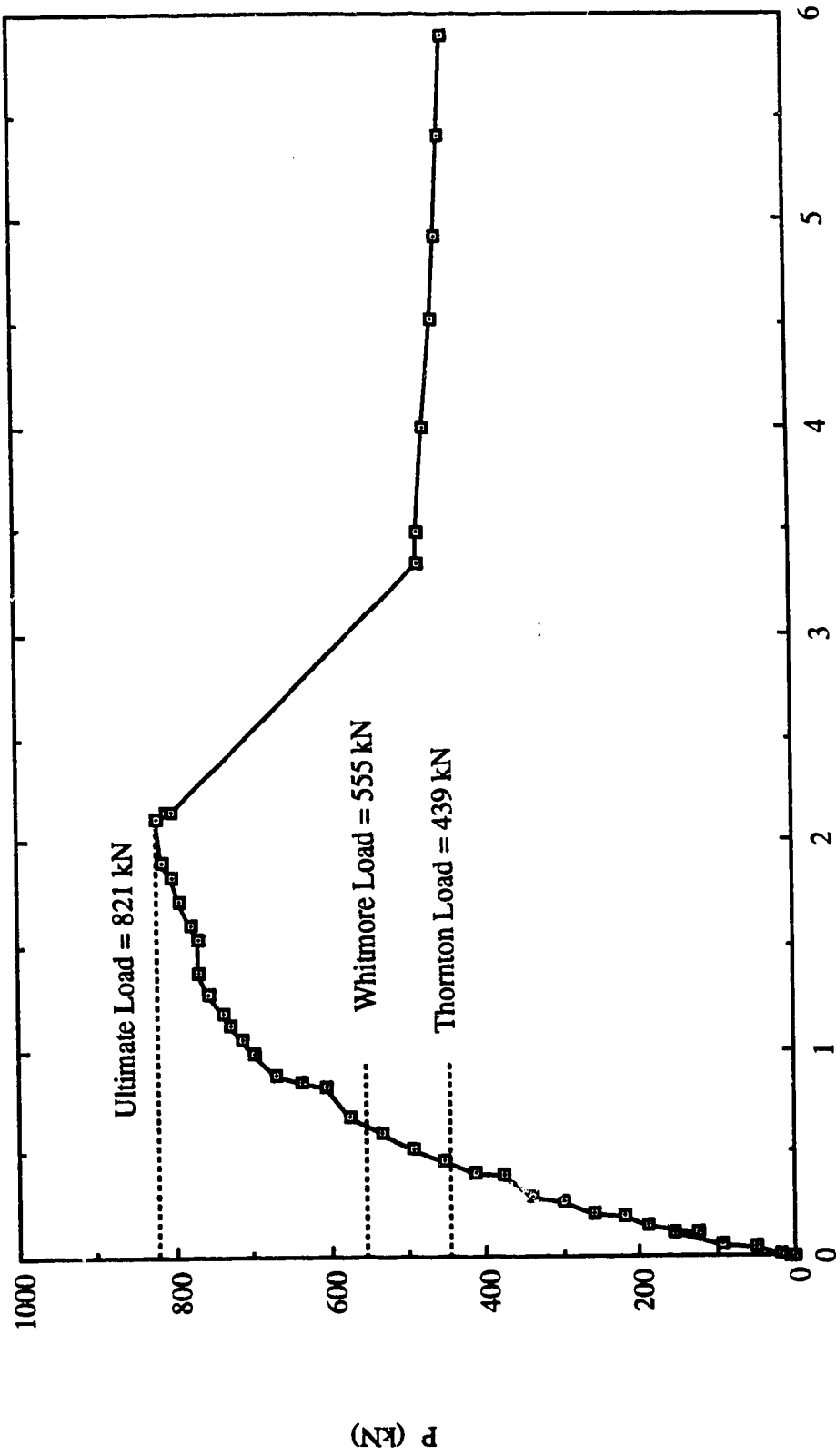
Vertical Deformation of Specimen Measured at End of Splice (mm)

Fig. 6.3 Load vs. In-Plane Deformation Measured at End of Splice for Specimen MP3



Vertical Deformation of Specimen Measured at End of Splice (mm)

Fig. 6.4 Load vs. In-Plane Deformation Measured at End of Splice for Specimen MP3A



Vertical Deformation of Specimen Measured at End of Splice (mm)

Fig. 6.5 Load vs. In-Plane Deformation Measured at End of Splice for Specimen MP3B

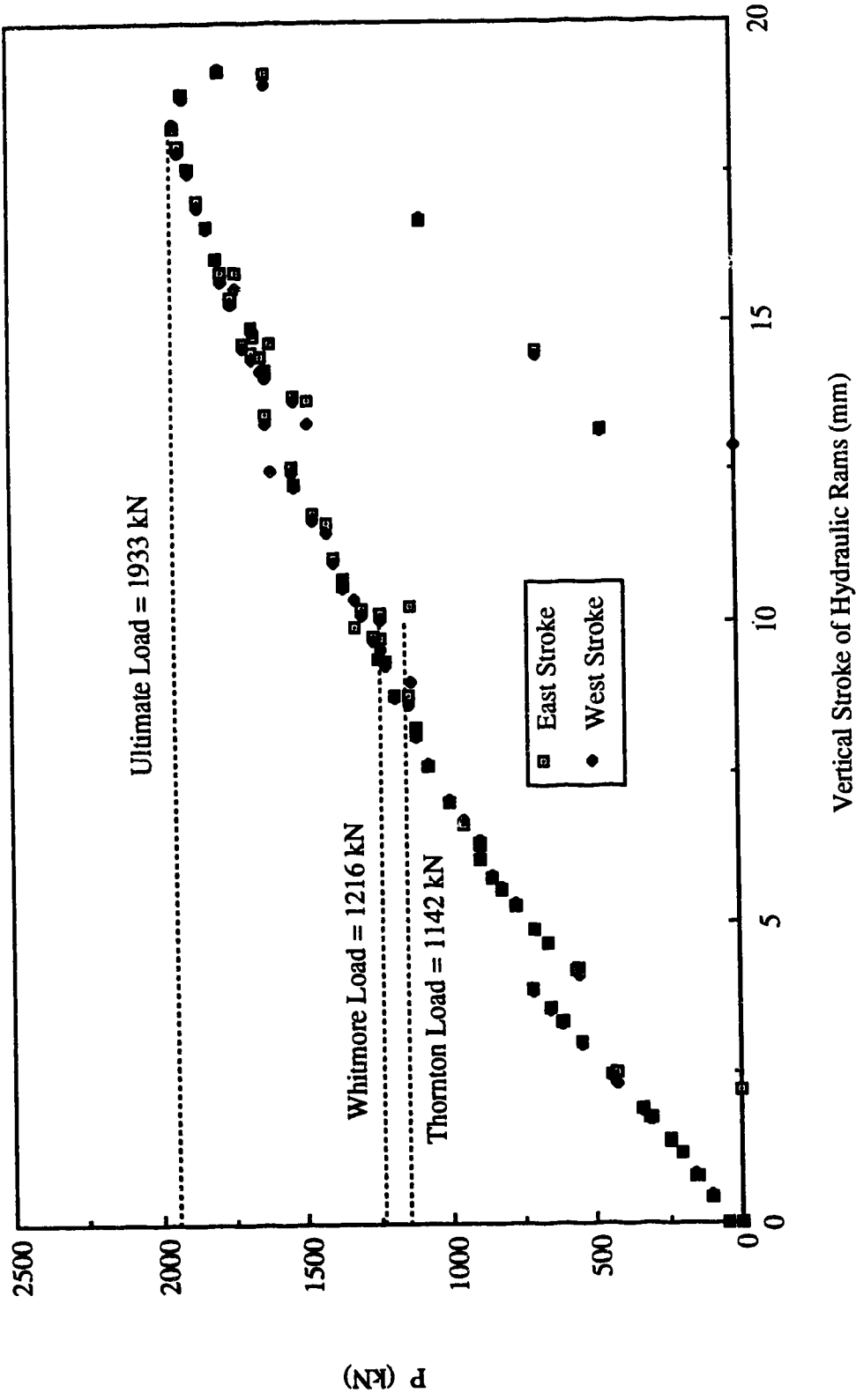


Fig. 6.6 Load vs. Vertical Strokes of Hydraulic Rams for Specimen MP1

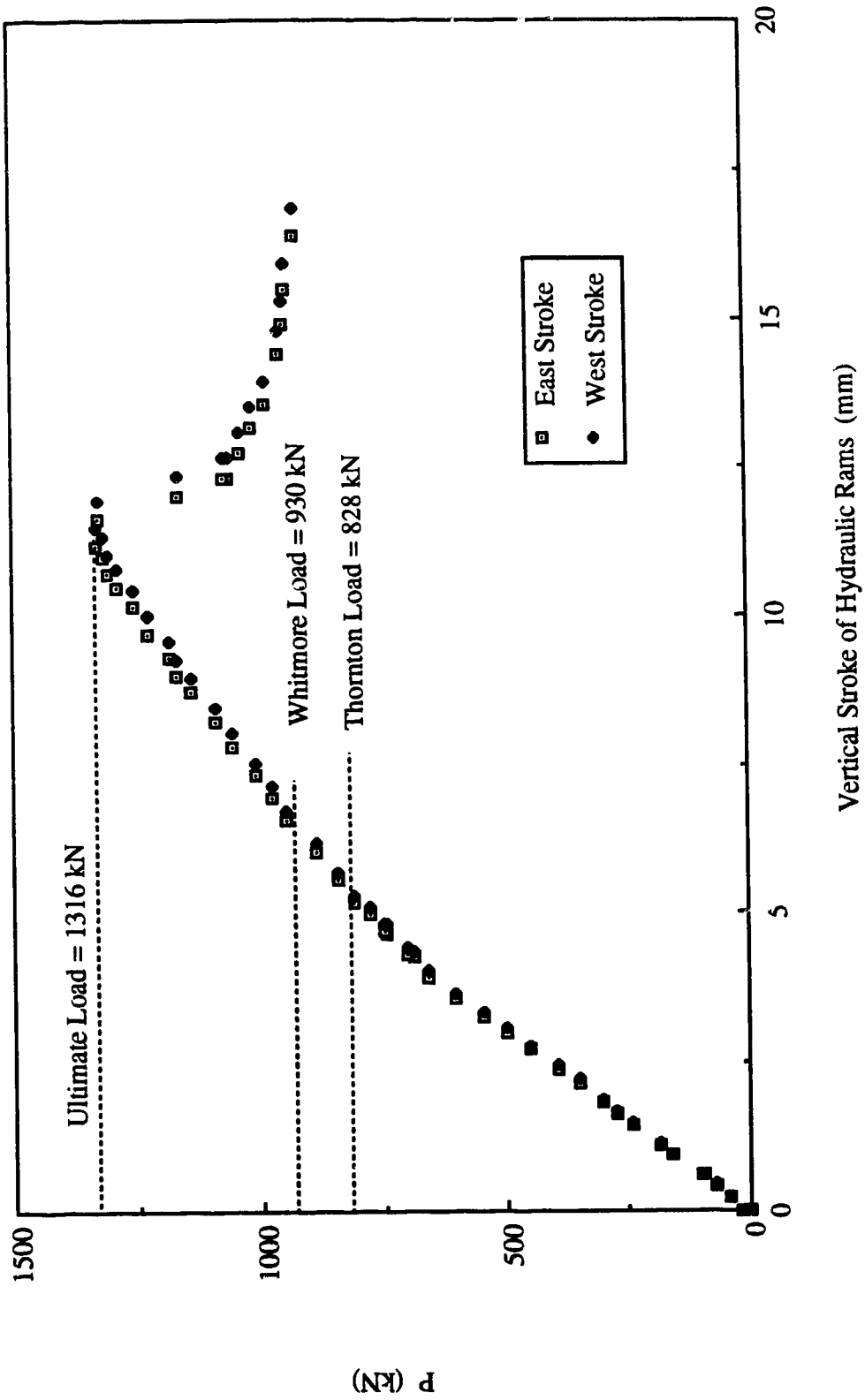


Fig. 6.7 Load vs. Vertical Strokes of Hydraulic Rams for Specimen MP2

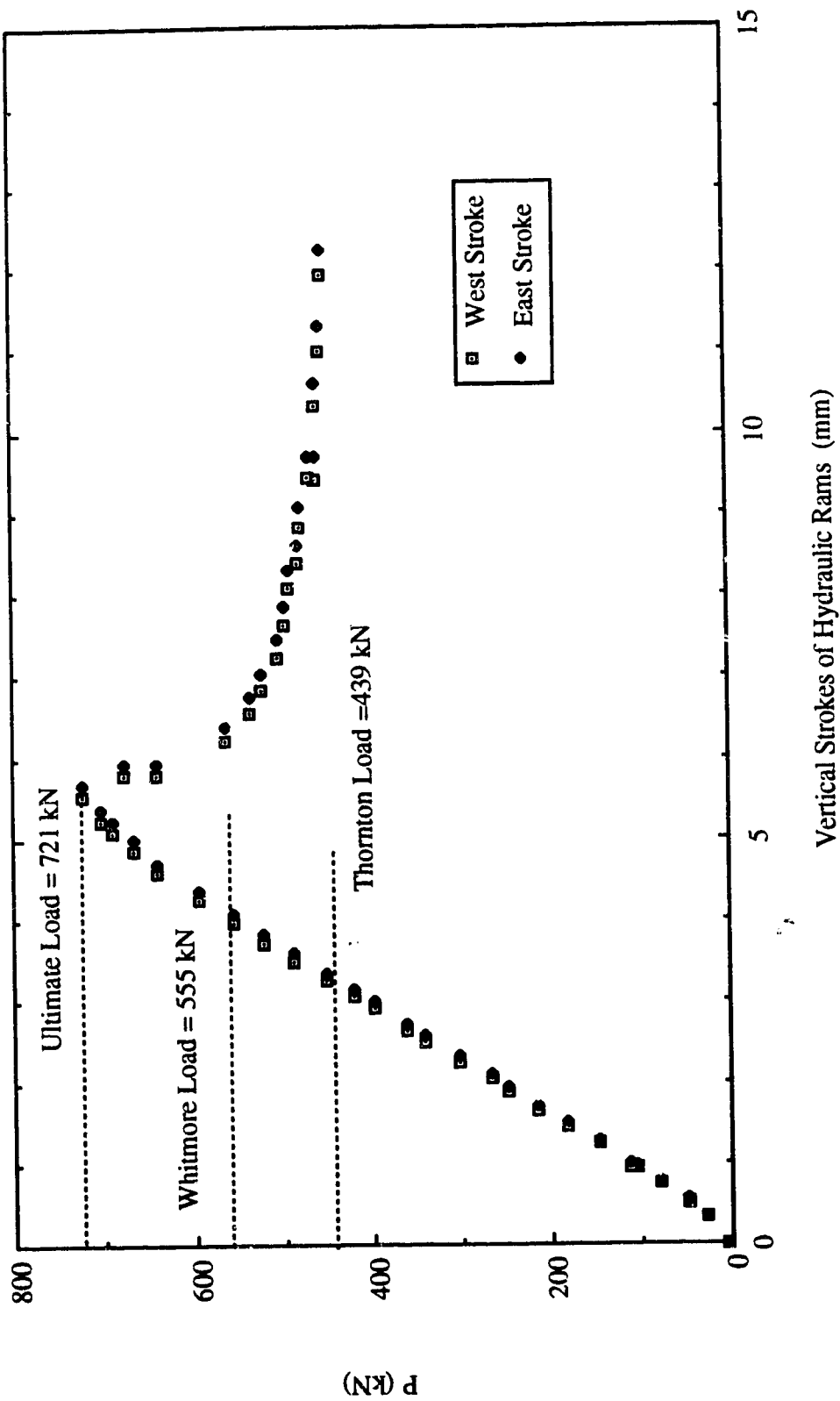


Fig. 6.8 Load vs. Vertical Strokes of Hydraulic Rams for Specimen MP3

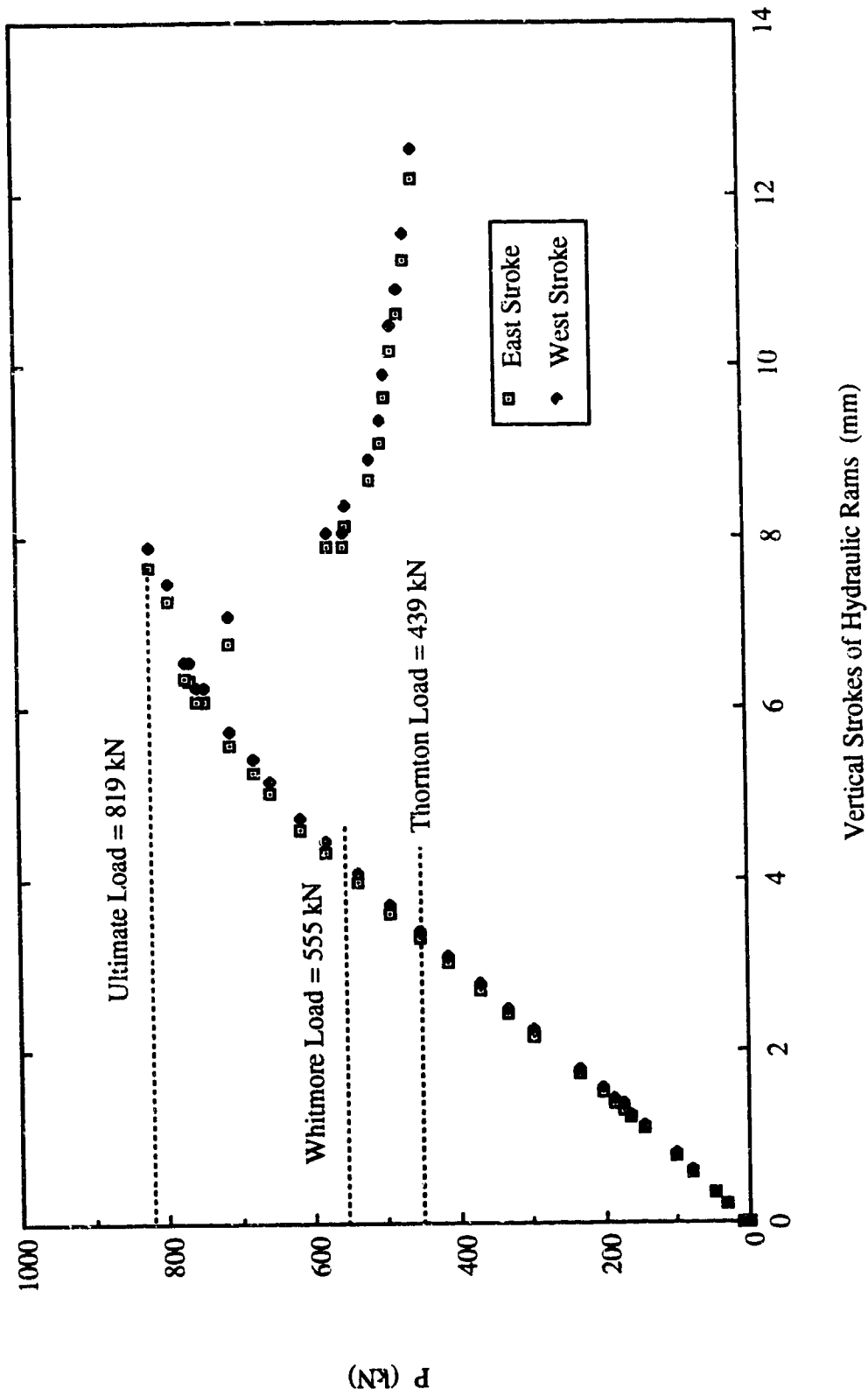


Fig. 6.9 Load vs. Vertical Strokes of Hydraulic Rams for Specimen MP3A

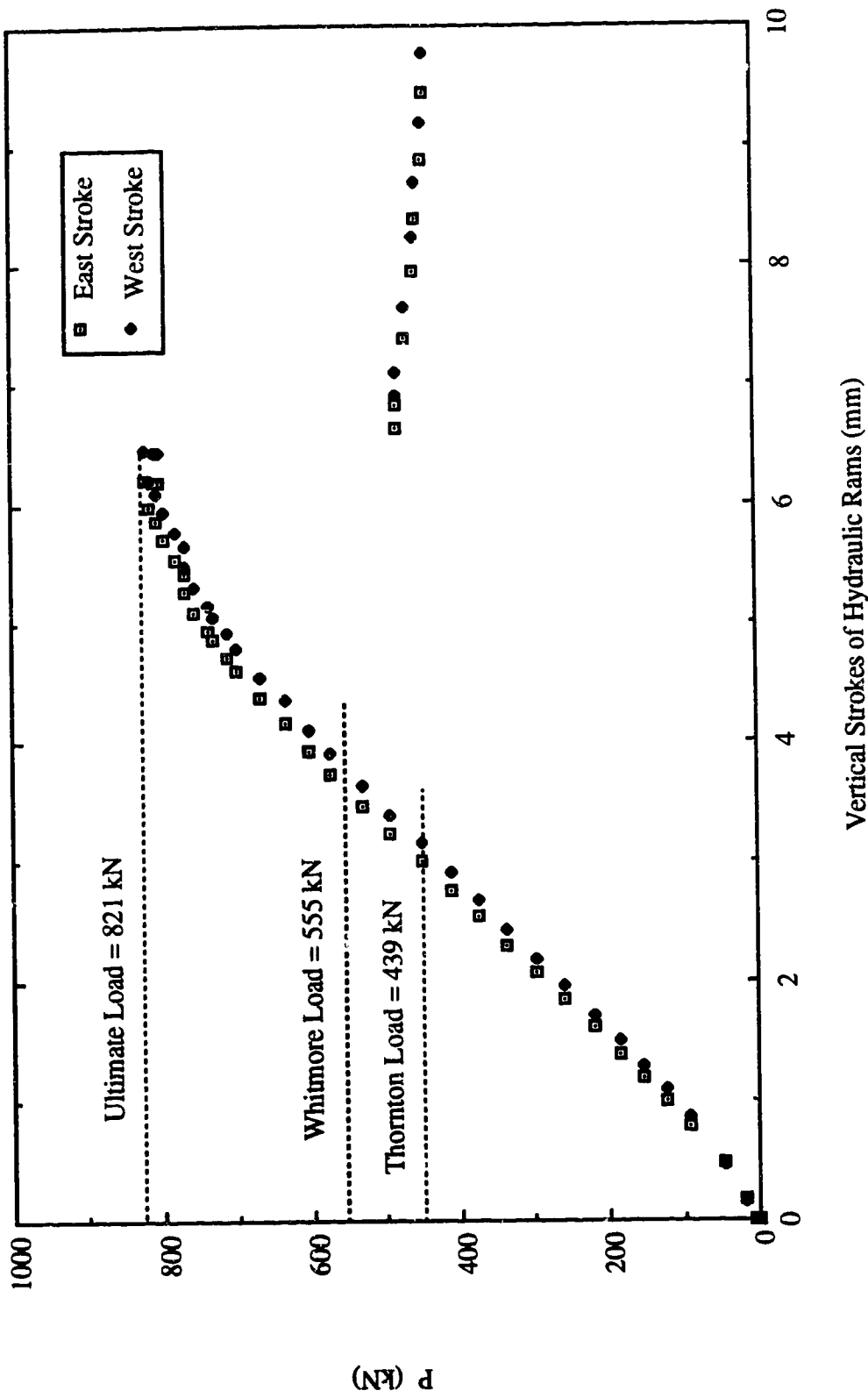


Fig. 6.10 Load vs. Vertical Strokes of Hydraulic Rams for Specimen MP3B



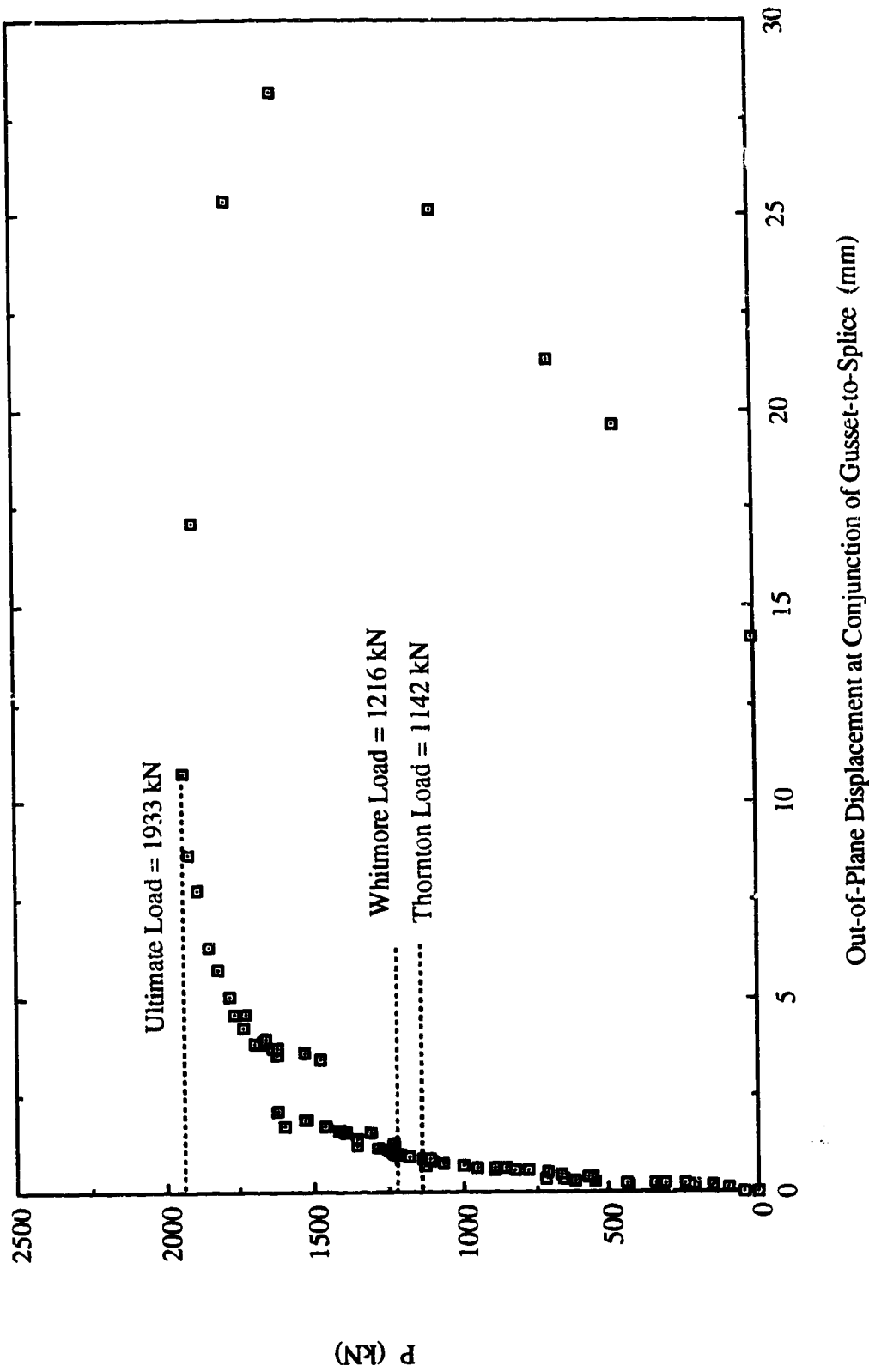


Fig. 6.11 Load vs. Out-of-Plane Displacement at Conjunction of Gusset-to-Splice for Specimen MP1

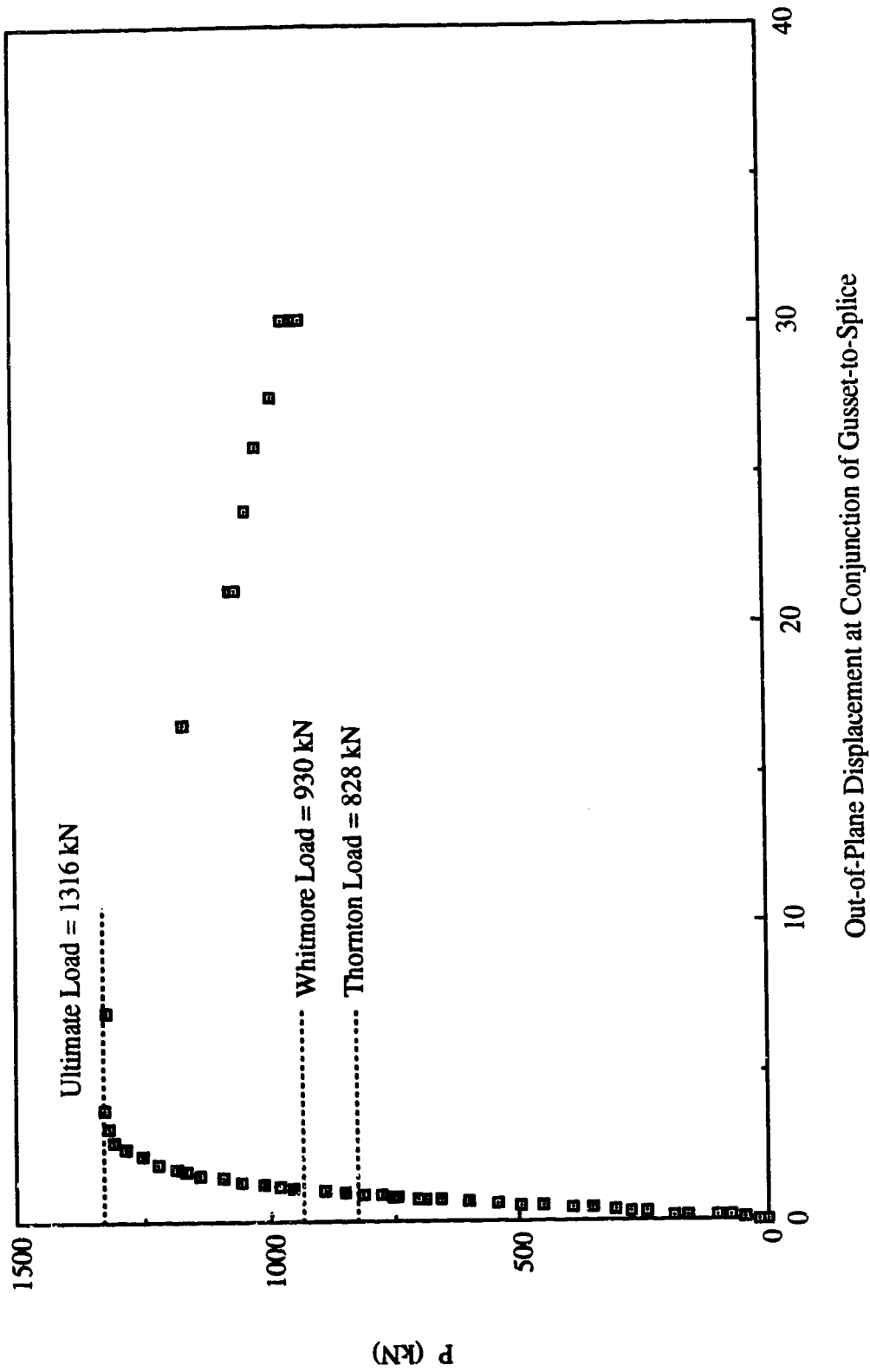


Fig. 6.12 Load vs. Out-of-Plane Displacement at Conjunction of Gusset-to-Splice for Specimen MP2

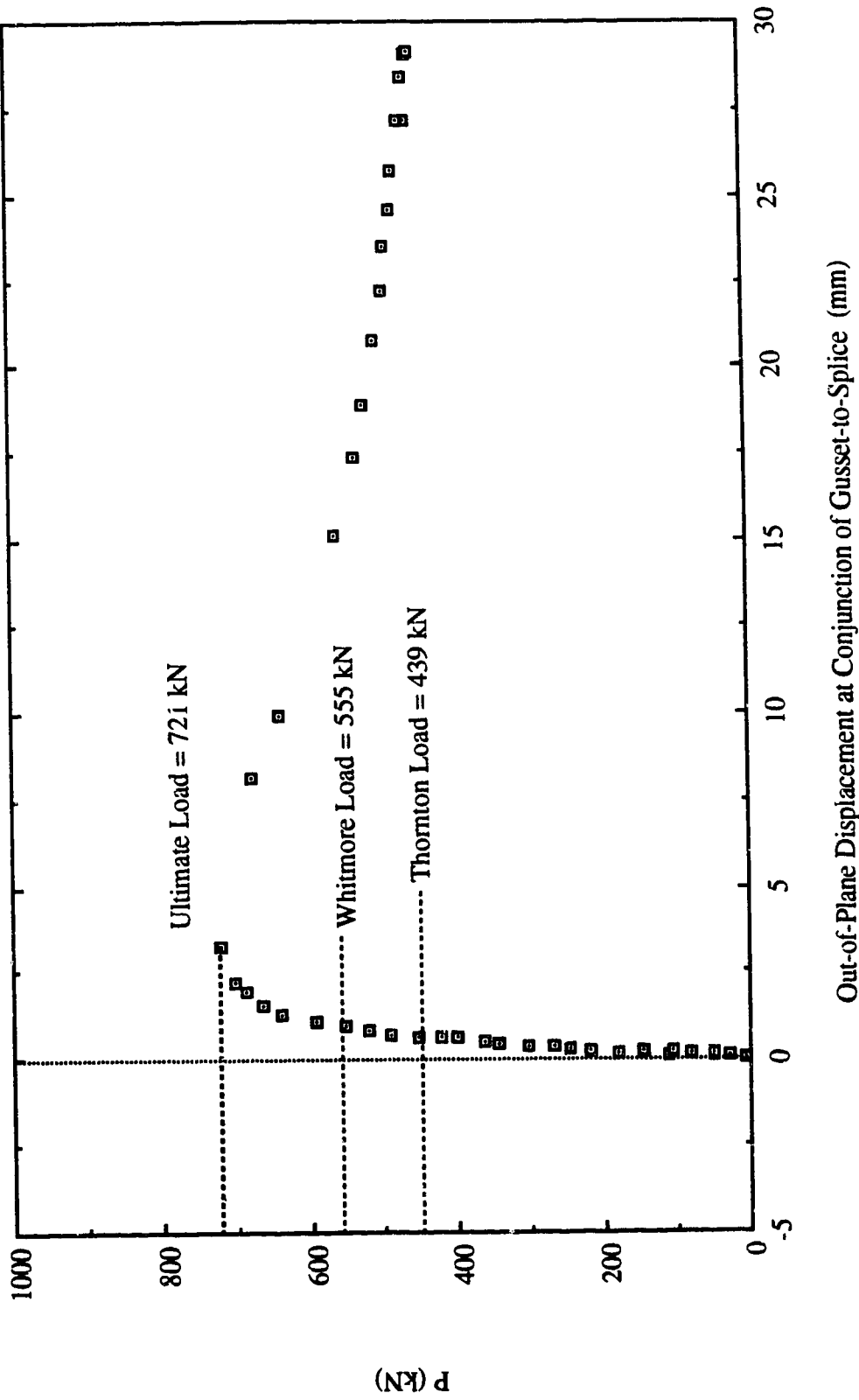


Fig. 6.13 Load vs. Out-of-Plane Displacement at Conjunction of Gusset-to-Splice for Specimen MP3

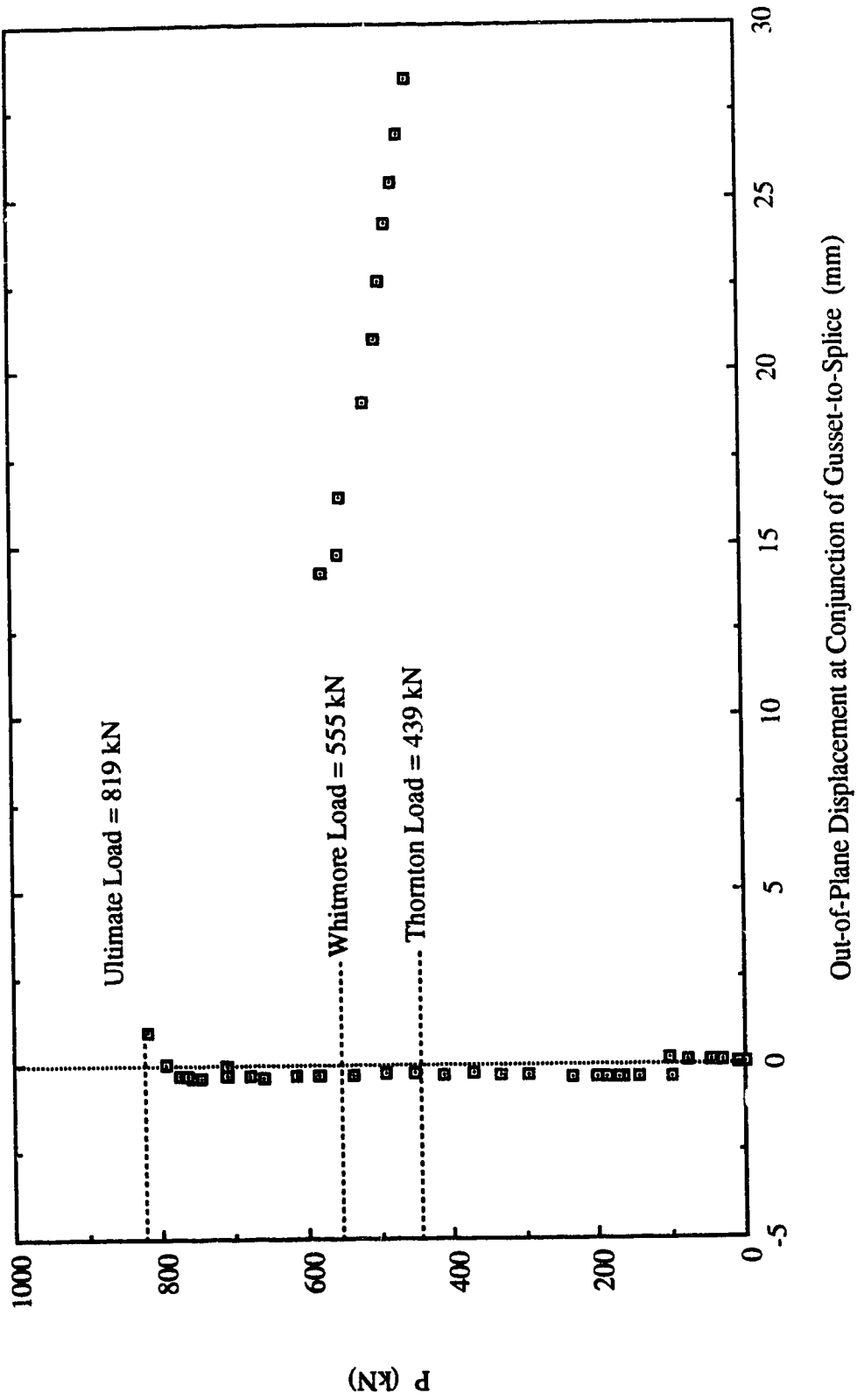


Fig. 6.14 Load vs. Out-of-Plane Displacement at Conjunction of Gusset-to-Splice for Specimen MP3A

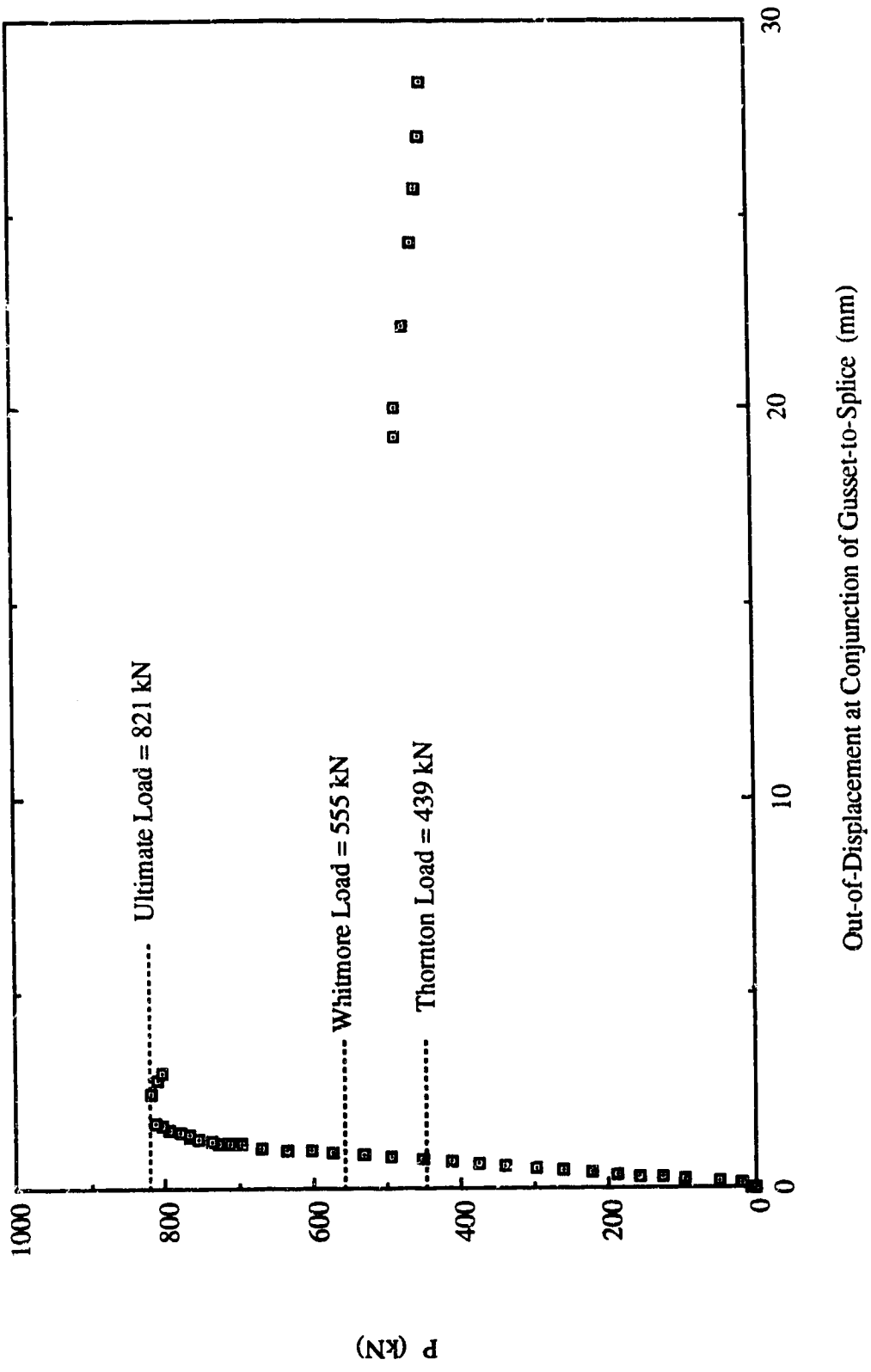


Fig. 6.15 Load vs. Out-of-Plane Displacement at Conjunction of Gusset-to-Splice for Specimen MP3B

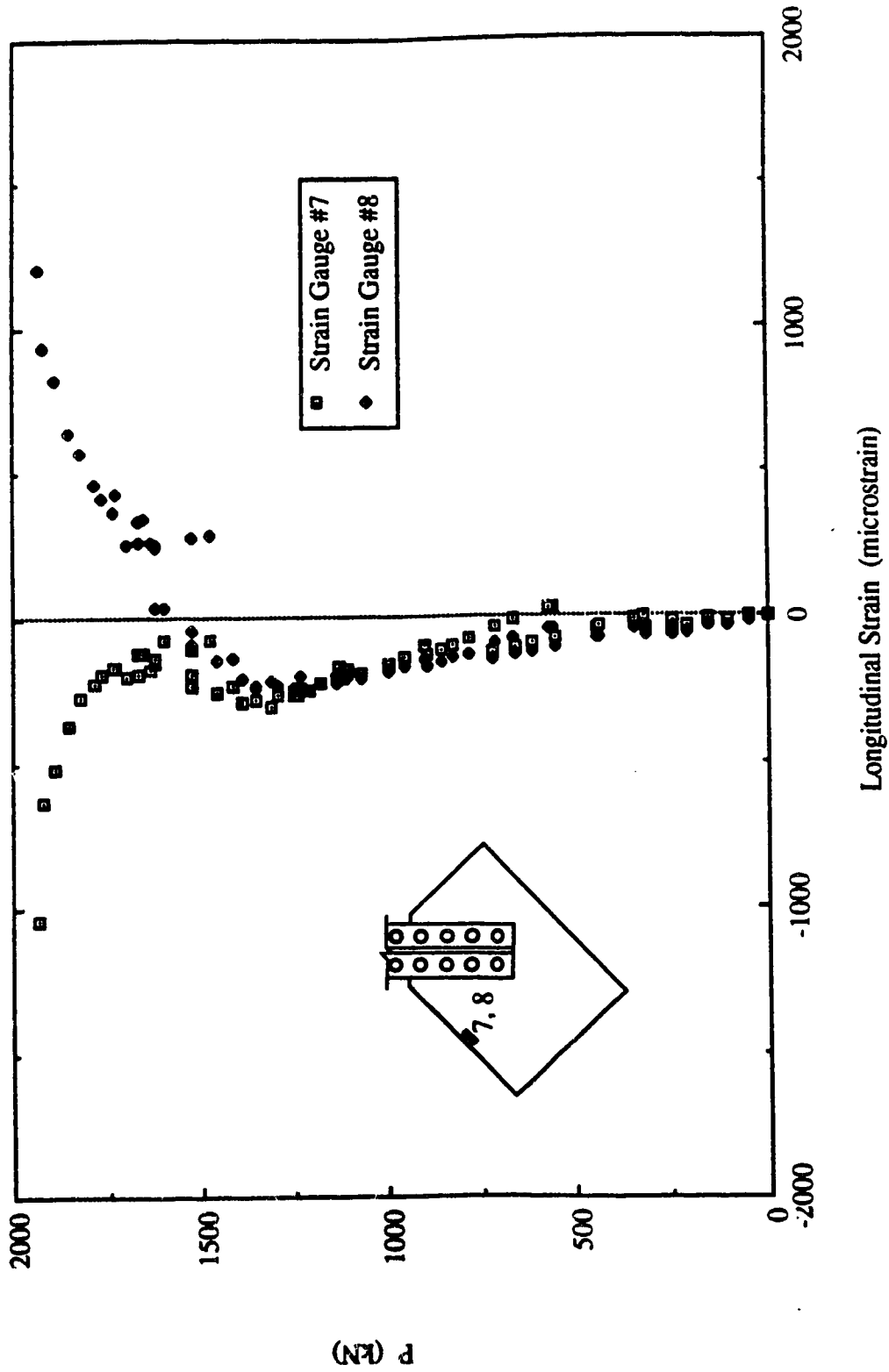


Fig. 6.16 Load vs. Strain Gauge Readings at Mid-Length of Long Free Edge for Specimen MP1

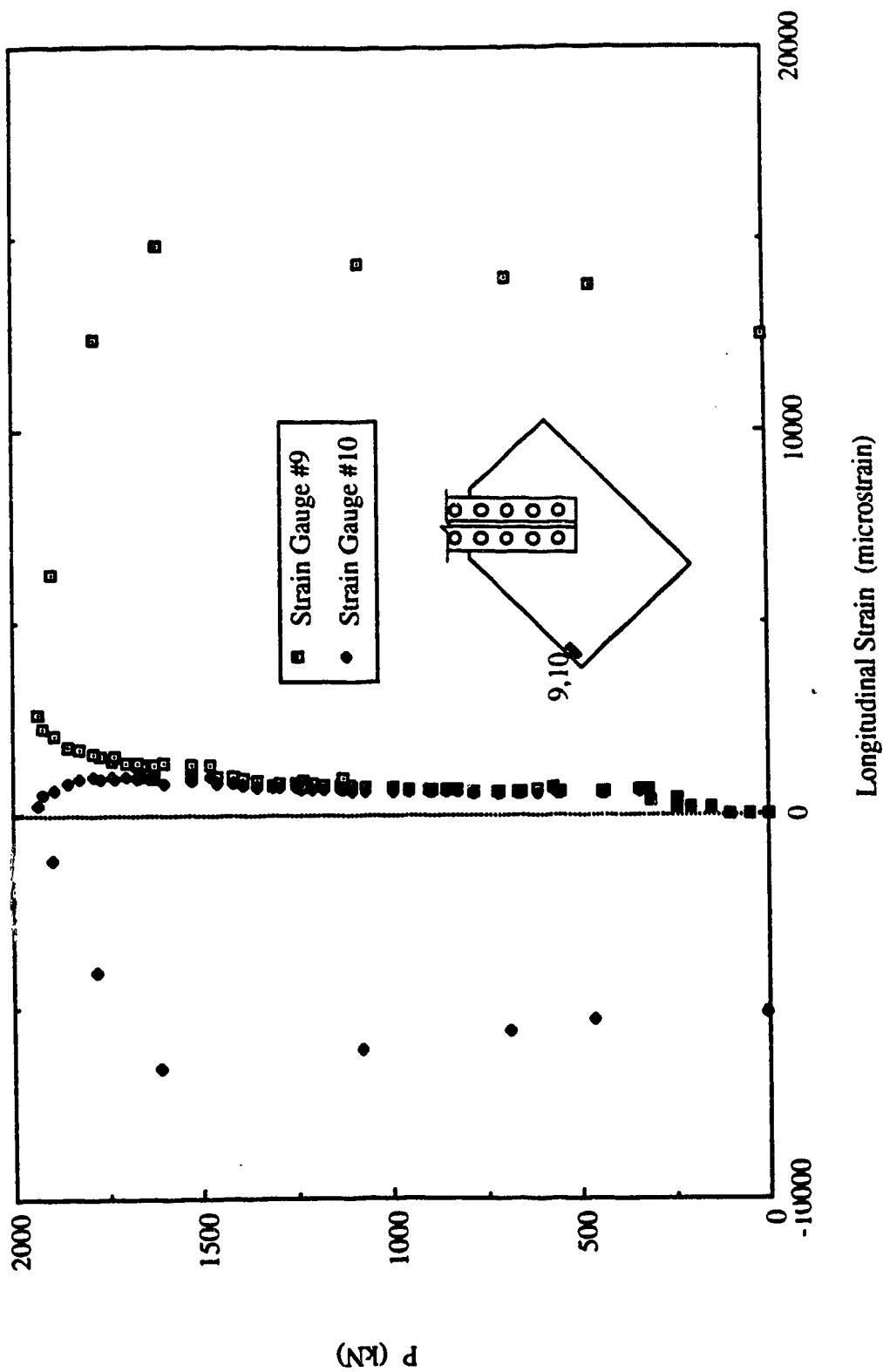


Fig. 6.17 Load vs. Strain Gauge Readings at End of Long Free Edge for Specimen MPI

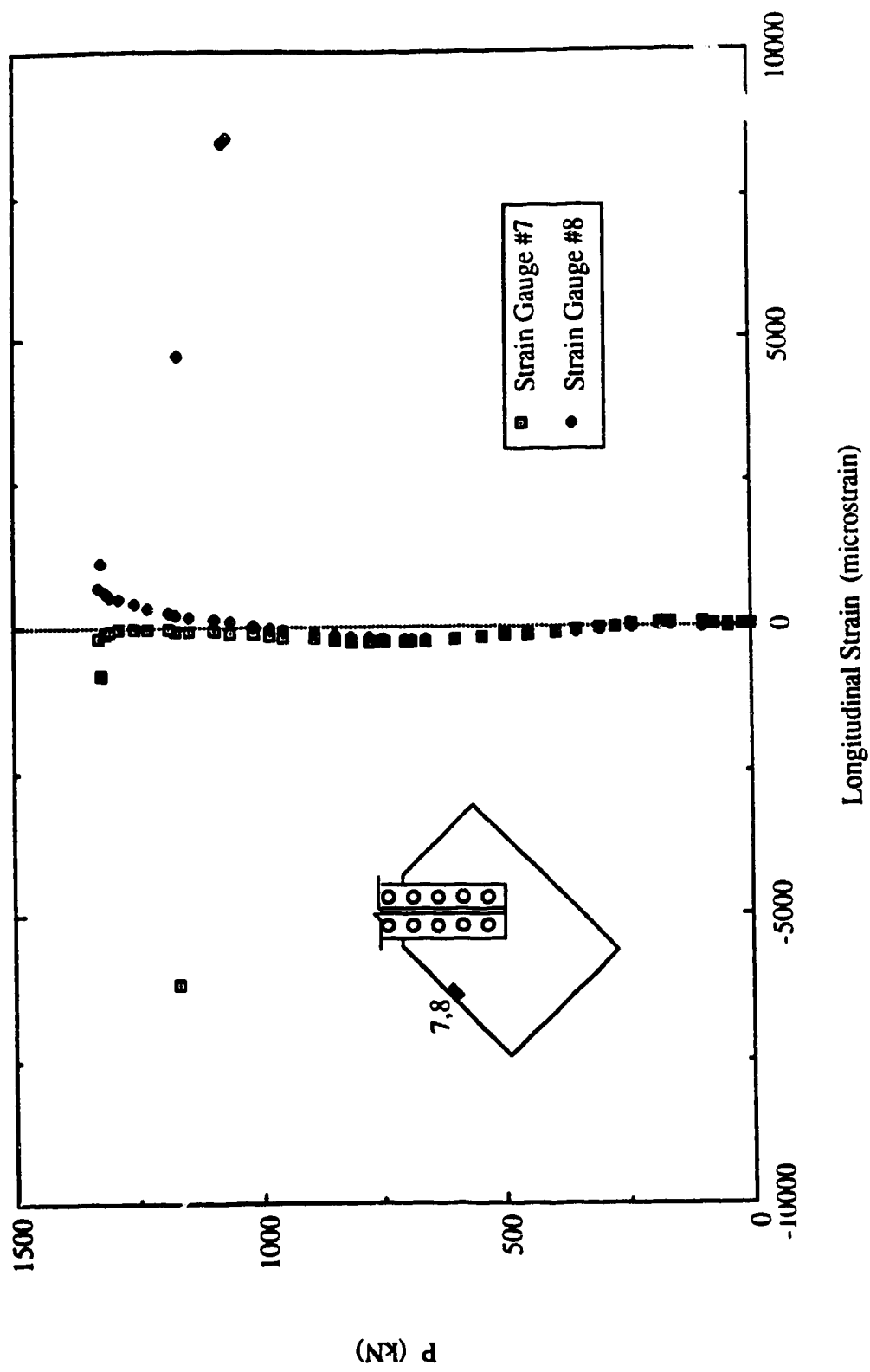


Fig. 6.18 Load vs. Strain Gauge Readings at Mid-Length of Long Free Edge for Specimen MP2



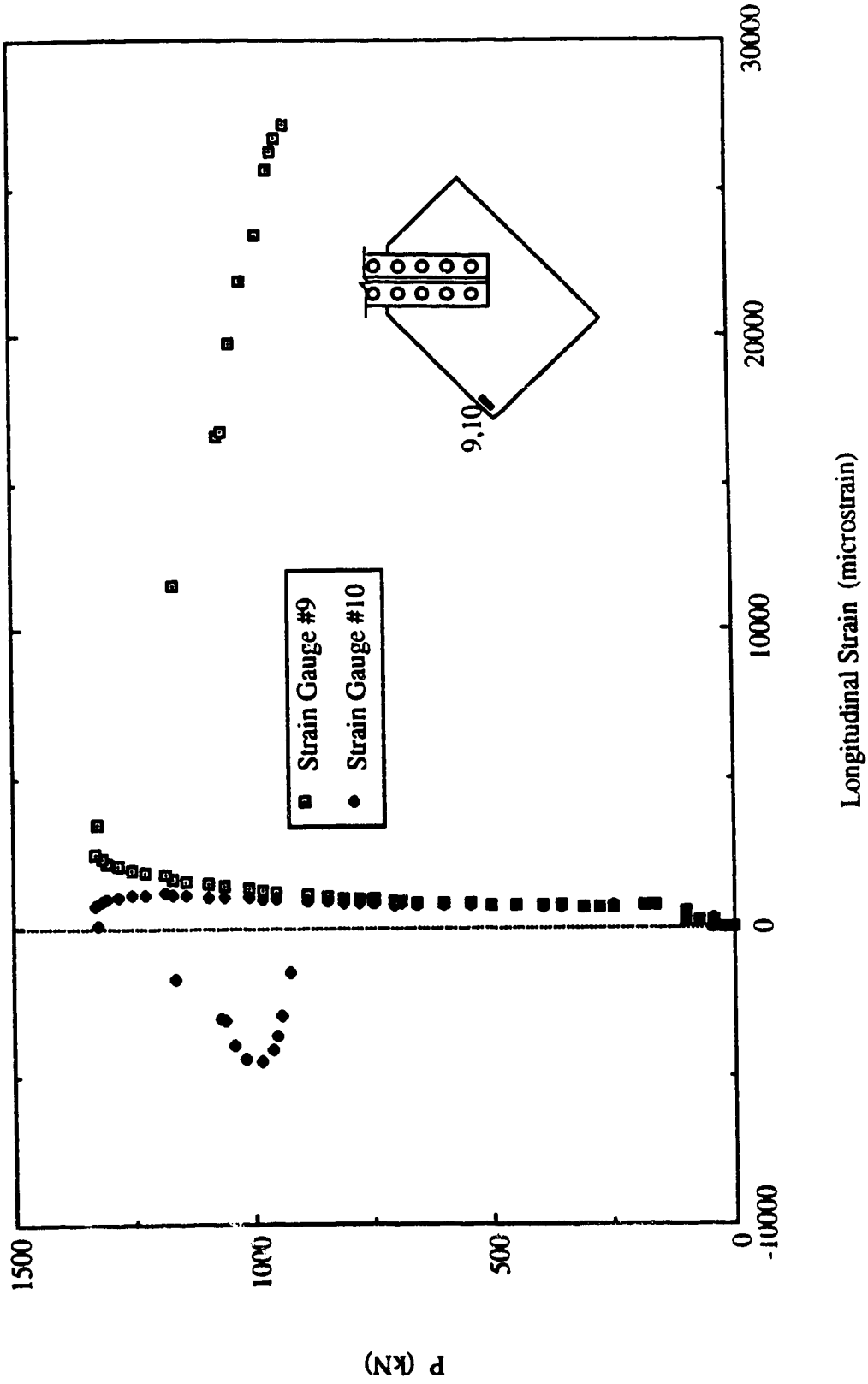


Fig. 6.19 Load vs. Strain Gauge Readings at End of Long Free Edge for Specimen MP2

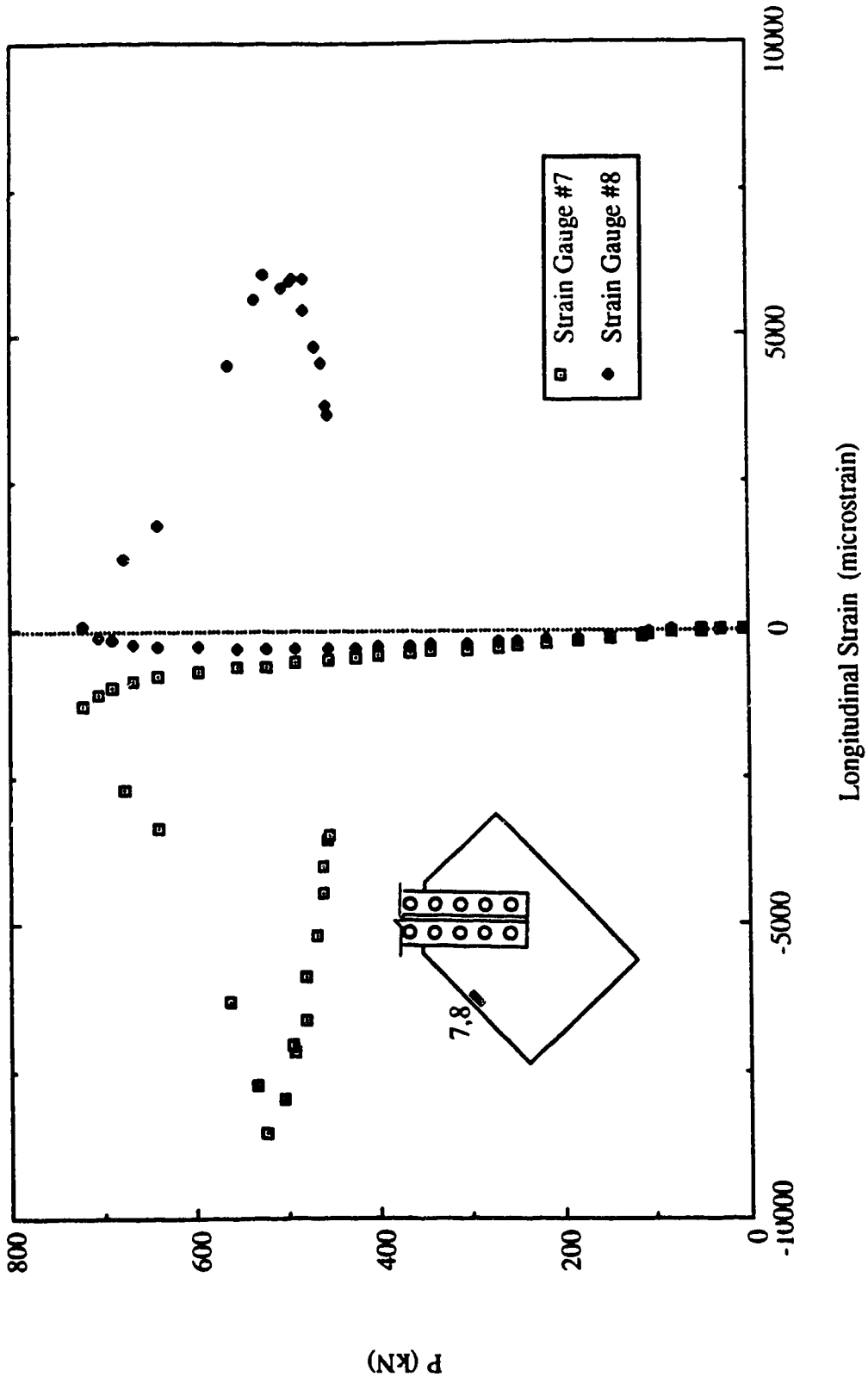


Fig. 6.20 Load vs. Strain Gauge Readings at Mid-Length of Long Free Edge for Specimen MP3

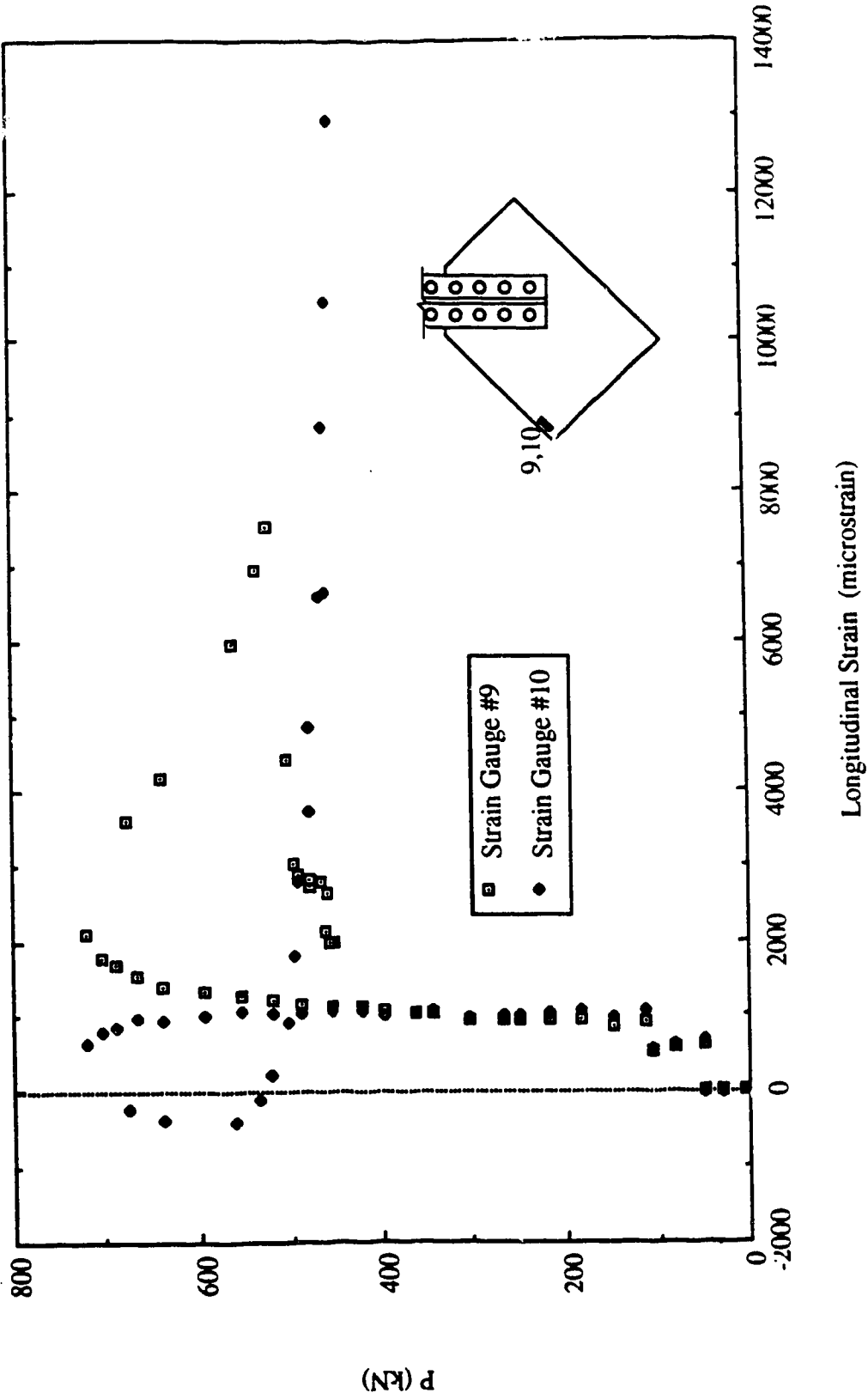


Fig. 6.21 Load vs. Strain Gauge Readings at End of Long Free Edge for Specimen MP3

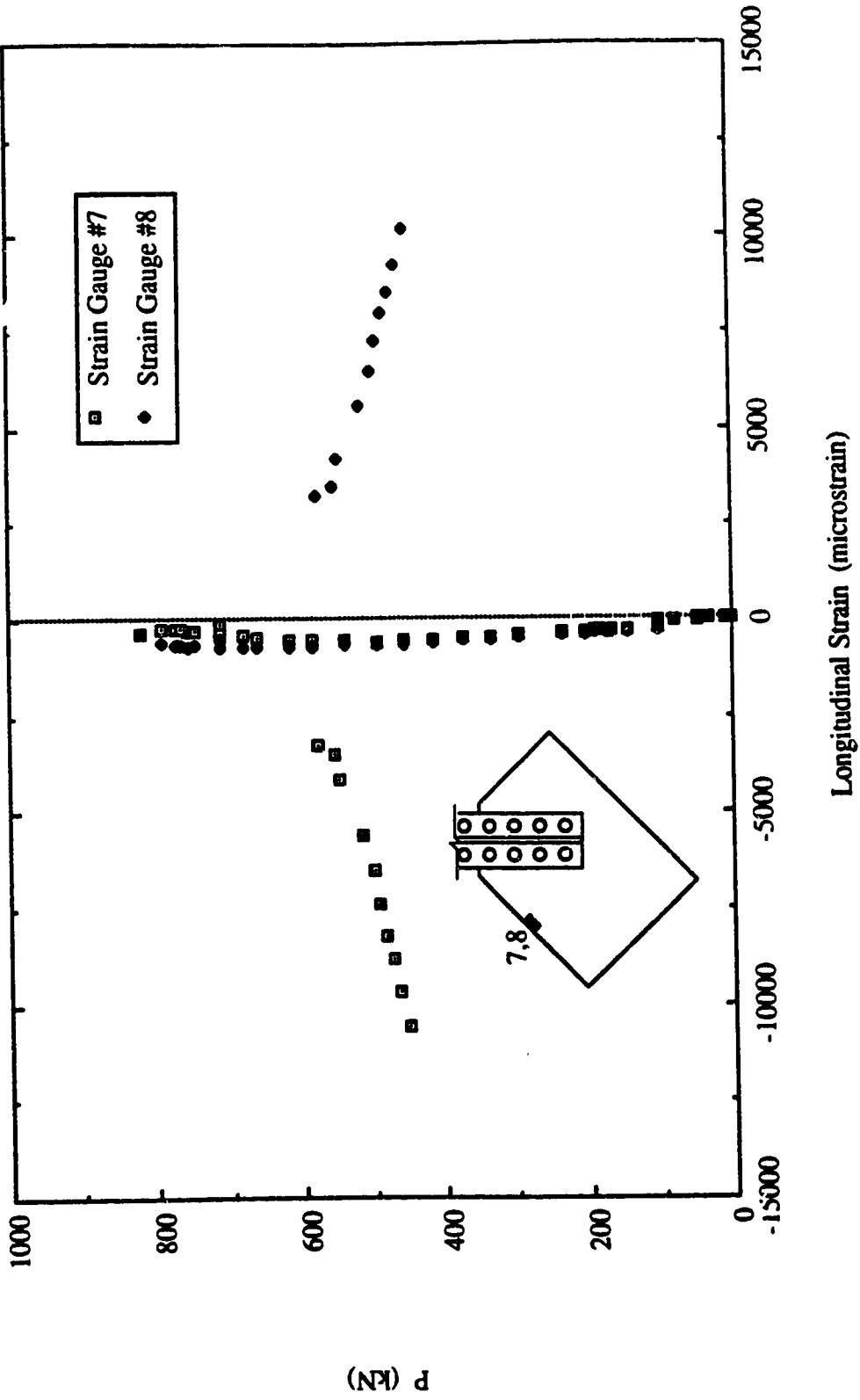


Fig. 6.22 Load vs. Strain Gauge Readings at Mid-Length of Long Free Edge for Specimen MP3A

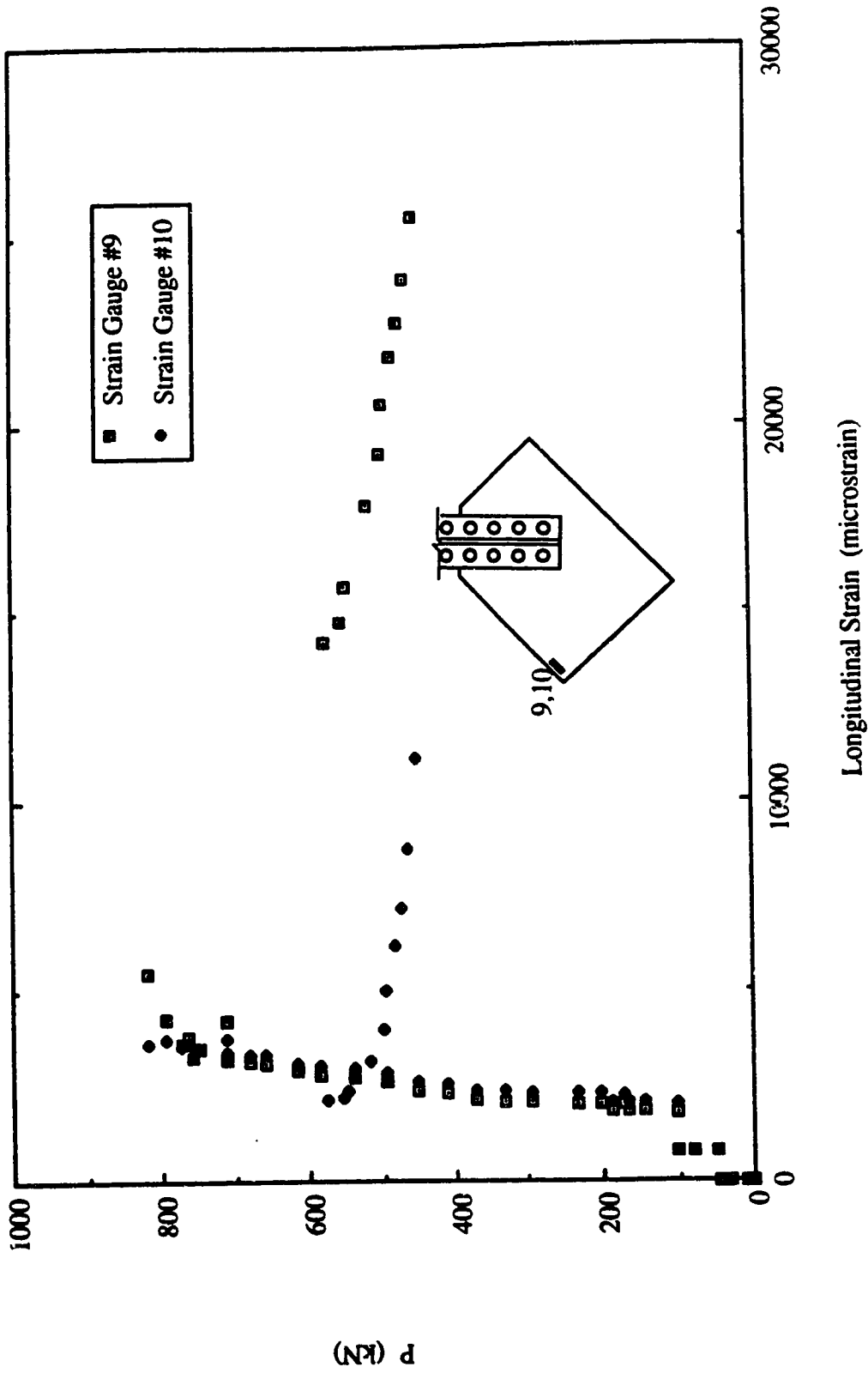


Fig. 6.23 Load vs. Strain Gauge Readings at End of Long Free Edge for Specimen MP3A

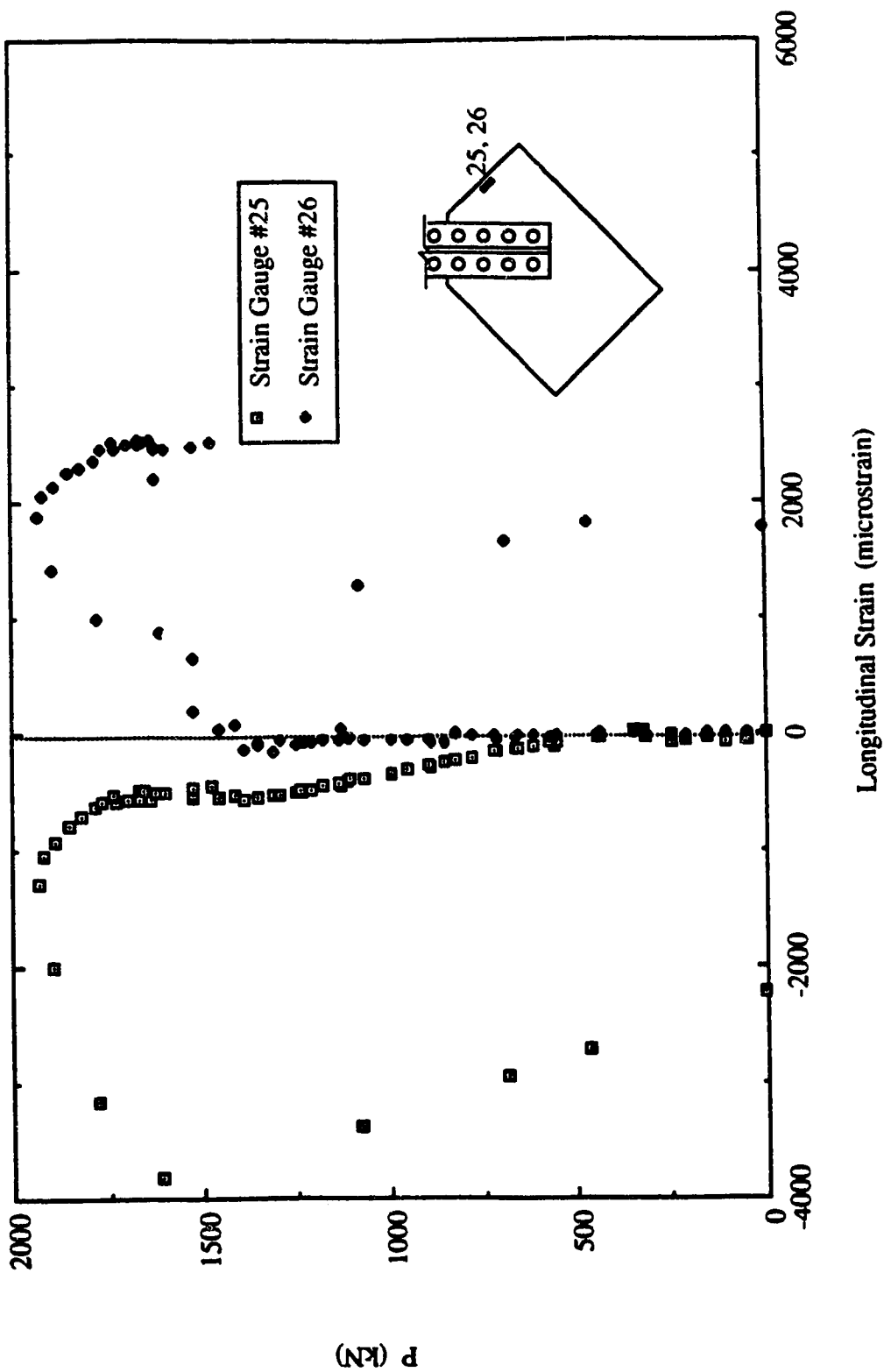


Fig. 6.24 Load vs. Strain Gauge Readings at Mid-Length of Short Free Edge for Specimen MP1

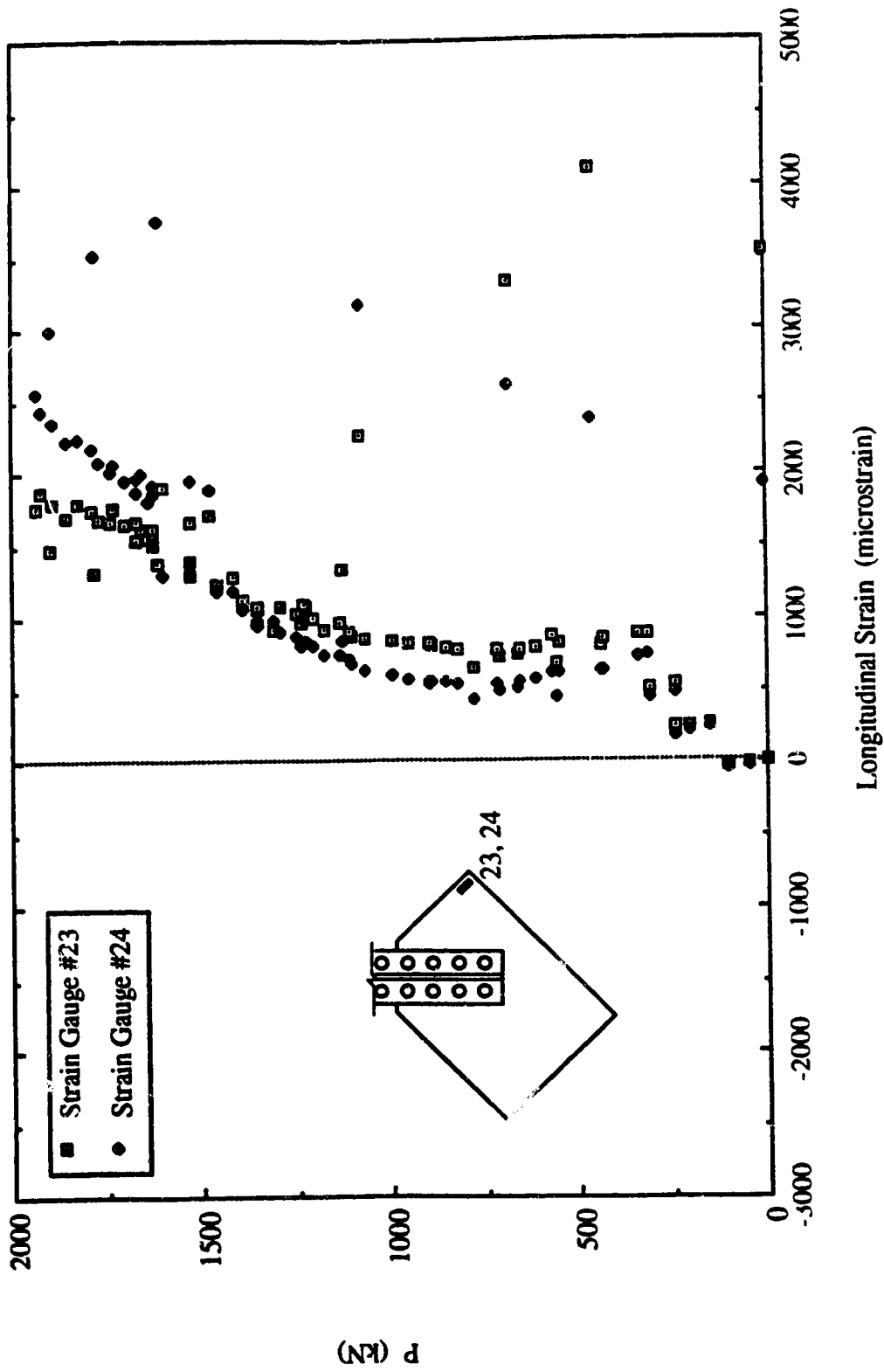


Fig. 6.25 Load vs. Strain Gauge Readings at End of Short Free Edge for Specimen MPI

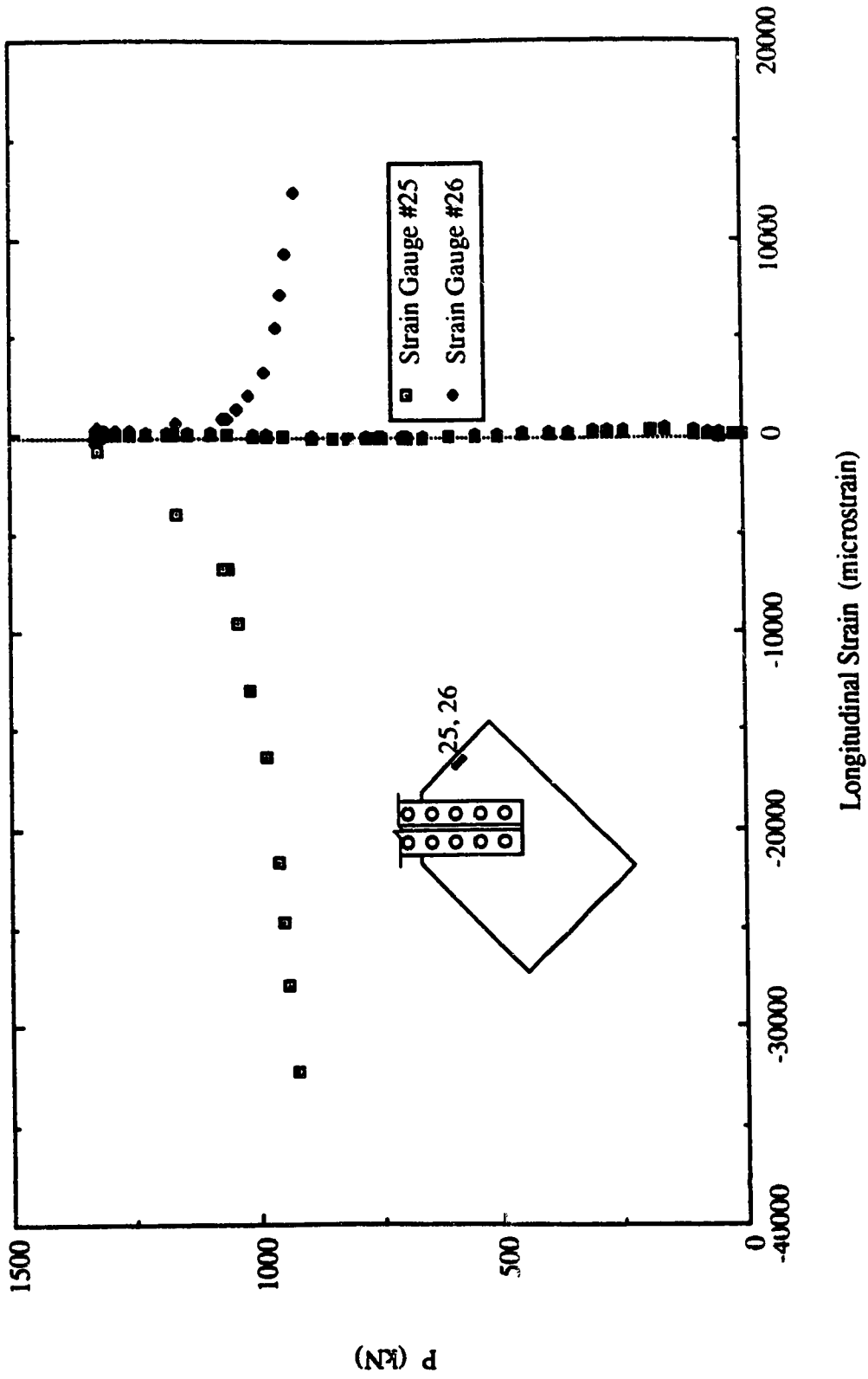


Fig. 6.26 Load vs. Strain Gauge Readings at Mid-Length of Short Free Edge for Specimen MP2



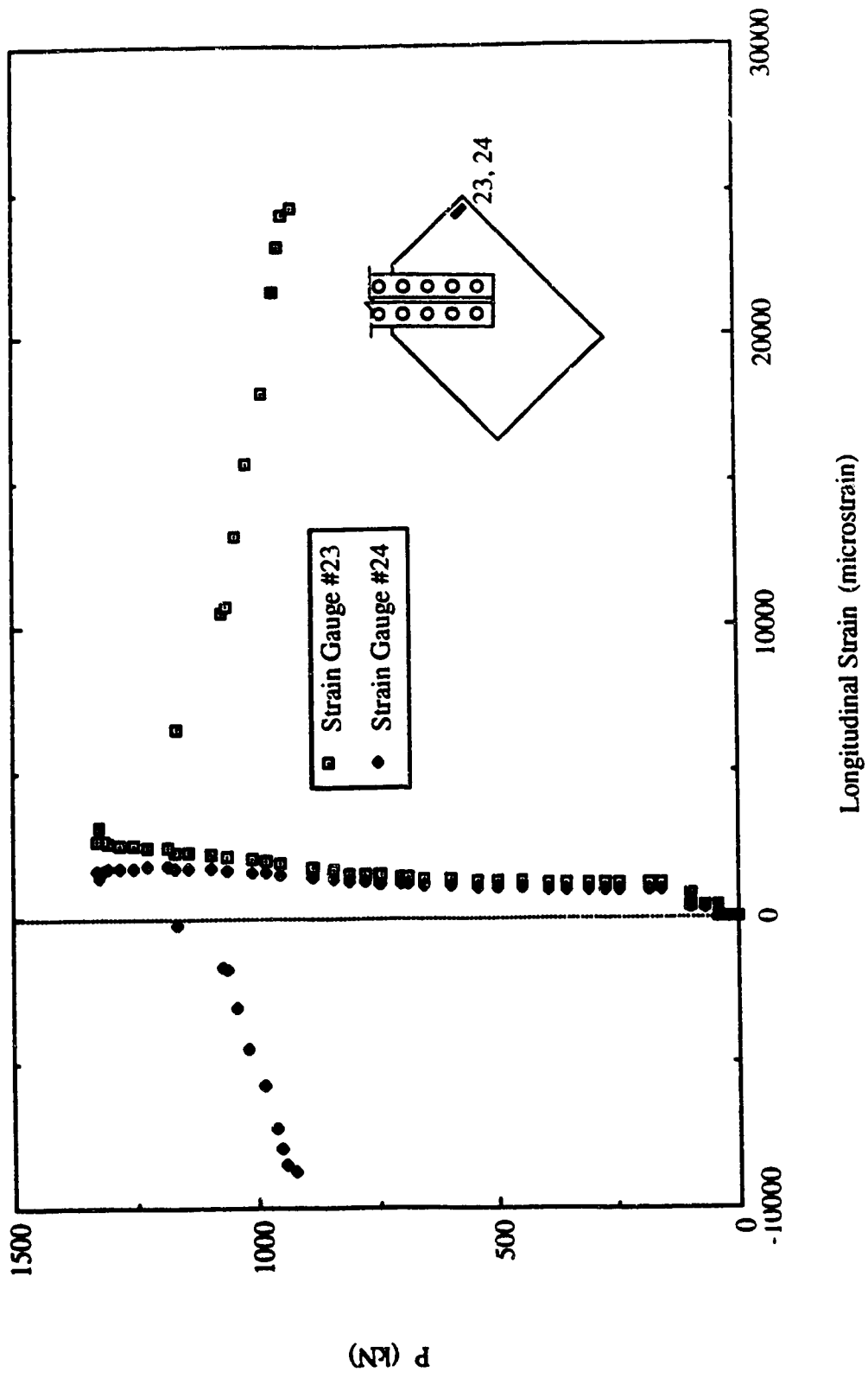


Fig. 6.27 Load vs. Strain Gauge Readings at End of Short Free Edge for Specimen MP2

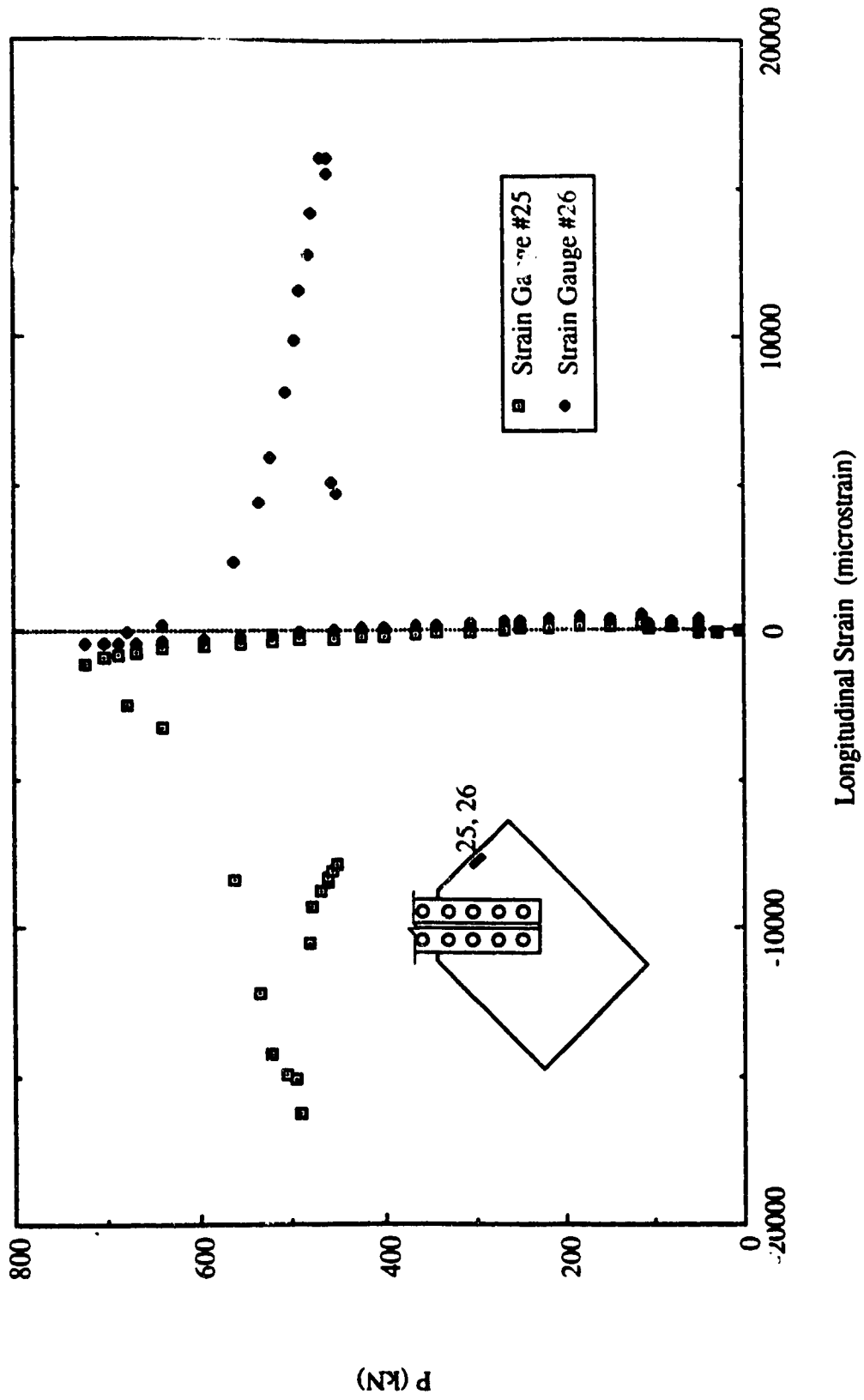


Fig. 6.28 Load vs. Strain Gauge Readings at Mid-Length of Short Free Edge for Specimen MP3

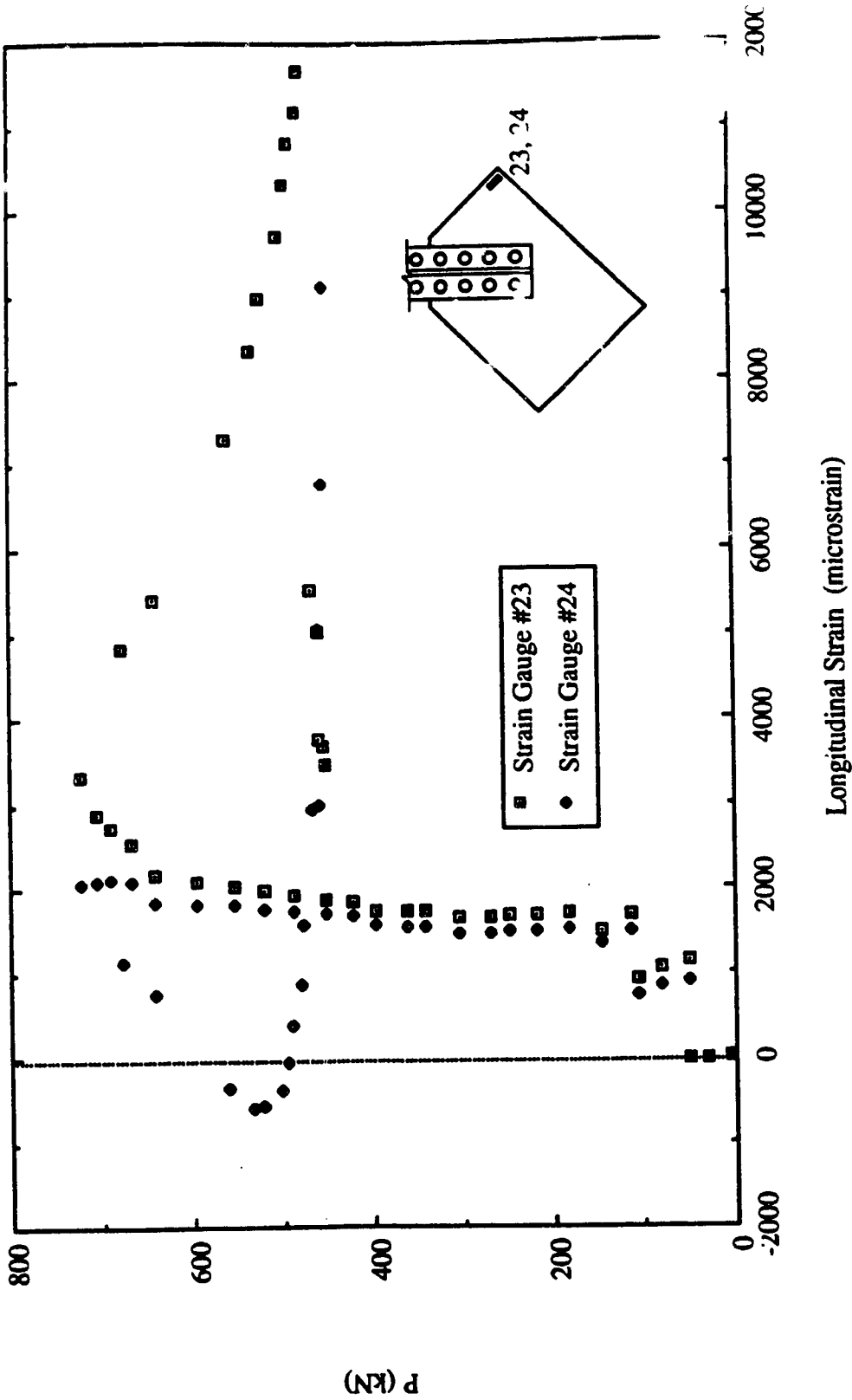


Fig. 6.29 Load vs. Strain Gauge Readings at End of Short Free Edge for Specimen MP3

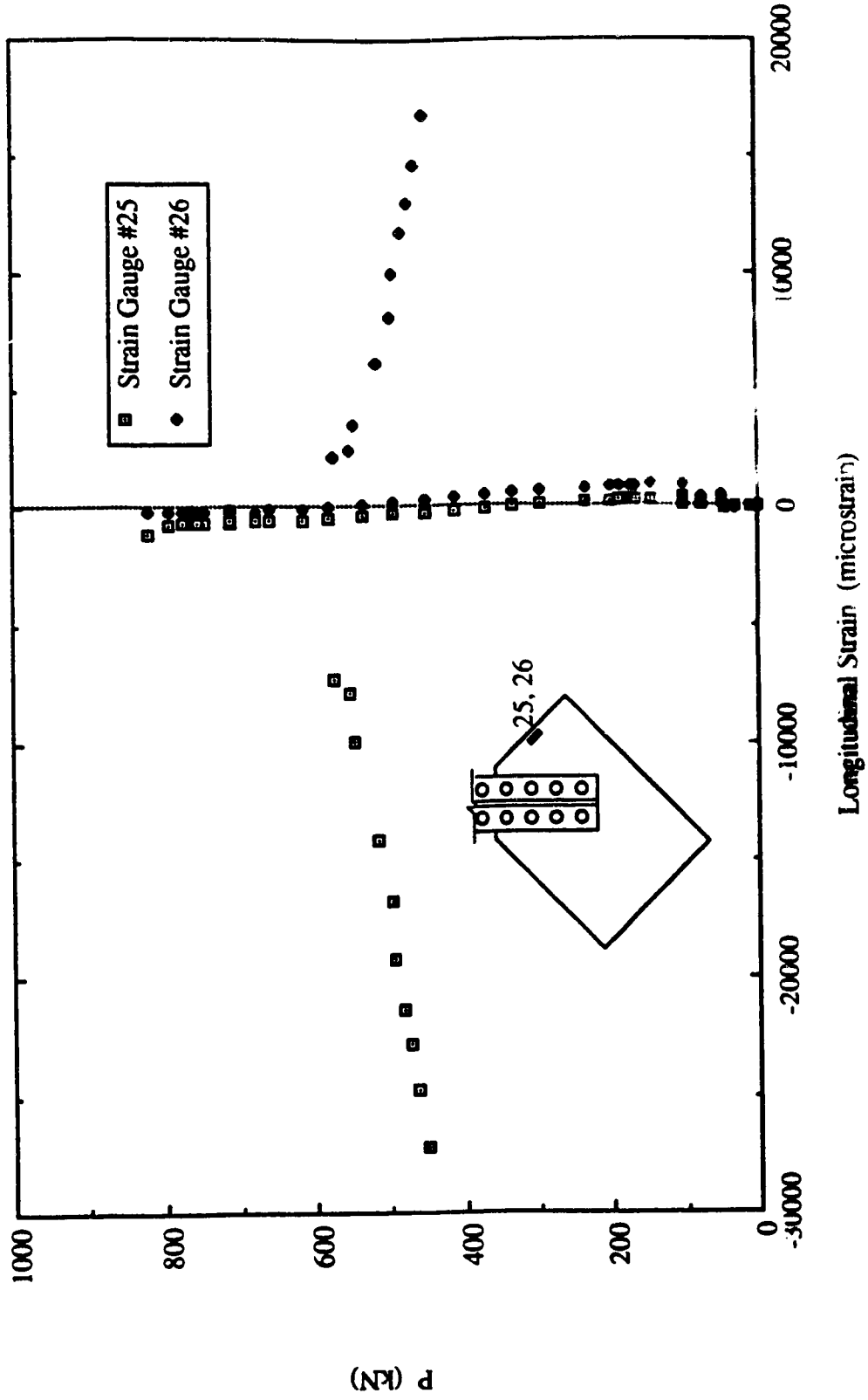


Fig. 6.30 Load vs. Strain Gauge Readings at Mid-Length of Short Free Edge for Specimen MP3A

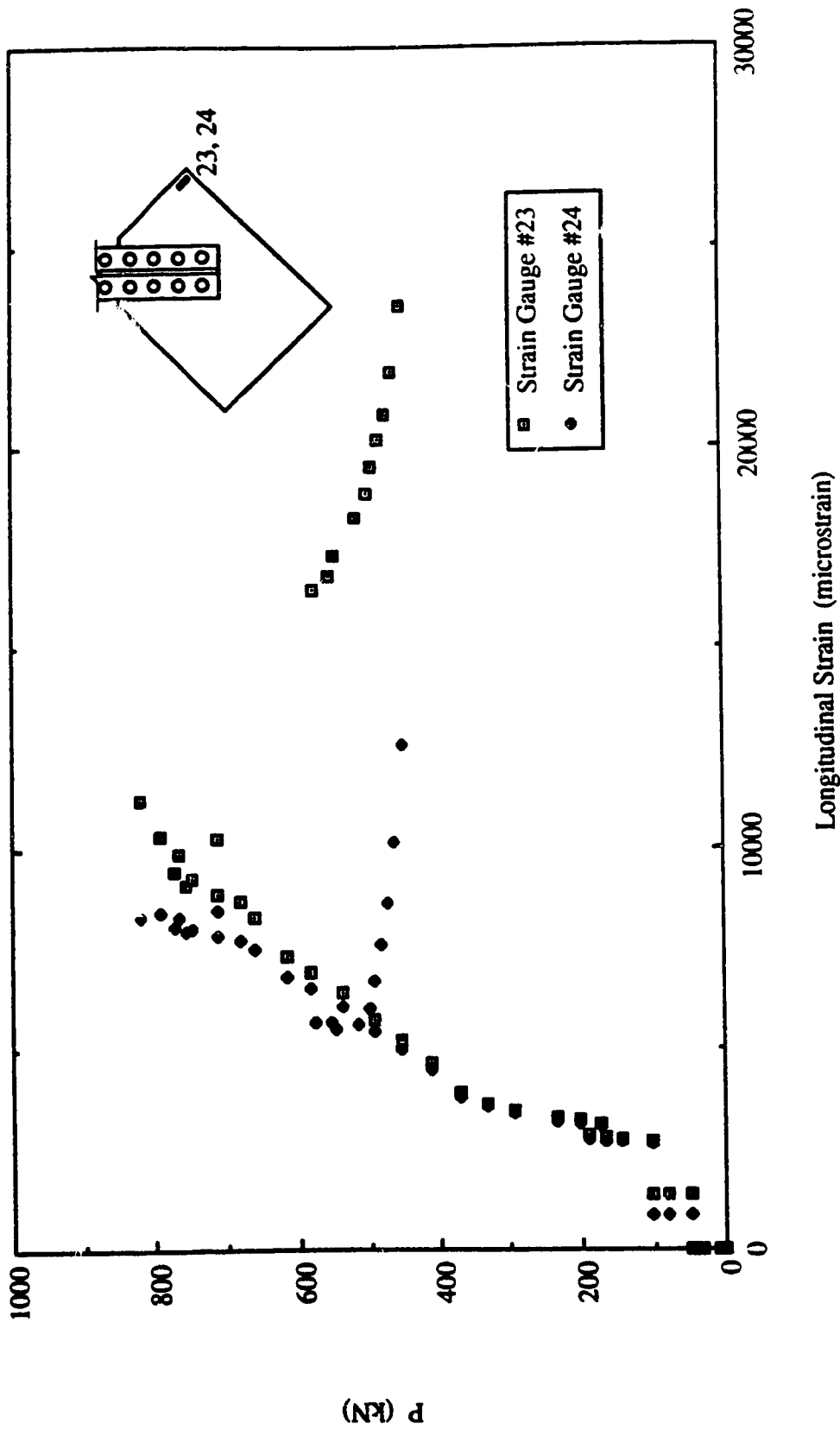


Fig. 6.31 Load vs. Strain Gauge Readings at End of Short Free Edge for Specimen MP3A

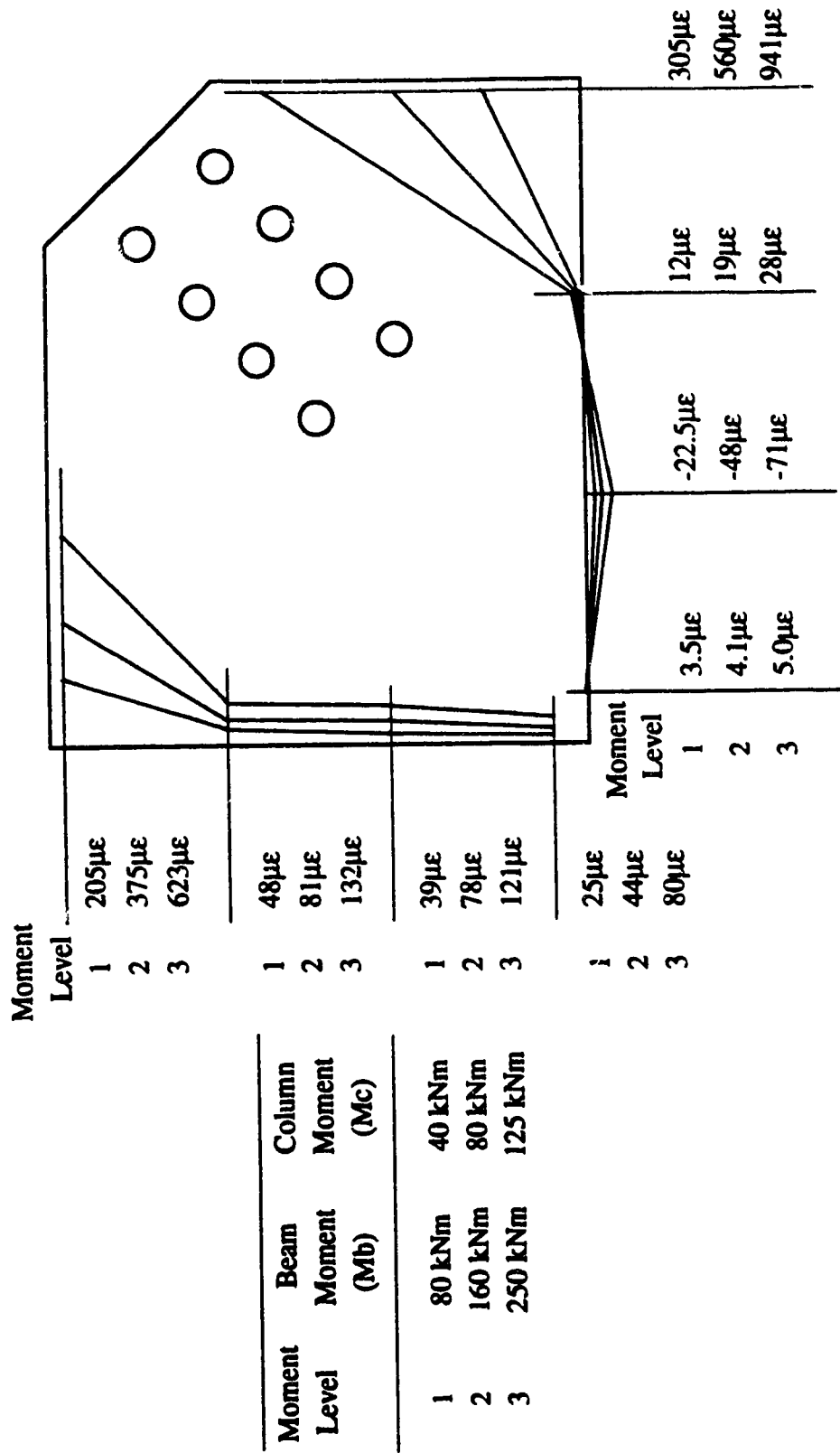


Fig. 6.32 Measured Strain Distribution Along Beam and Column Boundary at Gusset Plate for Specimen MP1



**Fig. 6.33** Picture of Failed Specimen MP1

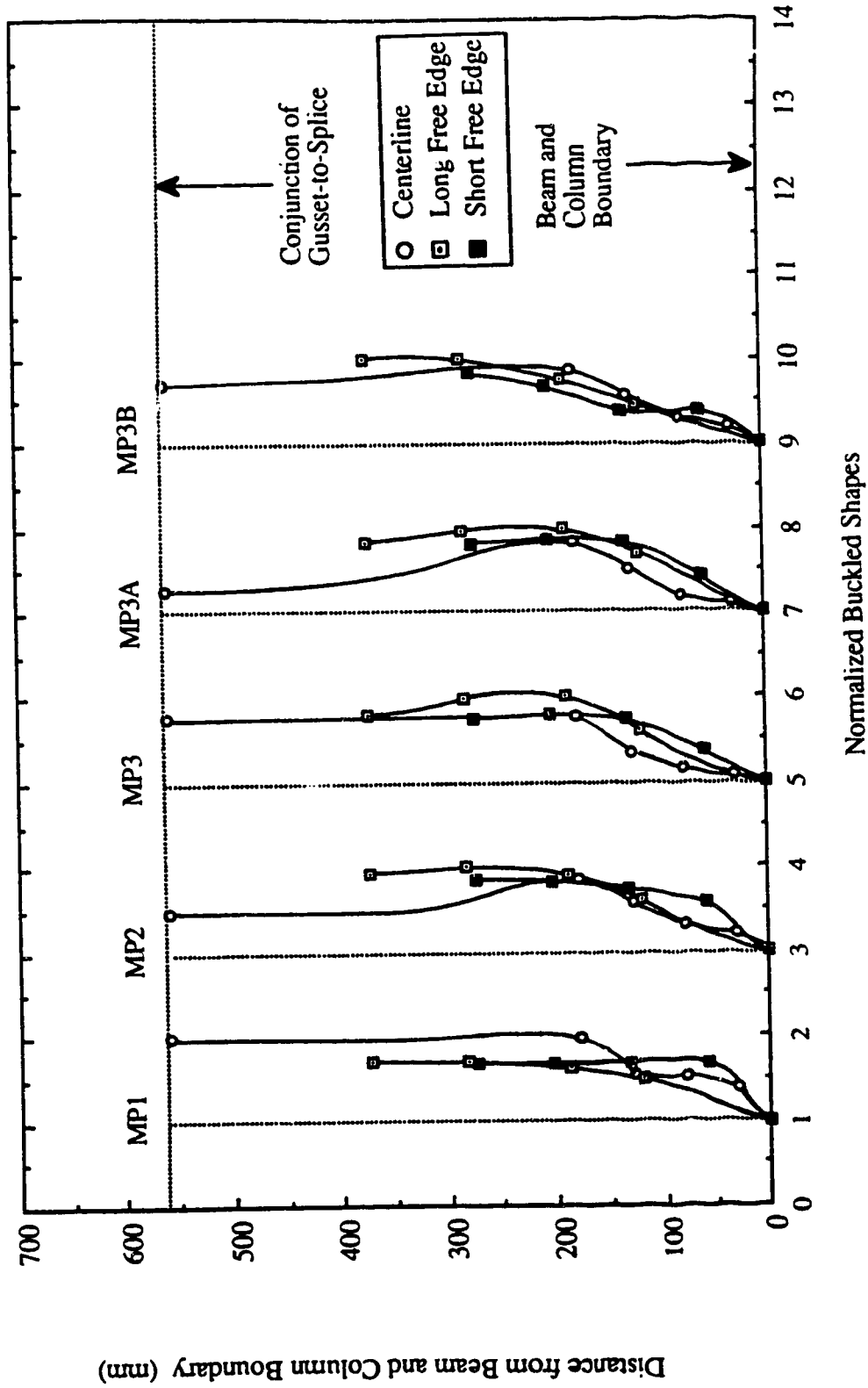
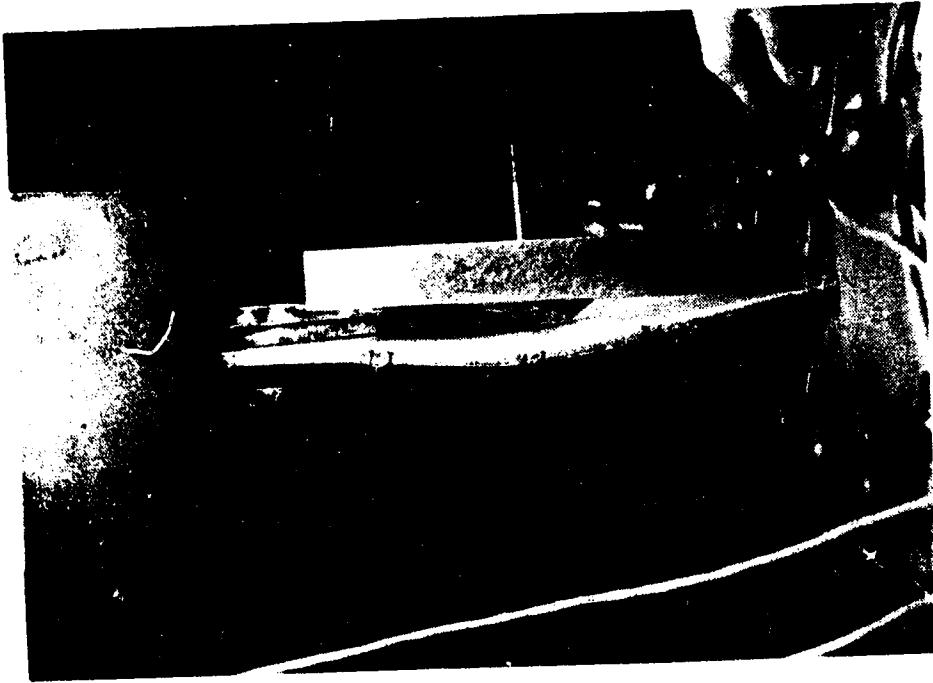


Fig. 6.34 Out-of-Plane Deflected Shapes at Free Edge and Along Centerline of Splice for MP Type Specimens





a) Long Free Edge



b) Short Free Edge

Fig. 6.35 Pictures of Out-of-Plane Deflected Shapes at Free Edges for Specimen MP3A

## **7. TEST RESULTS OF EP TYPE SPECIMENS**

### **7.1 General**

The EP type specimens were employed to study the compressive behavior of the eccentrically loaded gusset plate connections. As mentioned in Chapter 2, only one gusset plate thickness of 13.3 mm was used to conduct the tests. Three splice member sections were used to test the specimen, as shown in Table 2.2. As a reminder, scheme I test setup was used to perform the tests. In general, specimens failed by significant yielding in the splice section at the conjunction of gusset-to-splice. However, yielding in the gusset plate was also observed, depending on the specimens. In particular, extensive yielding was observed underneath the splice member close to the corner of the beam and column boundary for specimen EP3, as shown in Fig. 7.1. These yield lines originated from the end of the splice member close to the beam boundary and extended towards the ends of the free edges. For specimens EP1 and EP2, yield lines were also recorded near the beam boundary close to the short side free edge. The test results of the specimens are summarized in Table 7.1.

### **7.2 Behavior of Load versus In-Plane Deformation**

The in-plane behavior of the specimens can be illustrated by examining the curves of load versus the vertical stroke of the loading head, as shown in Figs. 7.2 to 7.4. In general, the specimens exhibited a linear load deflection behavior until about 60 percent of the corresponding ultimate loads. A similar in-plane stiffness was observed for both specimens EP1 and EP2. However, for specimen EP3, a higher in-plane stiffness was observed. Subsequently, the curves showed nonlinear behavior and gradually turned to the ultimate loads. It can be seen from the figures that specimen EP1 showed more rapid unloading than specimens EP2 and EP3, as shown in the figures.

### **7.3 Behavior of Load Versus Out-Of-Plane Displacement of Test Frame**

The curves of load versus out-of-plane displacement of the test frame for the specimens are shown in Figs. 7.5 to 7.7. The curve for specimen EP1 shows a typical load deflection curve for a beam column member. That is, linear behavior was observed in the initial loading stage and, subsequently, the curve gradually turned to the ultimate load, followed by rapid unloading. For specimens EP2 and EP3, however, the curves show a more gradual unloading path. It was also observed that specimens EP1 and EP2 reached the corresponding ultimate load at a deflection of about 20 mm. However, for specimen EP3, the ultimate load was attained at a deflection of about 10 mm, which illustrated the effects of stiffening the eccentrically loaded gusset plate. It was also observed that the out-of-plane stiffness of the specimen was greatly improved by providing a stiffer splice member.

### **7.4 Strain Gauges Results**

Since the primary failure mode of the specimens was yielding in the splice member at the conjunction of gusset-to-splice, it is important to examine the strain distribution at that conjunction and also in the gusset plate. The strain distribution and yielding pattern of each specimen will be presented individually. For specimen EP1, which employed a 9.5 mm thick splice plate, the curves of load versus the strain gauge readings recorded at the conjunction of gusset-to-splice and at the splice plate 50 mm above the end of bracing are shown in Figs. 7.8 and 7.9 respectively. As can be seen from the figures, bending was observed from the beginning of loading due to the loading eccentricity. Yielding was first observed at gauges #19 and 20 at an applied load of about 205 kN. However, no yield line was observed from the splice member. Unfortunately, strain gauge #19 malfunctioned after reaching the yield strain level, as shown in Fig. 7.9. At a load level of about 275 kN, yielding was observed at strain gauge #24, as shown in Fig. 7.9, and a slight flaking of the

whitewash at the south side of the conjunction was found. This yielding was mainly located in the splice member around the first row of bolts from the bracing member, as shown schematically in Fig. 7.10. As loading continued, the yielding progressed and yield lines were also observed at the north side of the splice plate around the first row of bolts from the gusset plate specimen. Yielding on the gusset plate specimen was only recorded at the strain gauges near the end of the splice member when the applied load was close to the ultimate load. However, yielding was observed near the beam and column boundary in the north side of the specimen, as shown in Fig. 7.11. These yield lines originated from the end of the splice plate and were caused by a significant bending of the gusset plate specimen. The failed splice plate for specimen EP1 is shown in Fig. 7.12a. It can be seen that a significant bending of the splice plate was observed at the conjunction with the formation of yield lines near the last row of bolts from the bracing member.

For specimen EP2, which used a 13 mm thick splice plate, yielding at the strain gauges was again recorded at the conjunction of gusset-to-splice at an applied load of 220 kN. The plots of strain gauges #19 and 20, which were located at the conjunction, are shown in Fig. 7.13. Figure 7.14 illustrates the curve for the strain gauge #24. Again, a bending behavior was observed from the beginning of loading. At a load level of 265 kN, the flaking of the whitewash was observed at the south side of the conjunction. As loading continued, the yielding at this region increased. When the applied load reached about the ultimate load yield lines were found on the gusset plate right underneath the splice plate. As out-of-plane displacement increased in the unloading stage, yielding near the beam and column boundary was observed. The failed splice plate for specimen EP2 is shown in Fig. 7.12b. It can be seen from the figure that significant yielding was observed in the splice member near the first row of bolts from the end of the brace.

For specimen EP3, yield lines were first observed at the gusset plate in the vicinity of the corner of beam and column boundary at an applied load of about 550 kN. At this loading

stage, strain gauges on the splice plate located at the conjunction of gusset-to-splice also showed yielding, but no yield lines were detected. A plot of load versus strain readings recorded at the web of the tee-section and on the south side of the splice plate at the conjunction is shown in Fig. 7.15. As expected, the strain reading from the web of the tee showed tension yielding, while compression yielding was observed for the strain gauge at the splice plate. The strain distribution recorded at an applied load of 400 kN across the depth of tee-section and the splice plate at the conjunction is shown in Fig. 7.16. This plot shows that the linear strain distribution existed across the depth of the tee-section. However, the location of the neutral axis was shifted away from the flange of the tee-section due to the compressive strain induced by the applied load. As loading continued, yielding in the vicinity of the corner of the beam and column boundary progressed. When the applied load approached the ultimate load, yielding was detected at the splice plate and at the tip of the web of the tee-section splice member at the conjunction.

### **7.5 Out-of-Plane Deflected Shapes of Free Edges and Along Centerline of Bracing Member**

The normalized out-of-plane deflected shapes for the EP type specimens are shown in Fig. 7.17. It can be seen that a similar deformed configuration was observed for the specimens. In addition, rotation was observed near the fixed ends of the free edges of specimens especially for specimen EP3. The figure also shows that maximum displacement occurred at about mid-height of the splice member length. The deformed shapes for specimen EP3 along the centerline of the splice indicated that the use of the tee-section splice member improved the out-of-plane stiffness of the connection. A slight local bending of the gusset plate underneath the splice member was observed for specimen EP3.

Table 7.1 Test Results of EP Type Specimens

Specimen Designation	Gusset Plate Size (mm x mm x mm)	Splice Member	Ultimate Load (kN)
EP1	500 x 400 x 13.3	9.5 mm Splice Plate	310
EP2	500 x 400 x 13.3	13.0 mm Splice Plate	334
EP3	500 x 400 x 13.3	WT 125 x 22.5 + 9.5 mm Splice Plate	890



**Fig. 7.1 Picture of Failed Specimen EP3**

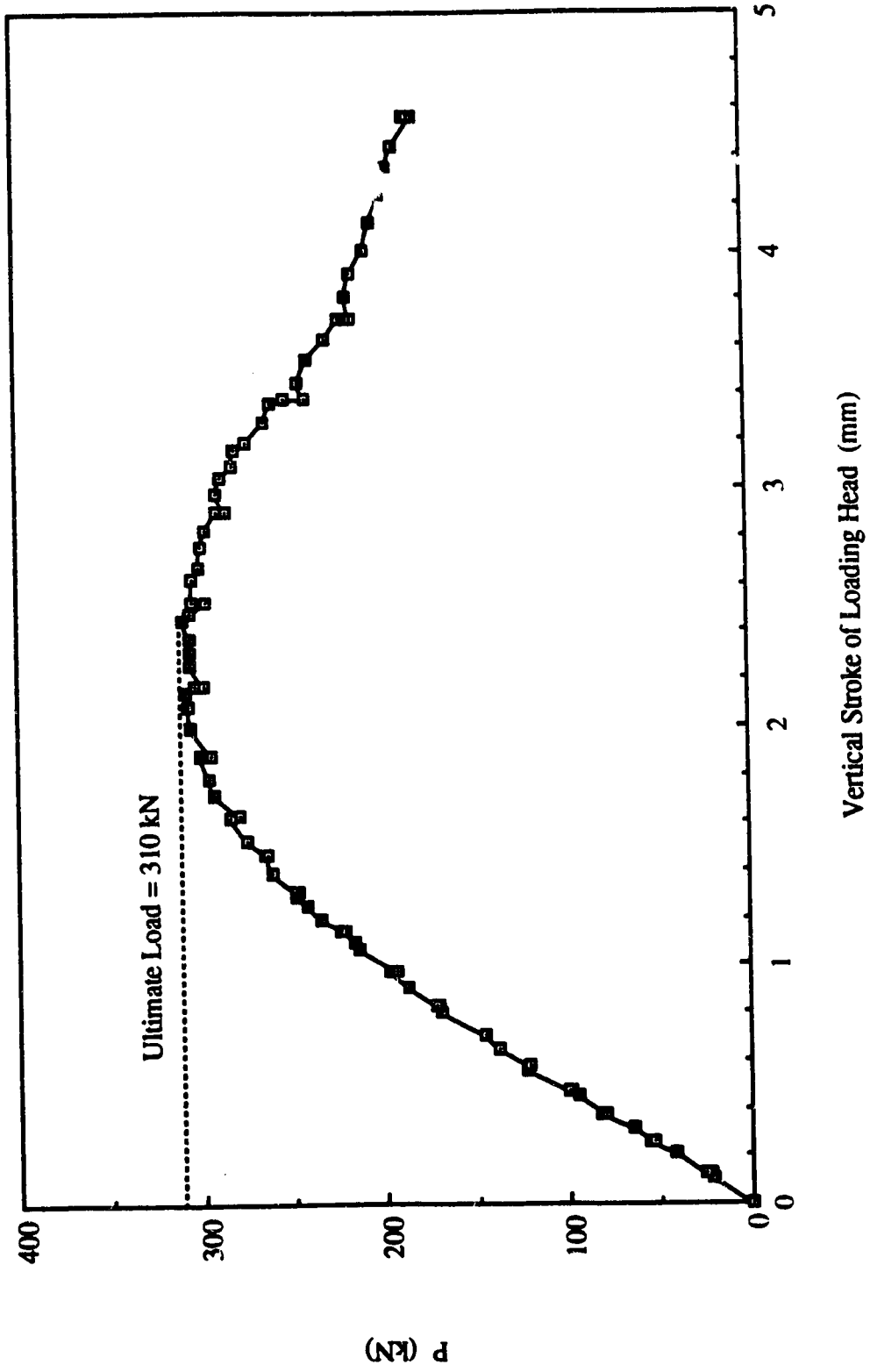


Fig. 7.2 Load vs. Vertical Stroke of Loading Head for Specimen EPI



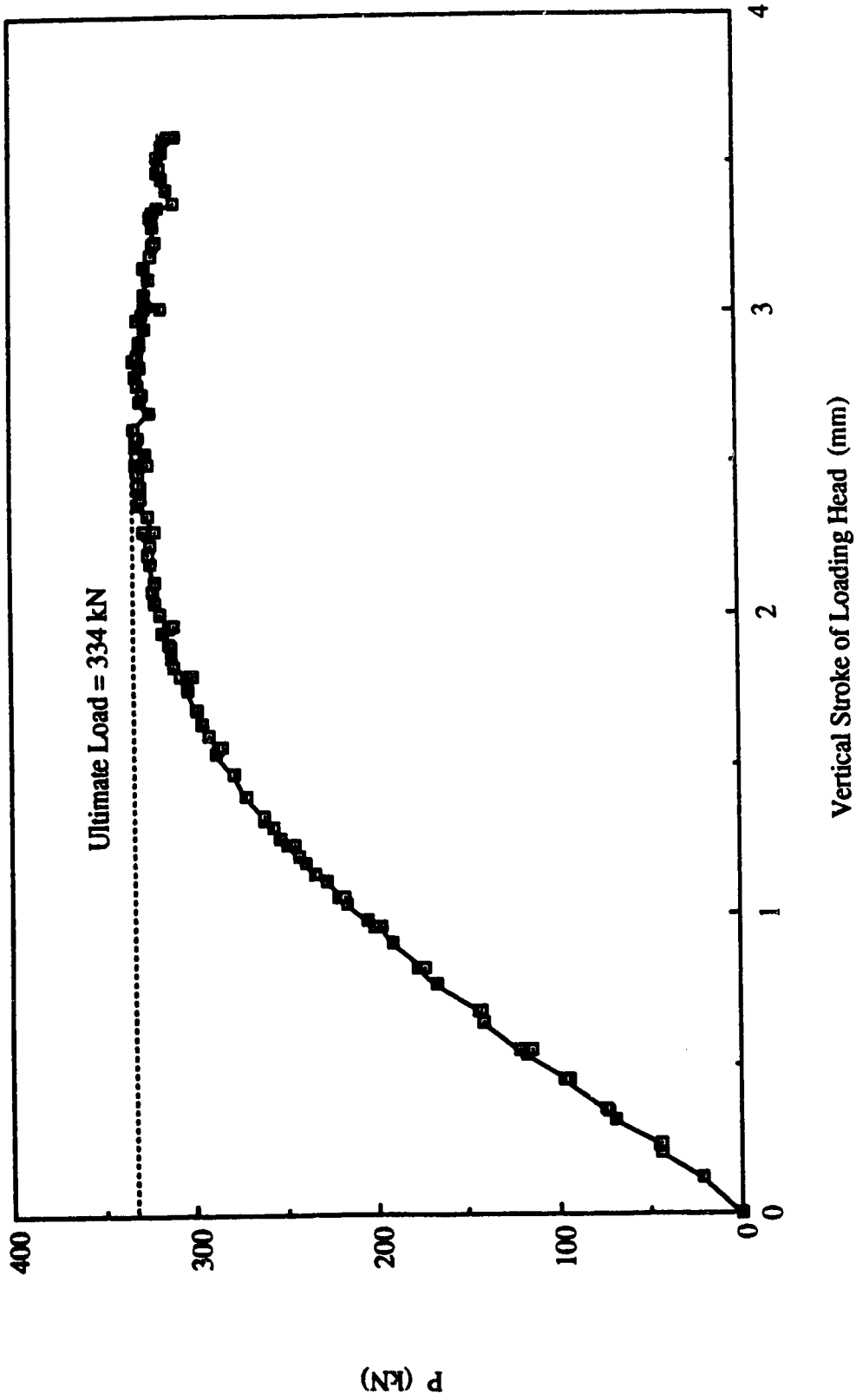


Fig. 7.3 Load vs. Vertical Stroke of Loading Head for Specimen EP2

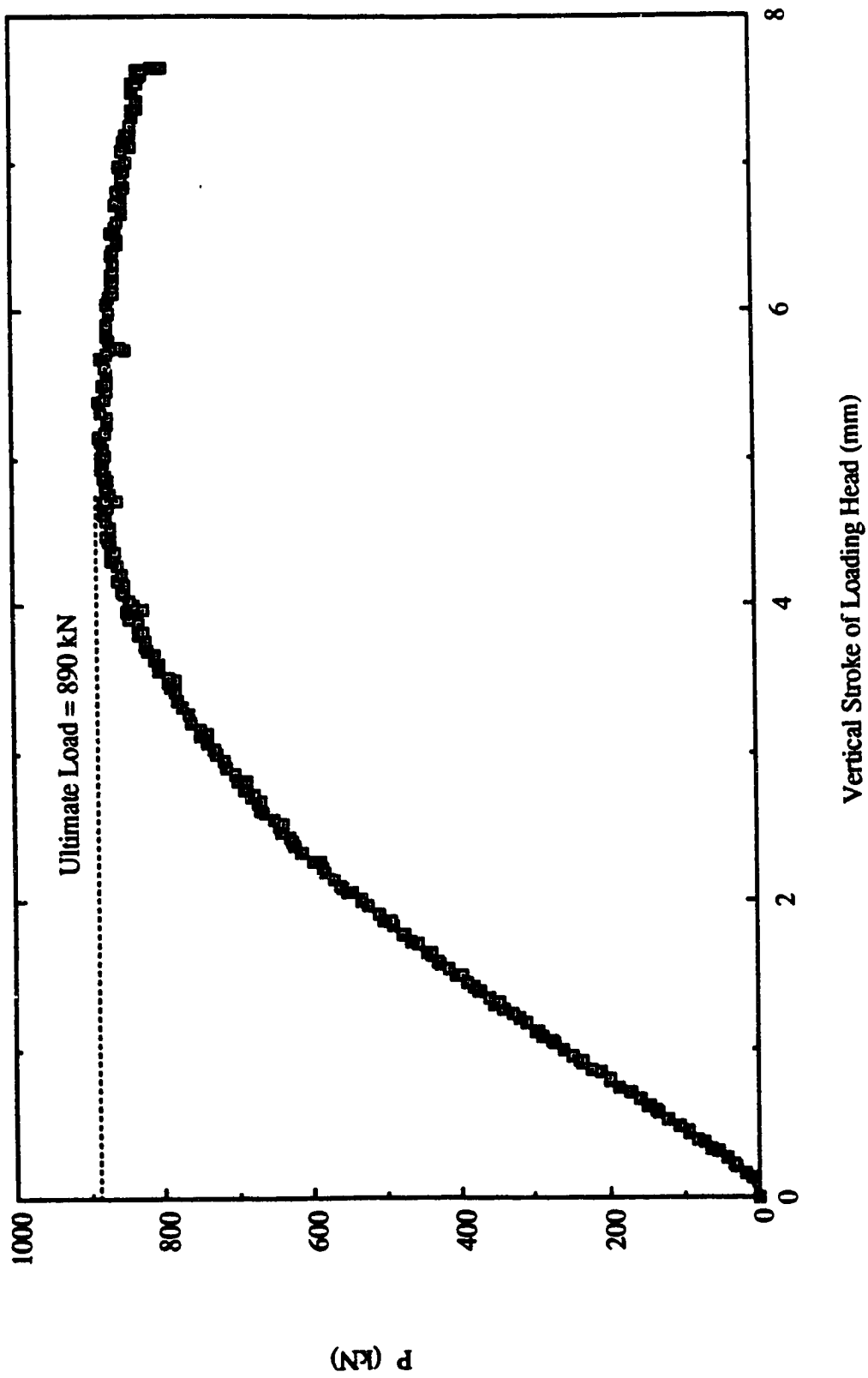


Fig. 7.4 Load vs. Vertical Stroke of Loading Head for Specimen EP3

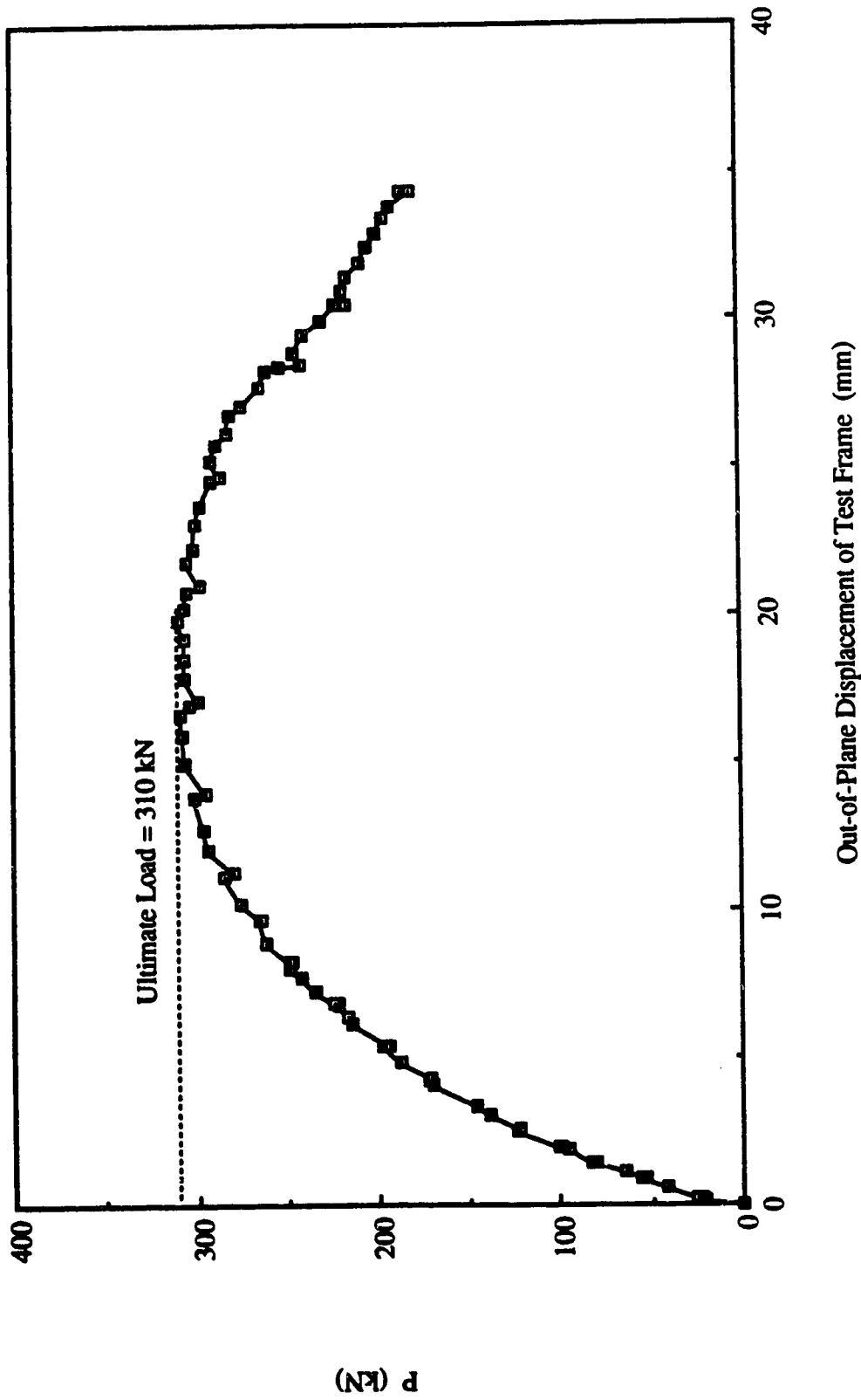


Fig. 7.5 Load vs. Out-of-Plane Displacement of Test Frame for Specimen EPI

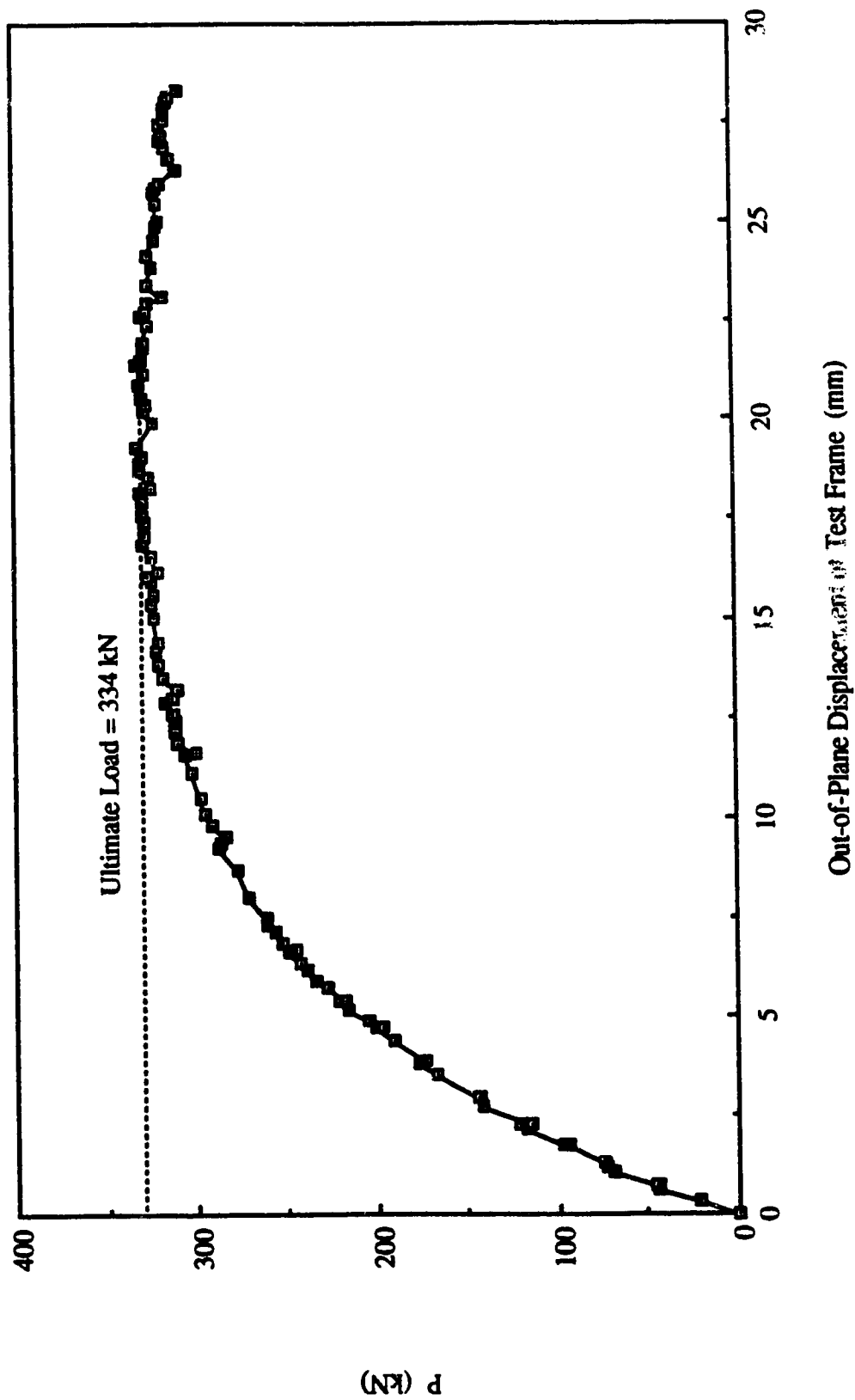


Fig. 7.6 Load vs. Out-of-Plane Displacement of Test Frame for Specimen EP2

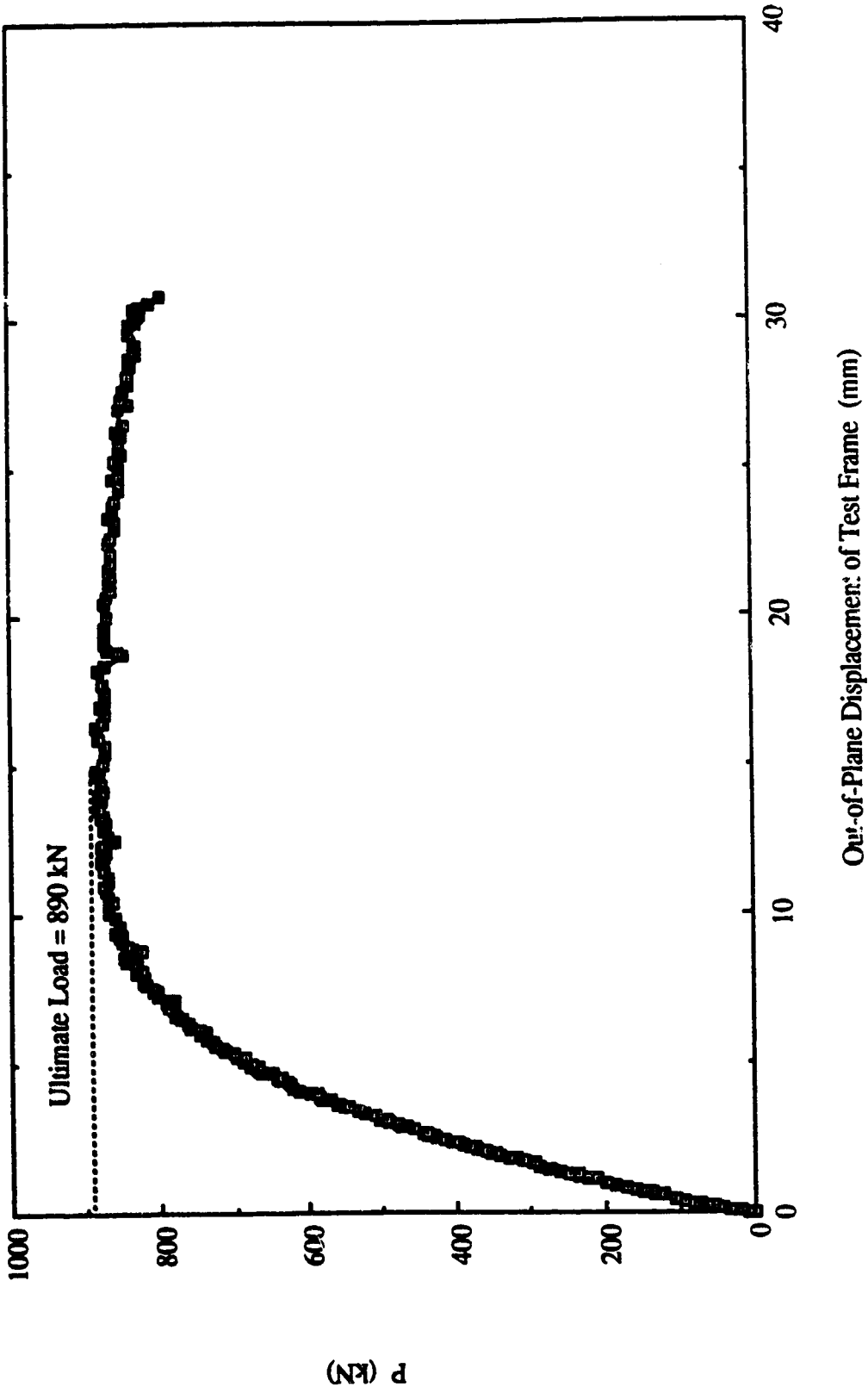


Fig. 7.7 Load vs. Out-of-Plane Displacement of Test Frame for Specimen EP3

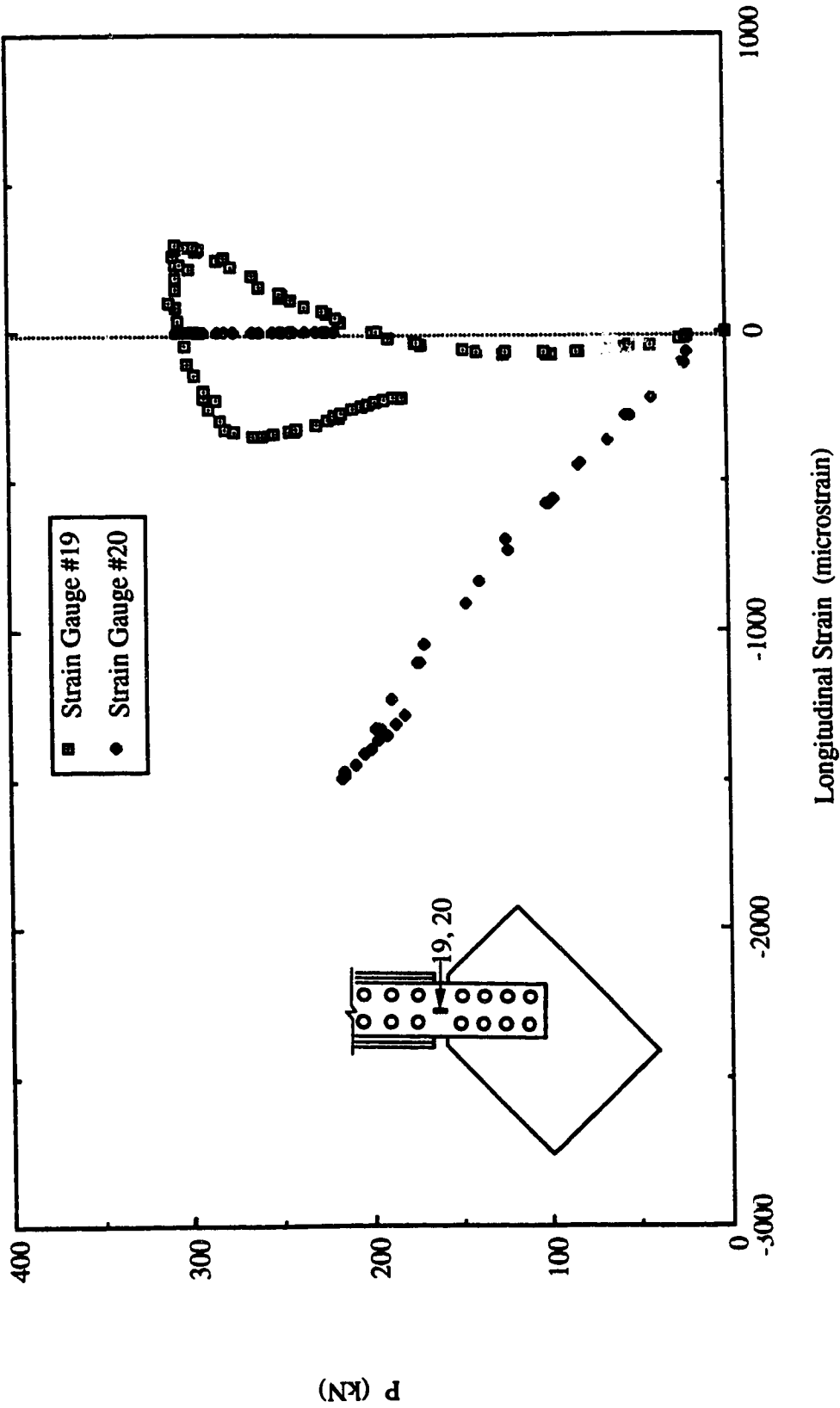


Fig. 7.8 Load vs. Strain Gauge Readings at the Conjunction of Gusset-to-Splice for Specimen EPI

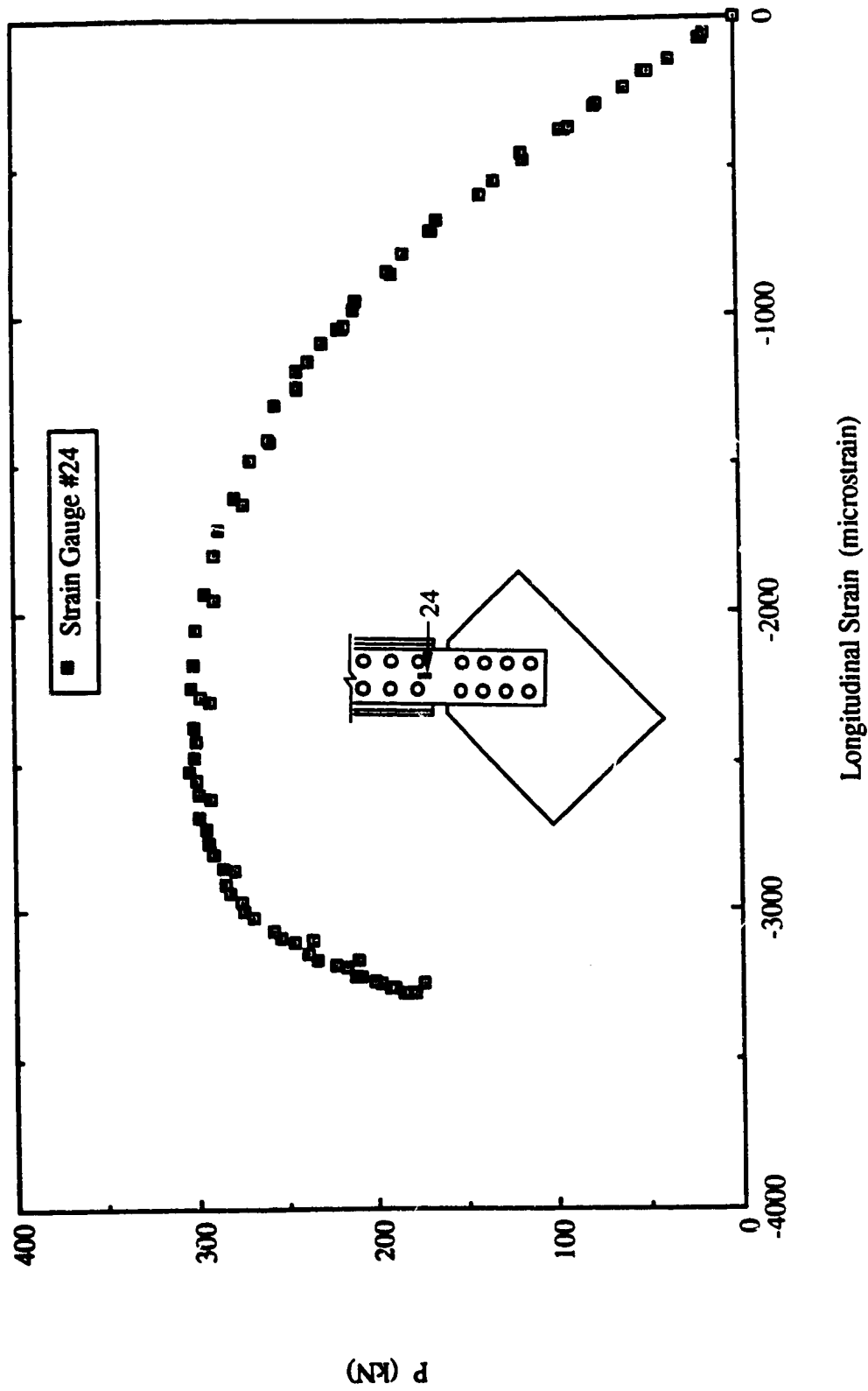
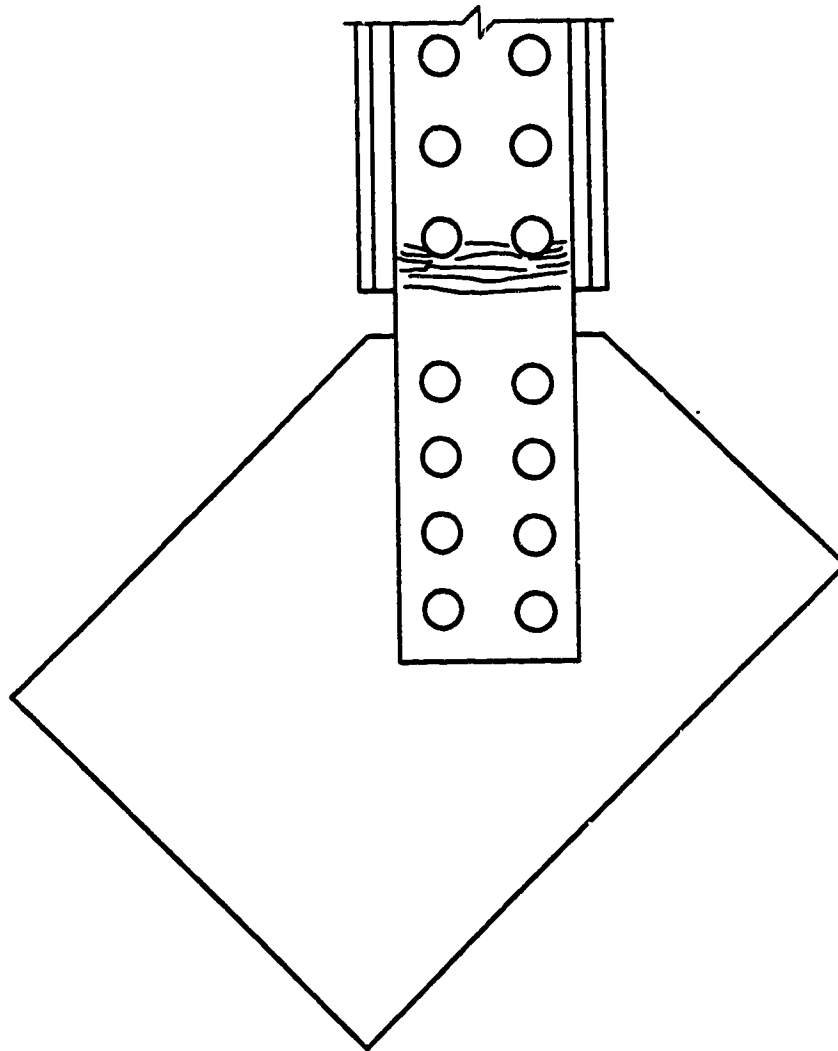


Fig. 7.9 Load vs. Strain Gauge Readings at Splice Member Near End of Brace for Specimen EP1



**Fig. 7.10 Schematic Yield Line Pattern on Splice Plate for EP Type Specimens**





**Fig. 7.11 Yielding Observed in Specimen EP1**

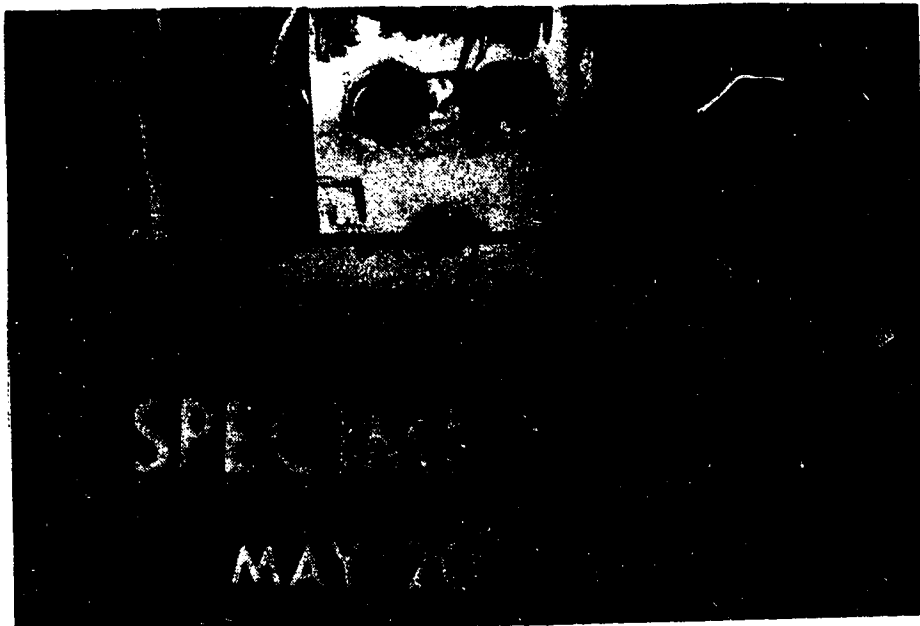


**Fig. 7.12a Failed Splice Member for Specimen EP1**

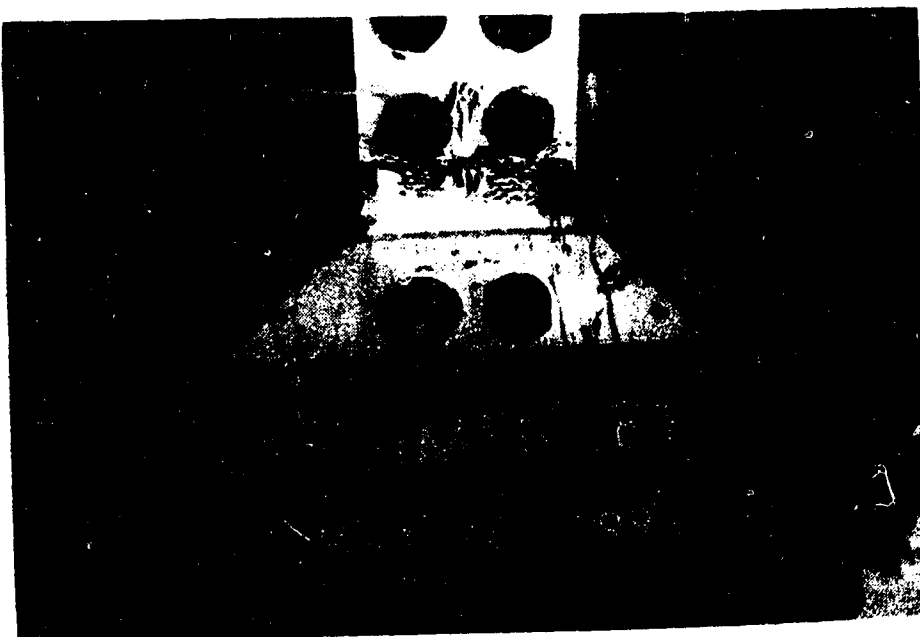


**Fig. 7.12b Failed Splice Member for Specimen EP2**

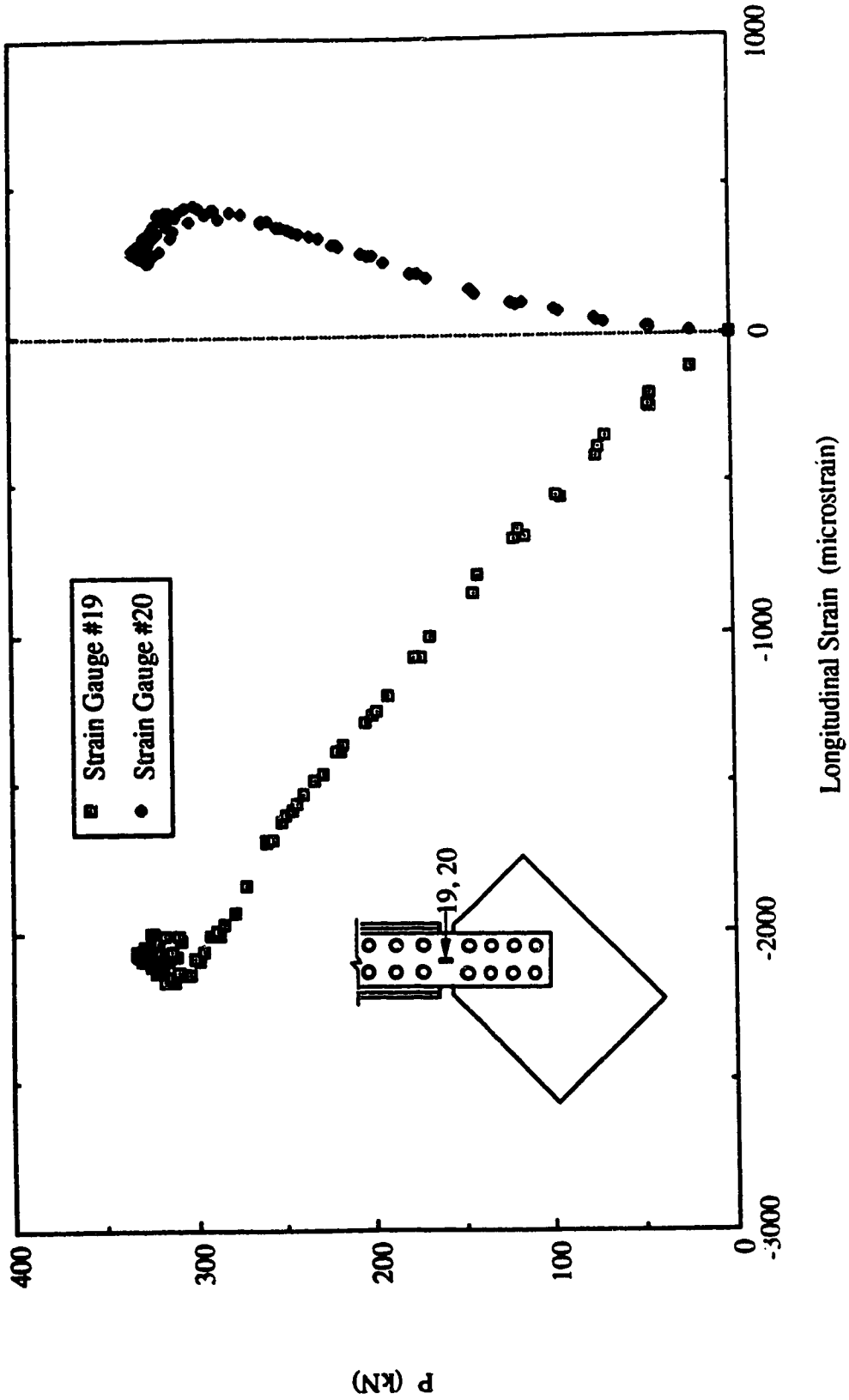


Fig. 7.13 Load vs. Strain Gauge Readings at the Conjunction of Gusset-to-Splice for Specimen EP2

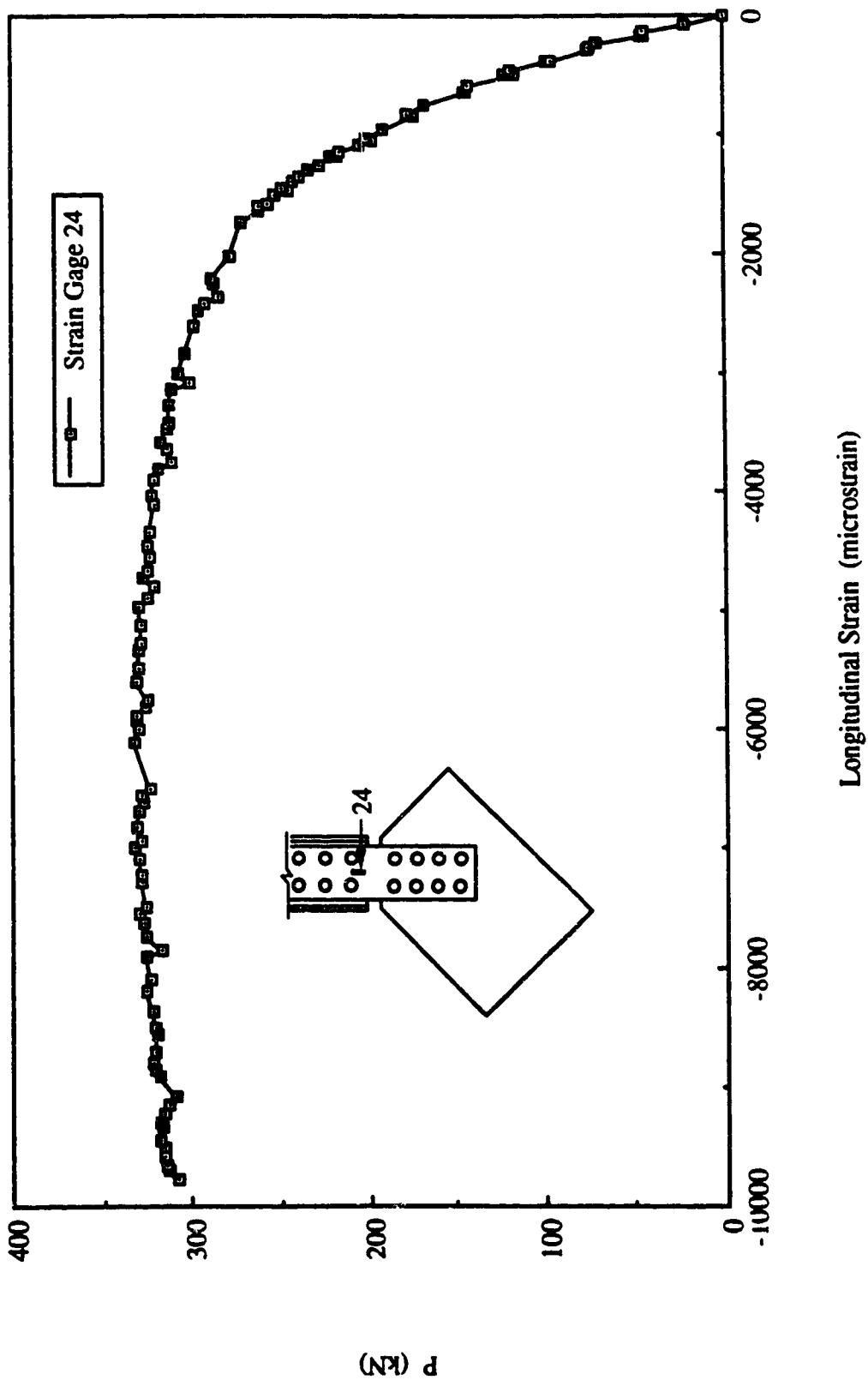


Fig. 7.14 Load vs. Strain Gauge Readings at Splice Near End of Brace for Specimen EP2

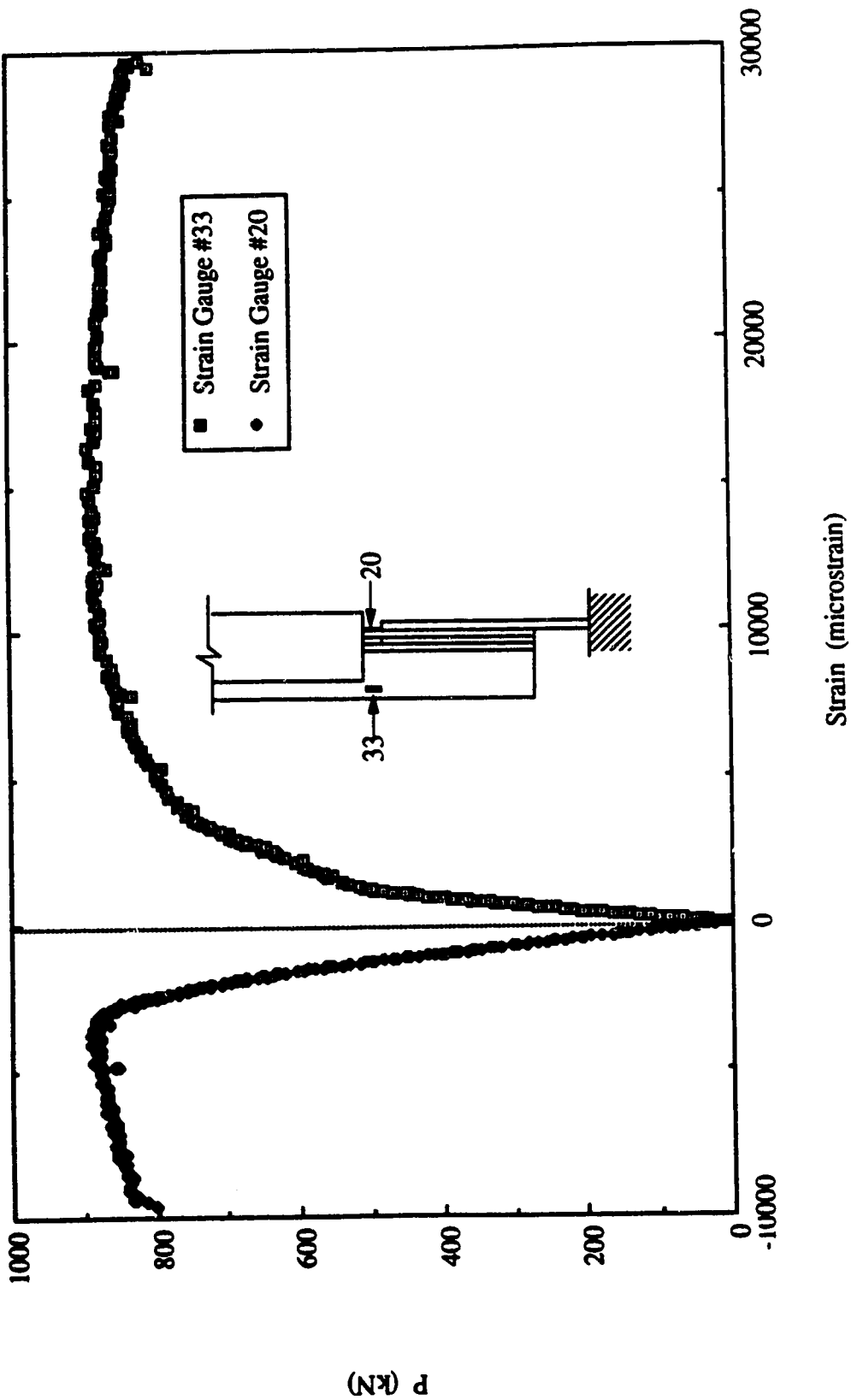


Fig. 7.15 Load vs. Strain Gauge Readings at Web of Tee-Section and Splice Plate for Specimen EP3

P = 400 kN

Strain Readings in microstrain

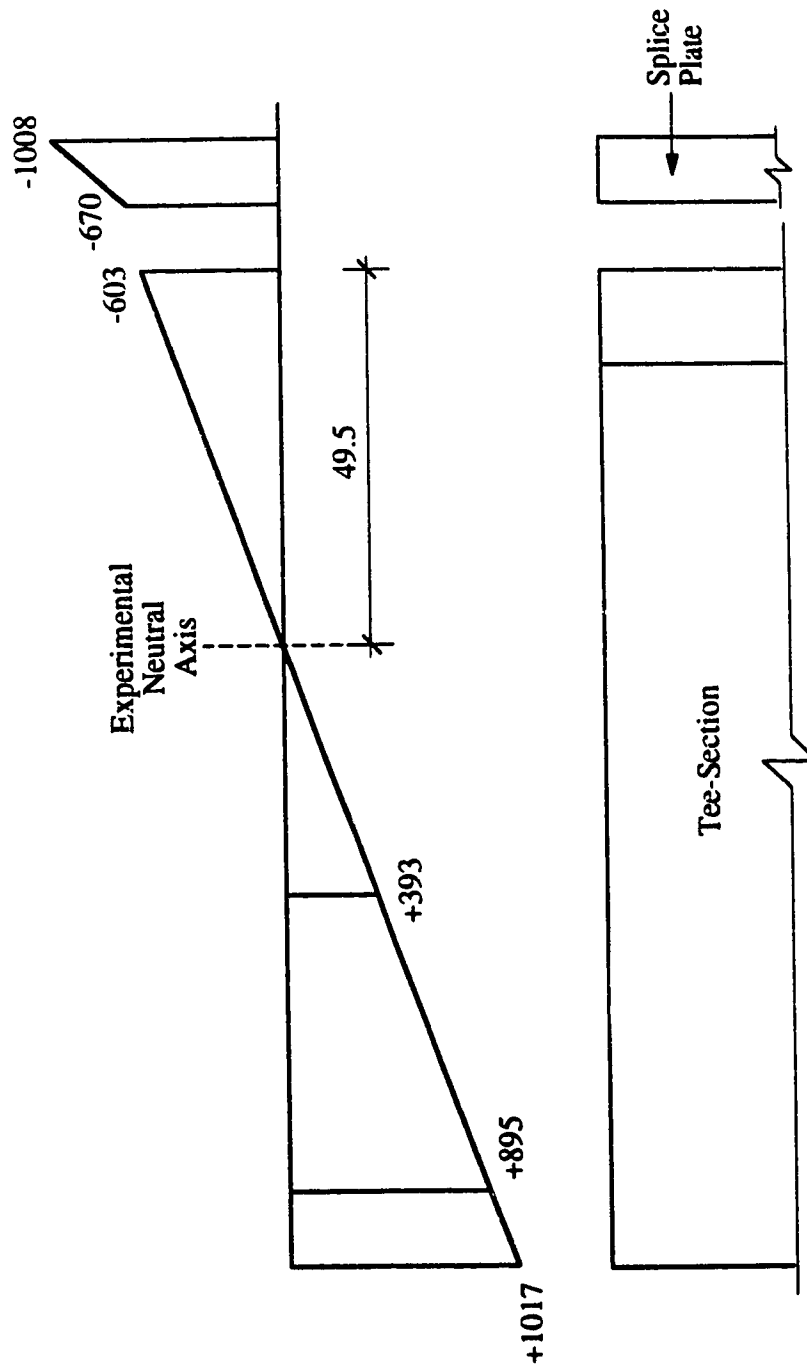


Fig. 7.16 Strain Distribution Across the Depth of the Splice Section For Specimen EP3

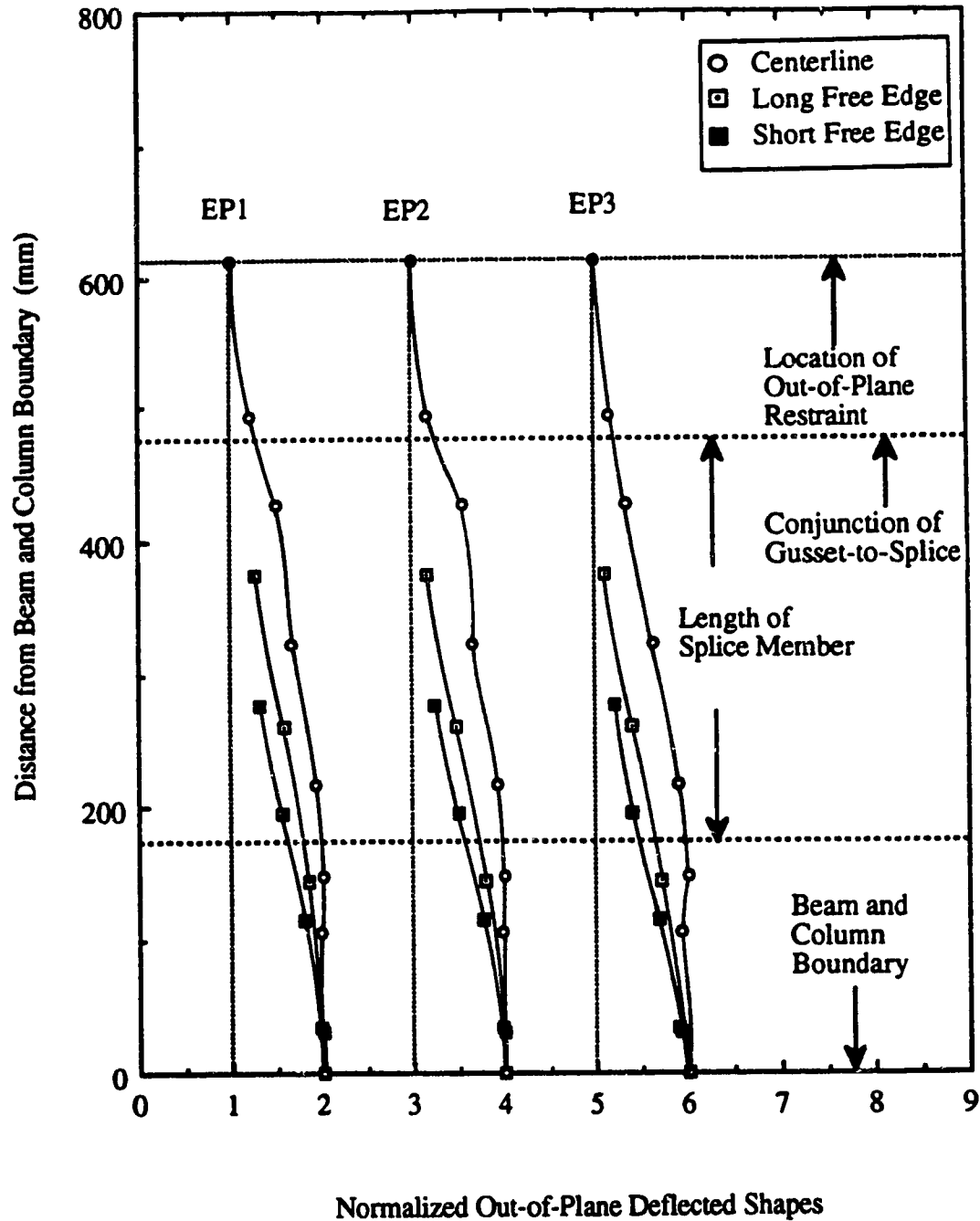


Fig. 7.17 Out-of-Plane Deflected Shapes at Free Edges and Along Centerline of Splice for EP Type Specimens

## **8. DISCUSSION AND COMPARISON OF TEST RESULTS**

### **8.1 Introduction**

This chapter presents the effects of the test parameters on the compressive behavior and ultimate strength of the specimens. The GP type specimens are only used to consider the general compressive behavior of a gusset plate connection with a plate size of 500 x 400 and brace angle of 45°; the effects of frame action were, however, not included. In order to examine the effects of each variable, the test results of the GP type specimens will be used as a reference to compare with the test results of other specimens. A general discussion of the test results is included in Section 8.2. The effects of each test variable on the behavior and strength of gusset plate connections will be discussed separately in each section. A summary of the test results is shown in Table 8.1.

### **8.2 General Discussion of Test Results**

The ultimate loads of all the specimens are illustrated in Table 8.1. It should be noted that this discussion excludes the test results of the EP type specimens since failure of these specimens occurred in the splice member at the conjunction of gusset-to-splice. The design loads of all the specimens estimated by the Whitmore method and the Thornton method were already presented in previous chapters. Table 8.1 includes the ratios of the ultimate load to the Whitmore loads and the ratios of the ultimate load to the Thornton loads. As can be seen from the table, the Whitmore method provided a conservative estimate of the design load for the specimens, except for the SP type specimens. The reason for this is that the SP type specimens, which had a plate size of 850 x 700, were relatively slender and, therefore, the connection experienced stability failure before even reaching the Whitmore yield load level. Test results from Cheng et al. (1994) with a gusset plate size of 850 x 700 and plate thicknesses of 6.7mm and 3.11mm also showed that the test specimens were failed by



elastic buckling. The elastic buckling loads of the test specimens were significantly lower than the corresponding Whitmore loads. The plot of the ratios of the experimental ultimate loads to the Whitmore design loads versus the gusset plate thicknesses for the GP, SP, AP and MP type specimens is shown in Fig. 8.1. As expected, it can be seen from this figure that the ratios are all above 1.0 except for the SP type specimens. Hence, in general the Whitmore method produces conservative estimates of the design load of the compact specimens. In addition, a higher ratio existed for the 13.3 mm thick specimens, as shown in the figure, which might indicate a more efficient use of the material for the compact specimens. Although the ratios for the SP type specimens were below 1.0, it can still be seen that the ratio for the specimen with a larger thickness was significantly higher than the one with a smaller plate thickness. However, the test data from Hu and Cheng (1987) showed that the ratio of the ultimate load to the Whitmore load did not increase with an increasing plate thickness. This was probably because a postbuckling strength existed in the 3.11 mm thick specimen, as shown by the finite element analysis (Cheng et al. 1994). If the theoretical elastic bifurcation buckling load had been used, the ratio of the buckling load to the Whitmore load would be 0.088 instead of 0.211 for the 3.11 mm thick specimen. Hence, the observation of the effect of gusset plate thickness to the ratio of the ultimate load to the Whitmore load is appropriate.

The plot of the ratio of experimental ultimate loads to the Thornton loads is shown in Fig. 8.2. It can be seen from the figure that the ratios for the specimens are all above 1.0. These ratios varied from 1.31 to 1.87, and it should be noted that the effective length factor,  $k$ , was chosen to be 0.65. For the MP type specimens, the ratio ranges from 1.59 to 1.87. Tests performed by Gross and Cheok (1988) on two gusset plate specimens subject to beam and column moments and failed by buckling showed a ratio of 1.5 and 1.7 between the experimental buckling load and the Thornton load. However, the effective length factor used to evaluate the Thornton load in this case was chosen to be 0.5. If a value of 0.5 had been used for  $k$  in evaluating the MP type specimens, the ratio of the

ultimate load to the Thornton load would have ranged from 1.50 to 1.71. Hence, it can be seen that the test results from two different testing programs showed similar test to predicted ratios and the Thornton method provides a simple procedure with conservative estimates to evaluate the buckling strength of the gusset plates.

In general, a similar yielding pattern was observed for the specimens. However, the final yielding pattern of each specimen type was influenced by the corresponding test parameter. For example, the beam and column moments caused tensile yielding at the fixed ends of the free edges for the MP type specimens. Nevertheless, the general yielding pattern of the specimens was still comparable to that of the GP type specimens. The influence on the yielding pattern by various test variables will be discussed in the following sections. The general yielding pattern involved the significant yielding occurring at the plate area underneath the splice member. This area was stressed severely during loading, regardless of the types of specimens. However, a load redistribution occurred in most of the specimens allowing the load to transfer to the other part of the plate once the plate underneath the splice member had yielded extensively. In order for load redistribution to occur, the specimens had to be stiff enough to avoid stability failure. In addition, due to the complex boundary conditions, the gusset plate connection was statically indeterminate. Hence, for the stocky specimens with a plate thickness of 13.3 mm and a plate size of 500 mm x 400 mm yielding was observed almost on the entire plate due to the load redistribution prior to stability failure. On the other hand, very minor yielding was observed in specimen SP2, which was quite slender, before buckling occurred. In fact, the preliminary finite element analysis indicated that specimen SP2 failed in elastic buckling.

The failure mode for the specimens without out-of-plane restraint was sway buckling of the plate, and local buckling was observed for specimens with out-of-plane restraint. The failed specimens indicated that yield lines occurred in the gusset plate. These yield lines allowed the specimens to form a mechanism such that a lower load level could be

maintained after the specimens reached the ultimate load. This behavior was evident when the curves of the load versus the in-plane deformation of the MP and AP type specimens were examined, as shown typically in Figs. 6.4 and 5.4. However, this behavior was not recorded for the GP and SP type specimens since the tests were terminated before the specimens were allowed to stabilize at a lower load level. The reason for terminating the tests at that stage was that the out-of-plane displacement of the specimens had reached the physical limit of the test setup and measuring devices, and the specimens were already in the unloading stage.

### **8.3 Effect of Plate Thickness and Size**

As can be seen from Table 8.1, the ultimate load of the specimens increased with an increasing plate thickness for the specimens tested without restraint. The plot of ultimate loads versus the plate thickness is shown in Fig. 8.3. This figure shows that the ultimate loads of the specimens increased almost linearly with respect to the plate thickness. In addition, the slopes of the curves are almost parallel except for those of the AP type specimens. The curves for the AP type specimens show a smaller slope than the rest of the curves, as shown in the figure.

For the specimens tested with restraint at the base of the test frame, specimen SP2 showed a similar ultimate load to that of specimen GP2, even though specimen SP2 was more slender, as shown in Fig. 8.4. The reason for this is that, for specimen SP2, the increase in the ultimate load because of the restraint was significant since the specimen was predominantly failed in elastic buckling. However, specimen GP2 already showed severe yielding in the test without restraint and the ultimate load in this case might be very close to the material strength of the gusset plate. Hence, specimen GP2 might not be sensitive to the change in the boundary condition, whereas specimen SP2 was susceptible to the restraint.

Again, the amount of yielding decreased with an increasing gusset plate size when the tests results of the GP type specimens are compared to those of the SP type specimens. Pictures of the failed specimens of GP1 and SP1 are shown in Figs. 3.15 and 4.11 respectively. Since the out-of-plane stiffness of the specimens also decreased with an increasing plate size, stability failure for the SP type specimens occurred before significant yielding could be developed in the specimens.

#### **8.4 Effects of Out-of-Plane Restraint at Conjunction of Gusset-to-Splice**

The ultimate loads of the specimens increased when out-of-plane restraint was provided at the conjunction of gusset-to-splice, as shown in Table 8.1. However, it can be seen that the increase in ultimate loads for the GP type specimens due to the restraint was not significant. A maximum of an increase of about 10% was recorded for specimen GP2. For the SP type specimens, a considerable increase was observed for specimen SP2 due to the restraint. A plot of load versus gusset plate thickness with the two restraint conditions is shown in Fig. 8.4. It can be seen from the figure that the curves for the GP type specimens are almost parallel, with only a minor increase in ultimate load due to the restraint.

As mentioned previously, the out-of-plane deflected shapes along the free edges and the centerline of the splice member for the GP and SP types specimens without restraint at the base of the test frame resembled the buckled shapes of a fixed-guided column. These deflected shapes are shown in Figs 3.16 and 4.12. However, when the restraint was applied to the base of the test frame, the deflected shapes were changed, as shown in Figs. 3.24 and 4.20 for the GP and SP types specimens, respectively. The deflected shapes shown in these figures indicated that an out-of-plane displacement was recorded at the conjunction of gusset-to-splice. This displacement, as mentioned in Chapter 3, was caused by a bending of the web of the brace member about the supports of the tension rods.

Hence, the restraint in the out-of-plane direction at the conjunction was reduced. Since the conjunction was not fully fixed, the restraint at the base of the test frame might not have a significant effect on the ultimate loads of the specimens. In addition, the GP type specimens were well within the inelastic range before they reached the ultimate loads; hence the restraint might not have a significant influence on the ultimate loads. On the other hand, specimen SP2 ( $t=9.8\text{mm}$ ) experienced only slight yielding prior to reaching the ultimate load. Therefore, the effects of the restraint might be considerable, as illustrated by the increase of the ultimate loads shown in Table 8.1. In general, the restraint did not affect the yielding pattern of the specimens.

### **8.5 Effects of Angle of Diagonal Brace Member**

The plot of ultimate loads versus gusset plate thickness for the GP and AP type specimens is shown in Fig. 8.5. It can be seen from the figure and Table 8.1 that the ultimate loads for the specimens with a  $30^\circ$  brace angle (AP) were slightly lower than those for the specimens with a  $45^\circ$  brace angle. The difference in ultimate loads for these two types of specimens ranges from 2 % to 12% . Hence, it can be seen that the brace angle did not affect the ultimate load of the specimens significantly. Figure 8.5 also shows that the curve for the GP type specimens was slightly steeper than for the AP type specimens. This indicates that the rate of the ultimate load increase with respect to the plate thickness for the GP type specimens was higher than to that of the AP type specimens. It should be noted that the test setup employed to perform the tests on the GP type specimens was different from that of the AP type specimens. However, it is believed that the test setups should not affect significantly the test results.

In general, the yielding pattern for the AP and GP types specimens was similar, except that yield lines were first observed near the beam and column boundary for the AP type specimens. It was observed from the tests that a significant yielding was recorded in the

area of the plate bounded by the beam boundary and the short side free edge. In fact, the failed AP type specimens showed that yield lines were observed in that entire area, as illustrated in Fig. 5.15. In-plane bending at the short side free edge of the AP type specimens was observed at the later stage of loading. To illustrate this, strain gauge readings recorded at the mid-length of the short side free edge for specimens GP3 and AP3 are shown in Fig. 8.6. It should be noted that average strains from the two sides of the plate were used to plot the curves. This figure shows that the strain readings from both specimens were almost identical until the load reached about 65% of the ultimate load. At this loading stage, a strain reversal was observed for specimen AP3, which indicated that in-plane bending had occurred at the short side free edge. As loading continued, the compressive strains at the short side free edge for specimen GP3 increased. However, a tensile strain was recorded for specimen AP3. This in-plane bending was probably caused by the smaller brace angle of  $30^\circ$ , which produced a larger horizontal component of applied force to the short side free edge.

### **8.6 Effects of Beam and Column Moments**

When the test results of the GP and MP types specimens are compared, it can be seen that beam and column moments had negligible effects on the ultimate loads of the specimens, as illustrated in Table 8.1. A plot of the ratio of ultimate load for the MP type specimens to that of the GP type specimens versus the beam moment is shown in Fig. 8.7. The ratio ranges from 0.97 to 1.11. This plot shows that negligible effects of the beam and column on the ultimate loads of the specimens were observed from the test results. As shown in Table 8.1, by increasing the beam and column moments from 250 kN·m and 125 kN·m (MP3) to 375 kN·m and 187.5 kN·m (MP3A), the ultimate load of the specimen was increased by 14%. However, the test results of specimen MP3B (no beam and column moment) showed a similar ultimate load to that of specimen MP3A. Hence, it can be seen

that the effects of beam and column moment on the ultimate load of the specimens should not be significant.

Although the beam and column moment did not affect the ultimate load of the specimens significantly, an early yielding in the plate area underneath the splice member was observed for the MP type specimens. As mentioned previously, yielding at the area underneath the splice occurred at a load level close to the one estimated by the Whitmore method for the specimens, without the effects of beam and column moments. However, for the MP type specimens, yielding at the area underneath the splice occurred at a load level significantly lower than that estimated by the Whitmore method. To examine these behaviors, a plot of load versus strain recorded at the rosette mounted underneath the splice for specimens GP3 and MP3 is shown in Fig. 8.8. It can be seen from this figure that similar strain readings were recorded for both specimens GP3 and MP3 at the initial loading stage. However, when the beam and column moment was applied to specimen MP3, a sudden increase in compressive strain for this specimen was observed. For specimen MP3, the full value of beam and column moment was applied at a load level of about 100 kN. It can also be seen from the figure that specimen GP3 showed yielding at approximately the load level slightly lower than the one estimated by the Whitmore method. However, for specimen MP3, yielding was observed at the early loading stage, after the full values of beam and column moment were applied, as shown in the figure. Hence, it can be seen that the beam and column induced early yielding at the plate area underneath the splice. It was also pointed out in the previous chapter that the beam and column moment also induced significant tensile stress at the ends of the gusset plate free edges, and a high tensile stress gradient was also observed along the beam and column boundary. However, for GP3 specimen, a compressive strain was observed along the beam and column boundary. Nonetheless, the tensile stress induced by the beam and column moment might have improved the compressive strength of the specimens. This is because, when the gusset plate specimens deformed out-of-plane, a component of the in-plane tensile stress perpendicular to the plane of the gusset plate would

act in the opposite direction of the out-of-plane deformation; hence the specimens were stiffened. This behavior is similar to that of membrane action; however, the in-plane tensile stress was produced by the beam and column moment. On the other hand, the early compressive yielding occurring underneath the splice due to presence of the beam and column moment might have counteracted these beneficial effects. Hence, on the whole the ultimate loads of the specimens were not affected significantly by the beam and column moment.

The beam and column moment also affected the load deflection behavior of the specimens. To illustrate this observation, the load deflection curves of specimens MP3, MP3A and MP3B, as shown in Figs 8.9 and 8.10, were examined. The load versus in-plane deformation of the gusset plate specimens recorded at the end of the splice member is shown in Fig. 8.9, which shows that the in-plane stiffness of the specimens decreased with increasing beam and column moments. When the curves for specimens MP3A and MP3B are examined, it can be seen that the curve for the specimen with a zero beam and column moment (MP3B) was linear up to approximately the Whitmore yield load level. However, for the specimen with a maximum beam and column moment (MP3A), nonlinearity of the curve was observed at about 350 kN, which was significantly lower than the Whitmore yield load. As a reminder, it can be observed from the figure that, regardless of the moment levels the specimens were all stabilized at the same lower load level after reaching the corresponding ultimate loads.

The out-of-plane load deflection behavior was also affected by the beam and column moment, as shown in Fig. 8.10. This figure illustrates that, as the beam and column moment increased, the out-of-plane stiffness of the specimen also increased. A significant increase in stiffness was observed when specimens MP3B and MP3A were compared. However, only slight increase in stiffness was recorded when specimens MP3 and MP3B



were compared. Nevertheless, this increase in out-of-plane stiffness was provided by the tensile stress due to the beam and column moment.

### **8.7 Effects of Loading Eccentricity**

As presented in the previous chapter, three tests with various splicing members were performed on a specimen similar to that of specimen GP1 in order to investigate the effect of loading eccentricity. Since the mode of failure for these specimens was yielding at the splice member, both the Whitmore and Thornton methods were not suitable to provide an estimate of the design load of these specimens. It can be seen from Table 8.1 that the ultimate loads of EP type specimens were significantly lower than those of the specimen GP1. The maximum load achieved by specimen EP3 was about 46% of the ultimate load of specimen GP1. It should be noted that in increasing the thickness of the splicing member, the loading eccentricity was also increased. For these specimens, the increase in loading eccentricity was 1.8 mm from specimens EP1 to EP2. In addition, the static yield strength for the 9.5 mm thick splice plate (EP1) was significantly higher than that of the 13.0 mm thick splice plate (EP2), as shown in Table 3.2. For specimen EP1, the static yield strength was 435 MPa, while the static yield strength for specimen EP2 was 285 MPa. When the test results of specimens EP1 and EP2 are compared, it can be seen that in increasing the splice plate thickness by approximately 40%, the ultimate load of specimen EP2 was only improved by 8%. This was probably due to the combined effects of the increased loading eccentricity for specimen EP2 and the higher static yield strength for specimen EP1.

When a tee-section and a 9.5 mm thick plate was used as the splicing member for specimen EP3, the ultimate load of specimen EP3 was increased to about 2.87 times that of specimen EP1. It should be noted that the tee-section provided an increase to the splice member in both the cross-sectional strength and the higher bending rigidity. However, it also created

additional loading eccentricity. Nevertheless, it can be seen that a significant improvement in the load carrying capacity of an eccentrically loaded gusset plate connection can be attained by employing a splicing member which has higher flexural stiffness. However, the maximum load of the eccentrically loaded specimen EP3 was still much less than that of the concentrically loaded specimen GP1.

The curves of load versus out-of-plane displacement of the test frame for the specimens are shown in Fig 8.11. As expected, the out-of-plane stiffness of the specimens increased with the increasing flexural stiffness of the splice member. The elastic range of the load deflection curve also increased with the splice member's increasing flexural stiffness. The curves were also similar to the typical load deflection curve for beam-column, which has an unloading path due to the effects of  $P\Delta$  moments. It can be observed from the figure that the rate of unloading for the specimens decreased as the flexural stiffness of the splicing member increased.

It can be seen from the failed specimens that the eccentric moment produced significant bending in both the splice member and the gusset plate. This bending effect caused yielding in the splice member at the conjunction and the gusset plate. In particular, for specimens EP1 and EP2, the yielding zones might have developed into a collapse mechanism. This will be further investigated in the following chapter of analysis.

Table 8.1. Summary of Test Results

Specimen Designation	Plate Size (mm)	Ultimate Load P (kN)	$\frac{P}{P_w}$	$\frac{P}{P_t}$
GP1	500 x 400 x 13.3	1956	1.61	1.71
GP2	500 x 400 x 9.8	1356	1.46	1.64
GP3	500 x 400 x 6.5	742	1.37	1.69
GP1R	500 x 400 x 13.3	2057	1.69	1.80
GP2R	500 x 400 x 9.8	1487	1.60	1.80
GP3R	500 x 400 x 6.5	790	1.42	1.80
SP1	850 x 700 x 13.3	1606	0.87	1.31
SP2	850 x 700 x 9.8	1010	0.71	1.58
AP1	500 x 400 x 13.3	1720	1.56	1.54
AP2	500 x 400 x 9.8	1210	1.55	1.51
AP3	500 x 400 x 6.5	728	1.31	1.80
MP1	500 x 400 x 13.3	1933	1.59	1.69
MP2	500 x 400 x 9.8	1316	1.42	1.59
MP3	500 x 400 x 6.5	721	1.30	1.64
MP3A	500 x 400 x 6.5	819	1.48	1.87
MP3B	500 x 400 x 6.5	821	1.48	1.87
EP1	500 x 400 x 13.3	310	0.25	0.27
EP2	500 x 400 x 13.3	334	0.27	0.29
EP3	500 x 400 x 13.3	890	0.73	0.78

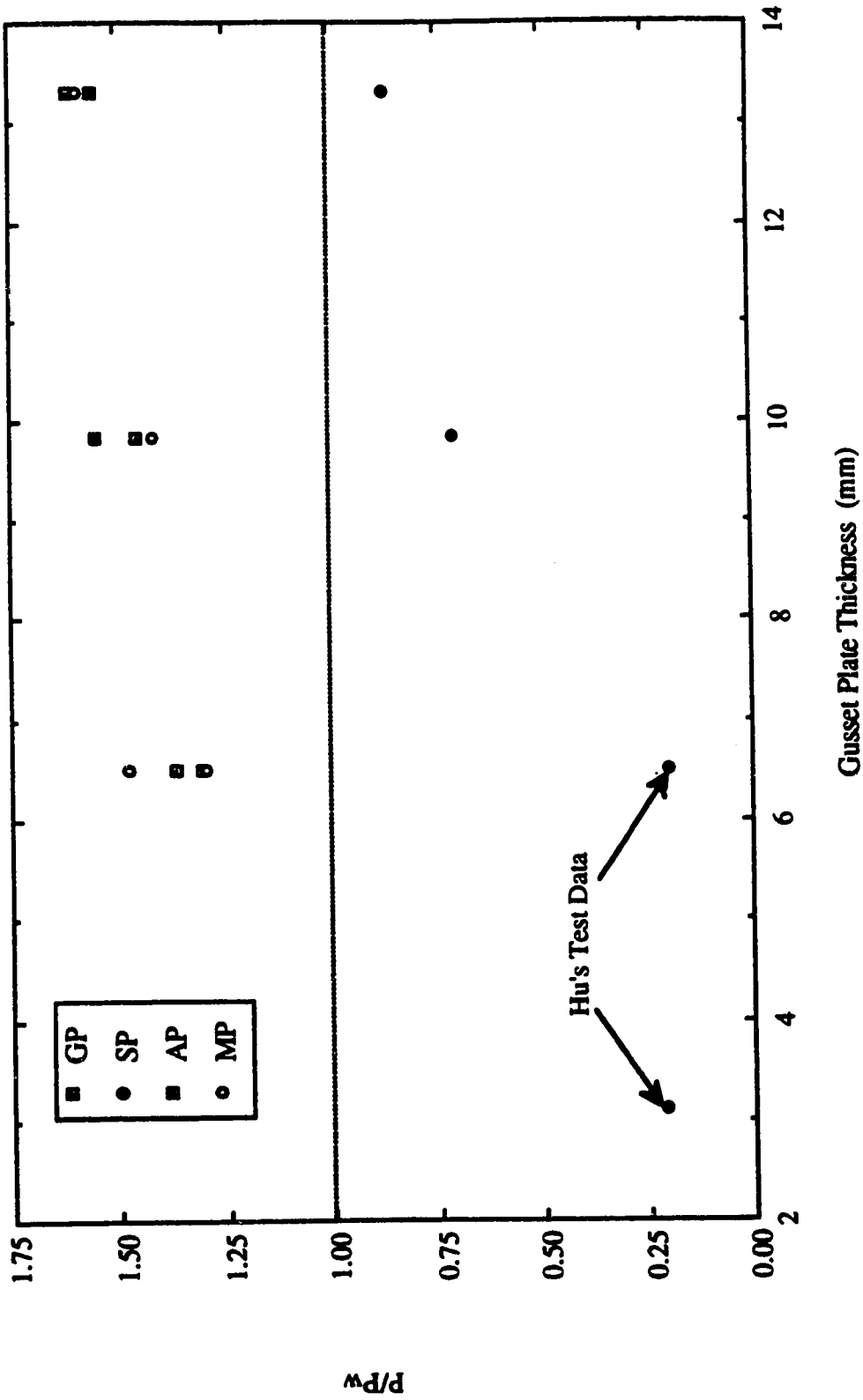


Fig. 8.1 Ratios of Ultimate Loads to Whitmore Loads vs. Gusset Plate Specimens Thickness

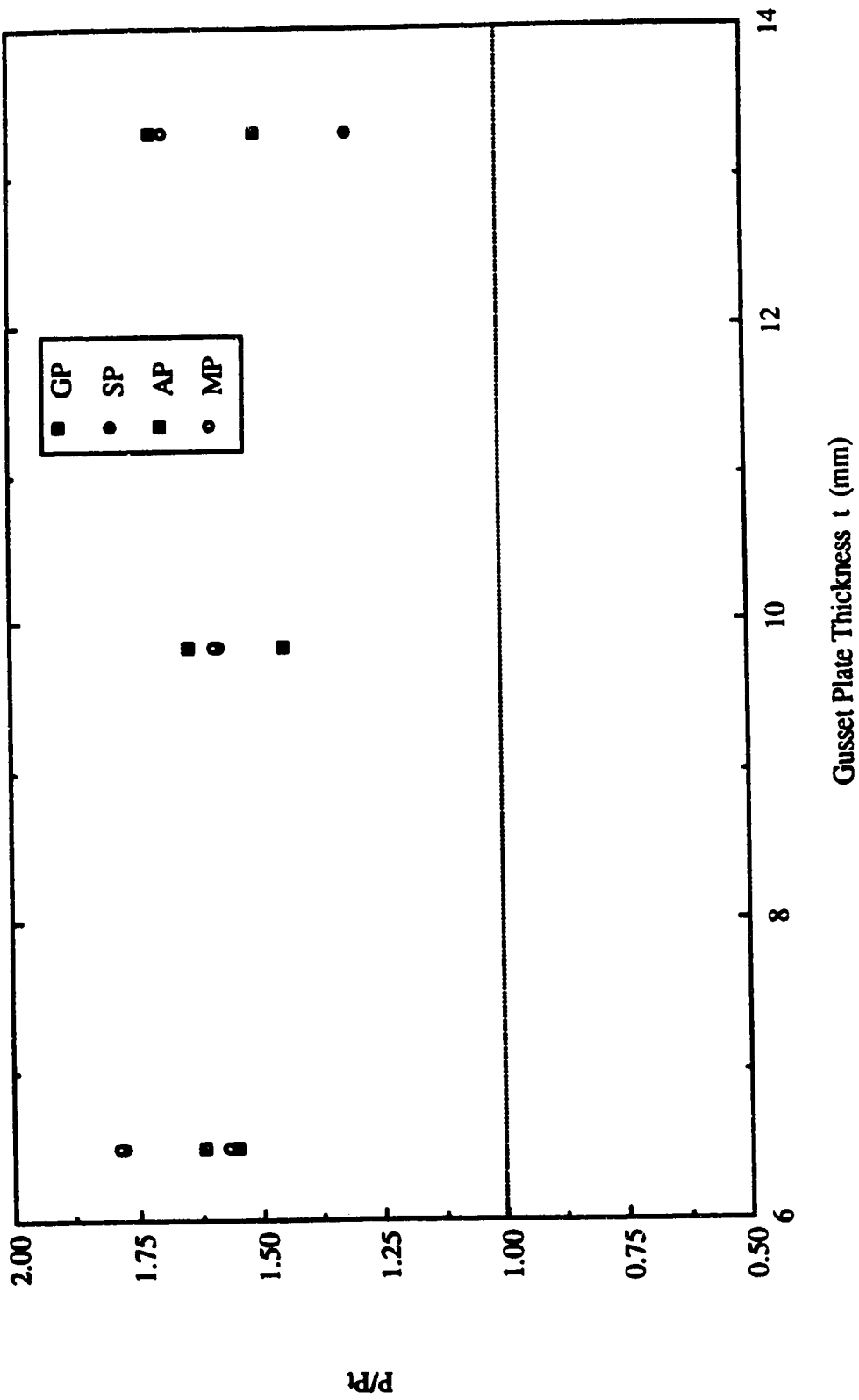


Fig. 8.2 Ratio of Ultimate Loads to Thornton Loads vs. Thickness of Gusset Plate Specimens

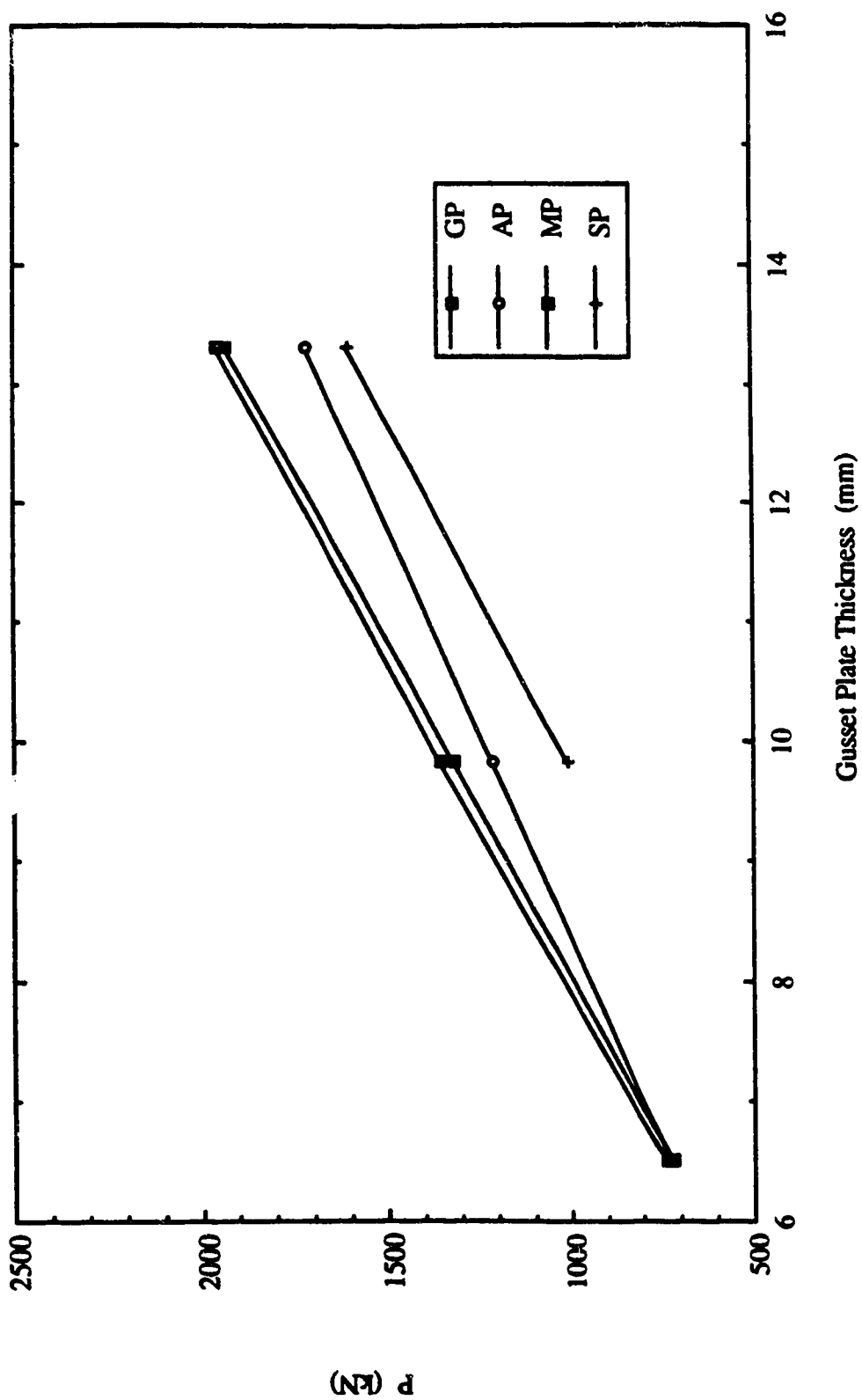


Fig. 8.3 Ultimate Loads vs. Thickness of Gusset Plate Specimens

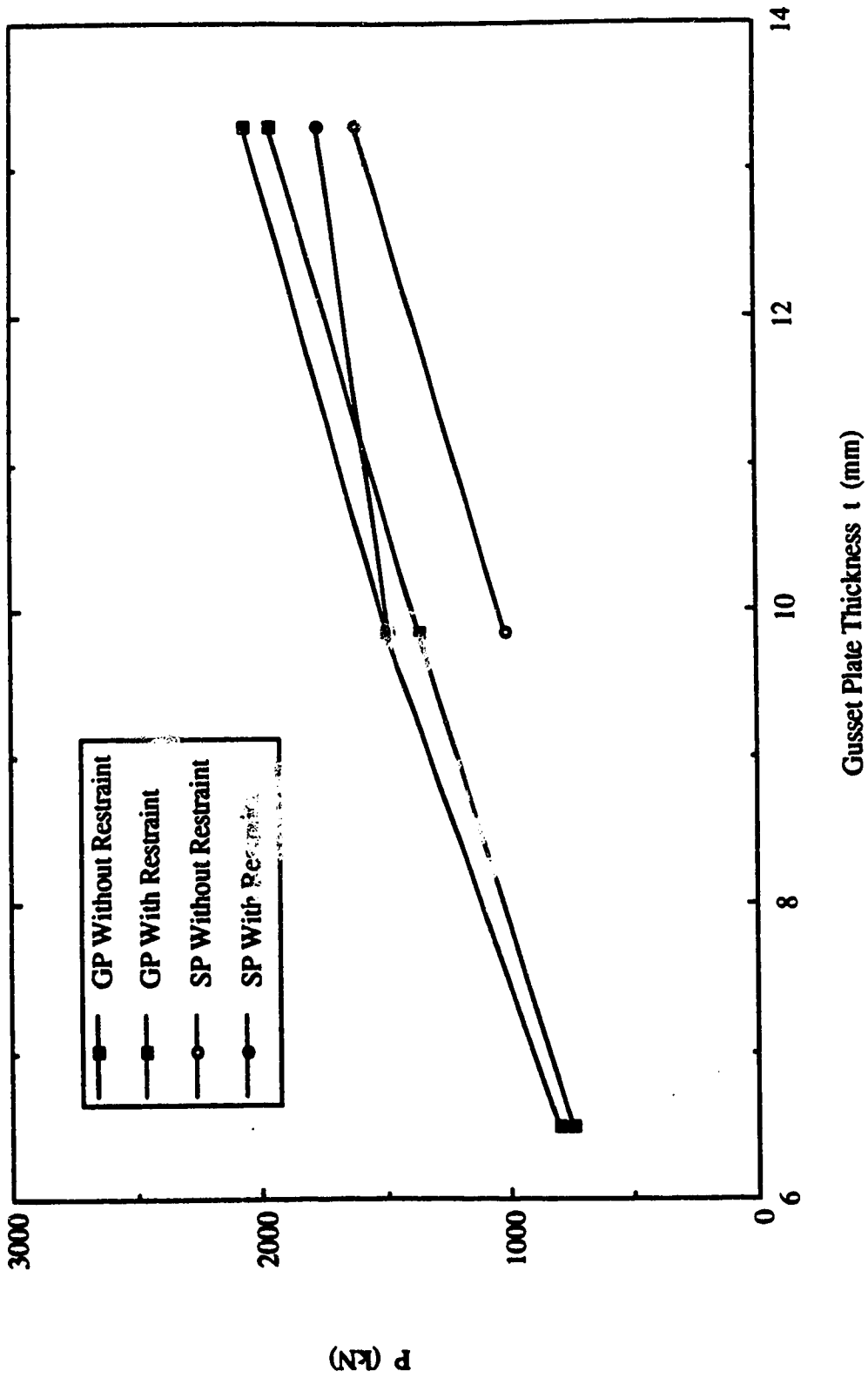


Fig. 8.4 Effects of Out-of-Plane Restraint on the Ultimate Loads of GP and SP Types Specimens

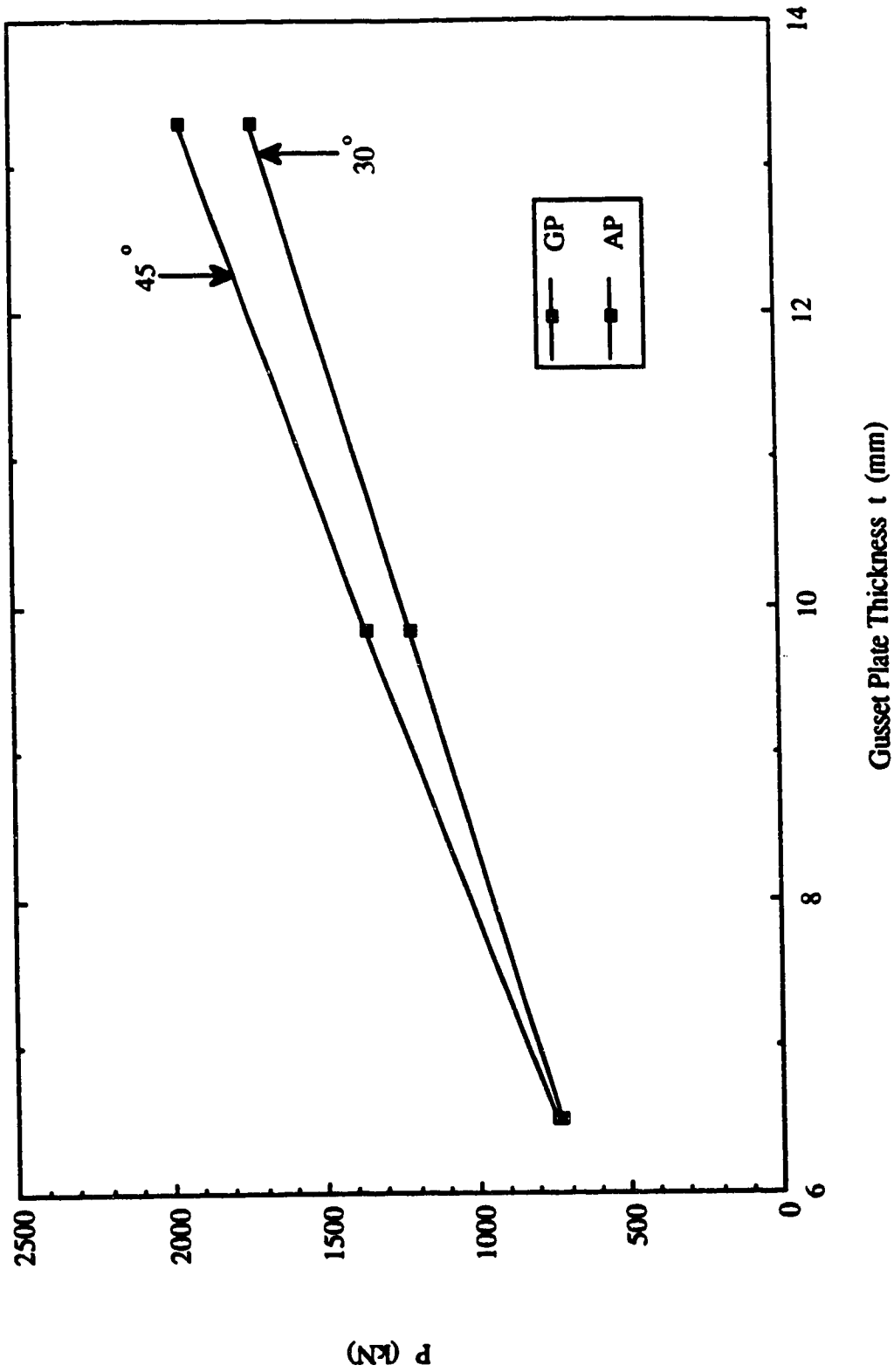


Fig. 8.5 Effects of Brace Angles on the Ultimate Loads of Specimens



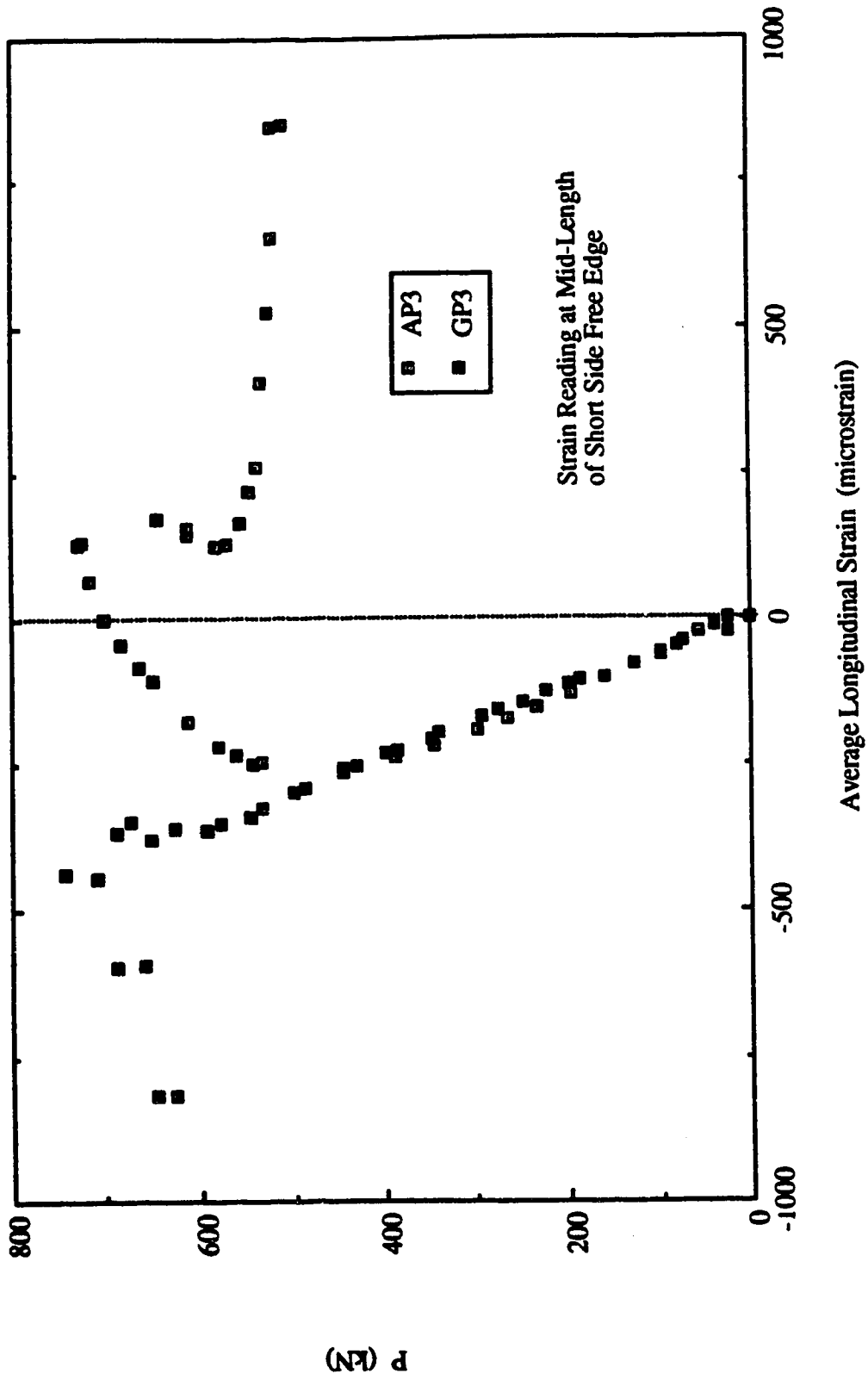


Fig. 8.6 Effects of Brace Angles on the Strain Readings Recorded at the Short Free Edge for Specimens AP3 and GP3

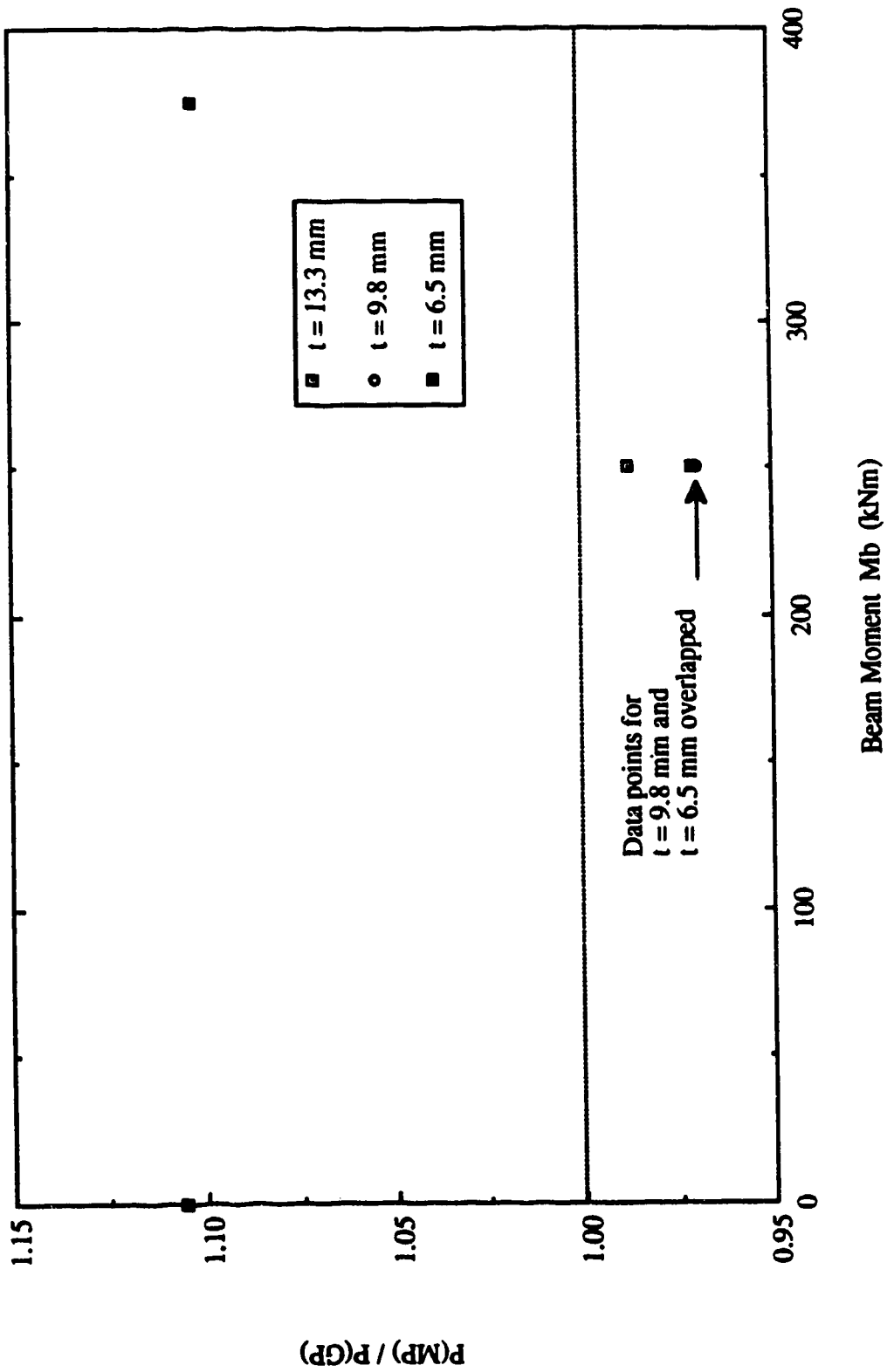


Fig. 8.7 Ratios of the Ultimate Loads of MP Type Specimens to GP Type Specimens vs. Beam Moment

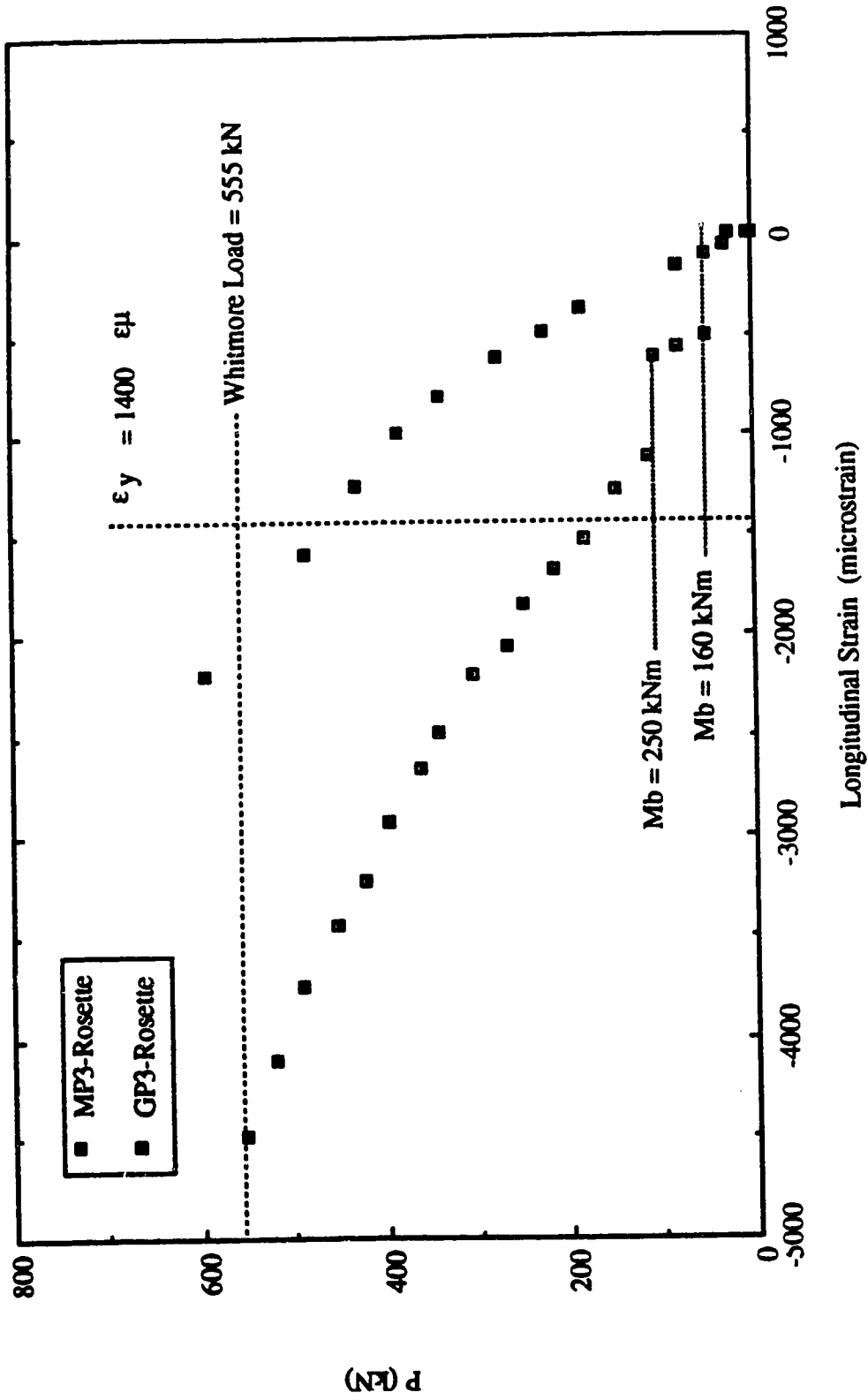


Fig. 8.8 Load vs. Strain Readings at Rosette underneath the Splice for Specimens MP3 and GP3

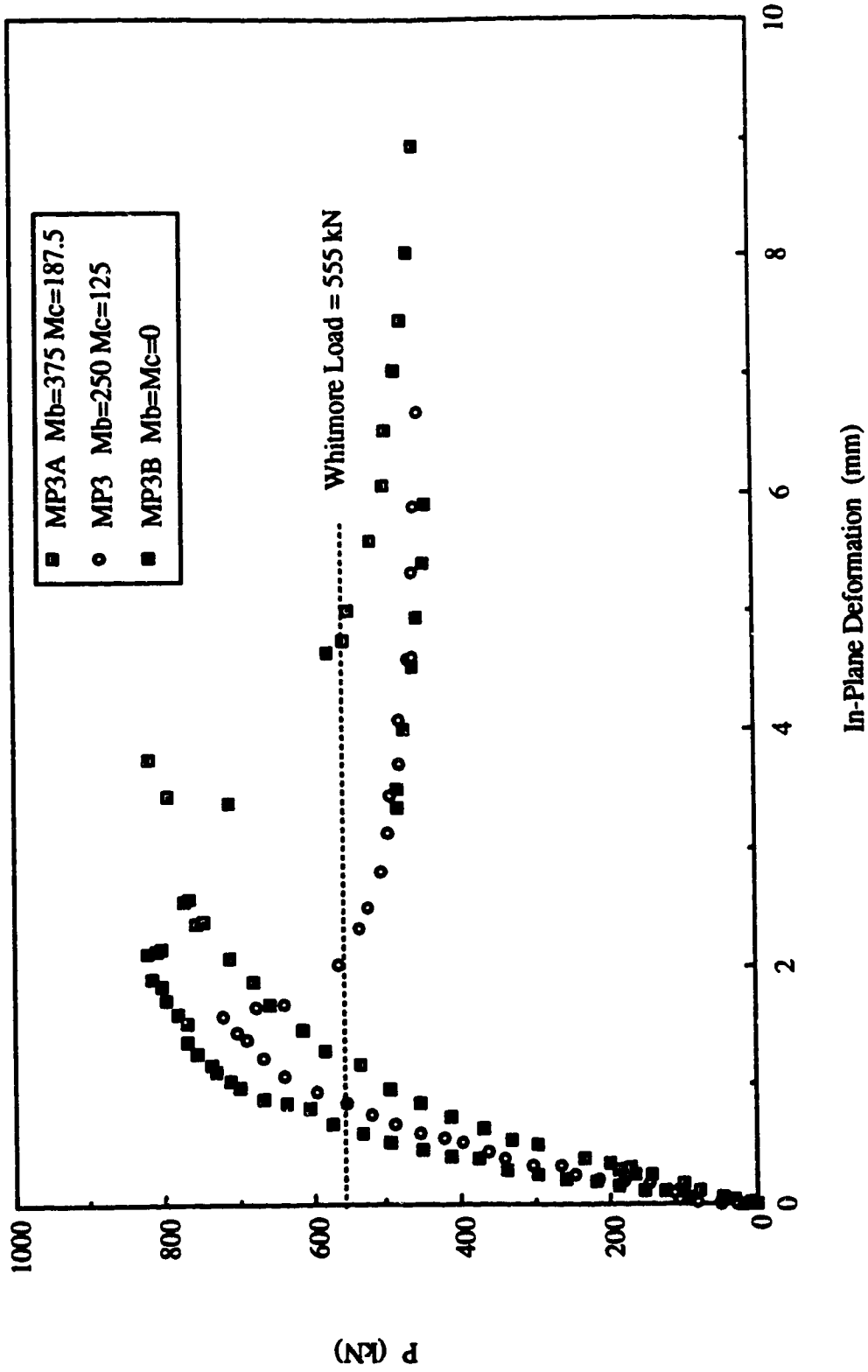


Fig. 8.9 Load vs. In-Plane Deformation Measured at End of Splice for Specimens MP3, MP3A and MP3B

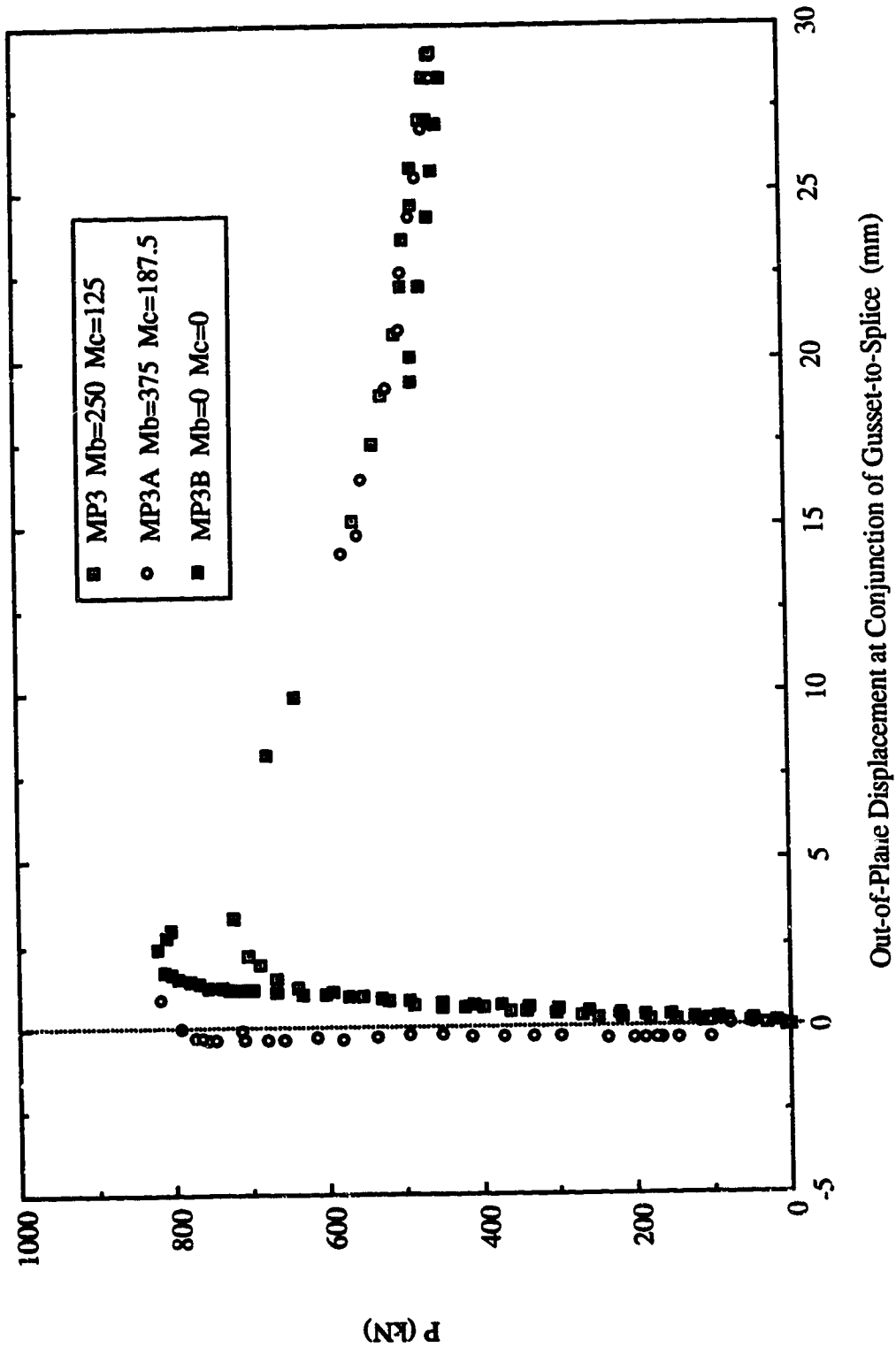


Fig. 8.10 Load vs. Out-of-Plane Displacement at Conjunction of Gusset-to-Splice for Specimens MP3, MP3A and MP3B

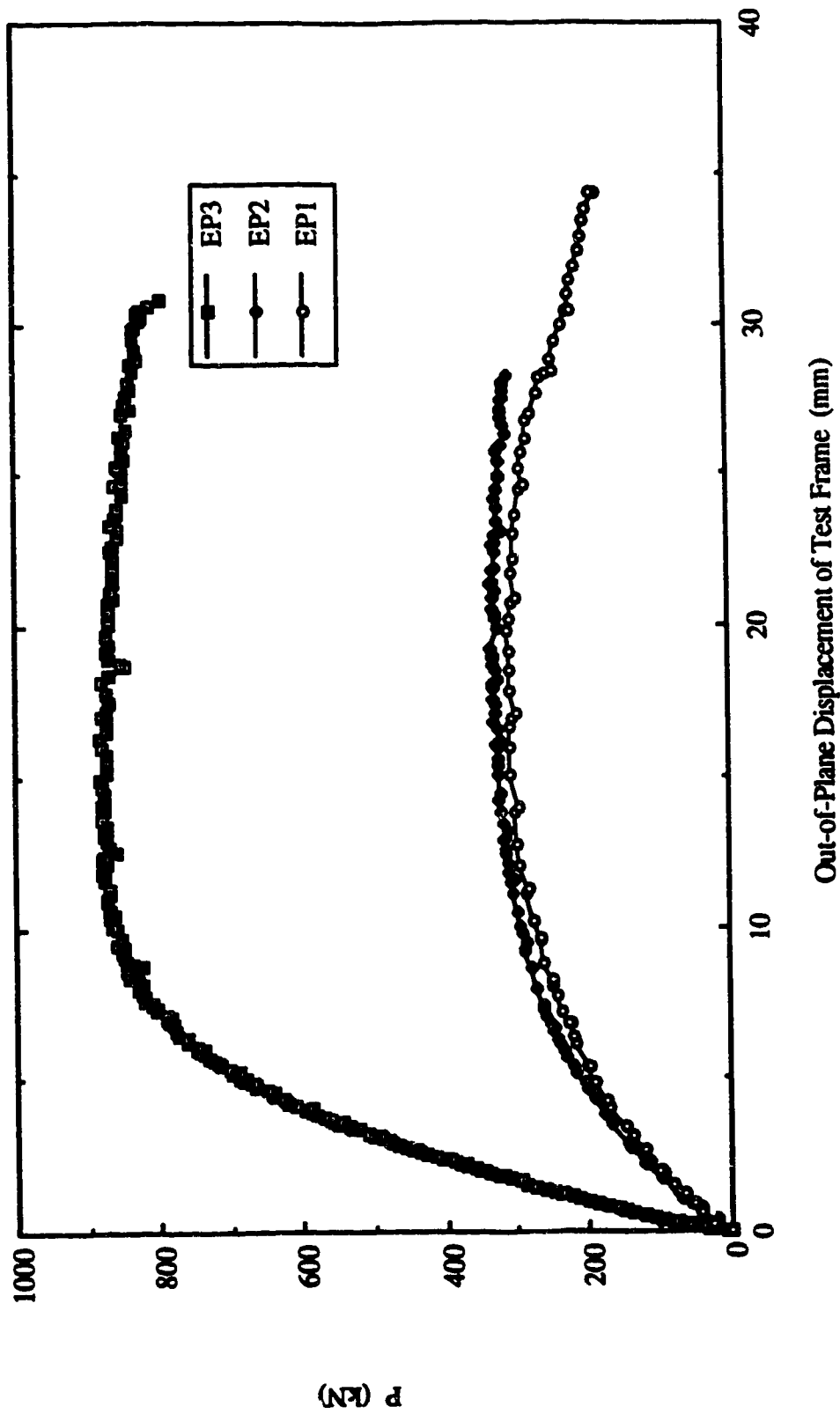


Fig. 8.11 Load vs. Out-of-Plane Displacement of Test Frame for EP Type Specimens

## **9. ANALYSIS OF TEST SPECIMENS**

### **9.1 General**

The compressive behavior of gusset plate connections has been investigated experimentally and the test results were presented in the previous chapters. To evaluate the ultimate strength of the specimens analytically, the finite element method was employed. It can be seen from the test results that the majority of the specimens experienced a significant yielding and out-of-plane deflection prior to reaching the ultimate loads. Since the failure mode of most of the specimens involved both a material nonlinearity and instability phenomenon, the most appropriate analysis is to trace the actual nonlinear load-deflection behavior of the specimens. However, the high computation expense of this approach prohibits its use in analyzing all the specimens. Therefore, it was decided to employ the method of plastic bifurcation buckling to evaluate the compressive strength of the GP, SP, AP, and MP type specimens. For the eccentrically loaded specimens (EP), a load deflection analysis was used to predict the ultimate strength of the specimens, since the main failure mode of the test specimens was yielding of the splice plate at the conjunction of gusset-to-splice. A rigid-plastic analysis was also performed on specimens EP1 and EP2 since a plastic collapse mechanism was observed from the test results of these specimens. The plastic bifurcation buckling method will be presented in detail in the following section.

### **9.2 Finite Element Analysis - Plastic Bifurcation Buckling**

The general bifurcation buckling analysis in the context of the finite element method will be discussed first, followed by the procedure of conducting plastic bifurcation buckling analysis. Bifurcation buckling is characterized by the fact that, as the load passes through its critical stage, the structure passes from its unbuckled equilibrium configuration to an

infinitesimally close buckled equilibrium configuration. The bifurcation buckling analysis in matrix form (Cook, Malkus and Plesha 1988) can be described as :

$$([K] + \lambda[K_{\sigma}]) \{D\} = \{0\} \quad [9.1]$$

where the matrix  $[K]$  is the conventional structural stiffness matrix,  $[K_{\sigma}]$  is the stress stiffness matrix to account for the in-plane stress distribution,  $\{D\}$  is the displacement vector corresponding to the buckling shape, and  $\lambda$  is an arbitrary scalar multiplier. This equation described the problem of classical buckling analysis (Chang and Chen 1986) in which the prebuckling rotations of the structure are either neglected or are zero. Equation [9.1] can also be described as an eigenvalue problem with  $\{D\}$  being the eigenvector and  $\lambda$  being the eigenvalue. To evaluate  $[K_{\sigma}]$ , a reference load level  $\{R\}$  is applied to the structure, and a standard linear static analysis is performed. The in-plane stress distribution resulting from this analysis is then used to generate  $[K_{\sigma}]$ . This  $[K_{\sigma}]$  is subsequently multiplied by  $\lambda$ , an arbitrary scalar multiplier, to account for the applied load level which causes bifurcation buckling to occur. It should be noted that, since  $[K_{\sigma}]$  is independent of displacement, multiplying  $[K_{\sigma}]$  by  $\lambda$  implies evaluating  $[K_{\sigma}]$  based on a stress intensity corresponding to the applied load level of  $\lambda\{R\}$ . However, the in-plane stress distribution remains the same. The lowest value of  $\lambda$  and the associated  $\{D\}$  (buckling shape) satisfying equation [9.1] defines the critical stage of the system, and the corresponding bifurcation buckling load is  $\lambda\{R\}$ .

In general, the method of plastic bifurcation buckling analysis is similar to the classical buckling analysis, except that material nonlinearity is considered in the former analysis method. In order to include the material nonlinearity existing prior to buckling, a nonlinear in-plane static analysis based on a applied trial load level and the actual material properties of the structure is performed. The resulting displacement field and the in-plane stress distribution from this analysis are used to evaluate the current values of  $[K]$  and  $[K_{\sigma}]$ ,



respectively. The matrix  $[K]$ , evaluated including the effects of material nonlinearity, is termed the tangent stiffness matrix. Then a classical buckling analysis based on these current stiffness values is conducted according to equation [9.1]. If  $\lambda$  evaluated based on the classical buckling analysis is equal to 1.0, then the applied trial load level is the critical load. However, if  $\lambda$  is greater than 1.0, a larger trial load level will be applied to the structure to perform the nonlinear in-plane static analysis again. A new set of current stiffness values is obtained and the classical buckling analysis is conducted to evaluate the new  $\lambda$ . This procedure continues until  $\lambda$  equals 1.0. This procedure is also illustrated schematically in Fig. 9.1.

### 9.3 Finite Element Model

The commercial program ANSYS (1989), version 4.4a, installed in a 486 personal computer was used to perform the analysis. A four node quadrilateral shell element (STIF 43 in ANSYS) with six degrees of freedom at each node was used to model the gusset plate. A beam element (STIF 4) and an elastic quadrilateral shell element (STIF 63) were used to model the flanges and webs of the beam and column respectively for the analysis of MP and AP types specimens. The STIF 43 element has the capability of handling plasticity, stress stiffening and large deflection problems. A multilinear stress-strain curve, based on the coupon tests results as mentioned in Chapter 3 was used as the material properties in the analysis. The von Mises yield criteria with the associated flow rule and isotropic hardening were employed in the multilinear material model. The full Newton-Raphson method was used to solve the nonlinear equilibrium equations in the static analysis. The full subspace iteration method was used to evaluate the eigenvector ( $D$ ) and eigenvalue ( $\lambda$ ) in the classical buckling analysis.

The typical finite element model of the GP and SP types specimens is shown in Fig. 9.2. Three-dimensional mesh was used to model the connection, with the splice plates placed on

both sides of the gusset plate, as shown in Fig. 9.2. The beam and column boundaries were fully restrained to simulate a rigidly welded connection. At the conjunction of the bracing member and gusset plate, infinite rotational restraint was assumed to be provided by the bracing member along the element x-axis. A load was applied as the element pressure on the splicing member and transferred from the splicing member to the gusset plate, at the bolt locations as shown in the figure. Constraint equations were used at the bolt locations to simulate a rigid line tied across the splice plates and the gusset plate such that the same in-plane displacements were shared at these locations and the connection rotated about the centerline of the gusset plate during buckling. It should be noted that the shear deformation of the bolts was neglected in the analysis due to its complex nonlinear behavior. It is also believed that this assumption will have negligible effects on the ultimate strength of the specimens. This belief is based on the fact that the critical region of the gusset plate at which inelastic buckling occurred is located directly underneath the splice member. Hence, the distribution of the bolt forces is believed to have insignificant effects on the stress distribution and intensity at this region.

For the AP and MP type specimens, a similar finite model as the GP type specimens was used; however, the beam and column supporting the gusset plate specimens were also included in the model, as shown in Fig. 9.3a. This particular model provides more realistic boundary conditions for the AP type specimens and allows the application of beam and column moment for the MP type specimens. Concentrated forces were applied at the end of the beam and column to produce the required moment at the connection. For the EP type specimens, the typical finite element mesh is shown in Fig. 9.3b. It can be seen from this figure that the bracing member was also included in the model in order to provide a more realistic boundary and loading conditions for the splice member. The bracing member was modeled by using a beam element (STIF 4) for the flanges and shell elements (STIF 43) for the web. The actual material properties of the gusset plate and the splice plate were used in the load deflection analysis.

Since plasticity introduced a nonconservative aspect to the problem, the applied load increment was selected to be as close to the actual loading sequence used in the experiments as possible. However, in some cases the incremental loads may have to be decreased in order for the nonlinear solution to converge. For the plastic bifurcation buckling analysis, in general, a single load step was applied to the gusset plate model such that the finite elements in the highly stressed area were almost beginning to yield. The load level was usually chosen as approximately 90% of the corresponding Whitmore load of the specimens. Then, load increments were applied to capture the effect of material nonlinearity. As the applied load approached about 90% of the experimental ultimate load, a classical buckling analysis was performed, based on the current stiffness values as mentioned above. This whole procedure was terminated when  $\lambda$ , evaluated by the classical buckling analysis, was equal to 1.05 or less. For the load vs. deflection analysis, a displacement controlled method was used to load the specimens in order to achieve the convergence of the solution, especially in the region of the ultimate load level and the unloading part of the curve. A uniform incremental displacement was imposed at the nodes of the bracing member, as shown in Fig. 9.3b.

The finite element mesh employed for this analysis was based on a mesh study of the GP type specimens. The plastic bifurcation buckling loads of the GP type specimens, evaluated using a coarse mesh, were within two percent of those of a fine mesh. However, since the computation time required to analyse the fine mesh was not significantly increased relative to the coarse mesh, the fine mesh was used for the analysis of the test specimens.

## **9.4 Finite Element Analysis Results**

### **9.4.1 General**

The analytical ultimate loads of the specimens, based on plastic bifurcation buckling analysis, are shown together with the test results in Table 9.1. However, the analytical

results of the specimens with out-of-plane restraint are not included, since the solution of the in-plane stress analysis for these specimens converged extremely slow. In fact, the load increment had to be made so small that it became impractical to continue the analysis. Hence, it was decided to abandon the analysis of the specimens with out-of-plane restraint. In general, it can be seen from the table that the analytical predictions are in reasonable agreement with the test results. The test to predicted ratios range from 0.76 (AP1) to 1.12 (MP3B), with a mean value of 0.94 and the corresponding standard deviation of 0.11. These ratios are also shown graphically in Fig. 9.4. For comparison purposes, the elastic buckling loads of all the specimens were also evaluated and are shown in Table 9.1. It can be observed that, in general, the elastic buckling loads of the specimens are significantly higher than the test ultimate loads, except for specimen SP2, which was governed by the elastic buckling mode.

To examine the analytical results, the in-plane stress contour plots, the principal stress vector plots, and the in-plane deformation plots of the specimens (except those of the EP type) will be discussed in the following sections according to the types of specimen. Since there is no significant difference in the buckling shapes for the specimens, only a general discussion of the buckling mode will be presented. The analytical results of the EP type specimens will be presented following the section of the discussion of buckling shapes. Comparisons of the analytical results among test parameters will also be included.

## **9.4.2 GP and SP Type Specimens**

### **9.4.2.1 In-Plane Stress Distribution**

To investigate the compressive behavior of the specimens, their in-plane stress distributions from the analyses are examined. The postprocessing routine of ANSYS allows the display of the in-plane stress distributions in terms of stress contour lines. In producing these contour plots, the von Mises effective stress was used. Since the experimental yielding

behavior of specimen GP1 was recorded thoroughly at various load levels during testing, the analytical yielding behavior of specimen GP1 will be examined in detail and compared with the test results. The effective stress contour plots of specimen GP1 are shown in Figs. 9.5a to 9.5e at various load levels as indicated. As a reminder, the unit of the effective stress is MPa. As can be seen from Fig. 9.5a, the yielding of the gusset plate area near the last row of bolts (Whitmore effective width section) was observed at a load level of 1370 kN. However, at this stage of loading most of the gusset plate area was still in the elastic range. It can also be seen that the short free edge was loaded more severely than the long free edge. At a load of 1500 kN, the effective stress distribution of the gusset plate changed moderately indicating that a redistribution of load had occurred due to inelastic action. The maximum effective stress at this stage occurred at the top right corner of the gusset plate, as indicated in Fig. 9.5b. A slight yielding was also observed at the plate area about the sides of the splicing member. Approximately 30% of the gusset plate area was in the inelastic range when the applied load was 1700 kN, as shown in Fig. 9.5c. General yielding of the plate was observed at the area around the last row of bolts and about the sides of the splice member. The yielding at the area around the last row of bolts extended towards the beam and column boundary when compared with the yielding zone at the previous load level. For the gusset plate area along the sides of the splicing member, the yielding progressed upwards and also towards the free edges. At a load of 1950 kN, about 65% of the area was in the inelastic range, as shown in Fig. 9.5d. A significant increase in stress levels when compared to that of the previous load level was also observed at the plate along the sides of the splicing member. Figure 9.5e shows the effective stress plot for specimen GP1 at an ultimate load of 2336 kN. It can be seen from this figure that about 85% of the gusset plate area was yielded. The yielding basically extended from the Whitmore effective width section to the entire area, except near the column boundary and the fixed end of the free edges. A similar yielding behavior and process were recorded during the testing of specimen GP1, as mentioned in Chapter 3 and shown in Fig. 3.14.

Based on the above discussion, it can be seen that a significant part of the gusset plate can reach the yield strength of the material. However, the connection must be stiff enough to avoid early instability failure. If the connection is relatively slender, elastic buckling may occur before the gusset plate can even reach the corresponding Whitmore load (Cheng et al. 1994).

For specimens GP2 and GP3, similar yielding patterns and stress distributions as those of specimen GP1 at the early loading stage were observed. However, the extent of yielding was not as significant. In particular, for specimen GP3, only minor yielding occurred at the plate area near the last row of bolts when the specimen reached the ultimate load. Since the analytical elastic buckling load of specimen GP3 was very close to the experimental ultimate load, it would not require a significant amount of inelastic deformation to cause plastic bifurcation buckling. For specimen SP1, a similar stress pattern to that of GP1 was observed since the same brace angle and similar plate aspect ratio were used for both types of specimens. However, for specimen SP2, no yielding developed and the plate was failed in elastic buckling.

To compare the stress prediction by ANSYS in the elastic range, the test result from specimen GP1 was used. The comparison was made at the rosette gages location in the elastic range at a load level of 1220 kN. The experimental strain readings were first converted to the principal values, and then these values were used with the two-dimensional Hook's law to evaluate the corresponding principal stresses. These principal stresses were then converted to the von Mises effective stress and compared to the ANSYS effective stress contour plot as shown in Fig. 9.6. It can be seen from this figure that a good prediction of stress was obtained from the analysis.

#### **9.4.2.2 Principal Stress Vector and In-Plane Deformation Plots**

The principal stress vectors plots produced by ANSYS were also used to examine the flow of force through the gusset plate to the beam and column boundary and also illustrated the behavior of in-plane bending. The stress vectors indicate a compression (tension) when the arrowheads of the vectors point inward (outward). Again, specimen GP1 was used for the illustration. The principal stress vectors plots at a load level of 1370 kN and the ultimate load level of 2336 kN were used for illustrational purposes, as shown in Figs 9.7a and 9.7b respectively. These figures show that the principal stress directions in the free edges area were almost parallel to the corresponding free edges especially in the lower load level. However, the direction of the principal stress vectors approached the angle of the bracing member, especially in the area around the end of the splicing member at which the stress vectors were almost aligned with the angle of the brace. In addition, this area was the most stressed one, as can be seen from the lengths of the stress vectors which were scaled to the actual stress values. The plate area near the last row of bolts and bounded by the beam boundary was also severely loaded, and the stress vectors were oriented at approximately  $60^\circ$  to the horizontal, as shown in the figures. It can be seen from these figures that the beam boundary attracted more load since it was closer to the last row of the bolts.

Transverse compression was observed at the top right part of the gusset plate, which was also the location of maximum stress at ultimate. This transverse compression was due to the significant in-plane deformation at the bolt points, as shown in Figs. 9.8a and 9.8b. The in-plane deformation mode and the principal stress plot of specimen GP1 shown in Fig. 9.8a and 9.7a respectively indicate that in-plane bending occurred at both free edges. This in-plane bending can also be observed in the stress contour plot, as shown in Fig. 9.5a, which illustrates that the stress gradient occurred in the free edges. The stress vector plot shown in Fig. 9.7b also indicates that compression occurred in the other principal direction perpendicular to the applied load direction. This compression was caused by the

displacement restraint applied to the beam and column boundary, which prohibited the lateral displacement of the plate due to Poisson's ratio effect. As will be seen in a later discussion, if the beam and column are allowed to deform (in-plane) when the load is applied to the gusset plate, tension instead of compression will occur.

### **9.4.3 AP Type Specimen**

#### **9.4.3.1 In-Plane Stress Distribution**

For this particular type of specimen, only the in-plane stress distribution for specimen AP1 at a load level of 1380 kN is discussed. It is believed that this is sufficient to demonstrate the in-plane stress behavior of this type of specimen. The in-plane stress distribution is shown in Fig. 9.9. It can be seen from this figure that the plate area underneath the splicing member was severely loaded. In addition, this highly stressed area was extended to the beam and column boundary. A high stress gradient was also observed at the short side free edge caused by the in-plane bending, as will be discussed in the following section. For this specimen, the maximum stress occurred at the top right part of the gusset plate, as shown in the figure.

#### **9.4.3.2 Principal Stress Vector and In-Plane Deformation Plots**

The principal stress vector plot and the in-plane deformation plot are shown in Figs. 9.10 and 9.11 respectively. It can be seen from Fig. 9.10 that the plate area underneath the splice member was highly stressed. Again, the principal compressive stress vectors in this area were almost aligned with the brace angle. Transverse tension was observed in the plate. As mentioned above, this tensile stress was developed due to the in-plane deformation of the supporting beam and column boundary when the axial load was applied. This in-plane deformation can be observed from the in-plane deformation plot of the gusset plate specimen, as shown in Fig. 9.11. This figure shows that the column boundary



deflected quite significantly when it is compared with the deformation at the beam boundary. It also illustrates that in-plane bending existed in both free edges, especially in the short free edge. The severity of this in-plane bending at the short free edge can also be observed from the principal stress vector plot where tensile stress existed in almost all the elements at the short free edge as, shown in Fig. 9.10.

#### **9.4.4 MP Type Specimens**

##### **9.4.4.1 In-Plane Stress Distribution**

The general discussion of the in-plane stress distribution for the MP type specimen will be based on specimen MP1. However, the effects of the beam and column moment will be presented in the following section of discussion and comparison of analytical results. Two load levels of 300 kN and 1500 kN were considered in this section. It should be noted that full beam and column moment values were applied to the specimen at these load levels. The stress contour plots for these load levels are shown in Figs. 9.12a and 9.12b. As can be seen from Fig. 9.12a when the applied load was relatively small (300 kN), the in-plane stress distribution was predominantly influenced by the beam and column moment. This can be illustrated by the fact that maximum tensile stress occurred at the fixed ends of the free edges due to the beam and column moment at the applied load of 300 kN. On the other hand, as the applied load increased to 1500 kN, the stress distribution was significantly altered, as shown in Fig. 9.12b. Again, the highly stressed area was located underneath the splicing member, although the maximum stress occurred at the top right part of the gusset plate. A high stress gradient also existed at the short free edge area, as shown in Fig. 9.12b.

#### **9.4.4.2 Principal Stress Vector and In-Plane Deformation Plots**

The principal stress vector plots and the in-plane deformation plots at the load levels of 300 kN and 1500 kN are shown in Figs. 9.13a and 9.13b respectively. It can be seen from Fig. 9.13a that the beam and column moment severely loaded the part of the plate closer to the beam and column boundary and produced principal tensile stress at this region, in particular in the area close to the fixed ends of the free edges. When the applied load increased to 1500 kN, the stress vector plot indicated that the axial load effect became more dominant. Again, the principal compressive stress vectors were almost aligned with the brace angle, especially in the area underneath the splicing member, as shown in Fig 9.13b. However, the elements near the fixed ends of the free edges still showed principal tensile stresses at this high load level.

The in-plane deformation at the load level of 300 kN is shown in Fig. 9.14a. This figure also includes the beam and column deflection. As can be seen from this figure, significant deflection was observed for the beam and column due to the applied concentrated loads at their ends. This figure also shows that the beam and column deformation stretched the gusset plate. The tensile stress produced by this stretching was oriented according to the principal tensile stress vector, as shown in Fig. 9.14a. The in-plane deformation plot at the load level of 1500 kN is shown in Fig. 9.14b. Again, in-plane deflection was observed at the beam and column boundary.

#### **9.4.5 Buckling Shapes of Specimens**

The typical buckling shapes of each type of specimens (except EP type) are shown in Figs. 9.15a to 9.15d. For illustrational purposes, the splicing members were removed from the model. It can be seen from these figures that, in general, similar buckling shapes were observed for the specimens. Since the bracing member was allowed to sway out-of-plane, the buckling shapes of these specimens at the free edges and the plate area underneath the

splicing member resembled the buckling shape of a fixed-guided column. However, a slight twisting at the conjunction of gusset-to-splice was observed, especially with the AP type specimens. This slight twisting was mainly caused by the unsymmetrical gusset plate section for all the specimens and, in addition, the  $30^\circ$  brace angle for the AP type specimens. However, it can be seen from these figures that the spliced region remains relatively straight for all the specimens.

#### **9.4.6 EP Type Specimens**

##### **9.4.6.1 Load Deflection Behavior**

As mentioned above, load deflection analysis was employed to evaluate the ultimate strength of the EP type specimens. The experimental and analytical load deflection curves for the specimens are shown in Figs. 9.16 to 9.18. It can be seen from these figures that the analysis predicts very well the experimental ultimate load of the specimens. The test to predicted ratios range from 0.97 to 1.05. However, the predictions by ANSYS show a stiffer load deflection behavior for the specimens. This may be due to the effects of the assumed idealized boundary conditions in the finite element model and the initial imperfections that could exist in the connection. Nevertheless, for specimens EP1 and EP2 the predicted load deflection curves are generally in good agreement with the test results.

##### **9.4.6.2 In-Plane Stress Distribution**

Since specimens EP1 and EP2 are similar, except for the splice plate thickness, only the discussion of the in-plane stress distribution of specimen EP1 will be presented. The in-plane stress distributions of the splice plate for specimen EP1 are shown in Figs 9.19 and 9.20. Fig 9.19 illustrates the in-plane stress for the top surface of the splice plate and Fig. 9.20 shows the bottom surface stress. The in-plane stress shown in these figures is in the local element x-axis, as illustrated in Fig. 9.3b. It can be seen from these figures that the

splice plate area near the last bolt line from the end of the brace member was stressed significantly. The bottom stresses at this location were well above the static yield strength of the material, and the top stresses were very close to yield. The test results also indicated that significant yield lines occurred in this region when the applied load was near ultimate. To illustrate that a significant bending stress existed in the splice plate, a plot of surface stresses along the centerline of the length of the splice plate is shown in Fig. 9.21. This figure shows that the bending of the splice plate was mainly concentrated in the vicinity of the last bolt line. It should be noted that high compressive stresses existed in the top surface of the splice plate for the part of the splice plate connected to the gusset plate, whereas the compressive stresses in the bottom surface were reduced in this region. This is due to the bending action of this region, which induced significant compressive bending stress to the top surface and tensile bending stress to the bottom surface of the splice plate.

The top and bottom surface in-plane stress distributions of the gusset plate are shown in Figs. 9.22 and 9.23. It can be seen from these figures that the gusset plate was stressed significantly from the effects of bending in a strip of area joining the two fixed ends of the free edges. The top stress levels in this strip of area were generally greater than the static yield strength of the gusset plate material. The test results also showed that yield lines in the gusset plate originating from the end of the splice plate to the beam boundary were observed as illustrated in Fig. 7.11. For the bottom surface stress, stress levels very close to yield were observed in this strip of gusset plate area. It can be seen from the analytical results of specimens EP1 and EP2 that plastic hinges were developed at the splice plate near the end of brace and along the strip of gusset plate area as mentioned above. These plastic hinges provided a failure mechanism for the connection, which was also observed in the test results. This plastic collapse mechanism will be discussed in the following section.

For specimen EP3, compressive yielding was observed for the 9.5 mm thick splice plate on both the top and bottom surfaces, as shown in Figs. 9.24a and 9.24b. The tee-section

splice member showed tensile yielding near the tip of the web at the conjunction of the gusset-to-splice at the ultimate load. As shown in Fig. 7.15, these observations compared well with the test results for the plot of load versus strain gauge readings recorded at the splice plate and the web of the tee-section. The gusset plate in-plane stress distributions for specimen EP3 are shown in Fig. 9.25a and 9.25b. Again, the strip of area joining the fixed ends of the free edges was highly stressed for both top and bottom surfaces. In particular, the gusset plate area underneath the splice members was severely stressed as indicated by the contour lines. This observation also confirms the test results wherein diagonal yield lines resulting from the applied axial load and yield lines resulting from the bending effects were observed, as shown in Fig. 7.1.

#### **9.4.6.3 Principal Stress Vector and Out-of-Plane Deformation Plots**

Since the principal stress vector plots for the gusset plate of the EP type specimens are similar, only specimen EP1 will be discussed. The principal stress vector plots for both the top and bottom surfaces of specimen EP1 are shown in Figs. 9.26 and 9.27. It can be seen from these figures that significant bending of the gusset plate was observed. The top surface of the gusset plate, which was connected to the bottom surface of the splice plate, was in severe compression, due to the combination of the axial compressive stress and the compressive bending stress. On the other hand, the bottom surface of the gusset plate was loaded in tension due to the significant bending effects.

The out-of-plane deformation plots for the EP type specimens are shown in Figs 9.28 to 9.30. It can be seen from these figures that significant bending deformation was observed at both the gusset plate and the splice member at the conjunction of gusset-to-splice. To examine closely the deformation mode of the splice member, a plot of out-of-plane displacement along the centerline of the splice plate for specimens EP1 and EP2 are produced, as shown in Figs. 9.31 and 9.32. These figures illustrate that a significant

rotation of the splice plate occurred in the vicinity of the location of gusset-to-splice and also at the gusset plate near the end of the splice plate. These observed rotations substantiated that plastic hinges were developed at these locations.

## **9.5 Discussion and Comparison of Analytical Results**

### **9.5.1 General**

As mentioned in the previous section, the predictions by ANSYS were in reasonable agreement with the test results. The test to predicted ratios varied from 0.76 to 1.12, as illustrated in Table 9.1 and Fig. 9.4. As can be seen from this figure, conservative predictions are always observed for the 6.5 mm thick specimens except for specimen MP3. However, the ultimate loads for the rest of the specimens were over-estimated. This is probably due to the use of the bifurcation buckling concept and also the nature of finite element method that usually produces a stiffer model of the structure. Nevertheless, these predictions do provide a reasonable estimate of the compressive strength of the specimens. A design method will be proposed, based on the test and analytical results and presented in the following chapter. The effects of various parameters on the compressive behavior and strength of the gusset plate specimens will be discussed in the following sections.

### **9.5.2 Effects of Gusset Plate Thickness and Size**

As can be seen in Table 9.1, as the gusset plate thickness increased, the ultimate load of the specimens increased. In order to compare with the test results, a linear regression line was fitted to the analytical results and the test results were also plotted on the same graph, as shown in Fig. 9.33. As mentioned above, the predictions were in general higher than the experimental ultimate loads, except for the 6.5mm thick specimens. This figure also shows that as the plate thickness increases, the difference between the test results and the analytical predictions increases. However, no reason can be found to explain this observation. In

general, for the same plate size the amount of yielding observed from the specimens in the analysis decreased with decreasing plate thickness, as described in the previous section. As the plate thickness decreases, the specimen may fail by instability before reaching the load level which causes inelastic deformation.

Table 9.1 shows that the predicted ultimate loads of the specimens decreases with increasing plate size. As expected, the slenderness of the gusset plate increases with increasing plate size and thus leads to a decrease in ultimate load. The amount of inelastic deformation also decreased with increasing plate size, as indicated from the analysis. It was also observed from both the tests and the analysis that elastic buckling occurred in specimen SP2 (850 x 700 x 9.8).

### **9.5.3 Effects of Angle of Diagonal Brace Member (45° and 30°)**

In general, the analytical ultimate loads of the AP type specimens (30° brace angle) are slightly lower than those of the corresponding GP type specimens (45° brace angle), except for specimen AP3. However, Table 9.1 illustrates that the test results showed an appreciable difference between the ultimate loads of the AP and GP type specimens. Nevertheless, it can be seen that the ultimate loads of the specimens were not significantly affected by changing the brace angle from 45° to 30°. On the other hand, changing the brace angle affected the in-plane stress distribution of the specimens.

The effective stress distribution of specimens GP1 and AP1 are shown in Figs. 9.5a and 9.9 respectively. It can be seen that for specimen AP1, the severely loaded area underneath the splicing member was significantly increased, when compared to that of specimen GP1. In addition, a higher stress gradient for specimen AP1 existed in the free edges, as shown in Fig. 9.9. In fact, tensile stress was observed at the fixed end of the short free edge as shown by the principal stress vector plot in Fig. 9.10. This observation was also recorded from the strain gage readings from the test results. As mentioned in the previous chapter of

test results, this tensile stress was probably caused by the in-plane bending resulting from the larger horizontal component of the applied force for the AP type specimens. However, this was not observed in the GP type specimens.

#### **9.5.4 Effects of Beam and Column Moments**

As can be seen from both the test and the analytical results, in general the beam and column moments did not significantly affect the ultimate loads of the specimens. In fact, the predictions by ANSYS showed very similar ultimate loads for the specimens with the same thickness and size, regardless of the presence of beam and column moments. The effects of beam and column moment levels on the ultimate loads of the specimens were also examined by varying the moments applied to the 6.5 mm thick MP type specimens. As can be seen from Table 9.1, the analytical ultimate loads of these specimens did not vary substantially when the beam and column moment levels were increased. However, as mentioned in the test results, the beam and column moments influenced the in-plane behavior of the specimens. To examine this observation in detail, the analytical results of MP3 specimens (MP3, MP3A and MP3B) are used. Figs 9.34a to 9.34c show the effective stress contour plots for the specimens at the same applied load level of 630 kN. One significant observation from these figures is that the effective stress increased when the applied beam and column moments increased. This explains the test results which demonstrate that when the beam and column moments were applied to the specimens, a significant additional increase in compressive strains was detected in the rosette gages. The additional increase in compression also contributed to the decrease in the in-plane stiffness of the specimens due to the early yielding initiated by this compression, as illustrated in the test results. The stress contour plots for specimens MP3 and MP3A also indicated that a high stress level existed at the fixed ends of the free edges due to the applied moments. Tensile strains close to yielding were also recorded at the strain gages located in the fixed ends of the free edges.



The principal stress vector plots shown in Figs. 9.35a to 9.35c indicate that a significant transverse tension due to the applied moments was observed in the specimens. As expected, this transverse tension increased with increasing applied moments, as indicated by the lengths of the stress vector. Again, significant tension was observed at the fixed ends of the free edges for the specimens (MP3 and MP3A) with applied moments. However, this tension was not observed from the specimen (MP3B) without applied moments, as shown in Fig. 9.35c. Different in-plane deformation modes are also observed for the specimens as shown in Figs. 9.36a to 9.36c. It can be seen from these figures that stretching of the plate was observed for the specimens with applied moments. This stretching is evident at the plate along the beam and column boundary and the free edges.

Based on the above discussion, it can be seen that beam and column moment produced both tensile and compressive stresses to the gusset plate. Since there was no significant increase or decrease in the ultimate loads of the specimens due to the applied moments, it is speculated that, although the increase in compression would have detrimental effects on the ultimate loads, the tensile stress would produce a beneficial stiffening effect on the specimens. Therefore, these two opposite stresses compensated each other and no significant change in ultimate loads was thus observed, due to the applied moments.

#### **9.5.5 Effects of Loading Eccentricity**

The test and analytical results both indicated that the presence of loading eccentricity significantly reduced the strength of the gusset plate connection and also produced a large out-of-plane deflection. It can be seen from the analysis that the loading eccentricity induced significant bending moment to both the splice member and the gusset plate. At the ultimate, plastic hinges were developed at the critical section of the splice member and also at the gusset plate. When the in-plane stress contour plots for specimens GP1 and EP3 are compared, it can be seen that the bending moment due to the loading eccentricity

significantly altered the in-plane stress distribution of the gusset plate. In particular, the gusset plate area underneath the splice member was stressed severely by both the axial load and the bending moment, which also produced high bending stresses in the vicinity of the fixed ends of the free edges, as typically shown by the stress vector plots of specimen GP1 in Figs. 9.25 and 9.26.

When the analytical load-deflection curves of the specimens were compared, it was found that the out-of-plane stiffness of the specimens increased as the thickness of the splice plate increased. In particular, the stiffness of specimen EP3 increased significantly due to the tee-section splice which provided bending rigidity to the connection.

## **9.6 Rigid Plastic Analysis of Specimens EP1 and EP2**

As mentioned above, both the test and analytical results indicated that plastic hinges were formed in the splice plate at the conjunction of gusset-to-splice and along a strip of gusset plate area joining the fixed ends of the free edges for specimens EP1 and EP2. Since a failure mechanism was developed by these plastic hinges, a rigid-plastic analysis of the specimens may provide useful information, especially in estimating the ultimate load of the connection. Kitipornchai et al. (1993) also employed the rigid plastic collapse analysis to evaluate the ultimate strength of the eccentrically loaded cleat plates. The rigid-plastic analysis provides an unloading line which represents the changes in the plastic collapse load due to the change in the plate geometry (Korol et al. 1972). The intersection of this unloading line with the elastic loading curve of the connection provides an upper bound estimate of the ultimate load of the structure.

The plastic collapse model for the specimens is shown in Fig. 9.37. The plastic hinges were assumed to be located at the splice plate and the gusset plate, as mentioned above. It should be noted that the plastic hinge in the gusset plate was assumed to be a horizontal line originating from the fixed end of the long free edge to the beam boundary (hinge A), as

shown in Fig. 9.37. A more appropriate plastic hinge would be the one labeled as hinge B, shown in Fig. 9.37. Nevertheless, the assumed plastic hinge (hinge A) provided a simple mechanism and also simplified the evaluation of the plastic moment capacity of the plate.

The equilibrium approach was used to derive the equation of the rigid-plastic unloading line of the connection. A free body diagram of the mechanism is shown in Fig. 9.37. The connection was assumed to have deflected  $\Delta$ , and plastic moment capacity was developed in both plastic hinges. However, the plastic moment capacity of the section was reduced by the interaction of the axial load and applied moment, according to:

$$M_{pc} = M_p \left( 1.0 - \left( \frac{P}{P_y} \right)^2 \right) \quad [9.2]$$

where  $P$  is the applied axial load,  $P_y$  is the yield load of the section,  $M_{pc}$  is the reduced plastic moment, and  $M_p$  is the plastic moment capacity of the section.  $M_{pcG}$  is the reduced plastic moment for the gusset plate and  $M_{pcS}$  is the reduced plastic moment for the splice plate, as shown in Fig. 9.37. The loading eccentricity produced an eccentric moment of  $P \cdot e$  as shown in the figure. Summing moment at the bottom plastic hinge gives:

$$M_{pcS} + M_{pcG} - P \cdot e - P \cdot \Delta = 0$$

therefore, 
$$P(e + \Delta) = M_{pcS} + M_{pcG} \quad [9.3]$$

According to eqn. 9.2, eqn 9.3 can be further reduced to:

$$P(e + \Delta) = M_{pS} \left( 1.0 - \left( \frac{P}{P_{yS}} \right)^2 \right) + M_{pG} \left( 1.0 - \left( \frac{P}{P_{yG}} \right)^2 \right)$$

where the subscripts S and G represent the splice plate and the gusset plate respectively. The above quadratic equation can be solved simply as:

$$P = \frac{-(e + \Delta) + \sqrt{(e + \Delta)^2 + 4 \left( \frac{M_{pS}}{P_{yS}^2} + \frac{M_{pG}}{P_{yG}^2} \right) (M_{pS} + M_{pG})}}{2 \left( \frac{M_{pS}}{P_{yS}^2} + \frac{M_{pG}}{P_{yG}^2} \right)} \quad [9.4]$$

The unloading line can be evaluated by assuming a  $\Delta$  and then solve for  $P$  from eqn. 9.3. A typical calculation of the unloading line for specimen EP1 is included in the appendix.

The rigid-plastic unloading lines for specimens EP1 and EP2 are shown in Figs. 9.38 and 9.39. As can be seen from these figures, an elastic curve was also included. The elastic curve was evaluated using ANSYS, which considered only the large deflection behavior of the connection. In general, the unloading lines for both specimens underestimated the unloading behavior of the specimens. However, for specimen EP1, the slope of the unloading curve was quite similar to that of the experimental curve. This underestimation of the unloading behavior was probably due to the assumption of the plastic hinge location in the gusset plate and also the strain-hardening of the material, aspects which were not included in the analysis. Murray (1981) investigated this effect of strain-hardening on the unloading line and concluded that if the static yield strength was increased by 20-30%, a better agreement between the tests and analysis would be achieved. To obtain an upper bound estimate of the ultimate load of the specimens, the intersection of the unloading line and the elastic curve was used. As can be seen from these figures, the intersection of the unloading line and the elastic curve for both specimens gives an ultimate load of approximately 10% higher than the test loads. The plastic collapse loads for these specimens are shown in Table 9.2. Hence, it can be seen that by employing the rigid-plastic analysis and the elastic analysis (both of which do not require enormous computation time)

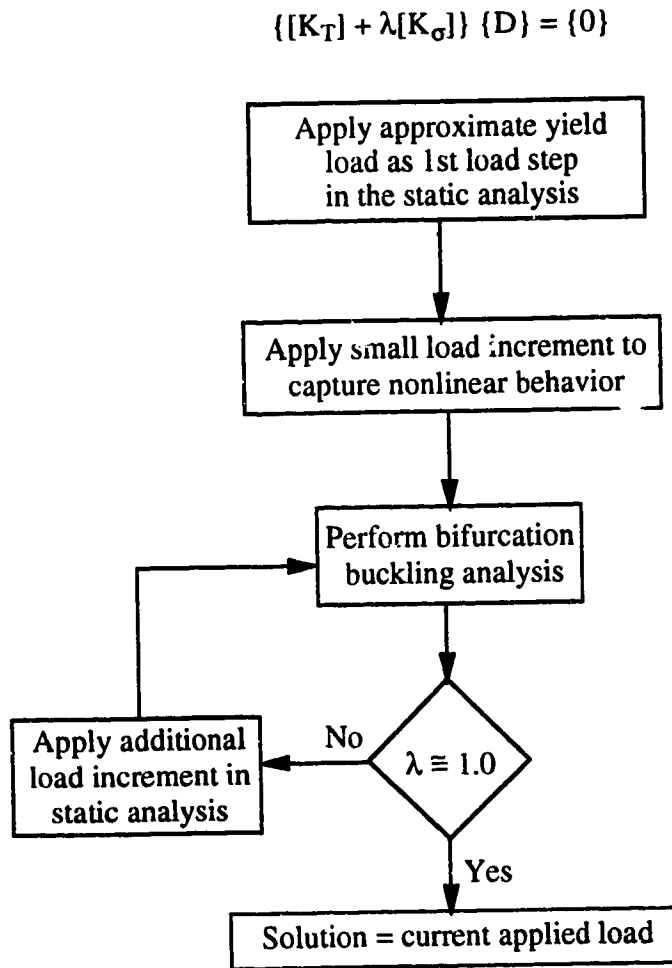
the upper bound of the ultimate load of the eccentrically loaded gusset plate connections can be evaluated.

Table 9.1 Analytical Plastic Bifurcation Buckling Loads of Test Specimens

Specimen	Ultimate Load		$\frac{P}{P_{ANSYS}}$	Elastic Buckling Load $P_E$
	P	$P_{ANSYS}$		
	(kN)	(kN)		(kN)
GP1	1956	2336	0.84	5428
GP2	1356	1483	0.91	2638
GP3	742	680	1.09	836
SP1	1606	1940	0.83	2169
SP2	1010	940	1.07	940
AP1	1720	2260	0.76	6476
AP2	1210	1460	0.83	3181
AP3	728	690	1.06	910
MP1	1933	2320	0.83	6075
MP2	1316	1450	0.91	3118
MP3	721	755	0.95	985
MP3A	819	765	1.07	985
MP3B	821	735	1.12	985
EP1	310	321	0.97	-
EP2	334	342	0.98	-
EP3	890	846	1.05	-

Table 9.2 Rigid-Plastic Collapse Load for Specimens EP1 and EP2

Specimen	Ultimate Load		$\frac{P}{P_{RPC}}$
	P	Rigid-Plastic Collapse Load $P_{RPC}$	
	(kN)	(kN)	
EP1	310	341	0.91
EP2	334	364	0.92

**Plastic Bifurcation Buckling Analysis****Figure 9.1** Flow Diagram for Plastic Bifurcation Buckling Analysis

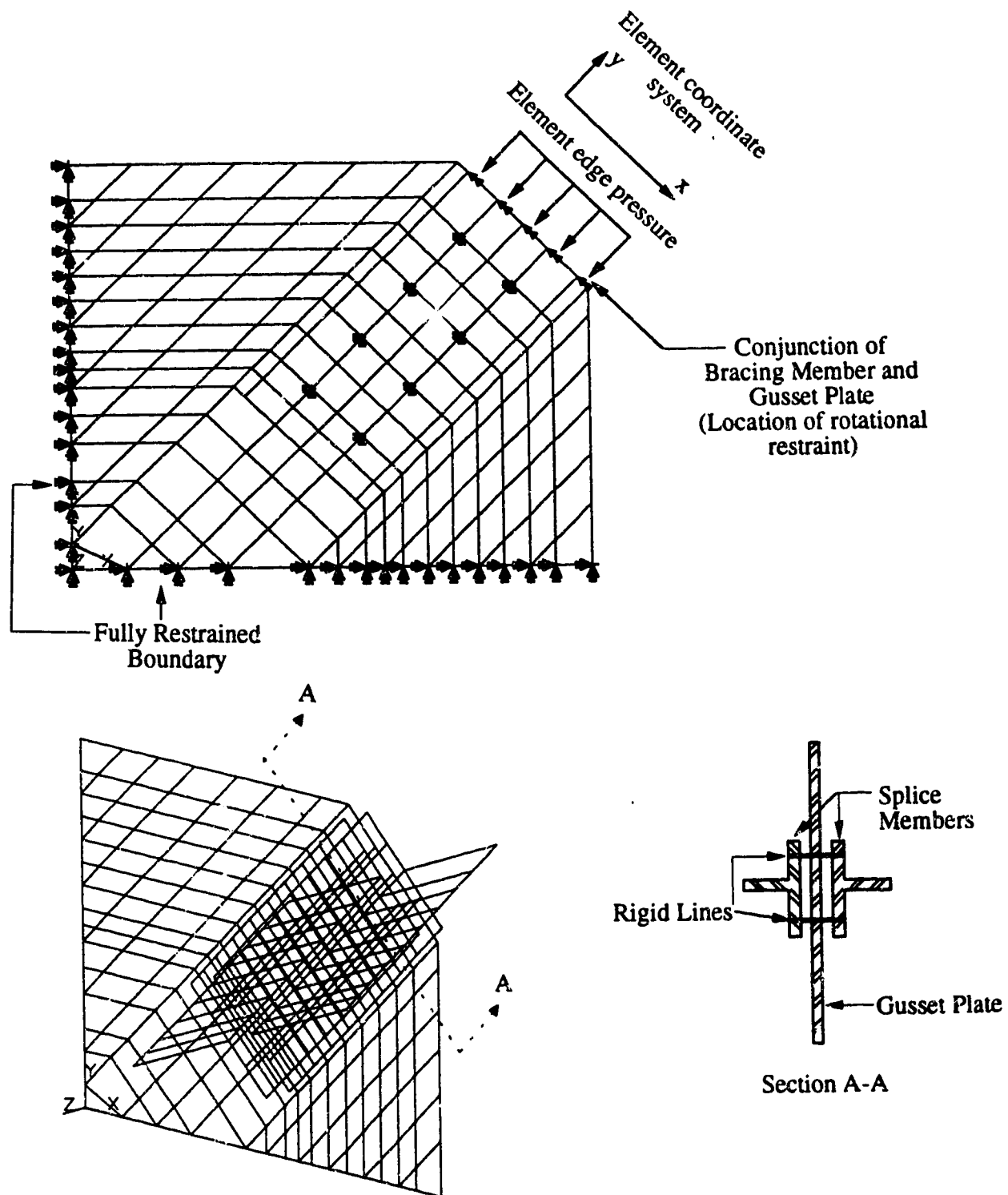


Fig. 9.2 Finite Element Model for GP and SP Type Specimens



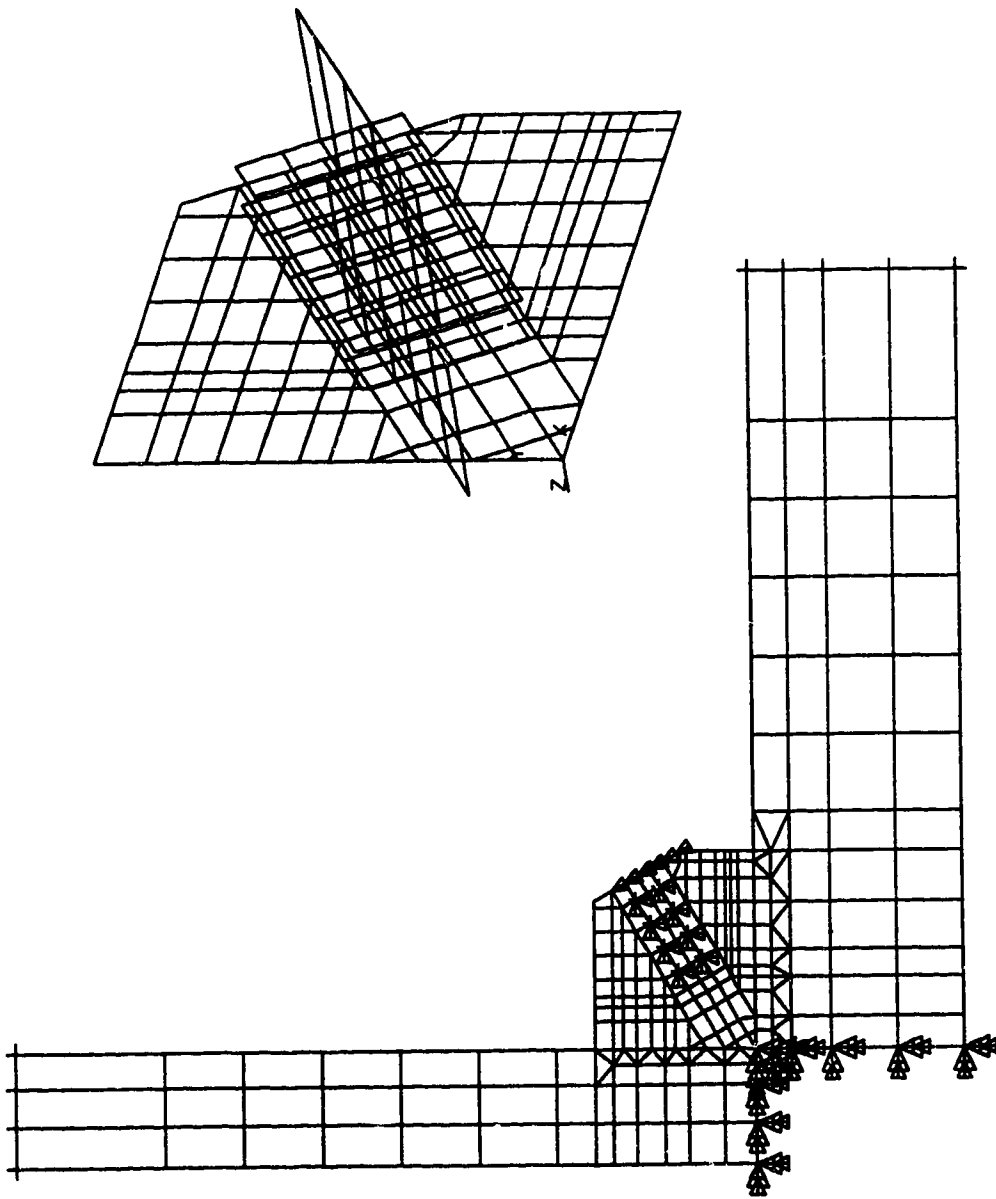


Fig. 9.3a Finite Element Model for AP and MP Type Specimens

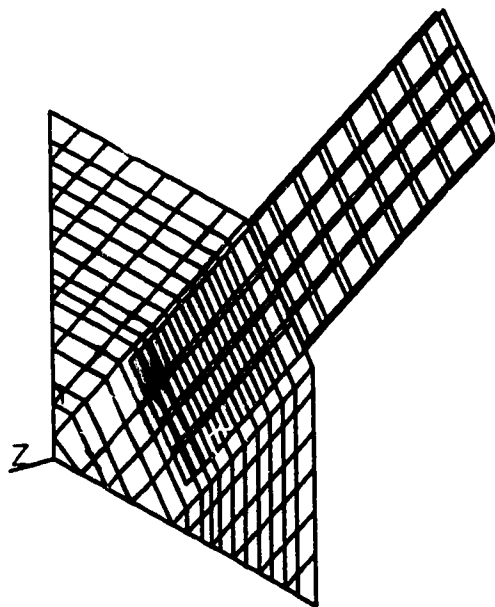
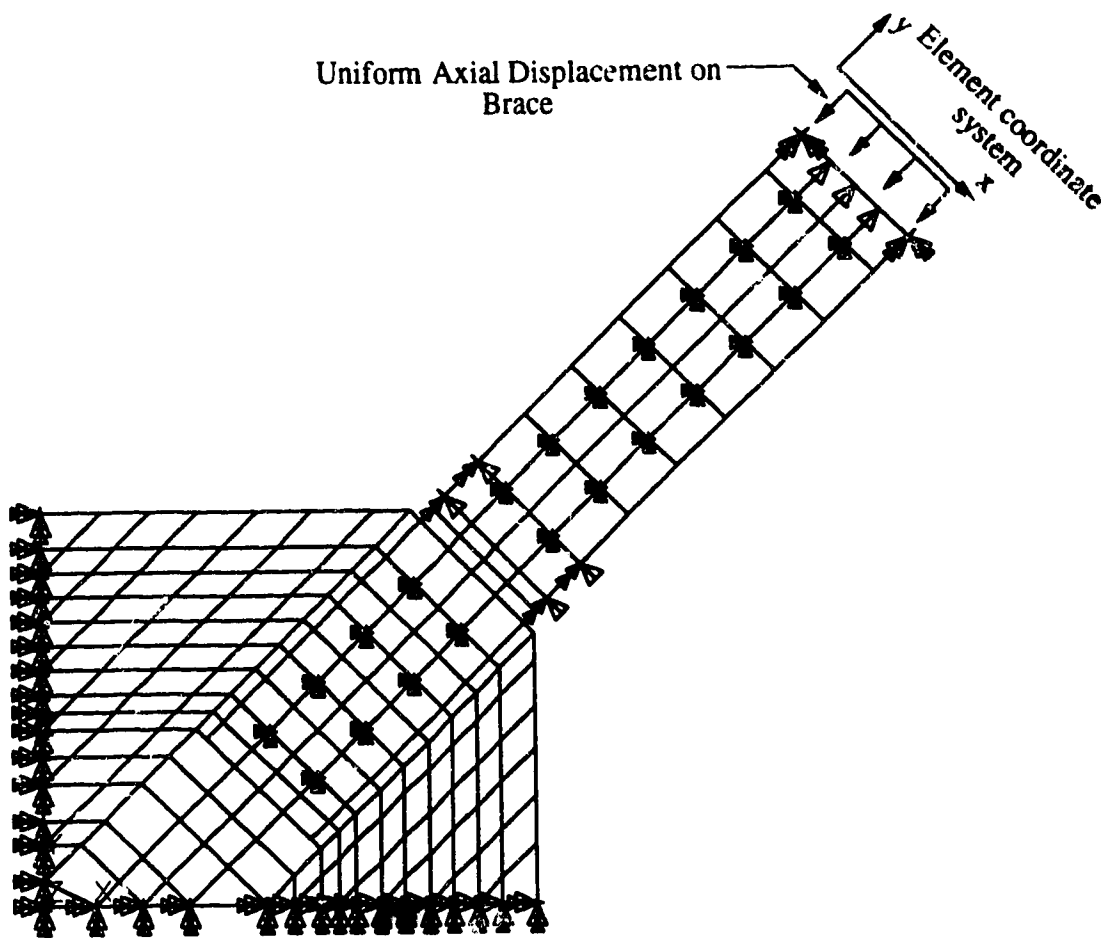


Fig. 9.3b Finite Element Model for EP Type Specimens

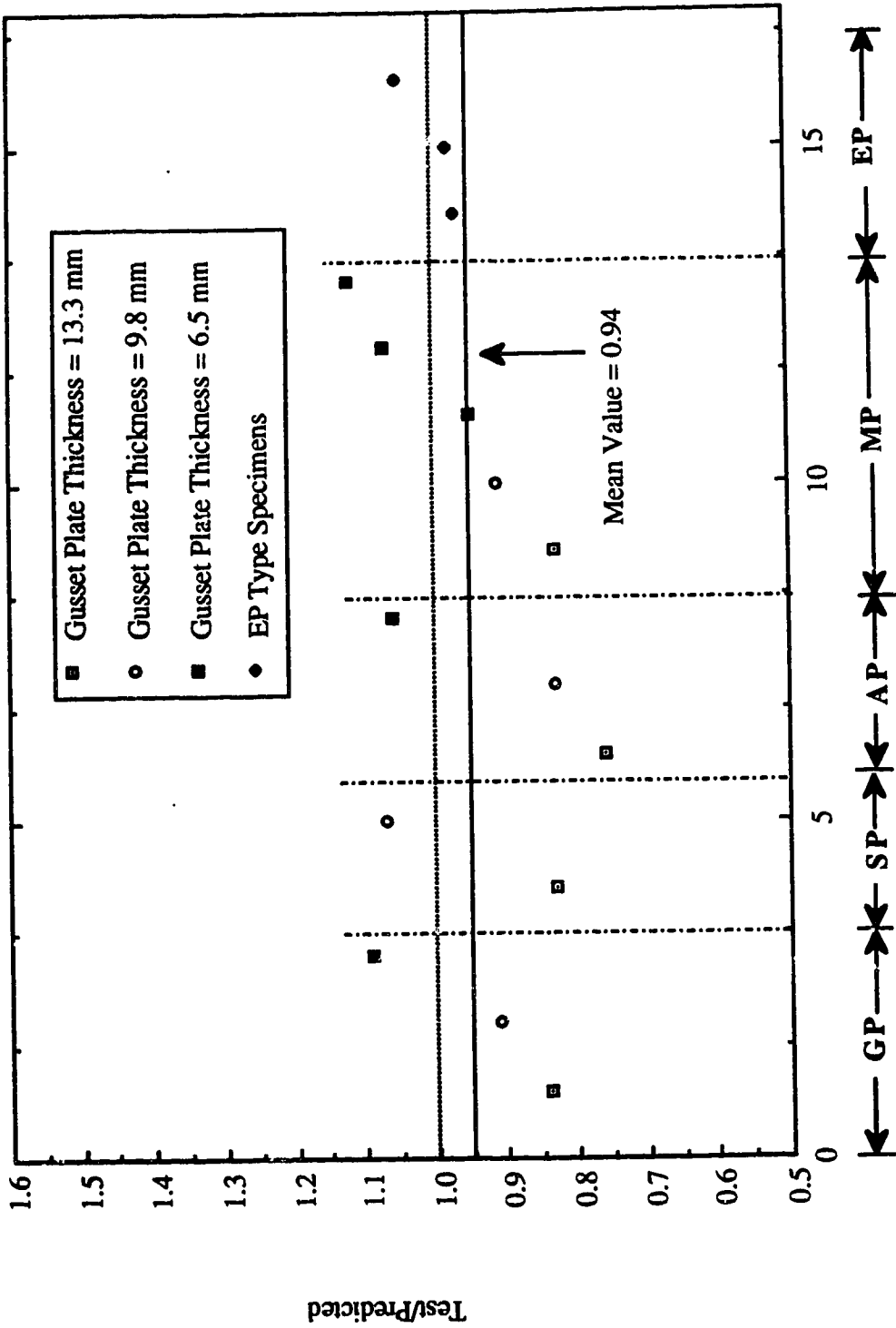


Fig. 9.4 A Plot of Test to Predicted(ANSYS) Ratios for Various Specimens

ANSYS 4.4A  
FEB 25 1993  
11:47:26  
PLOT NO. 1  
POST1 STRESS  
STEP=8  
ITER=15  
SIGE (AVG)  
MIDDLE  
SMX =329.293  
ZV =1  
DIST =275  
XYF =250  
=200  
=40  
=80  
=120  
=160  
=200  
=240  
=280  
=320  
ABCDEFGHI

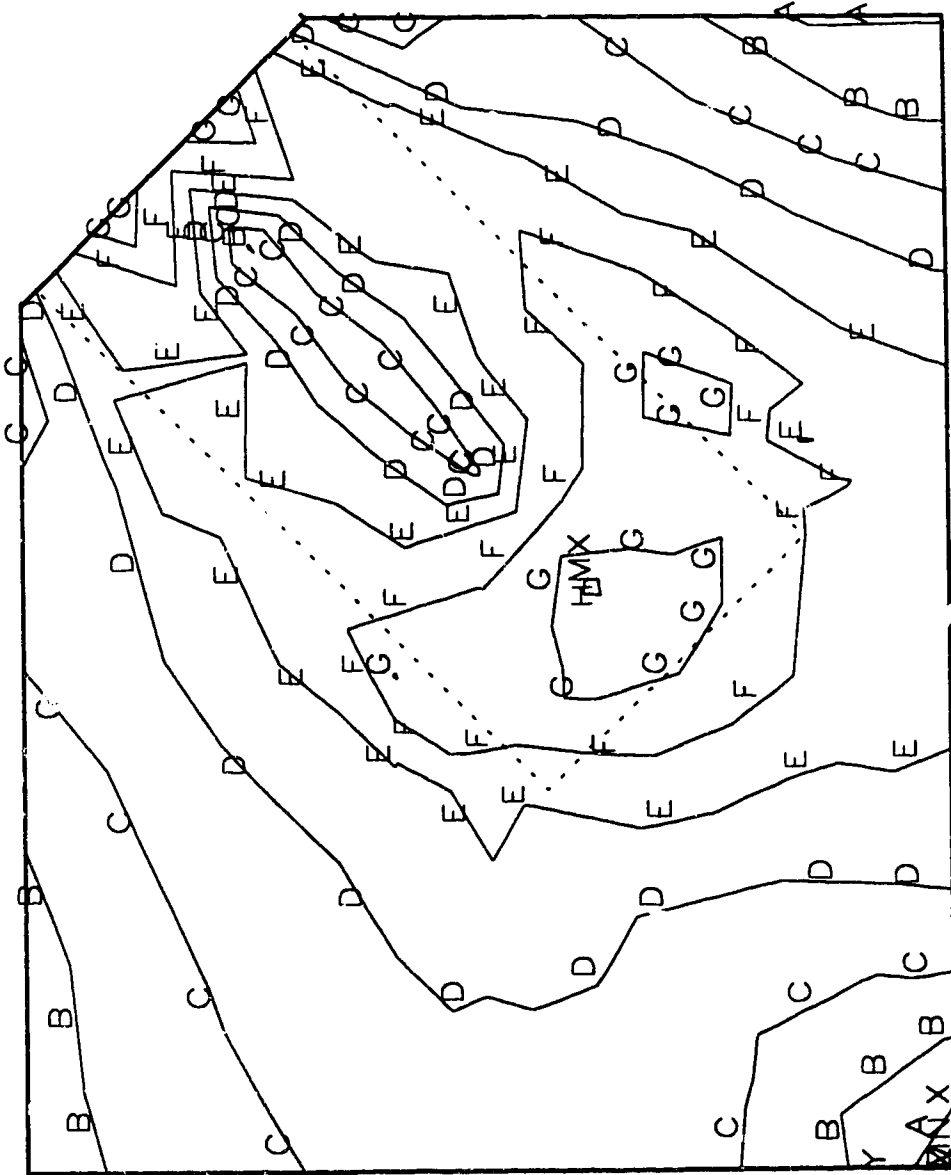


Fig. 9.5 a In-Plane Stress Contour for Specimen GP1 at P = 1370 kN

ANSYS 4.4A  
 FEB 25 1993  
 11:59:04  
 PLOT NO. 1  
 POST1 STRESS  
 STEP=14  
 ITER=15  
 SIGE (AVG)  
 MIDDLE  
 DMX =0.514726  
 SMX =400.109  
 ZV =1  
 DIST=275  
 XF =250  
 YF =200  
 A =50  
 B =100  
 C =150  
 D =200  
 E =250  
 F =300  
 G =350  
 H =400

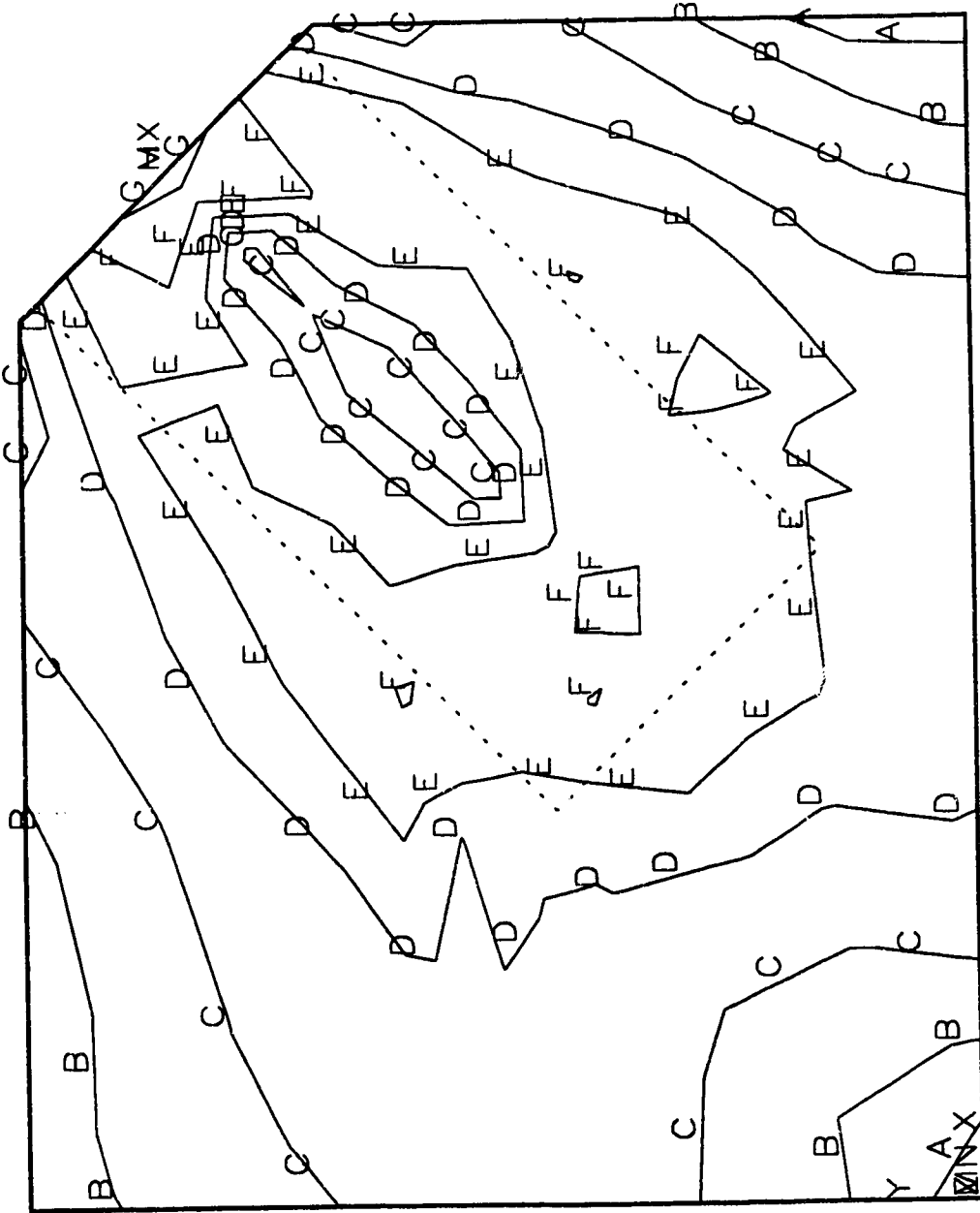


Fig. 9.5b In-Plane Stress Contour for Specimen GP1 at P = 1500 kN

ANSYS 4.4A  
FEB 25 1993  
12:04:39  
PLOT NO. 1  
POST1 STRESS  
STEP=22  
ITER=15  
SIGE (AVG)  
MIDDLE  
DMX =1.711  
SMX =430.275  
ZV =1  
DIST=275  
XF =250  
YF =200  
A =100  
B C D E F C H  
=150  
=200  
=250  
=300  
=350  
=400  
=450

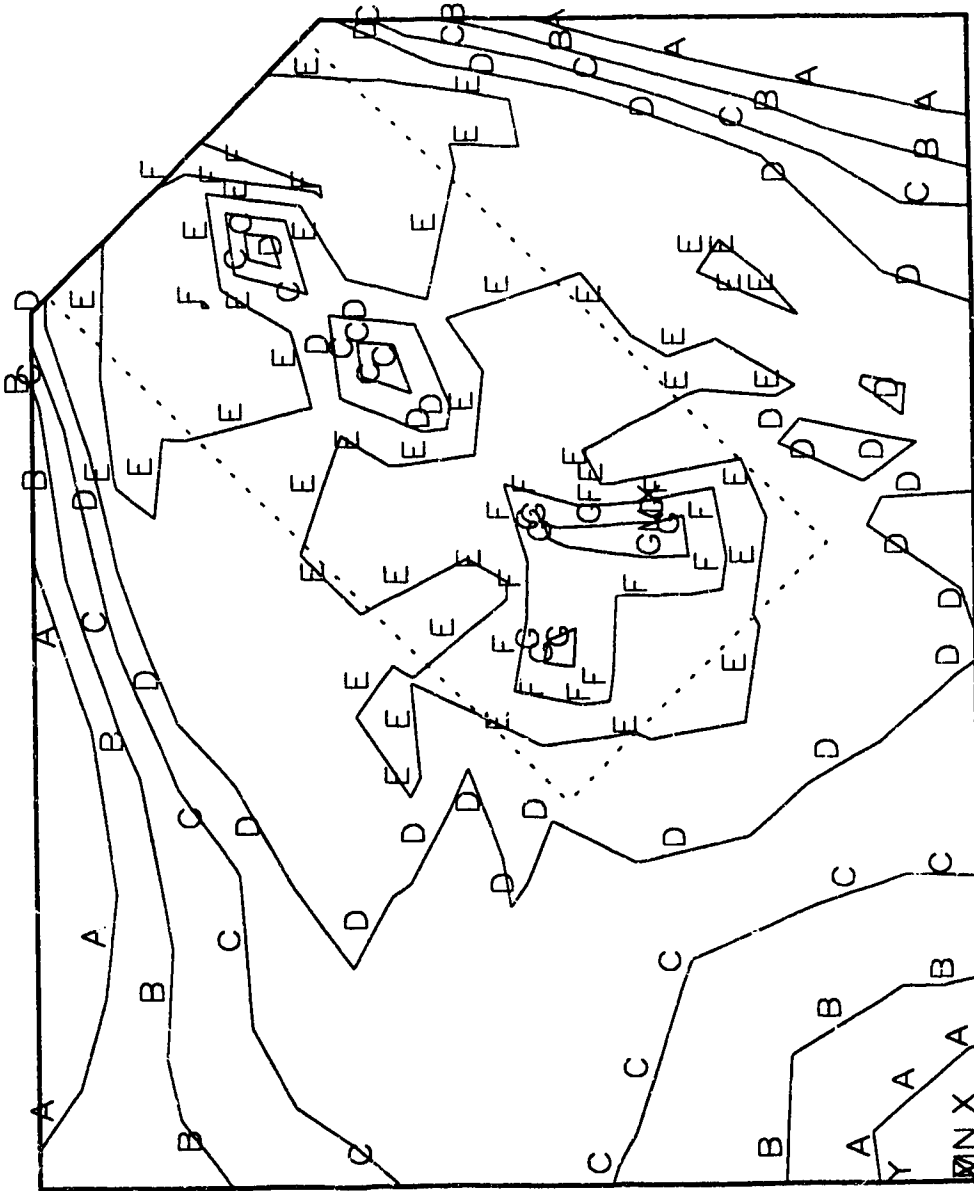


Fig. 9.5c In-Plane Stress Contour for Specimen GP1 at P = 1700 kN

ANSYS 4.4A  
 FEB 25 1993  
 12:45:08  
 PLOT NO. 1  
 POST1 STRESS  
 STEP=32  
 ITER=15  
 SIGE (AVG)  
 MIDDLE  
 DMX =3.463  
 SMX =480.215

ZV =1  
 DIST=275  
 XF =250  
 YF =200  
 =60  
 =120  
 =180  
 =240  
 =300  
 =360  
 =420  
 =480

A B C D E F G H I

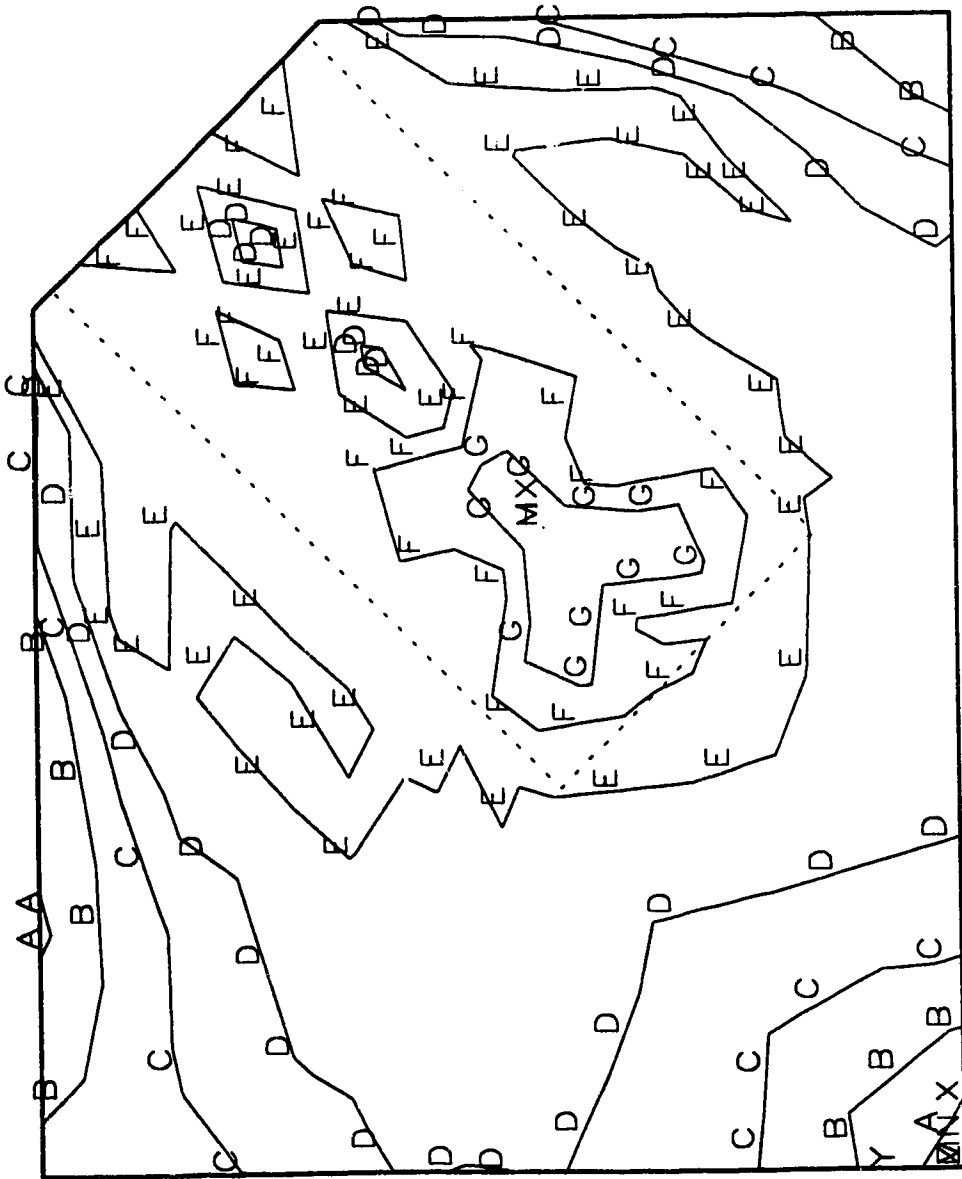


Fig. 9.5d In-Plane Stress Contour for Specimen GP1 at P = 1950 kN

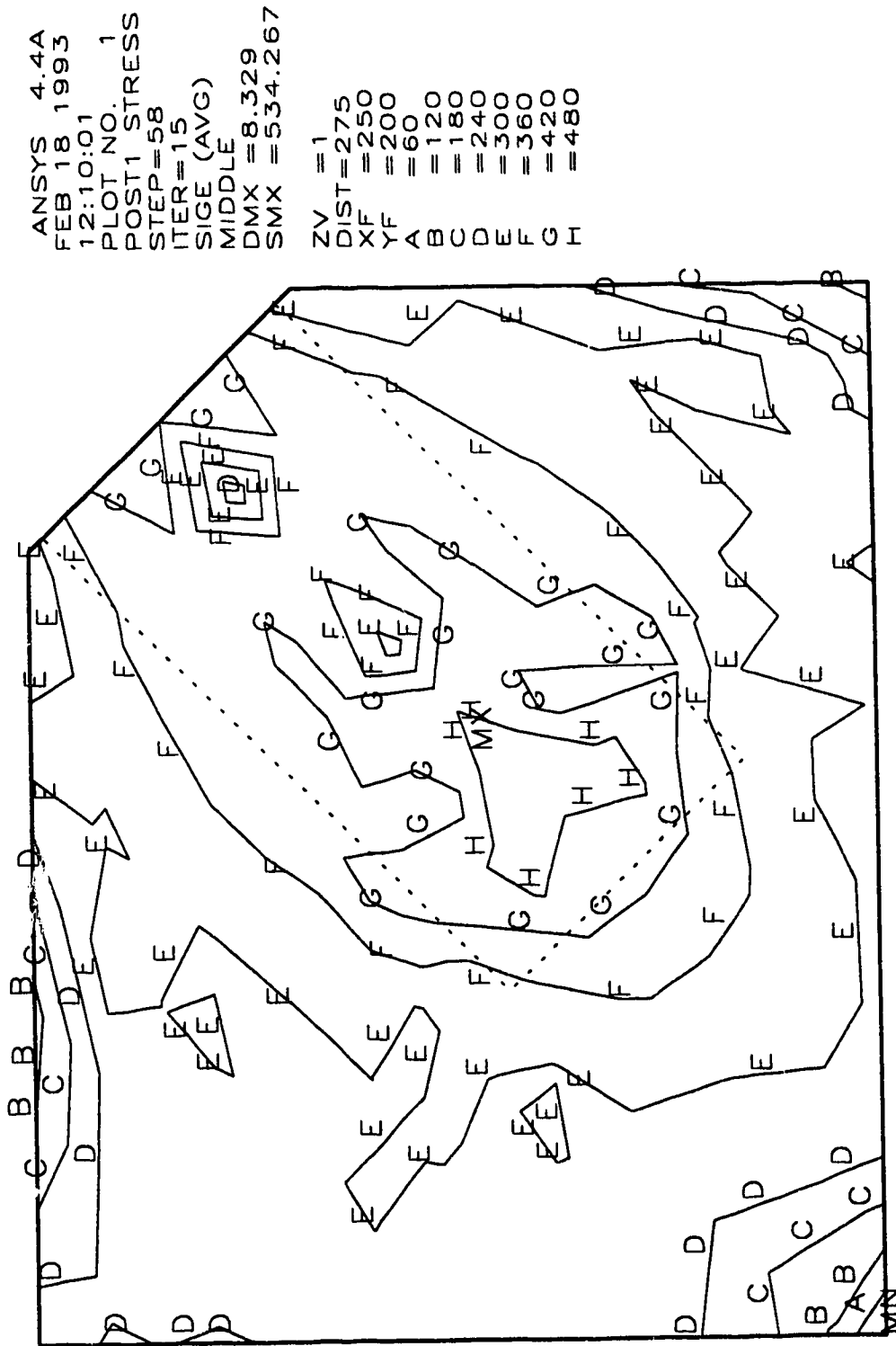


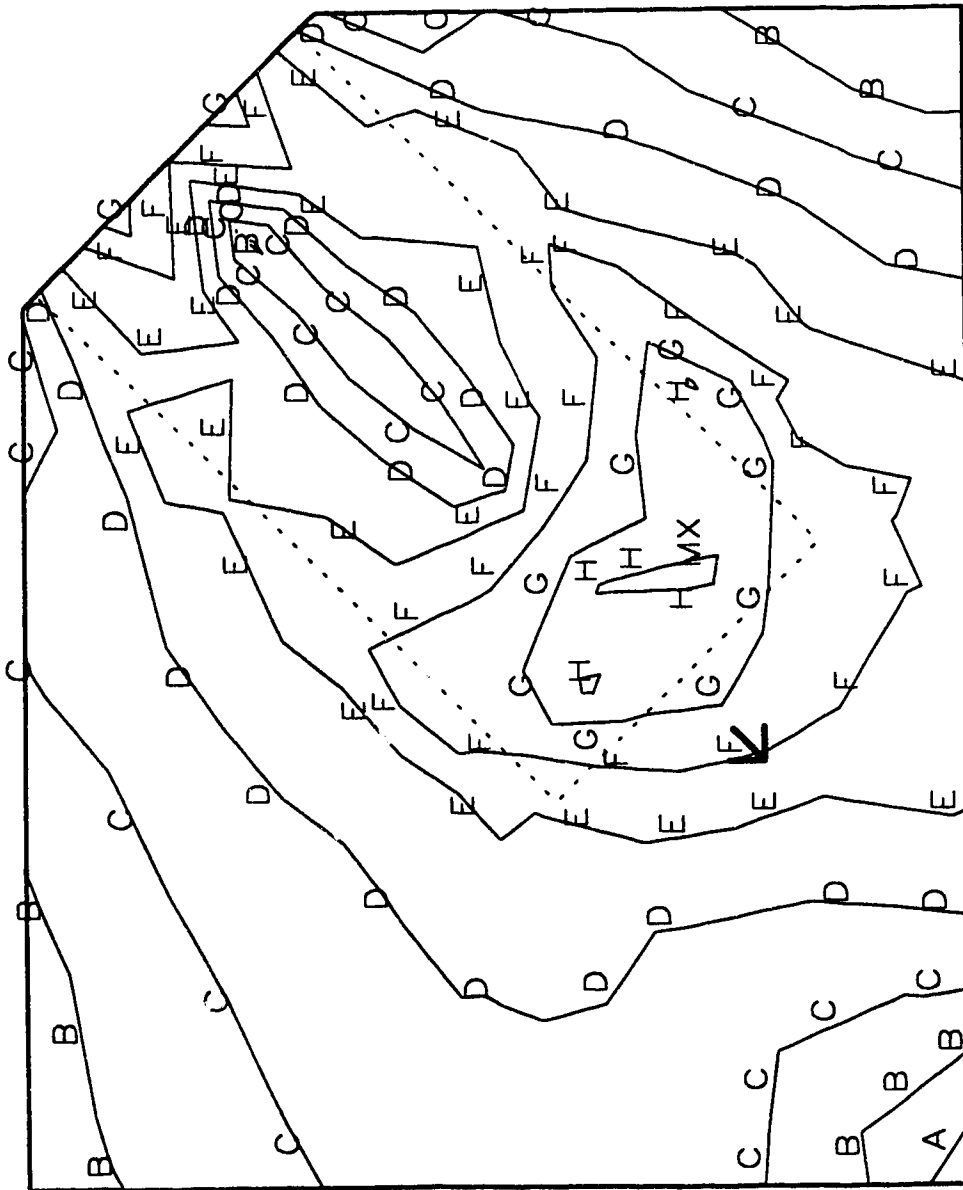
Fig. 9.5e In-Plane Stress Contour for Specimen GP1 at P = 2336 kN



```

ANSYS 4.4A
FEB 28 1993
10:56:42
PLOT NO. 1
POST1 STRESS
STEP=2
ITER=15
SIGE (AVG)
MIDDLE =0.332107
SMX =290.549
ZV =1
DIST=275
XF =250
YF =200
A =35
B =70
C =105
D =140
E =175
F =210
G =245
H =280

```



von Mises effective stress at rosette = 200 MPa

Fig. 9.6 In-Plane Stress Contour for Specimen GP1 at P = 1220 kN

ANSYS 4.4A  
FEB 25 1993  
11:48:03  
PLOT NO. 2  
POST1 VECTOR  
STEP=8  
ITER=15  
PDIR  
ZV =1  
DIST=275  
XF =250  
YF =200

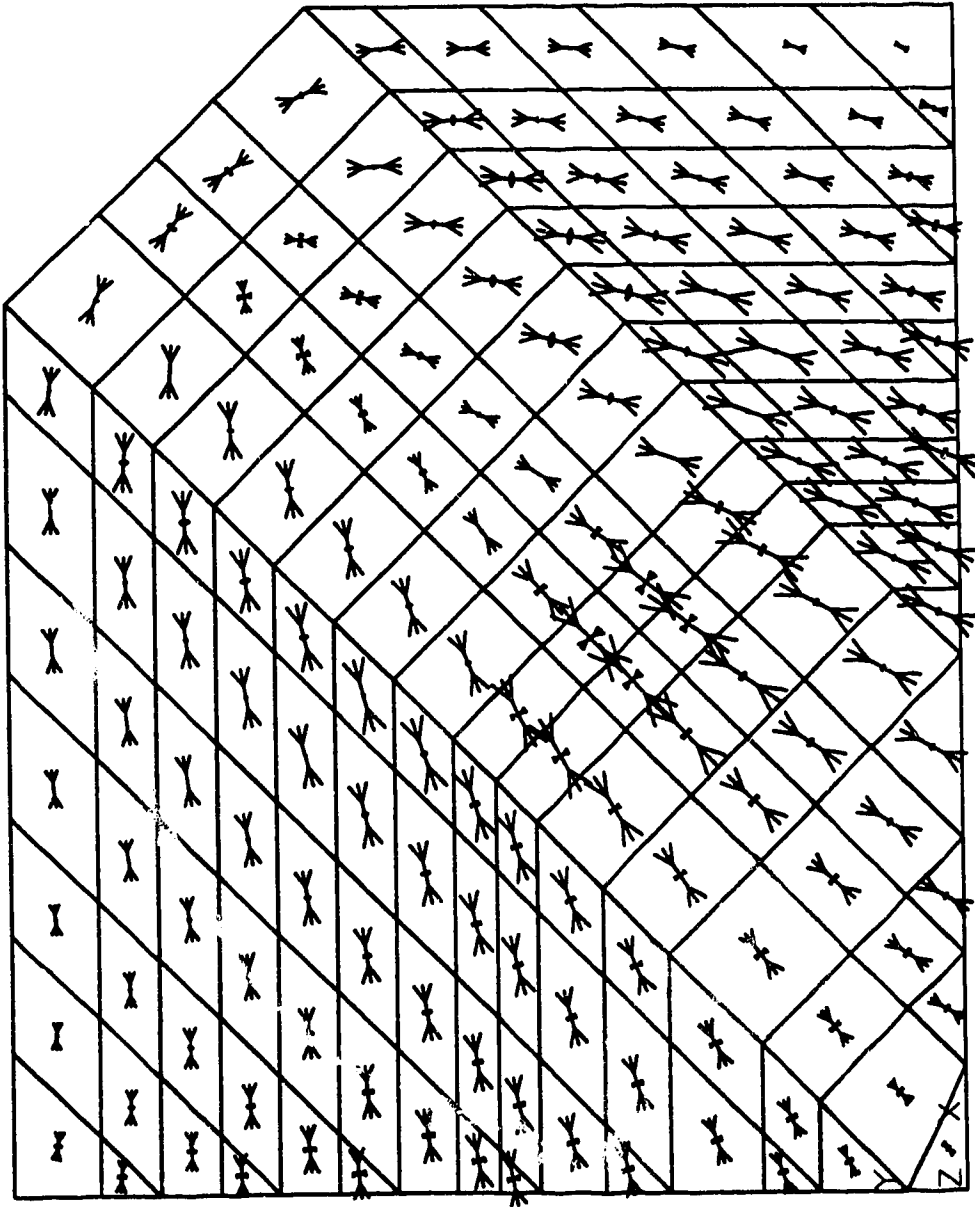


Fig. 9.7a Principal Stress Vector Plot for Specimen GP1 at P = 1370 kN

ANSYS 4.4A  
FEB 18 1993  
12:10:08  
PLOT NO. 2  
POST1 VECTOR  
STEP=58  
ITER=15  
PDIR  
ZV = 1  
DIST = 275  
XF = 250  
YF = 200

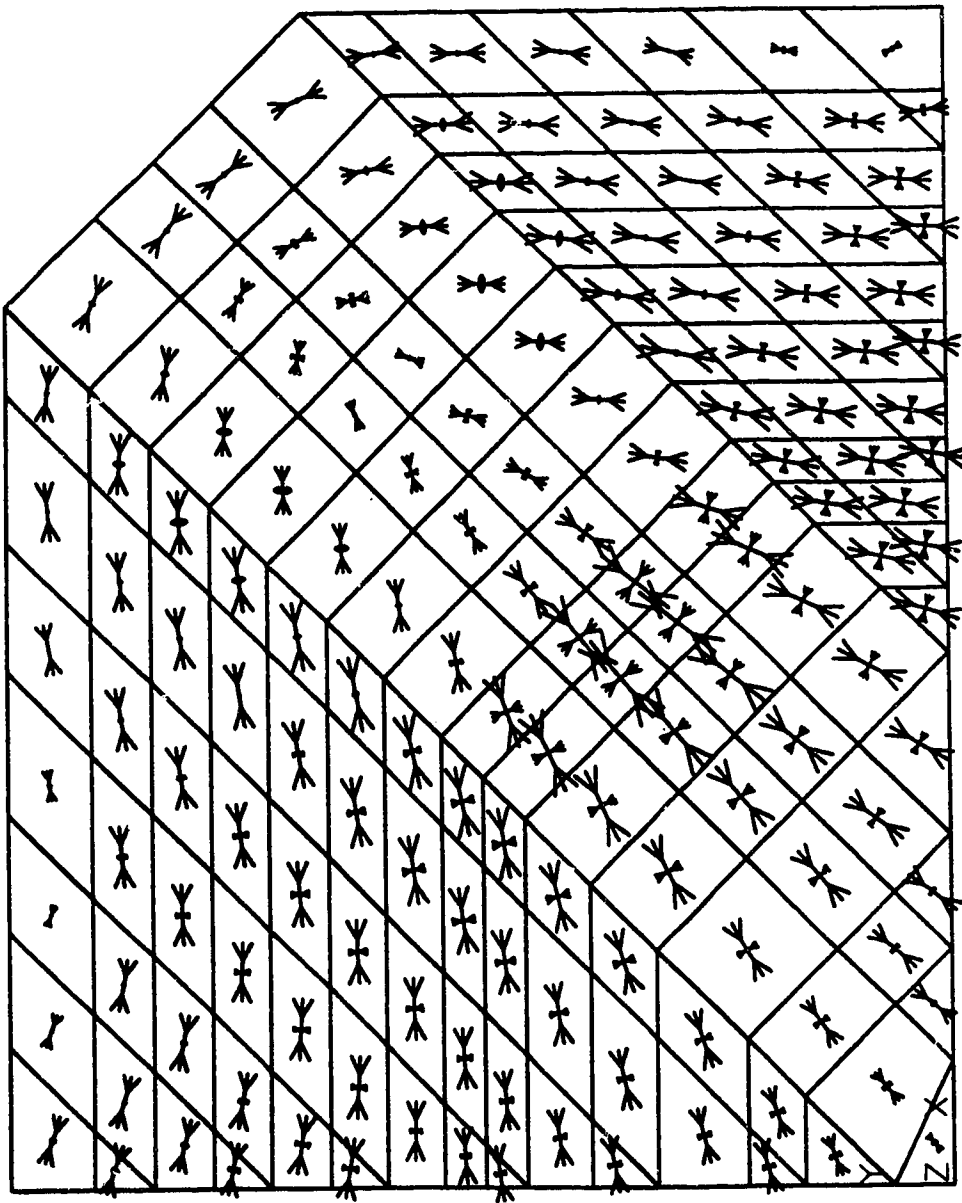


Fig. 9.7b Principal Stress Vector Plot for Specimen GP1 at P = 2336 kN

ANSYS 4.4A  
FEB 25 1993  
11:48:44  
PLOT NO. 3  
POST1 DISPL.  
STEP=8  
ITER=15

DSCA=69.933  
ZV =1  
DIST=275  
XF =250  
YF =200

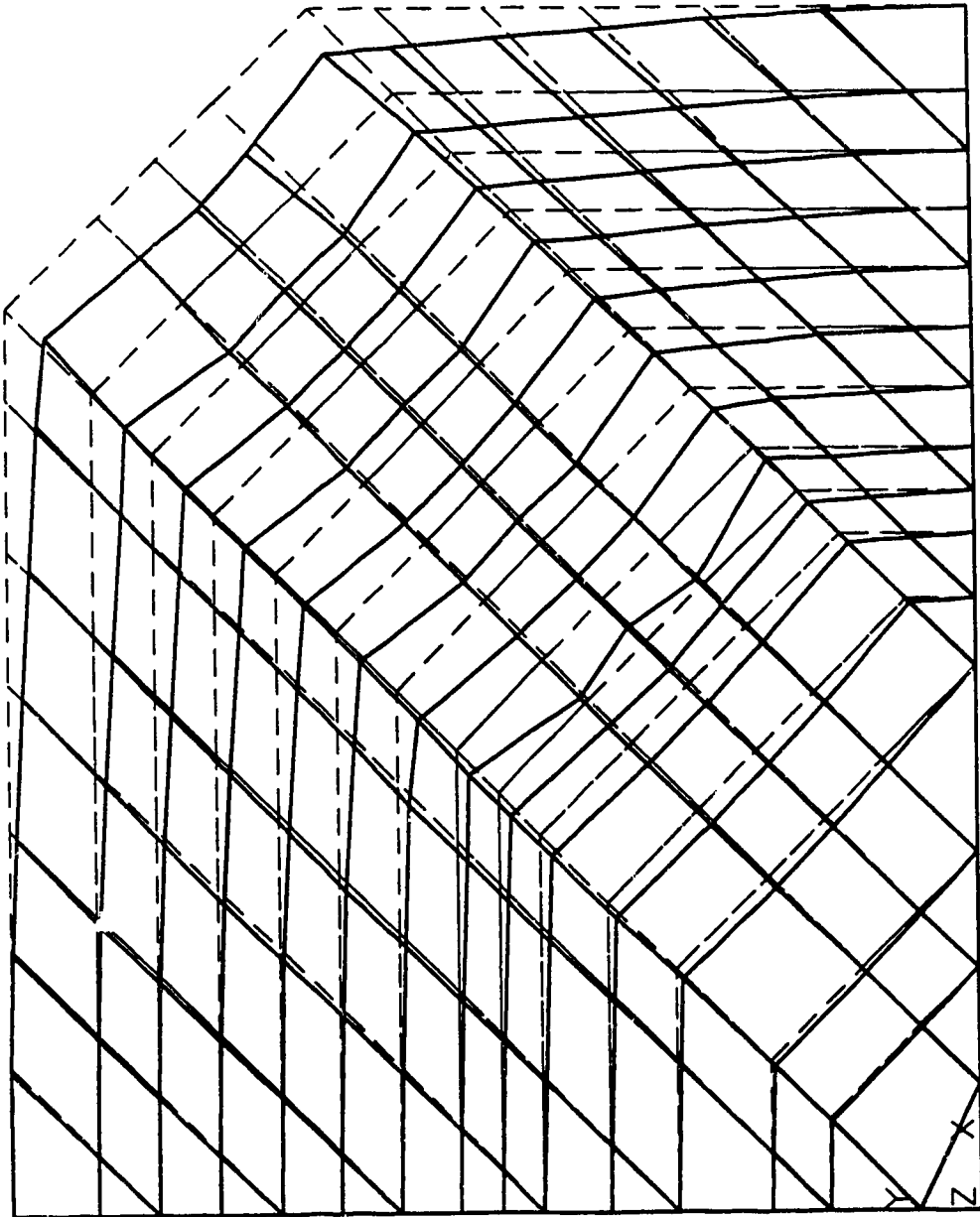


Fig. 9.8a In-Plane Deformation Mode for Specimen GP1 at P = 1370 kN

ANSYS 4.4A  
FEB 18 1993  
12:10:20  
PLOT NO. 3  
POST1 DISPL.  
STEP=58  
ITER=15  
DMX =8.329  
  
DSCA=3.302  
ZV =1  
DIST=275  
XF =250  
YF =200

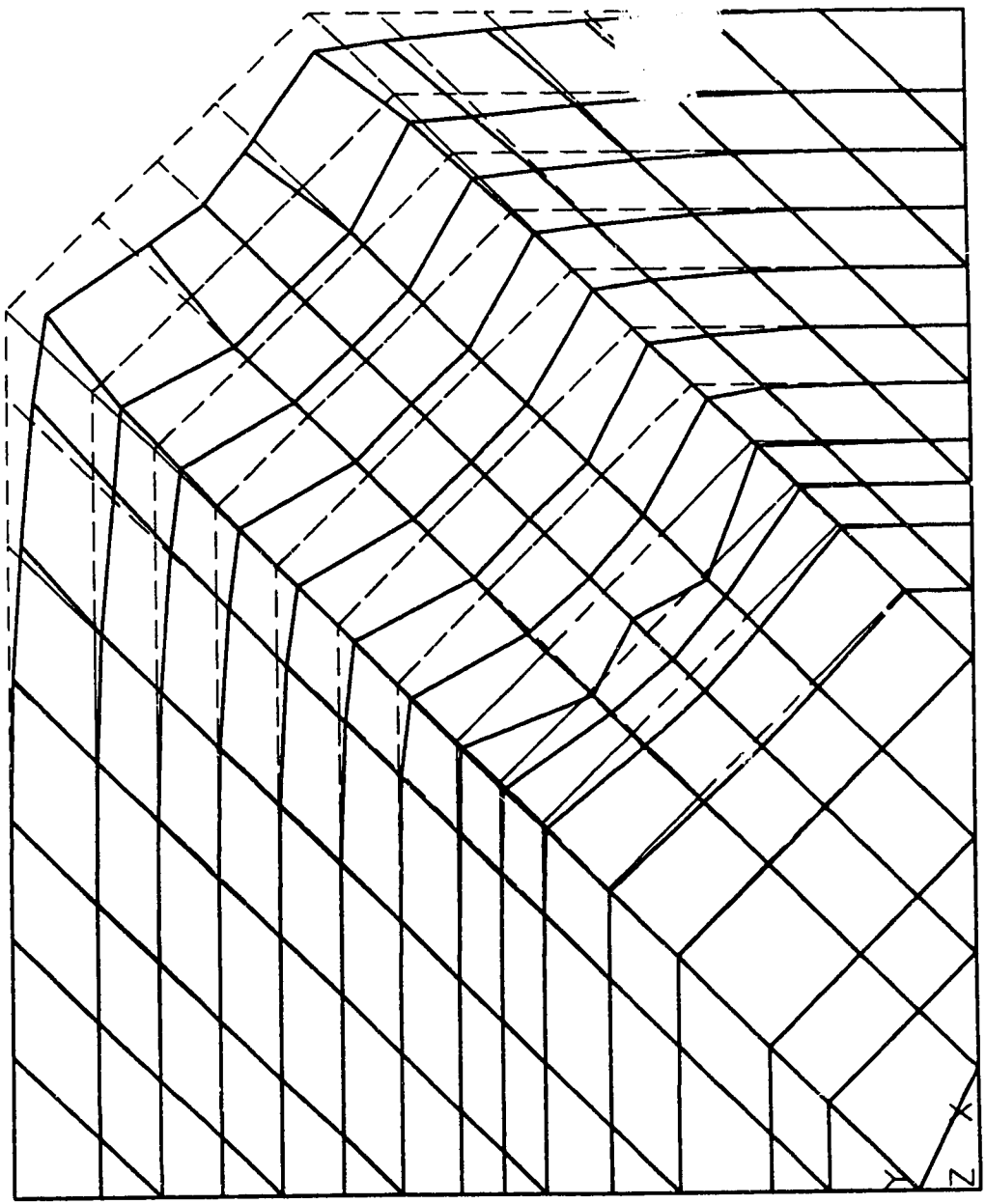


Fig. 9.8b In-Plane Deformation Mode for Specimen GP1 at P = 2336 kN

ANSYS 4.4A  
FEB 27 1993  
15:25:30  
PLOT NO. 1  
POST1 STRESS  
STEP=14  
ITER=15  
SICE (AVG)  
MIDDLE  
SMN = 18.51  
SMX = 341.773  
ZV = 1  
\*DIST=281.149  
\*XF =247.204  
\*YF =179.058  
A B C D E F G H I  
=36.469  
=72.387  
=108.305  
=144.223  
=180.142  
=216.06  
=251.978  
=287.896  
=323.814.

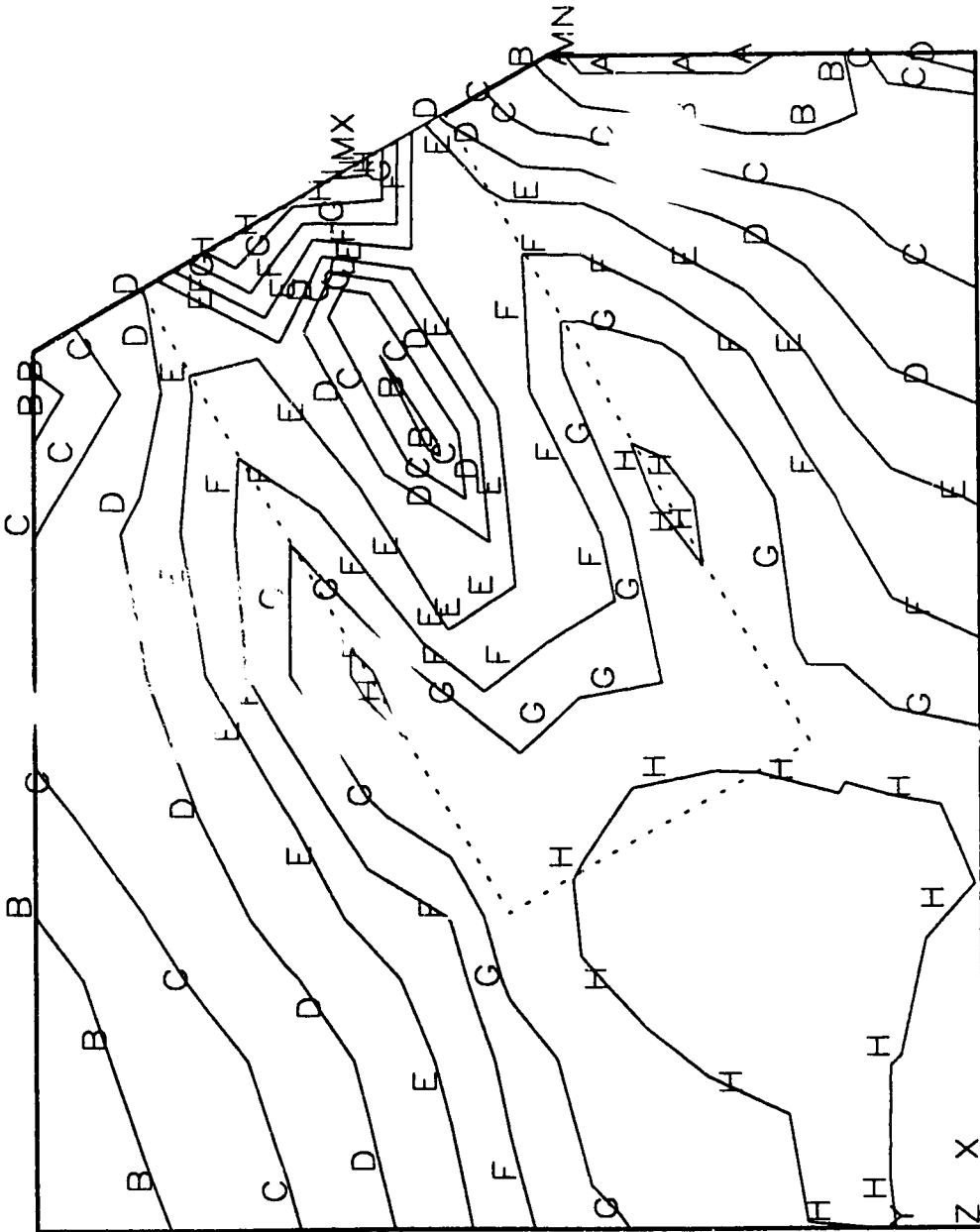


Fig. 9.9 In-Plane Stress Contour for Specimen AP1 at P = 1380 kN

ANSYS 4.4A  
FEB 27 1993  
15:25:42  
PLOT NO. 2  
POST1 VECTOR  
STEP=14  
ITER=15  
PDIR

ZV = 1  
\*DIST=281.149  
\*XF = 247.204  
\*YF = 179.058

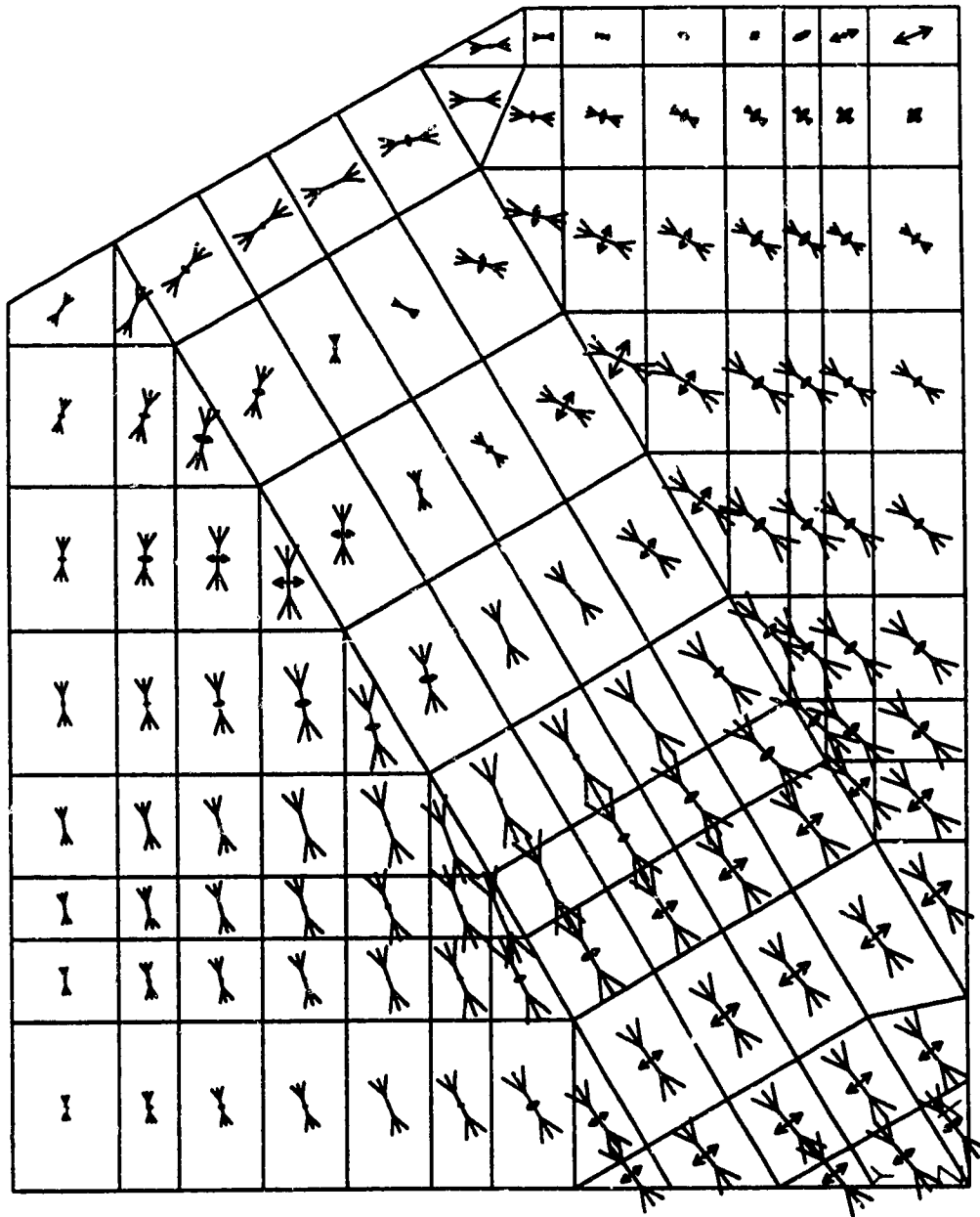


Fig. 9.10 Principal Stress Vector Plot for Specimen AP1 at P = 1380 kN

ANSYS 4.4A  
FEB 27 1993  
15:26:07  
PLOT NO. 3  
POST1 DISPL.  
STEP=14  
ITER=15  
DMX =0.652114  
  
DSCA=43.113  
ZV =1  
\*DIST=281.149  
\*XF =247.204  
\*YF =179.058

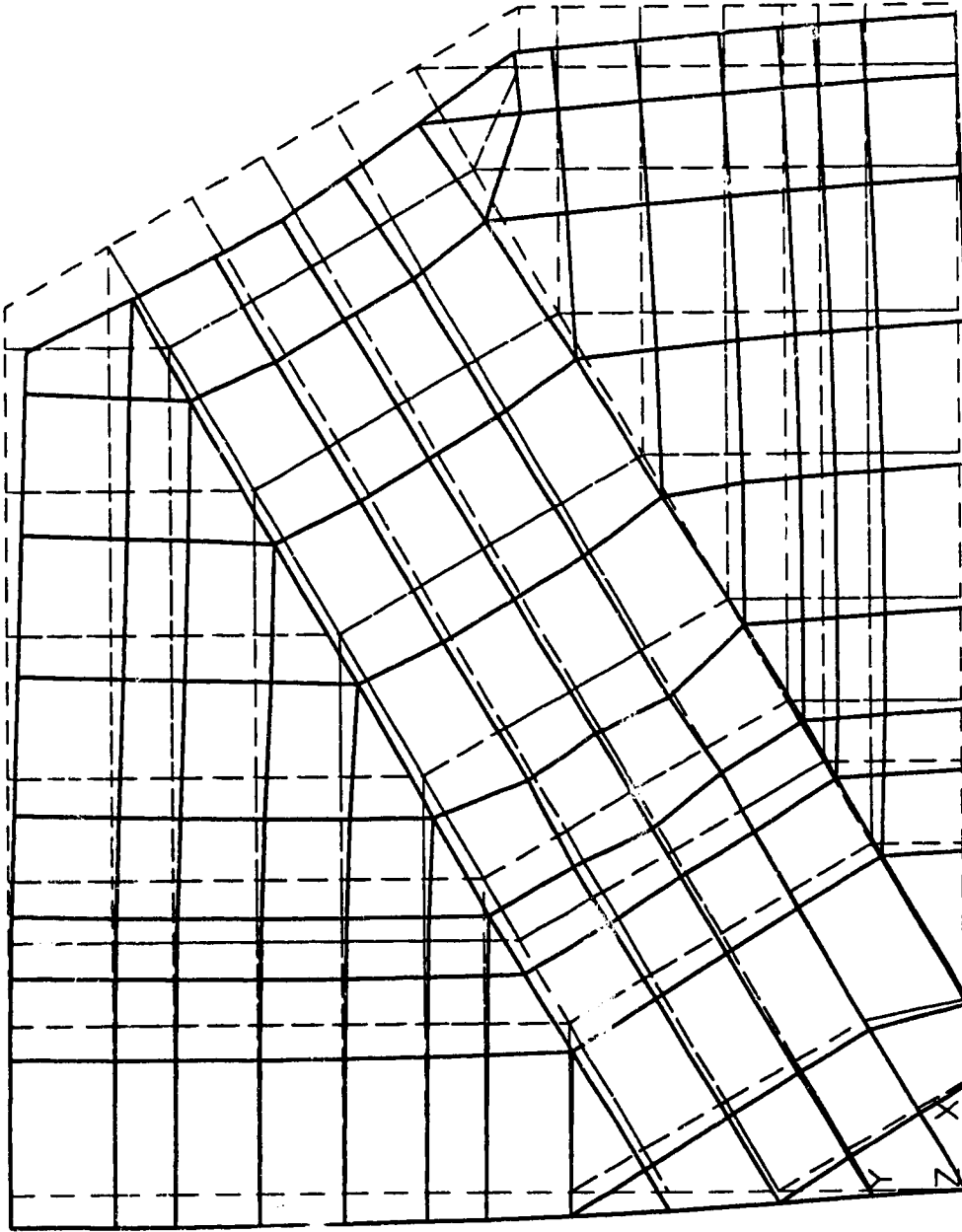


Fig. 9.11 In-Plane Deformation Mode for Specimen AP1 at P = 1380 kN



```

ANSYS  4.4A
FEB 28 1993
13:51:24
PLOT NO.  2
POST1  STRESS
STEP=12
ITER=15
SIGE (AVG)
MIDDLE
DMX =2.749
SMN =15.65
SMX =189.259

ZV  =1
*DIST=285.789
**XF  =231.543
**YF  =209.402
A  =10
B  =35
C  =60
D  =85
E  =110
F  =135
G  =160
H  =185

```

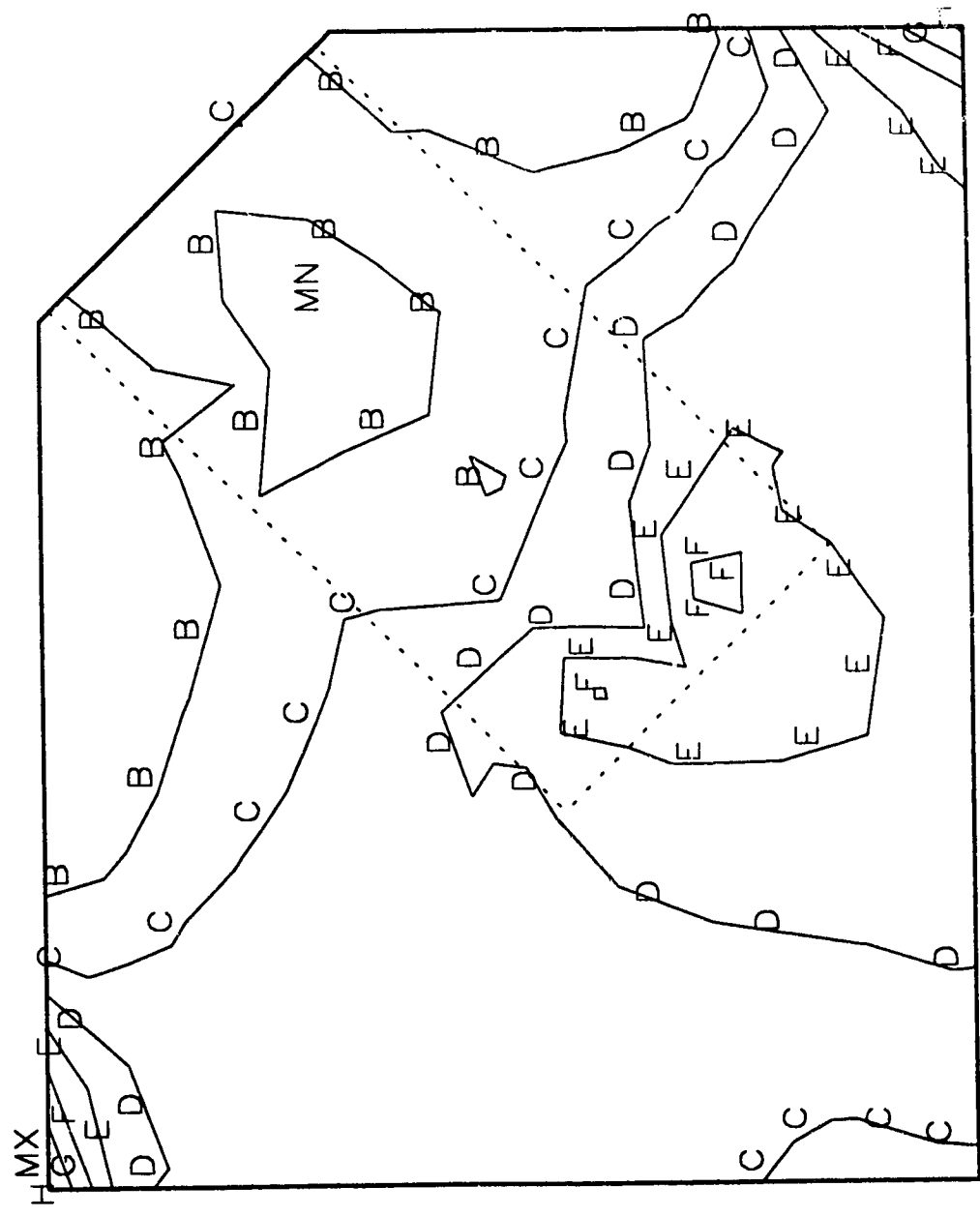


Fig. 9.12a In-Plane Stress Contour for Specimen MP1 at P = 300 kN

```

ANSYS 4.4A
FEB 28 1993
15:10:26
PLOT NO. 1
POST1 STRESS
STEP=22
ITER=15
SIGE (AVG)
MIDDLE
DMX =1.146
SMN =57.468
SMX =399.974
ZV =1
*DIST=285.467
**XF =246.674
**YF =180.628
A B C D E F G H
=80
=125
=170
=215
=260
=305
=350
=395

```

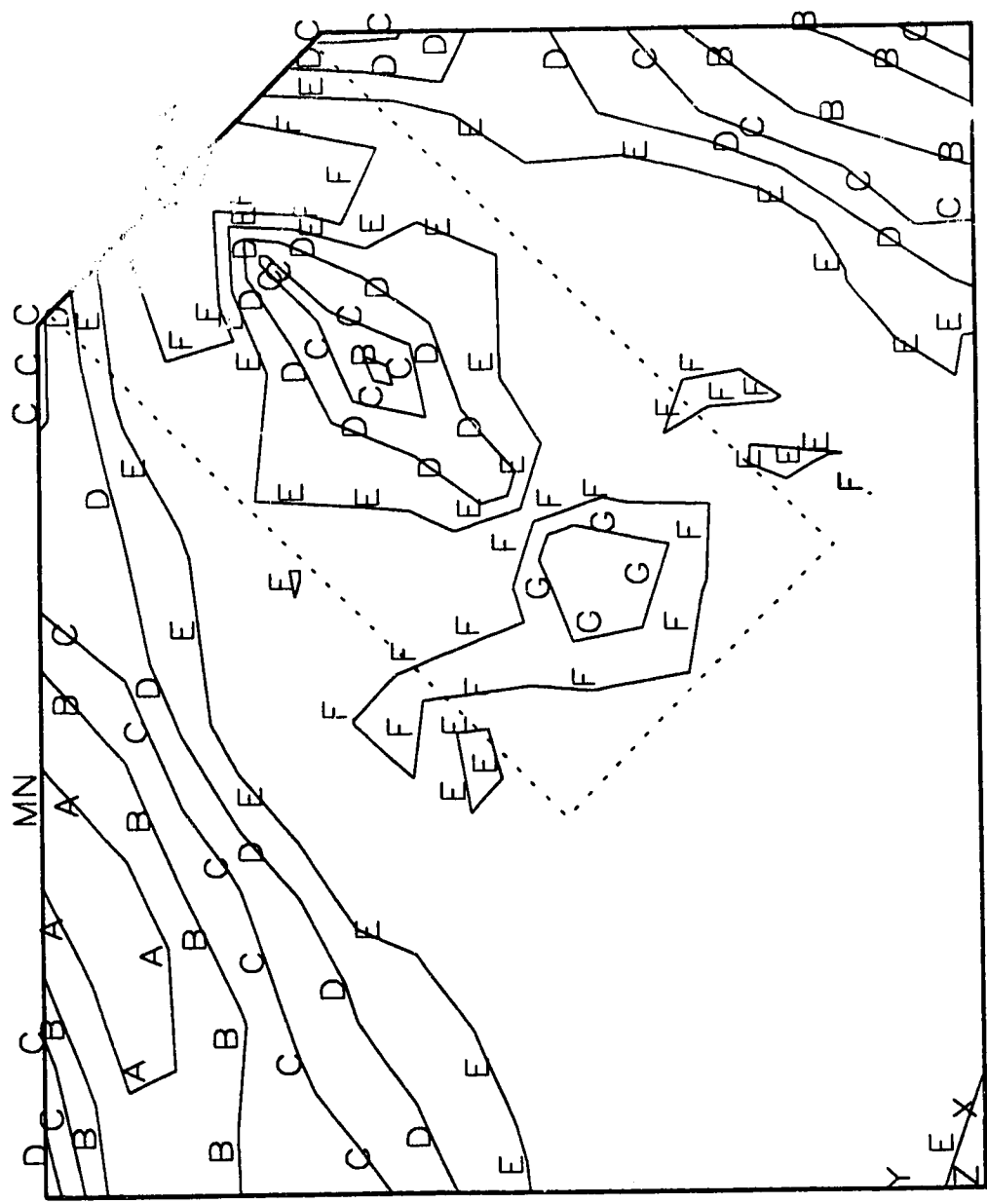


Fig. 9.12b In-Plane Stress Contour for Specimen MP1 at P = 1500 kN

ANSYS 4.4A  
FEB 28 1993  
13:51:31  
PLOT NO. 3  
POST1 VECTOR  
STEP=12  
ITER=15  
PDIR  
  
ZV =  
\*DIST = 0.59  
\*XF = 2.043  
\*YF = 209.402

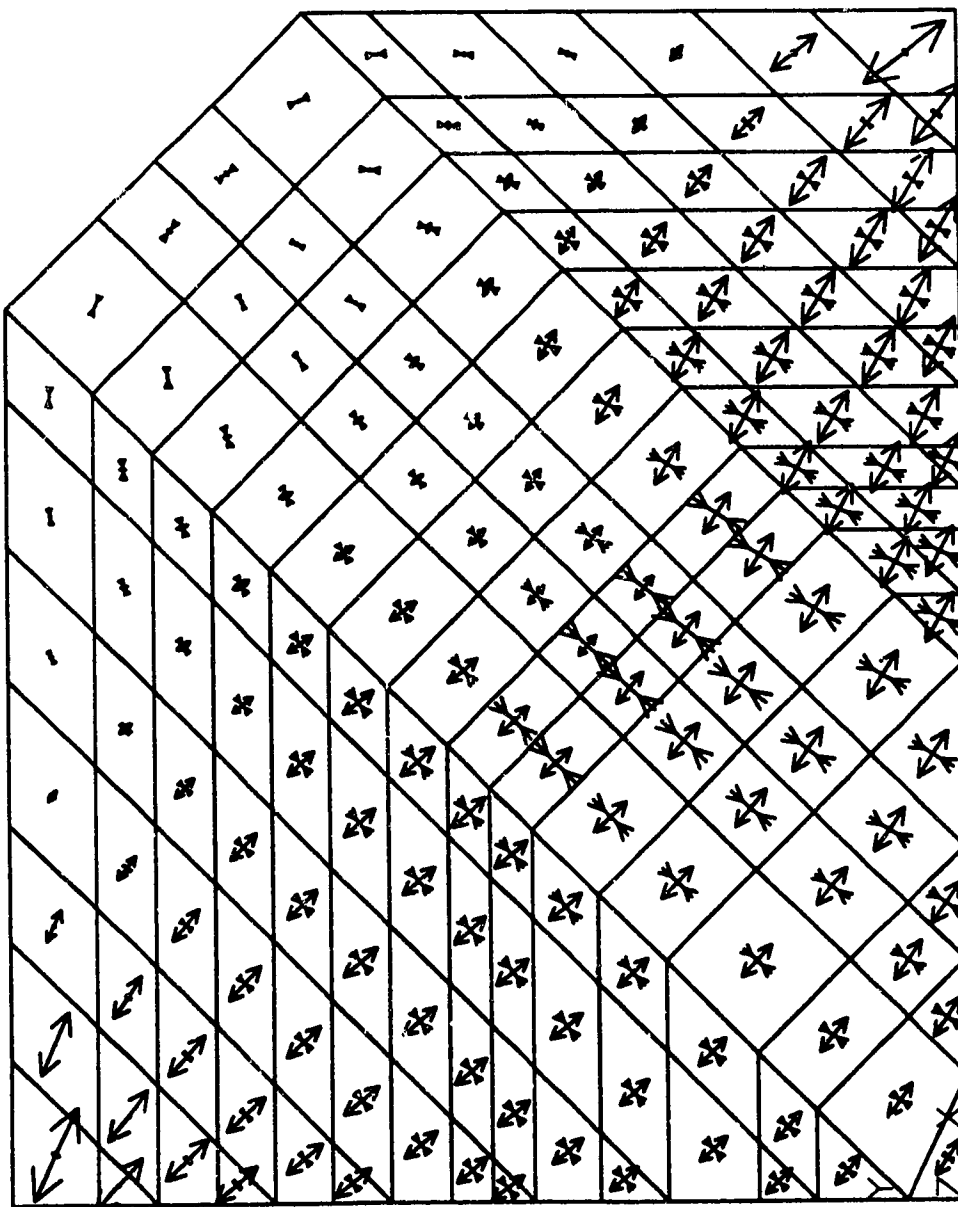


Fig. 9.13a Principal Stress Vector Plot for Specimen MP1 at P = 300 kN

ANSYS 4.4A  
FEB 28 1993  
15:10:31  
PLC NO. 2  
POST1 VECTOR  
STEP=24  
ITER=15  
PDIR  
ZV = 1  
\*D ST = 285.467  
\*XF = 246.674  
\*YF = 180.628

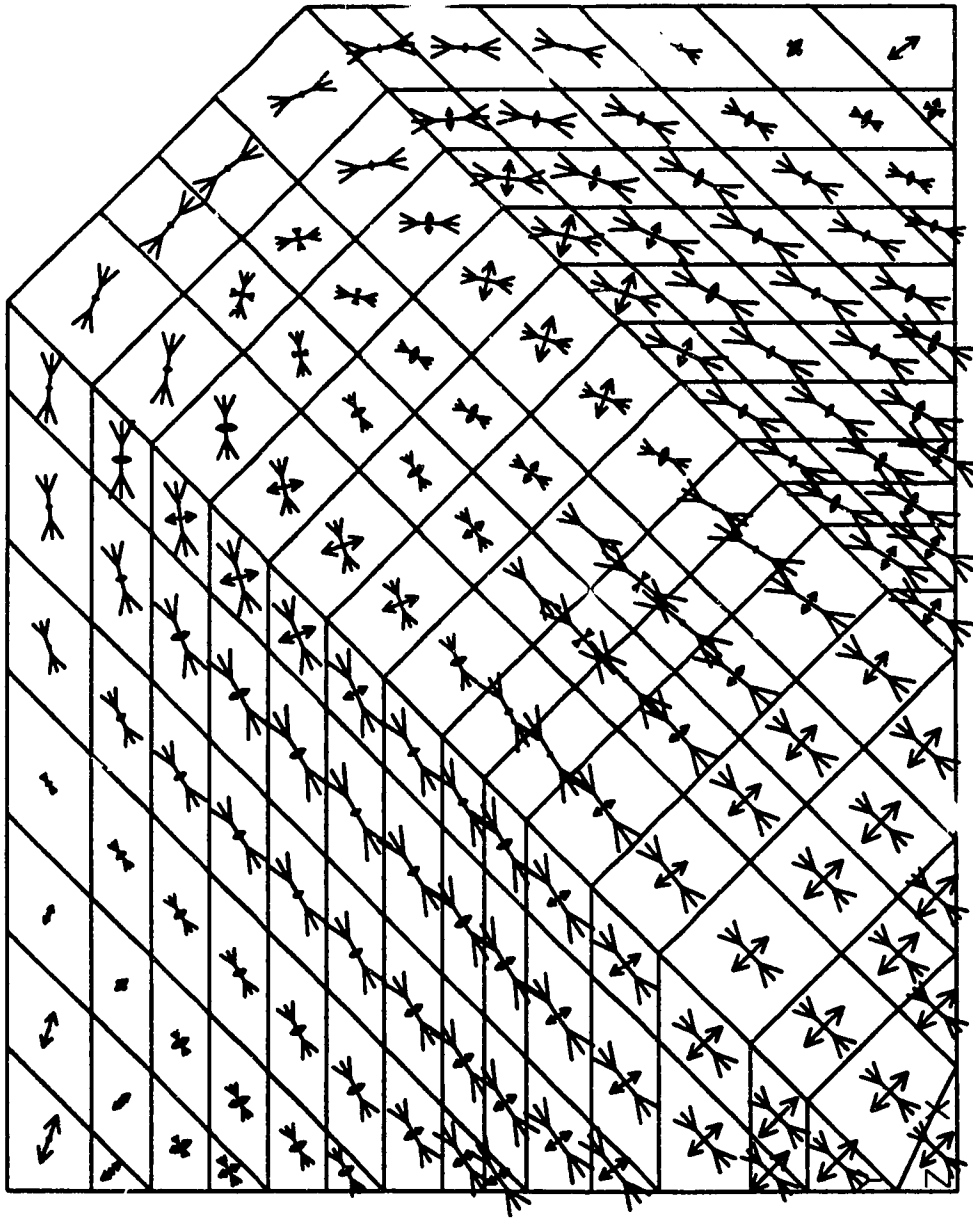
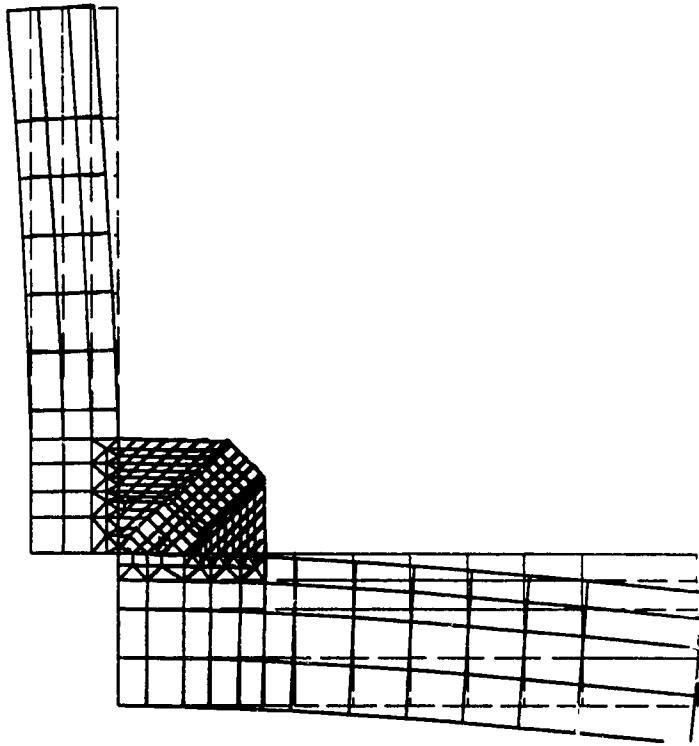
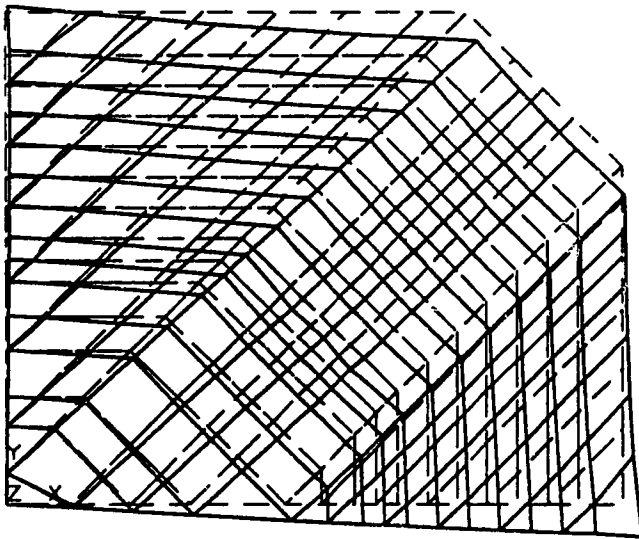


Fig. 9.13b Principal Stress Vector Plot for Specimen MPI at P = 1500 kN



Beam and Column In-Plane Deformation



Stretching of Gusset Plate Specimens Due to Beam and Column Moments

Fig. 9.14a In-Plane Deformation Mode for Specimen MP1 at  $P = 300$  kN

```
ANSYS 4.4A  
FEB 28 1993  
15:10:38  
PLOT NO. 3  
POST1 DISPL.  
STEP=22  
ITER=15  
DMX =3.124  
DSCA=9.138  
ZV =1  
*DIST=285.467  
*XF =-246.674  
*YF =180.628
```

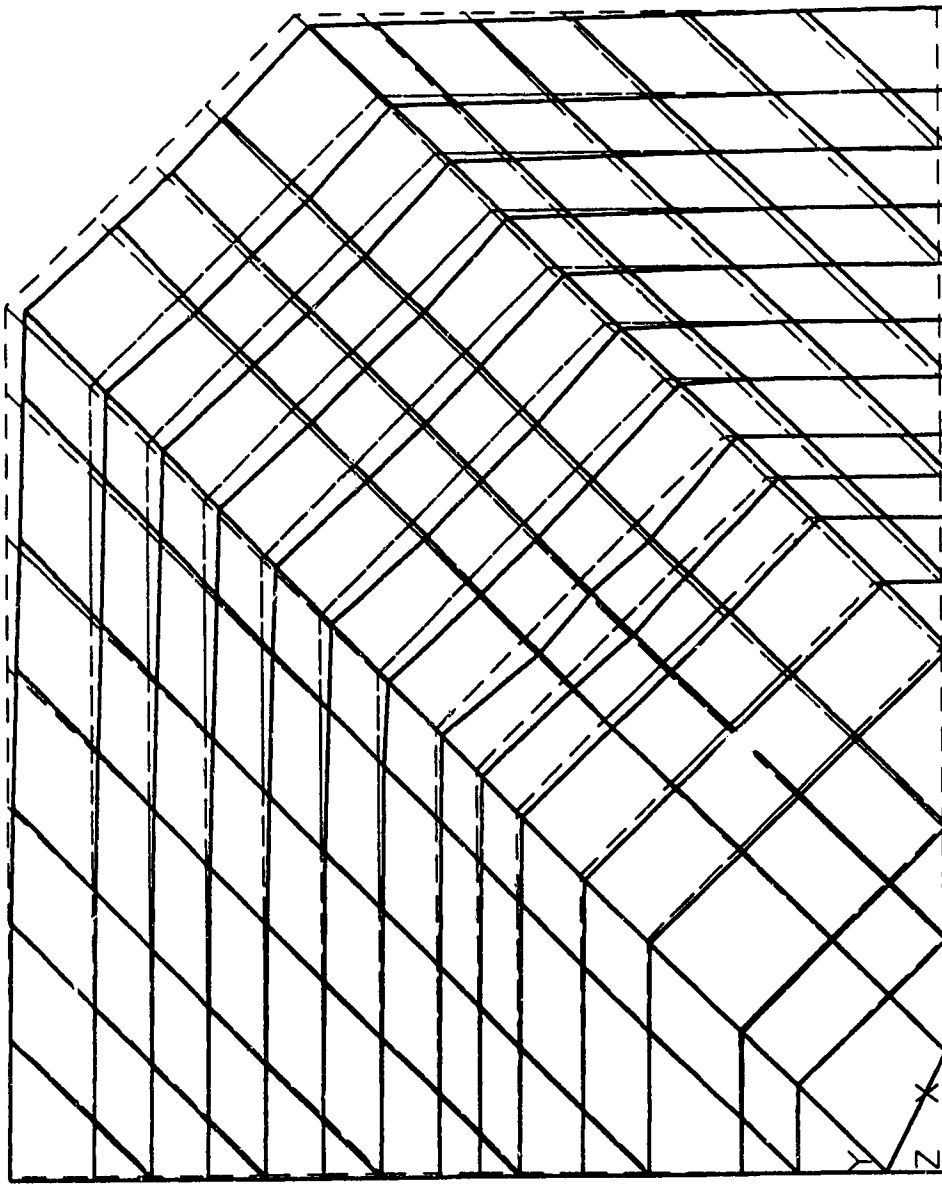


Fig. 9.14b In-Plane Deformation Mode for Specimen MPI at P = 1500 kN

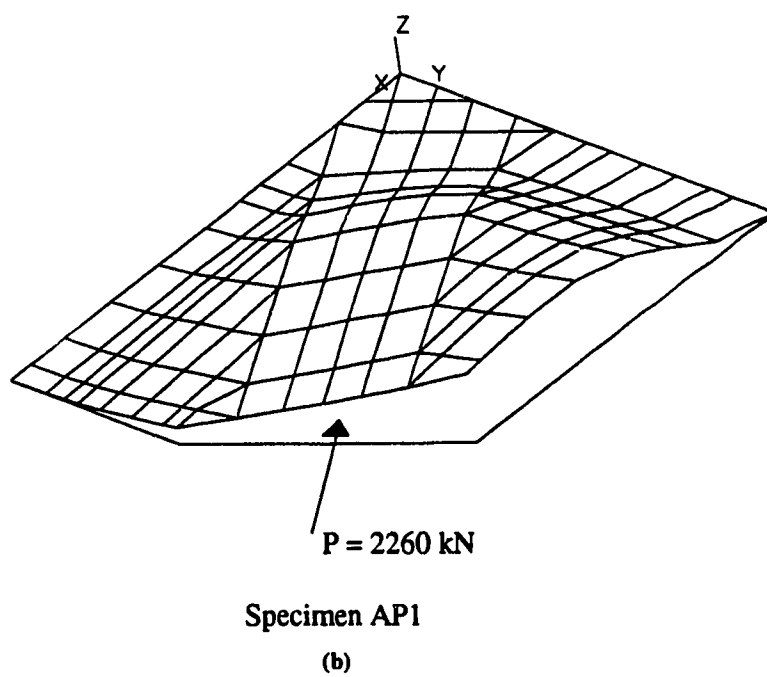
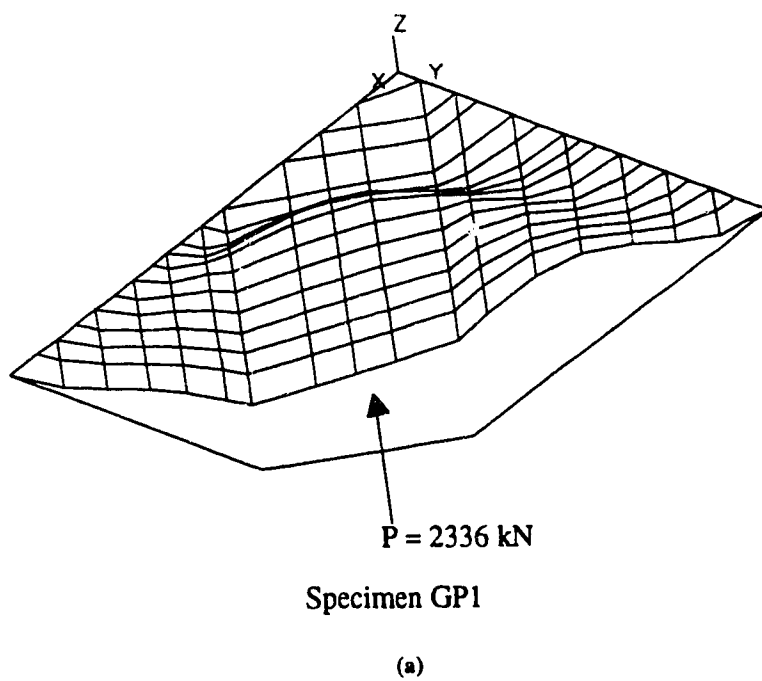


Fig. 9.15a,b Typical Buckling Shapes for Specimens GP1 and AP1

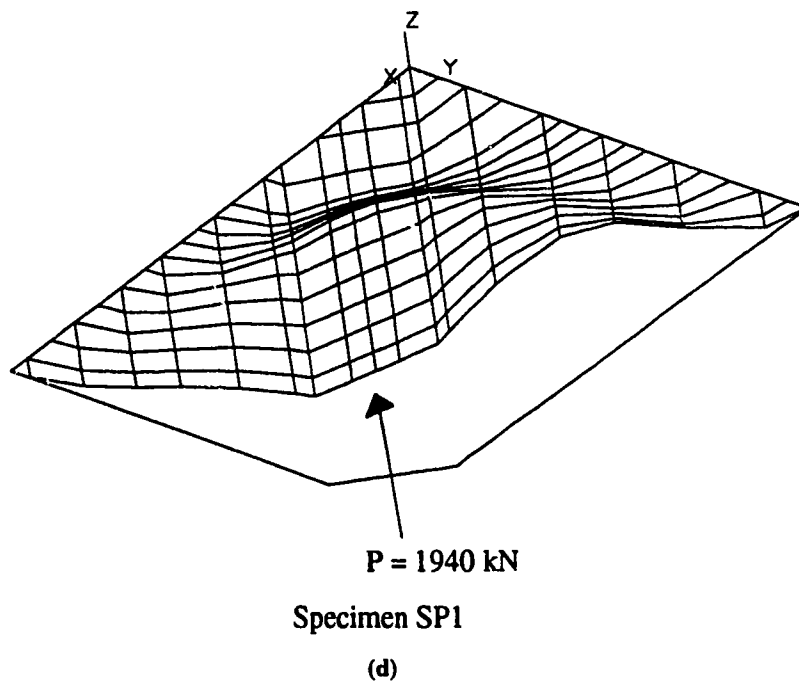
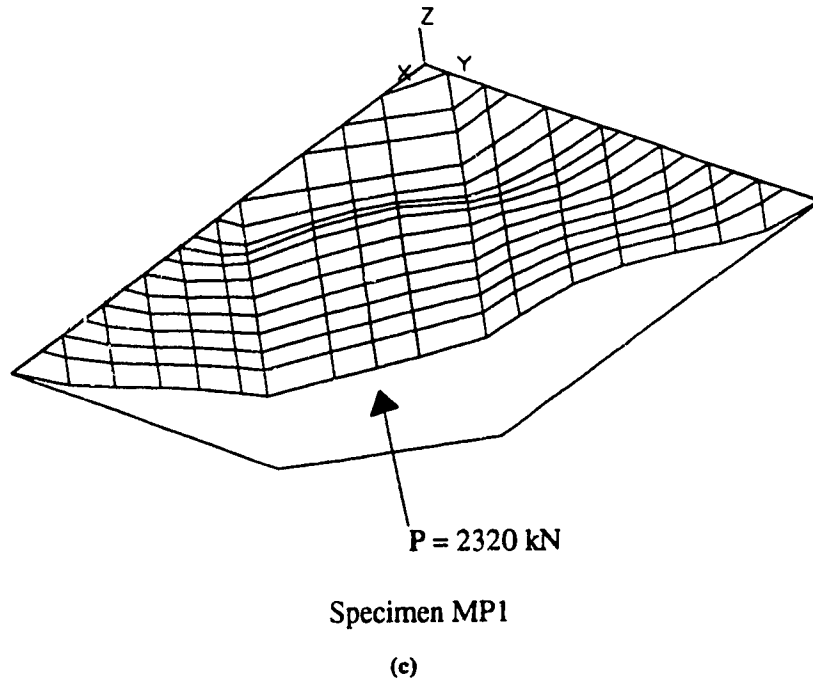


Fig. 9.15 c,d Typical Buckling Shapes for Specimens MP1 and SP1



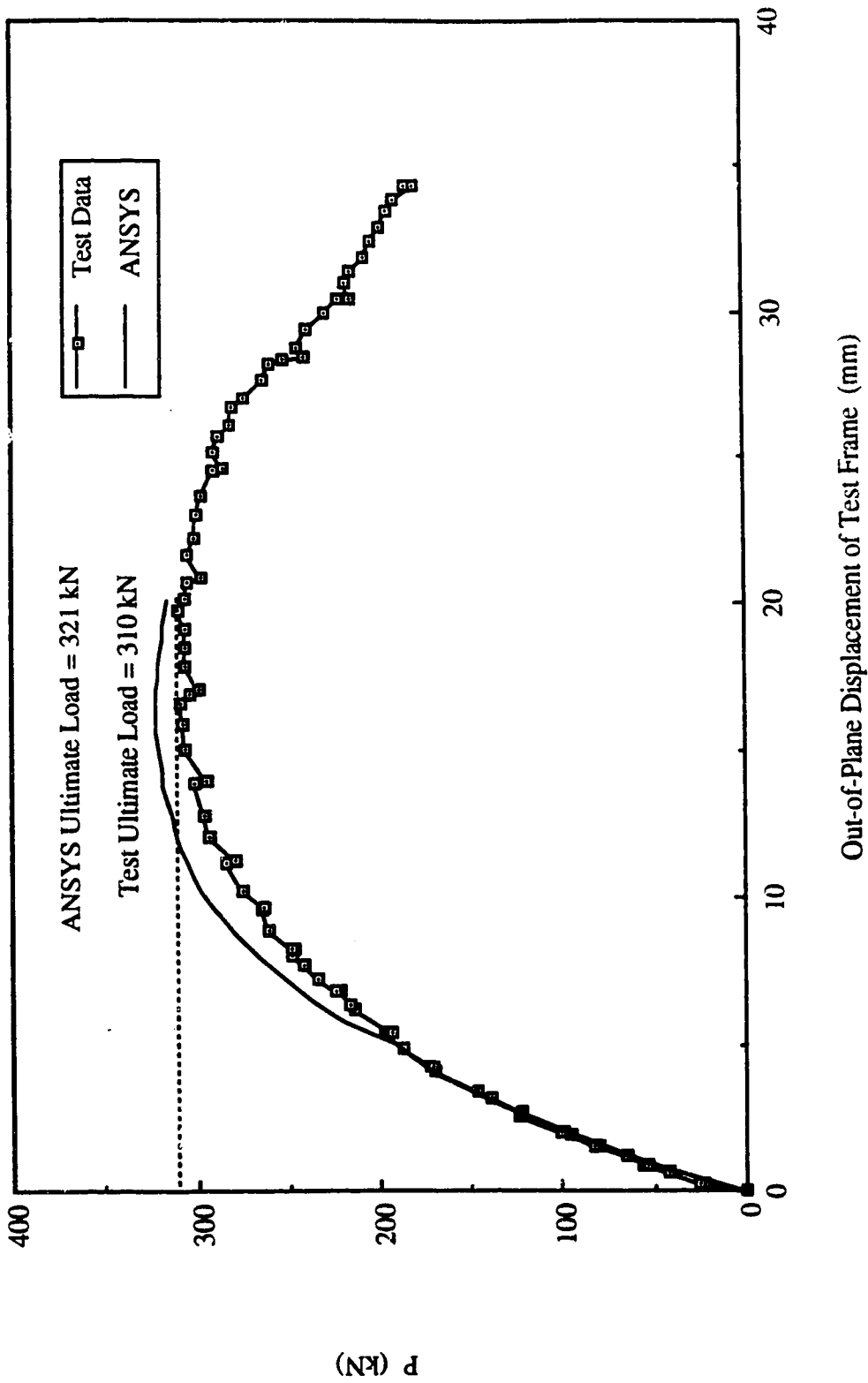
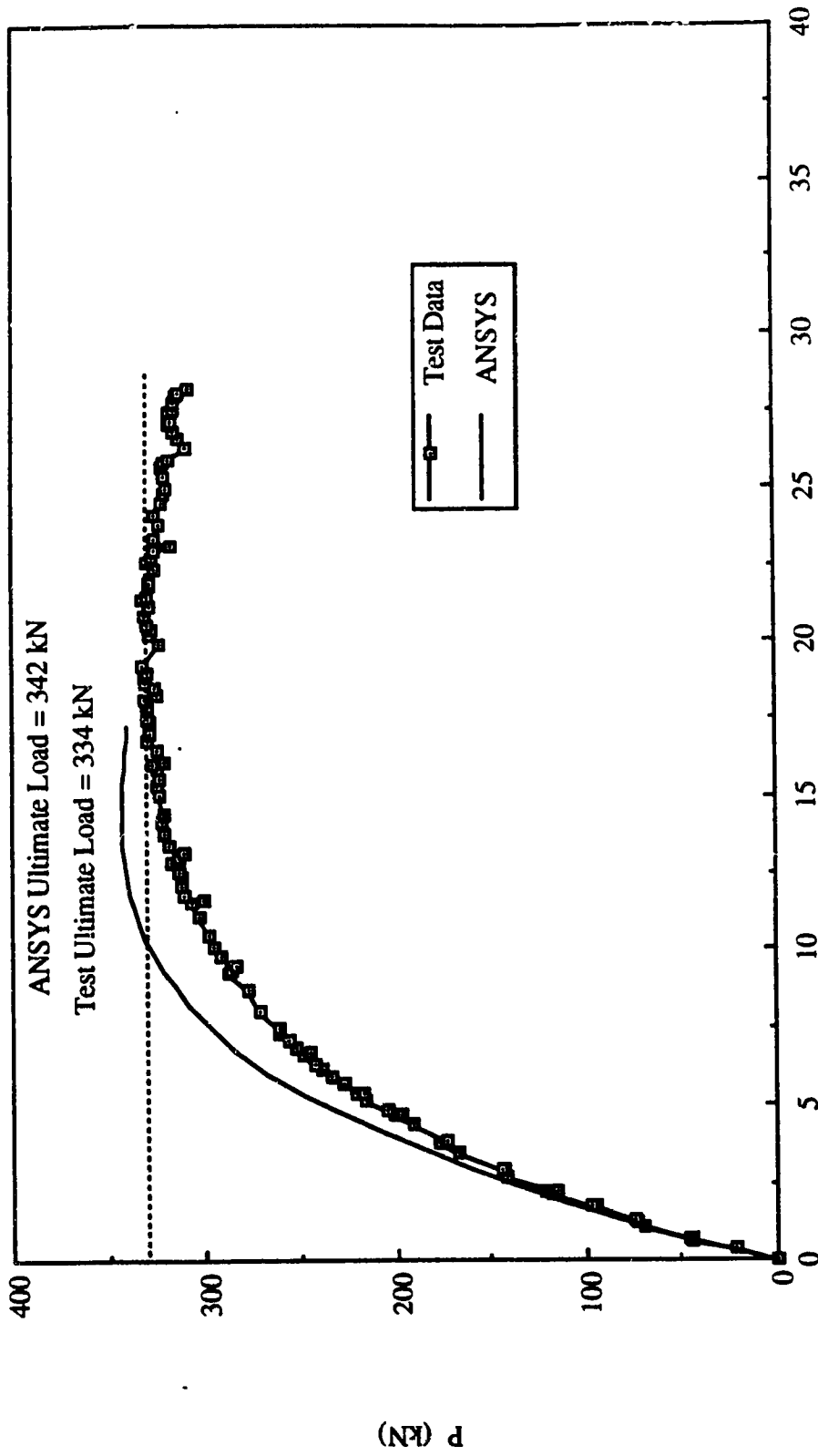
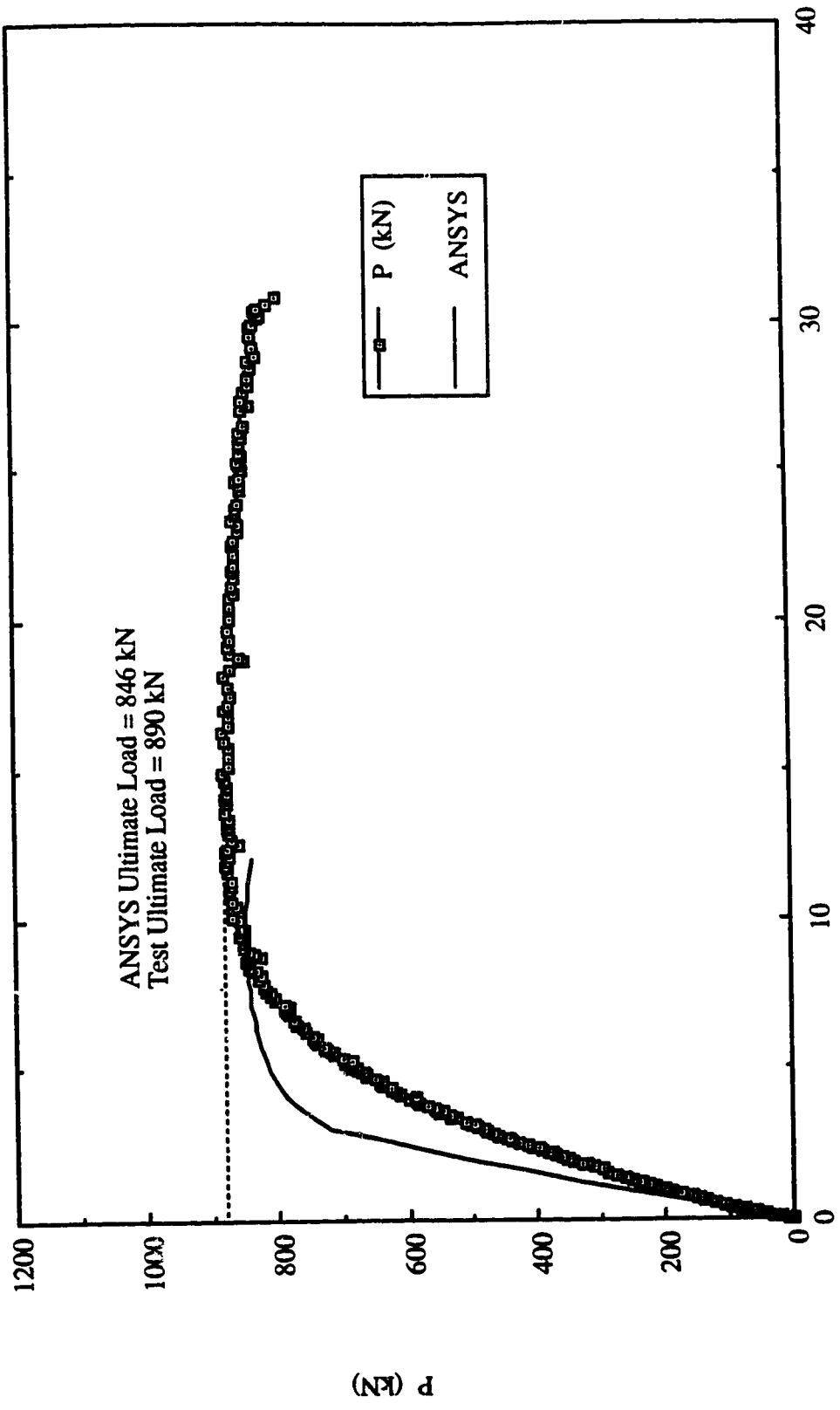


Fig. 9.16 Analytical Load Deflection Curve for Specimen EPI



Out-of-Plane Displacement of Test Frame (mm)

Fig. 9.17 Analytical Load Deflection Curve for Specimen EP2



Out-of-Plane Displacement of Test Frame (mm)

Fig. 9.18 Analytical Load Deflection Curve for Specimen EP3

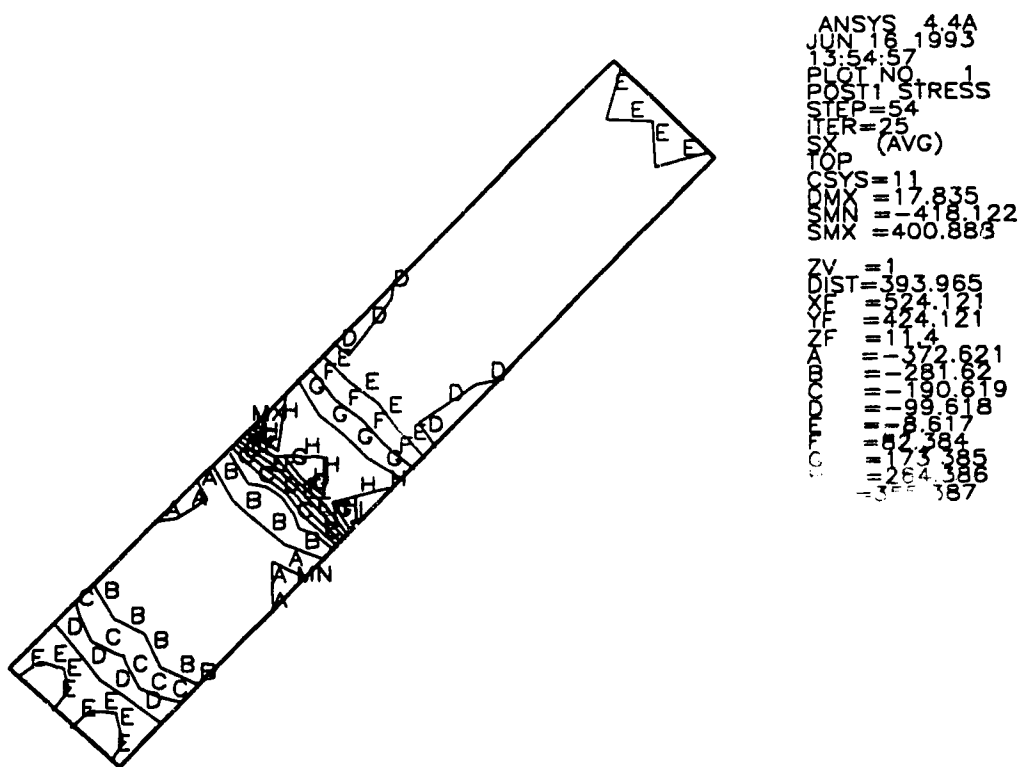


Fig. 9.19 In-Plane Stress Distribution of Splice Plate Top Surface for Specimen EP1 at Ultimate

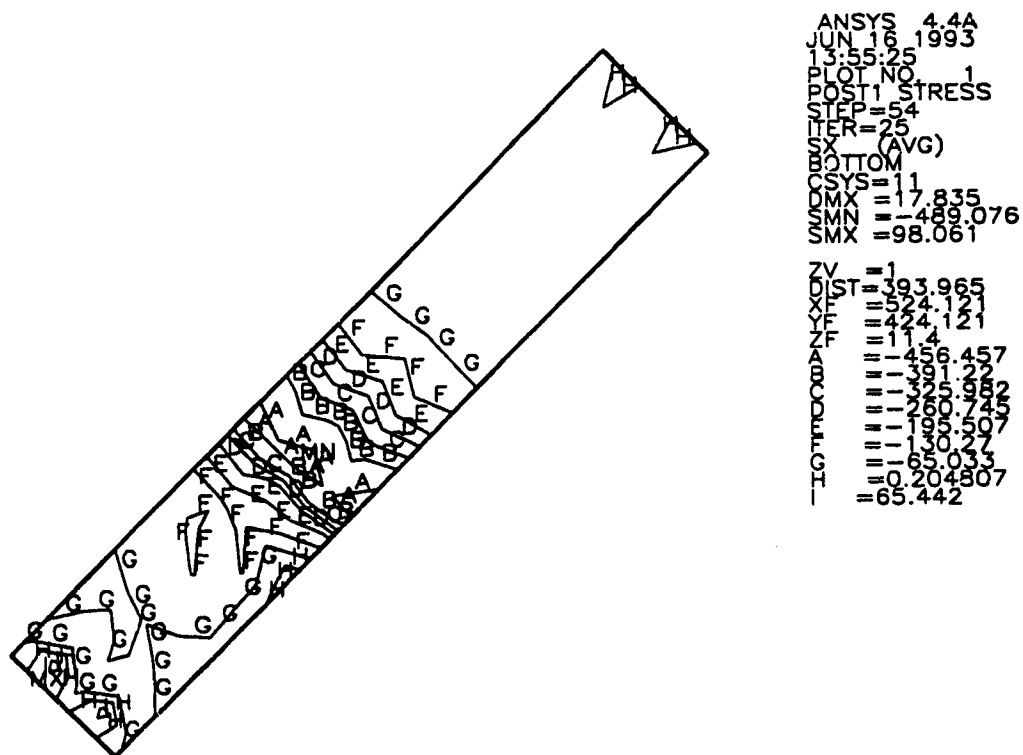


Fig. 9.20 In-Plane Stress Distribution of Splice Plate Bottom Surface for Specimen EP1 at Ultimate

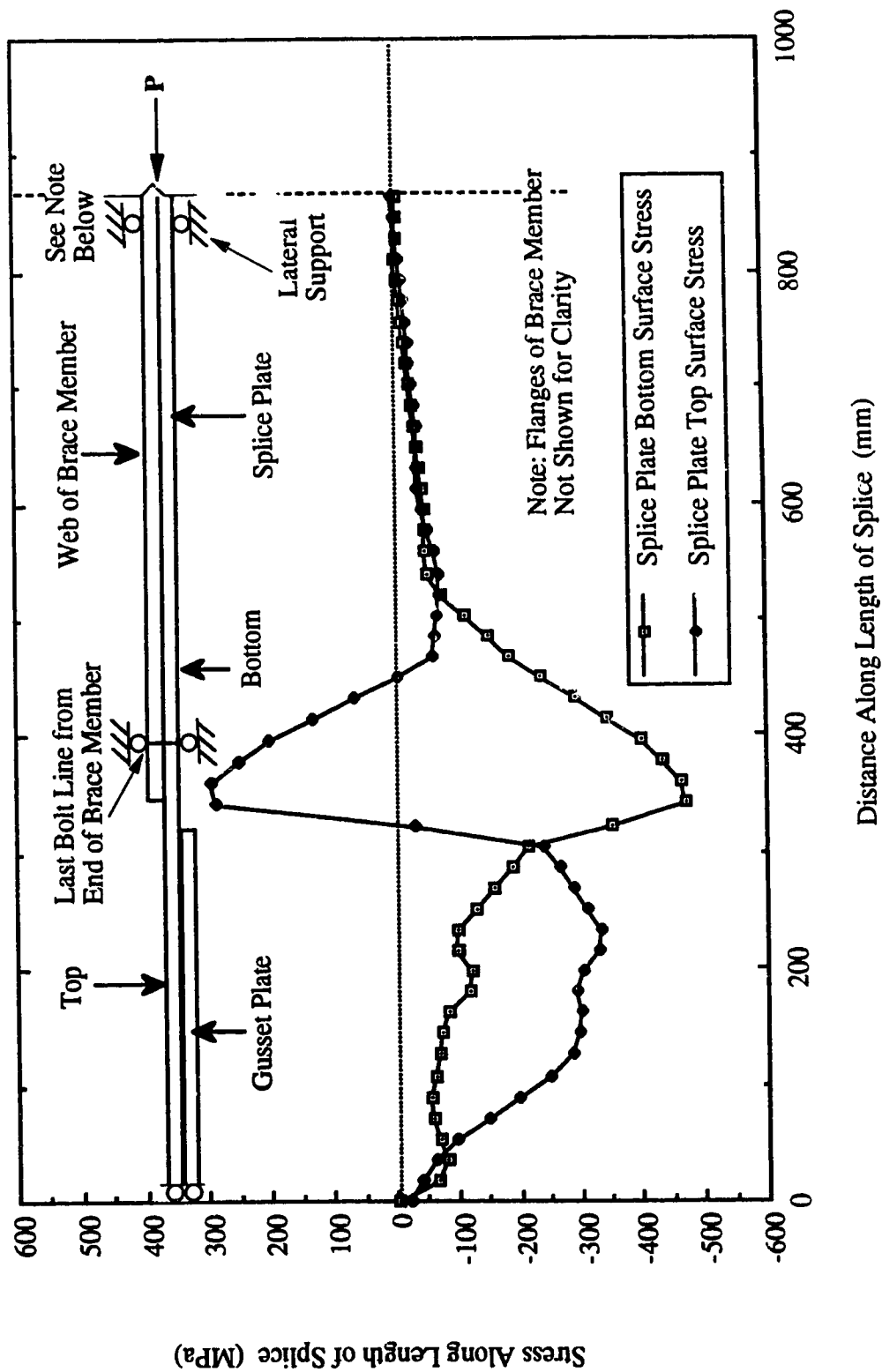


Fig. 9.21 In-Plane Stress Distribution at Centerline Along Length of Splice Plate for Specimen EP1

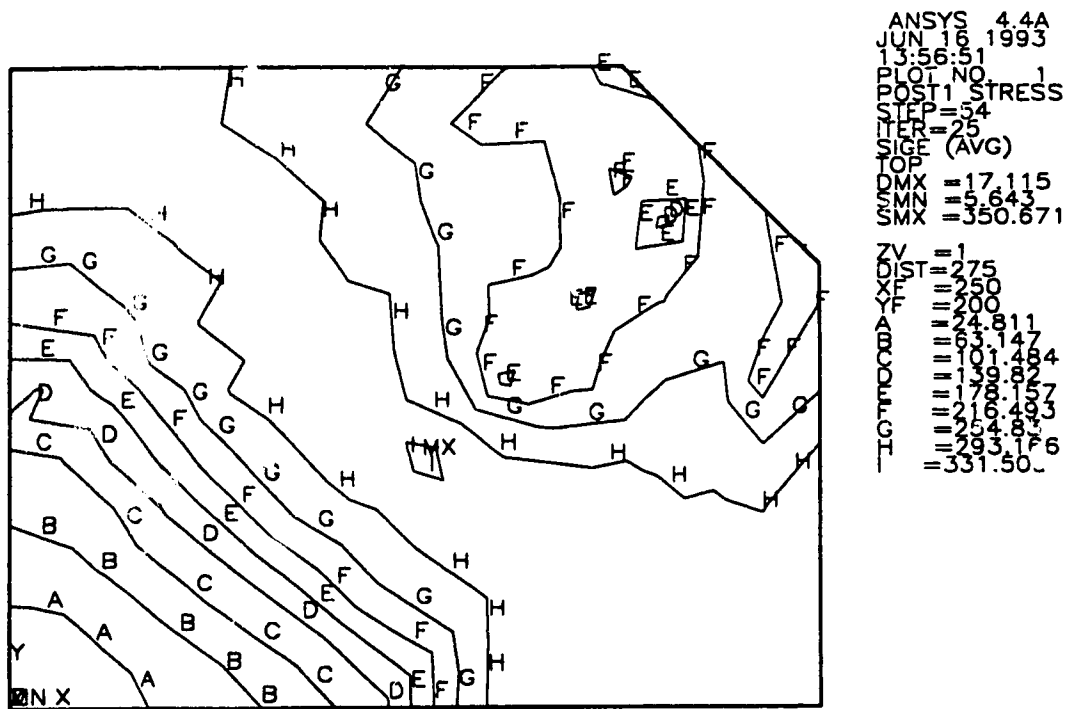


Fig. 9.22 In-Plane Stress Distribution of Gusset Plate Top Surface for Specimen EP1 at Ultimate

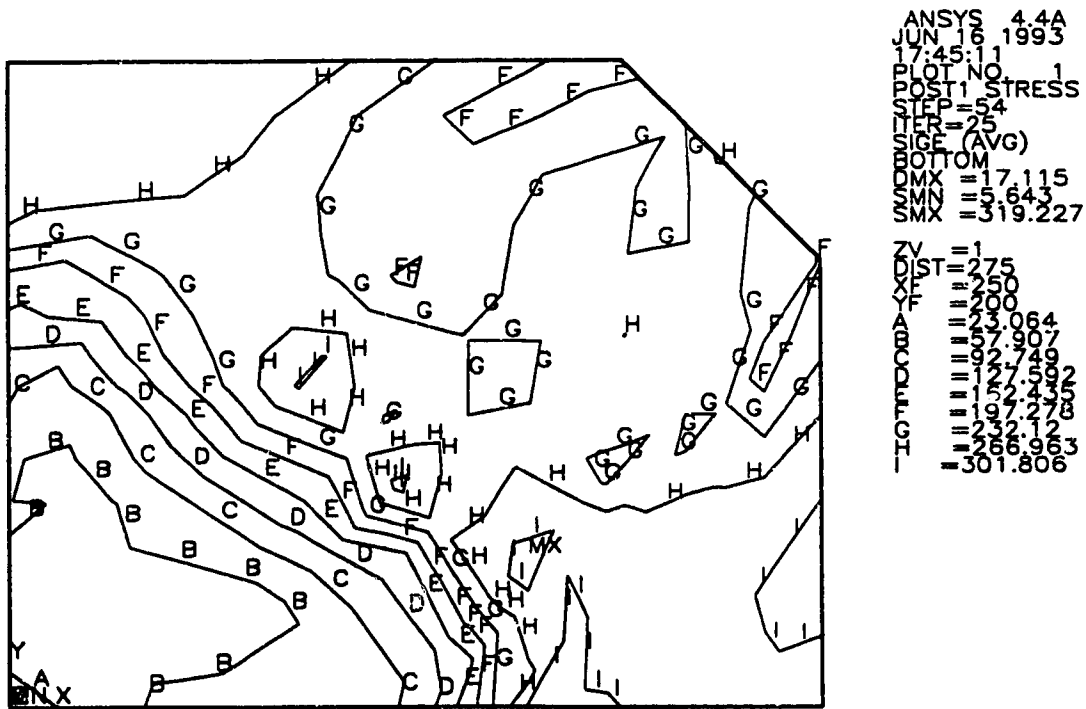
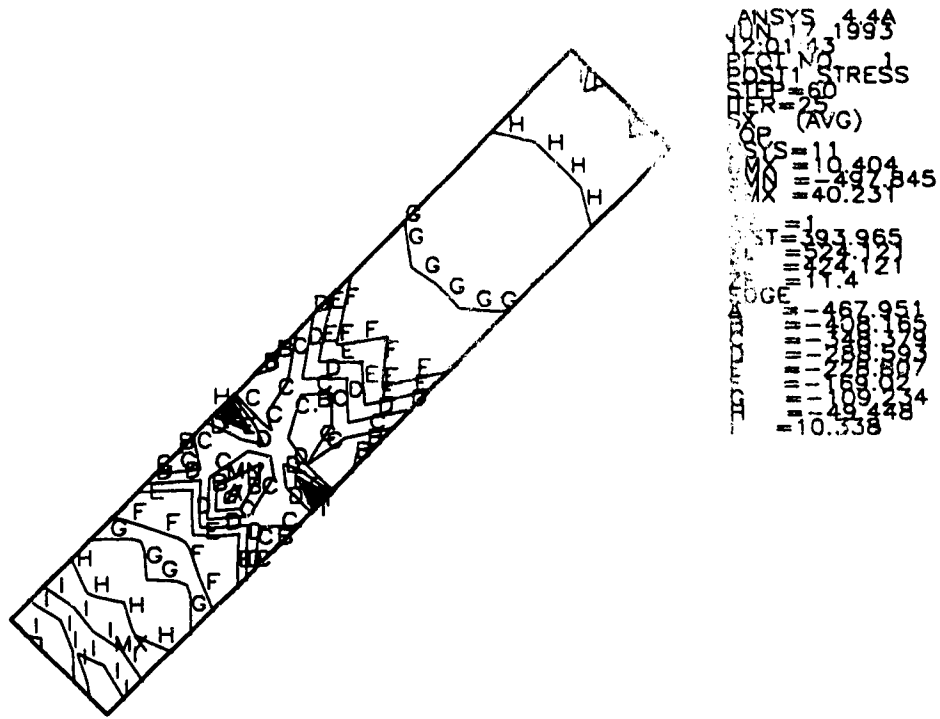
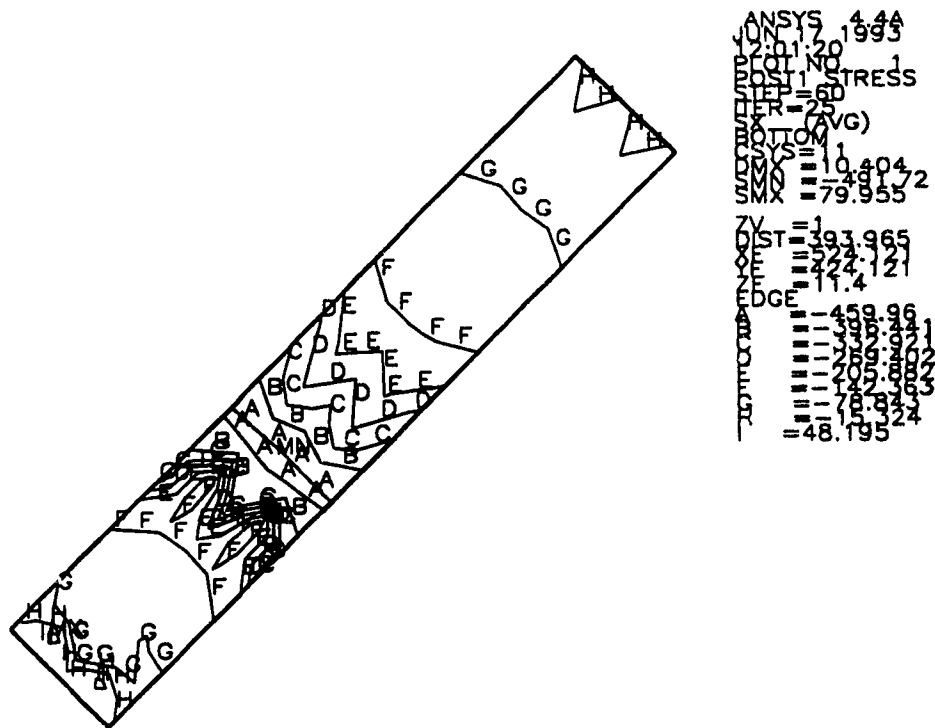


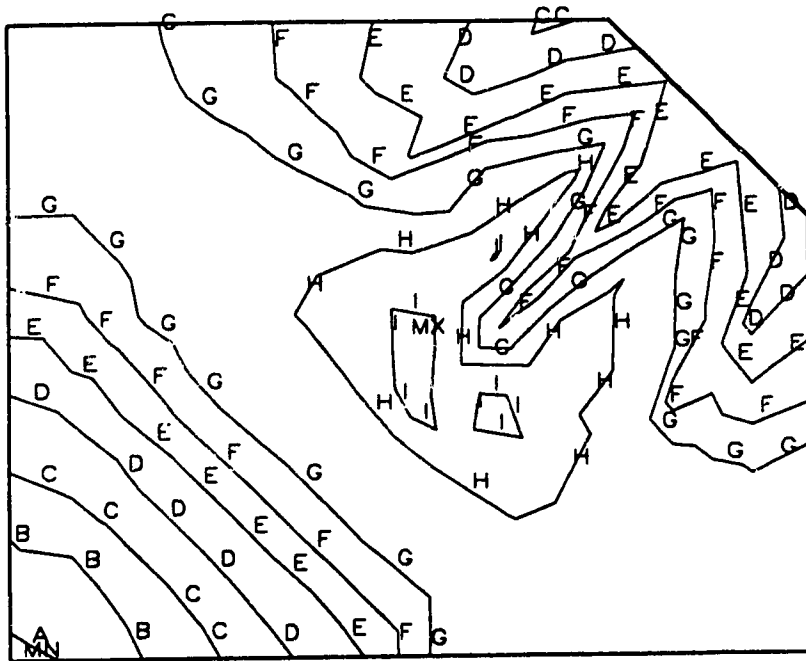
Fig. 9.23 In-Plane Stress Distribution of Gusset Plate Bottom Surface for Specimen EP1 at Ultimate



**Fig. 9.24a In-Plane Stress Distribution of Splice Plate Top Surface for Specimen EP3 at Ultimate**



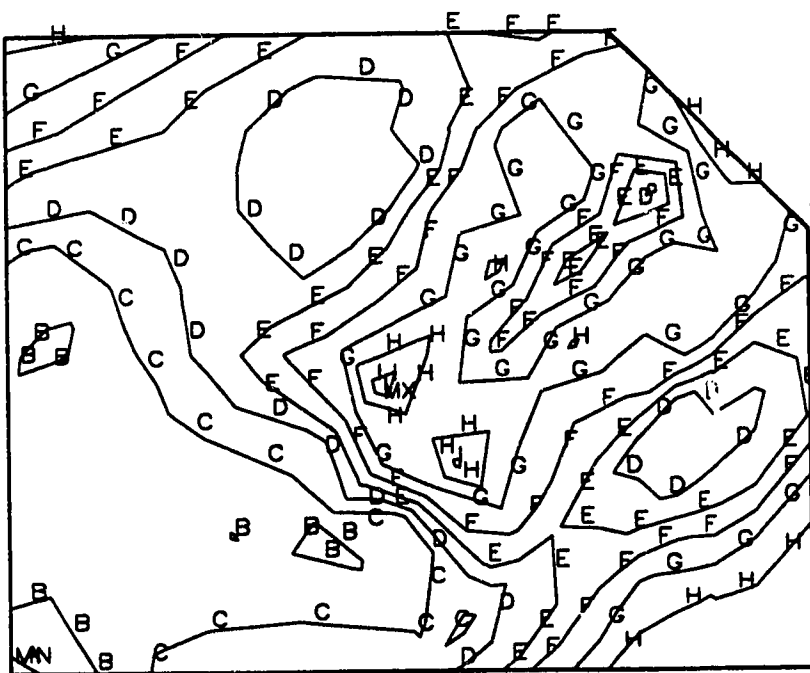
**Fig. 9.24b In-Plane Stress Distribution of Splice Plate Bottom Surface for Specimen EP3 at Ultimate**



```

ANSYS 4.4A
JUN 17 1993
12:30:47
PLOT NO 1
POST1 STRESS
STEP=60
ITER=25
SIGE (AVG)
TOP
DMX = 11.072
SMN = 0.096229
SMX = 369.231
ZV = 1
XST = 275
XYP = 250
XZP = 200
EDGE
DGE
= 20.604
= 61.619
= 102.634
= 143.649
= 184.664
= 225.679
= 266.694
= 307.709
= 348.724
    
```

Fig. 9.25a In-Plane Stress Distribution of Gusset Plate Top Surface for Specimen EP3 at Ultimate



```

ANSYS 4.4A
JUN 17 1993
12:31:11
PLOT NO 1
POST1 STRESS
STEP=60
ITER=25
SIGE (AVG)
BOTTOM
DMX = 11.072
SMN = 0.096229
SMX = 332.846
ZV = 1
XST = 275
XYP = 250
XZP = 200
EDGE
DGE
= 18.582
= 55.595
= 92.597
= 129.499
= 166.471
= 203.443
= 240.416
= 277.388
= 314.36
    
```

Fig. 9.25b In-Plane Stress Distribution of Gusset Plate Bottom Surface for Specimen EP3 at Ultimate



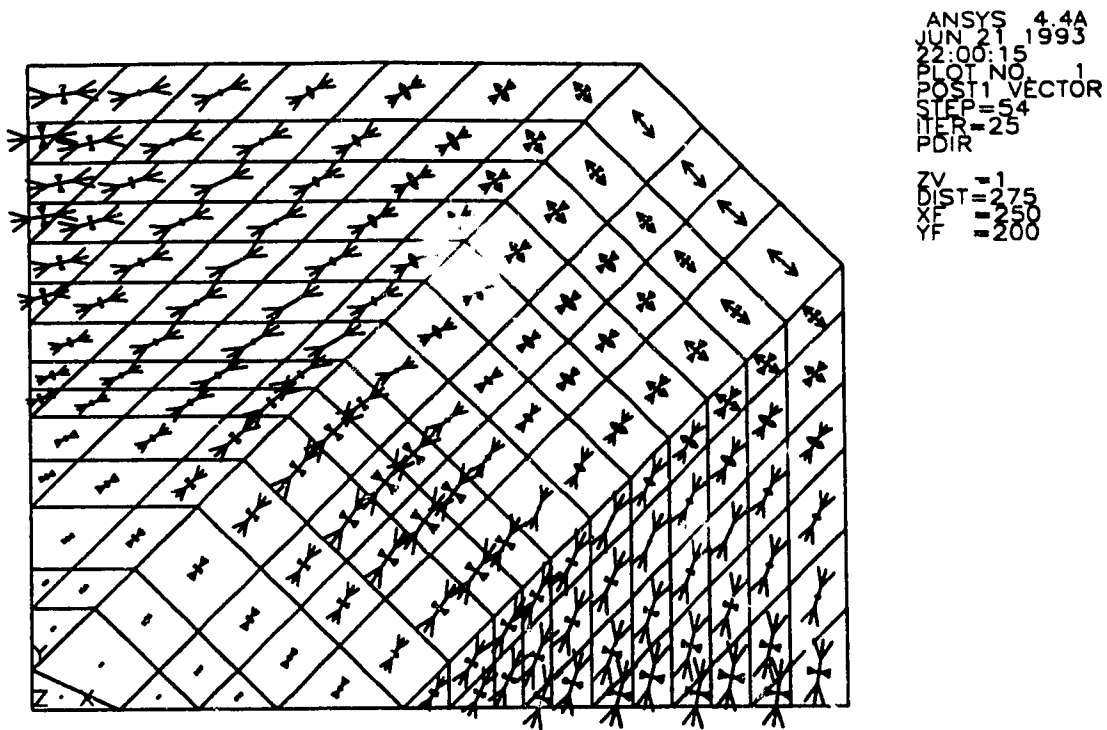


Fig. 9.26 Principal Stress Vector of Gusset Plate Top Surface for Specimen EP1 at Ultimate

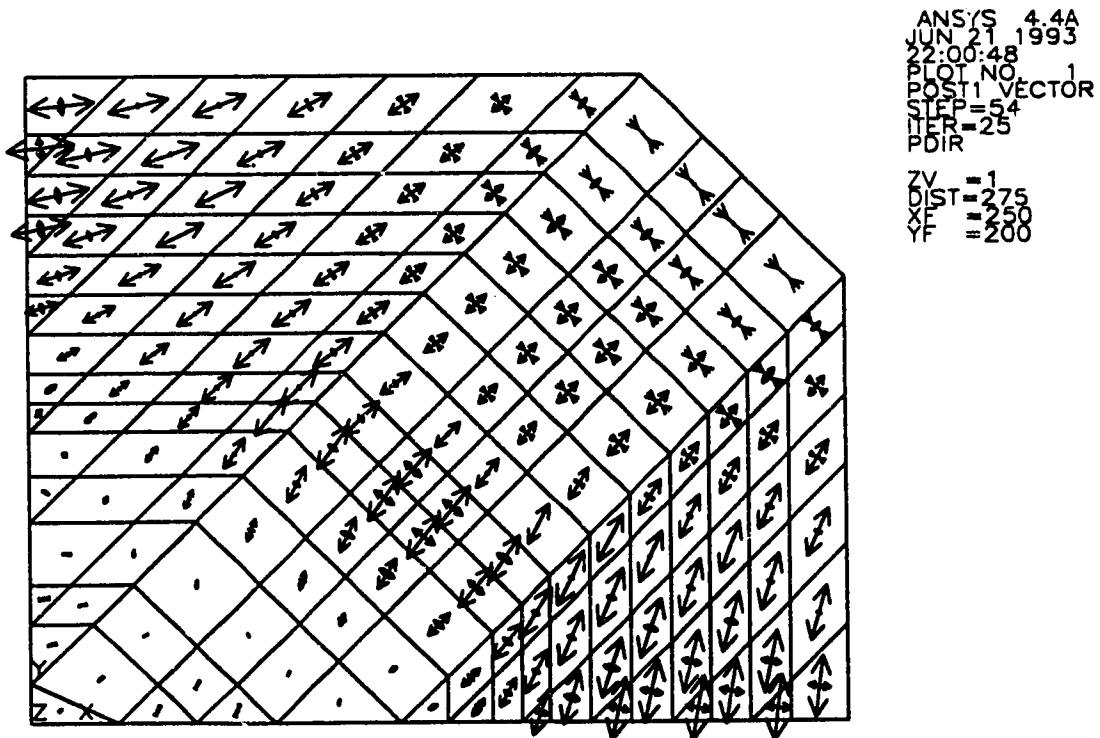


Fig. 9.27 Principal Stress Vector of Gusset Plate Bottom Surface for Specimen EP1 at Ultimate

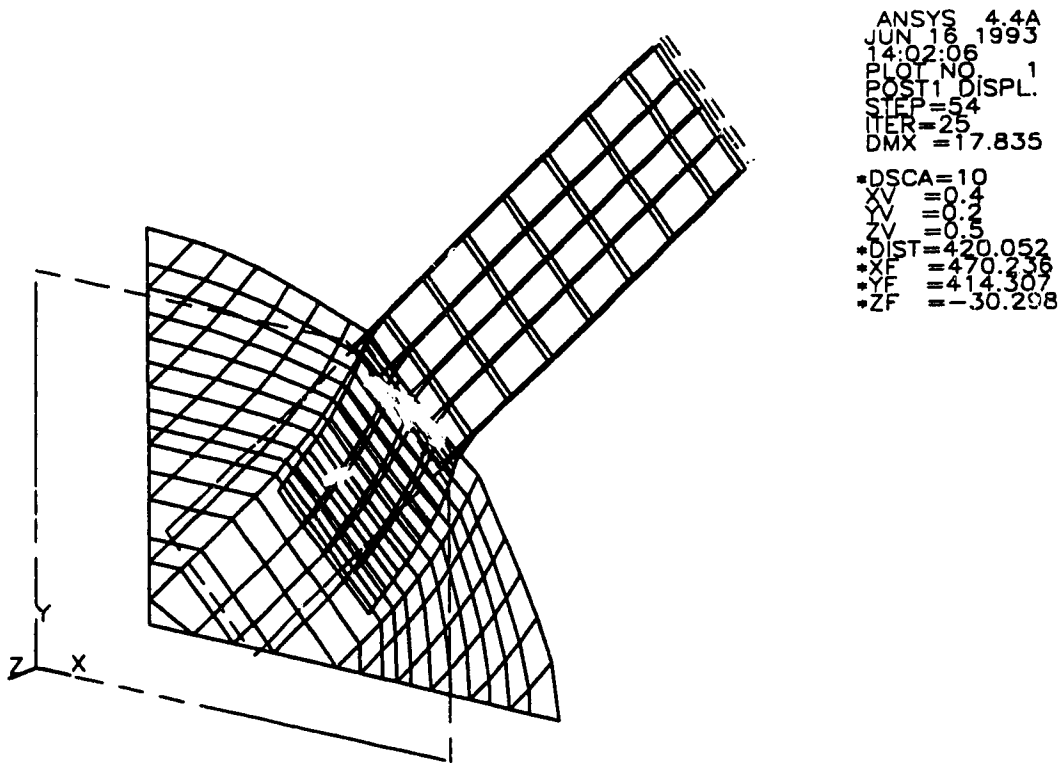


Fig. 9.28 Out-of-Plane Deformation for Specimen EP1

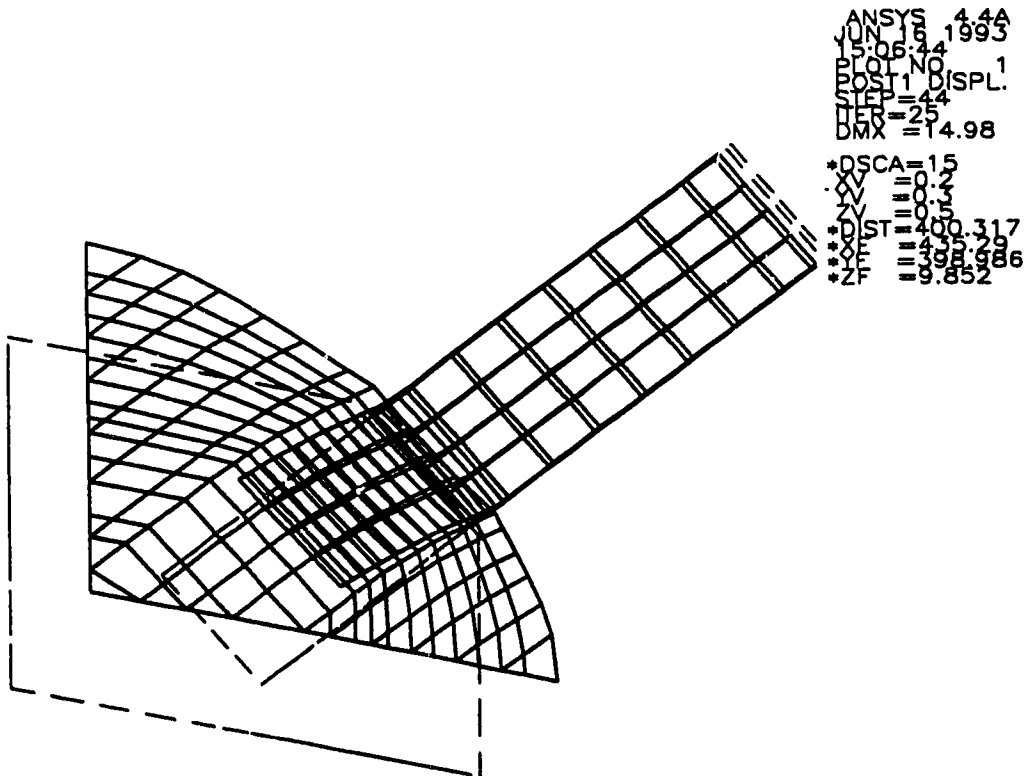


Fig. 9.29 Out-of-Plane Deformation for Specimen EP2

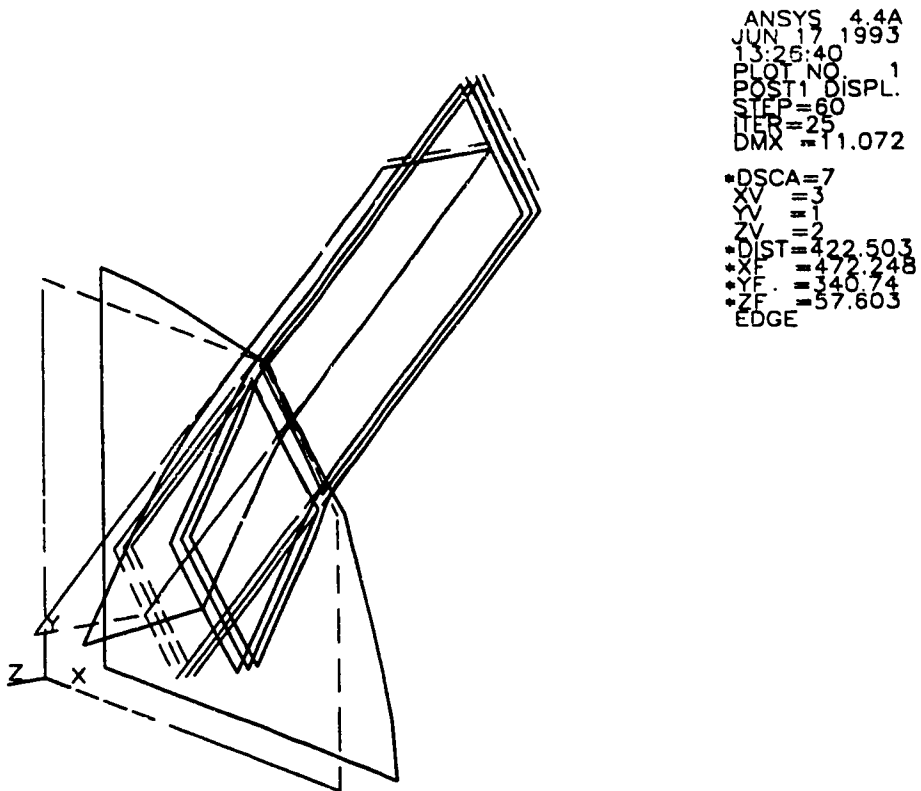


Fig. 9.30 Out-of-Plane Deformation for Specimen EP3

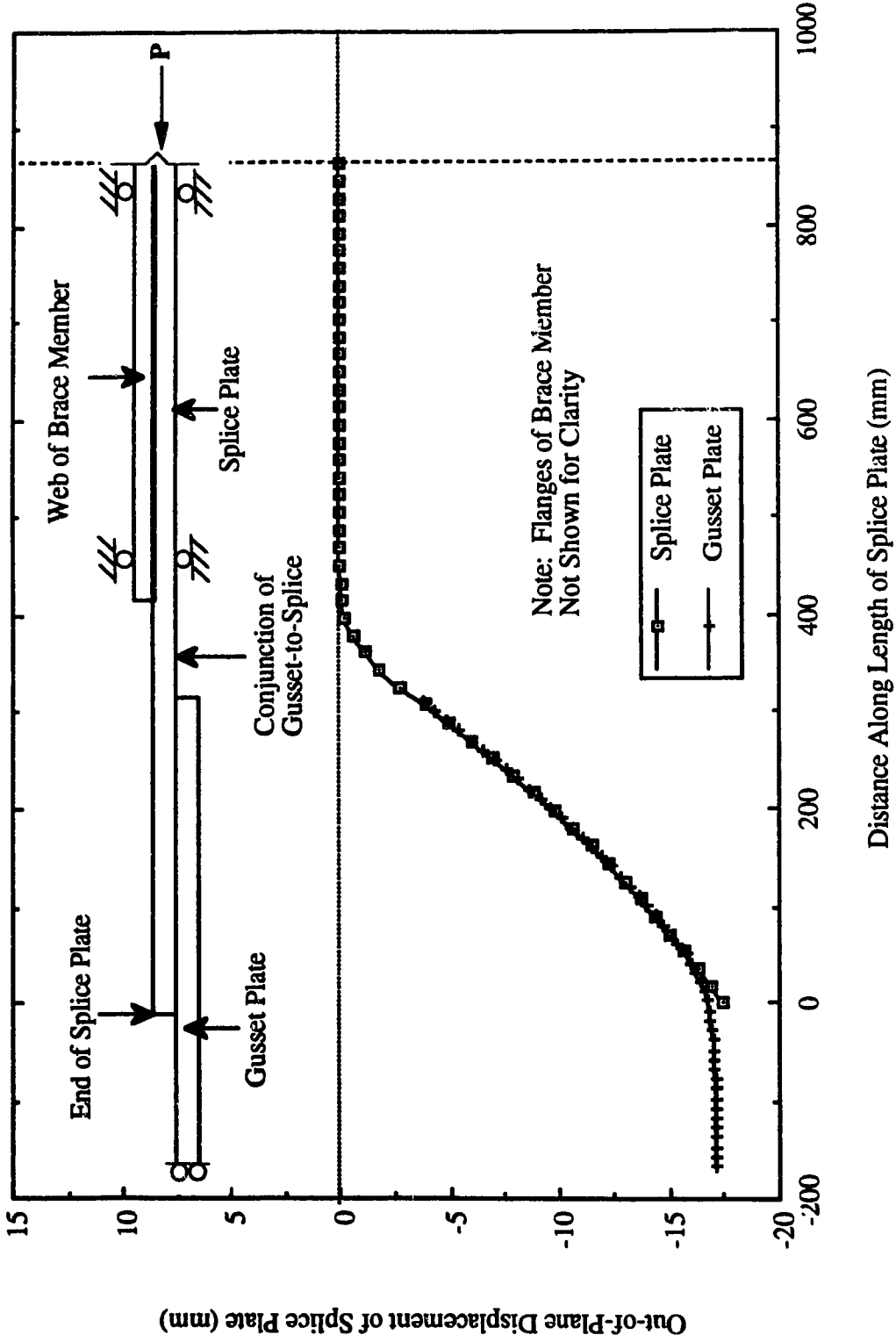


Fig. 9.31 Analytical Out-of-Plane Deflection at Centerline of Splice Plate for Specimen EP1

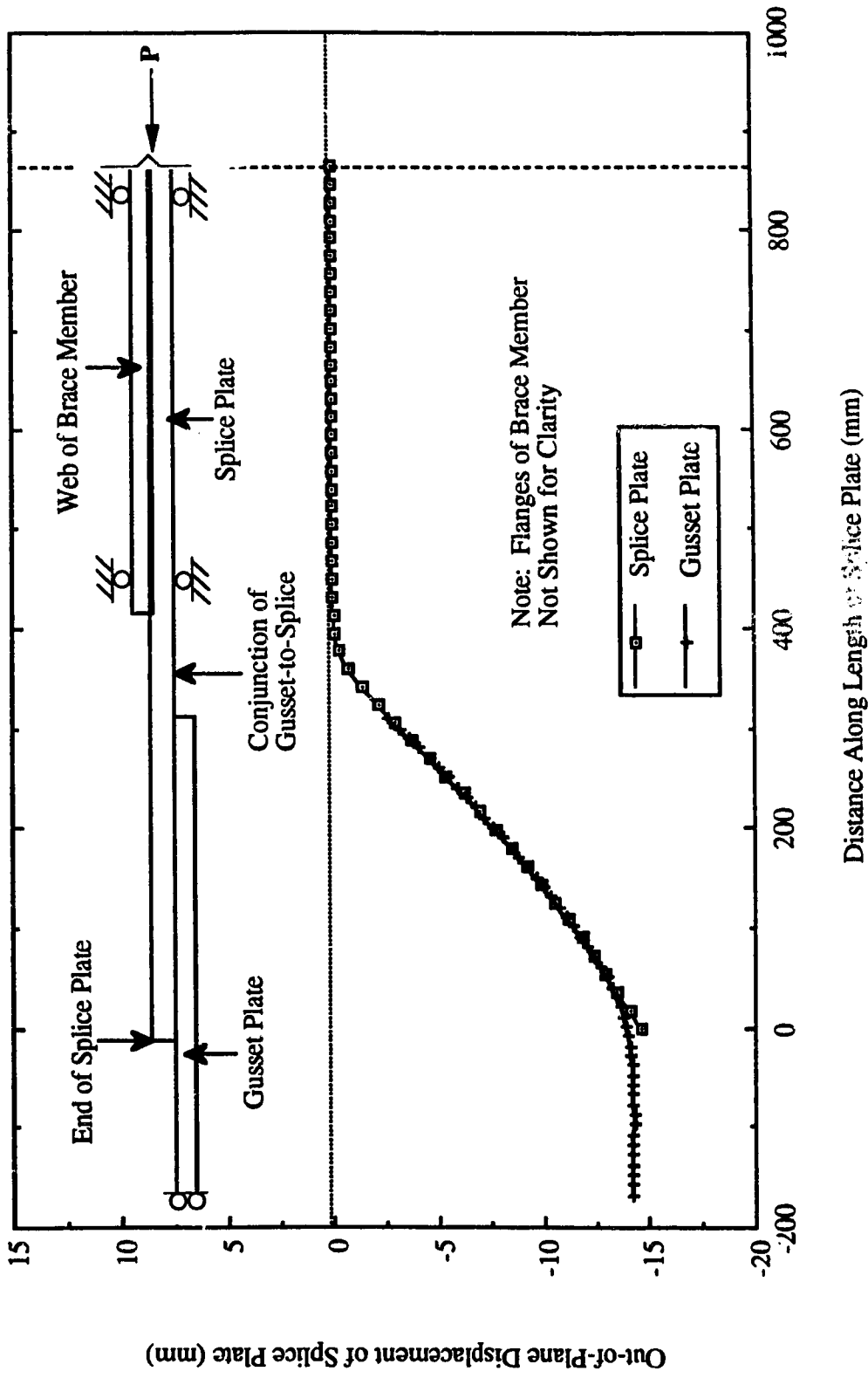


Fig. 9.32 Analytical Out-of-Plane Deflection at Centerline of Splice Plate for Specimen EP2

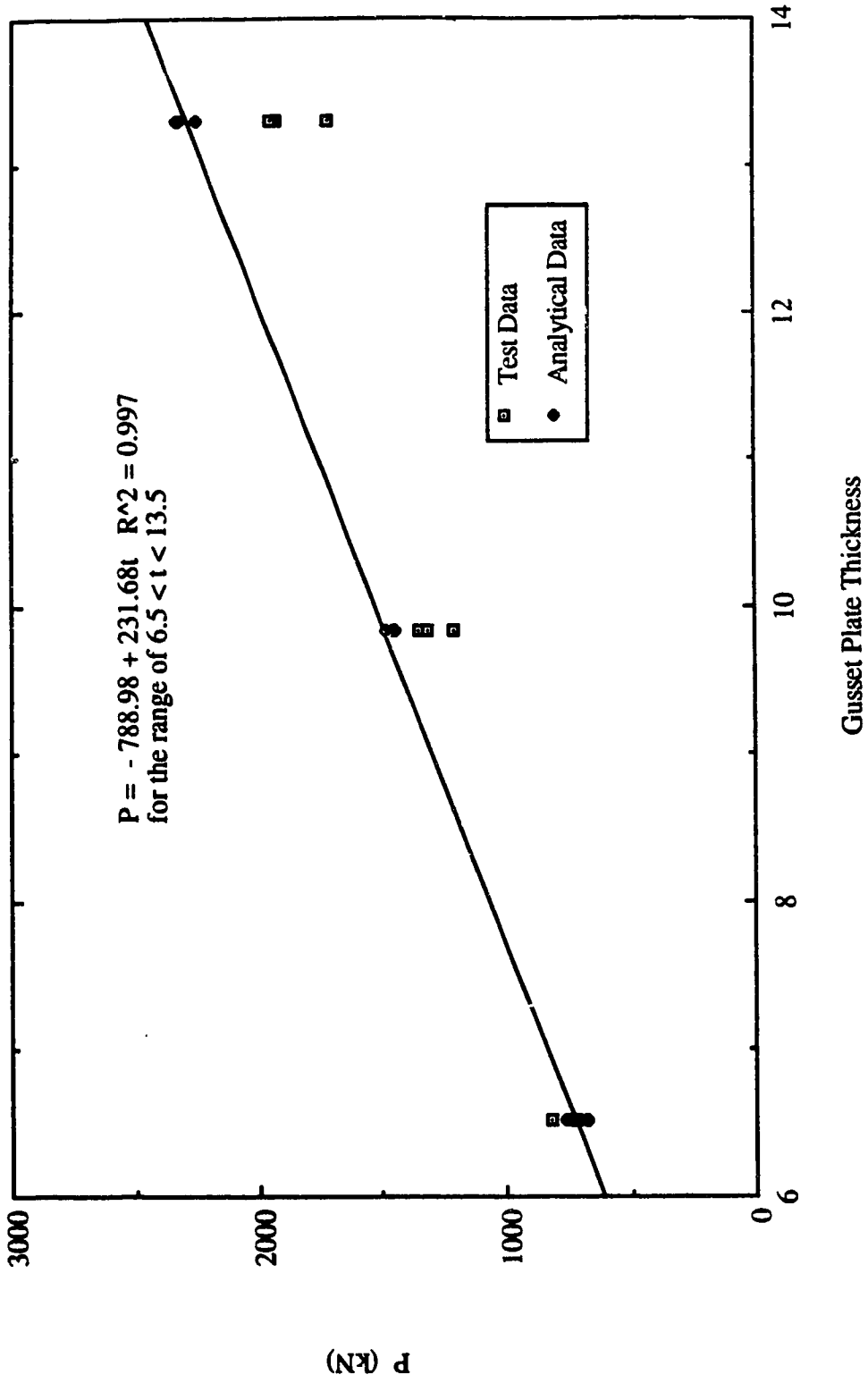


Fig. 9.33 Load vs. Gusset Plate Specimen Thickness

ANSYS 4.4A  
MAR 1 1993  
15:36:09  
PLOT NO. 1  
POST1 STRESS  
STEP=20  
ITER=15  
SIGE (AVG)  
MIDDLE  
SMN =53.388  
SMX =336.232  
ZV =1  
\*DIST=303.475  
\*XF =230.796  
\*YF =185.039  
A B C D E F G H

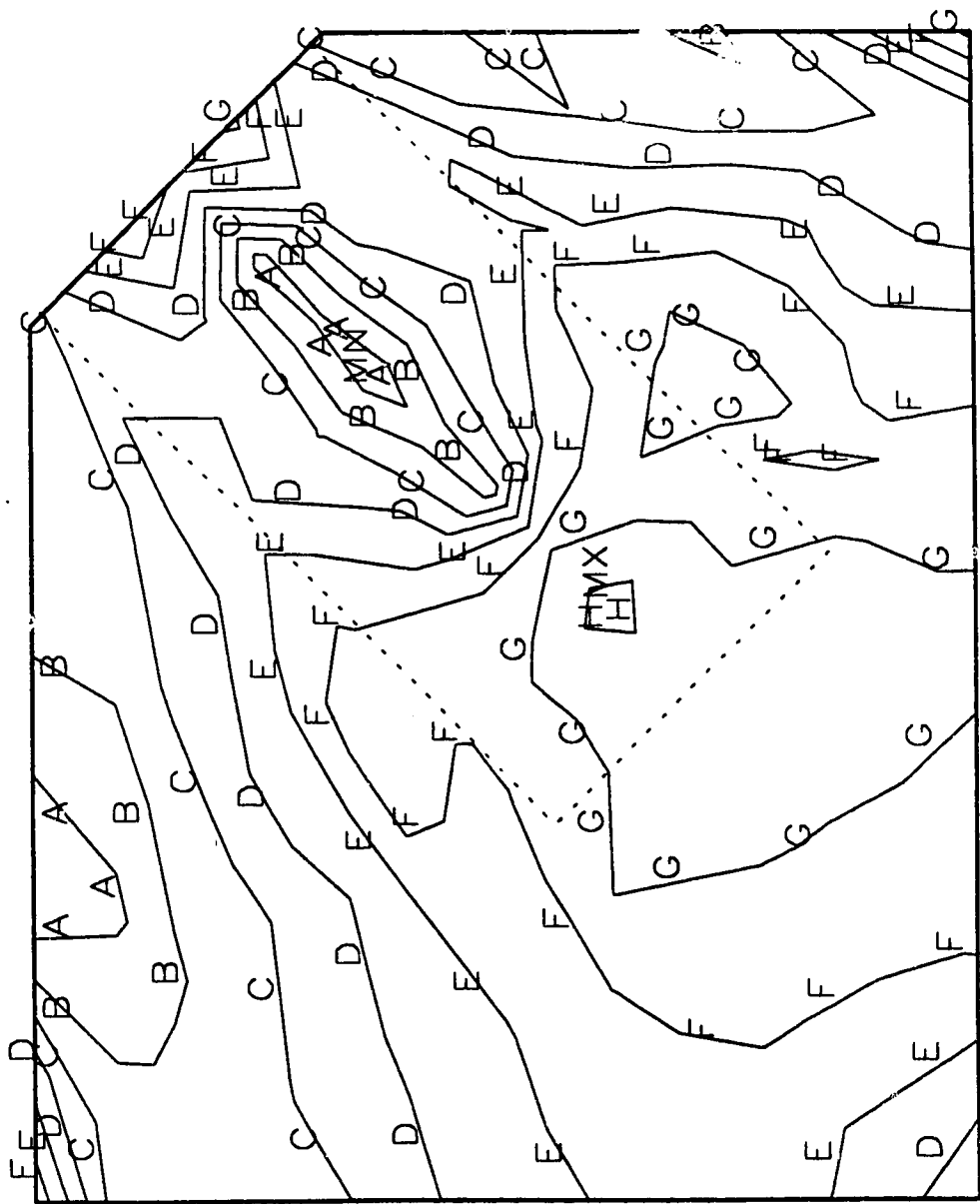


Fig. 9.34 a In-Plane Stress Contour for Specimen MP3 at P = 630 kN

```

ANSYS  4.4A
MAR  1 1993
17:46:57
PLOT NO.  1
POST1  STRESS
STEP=22
ITER=15
SIGE (AVG)
MIDDLE
SMN  =55.37
SMX  =354.47
ZV  =1
*DIST=295.229
*XF  =239.743
*YF  =201.699
      =75
      =110
      =145
      =180
      =215
      =250
      =285
      =320
      =355
      A B C D E F G H I
  
```

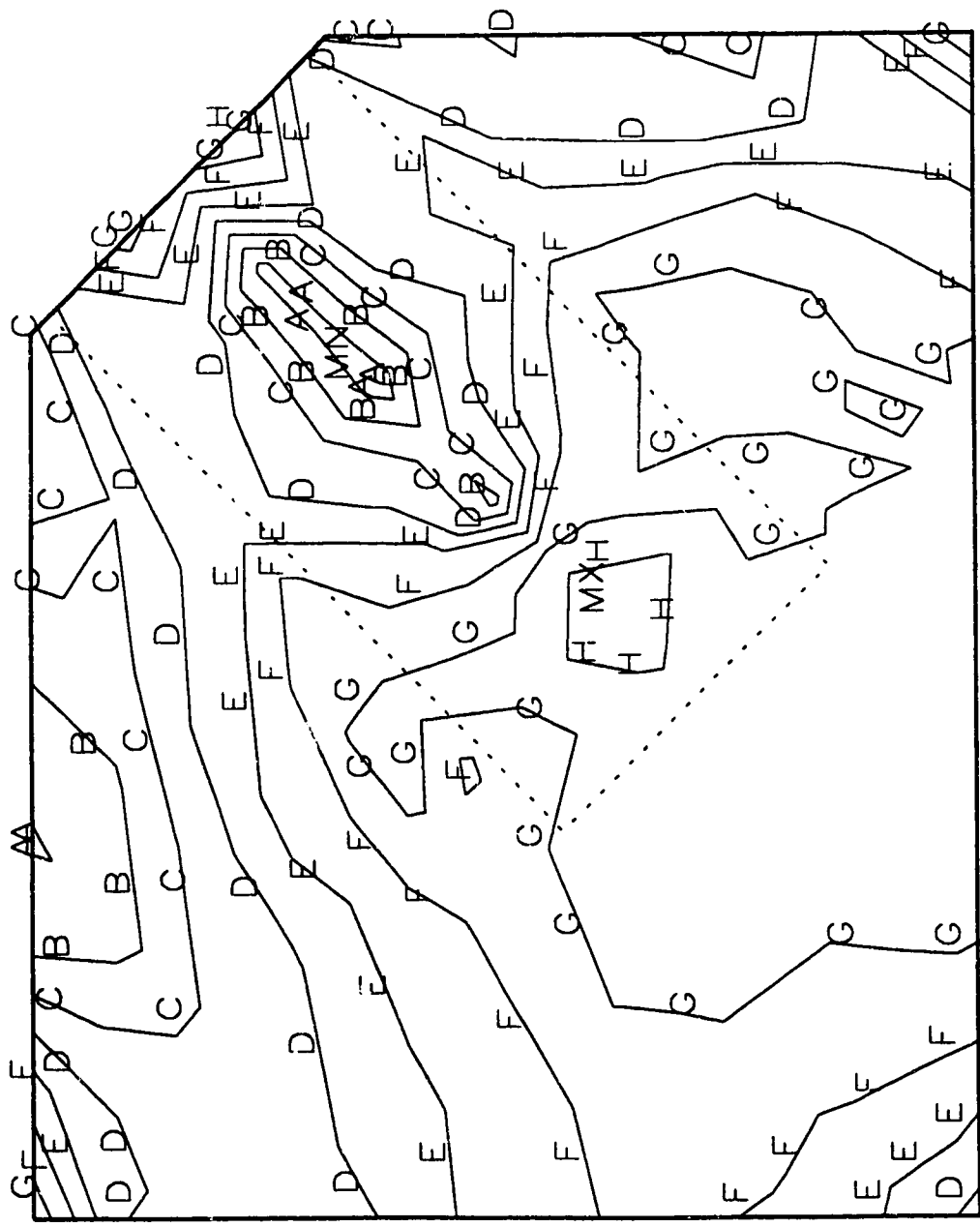


Fig. 9.34 b In-Plane Stress Contour for Specimen MP3A at P = 630 kN



ANSYS 4.4A  
MAR 1 1993  
18:00:09  
PLOT NO. 1  
POST1 STRESS  
STEP=8  
ITER=15  
SIGE (AVG)  
MIDDLE  
SMN =24.541  
SMX =322.738  
ZV =1  
\*DIST=295.473  
\*XF =242.276  
\*YF =195.779  
A =75  
B =110  
C =145  
D =180  
E =215  
F =250  
G =285  
H =320

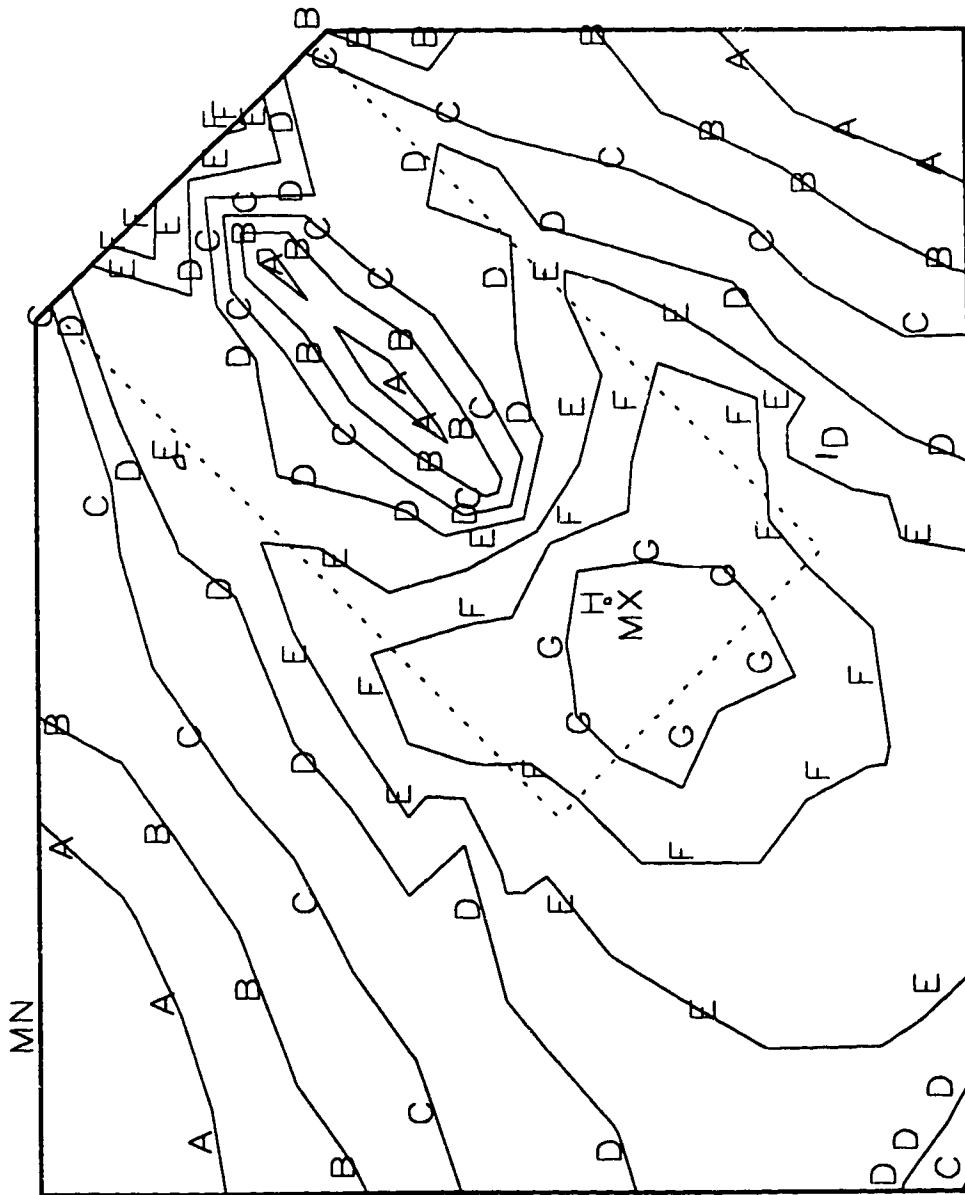


Fig. 9.34c In-Plane Stress Contour for Specimen MP3B at P = 630 kN

ANSYS 4.4A  
MAR 1 1993  
15:36:13  
PLOT NO. 2  
POST1 VECTOR  
STEP=20  
ITER=15  
PDIR  
  
ZV =1  
\*DIST=303.475  
\*XF =230.796  
\*YF =185.039

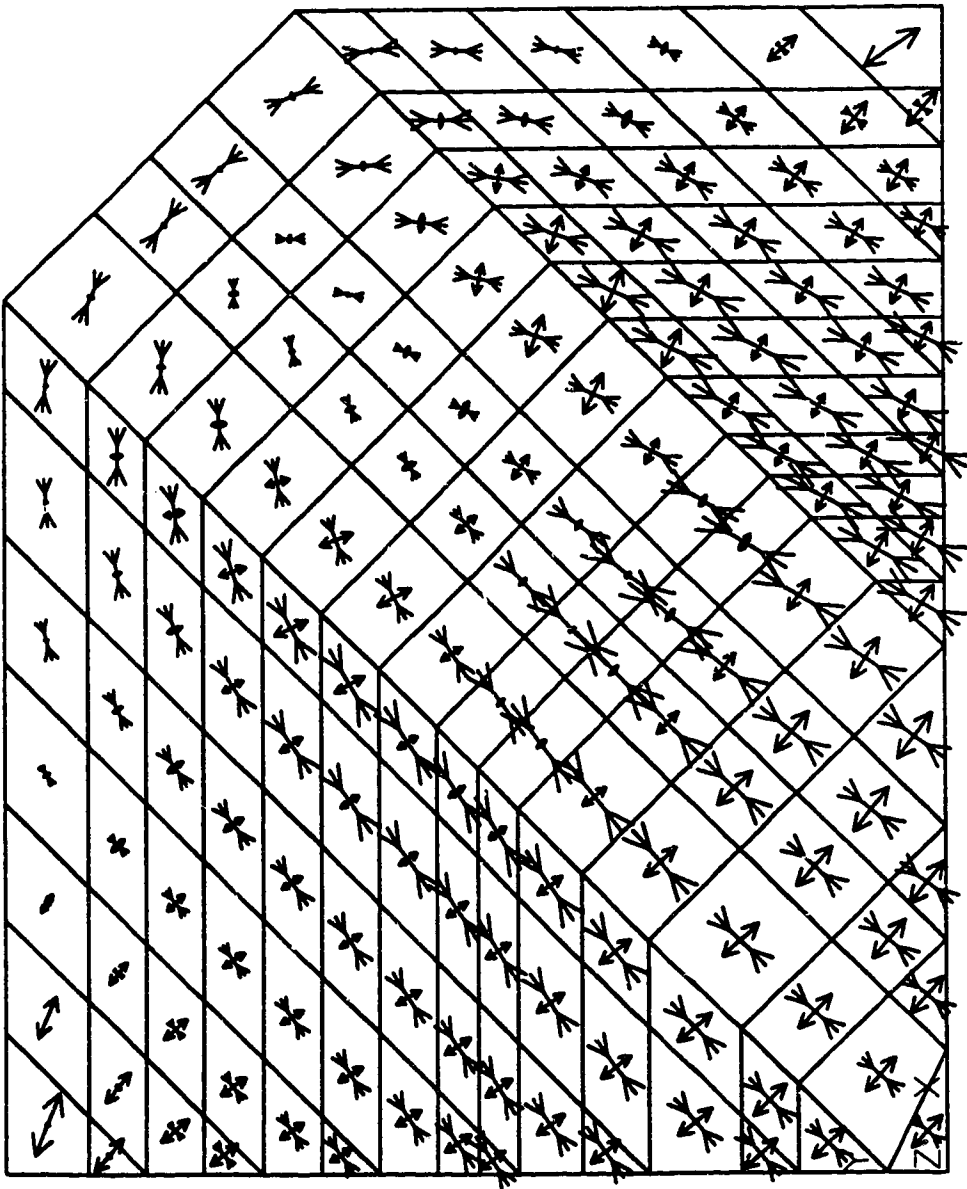


Fig. 9.35a Principal Stress Vector Plot for Specimen MP3 at P = 630 kN

ANSYS 4.4A  
MAR 1 1993  
16:08:27  
PLOT NO. 2  
POST1 VECTOR  
STEP=22  
ITER=15  
PDIR  
  
ZV = 1  
\*DIST=305.961  
\*XF = 260.124  
\*YF = 213.219

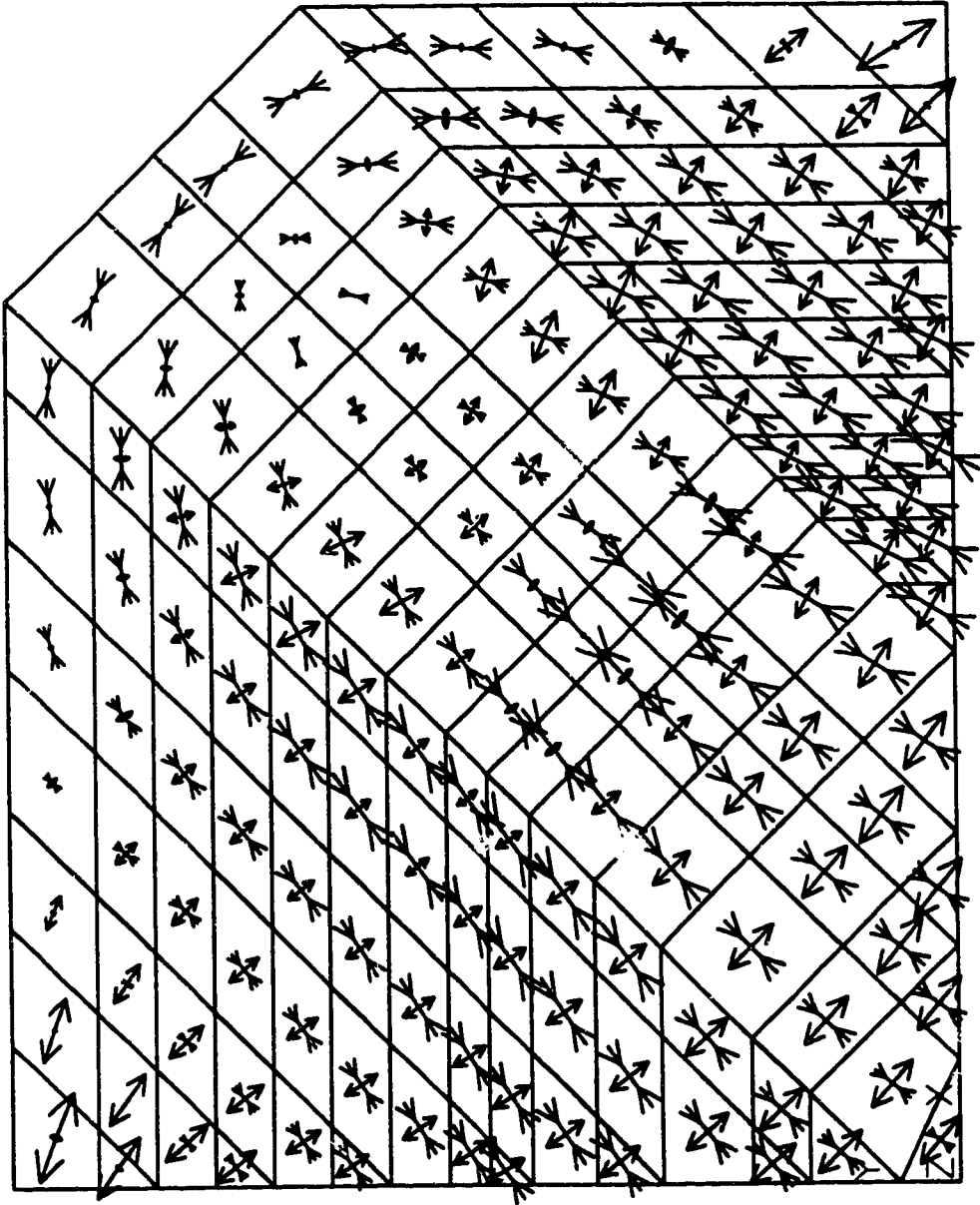


Fig. 9.35b Principal Stress Vector Plot for Specimen MP3A at P = 630 kN

ANSYS 4.4A  
MAR 1 1993  
13:41:06  
PLOT NO. 2  
POST1 VECTOR  
STEP=8  
ITER=15  
PDIR  
  
ZV =1  
\*DIST=297.677  
\*XF =264.022  
\*YF =184.309

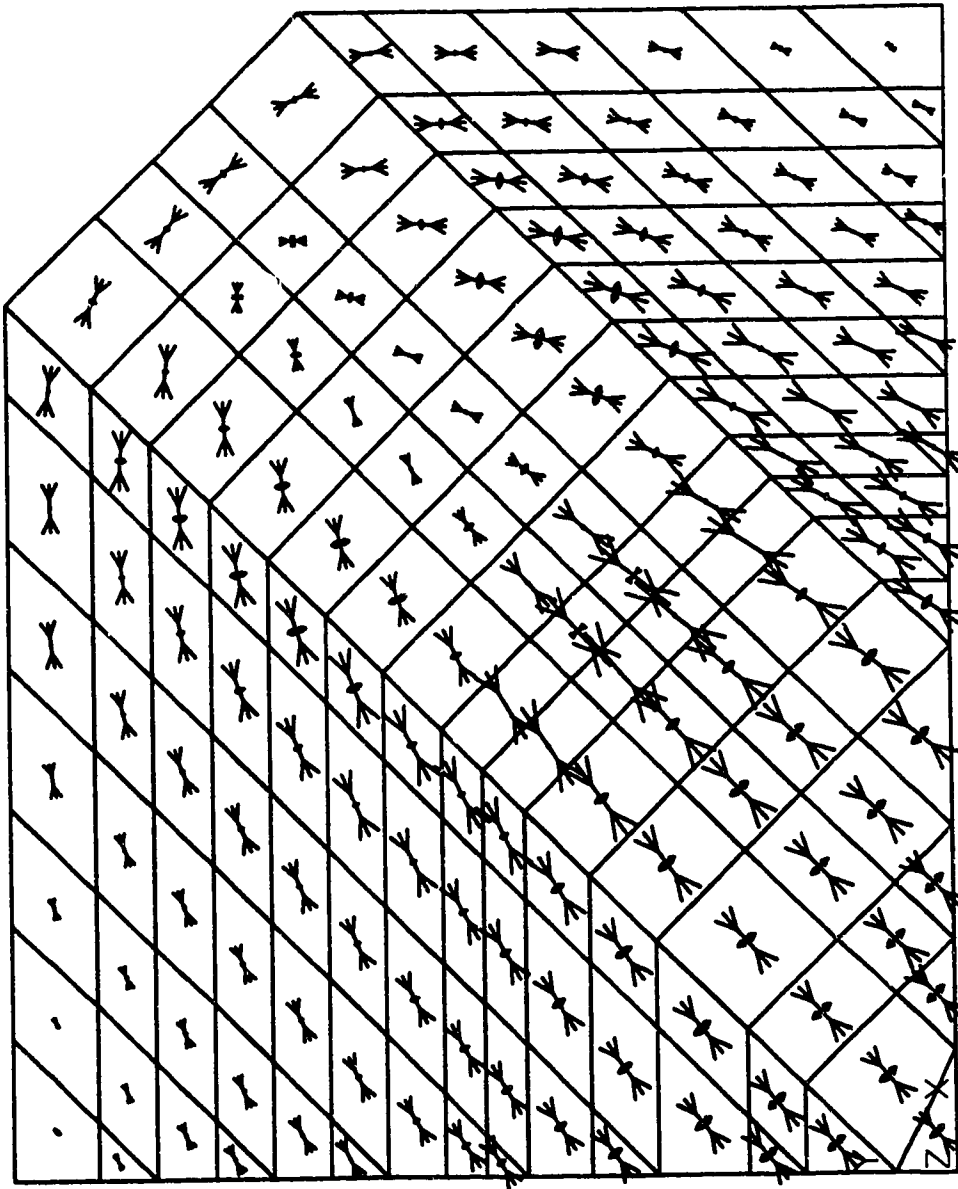


Fig. 9.35c Principal Stress Vector Plot for Specimen MP3B at P = 630 kN

ANSYS 4.4A  
MAR 9 1993  
17:19:49  
PLOT NO. 1  
POST1 DISPL.  
STEP=20  
ITER=15  
DMX =3.175  
\*DSCA=40  
ZV =1  
\*DIST=297.98  
\*XF =263.112  
\*YF =185.645

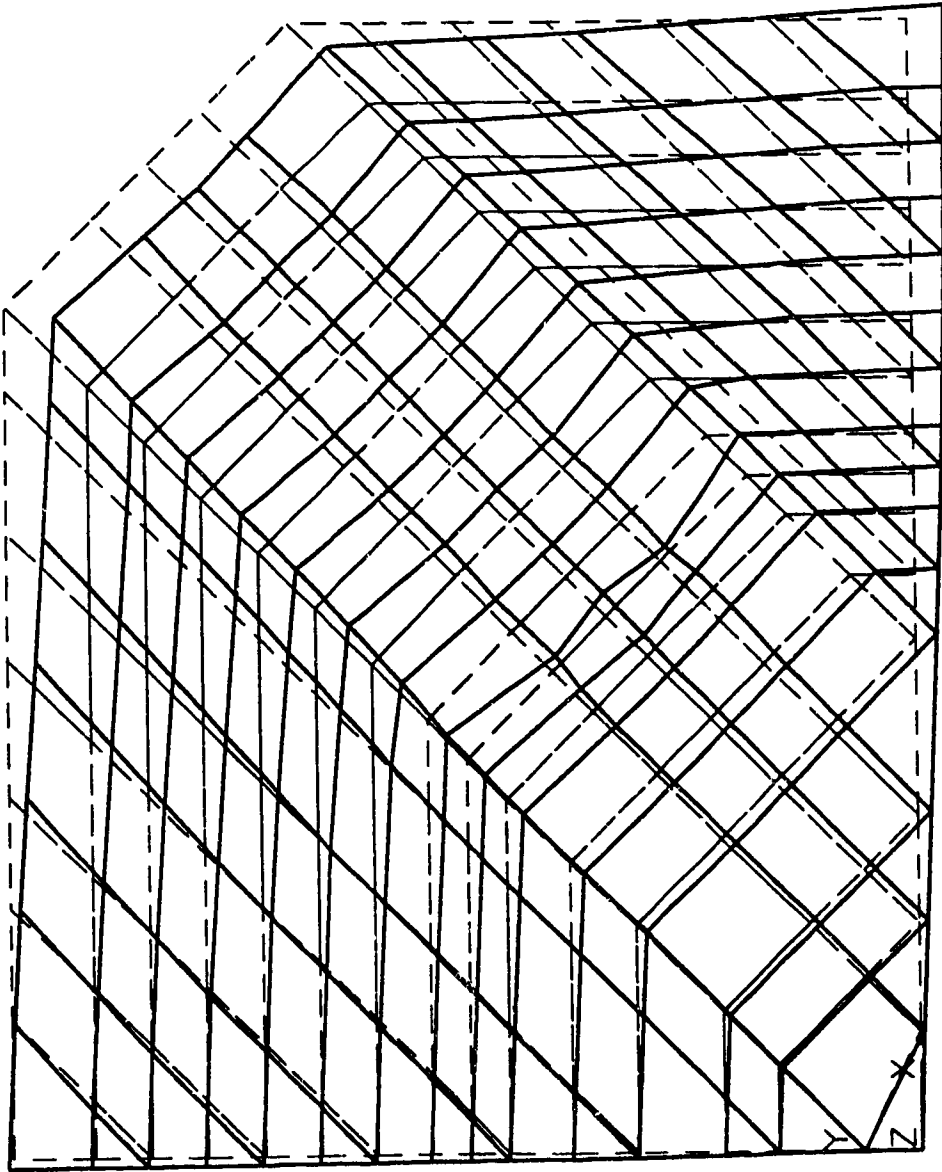


Fig. o 36a In-Plane Deformation Mode for Specimen MP3 at P = 630 kN

```
ANSYS 4.4A
MAR 9 1993
17:04:55
PLOT NO. 1
POST1 DISPL.
STEP=22
ITER=15
DMX =4.75

*DSCA=40
ZV =1
*DIST=350.508
**XF =244.59
**YF =214.637
```

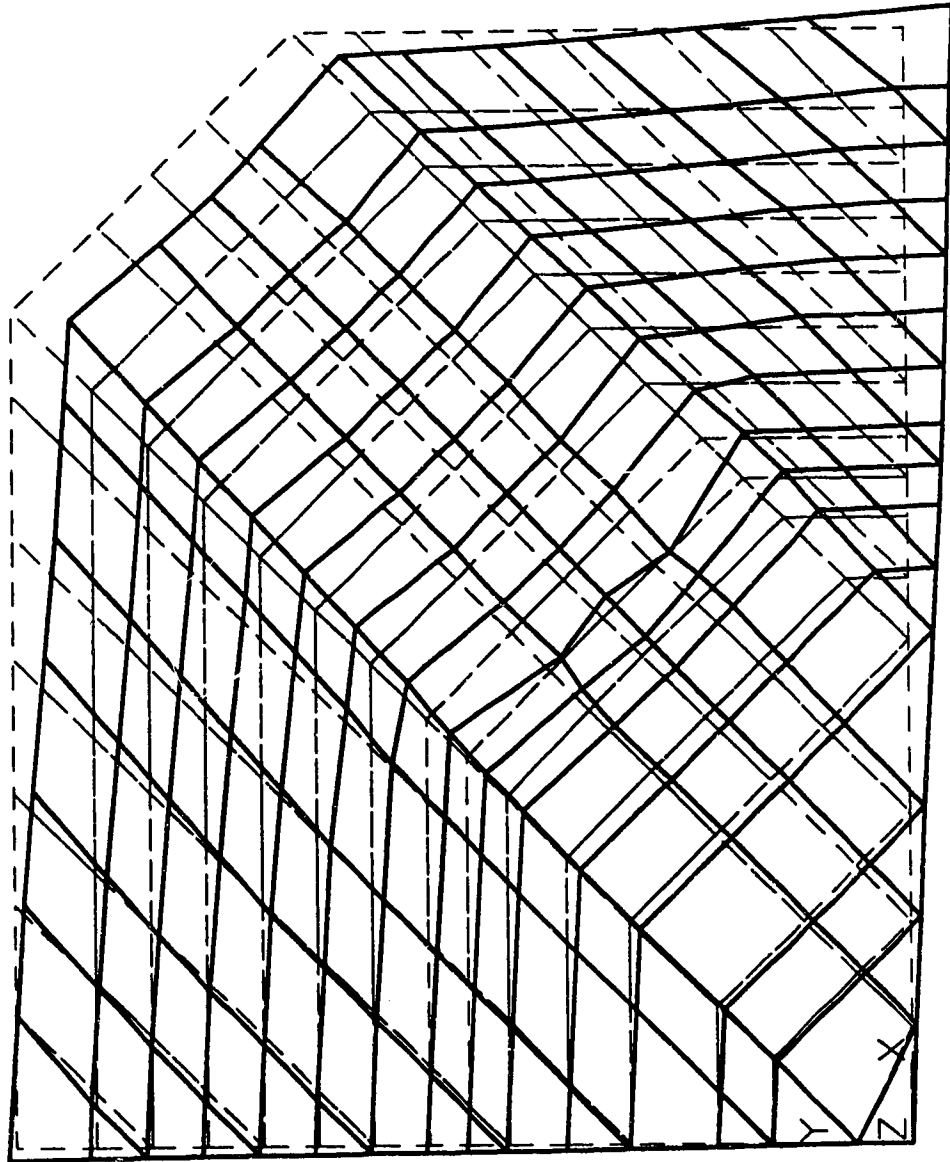


Fig. 9.36b In-Plane Deformation Mode for Specimen MP3A at P = 630 kN

ANSYS 4.4A  
MAR 1 1993  
13:41:11  
PLOT NO. 3  
POST1 DISPL.  
STEP=8  
ITER=15  
DMX =0.510306  
  
DSCA=58.333  
ZV =1  
\*DIST=297.677  
\*XF =264.022  
\*YF =184.309

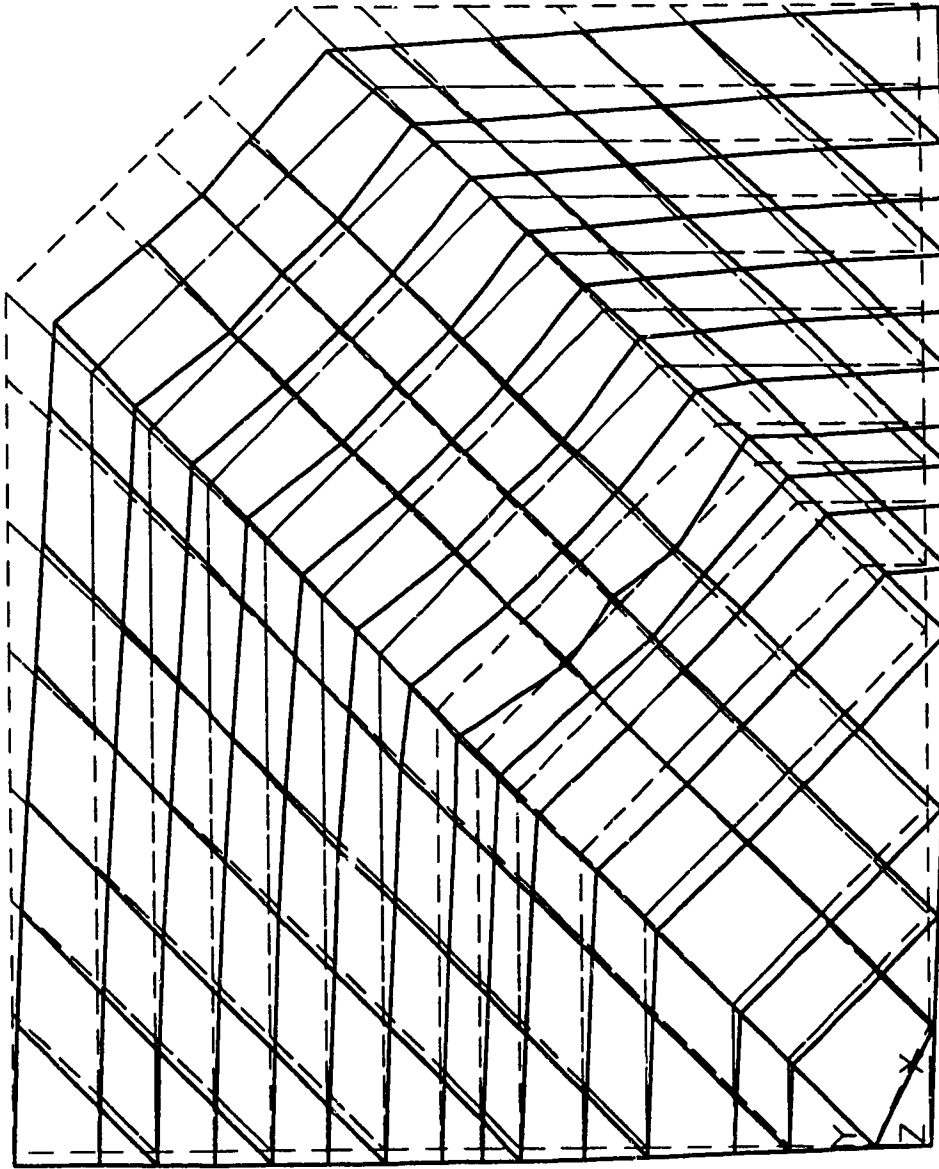


Fig. 9.36c In-Plane Deformation Mode for Specimen MP3B at P = 630 kN

Loading Eccentricity  $e = \frac{13.3 + 9.5}{2}$   
 = 11.4 mm

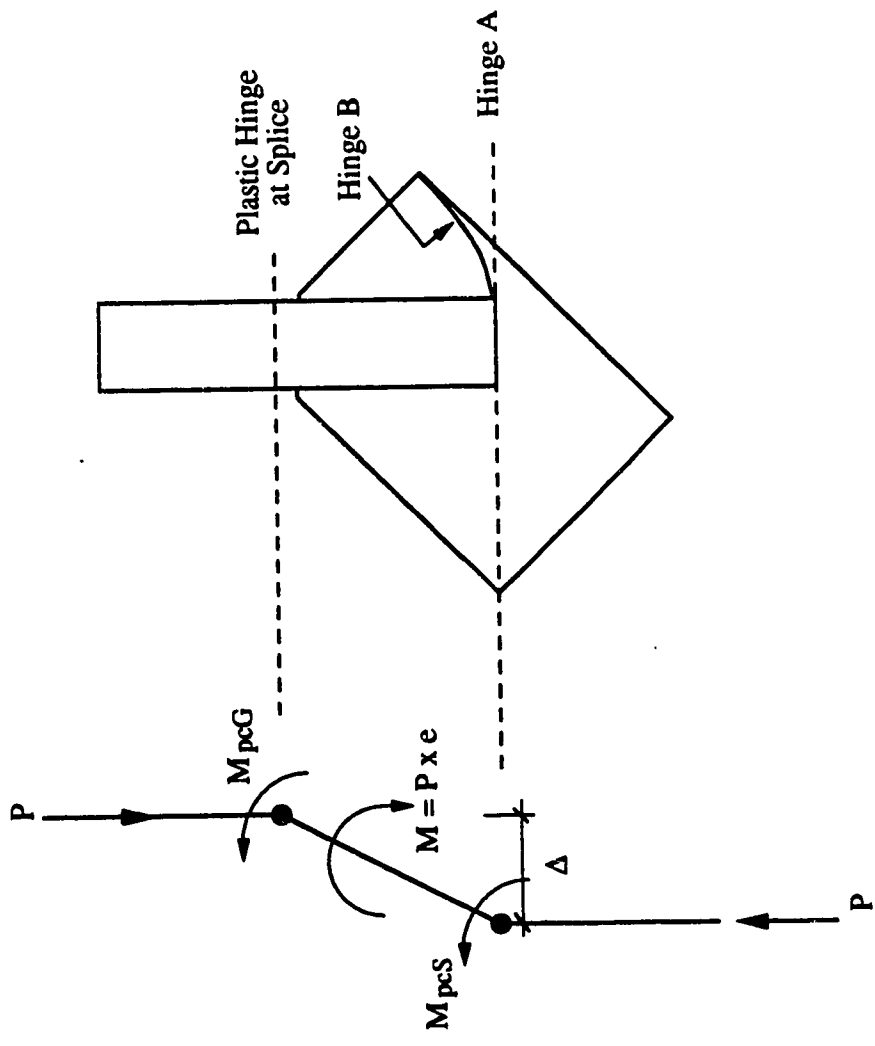
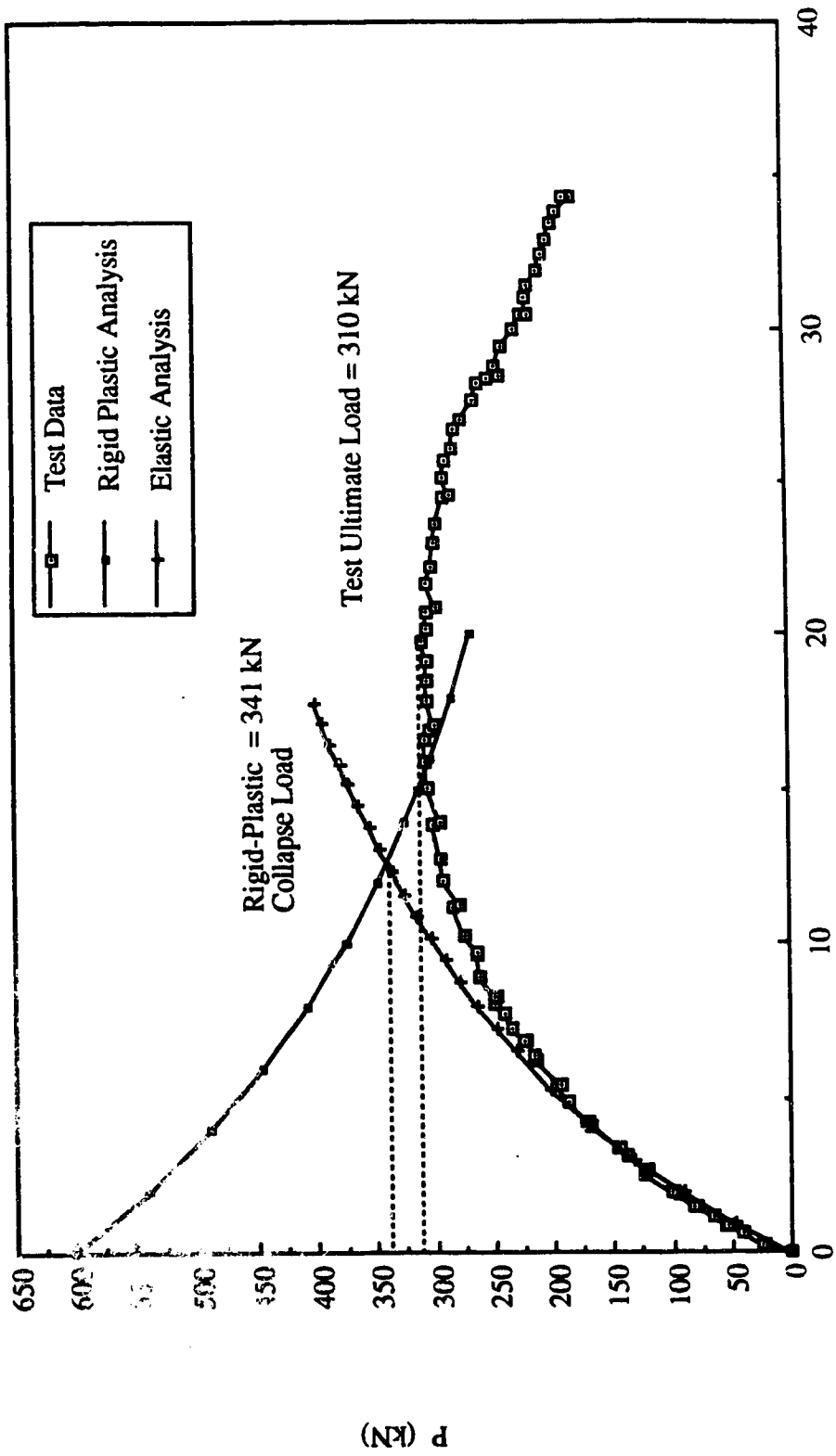


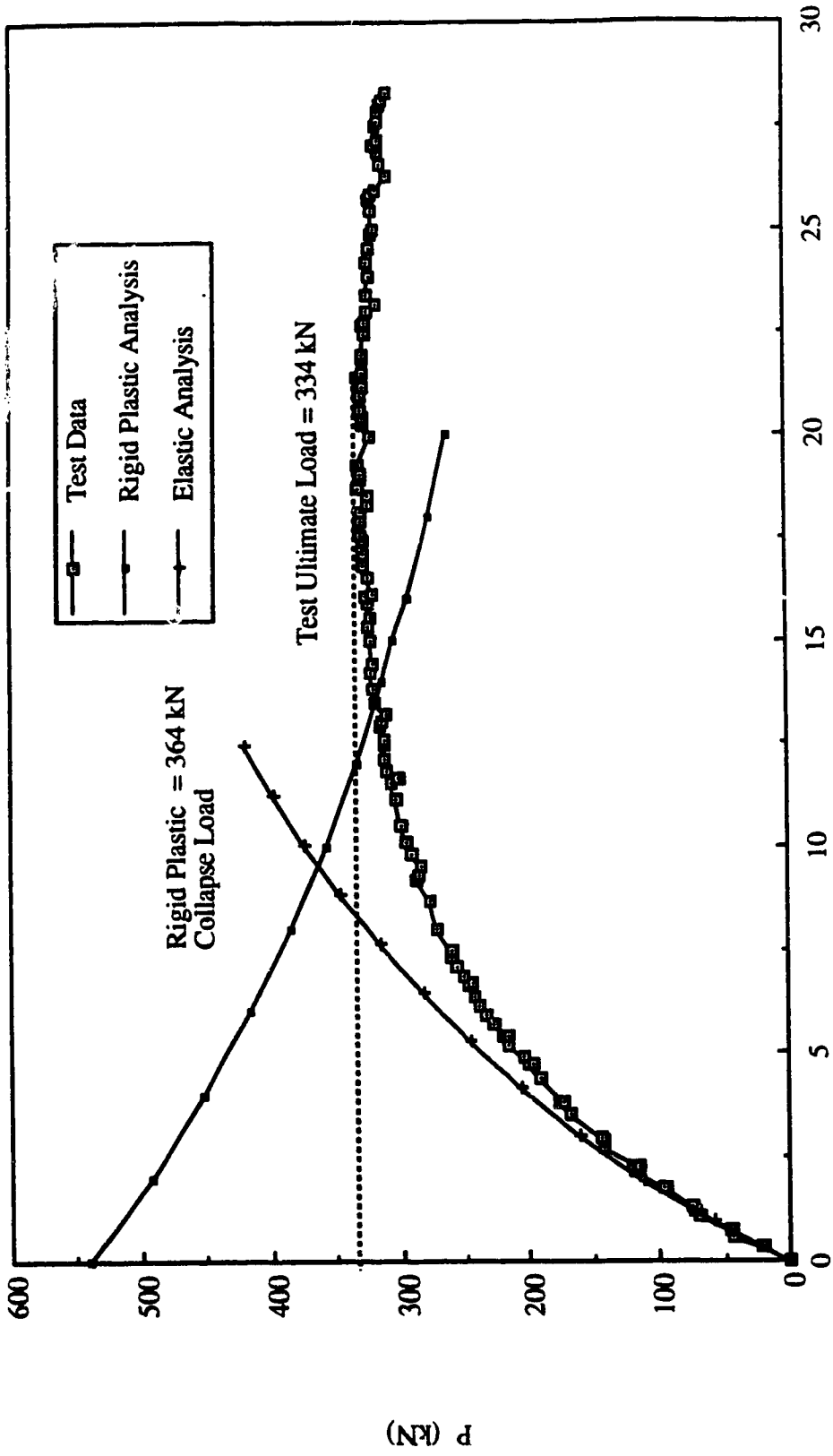
Fig. 9.38 Rigid-Plastic Collapse Mechanism for Specimens EP1 and EP2





Out-of-Plane Displacement of Test Frame (mm)

Fig. 9.39 Rigid-Plastic Unloading Line for Specimen EP1



Out-of-Plane Displacement of Test Frame (mm)

Fig. 9.40 Rigid Plastic Unloading Line for Specimen EP2

## **10. PROPOSED DESIGN GUIDELINES AND METHODS**

### **10.1 General**

A set of general design guidelines and methods are proposed in this chapter. The design guidelines are based on the parametric studies of the elastic buckling load of gusset plate connections (Cheng et al. 1994) which will be discussed in detail in the next section. The design method for gusset plate connections subject to compression is derived from the Thornton method (Thornton 1984), which has been examined in Chapter 1. For the eccentrically loaded gusset plate connections, which were failed by significant yielding at the splice member, the strength of the connections is examined using the beam-column equation of a rectangular section.

### **10.2 Elastic Parametric Studies of Gusset Plate Connections**

#### **10.2.1 General**

Hu and Cheng (1987) examined the compressive behavior and buckling strength of thin-walled gusset plate connections. The test setup for this experimental program is shown in Fig. 1.7. The test results of this investigation showed that elastic buckling of the gusset plate connection occurred in all the eccentrically loaded specimens. The experimental elastic buckling loads of these specimens are shown in Table 10.1.

The analytical elastic buckling load of these test specimens obtained using the finite element program ANSYS was studied by Cheng et al.(1994). The typical specimen size and the finite element model are shown in Fig. 10.1. The analytical results from this study are shown in Table 10.1. It can be seen from this table that the analytical results and the test results of specimens C2 and C3 are in reasonable agreement. However, a large discrepancy exists for specimens C1 and C4. For specimen C1, the discrepancy was due to the yielding that occurred in the splice plate at the conjunction of gusset-to-splice during

testing. This yielding reduced the rotational restraint at the conjunction; hence, the buckling load of the specimens was decreased. However, in the analytical model, a rigid rotational restraint was assumed at the conjunction. For specimen C4, the test buckling load was significantly higher than the analytical buckling load. This was due to the post-buckling strength of specimen C4. The details of a large deflection analysis that was employed to investigate this post-buckling behavior can be found in Cheng et al. (1994).

Hu and Cheng (1987) concluded that the splice plate thickness and length and the rotational restraint at the conjunction of the gusset-to-splice have significant effects on the elastic buckling load of gusset plate connections. In order to study the effects of these parameters, a parametric study was conducted. The finite element program ANSYS and the finite element model shown in Fig. 10.1 were used in the parametric study. This study will provide the general guidelines for designing the concentrically loaded gusset plate connections.

## 10.2.2 Parametric Studies

### 10.2.2.1 General

The parametric studies of the elastic buckling load of the gusset plate connections include the following parameters:

- 1) the thickness of the splice plate members;
- 2) the length of the splice plate members (SL; see Fig. 10.2) connected to the gusset plates;
- 3) the rotational restraint at the conjunction of the bracing member and the gusset plate.

Although this parametric study is limited to elastic analysis, the results can still illustrate the general influence of each parameter on the buckling load of the gusset plate connections.

### **10.2.2.2 Effects of Splice Plate Thickness**

The effects of splice plate thickness on the elastic buckling strength of the gusset plate connections are shown in Fig. 10.3. As shown in the figure, the investigation was conducted with two gusset plate sizes, 850 x 550 mm and 850 x 700 mm, three gusset plate thicknesses, 3.11 mm, 6.7 mm, and 9.5 mm, and two splice member lengths (SL), 297 mm and 447 mm. The splice plate length of 297 mm corresponds to the length of four rows of bolts connected to the gusset plate, and the splice plate length of 447mm corresponds to six rows of bolts connected to the gusset plate, as shown in Fig. 10.4.

It can be observed from Fig. 10.3 that the 3.11mm thick gusset plates with a splice plate thickness of 7 mm achieve 80% or more of the buckling load of the same gusset plate with infinite splice plate thickness. At a splice plate thickness of 13mm, the 3.11mm thick gusset plate is able to reach more than 97% of the buckling load of the same gusset plate with infinite splice plate thickness. Therefore, it can be seen that when the splice plate thickness is increased, the buckling load of the gusset plate increases until a critical value of the splice plate thickness is reached, after which increases in the splice plate thickness do not produce a significant additional increase in the buckling load. This implies that this critical value of splice plate thickness provides a rigid support to the gusset plate. The critical value ( $S_c$ ) is defined as the splice plate thickness at which a gusset plate specimen achieves 90% or more of the buckling load of the same specimen with infinite splice plate thickness. The critical values of the specimens shown in Fig. 10.3 are given in Table 10.2. It can be seen from the table that the critical splice plate thicknesses of the specimens range from about two to four times the corresponding gusset plate thickness. Therefore, it is believed that the elastic buckling load of a gusset plate connection with an infinite splice plate thickness can be achieved by providing a splice plate thickness of at least four times that of the gusset plate. It is also observed from Fig. 10.3 that, for the same gusset plate

size and the splice plate length, the buckling load of the gusset plates is proportional to the cube of the gusset plate thickness if infinitely thick splice plates are used.

### 10.2.2.3 Effects of Splice Plate Length

As can be seen from Fig. 10.3, for the same gusset plate size and thickness and splice plate thickness, the elastic buckling loads of the specimens increase with the increasing length of the splice member. The amount of the increase depends significantly on the splice plate thickness, as shown in the figure. To further investigate the effects of the splice plate length, the elastic buckling loads of the specimens with a splice plate thickness at least equal to the corresponding critical splice plate thickness are examined and are shown in Table 10.3a. As can be seen from this table, for the gusset plate size of 850 x 550, when the splice plate length is increased from 297 mm (4 rows of bolts) to 447 mm (6 rows of bolts), the elastic buckling loads are increased by approximately 2.4 times. It is also observed from this table that the same ratio of increase is recorded for all the gusset plate thicknesses examined. As mentioned above, since the elastic buckling loads of the specimens corresponding to each splice plate length increased proportionally to the cube of the gusset plate thickness if the critical splice plate thicknesses were used, the ratio of increase in the elastic buckling load due to an increase in the splice plate length was thus maintained with various gusset plate thicknesses. For the specimen with a plate size of 850 x 700 x 6.7 and the critical splice plate thickness of 20 mm, a 33% increase in the elastic buckling is observed when the splice plate length is increased from 447 mm (six rows of bolts) to 522 mm (seven rows of bolts), as shown in Table 10.3b. Hence, it can be seen that the length of the splice plate member has a significant effect on the elastic buckling load of the gusset plate connections.

The increase in the elastic buckling load due to an increase in the splice plate length can also be observed by examining Fig. 10.2. This figure shows a triangular area of the gusset

plate which is bounded by the beam and column boundary and a line (which will hereafter be referred to as the bending line) joining the extremities of the fixed edges. It is reasonable to assume that this triangular area provides out-of-plane and rotational supports to the connection if a significant part of the splice plate is extended beyond the bending line. Diagrams of the gusset plate specimens discussed above are shown in Fig. 10.4. This figure shows that, for the 850 x 500 mm specimens, increasing the number of rows of bolts from four to six moves the splice plate member from the outside of the triangular area to the inside of it with the first row of bolts extending beyond the bending line. The increase in buckling load due to this increase in splice plate length is 2.4 times, as mentioned above. Hence, it can be seen that in order to increase the buckling load of the gusset plate connections, the splice member should be extended beyond the bending line as close to the beam and column boundary as possible.

#### **10.2.2.4 Effects of Rotational Restraint at Conjunction of Bracing Member and Gusset Plate**

The effects of rotational restraint at the conjunction of the bracing member and the gusset plate are shown in Table 10.4. This table shows the elastic buckling load of a gusset plate connection with a plate size of 850 x 550 and a splice plate thickness of 13 mm. As can be seen from the table, providing infinite rotational restraint at the conjunction of the bracing member and the gusset plate significantly increases the elastic buckling load of the gusset plates. The ratios of the buckling loads of the gusset plates with infinite restraint to the buckling loads of the gusset plates without restraint range from 2.6 to 10.1, as shown in the table.

To further examine the effects of the rotational restraint on the elastic buckling load, a rotational spring is applied to the gusset plate at the conjunction; the analytical results are shown in Fig. 10.5. As can be seen from this figure, the elastic buckling load of the

specimens increases with increasing rotational spring stiffness. However, the rate of increase diminishes significantly when the rotational spring stiffness reaches a critical value of about 400 kN·m/rad for both specimens. At this value of rotational spring stiffness, the buckling loads of the specimens have already reached more than 90% of the buckling load of the same specimens with infinite rotational restraint. To compare the flexural stiffness of a bracing member to the critical value of rotational spring stiffness, a W250x67 section with a length of 5650 mm is chosen to be the diagonal bracing member (a 4 m x 4 m frame is assumed). The diagonal bracing member is assumed to be subject to equal end moments; therefore, the flexural stiffness of the member (neglecting the axial force effects) is  $2EI/L$ , where  $E$  is the modulus of elasticity (200 000 MPa),  $I$  is the moment of inertia of the section ( $I_y = 22.2 \times 10^6 \text{ mm}^4$ ) and  $L$  is the span length of the diagonal member. For this section, the flexural stiffness based on  $2EI/L$  is 1600 kN·m/rad. Hence, it can be seen that the chosen section, which is a reasonable size for a diagonal bracing member, provides sufficient rotational restraint to the gusset plate specimens examined in this section.

#### **10.2.2.5 General Design Guidelines**

A set of general design guidelines is proposed in this section. It should be noted that these are based on the elastic parametric studies cited above. Further analytical studies which take into account the inelastic behavior of the compact gusset plate connections would be required in order to refine the proposed design guidelines. The general design guidelines for designing concentrically loaded gusset plate connections subject to compression are:

- 1) To increase the buckling strength of the gusset plate connections, the use of splice members which have a high out-of-plane bending rigidity is recommended, e.g., a tee-section or a channel section. Based on the specimens examined in the parametric



studies, a splice plate member which has a thickness of four times the gusset plate thickness is recommended.

- 2) The splice member should always be extended beyond the bending line and as close to the beam and column boundary as possible.
- 3) The use of bracing members with high out-of-plane flexural rigidity is recommended. Based on the elastic parametric studies of the specimens, a flexural stiffness of 600 kN·m/rad is recommended for the diagonal bracing members. The reduction of the flexural stiffness of the bracing members due to the axial forces in the members should be considered in the design.

### **10.3 Modified Thornton Method**

#### **10.3.1 General**

The experimental results, the analytical plastic bifurcation buckling loads, the Whitmore loads, and the Thornton loads of the specimens are shown in Table 10.5. As can be seen from the table, the Thornton load ( $P_{130}$ ) predictions are generally very conservative: the ratio of the test loads to the Thornton loads ( $P/P_{130}$ ) varies from 1.31 to 1.87. This method recommends evaluating the critical buckling stress level at the Whitmore effective width (a  $30^\circ$  dispersion angle), as discussed in Chapter 1.

The tests results and the analyses showed that the yielding of the specimens usually extended beyond the Whitmore effective width, provided that the specimens were stiff enough to avoid early instability failure. This suggests that a load redistribution has occurred in the test specimens. In order to account for this load redistribution behavior in designing gusset plate connections subject to compression, it is proposed that a  $45^\circ$  dispersion angle be used to evaluate the effective width, instead of  $30^\circ$ , as shown in Fig. 10.6. The modified Thornton load is then calculated based on the extended effective width

and the appropriate column curves. It should be noted that the unsupported length of the unit column strip was evaluated from the end of the splicing member to the beam and column boundary, since a relatively rigid splicing member was used in the testing program (see Fig. 10.6). However, the unsupported length of the unit column strip measured from the effective width section can also be used for a more conservative estimate of the inelastic buckling strength.

The calculated design loads by the Thornton method based on a  $45^\circ$  dispersion angle, labeled as  $P_{145}$ , are shown in Table 10.5. Again, the effective length factor,  $k=0.65$  was used to evaluate the Thornton loads. However, the use of this value is intended to reflect the plate action that exists in the critical region bounded by the beam and column and not to account for a fixed-fixed boundary condition for the column strip as suggested by Thornton (1984). It can be seen from the table that a significant improvement in predictions is obtained using the modified Thornton method, except for specimen SP1. This discrepancy is attributed to the fact that the SP type specimens did not experience a significant amount of yielding prior to reaching the ultimate loads. In fact, the ultimate loads of the SP type specimens are lower than the corresponding Whitmore loads; hence, the load redistribution concept is not applicable for the SP type specimens.

As shown in Table 10.5, the ratio of test loads to the modified Thornton loads varies from 0.96 to 1.19, excluding SP type specimens. However, the ratio of the test loads to the Thornton loads, based on a  $30^\circ$  dispersion angle, varies from 1.51 to 1.87. For the purpose of comparison, the test specimens from Gross (1990) were also analyzed by the modified Thornton method and the results are shown in Table 10.5. It should be noted that, according to Gross (1990), a value of 0.5 was used for the effective length factor to account for the ideal no rotation end conditions occurring during his tests. Although three tests were conducted in the program, in only two tests did the gusset plate fail in compression. Table 10.5 shows that the test to predicted ratios which are 1.50 and 1.65

for the Thornton loads based on 30° dispersion angle, improve to 1.05 and 1.15 for the modified Thornton method. Hence, it can be seen that the modified Thornton method produces a better estimate of the compressive strength of the gusset plate specimens.

### 10.3.2 Proposed Design Method

It is important to note that the modified Thornton method is developed on the basis of load redistribution due to yielding occurring in the gusset plates prior to stability failure. To ensure that sufficient yielding occurs in the gusset plate, the elastic buckling load of the gusset plates must be significantly higher than the corresponding Whitmore load. As shown in Table 10.6, the ratio of analytical elastic buckling loads (based on finite element analyses) to the Whitmore loads ranges from 1.51 to 5.33 (excluding the SP type specimens). The lowest ratio, 1.51, corresponds to specimen GP3. The test results for specimen GP3 showed that moderate yielding occurred in the gusset plate prior to stability failure and the ultimate load of the specimen is comparatively higher than the corresponding Whitmore load. Therefore, it is reasonable to establish a limit for the applicability of the modified Thornton method: namely, that the ratio of the elastic buckling load to the Whitmore load has to be greater than about 1.5.

The evaluation of the elastic buckling loads of the gusset plate connections by the finite element method is not a practical design procedure. Therefore, it is proposed that the elastic buckling load of the gusset plate connections be estimated by the Thornton method (30° dispersion angle) along with the elastic buckling equation of a column, that is:

$$\sigma_{cr} = \frac{\pi^2 E}{\left(\frac{kL}{r}\right)^2} \quad [10.1]$$

where  $\sigma_{cr}$  is the critical stress of a column and  $r$  is the radius of gyration. The elastic buckling load estimated by this procedure will be termed the Thornton elastic buckling load ( $P_{TE}$ ). The Thornton elastic buckling loads of the test specimens are shown in Table 10.6. It can be seen from this table that the Thornton elastic buckling loads are generally higher than the corresponding elastic buckling loads evaluated by the finite element method. For specimen GP3, the ratio of the Thornton elastic buckling load to the Whitmore load increases to 2.1 from 1.51 (which is the ratio of the analytical elastic buckling load to the Whitmore load). Based on the estimation of the Thornton elastic buckling loads, the design method for designing concentrically loaded gusset plate connections subject to compression is:

$$P_{cr} = P_{t45} \quad \text{if} \quad \frac{P_{TE}}{P_w} \geq 2.0 \quad [10.2a]$$

$$P_{cr} = P_{t30} \quad \text{if} \quad \frac{P_{TE}}{P_w} < 2.0 \quad [10.2b]$$

where  $P_{cr}$  is the compressive strength of the gusset plates and all the other terms have been defined previously. It is assumed that the general design guidelines presented in Section 10.2.2.5 will also be followed when equation [10.2] is used. If the gusset plate shapes are significantly different from a rectangular shape, equation [10.2b] is recommended regardless of the ratio of the Thornton elastic buckling load to the Whitmore load and the length of the unit column strip as suggested by Thornton (1984) should be used. It should also be noted that the above design method is based on a limited number of test data and analytical study. Therefore, further experimental and analytical investigations are required to refine the design method.

The above design method has also been applied to the test results from Hu and Cheng (1987). The test results of this investigation are repeated in Table 10.7, along with the Whitmore loads ( $P_w$ ), the Thornton elastic buckling loads ( $P_{TE}$ ), the Thornton loads ( $P_{t30}$ )

and the analytical elastic buckling loads, assuming an infinite splice plate thickness for the test specimens. Since the ratios of  $P_{TE}$  to  $P_w$  for all the specimens are significantly less than 2.0, equation [10.2b] should be used to estimate the buckling strength of the specimens. The  $P_{B30}$  predictions of the specimens are conservative for three of the four cases. The overestimation of the buckling load for specimen C1 is because the splice plate used in the test of specimen C1 was only 13.0 mm thick, and this is not sufficient to provide the required stiffness as recommended in the general design guidelines. To further investigate this result, the analytical buckling loads (evaluated using ANSYS) with an infinite splice plate thickness ( $P_E$ ) are evaluated and shown in Table 10.7. The table shows that the analytical buckling load of specimen C1 is two times the corresponding test load; however, the  $P_{B30}$  prediction of specimen C1 is conservative relative to the analytical buckling load. Hence, it can be concluded that if the recommended general design guidelines are followed, the proposed design method will provide a conservative estimate of the compressive strength of gusset plate connections.

## **10.4 Eccentrically Loaded Gusset Plate Connections**

### **10.4.1 General**

The physical tests showed that the failure mode for the eccentrically loaded specimens was yielding at the splice member and the gusset plate. However, it should be noted that the yielding at the splice member was recorded during the loading stage whereas the yielding at the gusset plate was only observed when the applied load was very close to the ultimate load. Rigid plastic collapse analyses were conducted on specimens EP1 and EP2. These analyses, together with the elastic curves based on the large deflection assumption (evaluated using ANSYS), provided good estimates of the ultimate loads of the specimens, as discussed in Chapter 9. However, this method may not be practical in everyday design since a finite element analysis is required to evaluate the elastic curve.

According to Hu and Cheng (1987), the strength of the eccentrically loaded specimens can be evaluated using the beam-column equation for a rectangular cross-section. The beam-column formula for a rectangular section, as presented in the previous chapter is:

$$\left(\frac{P}{P_y}\right)^2 + \left(\frac{M_{pc}}{M_p}\right) = 1.0 \quad [10.3]$$

The ultimate strengths of the EP type specimens estimated by equation [10.3] are shown in Table 10.8. It should be noted that the beam-column equation only considers the cross-sectional strength of the splice member. It was also assumed that the total eccentric moment was resisted by the splice member at the conjunction of gusset-to-splice, which is a conservative approximation. The detail calculations are contained in the Appendix.

It can be seen from Table 10.8 that the beam-column equation produces conservative estimates of the strength of the specimens. The test to predicted ratios range from 1.16 to 2.54. (It should be noted that a linear beam-column equation which used the yield moment of the cross-section was employed to evaluate the strength of specimen EP3. In this case, the tee-section splicing member used is a Class 3 section according to the steel design specification (S16.1)). A reasonable prediction of the strength by the beam-column equation was obtained for specimen EP3. This is probably because the splice member for this specimen was relatively rigid and hence more moment was distributed to the splice member. Therefore, the assumption that the eccentric moment was resisted by the splice member was quite valid.

For specimens EP1 and EP2, which have relatively slender splice plates, if the assumption of the distribution of the eccentric moment is modified such that both the splice plate and the gusset plate share an equal amount of eccentric moment, the ultimate loads estimated by the beam-column equation are significantly improved. The beam-column ultimate loads of specimens EP1 and EP2 based on this modified assumption are shown in Table 10.8. It can be seen that the test to predicted ratios for specimens EP1 and EP2 are greatly

improved, decreasing from about 2.54 down to 1.42. It is believed that this modified assumption is still quite conservative since the bending rigidity of the gusset plate is usually larger than that of the splice plate member and hence more moment will be distributed to the gusset plate.

#### **10.4.2 General Design Guidelines**

Keeping in mind that the number of test data are limited, general design guidelines for designing the eccentrically loaded gusset plate connections can be set out as follows:

- 1) Eccentricity of load should be avoided in the gusset plate connections in order to prevent premature yielding failure of the splice member.
- 2) If the loading eccentricity cannot be avoided, splice members which have a high out-of-plane flexural rigidity (such as tee-sections and channel sections) are recommended. In this case, the beam-column equations for a rectangular cross-section can be used to evaluate the strength of the splice members. It should be assumed that the total eccentric moment is resisted by the splice members.
- 3) If a plate type splice member is used for the eccentrically loaded gusset plate connections, the beam-column equation for a rectangular cross-section can be used to evaluate the strength of the splice plate member. It should be assumed that half of the eccentric moment is resisted by the splice plate member.

Table 10.1 Buckling Loads of Test Specimens from Hu and Cheng (1987)

Specimen	Plate Size (mm x mm x mm)	Free Case	Finite Element	Whitmore Load
		Buckling Load P (kN)	Buckling Load P <sub>ANSYS</sub> (kN)	P <sub>w</sub> (kN)
C1	850 x 550 x 6.7	441.7	604.0	1922
C2	850 x 550 x 3.11	122.4	94.5	424
C3	850 x 700 x 6.7	380.1	332.0	1922
C4	850 x 700 x 3.11	89.6	37.3	424

Table 10.2 Critical Splice Plate Thickness for 850 x 550 and 850 x 700 Specimens

Specimen Size	Gusset Plate	Splice Plate	Critical Splice Plate	$\frac{S_c}{t}$
	Thickness t (mm)	Length SL (mm)	Thickness S <sub>c</sub> (mm)	
850 x 550	3.11	297	7	2.25
	3.11	447	13	4.18
	6.7	297	13	1.92
	6.7	447	26	3.88
	9.5	297	26	2.74
	9.5	447	35	3.68
850 x 700	6.7	447	20	2.99
	6.7	552	20	2.99



Table 10.3a Effects of Splice Plate Length on Buckling Loads for Specimens with a Plate Size of 850 x 550

Gusset Plate Size and Splice Plate Thickness	P SL = 297 4 Rows of Bolts (kN)	P SL = 447 Six Rows of Bolts (kN)	$\frac{P_{(SL=447)}}{P_{(SL=297)}}$
850 x 550 x 9.5 splice plate thickness = 35	1038	2526	2.43
850 x 550 x 6.7 splice plate thickness = 26	378	920	2.43
850 x 550 x 3.11 splice plate thickness = 13	38.8	95.9	2.47

Table 10.3b Effects of Splice Plate Length on Buckling Loads for Specimens with a Plate Size of 850 x 700

Gusset Plate Size and Splice Plate Thickness	P SL = 447 Six Rows of Bolts (kN)	P SL = 552 Seven Rows of Bolts (kN)	$\frac{P_{(SL=552)}}{P_{(SL=447)}}$
850 x 700 x 6.7 splice plate thickness = 20	353	471	1.33

**Table 10.4 Effects of Rotational Restraint at the Conjunction of Bracing Member and Gusset Plate**

Splice Plate Length (SL) (mm)	t Gusset Plate Thickness (mm)	P	P
		With Infinite Rotational Restraint (kN)	Without Rotational Restraint (kN)
297	12.7	1213	346
	9.50	758	152
	6.70	344	55.0
	3.11	38.3	5.60
447	12.7	1275	499
	9.50	849	237
	6.70	573	90.7
	3.11	95.9	9.65
522	12.7	1383	619
	9.50	888	315
	6.70	591	128
	3.11	144	14.2

Gusset Plate Size = 850 x 550 mm Splice Plate Thickness = 13.0 mm

E = 200 000 MPa

Table 10.5 Comparison of Test Loads with Analytical and Design Loads

Specimen	Ultimate Load		Whitmore Load		Thornton Load		Thornton Load		$\frac{P}{P_{ANSYS}}$	$\frac{P}{P_{130}}$	$\frac{P}{P_{145}}$
	P (kN)	$P_{ANSYS}$ (kN)	$P_w$ (kN)	$P_{130}$ (kN)	$P_{145}$ (kN)	Thornton Load (kN)	Thornton Load (kN)				
GP1	1956	2336	1216	1142	1792	1792	1792	0.84	1.71	1.09	
GP2	1356	1483	930	828	1300	1300	1300	0.91	1.64	1.04	
GP3	742	680	555	439	689	689	689	1.09	1.69	1.08	
SP1	1606	1940	1852	1228	1997	1997	1997	0.83	1.31	0.80	
SP2	1010	940	1416	640	1041	1041	1041	1.07	1.58	0.97	
AP1	1720	2260	1216	1119	1757	1757	1757	0.76	1.54	0.98	
AP2	1210	1460	930	801	1257	1257	1257	0.83	1.51	0.96	
AP3	728	690	555	404	634	634	634	1.06	1.80	1.15	
MP1	1933	2320	1216	1142	1792	1792	1792	0.83	1.69	1.08	
MP2	1316	1450	930	828	1300	1300	1300	0.91	1.59	1.01	
MP3	721	755	555	439	689	689	689	0.95	1.64	1.05	
MP3A	819	765	555	439	689	689	689	1.07	1.87	1.19	
MP3B	821	735	555	439	689	689	689	1.12	1.87	1.19	
Gross 1*	516	-	-	345	491	491	491	-	1.50	1.05	
Gross 2*	614	-	-	371	534	534	534	-	1.65	1.15	

\* Test specimens from Gross (1990)

Plate thickness = 6.35 mm

Table 10.6 Comparison of Elastic Buckling Loads with Whitmore Loads of Test Specimens

Specimen	Ultimate Load		Elastic Buckling Load (ANSYS) $P_E$ (kN)	Thornton Elastic Buckling Load $P_{TE}$ (kN)	Whitmore Load $P_w$ (kN)	$\frac{P_E}{P_w}$	$\frac{P_{TE}}{P_w}$
	P (kN)						
GP1	1956		5428	10568	1216	4.46	8.69
GP2	1356		2638	4333	930	2.81	4.65
GP3	742		836	1165	555	1.51	2.1
SP1	1606		2169	2206	1852	1.17	1.19
SP2	1010		940	905	1416	0.66	0.64
AP1	1720		6476	7751	1216	5.33	6.37
AP2	1210		3181	3178	930	3.42	3.42
AP3	728		910	854	555	1.64	1.54
MP1	1933		6075	10568	1216	5.00	8.69
MP2	1316		3118	4333	930	3.35	4.65
MP3	721		985	1165	555	1.77	2.1
MP3A	819		985	1165	555	1.77	2.1
MP3B	821		985	1165	555	1.77	2.1

Table 10.7 Design Loads for Test Specimens from Hu and Cheng (1987)

Specimen Size (mm x mm x mm)	P (kN)	PE (ANSYS) with infinite splice plate thickness (kN)	P <sub>TE</sub> Thornton Elastic Buckling Load (kN)	P <sub>w</sub> Whitmore Load (kN)	P <sub>T30</sub> Thornton Load (kN)	$\frac{P_{TE}}{P_w}$
C1: 850 x 500 x 6.7	441.7	982.0	928.0	1922	780	0.48
C2: 850 x 500 x 3.11	122.4	98.3	86.6	424	79.7	0.20
C3: 850 x 700 x 6.7	380.1	395.0	596.0	1922	275.0	0.31
C4: 850 x 700 x 3.11	89.6	37.3	27.6	424	27.6	0.07

Table 10.8 Design Loads for EP Type Specimens

Specimen	Ultimate	Beam-Column	Beam-Column	Beam-Column Load with 50% Eccentric Moment at Splice	$P_{MBC}$ (kN)	$\frac{P}{P_{MBC}}$
	Load	Load with Full Eccentric Moment at Splice	Load with Full Eccentric Moment at Splice			
	P (kN)	$P_{BC}$ (kN)	$P_{MBC}$ (kN)			
EP1	310	122	271			1.40
EP2	334	132	233			1.43
EP3	890	770	-			1.16

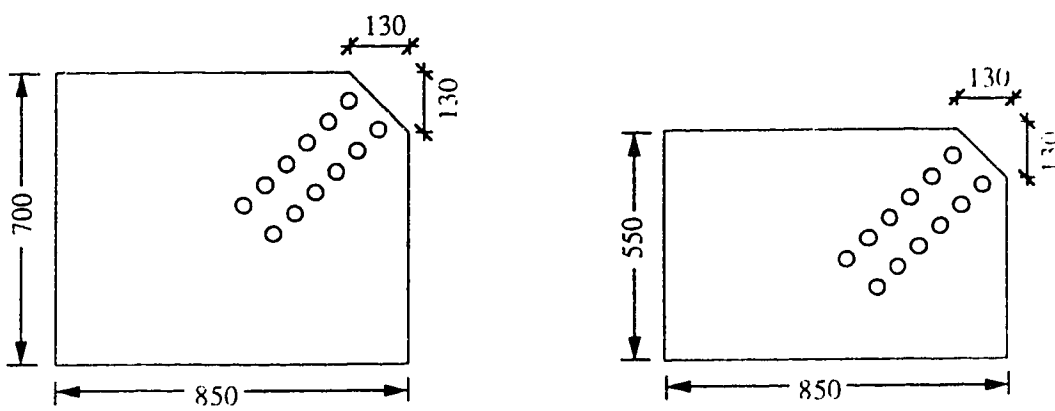
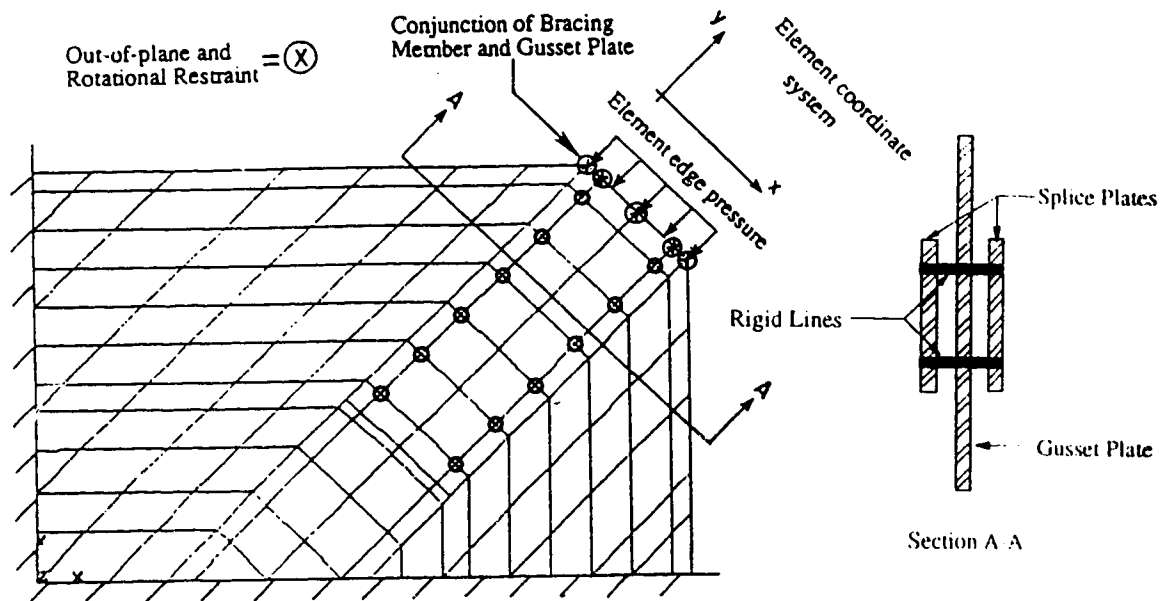


Fig. 10.1 Finite Element Model and Typical Specimens (Cheng et al., 1994)

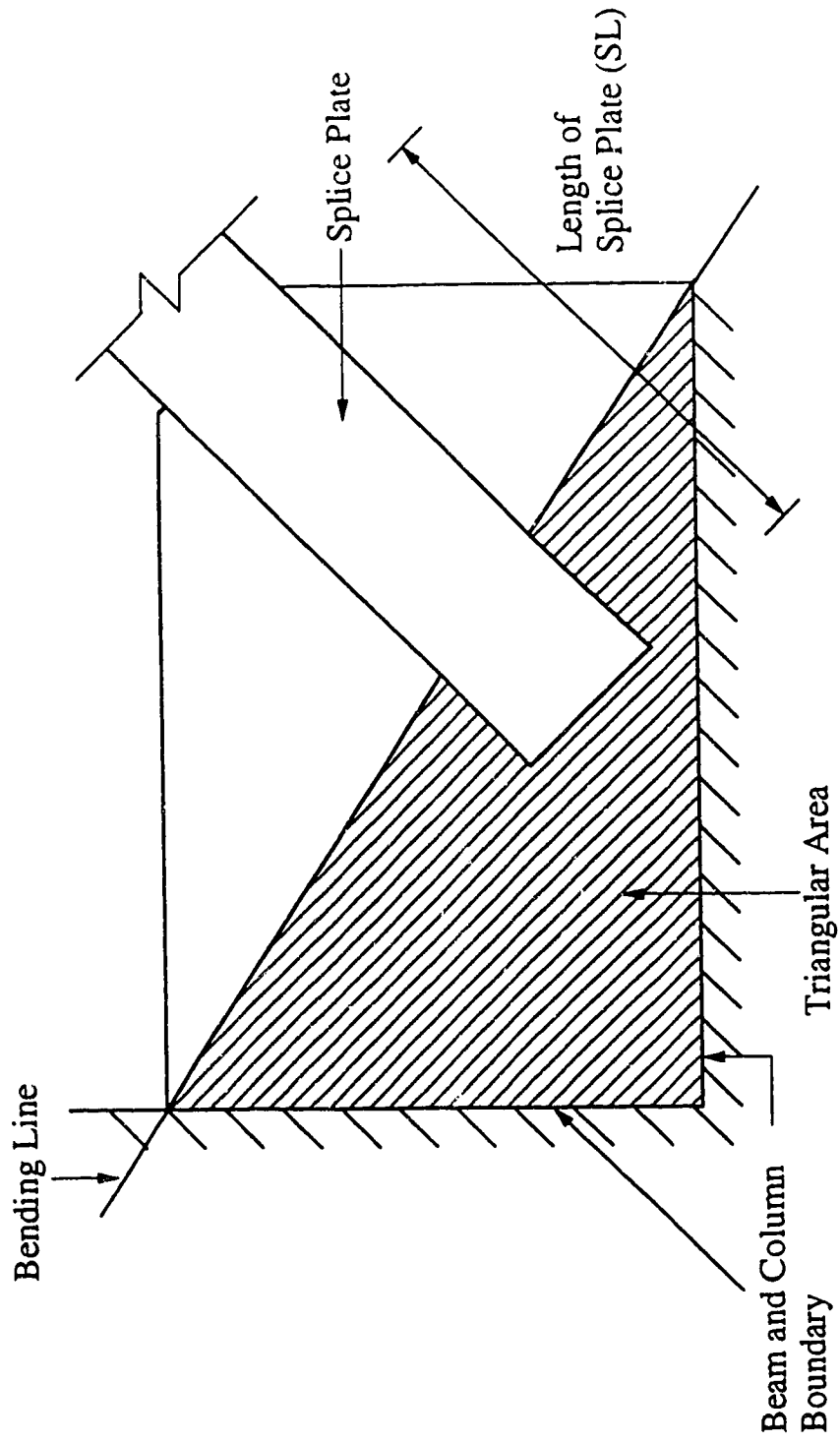


Fig. 10.2 Triangular Area of Gusset Plates



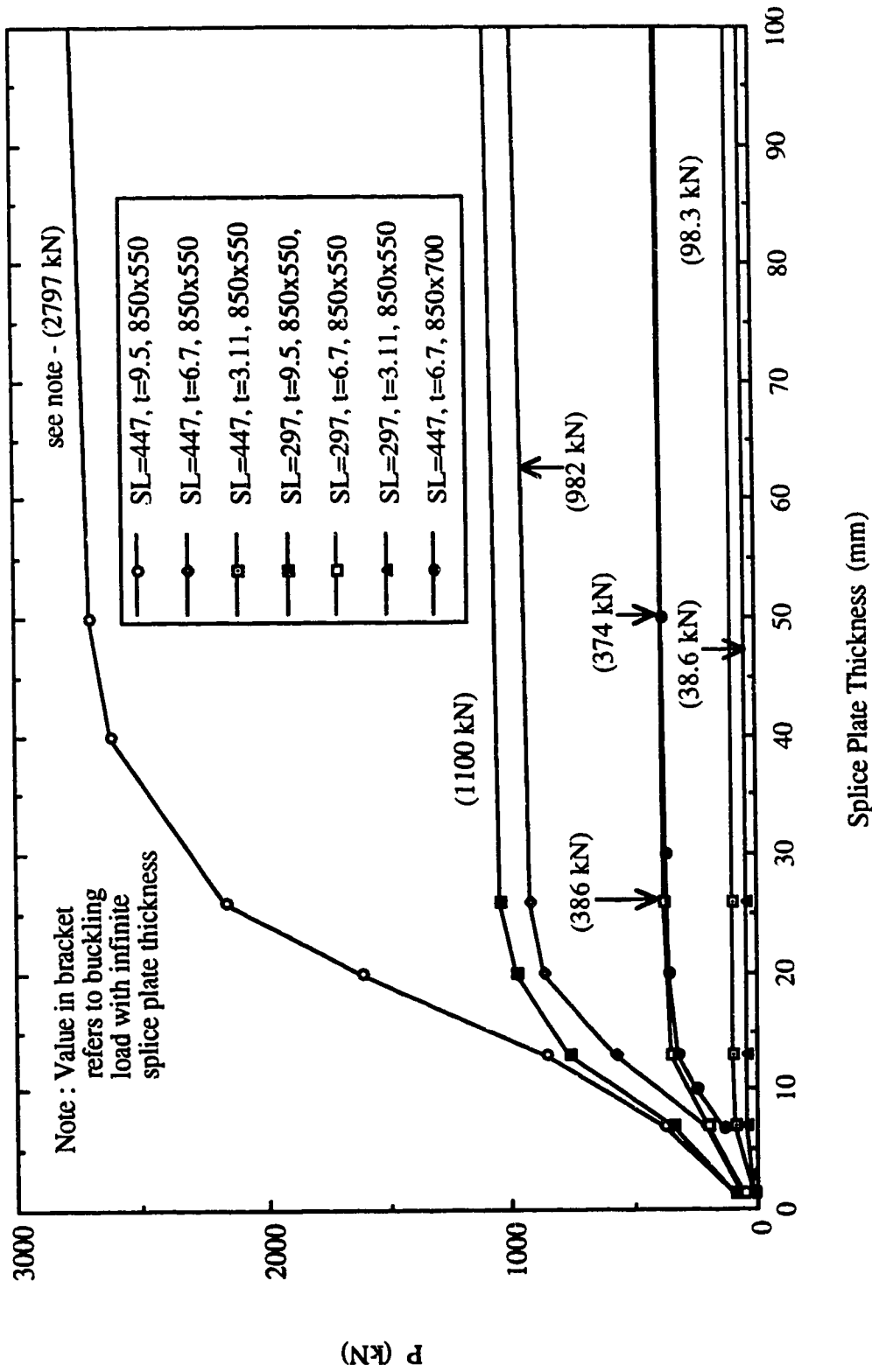
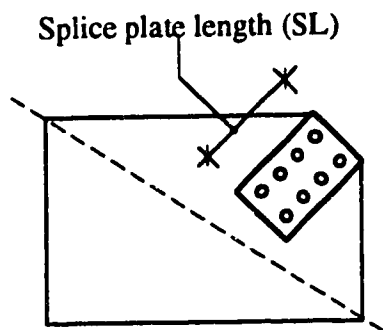
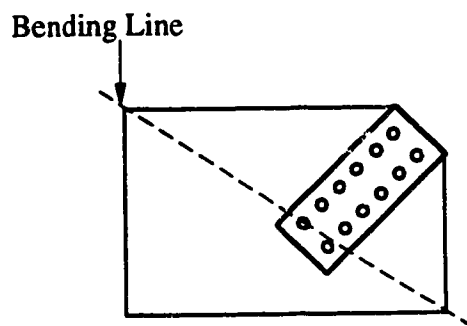


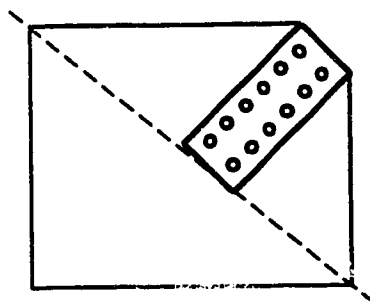
Fig. 10.3 Effects of Splice Plate Thickness on the Elastic Buckling Loads of Specimens



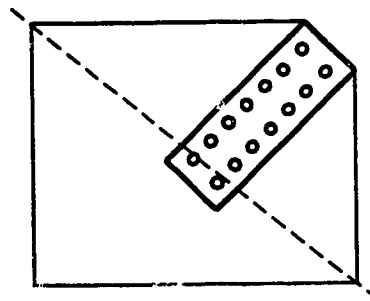
850 x 500  
Splice plate length = 297 mm



850 x 500  
Splice plate length = 447 mm



850 x 700  
Splice plate length = 447 mm



850 x 700  
Splice plate length = 552 mm

**Fig. 10.4 Various Splice Plate Lengths for the Specimens**

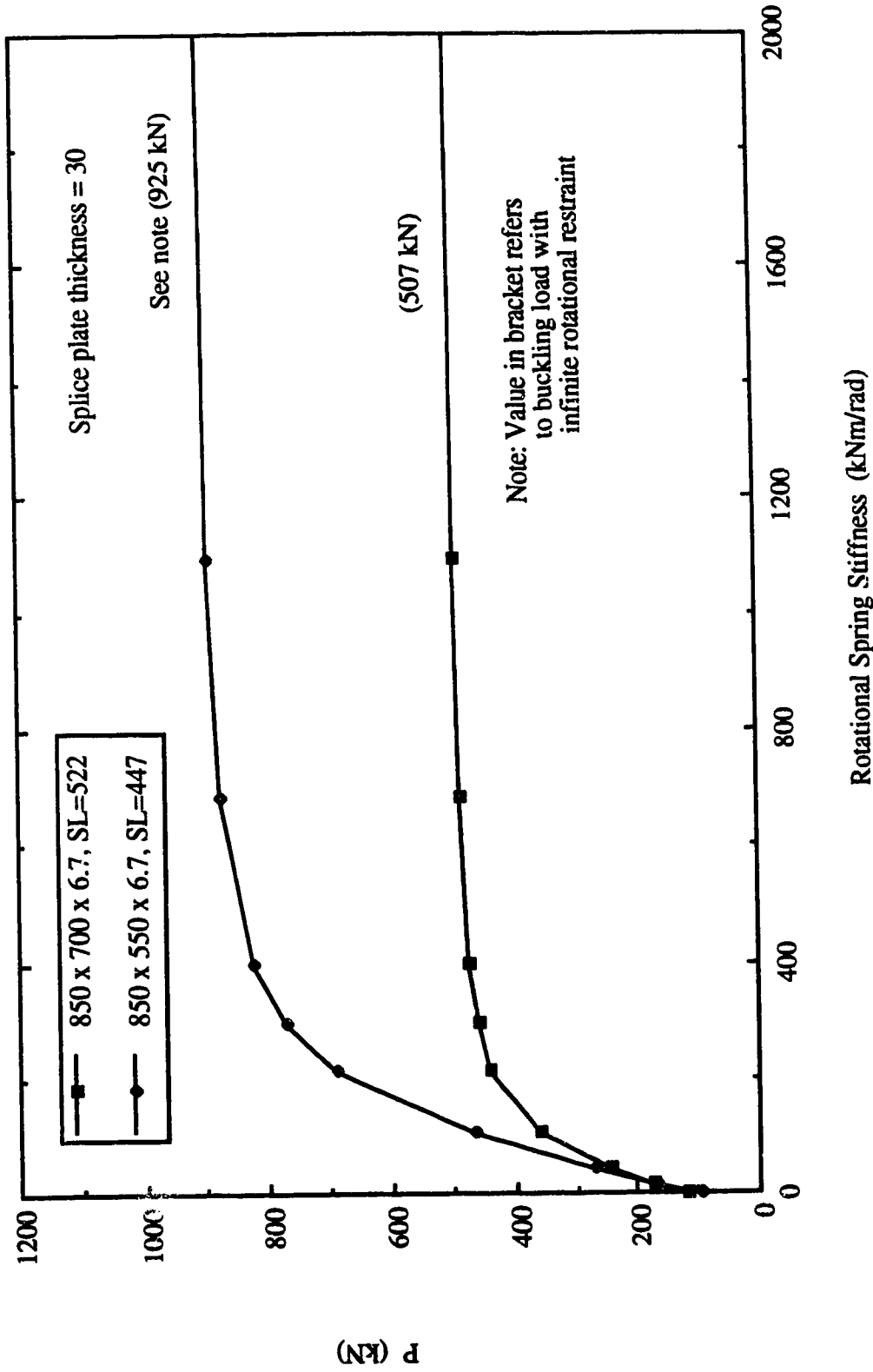


Fig. 10.5 Effects of Rotational Restraint on the Elastic Buckling Loads of Gusset Plate Specimens

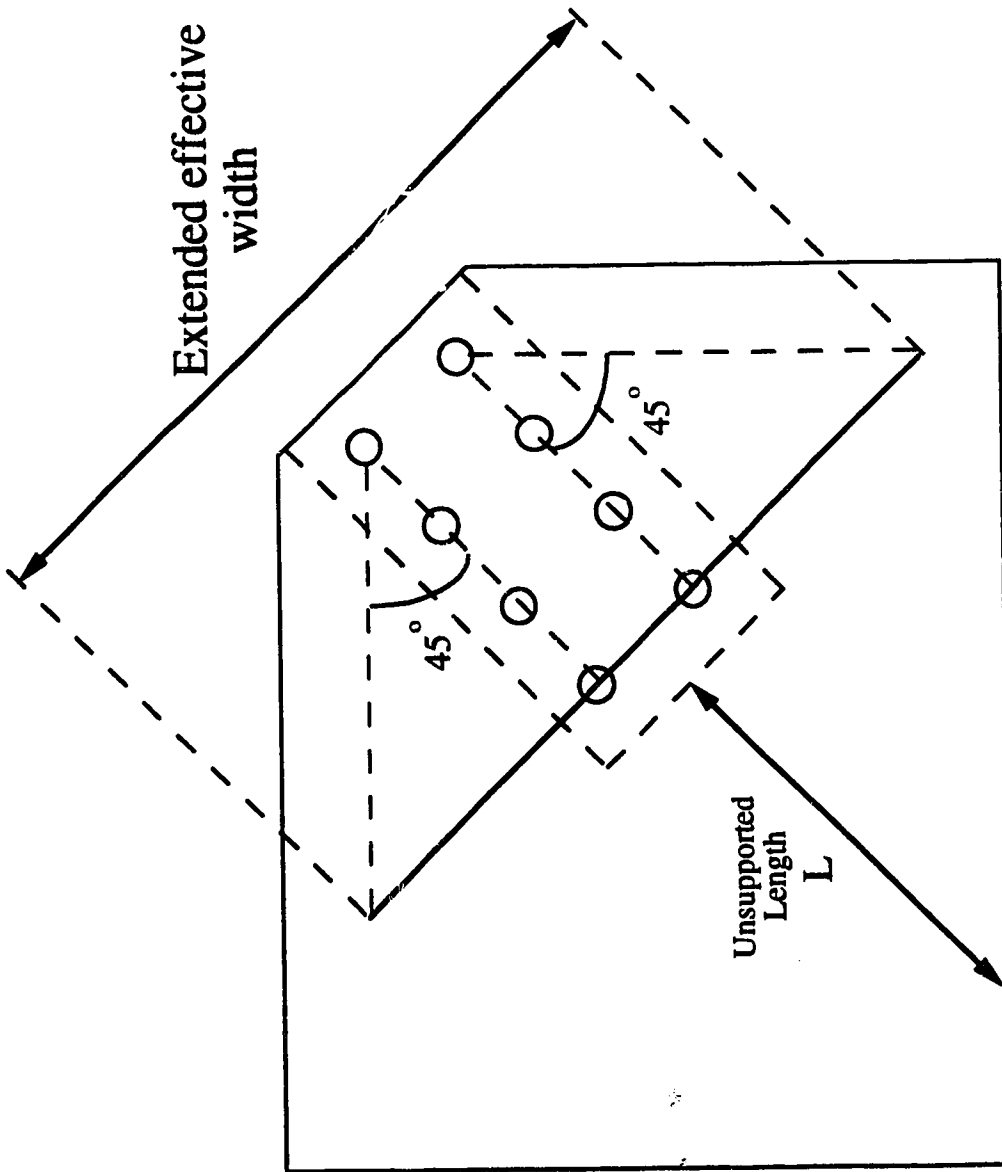


Figure 10.6 Modified Thornton Method

## 11. SUMMARY AND RECOMMENDATIONS

### 11.1 Summary

The compressive behavior and strength of steel gusset plate connections were investigated by testing full-scale diagonal bracing connections. In total, twenty-one tests were conducted on nineteen different specimens. The test parameters considered in the program were the gusset plate thickness and size, the out-of-plane restraint boundary conditions, the brace angle, the beam and column moments, and the loading eccentricity.

The finite element method was employed to analyze the test specimens. The finite element program ANSYS was used in these analyses. An elastic parametric study was conducted to examine the effects of splice plate thickness, splice plate length, and rotational restraint at the conjunction of the bracing member and the gusset plate upon the elastic buckling strength of the gusset plate connections.

The following is a summary of the research findings.

- 1) For specimens tested without the out-of-plane restraint boundary condition, the failure mode was sway buckling of the gusset plate connections. However, if an out-of-plane restraint boundary condition was imposed, a local buckling failure mode was observed.
- 2) In general, significant yielding was observed in the gusset plate specimens prior to their reaching the ultimate loads, except for the slender specimens (850 x 700 mm).
- 3) The ultimate loads of the specimens are almost linearly proportional to the gusset plate thickness.
- 4) Significant in-plane bending was observed for the specimens with a 30° brace angle. The ultimate loads of the 30° brace specimens were slightly lower than for the corresponding 45° brace specimens.

- 5) The presence of beam and column moments did not affect the ultimate loads of the gusset plate specimens. However, the in-plane stiffness of the specimens was reduced by the moments, and yielding was observed at a load level significantly lower than the corresponding yield load estimated by the Whitmore effective width method.
- 6) The ultimate loads of the compact specimens (500x400 mm) were significantly higher than the corresponding yield load levels estimated by the Whitmore effective width method.
- 7) The Thornton method ( $30^\circ$ ) produced conservative estimates of the ultimate loads of the specimens.
- 8) The eccentrically loaded specimens failed by extensive yielding at the splice member. The ultimate strength of the specimens was improved significantly when a tee-section splice member was used instead of a plate type splice member.
- 9) Plastic bifurcation buckling analyses done using ANSYS give reasonable predictions of the ultimate loads of the test specimens. The test to predicted ratios range from 0.76 to 1.12.
- 10) The ultimate loads of the eccentrically loaded specimens evaluated by the load-deflection analysis using ANSYS are in good agreement with the test results. The test to predicted ratios range from 0.97 to 1.05.
- 11) The rigid plastic analysis, together with the elastic curve evaluated using ANSYS, provided a good estimate of the ultimate loads of the eccentrically loaded specimens which used a plate as the splice member.

## **11.2 Design Recommendations**

### **11.2.1 Concentrically Loaded Gusset Plate Connections**

It should be noted that the design recommendations are based on a limited number of test data and analytical studies. Therefore, further experimental and analytical investigations are

required to refine these design recommendations. The method recommended for designing concentrically loaded gusset plate connections subject to compression is:

$$P_{cr} = P_{t45} \quad \text{if } \frac{P_{TE}}{P_w} \geq 2.0$$

$$P_{cr} = P_{t30} \quad \text{if } \frac{P_{TE}}{P_w} < 2.0$$

where  $P_{cr}$  = the compressive strength of gusset plates

$$P_{t45}(\text{modified Thornton load}) = \sigma_r \times (2 l_b \tan 45^\circ + s) t$$

$\sigma_r$  = compressive stress of the unit column strip (Fig. 11.1) evaluated using the column curves in CAN/CSA-S16.1-M89 (Clause 13.3.1)

$$P_{t30}(\text{Thornton load}) = \sigma_r \times (2 l_b \tan 30^\circ + s) t$$

$$P_{TE}(\text{Thornton elastic buckling load}) = \frac{\pi^2 E}{\left(\frac{kL}{r}\right)^2} \times (2 l_b \tan 30^\circ + s) t$$

$$k = 0.65$$

$$P_w(\text{Whitmore load}) = F_y \times (2 l_b \tan 30^\circ + s) t$$

The dimensions  $l_b$ ,  $s$ ,  $L$ , and  $t$  are defined in Fig. 11.1. It is assumed that the general design guidelines presented in Section 10.2.2.5, which are not repeated here, are followed when employing the above design recommendations. If the gusset plate shapes are significantly different from a rectangular shape, the Thornton load ( $P_{t30}$ ) is recommended, regardless of the ratio of the Thornton elastic buckling load to the Whitmore load, and the length of the column strip as suggested by Thornton (1984) should be used.

### 11.2.2 Eccentrically Loaded Gusset Plate Connections

Based on a limited number of test data and analyses, the following general design guidelines for designing eccentrically loaded gusset plate connections are recommended:

- 1) Loading eccentricity should be avoided in the gusset plate connections so as to prevent premature yielding failure at the splice member.
- 2) If loading eccentricity cannot be prevented, splice members that have a high out-of-plane flexural rigidity (such as tee-sections and channel sections) are recommended. The beam-column equations for a rectangular cross-section can be used to evaluate the strength of the splice members, assuming that the total eccentric moment is resisted by the splice members.
- 3) If a plate type splice member is used for the eccentrically loaded gusset plate connections, the beam-column equation for a rectangular cross-section can be used to evaluate the strength of the splice plate member, assuming that half of the eccentric moment is resisted by the splice plate member.

### **11.3 Recommendations for Future Research**

In order to develop a set of complete guidelines for designing the compressive strength of the gusset plate connections, the following areas should be further investigated:

- 1) More tests should be conducted to investigate the effects of gusset plate shape, types of splicing members, and types of bracing members on the ultimate strength and compressive behavior of gusset plate connections.
- 2) Parametric studies on the inelastic compressive behavior of gusset plate connections by the finite element method should be performed and important design variables should be identified in order to develop complete rational design procedures.
- 3) More tests should be conducted to investigate the compressive behavior of eccentrically loaded gusset plate connections. Test variables such as the relative stiffness of the



**gusset plate and the splice member, stiffener requirements, and the types of splicing members should be further investigated.**

- 4) Parametric studies of eccentrically loaded gusset plates should be conducted in order to develop rational design guidelines for this kind of connection.**

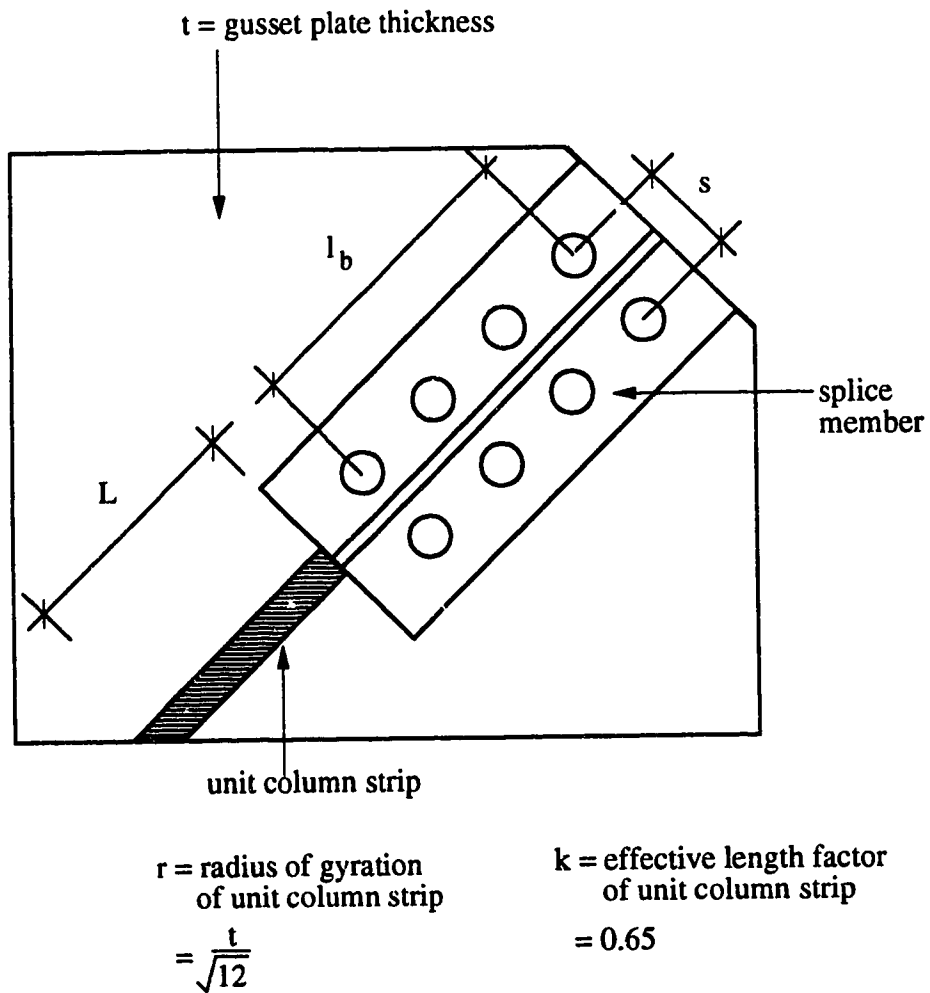


Fig. 11.1 Dimensions Required in the Design Method

## REFERENCES

- AISC, 1993. Load and Resistance Factor Design Specification for Structural Steel Buildings. American Institute of Steel Construction (AISC), Chicago, Illinois.
- Akay, H.U., Johnson, C.P. and Will, K.M., 1977. "Lateral and Local Buckling of Beams and Frames." *Journal of Structural Division, ASCE*, 103(9), 1821-1832.
- ANSYS User's Manual 4.4, 1989. Swanson Analysis System Inc.
- Bjorhovde, R and Chakrabarti, S.K., 1985. "Tests of Full-Size Gusset Plate Connections." *Journal of the Structural Division, ASCE* 111(3), 667-686.
- Chakrabarti, S.K. and Richard, R.M., 1990. "Inelastic Buckling of Gusset Plates." *Structural Engineering Review*, 2, 12-29.
- Chang, S.C. and Chen, J.J., 1986. "Effectiveness of Linear Bifurcation Analysis for Predicting the Nonlinear Stability of Structures." *Int. J. of Num. Meth. Engng.*, Vol. 23, No. 5, 831-846.
- Cheng, J.J.R., Yam, M., and Hu, S.Z., 1994. "Elastic Buckling Strength of Gusset Plate Connections." *Journal of Structural Engineering, ASCE*, 120(2), 538-559.
- Cook, R.D., Malkus D.S., and Plesha, M.E., 1989. *Concepts and Application of Finite Element Analysis*. 3rd edition, John Wiley & Sons.
- CSA, 1992. CAN/CSA-G40.21-M92 - Structural Quality Steel. Canadian Standards Association (CSA), Rexdale, Ontario.
- CSA, 1988. CAN/CSA-S6-88 - Design of Highway Bridges. Canadian Standards Association (CSA), Rexdale, Ontario.
- CSA, 1989. CAN/CSA-S16.1-M89 - Limit States Design of Steel Structures. Canadian Standards Association (CSA), Rexdale, Ontario.
- Davis, C.S. 1967. "Computer Analysis of the Stresses in a Gusset Plate." Thesis presented to the University of Washington, at Seattle, Wash., in partial fulfillment of the requirements for the degree of Master of Science.

- Fung, J.Y., and Richard, R.M. 1987. "Inelastic Finite Element Analysis of Gusset Plates." the University of Arizona.
- Gaylord, E.H., Gaylord, C.H., and Stallmeyer, J.E., 1992. Design of Steel Structures. 3rd edition, McGraw-Hill, New York.
- Gross, J.L. 1990. "Experimental Study of Gusseted Connections." Engineering Journal, AISC, Vol. 27, No. 3, 89-97.
- Hardash, S.G. and Bjorhovde, R. 1985. "New Design Criteria for Gusset Plates in Tension." Engineering Journal, AISC, Vol. 22, No. 2, 77-94.
- Hardin, B.O. 1958. "Experimental Investigation of the Primary Stress Distribution in the Gusset Plates of a Double Plane Pratt Truss Joint with Chord Splice at the Joint." Bulletin No. 49, Engineering Experiment Station, University of Kentucky.
- Horne, M.R. and Morris, L.J. 1981. Plastic Design of Low-rise Frames. Granada Publishing Limited - Technical Books Division, Great Britain.
- Hu, S.Z., and Cheng, J.J.R. 1987. "Compressive Behavior of Gusset Plate Connections." Structural Engineering Report No.153, University of Alberta.
- Irvan, W.G. 1957. "Experimental Study of Primary Stresses in Gusset Plates of a Double Plane Pratt Truss." Bulletin No.46, Engineering Experiment Station, University of Kentucky.
- Kitipornchai, S., Al-Bermani, F.G.A. and Murray, N.R. 1993. "Eccentrically Connected Cleat Plates in Compression." Journal of Structural Engineering, ASCE, 119(3), 761-781.
- Koroš, R.M. and Sherbourne, A.N. 1972. "Strength Predictions of Plates in Uniaxial Compression." Proceedings of ASCE, ST9, 1965-1985.
- Kulak, B.L., Fisher, J.W., and Struik, J.H.A. 1987. Guide to Design Criteria for Bolted and Riveted Joints. 2nd edition, Wiley-Interscience, New York, N.Y.
- Murray, N.W. and Khoo, P.S. 1981. "Some Basic Mechanisms in the Local Buckling of Thin-Walled Steel Structures." Int. J. Mech. Sci. Vol. 23, No. 12, 703-713.

- Rabinovitch, J.S. and Cheng, J.J. Roger. 1993. "Cyclic Behavior of Steel Gusset Plate Connections." Structural Engineering Report No. 191, University of Alberta.
- Richard, R.M., Rabern, D.A., Hormby, D.E., and Williams, G.C. 1983. "Analytical Models for Steel Connections." Behavior of metal structures, Proceedings of the W.H. Munse Symposium, ASCE, edited by W.J. Hall and M.P. Gaus, 128-155.
- Struik, J.H.A. 1972. "Applications of Finite Element Analysis to Non-Linear Plane Stress Problem." Ph.D. dissertation, Department of Civil Engineering, Lehigh University, Bethlehem, Pa.
- Thomnton, W.A. 1984. "Bracing Connections for Heavy Construction." Engineering Journal, AISC, 3rd Quarter, 139-148.
- Vasarhelyi, D.D. 1971 "Tests of Gusset Plate Models." Journal of the Structural Division, ASCE, 97(2), 665-678.
- Whitmore, R.E. 1952. "Experimental Investigation of Stresses in Gusset Plates." Bulletin No.16, Engineering Experiment Station, University of Tennessee.
- Williams, G.C. and Richard, R.M., 1986. "Steel Connection Design Based on Inelastic Finite Element Analysis." Report to the Department of Civil Engineering and Engineering Mechanics, the University of Arizona.
- Yamamoto, K., Akiyama, N., and Okumura, T. 1988. "Buckling Strength of Gusseted Truss Joints." Journal of the Structural Division, ASCE, 114(3), 575-590.

## **APPENDIX**

**Example calculation: Specimen EP1****Rigid-Plastic Unloading Line**

Splice Plate:

$$\sigma_y = 435 \text{ MPa}$$

$$P_{yS} = 435 \times 148 \times 9.5 \times 10^{-3}$$

$$= 611 \text{ kN}$$

$$M_{pS} = \sigma_y \left( \frac{bd^2}{4} \right)$$

$$= 435 \times \left( \frac{148 \times 9.5^2}{4} \right) \times 10^{-3}$$

$$= 1452 \text{ kNmm}$$

$$e = \frac{13.3 + 9.5}{2} = 11.4 \text{ mm}$$

From eqn. 9.4 :

$$P = \frac{-(e + \Delta) + \sqrt{(e + \Delta)^2 + 4 \left( \frac{M_{pS}}{P_{yS}^2} + \frac{M_{pG}}{P_{yG}^2} \right) (M_{pS} + M_{pG})}}{2 \left( \frac{M_{pS}}{P_{yS}^2} + \frac{M_{pG}}{P_{yG}^2} \right)} \quad [9.4]$$

$$\text{Therefore, } P = \frac{-(11.4 + \Delta) + \sqrt{(11.4 + \Delta)^2 + 4 \left( \frac{1452}{611^2} + \frac{7371}{2107^2} \right) (1452 + 7371)}}{2 \left( \frac{1452}{611^2} + \frac{7371}{2107^2} \right)}$$

$$P = \frac{-(11.4 + \Delta) + \sqrt{(11.4 + \Delta)^2 + 4 (5.45 \times 10^{-3})(8458)}}{(2)(5.45 \times 10^{-3})}$$

$\Delta$	0	2	4	6	8	10	12	14	15	16	18	20
P	581	521	471	429	393	362	335	312	302	292	274	258

**Beam-Column Equation**

$$\sigma_y = 435 \text{ MPa}$$

$$e = 11.4 \text{ mm}$$

$$P_{yS} = 611 \text{ kN}$$

$$M_{pS} = 1452 \text{ kNmm}$$

$$\left(\frac{P}{P_{yS}}\right)^2 + \left(\frac{M_{pS}}{M_{pS}}\right) = 1.0$$

$$\left(\frac{P}{611}\right)^2 + \left(\frac{P \times 11.4}{1452}\right) = 1.0$$

$$P^2 + 2931P = 373321$$

$$\Rightarrow P = \left( \frac{-2931 \pm \sqrt{2931^2 - 4 \times (-373321)}}{2} \right)$$

$$P = \underline{122 \text{ kN}}$$